

**Doctoral Dissertation**

**Advanced Geospatial-Based Risk Assessment of Water-Related Hazards  
Associated with SAR Interferometry Time Series of Land Deformation**

**March, 2019**

**Ni Made Pertiwi Jaya**

**Graduate School of Science and Engineering,  
Yamaguchi University**

## ACKNOWLEDGEMENT

Firstly, the author would like to express sincere gratitude to the Almighty “Ida Sang Hyang Widhi Wasa” for a grace, kindness and blessing in finishing this dissertation proposal. The title of this dissertation proposal is “Advanced Geospatial-Based Risk Assessment of Water-Related Hazards Associated with SAR Interferometry Time Series of Land Deformation”. This dissertation proposal is focused on the utilization of multitemporal satellite SAR data through interferometry processing of land deformation to assess risk of water-related hazards.

In this opportunity, the author would like to acknowledge:

1. Prof. Masaaki Oka as the President of Yamaguchi University.
2. Prof. Hiromori Tsutsumi as the Dean of the Graduate School of Sciences and Technology for Innovation.
3. Prof. Masato Shinji as the former Dean of the Graduate School of Science and Engineering.
4. Prof. Tasuku Tanaka as the international relation representative of Yamaguchi University.
5. Prof. Fusanori Miura as the former supervisor of this dissertation proposal.
6. Associate Professor DR. Eng. Masahiko Nagai as the supervisor of this dissertation proposal for the dedication, suggestion, and motivation.
7. Prof. Tsuyoshi Imai, Prof. Koji Asai, Prof. Motoyuki Suzuki, and Prof. Norikazu Shimizu as the examination committee members for the suggestions.
8. Academic section staffs in Yamaguchi University for providing all necessary information related to the master study.
9. Laboratory members of the Space Utilization Engineering Laboratory, Department of Environmental Science and Engineering, Faculty of Engineering and all Indonesian students in Yamaguchi University for the help and motivation in finishing this research.
10. Family members, especially mother, husband, older brother and younger brother for the love, support, and understanding.

The author realizes that this thesis is not yet perfect. Therefore, the author expects the constructive suggestion and criticism from readers.

Yamaguchi, March 2019

Author

## ABSTRACT

### **Advanced Geospatial-Based Risk Assessment of Water-Related Hazards Associated with SAR Interferometry Time Series of Land Deformation**

Water-related hazards have the implications for sustainable development, due to the social, economic, and environmental impacts they can cause, particularly in the urban coastal area. Evaluating the risk of the hazards is fundamental to maintain vulnerable regions. The improvement of risk assessments deals with the provision of adequate hazard-related information that can contribute to the risk reduction. Regarding this matter, there is a need to address existing challenges and prepare for future ones by focusing on risk assessment based on damage identification of related factors. In this study, the proposed risk assessment is comprehensively carried out through an advanced geospatial-based application. Considering the inter-correlation of land deformation with these types of hazards, this parameter is utilized to assess water-related hazard cases through time series analysis of SAR interferometry. In addition to providing a damage assessment, the analysis result is used as input for creating hazard-related risk maps in integration with several essentially related factors based on multi-criteria of AHP and GIS mapping.

The results of the Persistent Scatterer (PS) and Small Baseline Subset (SBAS) of time series interferometric SAR (InSAR) showed that both of the events have impacts in deformation on land. In the case of groundwater depression, the deformation analysis was performed in the area of Bali Island, Indonesia using 63 scenes of ALOS PALSAR for 2007 to 2010 analysis and 42 scenes of Sentinel 1A data for the analysis from 2014 to 2016. The deformation was obtained continuously during this period with the average of -12.08 mm/year. In particular for the land deformation due to groundwater depression, an evaluation using GNSS-CORS data was also performed which showed correlation with the InSAR analysis. The damage level of the groundwater environment can be considered from the presence or absence of the land deformation. Nevertheless, the factor has been neglected due to the insufficiency of the data. Moreover, an average deformation rate of -2.32 mm/year was estimated using five data sets of ALOS PALSAR before, during, and after the catastrophic tsunami disaster in Chile in 2010.

Furthermore, the study concerns itself with the improvement of risk assessment through multi-criteria Analytical Hierarchy Process (AHP) analysis. Besides the land deformation, land cover information generated from satellite optical data was used for the mapping. The tsunami inundation zone mapping was conducted by involving damaged areas and coastal proximity information to classify high, medium, and low vulnerability zones. The tsunami-damaged areas were identified by processing the surface reflectance values between pre- and post-disaster images of the satellite optical and SAR data due to the 2010 Chile

earthquake and tsunami. The DEM data was also employed to delineate areas according to the inundation height data. In this regards, local-based information collected from a participatory workshop called Disaster Imagination Game (DIG) was also utilized as a mapping input. Likewise, the map of the groundwater conservation was classified into protected, secure, vulnerable, and critical usage and groundwater depression information. The information was collected from institutional data and field observation. Fundamentally, the conservation zones of groundwater contain provisions related to the protection and utilization of the groundwater.

A corresponded map result compares with the available related map in the study area presented the potential use of the geospatial-based application for assessing water-related hazard risks. Moreover, taking the low operational cost and quick processing time of the technique, it is supposed to be a potential tool to assess local risk to support sustainable development in the area vulnerable with water-related hazards.

*Keywords:* Risk Assessment, Water-Related Hazards, Time Series SAR Interferometry, Tsunami Inundation Zone, Groundwater Conservation Map

## TABLE OF CONTENTS

	<b>Page</b>
COVER.....	i
ACKNOWLEDGEMENT .....	ii
ABSTRACT.....	iii
TABLE OF CONTENTS .....	v
LIST OF TABLE .....	ix
LIST OF FIGURE .....	xi
CHAPTER I INTRODUCTION .....	1
1.1 Background .....	1
1.2 Research Motivation .....	5
1.3 Research Problems .....	6
1.4 Research Objectives .....	9
1.5 Research Structure and Outline .....	9
CHAPTER II LITERATURE REVIEW.....	11
2.1 Fundamentals of Geographic Information System (GIS) and Remote Sensing.....	11
2.1.1 Geographic Information System (GIS) Technique .....	11
2.1.2 Data Collection and Remote Sensing Process.....	12
2.1.3 Passive and Active Sensor Systems.....	13
2.2 Optical Remote Sensing.....	14
2.2.1 Solar Radiation and Reflectance Spectrums .....	14
2.2.2 Interpreting Optical Remote Sensing Imageries.....	15
2.2.3 Very High Resolution (VHR) Optical Imageries of GeoEye-1 and QuickBird .....	18
2.2.4 High Resolution Optical Imagery of ALOS AVNIR-2 .....	19
2.2.5 Moderate Resolution Optical Imagery of Landsat .....	20
2.3 SAR Remote Sensing.....	22
2.3.1 SAR Principle and Geometry of SAR Image Acquisition .....	22
2.3.2 SAR Image Characteristics .....	23
2.3.3 SAR Signal Processing and Image Formation.....	25
2.3.4 Interpreting SAR Imageries .....	33
2.3.5 L-Band SAR Imagery of ALOS PALSAR.....	34
2.3.6 C-Band SAR Imagery of Sentinel-1A.....	35
2.4 Methods and Technique of SAR Interferometry .....	37

2.4.1 SAR Interferometry Processing of Deformation .....	38
2.4.2 SAR Interferogram Statistics .....	40
2.4.3 Uncertainty in DInSAR Deformation Measurement .....	43
2.4.4 Advanced Time-Series Technique of SAR Interferometry .....	45
2.4.5 Persistent Scatterer (PS) InSAR.....	46
2.4.6 Small Baseline Subsed (SBAS) .....	48
2.4.7 Merged PS and SBAS .....	51
2.5 Surface Topography .....	52
2.5.1 Global Navigation Satellite System (GNSS)	
Continuously Operating Reference Stations (CORS).....	53
2.5.2 Real Time Kinematic (RTK) Positioning Technique.....	55
2.5.3 Digital Elevation Model (DEM) of ASTER	
GDEM and SRTM.....	57
2.6 Supervised Classification Methods for Land Cover Mapping.....	60
2.6.1 Training Areas.....	61
2.6.2 Classes and Macroclasses .....	62
2.6.3 Classification Algorithms.....	62
2.7 Participatory Mapping of Disaster Imagination Game (DIG).....	67
2.8 Multi-Criteria Assessment.....	68
CHAPTER III RESEARCH METHOD .....	72
3.1 Framework of Research.....	72
3.2 Research Scheme.....	74
3.3 Research Area.....	81
3.4 Research Material.....	85
3.5 Instrument of Research.....	88
3.6 Data Analysis.....	98
3.6.1 Image Processing and Spatial Mapping.....	98
3.6.2 Time-Series InSAR Processing Using GMTSAR.....	112
3.6.3 GNSS Data Processing Using RTKLIB.....	122
3.6.4 Groundwater Depletion and Usage Analysis Using	
Groundwater Monitoring Data.....	127
3.6.5 Local Knowledge Tsunami Analysis Based on DIG	
Workshop .....	128
3.6.6 Geospatial-Based Multi-Criteria Analysis.....	129
3.6.7 Mapping Accuracy Assessment Using Confusion Matrix .....	133

CHAPTER IV RISK ASSESSMENT OF GROUNDWATER DEPLETION HAZARD ACCORDING TO GEOSPATIAL-BASED MULTI-CRITERIA ANALYSIS OF GROUNDWATER CONSERVATION MAP..... 135

4.1	Groundwater Conservation in Bali Island.....	135
4.2	Monitoring of Groundwater Level and Groundwater Usage .....	138
4.3	Land Subsidence Related to Groundwater Level Depletion.....	144
4.3.1	Application of Time Series InSAR Processing for Measuring Land Subsidence .....	144
4.3.2	Comparison Between InSAR and GNSS-CORS Measurements .....	171
4.3.3	Relationship Between Displacement and Rainfall.....	179
4.3.4	Estimation of Groundwater Level by Using InSAR Result.....	180
4.4	Classification of Land Coverage Using Optical Data in Combination with Interferometry Coherence .....	183
4.5	Groundwater Conservation Mapping in Bali Island .....	190
4.5.1	Zoning of Groundwater Conservation Through Multi-Criteria AHP Scheme .....	191
4.5.2	GIS Mapping of Groundwater Conservation in Bali Island .....	195

CHAPTER V RISK ASSESSMENT OF TSUNAMI INUNDATION HAZARD CORRESPONDING TO GEOSPATIAL-BASED MULTI-CRITERIA ANALYSIS OF TSUNAMI INUNDATION LEVEL MAP ..... 202

5.1	Tsunami Inundation in Chile .....	202
5.2	Tsunami Damage Assessment Based on Satellite Data Processing .....	205
5.2.1	Monitoring of Tsunami Damaged Locations Using VHR Optical Data .....	205
5.2.2	Extraction of Tsunami Damaged Areas by Integrating Satellite Optical and SAR Data.....	207
5.3	Land Subsidence Vulnerability Due to Tsunami Inundation .....	221
5.4	Land Cover Changes of Pre- and Post-Earthquake and Tsunami Disaster .....	226
5.5	Local Knowledge of Tsunami Inundation.....	227
5.6	Geospatial-Based Multi-Criteria Analysis by Integrating Spatial and Local Knowledge of Tsunami Inundation Zone in Talcahuano City .....	231

5.6.1 Framework of Integrated Spatial and Local Knowledge	
Analysis for Tsunami Inundation Level Mapping .....	233
5.6.2 Integrated Risk Assessment of Tsunami Inundation Zone .....	235
CHAPTER VI CONCLUSION .....	239
6.1 Conclusions .....	239
6.2 Suggestions .....	240
REFERENCES.....	241
APPENDIX A GMT5SAR PROCESSING	
APPENDIX B RTK-GNSS PROCESSING	



## LIST OF TABLE

	<b>Page</b>
Table 2.1 Types of Information in Optical Image.....	16
Table 2.2 Specifications of VHR optical satellite data of GeoEye-1 and QuickBird used in the study.....	19
Table 2.3 Characteristics and specifications of the AVNIR-2 instruments .....	20
Table 2.4 Landsat 7 ETM+ Bands .....	21
Table 2.5 Landsat 8 OLI and TIRS Bands .....	22
Table 2.6 ALOS PALSAR Characteristics .....	35
Table 2.7 Sentinel-1 operative modes .....	36
Table 2.8 Characteristics of time-series InSAR technique of PS and SBAS .....	46
Table 2.9 SRTM data naming conventions .....	59
Table 2.10 Product specifications of SRTM1 .....	60
Table 2.11 Example of Macroclasses .....	61
Table 2.12 Multi-criteria decision matrix .....	70
Table 3.1 Satellite-based data used for groundwater depletion case .....	85
Table 3.2 Secondary data used for groundwater depletion case .....	86
Table 3.3 List of satellite-based data used for tsunami inundation case .....	87
Table 3.4 List of secondary data used for tsunami inundation case .....	88
Table 3.5 Instrument list for groundwater depletion and tsunami inundation cases .....	89
Table 3.6 Mapping mark and evaluation according to the item and process step of DIG in Talcahuano City, Chile .....	93
Table 3.7 Calibration factors of spectral reflectance for the ALOS AVNIR-2 .....	100
Table 3.8 Calibration factors of spectral reflectance for the Landsat 7 ETM+ .....	100
Table 3.9 Calibration factors of spectral reflectance for the Landsat 8 OLI-TIRS in Bali Island for the groundwater depletion case.....	102
Table 3.10 Land cover macroclasses of ROIs in Bali Island and Talcahuano City.....	111
Table 3.11 Modules of GMTSAR for time-series InSAR processing in the study .....	118
Table 3.12 Characteristics of ALOS PALSAR data used in the study.....	119
Table 3.13 Characteristics of Sentinel 1A data used in this study .....	119
Table 3.14 Configuration parameters for the InSAR processing using GMTSAR.....	122
Table 3.15 An example of confusion matrix of a classification result.....	134

Table 3.16	An example of table of confusion for high risk class.....	134
Table 4.1	Potency of freshwater resource in Bali Province.....	136
Table 4.2	Groundwater conservation zones in Bali Province.....	137
Table 4.3	Field observation schedule of groundwater level measurement in Bali.....	139
Table 4.4	Groundwater level data in Bali area from 2008 to 2012 and 2017.....	141
Table 4.5	Groundwater depletion in Bali area from 2008 to 2012 and 2017.....	141
Table 4.6	Schedule of well check observation in Bali area .....	143
Table 4.7	Characteristics of time-series InSAR technique of PS and SBAS.....	147
Table 4.8	InSAR processing parameters for ALOS PALSAR and Sentinel-1A.....	149
Table 4.9	List of ALOS PALSAR data covering the entire study area in Bali.....	151
Table 4.10	Time series cumulative displacement and mean velocity of ALOS PALSAR in Bali from 2007 to 2010.....	158
Table 4.11	List of Sentine-1A Data.....	160
Table 4.12	Orbit data for Sentinel-1A InSAR processing.....	161
Table 4.13	Time series cumulative displacement and mean velocity of Sentinel-1A in Bali from 2014 to 2017.....	170
Table 4.14	List of the GNSS-CORS data in Bali Island.....	171
Table 4.15	Data input and parameter setting for RTKLIB processing.....	172
Table 4.16	Groundwater level in subsided and non-subsided areas.....	181
Table 4.17	Pairwise comparison matrix of groundwater conservation zoning.....	195
Table 4.18	Groundwater depletion and subsidence monitoring results .....	196
Table 5.1	Water heights and wave arrival times of tsunami in Chile.....	203
Table 5.2	Calibration factors of spectral reflectance for the ALOS AVNIR-2 .....	207
Table 5.3	List of time series SAR interferometry in Talcahuano due to the 2010 Chile earthquake and tsunami event .....	222
Table 5.4	Temporal and perpendicular baseline of the ALOS PALSAR data for tsunami inundation case in Talcahuano City, Chile .....	223

## LIST OF FIGURE

	<b>Page</b>
Figure 1.1	Flow chart of the background and research motivation..... 8
Figure 1.2	Outline of the dissertation..... 10
Figure 2.1	Data collection by using remote sensing ..... 13
Figure 2.2	Object classification through optical remote sensing ..... 14
Figure 2.3	Reflectance spectrums of five Types of Land covers ..... 15
Figure 2.4	Geometry's image for a typical strip-mapping SAR imaging system ..... 23
Figure 2.5	SAR backscattered intensity ..... 24
Figure 2.6	SAR image before and after applying speckle noise removal..... 25
Figure 2.7	SAR point target return..... 26
Figure 2.8	Digital SAR processing overview ..... 27
Figure 2.9	Geometry of radar passing over a point reflector ..... 29
Figure 2.10	Triangle of earth radius, satellite radius and range to a point on the surface of the earth used to compute look angle $\theta$ ..... 32
Figure 2.11	Satellite (red) in circular inclined orbit about the Earth ..... 32
Figure 2.12	Diagram of satellite-fixed coordinate system ..... 33
Figure 2.13	ALOS PALSAR observation characteristics ..... 34
Figure 2.14	Sentinel-1 product modes ..... 37
Figure 2.15	A schematic of how the change in phase of the EM wave relates to the change in surface deformation ..... 39
Figure 2.16	Processing flow to generate InSAR-based displacement ..... 40
Figure 2.17	Modelling of scattering mechanism inside a SAR resolution cell: (a) Point scatterer; (b) PSs with one (or more) dominating scatterer within a resolution element; and (c) DSs with multiple subscatterers within a resolution element..... 41
Figure 2.18	Example spatial versus temporal baseline plot with 3 small baselines ..... 49
Figure 2.19	Comparison between the number of scatterer obtained and the velocity values achieved using PS, SBAS, and merged (PS-SBAS) methods..... 52
Figure 2.20	The current status of the InaCORS managed by BIG..... 54
Figure 2.21	Pillars of InaCORS: (a) Pilar on the ground; (b) Pilar on the roof ..... 54
Figure 2.22	RTK measurement of range cycles..... 56
Figure 2.23	ASTER GDEM..... 57
Figure 2.24	Coverage of SRTM..... 59
Figure 2.25	Region Growing Example ..... 61

Figure 2.26	Maximum likelihood example.....	63
Figure 2.27	Spectral angle mapping example.....	64
Figure 2.28	Land cover signature classification .....	65
Figure 2.29	Plot of spectral ranges.....	66
Figure 2.30	The continuous rating scale used for the pairwise comparison of factors in multi-criteria analysis .....	69
Figure 2.31	Schematic procedures for spatial multi-criteria analysis on the AHP.....	69
Figure 3.1	General framework of the research.....	73
Figure 3.2	Research scheme of risk assessment of groundwater depletion case.....	77
Figure 3.3	Research scheme of risk assessment of tsunami inundation case.....	80
Figure 3.4	Study area of the groundwater depletion case in Bali Island, Indonesia.....	82
Figure 3.5	Groundwater level monitoring in the South Bali Area .....	83
Figure 3.6	Study area of tsunami inundation case in Talcahuano City, Chile.....	84
Figure 3.7	RTK RTKLAUNCH window and launcher icons for APs .....	90
Figure 3.8	Documentation instruments: (a) Camera; (b) Drone .....	90
Figure 3.9	Groundwater monitoring instruments: (a) Hands-on GPS; (b) Water level meter .....	91
Figure 3.10	Questionnaire for groundwater conservation zonation (based on multi-criteria analysis of AHP.....)	97
Figure 3.11	Buffer zones of overlapping areas with dissolved boundary .....	107
Figure 3.12	Spatial overlay using two input vectors (a_input is rectangle and b_input is circle) with vector layer result displayed in green color: Intersection; (b) Union; (c) Symmetrical difference; (d) Difference.....	107
Figure 3.13	Delaunay triangulation with circumcircles around the red sample data .....	108
Figure 3.14	A map production window in .....	115
Figure 3.15	Design of GMTSAR and preprocessors .....	117
Figure 3.16	Overview of the main processing steps of time-series InSAR using GMTSAR processing in the study .....	123
Figure 3.17	Main Window of RTKPOST .....	124
Figure 3.18	Time Dialog of RTKPOST .....	125
Figure 3.19	Text Viewer showing Solutions by RTKP .....	126
Figure 3.20	RTKPLOT Window executed by RTKPOST .....	126

Figure 3.21	Google Earth Converter Dialog of RTKPOST .....	131
Figure 3.22	Hierarchy of criteria and alternatives .....	133
Figure 3.23	Design and construction phases for a geo-spatial model.....	195
Figure 4.1	Modified Map of the Latest Groundwater Conservation Map of Bali in 2014.....	137
Figure 4.2	Documentation of groundwater level measurement using water level in Bali Island.....	140
Figure 4.3	Distribution of monitoring wells in Bali area.....	140
Figure 4.4	Groundwater depletion map in Bali area.....	142
Figure 4.5	Field observation documentation of wells location check.....	143
Figure 4.6	Groundwater usage map in Bali area.....	144
Figure 4.7	Schematic of the phase change of the EM wave associated with the land subsidence.....	145
Figure 4.8	Land subsidence estimation by combining time series InSAR and GNSS-CORS measurements in Bali Island.....	146
Figure 4.9	SAR Data of ALOS PALSAR and Sentinel-1A in Bali Island.....	148
Figure 4.10	Coherence map in Bali Island.....	150
Figure 4.11	Pair selection of ALOS PALSAR for path 422 row 7010 .....	152
Figure 4.12	Pair selection of ALOS PALSAR for path 422 row 7020 .....	152
Figure 4.13	Pair selection of ALOS PALSAR for path 423 row 7000 .....	153
Figure 4.14	Pair selection of ALOS PALSAR for path 423 row 7010 .....	153
Figure 4.15	Pair selection of ALOS PALSAR for path 423 row 7020 .....	154
Figure 4.16	Pair selection of ALOS PALSAR for path 424 row 7010 .....	154
Figure 4.17	Pair selection of ALOS PALSAR for path 424 row 7020 .....	155
Figure 4.18	Time series cumulative displacement of ALOS PALSAR in Bali.....	156
Figure 4.19	Mean velocity of displacement using ALOS PALSAR data from 2007 to 2010 .....	159
Figure 4.20	Pair selection of SENTINEL-1A data for sub-swath F1 .....	162
Figure 4.21	Pair selection of SENTINEL-1A data for sub-swath F2 .....	162
Figure 4.22	Time series cumulative displacement of Sentinel-1 in Bali from 2014 to 2016.....	162
Figure 4.23	Mean velocity of displacement using Sentinel-1A data from 2014 to 2016 .....	169
Figure 4.24	Changes of vertical deformation from InSAR and GNSS-CORS measurements at CDPN station .....	173
Figure 4.25	Changes of vertical deformation from InSAR and GNSS-CORS measurements at CPBI station .....	174

Figure 4.26	Changes of vertical deformation from InSAR and GNSS-CORS measurements at CSRJ station .....	175
Figure 4.27	Changes of vertical deformation from InSAR and GNSS-CORS measurements at TBN0 station.....	176
Figure 4.28	Changes of vertical deformation from InSAR and GNSS-CORS measurements at JMB0 station.....	177
Figure 4.29	Changes of vertical deformation from InSAR and GNSS-CORS measurements at KLG station.....	178
Figure 4.30	GNSS-CORS measurements using CDNP and CSRJ point from 2008 to 2010 .....	179
Figure 4.31	Modified soil investigation result at Estuary DAM of Badung region.....	181
Figure 4.32	Temporal groundwater level changes of integrated InSAR and well data analysis at MW-BD04 monitoring well .....	182
Figure 4.33	Land use classification in Bali Island in 2000 .....	185
Figure 4.34	Land use classification in Bali Island in 2003 .....	186
Figure 4.35	Land use classification in Bali Island in 2014.....	187
Figure 4.36	Land use classification in Bali Island in 2016.....	188
Figure 4.37	Land use classification for the groundwater vulnerability assessment.....	189
Figure 4.38	Vulnerability level of groundwater related to the groundwater utilization .....	190
Figure 4.39	Design and construction phases for a geo-spatial model in integration with AHP.....	192
Figure 4.40	Hierarchical decomposition of criteria, sub criteria, and alternatives of the groundwater conservation mapping .....	193
Figure 4.41	Interview with experts (a) Database Division of Ministry of Land and Spatial Planning, (b) Engineering Faculty of Udayana University, (c) Ministry of Mineral and Mining Resource in Bali Province, and (d) Water River Basin Agency of Bali-Penida.....	194
Figure 4.42	Rank of alternatives for groundwater conservation zoning.....	195
Figure 4.43	Modified rainfall map in Bali .....	197
Figure 4.44	Modified morphology map in Bali .....	198
Figure 4.45	Modified groundwater basin map in Bali.....	198
Figure 4.46	Groundwater conservation map in Bali Island .....	199
Figure 4.47	Field condition in the areas classified as safety zone of groundwater conservation without subsidence.....	200
Figure 4.48	Field condition in the areas classified as vulnerable zone of groundwater conservation with subsidence .....	200

Figure 4.49	Field condition in the areas classified as critical zone of groundwater conservation with subsidence .....	200
Figure 4.50	Field condition in the areas classified as damage zone of groundwater conservation with subsidence .....	201
Figure 5.1	Tsunami inundation level map due to the 2010 tsunami event in Talcahuano, Chile .....	204
Figure 5.2	Image processing of the VHR satellite optical imageries.....	205
Figure 5.3	Visual interpretation of damage locations due to tsunami inundation from pre-and post-disaster images of VHR satellite optical data.....	206
Figure 5.4	Image processing of the extraction of tsunami-damaged areas using ALOS AVNIR-2 imageries.....	209
Figure 5.5	ALOS AVNIR-2 true-color composite images: (a) Pre-disaster (2007/2/24); and (b) Post-disaster (2010/9/4) .....	210
Figure 5.6	ALOS AVNIR-2 false-color composite images: (a) Pre-disaster (2007/2/24); and (b) Post-disaster (2010/9/4) .....	210
Figure 5.7	Water area changes based on NDVI difference of pre- and post-disaster images of ALOS AVNIR-2 optical data .....	211
Figure 5.8	Image processing of the extraction of tsunami-damaged areas using ALOS PALSAR imageries.....	212
Figure 5.9	ALOS PALSAR raw images: (a) Pre-disaster (2009/3/11); and (b) Post-disaster (2010/3/14) .....	213
Figure 5.10	Image results of the registration and resize process: (a) Pre- disaster; and (b) Post- disaster .....	214
Figure 5.11	Image results after speckle noise removal: (a) Pre-disaster; and (b) Post- disaster .....	215
Figure 5.12	Result images after backscattering processing: (a) Pre-disaster; and (b) Post-disaster .....	216
Figure 5.13	The absolute difference of pre- and post-disaster images .....	216
Figure 5.14	The water mask processing: (a) Water mask; and (b) Image result after the water mask processing.....	218
Figure 5.15	The binary image result of water and other areas.....	218
Figure 5.16	The elevation mask processing: (a) Elevation mask and (b) Image result after the elevation mask processing .....	219
Figure 5.17	Inundated area according to the satellite data extraction and field survey reports .....	221
Figure 5.18	Coherence values based on correlation image result in Talcahuano City: (a) pre-disaster and (b) post-disaster .....	222

Figure 5.19	Plot of interferogram pairs based on PS and SBAS method .....	223
Figure 5.20	Time series cumulative displacement in Talcahuano City, Chile .....	224
Figure 5.21	Mean velocity of displacement in Talcahuano City before, during, and after the 2010 tsunami event.....	225
Figure 5.22	Comparison of the Pre- and Post-Disaster Land Classification in the Area of Talcahuano, Chile.....	227
Figure 5.23	DIG flowchart, which comprises pre-event and event stages.....	228
Figure 5.24	The DIG mapping activities in Talcahuano City .....	229
Figure 5.25	The evaluation result of DIG in Talcahuano city.....	230
Figure 5.26	Modified map of tsunami inundation zone based on the DIG.....	231
Figure 5.27	General framework of the integrated spatial and local knowledge analysis for tsunami inundation level mapping.....	234
Figure 5.28	Process scheme according to the framework of the integrated spatial and local knowledge analysis of tsunami risk assessment .....	234
Figure 5.29	Tsunami inundation zone map based on the integrated geospatial and local knowledge assessment .....	237



# CHAPTER I

## INTRODUCTION

### 1.1 Background

Water-related extreme events have aggravated the number of human losses and economic damages associated with human practices. Among all observed natural and anthropogenic adversities, water-related disasters are undoubtedly the most recurrent, and pose major impediments to achieving human security and sustainable socio-economic development (Adikari and Yoshitani, 2009). Many cities are currently facing severe water uncertainties (Bolognesi, 2015). Developing and poor urban areas are the most vulnerable to the issues. There are 21 of the world's 33 megacities are built on the coast. In Asia, more than a billion people live within 100 kilometers of the sea (UN, 2010). Climate change has already affected water resource and their management in various regions (Amarnath, *et. al.*, 2016). One fifth of the world's population or about 1.2 billion people are living in areas with water scarcity by 2010. In accordance to a projected urban and industrial water use, the number will be double by 2050 (UN, 2010).

Moreover, according to the Emergency Events Database (EM-DAT), water-related disasters were reported killing about 1 million people and inflicting a total amount of damages of USD 794 billion between 1980 and 2014 all over the world (Guha-Sapir et al., 2016). The number of water-related disasters such as floods, landslides, and droughts during the period of 2000 to 2006 was 2,163 events globally that afflicting more than 1.5 billion people (Adikari and Yoshitani, 2009). Besides the events, the awareness of tsunami risks has been increasing worldwide since the 2004 Indian Ocean Tsunami (Esteban et al., 2013). Although having a relatively low frequency (compared to other water-related disaster events), tsunamis have the power to cause massive loss of life, significant economic losses, and cascading effects from the destruction of critical facilities (UNISDR, 2015a). The 2004 Indian Ocean tsunami and the 2011 Tohoku tsunami caused more than 225,000 and 19,800 fatalities, and USD 9.9 billion and USD 210 billion in direct monetary losses, respectively (CRED, 2015). Considering inevitable impacts of ongoing global climate change in increasing and strengthening extreme weather events, it will possibly expand damages on human safety and economic activities (Amarnath et al., 2016).

When addressing disaster loss reduction, as stated on Sendai Framework for Disaster Risk Reduction (DRR) 2015-2030, the first of the four priorities of DRR is the understanding of disaster risk (UNISDR, 2015b). It is an essential requisite for the sustainable development of disaster-prone areas (UNISDR, 2016). The improvement of risk assessments deals with the provision of adequate disaster-related information that can contribute to the DRR (OOSA, 2013). Therefore, there is a need to address existing challenges and prepare for future ones by focusing on risk assessment based on damage identification.

Risk assessment is modestly an application of a methodology for evaluating risk, whereby risk is defined as the probability and frequency of occurrence of a hazardous event, exposure of people and property to the hazard and consequences of that exposure (Hu et al., 2009). An integration and development of pilot case studies on hazard-damage relationships in local or regional scales are essential to establishing risk management tools for related agency managers and policy makers (Karunaratne, 2001; Smith, 2001; UNISDR, 2016). Despite critical, the relationship between hazards and damages to identify risks of disasters are poorly studied (Karunaratne, 2001). Considering the inter-correlation of both natural and anthropogenic water-related hazards to damages on land changing, such as land subsidence and land cover, these parameters are considered advantageous in assessing the hazard risks.

Land subsidence can be defined as an environmental geological phenomenon that causes the slow lowering of ground surface elevation (Chen et al., 2014). In general, it is a result of the natural compaction of sediments and extraction of groundwater, geothermal fluids, oil, gas, coal and other solids through mining (Corapcioglu, 1989; Strozzi et al., 2001). It tends to change the topographic gradients and thus causes infrastructure damages in the land surface. There is also impact on water-related hazards, such as exacerbates flooding, induces inundation of land, and reduces the capacity of aquifers to store water (Holzer and Galloway, 2005). Therefore, it is necessary to assess land subsidence for decision and policy makers to prevent a huge potential disaster, particularly water-related disasters. Furthermore, water-related hazards and land subsidence are together associated with land cover changes. In case of disasters, land cover of land use is changed according to the type of the hazards (UN-HABITAT, 2010). Moreover, changes of land cover are effected by natural-anthropogenic induced damages that have considerable consequences to social-ecological systems (Sarukhán and Whyte, 2005). In some developing urban areas, land subsidence is obtained as one of the main causes of changing on land use (Sudiana et al., 2018). Nevertheless, the land subsidence parameter as well as its impact on land cover change has been neglected for water-related assessment due to the insufficiency of the data.

Referring to Integrated Coastal Area Management (ICAM) guidelines, the utilization of satellite remote sensing imageries through GIS technology is appropriate for estimating damage due to water-related hazards (Hoffman et al., 2013). Information of land deformation measurements can be extracted from Interferometric Synthetic Aperture Radar (InSAR) data processing (Rosen, et al., 2000; Hanssen, 2001). Advanced time-series InSAR analysis of persistent scatterer (PS) method (Bell et al., 2008; Schmidt and Brügmann, 2003) and Small Baseline Subset (SBAS) method (Chen et al., 2016; Chaussard et al., 2011; Reeves et al., 2014; Reeves et al., 2014) allow generation of a long-term of subsidence. The time-series analysis is considered effective to generate displacement information by removing de-correlations that typically occur on the conventional InSAR (Bouraoui et al., 2013). In case that continuous satellite navigation technologies, Global Positioning System (GPS) or

Global Navigation Satellite System (GNSS), are available in the study area, centimeter accuracy of elevation can be derived through Real Time Kinematic (RTK) measurement (Farah et al., 2008; Sickle, 2015). The measurement can be utilized as a reference to confirm the InSAR extracted subsidence information.

Moreover, satellite optical data have been widely used to provide land cover information by only performing a modest image processing (IOC, 2009). Damage detection can also be performed by integrating two or more different types of satellite data (Chini et al., 2013). Information produced from various satellite data can be integrated for assessing risks promptly, as well as assisting rehabilitation plans (Joyce et al., 2009). Taking the benefit of geospatial application into account, a multi-criteria analysis involving land subsidence criteria in combination with other related criteria is considered effective for providing hazard risk information.

There are two study cases provided in this study to evaluate the effectiveness of the proposed geospatial-based application for risk assessment, i.e. groundwater depletion and tsunami inundation. As stated previously, these sorts of water-related events have implications on land subsidence which together effect changes on land cover (Holzer and Galloway, 2005; UN-HABITAT, 2010; Sarukhán and Whyte, 2005). Groundwater depletion indicates a natural-anthropogenic water-related disaster which relates to water condition in the ground. Moreover, tsunami inundation corresponds to a natural disaster that associates with water on the surface. Tsunami is triggered by the occurrence of high magnitude earthquakes that cause inundation on land. Fundamentally, the inundation characteristics are identical with flood. The analysis is performed in areas prone to risks of the hazard exposures, i.e. Bali Island in Indonesia and Talcahuano City in Chile, that represent vulnerable areas of groundwater depletion and tsunami inundation, respectively.

The number of population in Bali are totaled 4,200,100 people based on projected population figures in year 2016, with 1.23% annual growth since year 2010 to 2015. Economic activities in the area are driven by agriculture, industries and services including tourism (BPS, 2017). In accordance with the utilization of groundwater, the water resource has been used largely to supply domestic water demand for the tourism accommodation, such as hotels, resorts, and private villas. Moreover, groundwater has been widely used for agriculture in the area which has a limited water resource (BWS of Bali-Penida, 2017). Over-usage of groundwater in Bali area has resulted in several problems, such as the risk of land subsidence as well as saline water intrusion (Bali Post, 2013a; Bali Post, 2013b; ESDM, 2013; Putra et al., 2014; Sukearsana et al., 2015; BWS of Bali-Penida, 2017). Groundwater level monitoring in the southern Bali area from 2001 to 2015 indicated groundwater depletion at wells located in five different area classifications, i.e. tourism, river basin, settlement area, and wetland (Sukearsana et al., 2015). Sea water intrusion was also observed as the cause of the increasing of the groundwater salinity in Candidasa region located in the eastern part of

Bali. Besides climate change, groundwater depletion and lowering of land surface are considered as causes the phenomenon (Putra et al., 2014). Scientific studies have revealed that unrestricted groundwater exploitation has the potential to cause a slow but significant land subsidence (Pratt et al., 1926; Bell et al., 1986; Shie et al., 2007). A large amount of groundwater extraction results in compaction of underlying sediments, such as fine-grained sediment, that ultimately triggers land subsidence (Perlman, 2016).

Concerning the critical of the issue, the Ministry of Mineral of Natural Resource of Bali Province produced a map of groundwater conservation in 2013. The map describes four level of risks of groundwater damage in the area, i.e. safety, vulnerable, critical, and damage zones. The purpose is to assist related government agencies as policy makers to maintain the appropriate amount of groundwater extraction according to the risk levels by establishing related regulations. Based on the report, a large number of primary and secondary data was utilized for the mapping, e.g. groundwater level, well number, groundwater usage, groundwater quality, hydro-climatology, land use, and impediments of groundwater extractions (ESDM, 2013). Despite essential, subsidence as a damage indicator of groundwater depletion was not utilized for the planning. Moreover, the program was not continued due to the high-cost and time-consuming of the process. Meanwhile, Bali, Bali-Penida River Basin Agency, a national government institution for water management in Bali has been carrying out planning for developing groundwater supply (BWS of Bali-Penida, 2017). In regard to support the actions or development strategies of the groundwater utilization, an adequate and continuous information related to groundwater depletion hazard and damage is fundamental. Therefore, a multi-criteria analysis of Analytic Hierarchy Process (AHP) based on geospatial application that integrates remote sensing and in situ data is introduced to perform groundwater conservation mapping. The proposed mapping criteria consist of land subsidence and land cover information extracted from remote sensing data processing and in situ data of groundwater level change and groundwater usage.

In the case of tsunami inundation in Chile, as the area is located on the so-called “Pacific Ring of Fire,” it has been affected by thirteen earthquakes with magnitudes equal to or greater than 7.0 since 1973 (UNISDR, 2015a). The February 27<sup>th</sup> Chile’s Maule M8.8 Earthquake, which triggered a tsunami, produced the largest insured losses of 2010 (Alarcon et al. 2010). This earthquake was the fifth largest earthquake measured in history (Koshimura et al., 2010). The tsunami generated by the 2010 Maule earthquake was also the most intense in this period, with 2 to 11-meters waves hitting coastal towns for periods of up to four hours (Siembieda and Guillermo, 2010). It caused severe damage to 45 coastal towns, with total economic damage of US\$ 30 billion (EM-DAT, 2015). The government reported casualties due to the earthquake and tsunami totaled 521, with a fourth of them being tsunami-related. Experiences over recent years regarding the impacts of tsunamis have shown that inadequate preparation for, and response to, emergency situations have contributed to widespread damage and the

avoidable loss of lives and livelihoods (Siembieda and Guillermo, 2010). In some instances, these shortcomings have been due to a poor regional identification of the risk as well as its dissemination to the community (Alarcon et al. 2010). It is crucial to identify and quantify tsunami disaster risks, particularly the potential extent of tsunami inundation (Arthurton, 2007).

A map was produced after the 2010 tsunami event representing tsunami inundated areas in the area of Talcahuano. The map was created based on field-observation conducted a few weeks after the disaster (Koshimura et al., 2010) and publicly published (*Comuna de Talcahuano*, 2010; *Sistema de Informacion Comunal*, 2017). Nevertheless, the map signifies inundation risk in areas prone to tsunami hazard regardless historical information that can be obtained from local community, as well as information regarding changing or displacement on land associate with the event. A Disaster Imagination Game (DIG) is an easy and cost-effective participatory mapping methodology invented in 1997 in Japan (Komura, 2002; Warner, 2015). In the context of disaster risk reduction, it can be very empowering at the community level, since it enables an assessment based on people's perception of risks and coping strategies (Samaddar et al., 2011). In regard to combine spatial and local knowledge, an alternative risk assessment procedure is proposed by integrating satellite data processing result and local community knowledge of tsunami inundation collected from DIG workshop. An inundation level map can be produced by utilizing using the tsunami inundation criteria in integration with land subsidence and land cover criteria based on geospatial-based multi-criteria analysis.

In accordance to the importance of hazard risk information and damage identification for DRR (UNISDR, 2015b), this study concerns itself with the development of geospatial-based application of multi-criteria analysis and mapping by comprising essential criteria able to be generated from remote sensing data, i.e. land subsidence and land cover. An evaluation of the mapping result can be conducted using available published map related to the disaster to confirm the accuracy. Taking the benefit of short-time and low-cost processing of the application, it is supposed to contribute an advanced alternative method in providing risk information of water-related hazard for maintaining vulnerable areas effectively.

## **1.2 Research Motivation**

Considering the advantage of remote sensing technique, i.e. InSAR and satellite optical image processing, to provide information of damages on land associated with water related hazard, and spatial mapping application, a geospatial-based multi-criteria analysis is introduced for assessing risk of water-related hazards. There are two study cases introduced in this study, i.e. groundwater depletion in Bali Island, Indonesia and tsunami inundation in Talcahuano City, Chile. According to the background, motivation of the research through the study cases is described as follow:

1. Utilization of multi-criteria analysis processing through geospatial application to identify risks related to groundwater depletion in Bali Island. Land subsidence and land cover criteria extracted from remote sensing data processing are combined with in situ data of groundwater level change and groundwater usage to classify groundwater conservation zones. Land subsidence and its impact on land cover change has not been used for risk assessment of groundwater depletion hazard in Bali. The land subsidence information can be measured by performing time-series InSAR analysis of PS and SBAS methods. The result can be evaluated with available continuous GNSS data through RTK processing. Moreover, the subsidence impacts on land cover associated with groundwater depletion is able to be identified through image processing of supervised classification using satellite optical data in combination with SAR data. The groundwater conservation map result can be evaluated with available groundwater conservation map produced by government agency as references to assess the accuracy.
2. Utilization of tsunami inundation information from satellite data analysis and local-knowledge collected from participatory mapping in combination with land-associated damage of land subsidence and land cover as criteria to generate tsunami inundation level map in Talcahuano City, Chile. The land subsidence and land cover related to tsunami inundation can be extracted from remote sensing data, i.e. time-series InSAR and supervised classification, respectively. Eventually, the map accuracy can be confirmed through evaluation with tsunami inundation maps published by Chile government.

The map results of groundwater conservation and tsunami inundation level which have a good agreement with the reference maps indicate an improved risk assessment based on the proposed method. Regardless the accuracy, the geospatial-based multi-criteria analysis map results involving land-related damage parameters of land subsidence and land cover are supposed to be able to present an alternative method of water-related hazard risk assessment. A flow-chart of the research motivation in correspondence to the research background is described in Figure 1.1.

### **1.3 Research Problems**

In regard to the research background and motivation, the research problems are stated as follow:

1. Risks assessment of groundwater depletion hazard in Bali Island according to zonation map of groundwater conservation produced from geospatial-based multi-criteria analysis by employing land subsidence criteria extracted from time-series InSAR technique and land cover criteria generated from satellite data processing of supervised classification, in combination with groundwater level change and groundwater usage.

2. Risk assessment of tsunami inundation hazard in Talcahuano City, Chile corresponding to zonation map of tsunami inundation level generated from geospatial-based multi-criteria analysis by integrating land subsidence criteria derived from time-series InSAR of PS and SBAS methods and land cover criteria obtained from satellite data processing, with spatial and local knowledge of tsunami inundation criteria.

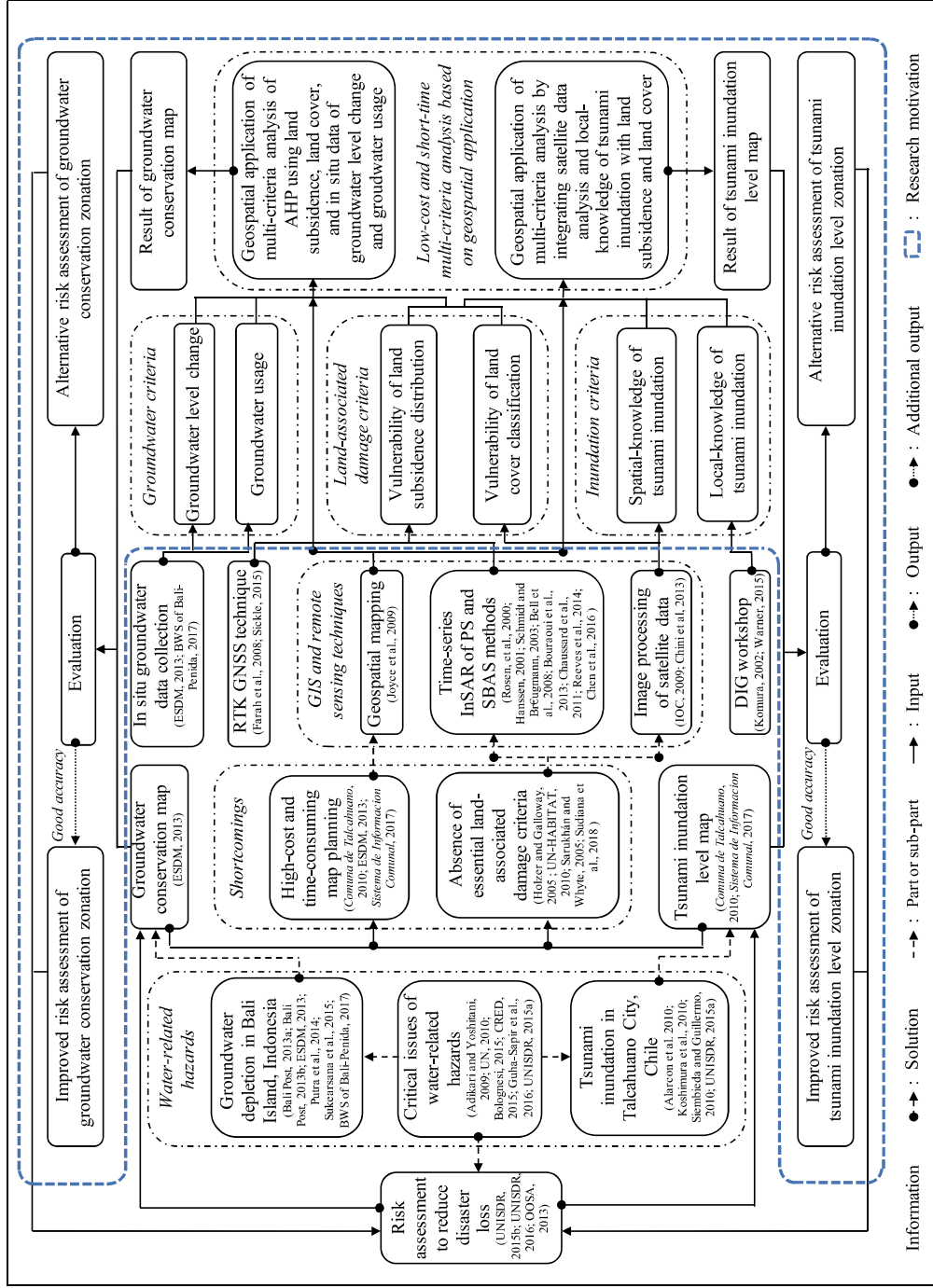


Figure 1.1 Flow chart of the background and research motivation



#### **1.4 Research Objectives**

According to the research problems, the objectives of the research are stated as follow:

1. To determine zonation map of groundwater conservation indicating risks assessment of groundwater depletion hazard in Bali Island based on multi-criteria analysis of geospatial application by employing land subsidence criteria extracted from time-series InSAR technique and land cover criteria generated from satellite data processing of supervised classification, in combination with groundwater level change and groundwater usage.
2. To establish zonation map of tsunami inundation level representing risk assessment of tsunami inundation hazard in Talcahuano City, Chile based on multi-criteria analysis of geospatial application by integrating land subsidence criteria derived from time-series InSAR and land cover criteria obtained from satellite data processing, with spatial and local knowledge of tsunami inundation criteria.

#### **1.5 Research Structure and Outline**

The research is dealing with risk assessment and mapping of water-related hazards. The water related hazards are devoted for cases of groundwater depletion in Bali Island, Indonesia and tsunami inundation in Talcahuano Chile signifying anthropogenic hazards in ground water and natural hazards on surface water, respectively. The hazards associated with damages on land, i.e. land subsidence and land cover, in which remote sensing approach using time-series InSAR and optical data processing, respectively, is able to be applied to provide the information. A multi-criteria analysis based on geospatial application involving the land-associated damage criteria are utilized to produce map as representation of risk assessment of the water-related. The study attempts to propose an alternative geospatial-based multi-criteria analysis for identifying risks of water-related hazards associated with damages of land subsidence and land cover.

The dissertation is divided into two parts. The first part contains introduction, literature review, and methodology of the research. Moreover, the second part discusses the research results of the study cases. The outline of the dissertation is described in Figure 1.2. The dissertation is structured into six chapters, as follows:

##### **1. Chapter 1**

Chapter 1 describes the introduction of the research. The introduction discusses the background of the research as well as the research motivation, research problem, research objectives, and research structure and outline.

##### **2. Chapter 2**

Chapter 2 focuses on the literature review related to the research. The literature review explains fundamentals of GIS and remote sensing techniques, optical remote sensing, SAR remote sensing, methods and technique of SAR interferometry, surface topography, supervised classification methods for land cover mapping, and multi-criteria assessment and

mapping.

### 3. Chapter 3

Chapter 3 discusses data and methodologies used in this research. The technical procedures and steps are also explained in this chapter. Technical procedures and steps comprise data sources, parameters, and data processing.

### 4. Chapter 4

Chapter 4 presents result and discussion of the study case of groundwater depletion hazard, i.e. land subsidence and land cover damages associated with the hazard, map of groundwater conservation zone, and evaluation with available reference data.

### 5. Chapter 5

Chapter 5 explains the result and discussion of the study case of tsunami inundation, i.e. pre- and post-disaster land subsidence and land cover change, tsunami inundation level map, and the assessment accuracy.

### 6. Chapter 6

Chapter 6 presents the conclusions and the future works of the research.

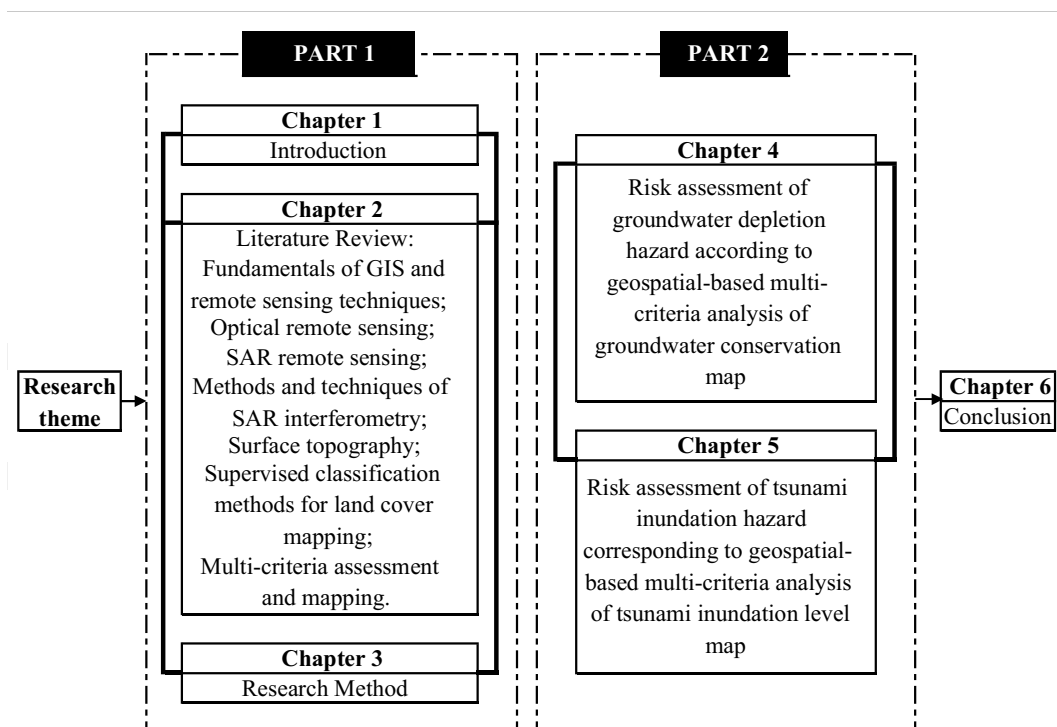


Figure 1.2 Outline of the dissertation

## **CHAPTER II**

### **LITERATURE REVIEW.**

#### **2.1 Fundamentals of Geographic Information System (GIS) and Remote Sensing**

Geographic Information System (GIS) have successfully been used in various applications, such as disaster monitoring as standalone systems, as database for planning and management, or in combination with related analysis data. The synergism between GIS and remote sensing allows representation and modelling of temporal and spatial variations due to disaster events efficiently. The integration of GIS and remote sensing with models derived from in situ information is today the technically most advanced and applicable approach (Baumgartner and Apfl, 2009).

GIS techniques are concerned with the digital capture of spatial data and spatially related attributes and their linkage relative to one another. Most importantly, geographic information processing deals with the query, analyses, reporting and output of these data. Remote sensing has always provided a primary source of geographic data to these systems. GIS applications have been developed to use raster images derived from remote sensing (Antenucci et al., 1991).

In general, the term of remote sensing is used to describe the science and art of identifying, observing, and measuring an object without coming into direct contact with it. The process involves detection and measurement of radiation from different wavelengths reflected or emitted from distant objects or materials, by which they may be identified and categorized by class or type, substance, and spatial distribution (Graham, 1999).

##### **2.1.1 Geographic Information System (GIS) Techniqiue**

A GIS is a system which is designed to collect, store, update, manage, manipulate, analyze and represent graphical and non-graphical spatial data. More precisely, the analysis procedures allow the user a wide variety of investigations such as (Antenucci et al., 1991):

1. Proximity analyses, neighborhood operations, e.g. identifying objects within a certain neighborhood fulfilling specific criteria;
2. Showing relationships between data sets within such a neighborhood;
3. Temporal operations and analyses;
4. Generating new information by combining several data layers and attributes, e.g. by splitting or aggregating, etc.

Furthermore, a GIS supports the import of external data such as remote sensing, and the selection and transfer of data into application-oriented, analytical models (Antenucci et al., 1991).

Basically, the data in a GIS can be subdivided into graphical and non-graphical data. Graphical data are digital descriptions of map features containing coordinates, symbols and

rules. Each map feature is separately stored in a layer and all the layers are geo-referenced enabling comparisons and evaluations between the different layers. For the description of the map features, several types of graphical elements are used such as points (including nodes), lines (including line segments, arcs etc.), regions (polygons), pixels and symbols. Non-graphical data (attributes) describe the characteristics, qualities or relationships of map features at a specific geographical location. Four attribute types are distinguished: attributes describing the quality and quantity of data; geographically referenced data at a specific location (excluding the map features themselves); description of spatial relationships of map features; geographical indices linking attribute data with graphical data via geocodes (Baumgartner and Apfl, 2009).

Graphical data can be stored in a raster or vector format, or some hybrid of the two. In some applications, raster-based GIS are often preferred to vector-based systems. The reason for this situation is that, very often, distributed parameter models are used where the basin is partitioned into unit elements of homogeneous hydrological parameters. In combination with the pixel structure of remote sensing data, the raster-based GIS is an ideal solution. Many investigations such as vertical analyses (i.e. logical operations) between several layers, or even more general, all geometrical and overlay operations can more easily be performed in the raster domain (Allen, 1994).

### **2.1.2 Data Collection and Remote Sensing Process**

Remote sensing relates to studying the environment from a distance using techniques such as satellite imaging, aerial photography, and radar (Hoang and Ashley, 2012). The process of data collection by using remote sensing can be seen in Figure 2.1. The detector of remote sensing is called sensor. Information about an object, an area, and a phenomenon are observed from the analysis of the data which are gathered by the sensor from the long distance. The sensor is installed to the vehicle (*platform*) that could have the shape of an aircraft, a rocket, an air balloon or a satellite. It will receive and record the reflection and electromagnetic radiation emission that came from the object. Further the data are analyzed in order to get the specific information. The integrity sizes of electromagnetic radiations that are reflected (*reflection*), passed (*transmission*) and broadcasted (*emission*) were different for each object. It depends on the characteristics of the object and the wavelength to the object (Campbell and Wynne, 2011).

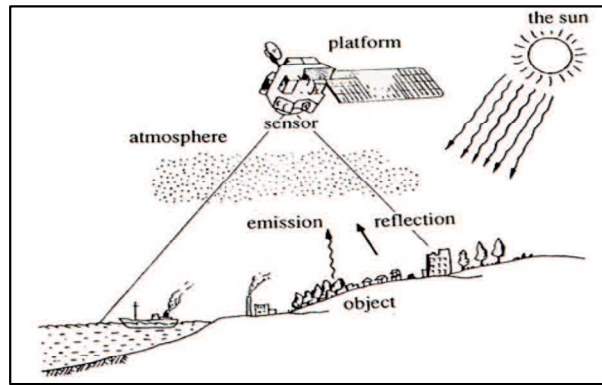


Figure 2.1 Data collection by using remote sensing  
(Source: Lilesand and Kiefer, 1993)

There are a number of important stages in a remote sensing process (Aggarwal, 2005):

- b. Emission of electromagnetic radiation (EMR) that is sun or self-emission.
- c. Transmission of energy from the source to the surface of the earth, as well as absorption and scattering.
- d. Interaction of EMR with the earth's surface such as reflection and emission.
- e. Transmission of energy from the surface to the remote sensor.
- f. Sensor data output.

### 2.1.3 Passive and Active Sensor Systems

Sensors of remote sensing that mounted on platforms gather information by measuring the electromagnetic radiation that is reflected, emitted and absorbed by objects in various spectral regions, from gamma-rays to radio waves. There are two types of sensors which are used to measure this radiation, namely active and passive remote sensors (Hoang and Ashley, 2012).

In the passive system, an array of sensors generally records the amount of electromagnetic radiation emitted by the surface being studied (Hoang and Ashley, 2012). The instruments sense only radiation emitted by the object being viewed or reflected by the object from a source other than the instrument. Reflected sunlight is the most common external source of radiation sensed by passive instruments. Passive radiometric methods of remote sensing technology include imaging radiometer, spectrometer and spectroradiometer (Graham, 1999).

Otherwise, active systems transmit a pulse of energy to the object being studied and measure the radiation that is reflected or backscattered from that object (Hoang and Ashley, 2012). The active instruments provide their own energy (electromagnetic radiation) to illuminate the object or scene they observe. They send a pulse of energy from the sensor to the object and then receive the radiation that is reflected or backscattered from that object.

Radar, scatter meter, lidar (light detection and ranging) and laser altimeter are examples of active remote sensor technologies (Graham, 1999).

Sensors mostly record information about the Earth's surface by measuring the transmission of energy from the surface in different portions of the electromagnetic (EM) spectrum. The transmitted energy varies because the Earth's surface varies in nature. This variation in energy allows images of the surface to be created. Sensors detect variations in energy in both the visible and non-visible areas of the spectrum. The ability of the atmosphere to allow energy waves to pass through it is referred to transmissivity and varies with the wavelength or type of the radiation (Baumann, 2010).

## 2.2 Optical Remote Sensing

Optical remote sensing makes use of visible, near infrared and short-wave infrared sensors to form images of the earth's surface by detecting the solar radiation reflected from targets on the ground (Figure 2.2). Different materials reflect and absorb differently at different wavelengths. Thus, targets can be differentiated by their spectral reflectance signatures in the remotely sensed images (Chini, 2015). High resolution and moderate resolution of satellite optical data are commonly used for earth monitoring, such as in case of disaster.

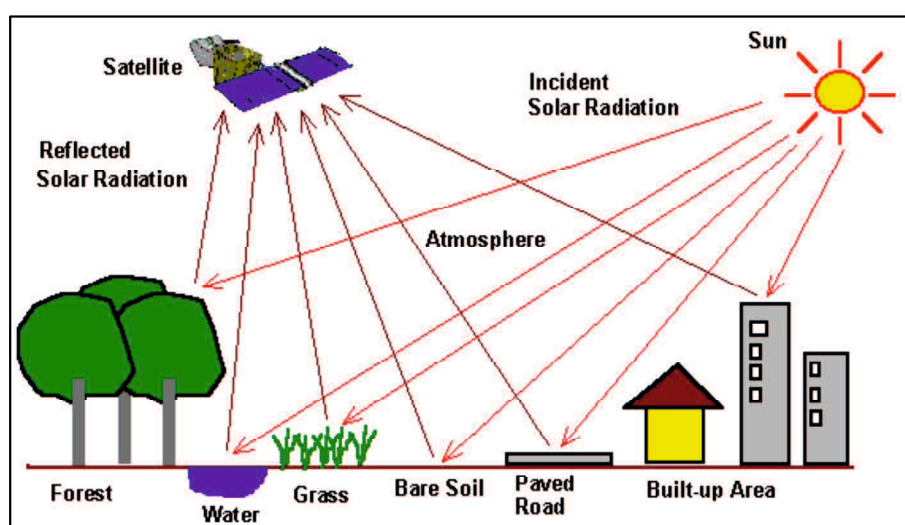


Figure 2.2 Object classification through optical remote sensing  
(Source: Liew, 2001)

### 2.2.1 Solar Radiation and Reflectance Spectrums

The solar irradiation spectrum above the atmosphere can be modeled by a black body radiation spectrum having a source temperature of 5900 K, with a peak irradiation located at about 500 nm wavelength. After passing through the atmosphere, the solar irradiation spectrum at the ground is modulated by the atmospheric transmission windows. Significant

energy remains only within the wavelength range from about 0.25 to 3  $\mu\text{m}$ . When solar radiation hits a target surface, it may be transmitted, absorbed or reflected. Different materials reflect and absorb differently at different wavelengths (Liew, 2001).

The reflectance spectrum of a material is a plot of the fraction of radiation reflected as a function of the incident wavelength and serves as a unique signature for the material. In principle, a material can be identified from its spectral reflectance signature if the sensing system has sufficient spectral resolution to distinguish its spectrum from those of other materials. This premise provides the basis for multispectral remote sensing. The following graph shows the typical reflectance spectra of five materials: clear water, turbid water, bare soil and two types of vegetation (Liew, 2001).

The reflectance of clear water is generally low. Vegetation has a unique spectral signature. The reflectance is low in both the blue and red regions of the spectrum, due to absorption by chlorophyll for photosynthesis. It has a peak at the green region which gives rise to the green color of vegetation. In the near infrared (NIR) region, the reflectance is much higher than that in the visible band due to the cellular structure in the leaves. Hence, vegetation can be identified by the high NIR but generally low visible reflectance. The shape of the reflectance spectrum can be used for identification of vegetation type (Suppasri, 2012). The reflectance spectra of five types of land covers are described in Figure 2.3.

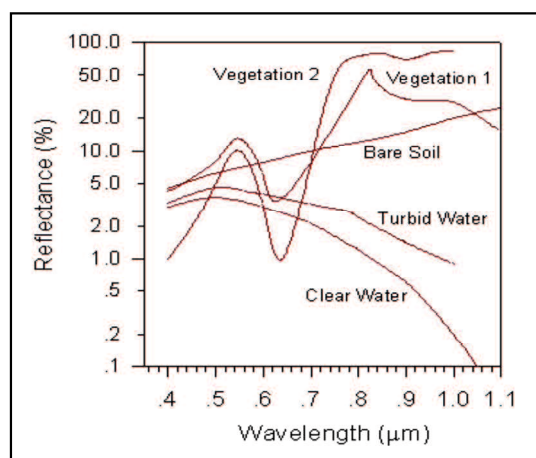






Figure 2.3 Reflectance spectra of five types of land covers  
(Source: Liew, 2001)

### 2.2.2 Interpreting Optical Remote Sensing Imageries

Information from optical image that commonly utilized for image interpretation consist of four main types, i.e. radiometric information, spectral information, textural information, and geometric and contextual information (Table 2.1). The radiometric information is the main information type utilized in the optical image interpretation. In general, it consists of only one band that displays a grey scale image. On the other hand, the spectral information is

generated by displaying several bands of data as a color-composite image using three primary colors, i.e. red, green, and blue. Moreover, texture is an important aid in visual image interpretation, especially for high spatial resolution imagery. In particular, using geometric and contextual features for image interpretation requires some a-priori information about the area of interest. The key of the texture interpretation commonly employed shape, size, pattern, location, and association with other familiar features (Liew, 2001).

Table 2.1 Types of information in optical image

No.	Types of information	Illustration image
1.	Radiometric information (brightness, intensity, and tone)	
2.	Spectral information (color, and hue)	
3.	Textural information	
4.	Geometric and contextual information	

(Source: Lilesand and Kiefer, 1993)

Types of images that represent the main information able to be interpreted from optical data are panchromatic images and multispectral images.

### 1. Panchromatic Images

A panchromatic image consists of only one band. It is usually displayed as a grey scale image, i.e. the displayed brightness of a particular pixel is proportional to the pixel digital



number which is related to the intensity of solar radiation reflected by the targets in the pixel and detected by the detector. Thus, a panchromatic image may be similarly interpreted as a black-and-white aerial photograph of the area that represents the radiometric information of an optical data (Liew, 2001).

## 2. Multispectral Images

A multispectral image consists of several bands of data. For visual display, each band of the image may be displayed one band at a time as a grey scale image, or in combination of three bands at a time as a color composite image. Interpretation of a multispectral color composite image will require the knowledge of the spectral reflectance signature of the targets in the scene. In this case, the spectral information content of the image is utilized in the interpretation (Liew, 2001).

Color composite images indicate multispectral images. In displaying a color composite image, three primary colors (red, green and blue) are used. When these three colors are combined in various proportions, they produce different colors in the visible spectrum. Associating each spectral band (not necessarily a visible band) to a separate primary color results in a color composite image (Liew, 2001).

### a. True Color Composite

If a multispectral image consists of the three visual primary color bands (red, green, blue), the three bands may be combined to produce a so-called true color image. For example, the bands 3 (red band), 2 (green band) and 1 (blue band) of a Landsat TM image or an IKONOS multispectral image can be assigned respectively to the R, G, and B colors for display. In this way, the colors of the resulting color composite image resemble closely what would be observed by the human eyes (Liew, 2001).

### b. False Color Composite

The display color assignment for any band of a multispectral can be done in an entirely arbitrary manner. In this case, the color of a target in the displayed image does not have any resemblance to its actual color. The resulting product is known as a false color composite image. There are many possible schemes of producing false color composite images. However, some scheme may be more suitable for detecting certain objects in the image (Liew, 2001).

Table 2.1 (Illustration image 2.) is an example of the false color composite of multispectral SPOT image. This false color composite scheme allows vegetation to be detected readily in the image. In this type of false color composite images, vegetation appears in different shades of red depending on the types and conditions of the vegetation, since it has a high reflectance in the NIR band as shown in the graph of spectral reflectance signature

(Figure 2.3). Clear water appears dark-bluish (higher green band reflectance), while turbid water appears cyan (higher red reflectance due to sediments) compared to clear water. Bare soils, roads and buildings may appear in various shades of blue, yellow or grey, depending on their composition (Lilesand and Kiefer, 1993).

c. Natural Color Composite

For optical images lacking one or more of the three visual primary color bands (i.e. red, green and blue), the spectral bands (some of which may not be in the visible region) may be combined in such a way that the appearance of the displayed image resembles a visible color photograph, i.e. vegetation in green, water in blue, soil in brown or grey, etc. Many people refer to this composite as a true color composite. However, this term is misleading since in many instances the colors are only simulated to look similar to the true colors of the targets. In this regard, the term natural color is preferred.

d. Vegetation Indices

Different bands of a multispectral image may be combined to accentuate the vegetated areas. One such combination is the ratio of the near-infrared (NIR) band to the red band. This ratio is known as the Ratio Vegetation Index (RVI) as follow:

$$RVI = NIR/Red \quad \text{(Equation 2.1)}$$

Since vegetation has high NIR reflectance but low red reflectance, vegetated areas will have higher RVI values compared to non-vegetated areas. Another commonly used vegetation index is the Normalised Difference Vegetation Index (NDVI) computed by:

$$NDVI = (NIR - Red)/(NIR + Red) \quad \text{(Equation 2.2)}$$

In the NDVI generated image, the bright areas represent vegetated while the non-vegetated areas (buildings, clearings, river, sea) are generally dark. The NDVI band may also be combined with other bands of the multispectral image to form a color composite image which helps to discriminate different types of vegetation.

### 2.2.3 Very High Resolution (VHR) Optical Imageries of GeoEye-1 and QuickBird

Very high resolution (VHR) optical satellites rotate in sun-synchronous orbit (400km-900km) which provides the proximity to Earth surface as well as consistent lightening. In addition, sun-synchronous orbit offers collecting images of the same point of the Earth's surface at the same local time each day. Moreover, VHR optical satellite data utilize the linear array charge-coupled device (CCD) technology sensors in push-broom mode (Jenson. 2004; Zhang and Gruen, 2006). In push-broom sensors also called survey or wide field devices, the different areas of target are imaged as the satellite moves forward by using an arranged line of sensors which are perpendicular to the flight direction. The advantages of push-broom sensors over other types are, first, low noise in received signals due to longer

dwelt time; second, there are no moving parts; hence, scan speeds of less than 1  $\mu$ s access time are possible (Hashim and Deilami, 2011). GeoEye-1 launched by GeoEye and QuickBird launched by DigitalGlobe are VHR optical data are used for this study, particularly for analysis of tsunami damaged areas. Specifications of contemporary VHR optical satellite data of GeoEye-1 and QuickBird with the capability of producing stereo images were summarized in Table 2.2.

Table 2.2 Specifications of VHR optical satellite data of GeoEye-1 and QuickBird used in the study

<b>Specifications</b>	<b>GeoEye-1</b>	<b>QuickBird</b>
Country/company	USA/GeoEye	USA/DigitalGlobe
Date of lunch	6 September 2008	18 October 2001
Resolution (stereoimage)	Pan (N) 0.5	Pan 0.61
Min/Max (m)	Multi (N) 2 Pansharpened 15.2	Multi 2.4
Swath width min/max (km)	Contiguous area 224*28	16.5*16.5
Mission	Commercial	Commercial
Stereo	Along-track	Along -track
B/H	Variable	0-6 to 2.0 most collections between 0.9 and 1.2

(Source: Hashim and Deilami, 2011)

#### **2.2.4 High Resolution Optical Imagery of ALOS AVNIR-2**

High-resolution satellite data with a resolution of 5 to 10 meters in the panchromatic and 10 to 30 meters in the multi-spectral imaging mode may be suited to generate map products in the scale of 1: 50000 and 1: 100000 in the fields of cartography (Joanneum Research Digital, 2017). ALOS offers the largest available combination of spectral, spatial and radiometric characteristics that able to acquire optical data from the Advance Visible Near-Infrared (AVNIR-2) sensor. The on-board AVNIR-2 is a high-resolution imaging spectrometer operating in the visible and NIR spectrum and a successor to AVNIR on-board the Advances Earth Observation Satellite (ADEOS). It mainly observes land and coastal areas in visible and near-infrared bands. AVNIR-2 data are available in Level 1 A, Level 1B1 and Level 1B2, which are generated by applying radiometric and geometric corrections to the acquired data (ESA, 2007). The sensor is a 4-band multispectral sensor that can be steered 44° on either side of the ground track and has a revisit rate of 2 days. Imagery is acquired at a resolution of 10 m. Characteristics and specifications of the AVNIR-2 instruments are described in Table 2.3.

Table 2.3. Characteristics and specifications of the AVNIR-2 instruments

<b>Items</b>	<b>Characteristics</b>
Number of Bands	4
Wavelength	Band1 : 0.42 - 0.50 micrometers Band2 : 0.52 - 0.60 micrometers Band3 : 0.61 - 0.69 micrometers Band4 : 0.76 - 0.89 micrometers
Spatial Resolution	10 m (at Nadir)
Swath Width	70 km (at Nadir)
S/N	>200
MTF	Band 1~3 : >0.25 Band 4 : >0.20
Number of Detectors	7000 / band
Pointing Angle	- 44 to + 44 deg.
Bit Length	8 bits
Data rate	About 160 Mbit/s of raw data, a quasi-lossless (DPCM) data compression technique reduces the actual downlink data rate of AVNIR-2 to 120 Mbit/s (3/4 reduction)

(Source: ESA, 2007)

### 2.2.5 Moderate Resolution Optical Imagery of Landsat

Moderate resolution optical imageries are integral to a wide variety of sectors, including land use planning, agriculture, and forestry, at local, regional, and global scales. Of the suite of moderate resolution satellites, Landsat is the most widely used for earth observation applications. It has been used as the primary source of moderate resolution satellite data (ASPRS, 2006).

The popularity of Landsat data can be attributed to several key characteristics of the Landsat program, including a systematic data acquisition plan and archive that ensures global coverage and data availability. Further, low imagery costs and free data distribution facilitate widespread use. The keys to the popularity of Landsat also include its data characteristics, namely its large footprint, and a spatial resolution fine enough to characterize typical land cover dynamics related to land management (Chien and Goward, 2004)

Landsat data have been collected and archived from six Landsat missions spanning nearly 35 years. The Landsat suite of satellites was initiated in 1972 with the launch of Landsat 1 Multispectral Scanner (MSS), and continues to this day with the operation of Landsat 5 Thematic Mapper (TM), Landsat 7 Enhanced Thematic Mapper Plus (ETM+)

(Scott et al., 2007). Lastly, Landsat 8 Operational Land Imager (OLI) and Thermal Infrared Sensor (TIRS) with temporal resolution of 16 days has also been developed by NASA. Images of Landsat are identified with the paths and rows of the Worldwide Reference System (WRS) for Landsat. A vast archive of images is freely available from the U.S. Geological Survey (NASA, 2013).

In regards to the study, Landsat 7 ETM+ and Landsat 8 OLI-TIRS are utilized for satellite optical processing. Landsat 7 ETM+ images consist of seven spectral bands with a spatial resolution of 30 meters for Bands 1-5, and 7. The resolution for Band 8 (panchromatic) is 15 meters. All bands can collect one of two gain settings (low or high) for increased radiometric sensitivity and dynamic range, while Band 6 collects both low and high gain (Bands 6-1 and 6-2, respectively) for all scenes. The approximate scene size is 170 km north-south by 183 km east-west (106 mi by 114 mi). The band wavelength and resolution of Landsat 7 ETM essential for image representation are described in Table 2.4.

Table 2.4 Landsat 7 ETM+ Bands

<b>Landsat 7 Bands</b>	<b>Wavelength (micrometers)</b>	<b>Resolution (meters)</b>
Band 1 - Blue	0.45 - 0.52	30
Band 2 - Green	0.52 - 0.60	30
Band 3 - Red	0.63 - 0.69	30
Band 4 - Near Infrared (NIR)	0.77 - 0.90	30
Band 5 - SWIR	1.57 - 1.75	30
Band 6 - Thermal Infrared	10.40 - 12.50	60 (resampled to 30)
Band 7 - SWIR	2.09 - 2.35	30
Band 8 - Panchromatic	0.52 - 0.90	15

(Source: Barsi, et. al., 2014)

Moreover, Landsat 8 OLI-TIRS images consist of nine spectral bands with a spatial resolution of 30 meters for Bands 1 to 7 and 9. The ultra blue band 1 is useful for coastal and aerosol studies. Band 9 is useful for cirrus cloud detection. The resolution for Band 8 (panchromatic) is 15 meters. Thermal bands 10 and 11 are useful in providing more accurate surface temperatures and are collected at 100 meters. The approximate scene size is 170 km north-south by 183 km east-west (106 mi by 114 mi) (Barsi, et. al., 2014). The band wavelength and resolution of Landsat 8 OLI-TIRS are described in Table 2.5.

Table 2.5 Landsat 8 OLI and TIRS Bands

<b>Landsat 7 Bands</b>	<b>Wavelength (micrometers)</b>	<b>Resolution (meters)</b>
Band 1 - Coastal aerosol	0.435 - 0.451	30
Band 2 - Blue	0.452 - 0.512	30
Band 3 - Green	0.533 - 0.590	30
Band 4 - Red	0.636 - 0.673	30
Band 5 - Near Infrared (NIR)	0.851 - 0.879	30
Band 6 - SWIR 1	1.566 - 1.651	30
Band 7 - SWIR 2	2.107 - 2.294	30
Band 8 - Panchromatic	0.503 - 0.676	15
Band 9 - Cirrus	1.363 - 1.384	30
Band 10 - Thermal Infrared (TIRS) 1	10.60 - 11.19	100 (resampled to 30)
Band 11 - Thermal Infrared (TIRS) 2	11.50 - 12.51	100 (resampled to 30)

(Source: Barsi, et. al., 2014)

## 2.3 SAR Remote Sensing

In the last two decades, satellite systems of SAR have provided a wealth of information on Earth observation. Indeed, SAR has become the premier sensor for the coverage necessary to observe some phenomena because it is sensitive to small surface roughness changes on the order of the radar wavelength. It is also independent of solar illumination and is generally unaffected by cloud cover. In addition, SAR has the advantage of providing control over such factors as power, frequency, phase, polarization, incident angle, spatial resolution and swath width, all of which are important when designing and operating a system for the extraction of quantitative information (McCandless and Jackson, 2004).

### 2.3.1 Principle and Geometry of SAR Image Acquisition

SAR is the most common form of active microwave radar sensors. The active radar sensors record the intensity of the transmitted microwave energy backscattered to the sensor. In SAR imaging, microwave pulses are transmitted by an antenna towards the earth surface. The microwave energy scattered back to the spacecraft is measured. When microwaves strike a surface, the proportion of energy scattered back to the sensor depends on many factors, such as physical factors, geometric factors, the types of land cover, and microwave frequency, polarization and incident angle. An example of geometry's image for a typical strip-mapping SAR imaging system is described in Figure 2.4.

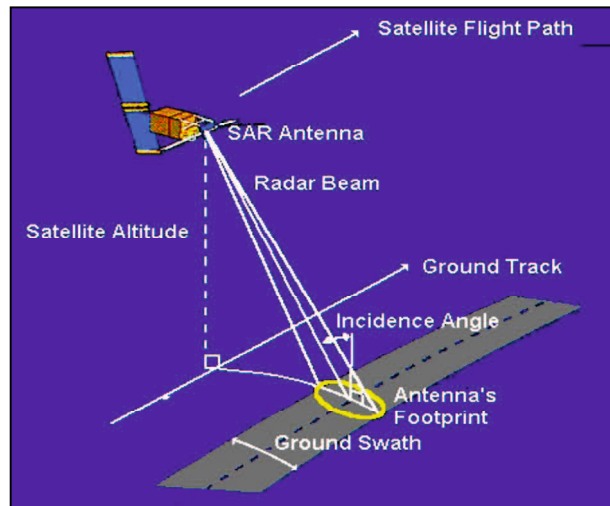


Figure 2.4 Geometry's image for a typical strip-mapping SAR imaging system  
(Source: Liew, 2001)

The SAR makes use of the radar principle to form an image by utilizing the time delay of the backscattered signals. Moreover, SAR capitalizes on the motion of the space craft which has a limitation to carry a very long antenna to emulate a large antenna from the small antenna it actually carries on board for a high resolution imaging of the Earth surface (Matsuoka and Yamazaki, 2000).

### 2.3.2 SAR Image Characteristics

A SAR image has several characteristics that make it different with the other image. The position and proportions of objects in the image can appear distorted and also grain, due to the presence of many black and white pixels randomly distributed throughout the image.

#### 1. Microwave Frequency

The ability of microwave to penetrate clouds, precipitation, or land surface cover depends on its frequency. Generally, the penetration power increases for longer wavelength (lower frequency). The SAR backscattered intensity generally increases with the surface roughness. In SAR imaging, the reference length scale for surface roughness is the wavelength of the microwave. If the surface fluctuation is less than the microwave wavelength, then the surface is considered smooth. The short wavelength radar interacts mainly with the top layer of the forest canopy while the longer wavelength radar is able to penetrate deeper into the canopy to undergo multiple scattering between the canopy, trunks and soil (McCandless and Jackson, 2004).

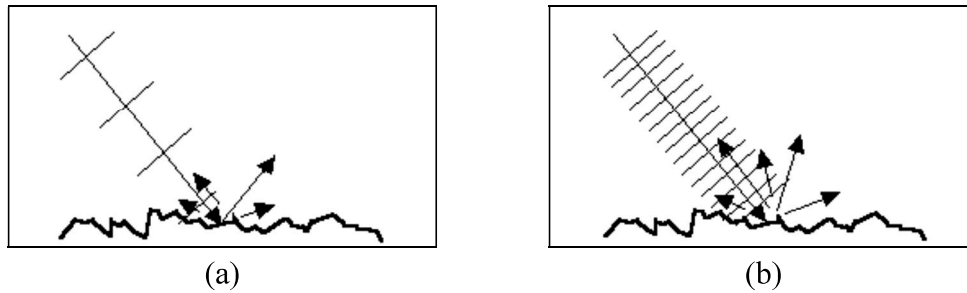


Figure 2.5 SAR backscattered intensity

(a) Long Wavelength Radar and (b) Short Wavelength Radar

(Source: Liew, 2001)

Figure 2.5 (a) above showed that the surface appears smooth to a long wavelength radar. Little radiation is backscattered from the surface. Otherwise, the same land surface appears rough to the short wavelength radar as can be seen on Figure 2.5 (b). The surface appears bright in the radar image due to increased backscattering from the surface (Liew, 2001).

### 3. Polarization Wave

The microwave polarization refers to the orientation of the electric field vector of the transmitted beam with respect to the horizontal direction. If the electric field vector oscillates along a direction parallel to the horizontal direction, the beam is said to be “H” polarized. On the other hand, if the electric field vector oscillates along a direction perpendicular to the horizontal direction, the beam is “V” polarized. After interacting with the earth surface, the polarization state may be altered. There are four possible polarization configurations for a SAR system, namely “HH”, “VV”, “HV” and “VH”. It depends on the polarization states of the transmitted and received microwave signals (McCandless and Jackson, 2004).

### 4. Incident Angles

The incident angle refers to the angle between the incident radar beam and the direction perpendicular to the ground surface. The interaction between microwaves and the surface depends on the incident angle of the radar pulse on the surface. A small incident angle is optimal for detecting ocean waves and other ocean surface features. While a larger incident angle may be more suitable for other applications. For example, a large incident angle will increase the contrast between the forested and clear cut areas. Acquisition of SAR images of an area using two different incident angles will also enable the construction of a stereo image for the area (Baumann, 2010).

### 5. Slant Plane/ Ground Plane

Slant plane is the distance that measured along the line between the radar and surface of the earth where the pulse travels. The distances were converted from the delay time



associated with a particular reflection. The resolution in the ground plane image is coarser than the corresponding slant plane image. To make a SAR image appear like a map, the sampling along the slant plane must be converted to the ground plane. Slant to ground range distortions are often small for the space-based SARs because of the small variation in incident angle from the near side of the swath (Liew, 2001).

## 6. Speckle Noise

Unlike optical images, radar images are formed by coherent interaction of the transmitted microwave with the targets. Hence, it suffers from the effects of speckle noise which arises from coherent summation of the signals scattered from ground scatters distributed randomly within each pixel. A radar image appears noisier than an optical image. The speckle noise is sometimes suppressed by applying a speckle removal filter on the digital image before display and further analysis. The vegetated areas and the clearings appear more homogeneous after applying a speckle removal filter to the SAR image (Liew, 2001). The difference of images before and after removing speckle noise is shown in Figure 2.6.

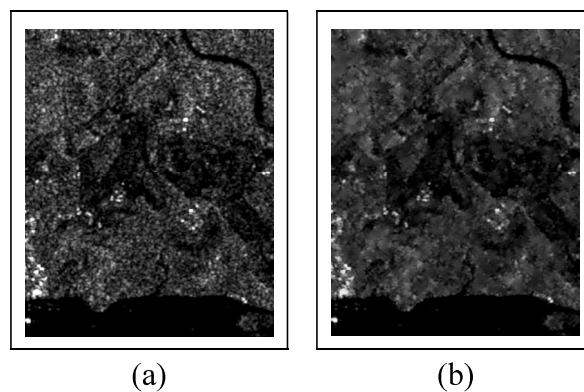


Figure 2.6 SAR image before and after applying speckle noise removal (Liew, 2001)

### 2.3.3 SAR Signal Processing and Image Formation

In a SAR signal processor there is specific operations required to convert a raw data set into an interpretable image. The raw SAR data is not an image since point targets are spread out in range and in the along-track dimension. Figure 2.7 illustrates the raw data trace of a typical point-target as the beam moves in the along-track or azimuth direction. As the radar moves by the target, the radar-to-target range varies, forming the curved trace. This translation also produces an along-track frequency/ time trace in azimuth, induced by Doppler, and range pulse encoding produces a somewhat similar time or frequency trace in range. The SAR signal processor compresses this distributed target information in two dimensions (range and along-track) to create the image (Baumann, 2010).

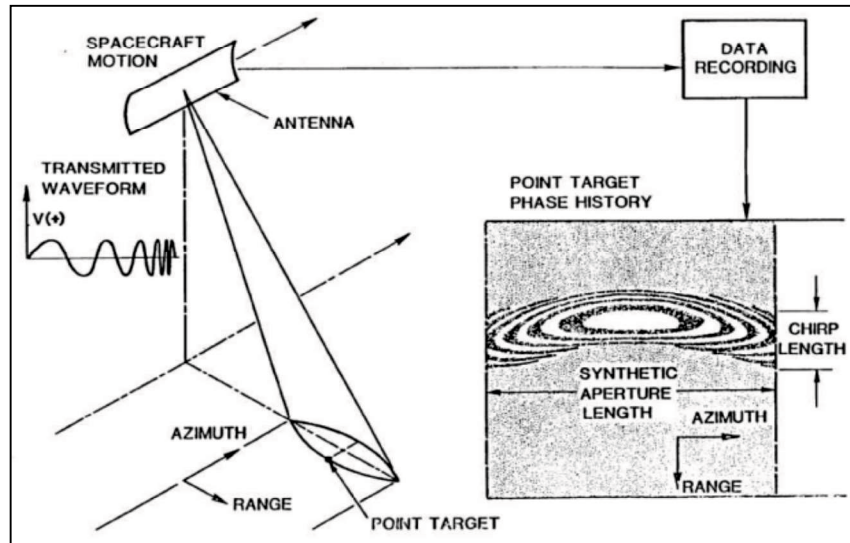


Figure 2.7 SAR point target return  
(Source: McCandless and Jackson, 2004)

Several computation techniques may be used to form a SAR image. One method is to use Fourier spectrum estimation techniques, commonly implemented through a Fast Fourier Transform (FFT). Time domain matched filters may also be used. The choice is applications dependent and usually made based on computational efficiencies. In summary, SAR image formation requires many rote process and computation intensive signal processing of coherent radar return phase histories (Curlander and McDonough, 1991).

The most difficult part of the inner workings of the SAR processor problem is related to the coupling between the azimuthal compression and the orbital parameters (Sandwell et al., 2016). Conventional techniques such as *clutterlock* and *autofocus* to derive the orbital parameters from a data is no longer necessary due to the availability of high accuracy orbits. A standard processing sequence follows where the first two steps are done onboard the satellite while the remaining 4 steps are done by the user with a digital SAR processor. The digital SAR processor is a computer program that converts the raw signal data into a single-look complex (SLC) image. An overview of digital SAR processing overview is provided in Figure 2.8

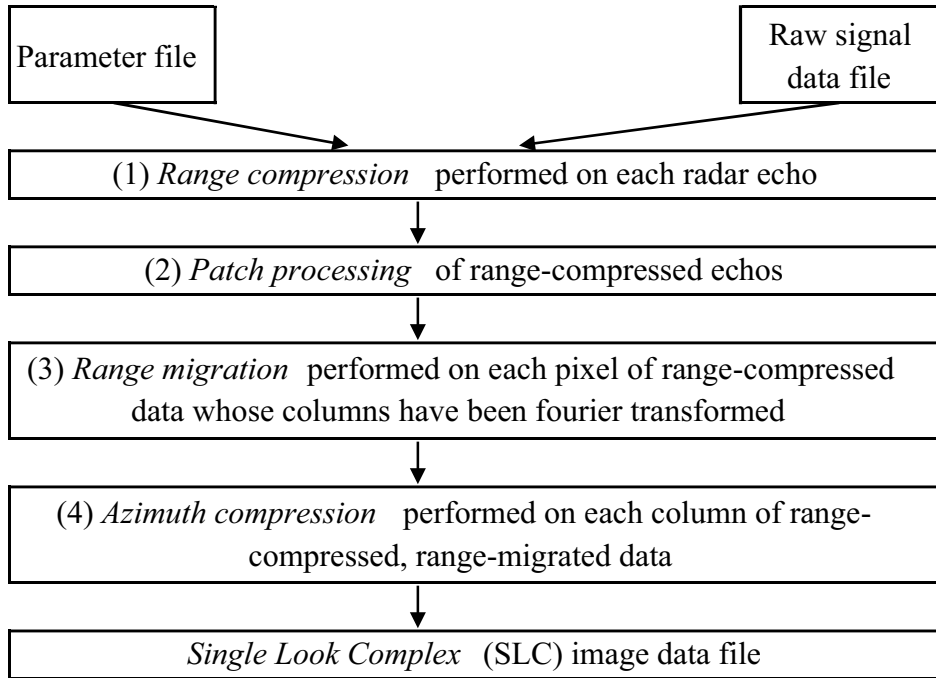


Figure 2.8 Digital SAR processing overview  
(Source: Sandwell et al., 2016)

### 1. Range Compression

A sharp radar pulse is recovered by deconvolution of the chirp. This is done with Fast Fourier Transform (FFT). To reduce the peak power of the radar transmitter associated with a short pulse, a long frequency-modulated chirp is emitted by the radar. This chirp propagates to the ground where it reflects from a swath typically 100 km wide. When it returns to the radar, the raw signal data consists of the complex reflectivity of the surface convolved with the chirp. In order to recover the complex reflectivity by deconvolution of the chirp, the frequency-modulated chirp is calculated as follow (Sandwell et al., 2016):

$$f_s(t) = e^{i\pi kt^2} \quad |t| < \tau_p/2 \quad \text{(Equation 2.3)}$$

Where  $k$  is chirp slope,  $\tau_p$  is pulse duration, and  $f_s$  is range sampling rate. The bandwidth of the chirp is indicated by  $B = k\tau_p$ . A matched filter is used to deconvolve the chirp from the data. In this case, the matched filter is simply the complex conjugate of the chirp or  $s^*(t) = e^{-i\pi kt^2}$  (Sandwell et al., 2016).

### 2. Patch Processing

The next step is to focus the image in the along-track or *azimuth* direction. This is also done by FFT, but now we need to process columns rather than rows. A 4096 x 5616 patch requires at least 184 Mbytes of computer memory for single precision real numbers. In the old days before this large memory space was available, each patch was transposed (corner

turning) using high-speed disks so the data could be processed on a column-by-column basis (Sandwell et al., 2016).

### 3. Range Migration

A point target will appear as a hyperbolic- shaped reflection as it moves through the synthetic aperture. In addition, there could be a pronounced linear drift due to an elliptical orbit and earth rotation. In other words, the target will migrate in range cell as a linear trend plus a hyperbola. The shape of this migration path is calculated from the precise orbital information and is approximated by a parabola. Prior to focusing the image along a single column, these signals must be migrated back to a constant range cell. This is called “range migration” and the fastest way to do this is by Fourier transforming the columns first. Each Fourier component corresponds to a unique Doppler shift and also a unique value of range migration. In case of an ideal radar, the first component will have zero Doppler and will correspond to the point on the earth that is perpendicular to the spacecraft velocity vector. The second component will have a small positive Doppler shift and a small migration of the range cells will be needed and so forth all the way through the positive and negative Doppler spectrums (Sandwell et al., 2016).

### 4. Azimuth Compression

The final step in the processing is to focus the data in azimuth by accounting for the phase shift of the target as it moves through the aperture. The azimuth compression relies on the same theory although an opposite calculation is conducted for the process, the shape of the aperture (reflectivity of the target) is calculated by given the illumination pattern. This is done by generating a second frequency-modulated chirp whereby the chirp parameters depend on the velocity of the spacecraft, the pulse repetition frequency (PRF), and the absolute range. The chirp is Fourier transformed into Doppler space and multiplied by each column of range-migrated data. The product is inverse Fourier transformed to provide the focused image (Sandwell et al., 2016). The geometry of the strip-mode acquisition of azimuth compression or azimuth focusing that involves coherent summation of echoes at a constant range from the point reflector is shown in Figure 2.9.

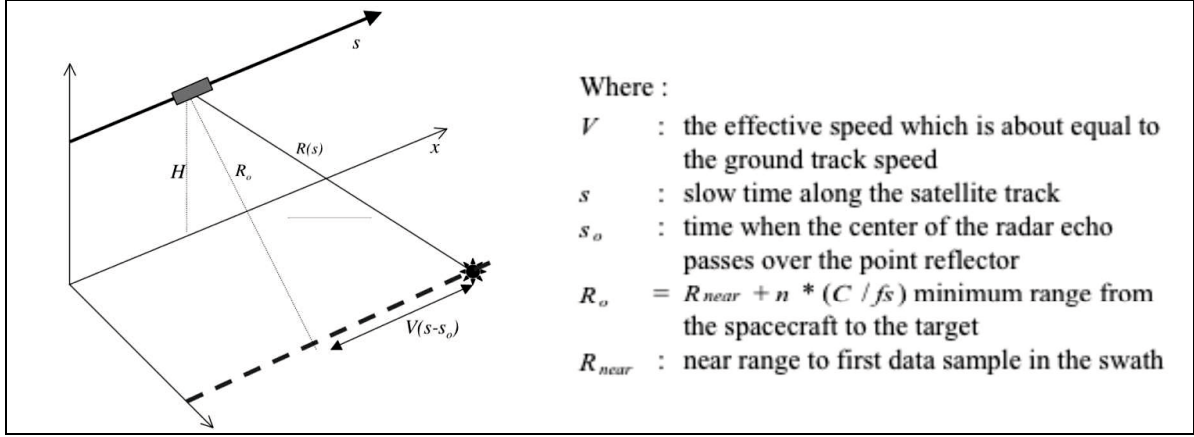


Figure 2.9 Geometry of radar passing over a point reflector  
(Source: Sandwell et al., 2016)

The following is the formula to calculate the range to the point reflector evolves with time (Curlander and McDonough, 1991):

$$R^2(s) = R_o^2 + V^2(s - s_o)^2 \quad (\text{Equation 2.4})$$

The complex phase of the return echo is described in Equation 2.5 as follow (Curlander and McDonough, 1991):

$$C(s) = \exp \left[ -i \frac{4\pi}{\lambda} R(s) \right] \quad (\text{Equation 2.5})$$

The range versus slow time is approximately a hyperbola but for mathematical convenience it is approximated using a parabola as follow (Curlander and McDonough, 1991):

$$R(s) = R_o + \dot{R}_o(s - s_o) + \frac{\ddot{R}_o}{2}(s - s_o)^2 + \dots \quad (\text{Equation 2.5})$$

Where the dot indicates derivative with respect to slow time  $s$  discuss the accuracy of this polynomial approximation. The approximation is good enough for strip-mode SAR but may be inadequate for the much longer apertures associated with spotlight-mode SAR. Furthermore, the phase of the return signal as a function range, range rate, and range acceleration can be written as follow (Curlander and McDonough, 1991):

$$C(s) = \exp \left\{ -i \frac{4\pi}{\lambda} \left[ R_o + \dot{R}_o(s - s_o) + \frac{\ddot{R}_o}{2}(s - s_o)^2 / 2 \right] \right\} \quad (\text{Equation 2.6})$$

It is more common to describe the parameters for focusing the SAR image as the Doppler centroid  $f_{Dc}$  and the Doppler frequency rate  $f_R$ . The relationships are described in the following equation (Curlander and McDonough, 1991):

$$f_{Dc} = \frac{-2\dot{R}}{\lambda} \quad \text{and} \quad f_R = \frac{-2\ddot{R}}{\lambda} \quad (\text{Equation 2.7})$$

or

$$C(s) = \exp \left\{ -i \frac{4\pi R_o}{\lambda} \right\} \exp \{ i 2\pi [ f_{Dc}(s - s_o) + f_R(s - s_o)^2 / 2 ] \} \quad (\text{Equation 2.8})$$

It should be noted that this function is another frequency-modulated chirp where the parameters are the Doppler centroid and the Doppler frequency rate.

Proper focus of the image requires accurate estimates of the three parameters given in Equation (2.6) and Equation (2.7). In regard to the equations, there are two parameters necessary to be estimated to sweep through the range cells  $n$  in the raw data file and focus the image at each range  $R_o = R_{near} + n*(C/f_s)$  where  $C$  is the speed of light and  $f_s$  is the sampling rate. Ideally the beam of the radar would be steered so that it is centered at a point on the ground where the range is minimum so the Doppler centroid is zero or at least small. The approach of Masden (1989) is used to calculate the Doppler centroid directly from the raw data file by computing the average change in phase between adjacent rows of the raw data file. This assumes that the Doppler centroid does not vary with slow time although it could vary slightly with increasing range. This estimated Doppler centroid is employed to focus the image or select a similar Doppler centroid that is close to the mean of a stack of repeated SAR images (Sandwell et al., 2016).

Finally, as discussed below, the precise orbit can be used to calculate the third parameter, the range acceleration  $\ddot{R}$ . The parameter decreases with the increasing of range. One approach would be to use the precise orbit to calculate range acceleration for each range but this is unnecessary because there is a good formula for range acceleration as a function of range that involves a parameter called the effective speed  $V$  of the spacecraft. Indeed the SAR processor code takes effective speed and converts this to  $\ddot{R}$  to focus the image. The derivation of the effective speed parameter is described in Equation (2.9) by taking the first derivative of the range versus slow time given in Equation (2.5).

$$\frac{\partial R^2(s)}{\partial s} = 2R\dot{R} = 2V^2s \quad (\text{Equation 2.9})$$

The second derivative is

$$\dot{R}\dot{R} + R\ddot{R} = V^2 \quad (\text{Equation 2.10})$$

Assuming that the radar antenna is oriented nearly perpendicular to the velocity vector of the satellite so  $\dot{R} \ll V$ . Note that to achieve interferometric coherence the radar beams of the reference and repeat images must overlap spatially which essentially requires that the Doppler centroid be less than half of the pulse repetition frequency (PRF). Given a typical PRF for a spaceborne SAR of 2000 and using Equation (2.7) and a wavelength of 0.05 m the range rate must be less than  $\sim 25$  m/s. This is much less than the typical spacecraft velocity of 7800 m/s so that we can safely ignore the first term on the left hand side of Equation (2.10). So that, the approach is to use the precise orbit to calculate the range acceleration  $\ddot{R}$  at a single range  $R_o$  within the image. These two numbers are used to calculate the effective speed as follow (Sandwell et al., 2016):

$$V = \sqrt{R_o\ddot{R}} \quad (\text{Equation 2.11})$$

Finally, this parameter is used by the SAR processing code to calculate the range acceleration at all the other ranges in the swath as described in Equation 2.12.

$$\ddot{R} = V^2 / R \quad (\text{Equation 2.12})$$

The effective speed, which is reported as SC\_vel in the PRM-file, can be used to compute the ground track speed  $V_g$  of the satellite as follow:

$$V_g = \frac{V}{\left(1 + \frac{H}{R_e}\right)^{1/2}} \quad (\text{Equation 2.13})$$

In case of a long aperture, several factors must be considered such as the curvature and ellipticity of the orbit as well as the rotation rate of the Earth. This complexity is bypassed by computing the effective speed from a polynomial fit of range versus time.

Estimation of the range acceleration from the orbit seems conceptually trivial although there is one complication that requires a bit of geometry. The complication is to find a point on the surface of the earth, at a prescribed range, and convert that location to Cartesian coordinates. Consider the following three vectors which form a triangle (Sandwell et al., 2016):

$\vec{R}_s$  : the vector position of the satellite in the Earth-fixed coordinate system;

$\vec{R}_e$  : the vector position of a point scatterer on the Earth and somewhere in the SAR scene;

$\vec{R}_o$  : the line-of-sight vector between the satellite and the point scatterer.

The three vectors form a triangle such that  $\vec{R}_e = \vec{R}_s + \vec{R}_o$  (Figure 2.9). The scalar range, which is a function of slow time, is given by (Sandwell et al., 2016):

$$R(s) = \left| \vec{R}_s(s) - \vec{R}_e \right| \cong R_o + \dot{R}_o(s - s_o) + \frac{\ddot{R}_o}{2}(s - s_o)^2 + \dots \quad (\text{Equation 2.14})$$

Measurements of scalar range versus slow time can be used to estimate the coefficients of the parabolic approximation. The algorithm uses the precise orbit to calculate the position vector of the satellite and compute a time series  $R(s)$  over the length of the aperture, perform a least-squares parabolic fit to this time series to estimate  $R_o$ ,  $\dot{R}_o$ , and  $\ddot{R}_o$ , and compute the effective speed as  $V_e^2 = R_o \ddot{R}_o$ .

The only remaining step is to calculate the position of the point target  $\vec{R}_e = \vec{R}_s + \vec{R}_o$ . Actually, this can be any point in the image so the selection criteria is that the point lie at the proper radius of the surface of the Earth  $R_e = \left| \vec{R}_e \right|$  and the  $\vec{R}_o$  vector is perpendicular to the velocity vector of the satellite  $\vec{V}$ . By prescribing the length of the  $R_o$  - vector then the angle between the satellite position vector and the line-of-sight vector is given by the law of cosines (Sandwell et al., 2016), as shown in Figure 2.10.

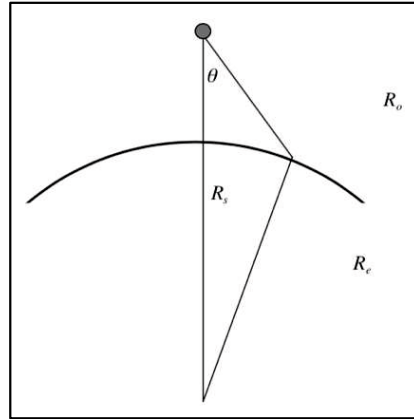


Figure 2.10 Triangle of earth radius, satellite radius and range to a point on the surface of the earth used to compute look angle  $\theta$   
 (Source: Sandwell et al., 2016)

This diagram has the satellite at the gray dot with the velocity vector pointing into the page. The cosine of the look angle is described in the following equation:

$$\cos\theta = \frac{R_s^2 + R_o^2 - R_e^2}{2R_s R_o} \quad (\text{Equation 2.15})$$

Further, consider a local coordinate system where the  $q_2$  axis is aligned with the velocity vector of the satellite as shown in the diagram of Figure 2.11.

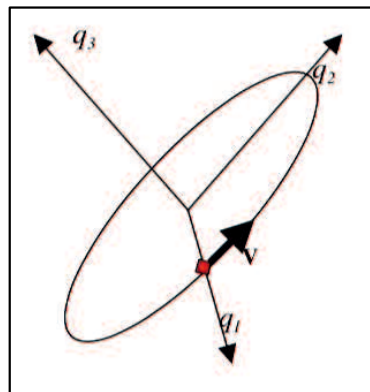


Figure 2.11 Satellite (red) in circular inclined orbit about the Earth  
 (Source: Sandwell et al., 2016)

In this coordinate system, the  $q_1$ -axis is parallel to  $\vec{R}_s$ , the  $q_2$  axis is parallel to  $\vec{V}$ , and the  $q_3$  axis is perpendicular to both and is given by their cross product as follow:

$$q_3 = \frac{\vec{R}_s}{|\vec{R}_s|} \times \frac{\vec{V}}{|\vec{V}|} \quad (\text{Equation 2.16})$$

The following diagram has the velocity vector of the satellite going into the page and aligned with the  $q_2$  coordinate. The  $q_1$  vector is the radial vector from the center of the earth.



The line-of-sight right-look vector is in the  $q_1$ - $q_3$  plane as described in Figure 2.12 where  $q_1$  is the vector from the center of the earth to the spacecraft,  $q_2$  is parallel to the velocity vector of the spacecraft, and the bold vector is the look vector of the radar where  $\theta$  is the look angle.

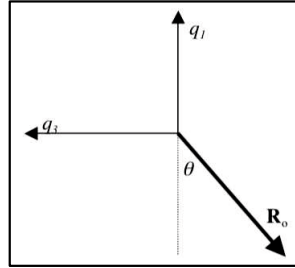


Figure 2.12 Diagram of satellite-fixed coordinate system  
(Source: Sandwell et al., 2016)

After going through this geometry, the line of sight (LOS) vector to a point on the surface of the earth at the prescribed range for a right-looking and left-looking radar are described in Equation 2.17 and Equation 2.18, respectively (Sandwell et al., 2016):

$$\vec{R}_o = R_o(-\cos\theta\hat{q}_1 \ 0 \ \hat{q}_2 \ -\sin\theta\hat{q}_3) \quad (\text{Equation 2.17})$$

$$\vec{R}_o = R_o(-\cos\theta\hat{q}_1 \ 0 \ \hat{q}_2 \ -\sin\theta\hat{q}_3) \quad (\text{Equation 2.18})$$

### 2.3.4 Interpreting SAR Imageries

Interpretation of a radar image is not a straightforward task. In general, it requires some familiarity with the ground conditions of the areas imaged. As a useful rule of thumb, the higher the backscattered intensity, the rougher is the surface being imaged. Based on the backscattered of radar images, flat surfaces such as paved roads, runways or calm water normally appear as dark areas in a radar image since most of the incident radar pulses are commonly reflected away. Calm sea surfaces appear dark in SAR images. However, rough sea surfaces may appear bright especially when the incidence angle is small. Trees and other vegetation are usually moderately rough on the wavelength scale. Hence, they appear as moderately bright features in the image. The tropical rain forests have a characteristic backscatter coefficient of between -6 and -7 dB, which is spatially homogeneous and remains stable in time. For this reason, the tropical rainforests have been used as calibrating targets in performing radiometric calibration of SAR images (Lilesand and Kiefer, 1993).

Very bright targets may appear in the image due to the corner-reflector or double-bounce effect where the radar pulse bounces off the horizontal ground (or the sea) towards the target, and then reflected from one vertical surface of the target back to the sensor. Examples of such targets are ships on the sea, high-rise buildings and regular metallic objects such as cargo containers. Built-up areas and many man-made features usually appear as bright patches in a radar image due to the corner reflector effect (Lilesand and Kiefer, 1993).

### 2.3.5 L-Band SAR Imagery of ALOS PALSAR

One of the ALOS remote sensing instruments is the Phased Array type L-band Synthetic Aperture Radar (PALSAR) for day-and-night and all-weather land observation (Shimada, 2007). The PALSAR is an enhanced version of the Synthetic Aperture Radar on JERS-1 (L-band, HH-polarization, 35° off-nadir angle), like its predecessor, PALSAR was developed jointly by JAXA and the Japan Resources Observation Systems Organization (JAROS). PALSAR is a fully polarimetry instrument, operating in fine-beam mode with single polarization (HH or VV), dual polarization (HH+HV or VV+VH), or full polarimetry (HH+HV+VH+VV). The characteristics of fine, scanSAR, and polarimetric modes of ALOS PALSAR observation are pictured in Figure 2.13.

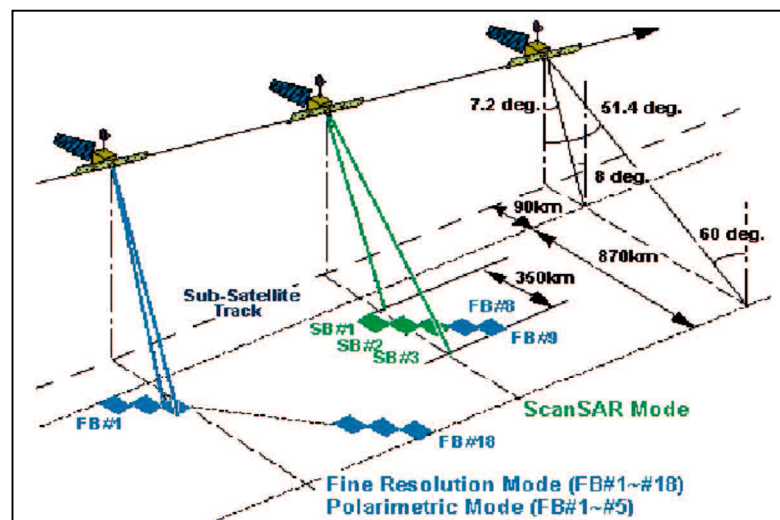


Figure 2.13 ALOS PALSAR observation characteristics  
(Source: Rosenqvist, et. al., 2004)

It also features wide-swath ScanSAR mode, with single polarization (HH or VV). The center frequency is 1270 MHz (23.6 cm), with a 28 MHz bandwidth in fine beam single polarization mode, and 14 MHz in the dual-, quad-pol and ScanSAR modes. The off-nadir angle is variable between 9.9° and 50.8° (at mid-swath), corresponding to a 7.9 - 60.0° incidence angle range. In 5-beam ScanSAR mode, the incidence angle range varies from 18.0° to 43.0° (Rosenqvist, et. al., 2004). The characteristics are described in detail in Table 2.6.

Table 2.6 ALOS PALSAR Characteristics

Mode	Fine		ScanSAR	Polarimetric (experimental mode)*1
Center frequency	1270 MHz (L-band)			
Chirp bandwidth	28MHz	14MHz	14MHz, 28MHz	14MHz
Polarization	HH or VV	HH+HV or VV+VH	HH or VV	HH+HV+VH+VV
Incident angle	8 to 60deg.	8 to 60deg.	18 to 43deg.	8 to 30deg.
Range Resolution	7 to 44m	14 to 88m	100m (multi look)	24 to 89m
Observation swath	40 to 70km	40 to 70km	250 to 350km	20 to 65km
Bit length	5 bits	5 bits	5 bits	3 or 5bits
Data rate	240Mbps	240Mbps	120Mbps, 240Mbps	240Mbps
NE sigma zero		< -23dB (Swath Width 70km) < -25dB (Swath Width 60km)	< -25dB	< -29dB
S/A		> 16dB (Swath Width 70km) > 21dB (Swath Width 60km)	> 21dB	> 19dB
Radiometric accuracy	scene: 1dB / orbit: 1.5 dB			

(Source: Rosenqvist, *et. al.*, 2004)

### 2.3.6 C-Band SAR Imagery of Sentinel-1A

Sentinel-1 is an imaging radar mission providing continuous all-weather, day-and-night imagery at C-band. It is a two-SAR satellite constellation designed to guarantee global coverage with a revisit time of 6 days (Amitrano et al., 2014). Moreover, it is able to provide high reliability, improved revisit time, geographical coverage and rapid data dissemination to support operational applications in the priority areas of marine monitoring, land monitoring and emergency services. The satellite potentially images all global landmasses, coastal zones and shipping routes in European waters in high resolution and covers the global oceans at regular intervals. Having a primary operational mode over land and another over open-ocean allows for a pre-programmed conflict-free operation. The main operational mode features a wide swath (250 km) with high geometric (typically 20 m Level-1 product resolution) and radiometric resolutions, suitable for most applications (ESA, 2000).

The first satellite (Sentinel-1A) was launched on 3 April 2014. A 12-meter long radar working in C-band was successfully deployed and is starting to acquire images all over the world. Sentinel-1A is placed in a near-polar, sun-synchronous orbit with a 12-day repeat

cycle and 175 orbits per cycle. Both the satellites of the Sentinel-1 constellation share the same orbit plane with a 180° orbital phasing difference (Amitrano et al., 2014).

Sentinel-1 instrument is designed to work with four different operative modes, i.e. stripmap (SM), wave (WV), Interferometric wide swath (IW), and Extra wide swath (EW) (ESA, 2000). The operative modes are summarized in Table 2.7

1. Stripmap (SM) - A standard SAR stripmap imaging mode where the ground swath is illuminated with a continuous sequence of pulses, while the antenna beam is pointing to a fixed azimuth and elevation angle.
2. Wave (WV) - Data is acquired in small stripmap scenes called "vignettes", situated at regular intervals of 100 km along track. The vignettes are acquired by alternating, acquiring one vignette at a near range incidence angle while the next vignette is acquired at a far range incidence angle. WV is Sentinel-1's operational mode over open-ocean.
3. Interferometric Wide swath (IW) - Data is acquired in three swaths using the Terrain Observation with Progressive Scanning SAR (TOPSAR) imaging technique. In IW mode, bursts are synchronised from pass to pass to ensure the alignment of interferometric pairs. IW is Sentinel-1's primary operational mode over land.
4. Extra Wide swath (EW) - Data is acquired in five swaths using the TOPSAR imaging technique. EW mode provides very large swath coverage at the expense of spatial resolution.

Table 2.7 Sentinel-1 operative modes

<b>Mode</b>	<b>Swath (km)</b>	<b>Resolution (m x m)</b>	<b>Polarization</b>
Stripmap (SM)	80	5 x 5	Dual
Wave (WV)	20	5 x 5	Dual
Interferometric Wide swath (IW)	250	5 x 20	Dual
Extra Wide swath (EW)	400	20 x 40	Single

(Source: Amitrano et al., 2014)

Sentinel-1 with C-band SAR active sensor can observe the surface of the Earth at any time of the day or night, regardless of weather and environmental conditions. Since SAR has the advantage of operating at wavelengths not impeded by cloud cover or lack of illumination. C-band is a nominal frequency range, from 8 to 4 Ghz (3.75 to 7.5 cm wavelength) within the microwave (radar) portion of the electromagnetic spectrum. Imaging radars equipped with C-band are generally not hindered by atmospheric effects and are capable of viewing through tropical clouds and rain showers. Its penetration capability with regard to vegetation canopies or soils is limited and is restricted to the top layers.

Sentinel-1 potentially operates in four exclusive acquisition modes, i.e. Stripmap (SM), Interferometric Wide swath (IW), Extra-Wide swath (EW), and Wave (WV). The Sentinel-1 C-band SAR instrument supports operation in single polarisation (HH or VV) and dual polarisation (HH+HV or VV+VH), implemented through one transmit chain (switchable to H or V) and two parallel receive chains for H and V polarisation. SM, IW and EW are available in single (HH or VV) or dual polarisation (HH+HV or VV+VH). WV is single polarisation only (HH or VV). The primary conflict-free modes are IW, with VV+VH polarisation over land, and WV, with VV polarisation, over open ocean. EW mode is primarily used for wide area coastal monitoring including ship traffic, oil spill and sea-ice monitoring. SM mode will only be used on request for extraordinary events such as emergency management.

Having the Interferometric Wide swath mode as the one main operational mode satisfies most currently known service requirements, avoids conflicts and preserves revisit performance, simplifies mission planning, decreases operational costs and builds up a consistent long-term archive. For each mode, it will be possible to produce products at SAR Level-0, Level-1 SLC, Level-1 GRD and Level-2 OCN (ESA, 2000). The product modes of Sentinel-1 are described in Figure 2.14.

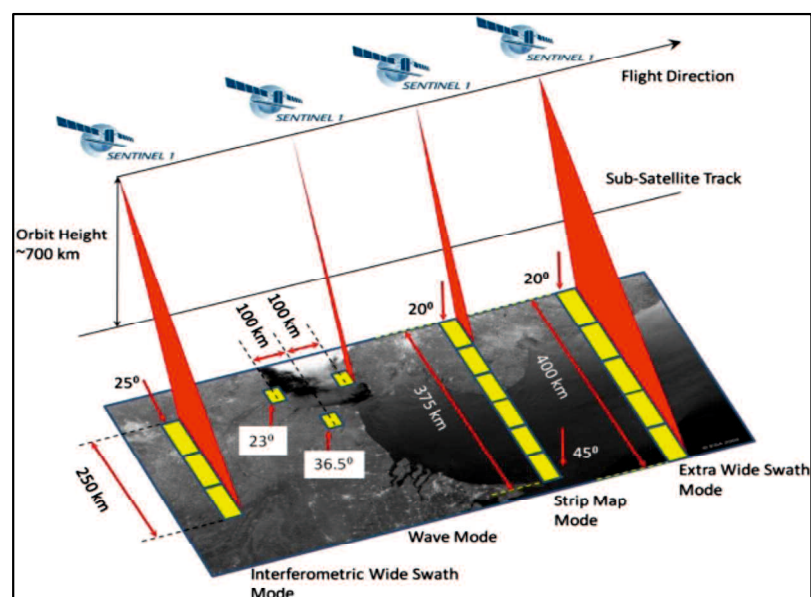


Figure 2.14 Sentinel-1 product modes  
(Source: ESA, 2000)

## 2.4 Methods and Technique of SAR Interferometry

Firstly, the basic of InSAR processing are described regarding the generation of SAR interferogram to extract displacement information. The limitation of conventional InSAR technique is emphasized by signifying uncertainties from DInSAR displacement measurement prior to the explanation of advanced time-series InSAR technique.

### 2.4.1 SAR Interferometry Processing of Deformation

Standard InSAR processing techniques combine two SAR scenes of the same area, acquired at different times. Calculating the difference in the phase component ( $\Delta\phi$ ) of the reflected signals is known as radar interferometry, and the image of  $\Delta\phi$  for all pixels is known as an interferogram (Zebker et al., 1994). Data are collected along the line-of-sight (LOS) direction, from the antenna to Earth's surface. The look angle is defined as the angle between the LOS and the normal to Earth's surface. In case of Fine-Beam Mode of ALOS PALSAR which has incident angle of about  $23.6^\circ$ , the change in LOS distance from the antenna to the surface is approximately equal to the change in vertical distance to the surface.

If the effects to topography are removed, then the result can provide an accurate measure of the change in the elevation of the land surface. Pixels are often spatially averaged to correspond to a 50 m by 50 m resolution cell to improve the signal-to-noise ratio of the observed interferometric phase. Because of the cyclic nature of phase,  $\Delta\phi$  will only be known within radians; this is called wrapped phase. The process of estimating and adding the unknown correct integer multiple of  $2\pi$  to  $\Delta\phi$  is called phase unwrapping (Chen and Zebker, 2002).

The measured difference in the phase of the two signals  $\Delta\phi$  is the sum of six parts (Zebker et al., 1994; Ferretti et al., 2000):

$$\Delta\phi = \Delta\phi_{def} + \Delta\phi_{topo} + \Delta\phi_{orb} + \Delta\phi_{ip} + \Delta\phi_{atm} + \Delta\phi_n \quad (\text{Equation 2.3})$$

Where  $\Delta\phi_{def}$  is the phase change due to the deformation of the ground surface,  $\Delta\phi_{topo}$  is the phase change due to topography,  $\Delta\phi_{ip}$  is the phase change due to integer phase ambiguities,  $\Delta\phi_{orb}$  is the phase change due to orbital errors,  $\Delta\phi_{atm}$  is the phase change due to atmospheric phase effects and  $\Delta\phi_n$  is the phase change due to random phase noise. The different components can be considered signal or noise in different applications, however for this study we are interested in the phase change due to the deformation of the ground surface.  $\Delta\phi_{def}$  is related to the deformation ( $\Delta d$ ) by:

$$\Delta\phi_{def} = \frac{2\pi}{\lambda}(2\Delta d) = \frac{4\pi}{\lambda}\Delta d \quad (\text{Equation 2.4})$$

where  $\lambda$  is the wavelength of the radar system (Figure 2.15). The noise components  $\Delta\phi_{topo}$  and  $\Delta\phi_{orb}$  must be removed and the noise components  $\Delta\phi_{ip}$ ,  $\Delta\phi_{atm}$ , and  $\Delta\phi_n$  must be mitigated in order to accurately determine  $\Delta\phi_{def}$ . To follow is a description of how the components  $\Delta\phi_{topo}$  and  $\Delta\phi_{orb}$  can be removed from the measurement of the change in phase. We will reserve the detailed discussion about quantification of the change in phase as well as the other components of uncertainty (Zebker et al., 1994; Ferretti et al., 2000).

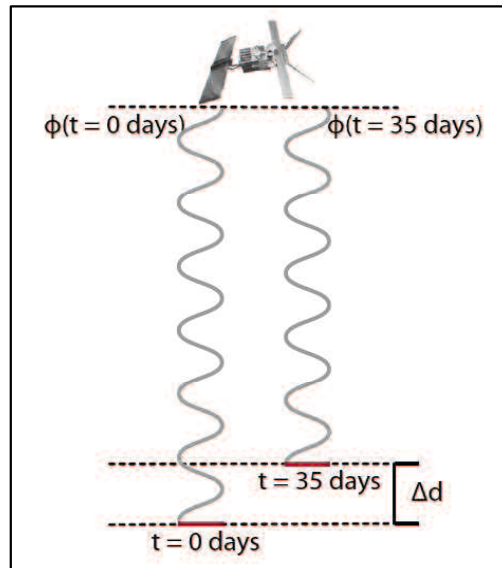


Figure 2.15 A schematic of how the change in phase of the EM wave relates to the change in surface deformation

(Source: Chen and Zebker, 2002)

$\Delta\phi_{topo}$  arises if the satellite views the surface from a slightly different parallax angle at the two acquisition times. This means that different points on the surface will be at different positions from the antenna.  $\Delta\phi_{topo}$  can easily be removed if there is accurate information about the imaging geometry and the surface topography from a digital elevation model (DEM) that has an elevation accuracy between 10 and 100 m. If there are significant errors in the DEM, advanced processing techniques are used to correct for this effect. This correction is called the topographic correction (Zebker et al., 1994; Hanssen, 2001).

Using incorrect orbital parameters to process SAR data also adds uncertainty to the InSAR deformation measurement ( $\Delta\phi_{orb}$ ). Modest orbital parameter errors result in a nearly planar change in phase across the interferogram that can be much larger than the deformation component of the phase. This planar trend can be removed by subtracting a best-fit plane from each interferogram (Lauknes et. al., 2005).

The processing flow to go from SAR images to deformation images is outlined in Figure 2.16. First, the two SAR images are co-registered, which means that they are spatially aligned using the amplitude returns of the radar. The interferogram is formed by subtracting the phase of scene 1 from the phase of scene 2 for all pixels.  $\Delta\phi_{topo}$  is removed using a digital elevation model, as discussed previously in this section. The phase unwrapping is applied, where the modulo  $2\pi$  phase is converted into an absolute phase measurement. On the unwrapped phase the  $\Delta\phi_{orb}$  is removed as described in this section. Eventually, the result is geocoded, latitude and longitude co-ordinates are determined, so that the exact location of the deformation at each pixel is known (Hanssen, 2001).

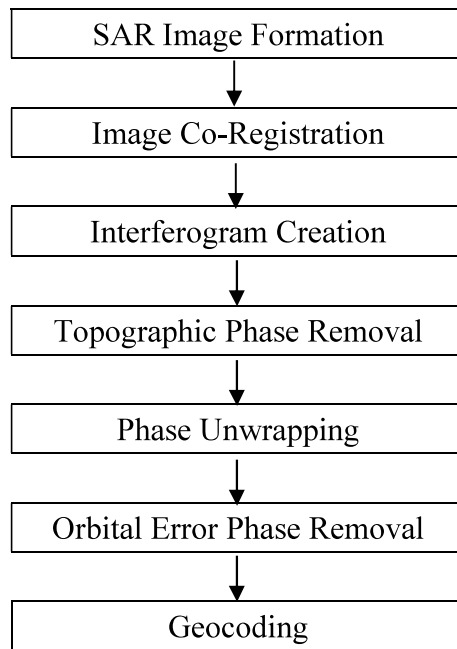


Figure 2.16 Processing flow to generate InSAR-based displacement  
(Source: Lauknes et. al., 2005)

#### 2.4.2 SAR Interferogram Statistics

Scattering mechanism inside a SAR resolution cell can be categorized as point scatterer (PSs) and distributed scatterers (DSs) within a resolution element. The ideal case of interferometric return is due to a *point scatterer* (Figure 13 (a)). If the resolution element contains a single point scatterer, the phase contributions due to the scattering inside the resolution cell,  $\phi_{scat}$ , shows almost no variation with time. In such a case, the topography and deformation information can be estimated from the interferogram without any error. However, such scatterers rarely exist in reality (Goel, 2014).

Nevertheless, on man-made structures like roofs, building facades, metallic structures etc. in urban areas, there do exist PSs. A PSs is characterized by one (or a few) dominating scatterer inside a resolution cell (Figure 2.17 (b)). It exhibits a small variation of  $\phi_{scat}$  with time and can also be used for topography and deformation mapping of the dominating scatterer. The phase stability of a PS is characterized by the Signal to Clutter Ratio (SCR) (clutter is the contribution of the echo from all the non-PSs scattering elements within the cell). Such pixels form the basis of Persistent Scatterer (PS) for topography and deformation time series estimation. PS exploits interferograms at the highest possible resolution (single-look data) to identify such scatterers (Goel, 2014).

On the other hand, in natural terrains, the scattering is generally the coherent sum of many subscatterers within a resolution cell (where no single sub-scatterer dominates the others) (Goodman, 1976). Such a scattering object is a Gaussian (or Rayleigh) scatterer, also



called a DSs (Figure 2.17 (c)). It obeys circular Gaussian statistics. The variation of  $\phi_{scat}$  with time is randomly distributed in the interval  $(-\pi, \pi)$  (Bamler and Hartl, 1998).

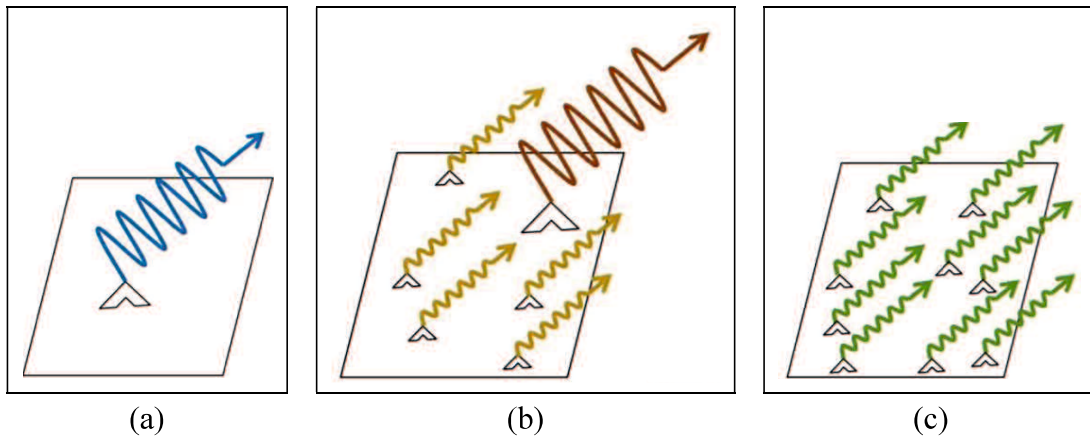


Figure 2.17 Modelling of scattering mechanism inside a SAR resolution cell:  
(a) Point scatterer; (b) PSs with one (or more) dominating scatterer within a resolution element; and (c) DSs with multiple subscatterers within a resolution element  
(Source: Goel, 2014)

InSAR stacking methods based on DSs include the SBAS and SqueeSAR. These methods exploit interferograms at a lower resolution (multi-look data). Essentially, the DSs are characterized by a low SNR, which has to be improved by a local spatial averaging (i.e. multi-looking). In other words, the statistics of interferograms characterized by DSs are governed by the complex covariance (Just and Bamler, 1994) and this has to be estimated by sample means.

The covariance between two complex SAR images  $s_1$  and  $s_2$  for a pixel is defined as the expectation of the product of the first with the complex conjugate of the second (Bamler and Hartl, 1998):

$$c = E(s_1 \cdot (s_2)^*) \quad (\text{Equation 2.19})$$

The complex correlation coefficient (also referred to as the complex coherence)  $\gamma$  of the two SAR images for a pixel is obtained by normalizing the covariance by the standard deviation of the two images and is given by the following equation (Bamler and Hartl, 1998):

$$\gamma = \frac{E(s_1 \cdot (s_2)^*)}{\sqrt{E(|s_1|^2) \cdot E(|s_2|^2)}} \quad (\text{Equation 2.20})$$

The Maximum Likelihood (ML) estimate  $\hat{\gamma}$  of the correlation is obtained from  $L$  independent samples such as looks (Bamler and Hartl, 1998):

$$\hat{\gamma} = \frac{\sum_{i=1}^L s_1^i \cdot (s_2^i)^*}{\sqrt{\sum_{i=1}^L |s_1^i|^2 \cdot \sum_{i=1}^L |s_2^i|^2}} \quad (\text{Equation 2.21})$$

Usually, the samples are selected from a local spatial estimation window, for example, a rectangular patch around the pixel of interest (although, it is possible to do an ensemble average for a pixel by including spatial as well as temporal samples). The magnitude  $\hat{\gamma}$  of the correlation, usually called coherence, is a measure of the phase noise of the pixel under consideration. It ranges from 0 to 1, 1 being the coherence for a noise-free interferometric pixel. The coherence describes the SNR as follow (Goel, 2014):

$$SNR = \frac{|\hat{\gamma}|}{1-|\hat{\gamma}|} \quad (\text{Equation 2.22})$$

The phase  $\arg\{\hat{\gamma}\}$  of the correlation is the expected interferometric phase of the pixel. The phase standard deviation  $\sigma_\phi$  of a pixel is a function of the coherence and the number of looks. It is worth mentioning that the estimator in Equation (2.5) is biased, it tends to overestimate low coherence. It becomes asymptotically unbiased for large number of looks, but this decreases the resolution. There are approaches available for unbiased coherence estimation (Touzi et al., 1999). The estimator also underestimates the coherence in case of interferometric fringes present due to residual digital elevation model (DEM), local slope, and so forth. Moreover, a rectangular estimation window can lead to averaging of pixels arising from different distributions leading to a wrong estimation of the correlation. The decorrelation in SAR interferograms (i.e. decrease in coherence) occurs due to various factors such as geometric and Doppler decorrelation, temporal decorrelation and thermal noise (Zebker and Chen, 2005).

The geometric decorrelation happens because the same ground resolution element is imaged from two slightly different look directions. It leads to a shift in the range spectra of the two SAR images. There exists a critical perpendicular baseline for every SAR system, above which there is a complete loss of coherence. The geometric decorrelation can be compensated in the Fourier transform domain via spectral shift filtering. The Doppler decorrelation occurs due to different Doppler centroids for the two images as they are taken with different squint angles. It can be mitigated in the Fourier transform domain by common band filtering.

When two SAR acquisitions are taken at different times, the reflectivity of the resolution cell might change. Since the backscattering depends on the terrain composition and roughness, any change in the terrain properties leads to a change in the reflectivity. This leads to temporal decorrelation. It is dependent on the wavelength used and the land coverage (e.g. water decorrelates in fractions of seconds, vegetation decorrelates in a few days, whereas buildings remain long-time coherent). Temporal decorrelation is difficult to model as it could occur due to changes in weather, anthropogenic activities or even natural hazards. Thermal noise is mostly due to internal circuitry of the SAR instrument.

### 2.4.3 Uncertainty in DInSAR Deformation Measurement

Three major components remain and contribute to uncertainty in the measurement of interferometric phase: integer phase ambiguities ( $\Delta\phi_{ip}$ ), atmospheric phase effects ( $\Delta\phi_{atm}$ ) and decorrelation of radar signals ( $\Delta\phi_n$ ). Without removing these uncertainty components, Equation (2.9) describes that this uncertainty will propagate through to an uncertainty in the InSAR deformation measurement. These components were discussed at length in *Hanssen* (2001):

$$\Delta d = \frac{\lambda}{4\pi} \Delta\phi = \frac{\lambda}{4\pi} (\Delta\phi_{ip} + \Delta\phi_{atm} + \Delta\phi_n) \quad (\text{Equation 2.23})$$

InSAR data processing includes a step called phase unwrapping, in which phases measured modulo  $2\pi$  are converted into a relative phase measurement by estimating and adding the correct number of integer cycles of phase into the measurement. If there is a considerable amount of noise in the data the algorithm will incorrectly estimate the phase by some integer multiple of  $2\pi$ , this is known as an integer phase ambiguity ( $\Delta\phi_{ip}$ ). Usai (2003) proposed a method for estimating this component of uncertainty by recognizing the “closed-loop” condition of the change in phase in three interferograms:

$$\phi_{t_1 t_2} + \phi_{t_2 t_3} + \phi_{t_3 t_1} = 0 \quad (\text{Equation 2.24})$$

Where  $\phi_{t_i t_j}$  is the interferometric phase from scene  $i$  and scene  $j$ . However, using this method with more interferograms is not simple and has not been attempted on datasets with a large number of interferograms (Gonzalez and Fernandez, 2011). As in Gonzalez and Fernandez (2011), poor quality interferograms from the SLV were omitted, allowing us to assume that this component of uncertainty is small.

If the atmospheric humidity, temperature, and pressure change significantly between the two SAR scenes, the refractive index of the atmosphere will change. As the EM wave passes through the atmosphere, the velocity of the EM wave will change and affect the measured phase. The phase change due to atmospheric effects ( $\Delta\phi_{atm}$ ) is uncorrelated in time, because the atmosphere changes randomly from one acquisition day to the next, but correlated in space, because cloud cover, temperature, and pressure are continuous in space over distances on the order of hundreds of meters (Hanssen, 1998; Hanssen, 2001). In regard to these reasons, it is common to use temporal and spatial filtering to remove this error component (Zebker et al., 1997; Ferretti et al., 2001). However, these atmospheric effects are highly variable, often dominating the change in phase observed in interferograms. The limited number of scenes used in any single analysis makes the associated uncertainty difficult to quantify. Simons et al. (2002) estimated the uncertainty due to atmospheric phase effects by looking at the root mean squared (RMS) difference between each interferogram and all other interferograms in one data set. Because they knew that any surface deformation in their study area was occurring slowly, they were able to attribute the RMS difference to the uncertainty

due solely to atmospheric phase effects. However, this method assumes the same amount of uncertainty for every pixel in a given interferogram and does not accurately represent the spatial variations in the uncertainty. Onn and Zebker (2006) used Global Positioning System (GPS) estimates of water vapor to decrease the amount of uncertainty in the InSAR deformation measurements, in some cases as much as 31%. However, this analysis involves having a network of GPS measurements available, which is not the case for many field sites.

A more recent study by Knospe and Jonsson (2010) investigated how atmospheric phase effects vary spatially. In order to isolate the uncertainty due to atmospheric phase effects they processed two interferograms that spanned a single day. They assumed that no deformation was taking place over the time span of that day ( $\Delta\phi_{def} = 0$ ), and that  $\Delta\phi_{ip}$  and  $\Delta\phi_n$  were also very small. This means that the measure phase change was all due to changes in atmospheric conditions. They then created two variogram models that quantified the spatial variability of the uncertainty. The variogram models were then used to represent the uncertainty due to atmospheric phase effects for a synthetic data set. They showed that the uncertainty in the final deformation estimates was less when the variogram models were used to estimate the uncertainty due to atmospheric phase effects. However, they stated that it is important to know which variogram model best represents the uncertainty due to atmospheric phase effects for a given data set. Many applications would not have a set of interferograms that span a single day, and hence would not produce an appropriate variogram model of the uncertainty due to atmospheric phase effects.

The phase change due to phase noise ( $\Delta\phi_n$ ) is caused by signal decorrelation and cannot readily be compensated for without sacrificing spatial resolution. For a given pixel in an interferogram the coherence is calculated as a quality measure for the phase difference  $\Delta\phi_n$  between two SAR scenes at that point. The complex coherence ( $\gamma$ ) is defined as follows:

$$\gamma = \frac{\langle S_1 S_2^* \rangle}{\sqrt{\langle S_1 S_1^* \rangle \langle S_2 S_2^* \rangle}} \quad (\text{Equation 2.25})$$

where  $\langle \rangle$  denotes the expected value  $S_1$  and  $S_2$  are the complex values of SAR scene and SAR scene 2 and  $S_1^*$  and  $S_2^*$  are the complex conjugates of SAR scene 1 and SAR scene 2 for a small sample of pixels around the pixel in question. Often the magnitude of the complex coherence is used, referred to as only the coherence, which can range from 0 to 1. An interferogram is described as coherent/well correlated, if many of the pixels have coherence near 1; or as incoherent/decorrelated, if many of the pixels have coherence near 0.

The coherence can be described as the product of the thermal coherence  $\gamma_{therm}$  coherence  $\gamma_{spat}$  and the temporal coherence  $\gamma_{temp}$  (Zebker and Villasenor, 1992):

$$\gamma = \gamma_{therm} \cdot \gamma_{spat} \cdot \gamma_{temp} \quad (\text{Equation 2.26})$$

Where  $\gamma_{therm}$  quantifies the system noise, a characteristic of the system configuration;  $\gamma_{spat}$  is a factor corresponding to the viewing angle of the satellite between the acquisition of the two scenes, as described above as a parallax effect. The reflection from a scattering area viewed

at one angle will be different when viewed at another angle. This change in viewing angle is quantified by the spatial distance between the two satellite positions, the spatial baseline.

The most difficult effect to deal with is the temporal coherence  $\gamma_{temp}$ . Temporal decorrelation follows from wavelength-scale changes in the positions of scatterers within each resolution cell between the acquisition times of the two scenes. The time between two scenes is called the temporal baseline; long temporal baselines tend to decrease  $\gamma_{temp}$ . A surface can de-correlate with time due to processes or activities such as seasonal vegetation changes, erosion of the land surface, agricultural activity, or construction. The best way to mitigate this effect is to form interferograms from scene pairs with small temporal baselines.

#### **2.4.4 Advanced Time-Series Technique of SAR Interferometry**

DInSAR is quite efficient in various applications of remote sensing. Nevertheless, this conventional InSAR processing involve decorrelation of the interferometric signal caused by the difference in orbital position between the two SAR acquisitions, topography changes, atmospheric delay (ionosphere), atmospheric condition changes. In addition, the changes in dielectrical characteristics of scatterers favor the presence of temporal and geometric (baseline) decorrelations presented in conventional DInSAR interferograms. The atmospheric and topographic errors are correlated and to attenuate these decorrelations phenomena, the multi-temporal processing also known as time series analysis aims to reduce the signal decorrelation and residuals with the processing of multiple SAR images over the same track in order to get the best signal-to-noise ratio and then obtain the best phase signal correlation matrix. Fundamentally, time-series InSAR use one set of images (for phase values) and the reflected signal from each element in the ground (depending on it is resolution) is obtained with the sum of all individual wavelets reflected by the scattering centers of each elements. Nowadays, there are two time-series InSAR that have been widely applied for related analysis, i.e. Persistent Scatterer (PS) and Small BASline (SBAS) methods. Each of these two methods gives temporal solution to the uncorrelated phenomena based on the principle of dominant reflectivity of centers of permanent scatterers.

In PS InSAR, PSs are exploited and differential interferograms with respect to a single master image are formed (Ferretti et al., 2000; Ferretti et al., 2001). The main idea behind PS InSAR is that some of these interferograms might have a large perpendicular baseline or a large temporal baseline, and are hence affected by strong decorrelation noise. Thus, only points which do not change their scattering characteristics in time can preserve the interferometric phase information. It is thus implied that only the signal phases of permanently coherent PSs can be retrieved for interferometry in PS method. The interferograms are analysed at PSs to maximize the SCR. PS InSAR uses a deformation model for the estimation.

One of the DS-based techniques include SBAS. The SBAS method exploits only small baseline (temporal and spatial) unwrapped differential interferograms, so as to limit the effects of uncompensated geometric decorrelation and temporal decorrelation on the DSs (Berardino et al., 2002). These interferograms are multi-looked to reduce the phase noise and improve the phase estimate. SBAS estimates the non-linear deformation time series via the Singular Value Decomposition (SVD) without using any deformation model (Golub and Loan, 1996).

In this study, PS and SBAS methods are introduced to generate information of subsidence in the study area. The characteristics of stacking or multi-temporal or time-series InSAR technique of PS and SBAS used in the study are presented in Table 2.8. The PS algorithms are able to resolve double scatterers inside a resolution cell. Moreover, the SBAS method exploits only small temporal and spatial baseline to unwrap differential interferograms, to limit the effects of uncompensated geometric decorrelation and temporal decorrelation on the DSs.

Table 2.8 Characteristics of time-series InSAR technique of PS and SBAS

<b>Methods</b>	<b>Baseline configuration</b>	<b>Pixel Selection Criterion</b>	<b>Deformation Mode</b>
PS*	Single master	Amplitude dispersion	Linear deformation in time
SBAS**	Small baseline	Coherence	Spatial smoothness

(Source: \*Bouraoui, 2013; Crosetto et al., 2016; Ferretti et al., 2001; \*Kampes, 2005; \*Hooper et al., 2004; \*\*Kooij et al., 2006; \*\*Berardino et al., 2002)

#### 2.4.5 Persistent Scatterer (PS) InSAR

Persistent scatterer InSAR (PS) (Ferretti et al., 2000, 2001; Kampes, 2005; Hooper et al., 2004; van der Kooij et al., 2006) marks the second generation of InSAR processing systems that belong to the family of time series analysis and time-series InSAR techniques. PS was developed to give solutions to the conventional InSAR decorrelation especially those due to temporal and geometric effects (Ferretti et al., 2001). The errors due to spatial and temporal variations cause the temporal and spatial phase errors producing disconnected areas in space and time (Hooper, 2006). This makes the interpretation of geodetic measurements from interferograms difficult and sometimes ambiguous by reducing the signal-to-noise ratio (SNR). Man-made structures can be used as corner reflectors and reference to calibrate the InSAR system due to their coherent phase center.

The principle of permanent reflector method is to identify points (scatterers) from a series of InSAR images that preserve their coherence (in term of signal backscattered) in time and space. These scatterers will form a connected network from their phase measurements (Hooper, 2006). The interferometric phase distribution ranging between  $[\pi -\pi]$ , to improve the

phase signal, one of the existing solutions is to choose the dominant element from the interferometric phase by statistical estimations from the brightness of each reflector and the dominant signal with its corresponding dominant scatterer.

This method guarantees that the obtained signal is less affected by the decorrelations phenomena using the one signal of the dominant scatterer for each pixel to perform the time series evolutions of the studied phenomena. The chosen pixels have invariance in their amplitude values and/or their phase values over a set of PS SAR images. Note that the variance correlates with the brightness of the non-selected scatterers of the same pixel. In fact, as their brightness raises, the variance of the pixel grows. The signal-to-clutter ratio (SCR) is obtained in this case by measuring the ratio between the echo of the dominant scatterer and to separate the noise signals and extract the signal of deformation ( $\phi_{def}, \Delta t_i$ ) from Equation (2.3).

In order to remove interferograms, the phase contribution due to the topography and the imaging geometry  $\phi_{topo}, \Delta t_i$ , PS use the flattening correction. The principle is to suppose that all scatterers are in the WGS-84 projection system of the digital elevation model (DEM) in radar coordinate and calculate the topographic contribution and then remove it. Most common way it to use the SRTM data (Farr et al, 2007). Following Kampes (2006), the DEM error is estimated from the phase signal using:

$$\phi_{topo}, \Delta t_i = \frac{4\pi}{\lambda} B_{\perp}(\theta) \frac{\Delta h \sin(\theta)}{r} \quad (\text{Equation 2.27})$$

Where  $r$  is the distance from the satellite to the pixel on the ground.  $\theta$  is the look angle of the satellite, and  $B_{\perp}$  is the perpendicular baseline.

One of the typical characteristics of the SAR images is the range and azimuth resolutions. Using the time series methods, these two parameters belong to dominant scatterer positions in the pixel. We may then estimate the error in the range and in azimuth position of sub-pixel as following (Kampes, 2006):

$$\phi_{\varepsilon}, \Delta t_i = \frac{4\pi}{\lambda} B_{\perp}(\theta) \frac{\varepsilon \cos(\theta)}{r} \quad (\text{Equation 2.28})$$

$$\phi_{\nu}, \Delta t_i = \frac{2\pi}{\delta} \Delta F_{DC} \omega \quad (\text{Equation 2.29})$$

Where  $\varepsilon$  indicates the distance between the dominant scatter and the center of the pixel,  $\nu$  is the velocity of the satellite,  $\omega$  is the azimuthal offset component of the dominant scatterer from the center of the pixel,  $\Delta F_{DC}$  the difference in the Doppler centroid frequencies between the Master and Slave SAR images. Hooper (2006) considers the phase signal due to the atmospheric delay  $\phi_{atm}, \Delta t_i$  as a long wavelength observed from the unwrapped phase which characterizes a significant gradual variation in space.

PS are therefore obtained from SAR images that are less affected by noises due to the Master and Slave SAR images. Hooper (2006) considers the phase signal due to the atmospheric delay, atmospheric delay, topographic artifact, and orbital error and also from the scatterer

noise in addition to the scatterer signal models. PS algorithms have two scattering signal models that are, the constant signal model and the Gaussian signal model. The probability distribution functions (PDFs) are calculated for each SAR pixel respectively from their amplitude and phase.

Ferretti et al. (2001) propose a signal model:  $z_i = g + n_i (i = 1, \dots, K + 1)$  where  $g$  is the complex reflectivity taken as  $g=1$ ,  $n_i$  represents the noise sources and  $K+1$  the number of used SAR data. The amplitude of the SAR signal after Ferretti et al. (2001) is given by:

$$f_A(a) = \frac{a}{\sigma_n^2} I_0 \left( \frac{ag}{\sigma_n^2} \right) e^{-(a^2+g^2)/2\sigma_n^2} \quad a > 0. \quad (\text{Equation 2.30})$$

Where  $I_0$  is the modified Bessel function. The complex circular Gaussian noise variance  $\sigma_n^2$  is  $\text{SNR} = g/\sigma_n$  (Equation 2.31)

The quality of the PS analysis depends on the number of available images and the density of PSs. A minimum of about 25 images and a PS density of approximately 5-10 PS/km<sup>2</sup> are needed (Colesanti et al., 2003). In addition, a deformation model has to be defined prior to deformation estimation. Typically, a linear model is assumed, although it is also possible to use seasonal or some other non-linear deformation models (Ferretti et al., 2000; Colesanti et al., 2003). PS algorithms have been proposed to resolve double scatterers (i.e. two dominant scatterers located at different elevations) inside a resolution cell (Ferretti et al., 2005; Adam et al., 2005).

#### 2.4.6 Small Baseline Subset (SBAS)

An agricultural area where crop growth, irrigation, land erosion and harvesting cycles can all change the height of the imaged surface between the acquisition of any two SAR scenes, leading to decorrelation of the signals. A recently developed technique, Small Baseline Subset (SBAS) analysis, combines the coherent areas in a series of interferograms to produce a map of deformation time-series (Berardino et al., 2002). Phase decorrelation is minimized by imposing constraints on the temporal and spatial baselines for each pair of scenes that are interfered.

The basic principle underlying SBAS is proper interferogram selection combined with a least squares (LS) analysis of the phases in the resulting unwrapped interferograms. Interferogram selection is illustrated in Figure 2.18, a plot of spatial versus temporal baseline for all available SAR scenes from an area. Each scene is shown as a circle with the spatial and temporal baselines plotted relative to the first scene. Lines, which signify an interferogram, connect scenes if the spatial and temporal baselines are below some selected threshold. In general, a smaller spatial baseline leads to better coherence, therefore the goal is to minimize the spatial baseline threshold for the set of interferograms. The temporal baseline threshold is dependent on how rapidly the height of the vegetation changes with time in a



given area and so, for example, could be 6 years for areas in an arid climate, but a few months for vegetated areas. Each group of connected scenes is known as a small baseline subset. As long as the subsets overlap for some period of time, a singular value decomposition (SVD) can be used to solve for a time-series of deformation, relative to the first scene.

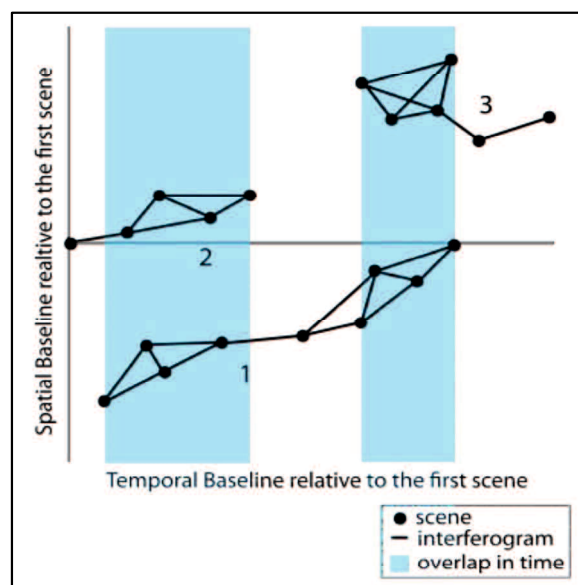


Figure 2.18 Example spatial versus temporal baseline plot with 3 small baselines  
(Source: Reeves, 2013)

The mean coherence for every pixel is then calculated and a threshold applied, such that only highly coherent pixels are used in the remainder of the analysis. In the development of the SBAS method, Berardino et al. (2002) and Lauknes (2004) determined values for the threshold: they set thresholds  $\gamma > 0.25$  in at least 30% of the interferograms and  $\gamma > 0.3$  in at least 30% of the interferograms respectively. The goal of setting this threshold is to select pixels that have high coherence through time while still selecting enough pixels to properly unwrap the interferometric phase.

SBAS method (Berardino et al., 2002; Lanari et al., 2004) is one of the differential synthetic aperture radar interferometry algorithms for studying temporal evolution of ground deformation characterized by the small baseline separation between the SAR pairs used to generate interferograms (Sandwell et al., 1998; Berardino et al., 2002; Schmidt and Burgmann, 2003). This algorithm aims to limit the spatial decorrelation taking into account the spatial and the temporal information from the SAR data (Berardino et al., 2002). The generation of time series is the principle of time-series InSAR algorithms.

The small baseline processing method was introduced for the first time by Sandwell et al. (1998) and defined as an InSAR stacking method. This method is able to calculate the average

velocity (mean-velocity) by measuring the average displacements obtained with the set of interferograms respecting a short baseline. The SBAS algorithm relates the different SAR acquisitions having a short baseline (short spatial separation) in order to generate series of interferograms under some circumstances: By reducing the spatial separation between SAR images, we reduce the decorrelations especially due to the large baseline separation and obtain correlated interferograms (Berardino et al., 2002)

According to the process application of SBAS algorithm by Bernardino et al (2002), After InSAR processing, the interferometric phase distribution ranges between  $[\pi -\pi]$  (wrapped phase). In order to improve the phase signal quality, one of the existing solutions from MT-InSAR algorithms is to measure the average value of the scatterers for each pixel, by taking into account the neighbored reflectors value. This method can attenuate the exhibited large random phase difference observed in time and takes into account the average from all scatterers of each averaged elements.

In order to review the mathematical formulation from Berardino et al. (2002), SBAS technique is on the selected pixels by considering  $N + 1$  SAR scenes acquired at times  $(t_0, t_1, \dots, t_N)$ . Each scene must be able to interfere with one other scene, so the minimum number for each subset is two scenes. If  $N$  is odd, the number of different interferograms  $M$  is given by the following formula:

$$\frac{N+1}{2} \leq M \leq N \left( \frac{N+1}{2} \right) \quad (\text{Equation 2.32})$$

In case the  $j^{\text{th}}$  interferogram made with SAR scenes at  $t_A$  and  $t_B$ , the change in phase measured at each pixel position in terms of range direction and azimuth direction  $(x,r)$  can be defined as follows:

$$\begin{aligned} \Delta\phi(x, r) &= \phi(t_B, x, r) - \phi(t_A, x, r) \\ &\cong \frac{4\pi}{\lambda} [d(t_B, x, r) - d(t_A, x, r)] \end{aligned} \quad (\text{Equation 2.33})$$

where  $d(t_B, x, r)$  is the deformation at time  $t_B$  relative to zero deformation at time  $t_0$  and  $d(t_A, x, r)$  is the deformation at time  $t_A$  relative to zero deformation at time  $t_0$ .

The SBAS algorithm uses series of SAR to perform interferograms having a short baseline separation. These interferograms obtained with the conventional D-InSAR method are used as inputs to calculate the unwrapping stage, from which we estimate the topographic contribution and extract the low-pass (LP) temporal deformation that will be subtracted from the wrapped interferograms modulo- $2\pi$ . After extraction of the residual topographic contribution and LP component from the wrapped interferograms, they will be considered as residual phase and be unwrapped. The next step is to apply spatial and temporal filtering to the unwrapping residual file that contains the temporal deformation and the topographic phase residual. Finally, the inversion of the stack of interferograms is assured using the singular value decomposition (SVD) method.

### 2.4.7 Merged PS and SBAS

Since the appearance of time-series methods (PS and SBAS), the advantage of the methods has been developed on several software solutions. In general, PS algorithm use the information from SAR amplitude dispersion (Ferreti et al., 2001) with threshold value of  $\sim 0.4$  in order to select the candidate scatterers. According to (Hooper, 2008) the pixels of filtered phase that exhibit small decorrelation in short time and are denoted as slowly-decorrelating filtered phase (SDFP), are selected by SBAS method. The merged method selects pixel from the PS and SDFP groups that are coincidence to improve the spatial sampling of the signal. The used PS algorithm from Hooper (2007) requires a minimum constraint of five SAR data. In order to have possibility to process large areas, Hooper (2007) proposes to divide the whole area into small patches (in azimuth and in range) and process InSAR separately. The final map will be reconstituted from the processed patches.

The combination between PS-SBAS calculates the equivalence from SBAS interferograms to PS single Master interferogram. When pixel has both PS and SB values, the system set to the pixel mean values from the phase and the amplitude obtained by PS and SBAS algorithms. The merged method has two highlights, it increases the number obtained scatterer and also increase the SNR (Hooper, 2008). According to (Hooper, 2008), the merged pixels are obtained by measuring the mean of both PS and SBAS sets of results for each pixel and SNR is defined by:

$$\widehat{SNR} = \frac{1}{Y_x^{-1} - 1} \quad (\text{Equation 2.34})$$

Figure 2.19 showed comparison between the number of scatterer obtained and the velocity values achieved using Persistent Scatterer (PS) method, Small Baseline (SB) and Merged (PS-SBAS) based on a study conducted using combined method from both PS and SBAS results provided on STAMPS/MTI software package for landslide case in Constantine (Bouraoui, 2013).

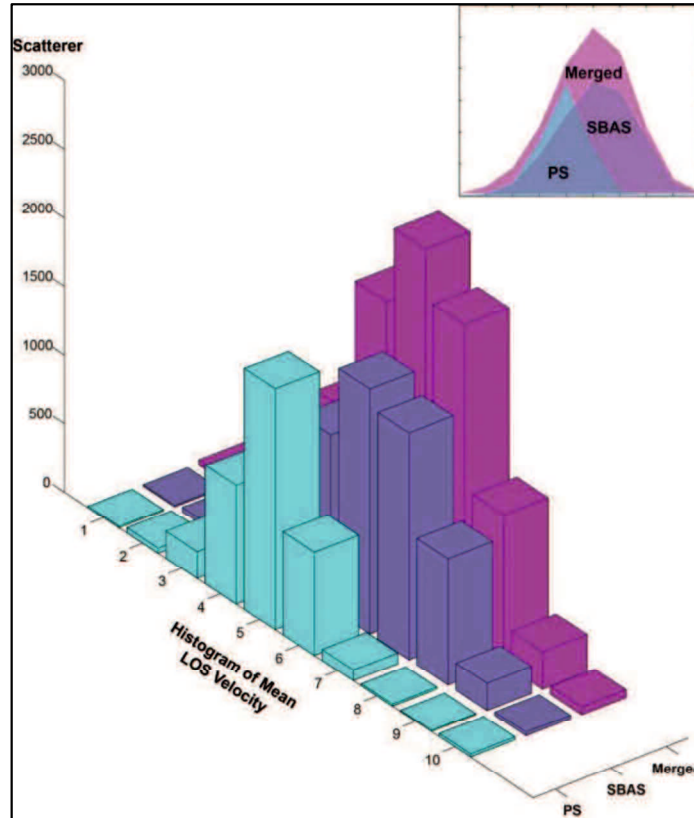


Figure 2.19 Comparison between the number of scatterer obtained and the velocity values achieved using PS, SBAS, and merged (PS-SBAS) methods  
(Source: Bouraoui, 2013)

## 2.5 Surface Topography

Topography is one of the most important of the physical characteristics of surfaces influencing their significant technical properties. The study is a branch of geodesy which deals with the measurement technique of a portion of Earth's shell, with determining the position of earth elements on small surfaces that considered flat, as well as graphical or numerical representation technique of the measured surfaces, for drawing up maps and plans; detailed description of a place in terms of placement, configuration, etc.; and how elements of an ensemble are arranged in space. The systematic study of the fine structure of surfaces only became possible when instruments with sufficient magnification to resolve the vertical structures became available (Thwaite, 1982). In this study, Digital Elevation Model (DEM) and Global Navigation Satellite System (GNSS) Continuously Operating Reference Stations (CORS) are used as data source to obtain surface topography information. A Real Time Kinematic (RTK) processing is applied particularly for the GNSS CORS.

### **2.5.1 Global Navigation Satellite System (GNSS) Continuously Operating Reference Stations (CORS)**

Global Navigation Satellite System (GNSS) is the worldwide standard generic term for satellite navigation systems that provide autonomous geospatial positioning with global coverage. This term includes e.g. the GPS, GLONASS, Galileo, Beidou and other regional systems. GPS is currently the world's most utilized satellite navigation system. It consists of up to 32 medium Earth orbit satellites in six different orbital planes, with the exact number of satellites varying as older satellites are retired and replaced (Venezia, 2015; Sickle, 2015).

GPS/GNSS observations are increasingly used for a wide range of applications. Today, many countries have established active primary networks of GPS/GNSS Continuously Operating Reference Stations (CORS) to monitor the stability and integrity of their datums. This is particularly the case for countries located on or near tectonic plate boundaries that cause their datum (or to be more correct, the realization of their datum in the form of 3D coordinates of ground marks and reference stations) to undergo deformation (or coordinate change) with time (Rizos and Satirapod, 2011).

Networks of CORS have also been rapidly installed in Indonesia by several institutions to provide high level positioning and practice needed users. One of the Indonesian government agency responsible for the management and operating of CORS is Geospatial Information Agency (BIG). BIG currently manages and operates 124 CORS, 19 of them in collaboration with GeoForschungsZentrum (GFZ) Germany in support of the Tsunami Early Warning System, 3 GNSS Stations in collaboration with TU Delft Netherland. Indonesian Continuously Operating Reference Stations (InaCORS) is GNSS network that covers the territory of Indonesia. GNSS-based technology began in 1995 with the establishment of IGS stations BAKO. In 2007, GNSS CORS infrastructure developed rapidly until today. Infrastructure development of InaCORS is financial supported by the national budget and is managed by BIG. Communication technologies used include virtual private network and radio. InaCORS divided in different groups by using virtual server for sites management in a variety of areas in Indonesia (Adhitya et al., 2014).

The main purpose of Indonesian Continuously Operating Reference Station (InaCORS) is to maintain an accurate and precise geodetic reference frame over Indonesian region, and also to support a wide range of scientific and practical applications such as geodynamics and deformation monitoring, meteorological and ionospheric studies and other needs in the frame of surveys and mapping (Abidin et al. 2010). The current status of the InaCORS managed by BIG is described in Figure 2.20.

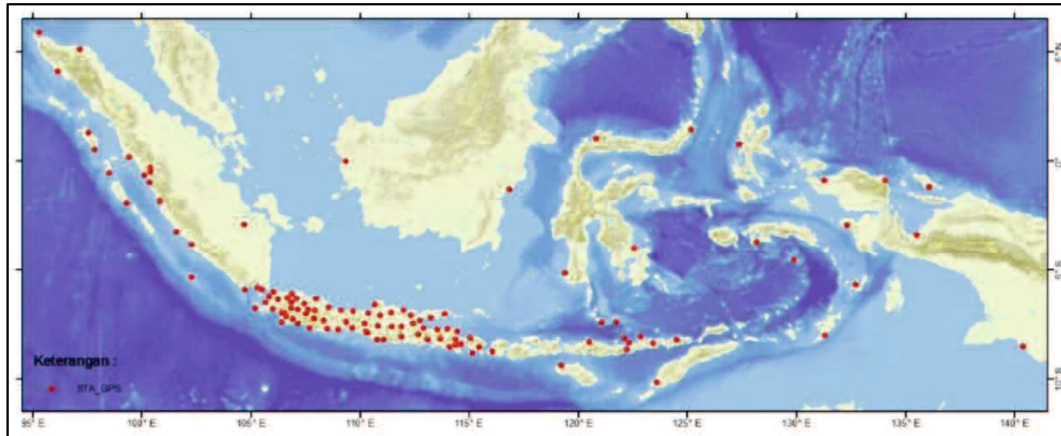
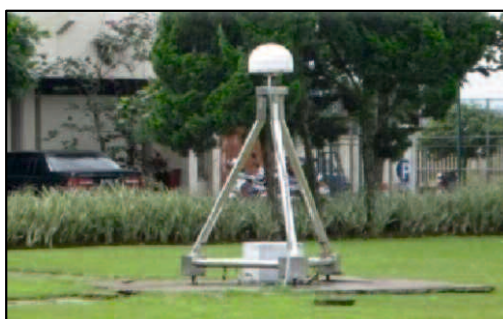


Figure 2.20 The current status of the InaCORS managed by BIG  
(Source: Adhitya et al., 2014)

The current status of all stations of Indonesian CORS receivers system incorporates the high- precision L1/L2 geodetic type (i.e. GRX1200 family, Topcon NetG3/NetG3A, and Septentrio) with standard Choke Ring antenna and most of the GPS receivers equipped with meteorological sensors (Matindas and Subarya, 2009). In 2013, several broken receivers were replaced with Leica GR10. Figure 2.21 (a) and (b) show several pillars of InaCORS on the ground and on the roof, respectively. Average height concrete pillar in the ground surface is 3.5 meters. They use identification marker contain ID site and site owner information.

The data communication of CORS system is very important. By good communication support, data can be sent optimum. Reliability of the data flows from CORS sites could expect that the real or near real time tracking data should deliver to the processing or operational center with a sufficiently small delay. The data communication link from CORS sites streaming real time to operational center by using a license free Spread Spectrum radio operating in the band from 2.400 GHz to 2.4835 GHz in combination with VPN-IP (Matindas and Subarya, 2009).



(a)



(b)

Figure 2.21 Pillars of InaCORS: (a) Pilar on the ground; (b) Pilar on the roof  
(Source: Adhitya, et al., 2014)

Besides the national GPS CORS established and maintained by Bakosurtanal, other national agencies, such as the Ministry of Land and Spatial Planning (BPN) have also started establishing their own GPS CORS network. In order to speed up the land administration process in Indonesia, BPN has started to establish GPS CORS, consisting of Class-A and Class-B type stations. In 2010, other 33 CORS stations was established in Java Island, Bali Island, and other strategic areas outside Java and Bali (Abidin et al., 2010).

The long line accuracy, convenience and relative low-cost of GNSS positioning have revolutionized operations for surveying and mapping agencies. Modern nationwide geodetic datums are now underpinned by GNSS surveying and CORS networks provide a cost-effective means of densifying coordinate reference frames. The advantages to land authorities include a reduced overhead on physical survey mark maintenance, a more homogeneous coordinate set and the opportunity to provide positioning services to a range of new users across the public and private sector (Roberts, C. and Stanaway, 2009). In particular, GPS CORS in Indonesia will be useful for various existing applications in Indonesia and also will create more innovative applications, both in real-time and post-processing modes (Abidin et al., 2010)

### **2.5.2 Real Time Kinematic (RTK) Positioning Technique**

The development of Real Time Kinematic (RTK) positioning technique has allowed any application, including surveying and navigation, to meet the accuracy requirements of real-time surveying and high-precision navigation (Langley, 1998). Real time kinematic (RTK) GPS/GNSS employs a method of real time carrier-phase (CPH) differential GPS/GNSS positioning whereby users can obtain centimeter-level position accuracies in real time (Riley et al., 2000). The carrier phase is the more precise sibling of the pseudorange. It is the phase of the receiver carrier with respect to the phase of a carrier generated by an oscillator in the GPS receiver (Langley, 1998).

Fundamentally, RTK positioning uses a static GPS receiver as a reference station located at a known point. Another receiver is used as the rover which can move and survey any points of interest. Both receivers make observations of the GPS signals at the same time and a radio data link between the two receivers permits data to be sent from reference to rover, where the calculation of coordinates is carried out. For the desire of cost saving, when there is no need for instantaneous point coordinates, post processed kinematic GPS systems could be used as well. In this case there is no need for transmitting data between two receivers, instead the two data files from reference station and the rover are processed later on (Farah et al., 2008).

At a very basic conceptual level, the range is calculated by determining the number of carrier cycles between the satellite and the rover station, then multiplying this number by the carrier wavelength. The calculated ranges still include errors from such sources as satellite

clock and ephemerides, and ionospheric and tropospheric delays. To eliminate these errors and to take advantage of the precision of carrier-based measurements, RTK performance requires measurements to be transmitted from the base station to the rover station. A complicated process called “ambiguity resolution” is needed to determine the number of whole cycles. Despite being a complex process, high precision GNSS receivers can resolve the ambiguities almost instantaneously (NovAtel, 2017). Figure 2.22 describes RTK measurement of range cycles.

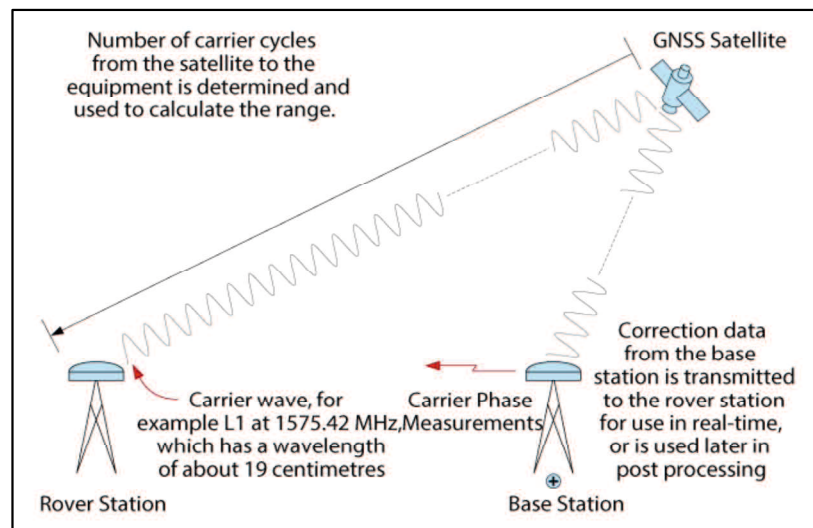


Figure 2.22 RTK measurement of range cycles  
(Source: NovAtel, 2017)

Rovers determine their position using algorithms that incorporate ambiguity resolution and differential correction. Like differential GNSS, the position accuracy achievable by the rover depends on, among other things, its distance from the base station (referred to as the baseline) and the accuracy of the differential corrections. Corrections are as accurate as the known location of the base station and the quality of the base station’s satellite observations. Site selection is important for minimizing environmental effects such as interference and multipath, as is the quality of the base station and rover receivers and antennas (NovAtel, 2017).

Network RTK is based on the use of several widely spaced permanent stations. Depending on the implementation, positioning data from the permanent stations is regularly communicated to a central processing station. On demand from RTK user terminals, which transmit their approximate location to the central station, the central station calculates and transmits correction information or corrected position to the RTK user terminal. The benefit of this approach is an overall reduction in the number of RTK base stations required. Depending on the implementation, data may be transmitted over cellular radio links or other wireless medium (NovAtel, 2017).



### 2.5.3 Digital Elevation Model (DEM) of ASTER GDEM and SRTM

A topographical map is the main type of map used to depict elevation, often through use of contour lines. In a GIS, Digital Elevation Model (DEM) are commonly used to represent the surface (topography) of a place, through a raster (grid) dataset of elevations. Fundamentally, the term DEM is used to mean the digital cartographic representation of the elevation of the earth surface in any form. It is sometimes also referred as a Digital Terrain Model (DTM). The horizontal spacing is specified in arc-seconds, with a smaller horizontal spacing usually implying a better resolution in height, although the height accuracy is actually a function of the production methods (Mikhail et al., 2001).

A DEM represents ground surface topography or terrain digitally with different accuracies for different application fields. A wide range of civil engineering and military planning tasks have utilized DEM products (Habib, 2005). In general, it is obtained using a number of techniques such as photogrammetry, digitizing, laser scanning, radar interferometry, classical survey and GPS techniques (Blomgren, 1999; Sugumaran et al., 2000). DEM data generated from radar interferometry of SAR data used in this study are ASTER-GDEM and SRTM.

#### 1. Advanced Spaceborne Thermal Emission and Reflection Radiometer (ASTER) Global Digital Elevation Model (GDEM)

The ASTER Global Digital Elevation Model (ASTER GDEM) is a joint product developed and made available to the public by the Ministry of Economy, Trade, and Industry (METI) of Japan and the United States National Aeronautics and Space Administration (NASA). It is generated from data collected from the Advanced Spaceborne Thermal Emission and Reflection Radiometer (ASTER), a spaceborne earth observing optical instrument. The ASTER GDEM is the only DEM that covers the entire land surface of the Earth (Figure 2.23) at high resolution. Moreover, the ASTER GDEM is available at no charge to users worldwide via electronic download from ERSDAC and from NASA's Land Processes Distributed Active Archive Center (LP DAAC) (JSS, 2017).

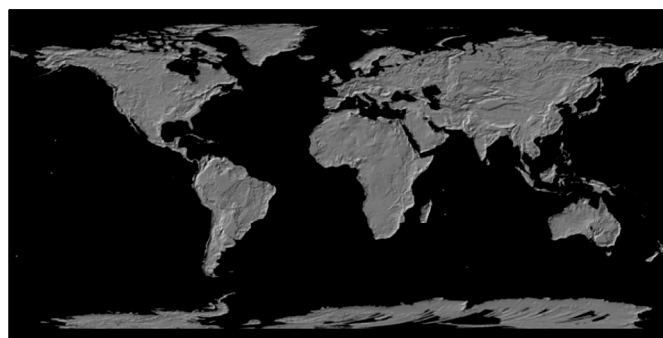


Figure 2.23 ASTER GDEM  
(Source: JSS, 2017)

The ASTER instrument was built by METI and launched onboard NASA's Terra spacecraft in December 1999. It has an along-track stereoscopic capability using its near infrared spectral band and its nadir-viewing and backward-viewing telescopes to acquire stereo image data with a base-to-height ratio of 0.6. The spatial resolution is 15 m in the horizontal plane. One nadir-looking ASTER VNIR scene consists of 4,100 samples by 4,200 lines, corresponding to about 60 km-by-60 km ground area (JSS, 2017).

The methodology used to produce the ASTER GDEM involved automated processing of the entire 1.5-million-scene ASTER archive, including stereo-correlation to produce 1,264,118 individual scene-based ASTER DEMs, cloud masking to remove cloudy pixels, stacking all cloud-screened DEMs, removing residual bad values and outliers, averaging selected data to create final pixel values, and then correcting residual anomalies before partitioning the data into 1°-by-1° tiles. It took approximately one year to complete production of the beta version of the ASTER GDEM using a fully automated approach (JSS, 2017).

The ASTER GDEM covers land surfaces between 83°N and 83°S and is composed of 22,600 1°-by-1° tiles. Tiles that contain at least 0.01% land area are included. The ASTER GDEM is in GeoTIFF format with geographic lat/long coordinates and a 1 arc-second (30 m) grid of elevation postings. It is referenced to the WGS84/EGM96 geoid. Pre-production estimated accuracies for this global product were 20 meters at 95 % confidence for vertical data and 30 meters at 95 % confidence for horizontal data. Initial validation studies concluded that the ASTER GDEM generally meets the pre-production accuracy predications, but results do vary and include areas where GDEM accuracy does not meet the pre-production estimates (JSS, 2017).

The topography of the land surface is one of the most fundamental geophysical measurements of the Earth, and it is a dominant controlling factor in virtually all physical processes that occur on the land surface. Topography of the land surface also significantly controls processes within the overlying atmosphere, and it reflects the processes within the underlying lithosphere. Consequently, topographic information is important across the full spectrum of earth sciences, and the availability of an up-to-date, high resolution (1-arc-sec or less) global DEM has been a priority of earth scientists for a long time. The ASTER GDEM, with 30m grid postings and produced from a consistent primary data source, is expected to meet the requirements of many users for global topographic information (JSS, 2017).

## 2. Shuttle Radar Topography Mission (SRTM)

The Shuttle Radar Topography Mission (SRTM) data sets result from a collaborative effort by the National Aeronautics and Space Administration (NASA) and the National Geospatial-Intelligence Agency (NGA - previously known as the National Imagery and Mapping Agency, or NIMA), as well as the participation of the German and Italian space

agencies, to generate a near-global digital elevation model (DEM) of the Earth using radar interferometry. The SRTM explored the structure of the earth surface in February 2000. The instrument consisted of the Spaceborne Imaging Radar-C (SIR-C) hardware set modified with a Space Station-derived mast and additional antennae to form an interferometer with a 60 m long baseline (Farr and Kobrick, 2000).

Synthetic aperture radars are side-looking instruments and acquire data along continuous swaths. The SRTM swaths extended from about 30 degrees off-nadir to about 58 degrees off-nadir from an altitude of 233 km, and thus were about 225 km wide. During the data flight the instrument was operated at all times the orbiter was over land and about 1000 individual swaths were acquired over the ten days of mapping operations. Length of the acquired swaths range from a few hundred to several thousand km. Each individual data acquisition is referred to as a “data take” (Farr and Kobrick, 2000).

The SRTM data have undergone a sequence of processing steps resulting in several data versions having slightly different characteristics. In addition, there are difference naming conventions used by the NGA and NASA for the SRTM products (USGS, 2015). Coverage of SRTM is describes in Figure 2.24. Table 2.9 summarizes the naming conventions used to differentiate the SRTM products.

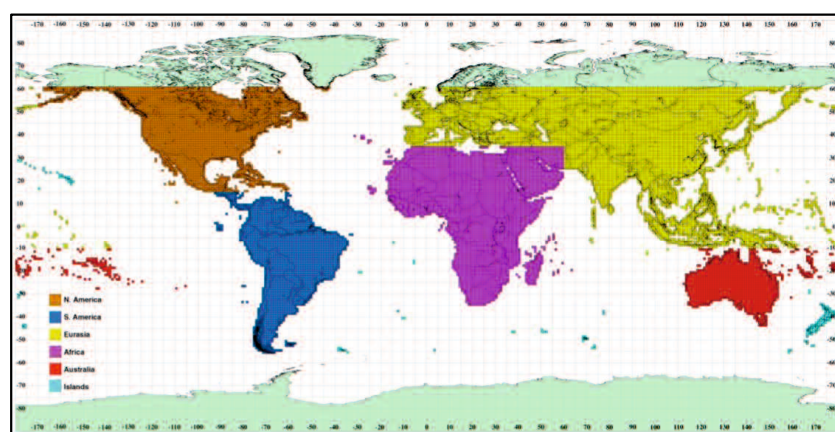


Figure 2.24 Coverage of SRTM

(Source: USGS, 2015)

Table 2.9 SRTM data naming conventions

Posting (Sample Spacing)	SRTM name	DTED equivalent	Other data sets
1 arc-second	SRTM1	DTED2 (indicating “level 2”)	
3 arc-seconds	SRTM3	DTED1	
30 arc-seconds	SRTM30	DTED0	GTOP30

(Source: USGS, 2015)

SRTM data are organized into individual rasterized cells, or tiles, each covering one degree by one degree in latitude and longitude. Sample spacing for individual data points is either 1 arcsecond, 3 arc-seconds, or 30 arc-seconds, referred to as SRTM1, SRTM3 and SRTM30, respectively. Since one arc-second at the equator corresponds to roughly 30 meters in horizontal extent, the SRTM1 and SRTM3 are sometimes referred to as “30 meter” or “90 meter” data (USGS, 2015). Table 2.10 described the product specification of SRTM1 used for the study.

Table 2.10 Product specifications of SRTM1

<b>Item</b>	<b>Specifications</b>
Projection	Geographic
Horizontal datum	WGS84
Vertical datum	EGM96 (Earth Gravitational Model 1996)
Vertical units	Meters
Spatial resolution	1 arc-second for global coverage (~30 meters) 3 arc-seconds for global coverage (~90 meters)
Raster size	1 degree tiles
C-band wavelength	5.6 cm

(Source: USGS, 2015)

## **2.6 Supervised Classification Methods for Land Cover Mapping**

Land cover is the material at the ground, such as soil, vegetation, water, asphalt, and so forth. Depending on the sensor resolutions, the number and kind of land cover classes that can be identified in the image can vary significantly. A supervised classification is an image processing technique that allows for the identification of materials in an image, according to their spectral signatures. There are several kinds of classification algorithms, but the general purpose is to produce a thematic map of the land cover.

### **2.6.1 Training Areas**

In general, supervised classifications require the user to select one or more Regions of Interest (ROIs, also training areas) for each land cover class identified in the image. ROIs are polygons drawn over homogeneous areas of the image that overlay pixels belonging to the same land cover class (Fisher and Unwin, 2005). Region growing algorithm is the algorithm used for determining training areas in supervised classification

The region growing algorithm allows to select pixels similar to a seed one, considering the spectral similarity (i.e. spectral distance) of adjacent pixels. In supervised classification, the region growing algorithm is available for the training area creation. The parameter

distance is related to the similarity of pixel values (the lower the value, the more similar are selected pixels) to the seed one (i.e. selected clicking on a pixel). An additional parameter is the maximum width, which is the side length of a square, centred at the seed pixel, which inscribes the training area. If all the pixels had the same value, the training area would be this square. The minimum size is used as a constraint (for every single band), selecting at least the pixels that are more similar to the seed one until the number of selected pixels equals the minimum size (Congedo, 2012). In Figure 2.25, region growing exemplified the central pixel is used as a seed (image a) for the region growing of one band (image b) with the parameter spectral distance equal to 0.1. Similar pixels are selected to create the training area (image c and image d).

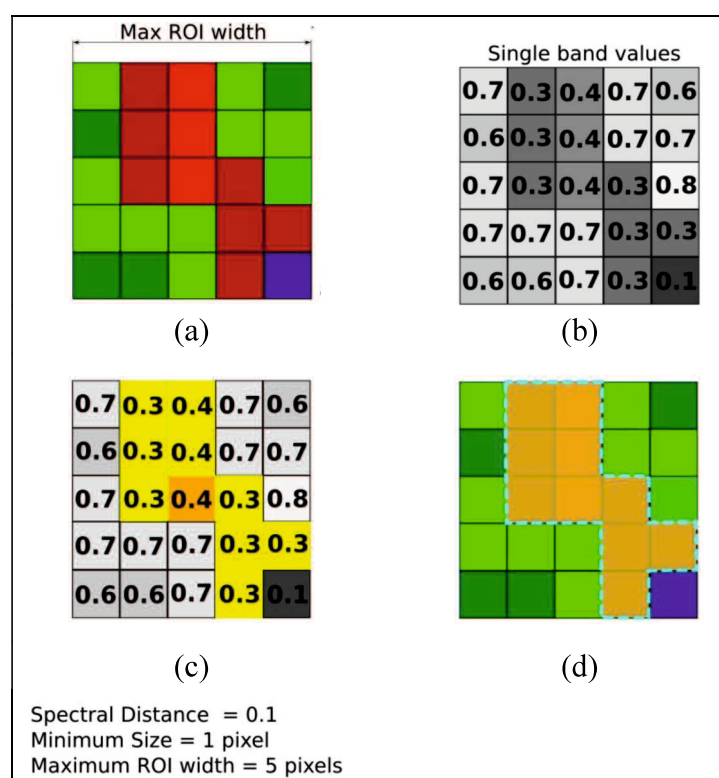


Figure 2.25 Region Growing Example

(Source: Congedo, 2012)

## 2.6.2 Classes and Macroclasses

Land cover classes are identified with an arbitrary ID code (i.e. Identifier). A macroclass is a group of ROIs having different Class ID, which is useful when one needs to classify materials that have different spectral signatures in the same land cover class (Congedo, 2012). For instance, one can identify grass (e.g. ID class = 1 and Macroclass ID = 1) and trees (e.g. ID class = 2 and Macroclass ID = 1) as vegetation class (e.g. Macroclass ID = 1). Multiple Class IDs can be assigned to the same Macroclass ID, but the same Class ID cannot be assigned to multiple Macroclass IDs, as shown in the Table 2.11.

Table 2.11 Example of Macroclasses

Macroclass name	Macroclass ID	Class name	Class ID
Vegetation	1	Grass	1
Vegetation	1	Trees	2
Built-up	2	Buildings	3
Built-up	2	Roads	4

(Source: Congedo, 2012)

### 2.6.3 Classification Algorithms

The spectral signatures (spectral characteristics) of reference land cover classes are calculated considering the values of pixels under each ROI having the same Class ID (or Macroclass ID). Therefore, the classification algorithm classifies the whole image by comparing the spectral characteristics of each pixel to the spectral characteristics of reference land cover classes. There are several classification algorithms in supervised classification, i.e. minimum distance, maximum likelihood, spectral angle mapping, parallelepiped classification, land cover signature classification, and algorithm raster (Congedo, 2012).

#### 1. Minimum Distance

Minimum Distance algorithm calculates the Euclidean distance  $d(x,y)$  between spectral signatures of image pixels and training spectral signatures, according to the following equation (Richards and Jia, 2006):

$$d(x, y) = \sqrt{\sum_{i=1}^n (x_i - y_i)^2} \quad (\text{Equation 2.35})$$

where:

$x$  = spectral signature vector of an image pixel;

$y$  = spectral signature vector of a training area;

$n$  = number of image bands.

Therefore, the distance is calculated for every pixel in the image, assigning the class of the spectral signature that is closer, according to the following discriminant function (Richards and Jia, 2006):

$$x \in C_k \Leftrightarrow d(x, y_k) < d(x, y_j) \quad \forall k \neq j \quad (\text{Equation 2.36})$$

where:

$C_k$  = land cover class  $k$ ;

$y_k$  = spectral signature of class  $k$ ;

$y_j$  = spectral signature of class  $j$ .

It is possible to define a threshold  $T_i$  in order to exclude pixels below this value from the classification:

$$x \in C_k \Leftrightarrow d(x, y_k) < d(x, y_j) \quad \forall k \neq j \text{ and } d(x, y_k) < T_i \quad (\text{Equation 2.37})$$

## 2. Maximum Likelihood

Maximum Likelihood algorithm calculates the probability distributions for the classes, related to Bayes' theorem, estimating if a pixel belongs to a land cover class. In particular, the probability distributions for the classes are assumed the of form of multivariate normal models (Richards and Jia, 2006). In order to use this algorithm, a sufficient number of pixels is required for each training area allowing for the calculation of the covariance matrix. The discriminant function, described by Richards and Jia (2006), is calculated for every pixel as follow:

$$g_k(x) = \ln p(C_k) - \frac{1}{2} \ln |\Sigma_k| - \frac{1}{2} (x - y_k)^t \Sigma_k^{-1} (x - y_k) \quad (\text{Equation 2.38})$$

where:

$C_k$  = land cover class  $k$ ;

$x$  = spectral signature vector of an image pixel;

$p(C_k)$  = probability that the correct class is  $C_k$ ;

$|\Sigma_k|$  = determinant of the covariance matrix of the data in class  $C_k$ ;

$\Sigma_k^{-1}$  = inverse of the covariance matrix;

$y_k$  = spectral signature vector of class  $k$ .

Therefore:

$$x \in C_k \Leftrightarrow g_k(x) > g_j(x) \quad \forall k \neq j \quad (\text{Equation 2.39})$$

The example of maximum likelihood histogram is described in Figure 2.26.

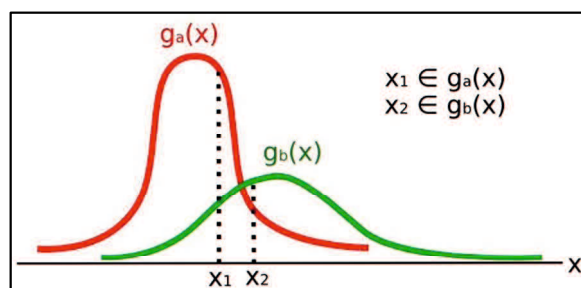


Figure 2.26 Maximum likelihood example

(Source: Richards and Jia, 2006)

In addition, it is possible to define a threshold to the discriminant function in order to exclude pixels below this value from the classification. Considering a threshold  $T_i$  the classification condition becomes (Richards and Jia, 2006):

$$x \in C_k \Leftrightarrow g_k(x) > g_j(x) \quad \forall k \neq j \text{ and } dg_k(x) > T_i \quad (\text{Equation 2.40})$$

Maximum likelihood is one of the most common supervised classifications, however the classification process can be slower than minimum distance.

### 3. Spectral Angle Mapping

The spectral angle mapping calculates the spectral angle between spectral signatures of image pixels and training spectral signatures. The spectral angle  $\theta$  is defined as (Kruse et al., 1993):

$$\theta(x, y) = \cos^{-1} \left( \frac{\sum_{i=1}^n x_i y_i}{\left( \sum_{i=1}^n x_i^2 \right)^{\frac{1}{2}} \left( \sum_{i=1}^n y_i^2 \right)^{\frac{1}{2}}} \right) \quad (\text{Equation 2.41})$$

Where:

$x$  = spectral signature vector of an image pixel;

$y$  = spectral signature vector of a training area;

$n$  = number of image bands.

Therefore a pixel belongs to the class having the lowest angle, that is (Kruse et al., 1993):

$$x \in C_k \Leftrightarrow \theta(x, y_k) < \theta(x, y_j) \quad \forall k \neq j \quad (\text{Equation 2.42})$$

where:

$C_k$  = land cover class  $k$ ;

$y_k$  = spectral signature of class  $k$ ;

$y_j$  = spectral signature of class  $j$

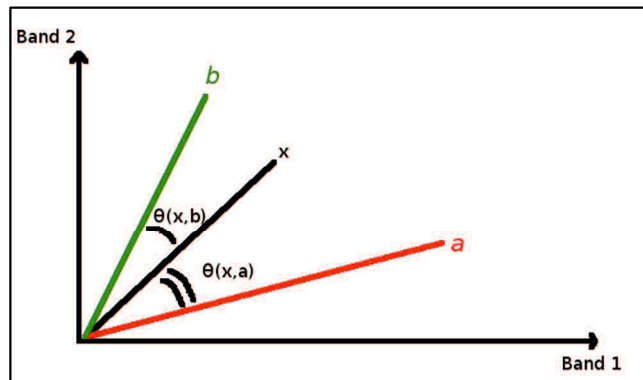


Figure 2.27 Spectral angle mapping example  
(Source: Kruse et al., 1993)

Figure 2.27 shows an example of spectral single mapping. In order to exclude pixels below this value from the classification it is possible to define a threshold  $T_i$  (Kruse et al., 1993):

$$x \in C_k \Leftrightarrow \theta(x, y_k) < \theta(x, y_j) \quad \forall k \neq j \text{ and } \theta(x, y_k) < T_i \quad (\text{Equation 2.43})$$

Spectral angle mapping is largely used, especially with hyperspectral data (Kruse et al., 1993).

### 4. Parallelepiped Classification

Parallelepiped classification is an algorithm that considers a range of values for each band, forming a multidimensional parallelepiped that defines a land cover class. A pixel is



classified if the values thereof are inside a parallelepiped. One of the major drawbacks is that pixels whose signatures lie in the overlapping area of two or more parallelepipeds cannot be classified (Richards and Jia, 2006).

## 5. Land Cover Signature Classification

Land cover signature classification allows for the definition of spectral thresholds for each training input signature (a minimum value and a maximum value for each band). The thresholds of each training input signature define a spectral region belonging to a certain land cover class. In this classification, spectral signatures of image pixels are compared to the training spectral signatures. A pixel belongs to class X if pixel spectral signature is completely contained in the spectral region defined by class X. In case of pixels falling inside overlapping regions or outside any spectral region. It is possible to use additional classification algorithms (i.e. minimum distance, maximum likelihood, spectral angle mapping) considering the spectral characteristics of the original input signature (Congedo, 2012).

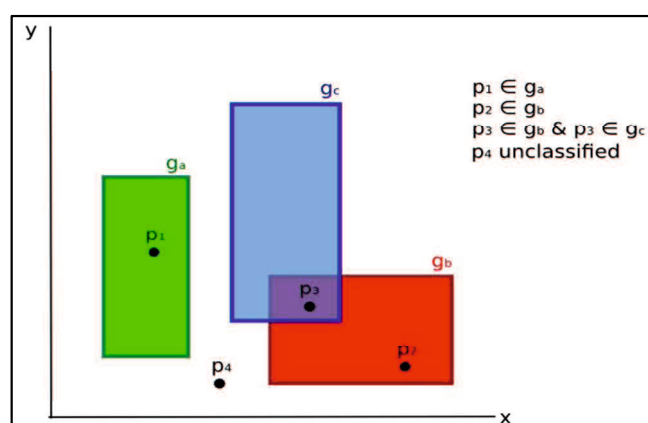


Figure 2.28 Land cover signature classification

(Source: Congedo, 2012)

In Figure 2.28, a scheme illustrates the land cover signature classification for a simple case of two spectral bands  $x$  and  $y$ . User defined spectral regions define three classes ( $g_a$ ,  $g_b$ , and  $g_c$ ). Point  $p_1$  belongs to class  $g_a$  and point  $p_2$  belongs to class  $g_b$ . However, point  $p_3$  is inside the spectral regions of both classes  $g_b$  and  $g_c$  (overlapping regions); in this case, point  $p_3$  will be unclassified or classified according to an additional classification algorithm. Point  $p_4$  is outside any spectral region, therefore it will be unclassified or classified according to an additional classification algorithm. Given that point  $p_4$  belongs to class  $g_c$ , the spectral region thereof could be extended to include point  $p_4$  (Congedo, 2012).

This classification is similar to parallelepiped classification, with the exception that spectral regions are defined by user, and can be assigned independently for the upper and

lower bounds. One can imagine spectral regions as the set of all the spectral signatures of pixels belonging to one class (Congedo, 2012).

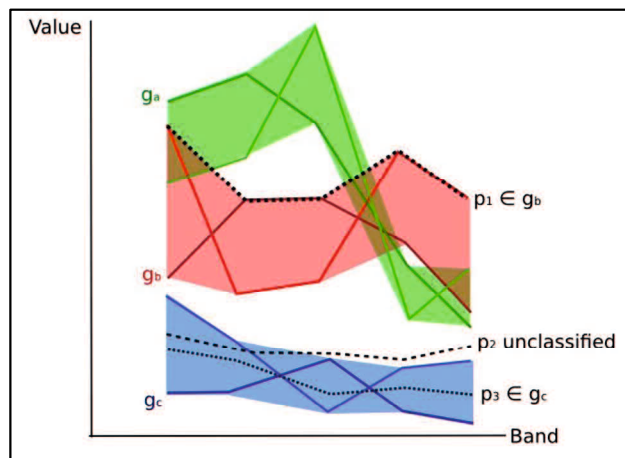


Figure 2.29 Plot of spectral ranges  
(Source: Congedo, 2012)

In Figure 2.29 plot of spectral ranges the spectral ranges of three classes ( $g_a$ ,  $g_b$ , and  $g_c$ ) are displayed. The colored lines inside the ranges (i.e. semi-transparent area) represent the spectral signatures of pixels that defined the upper and lower bounds of the respective ranges. Pixel  $p_1$  (dotted line) belongs to class  $g_b$  because the spectral signature thereof is completely inside the range of class  $g_b$  (in the upper limit); pixel  $p_2$  (dashed line) is unclassified because the spectral signature does not fall completely inside any range; pixel  $p_3$  (dotted line) belongs to class  $g_a$  (Congedo, 2012).

It is worth noticing that these spectral thresholds can be applied to any spectral signature, regardless of spectral characteristics thereof; this function can be very useful for separating similar spectral signatures that differ only in one band, defining thresholds that include or exclude specific signatures. In fact, classes are correctly separated if the spectral ranges thereof are not overlapping at least in one band. It is certain that even if spectral regions are overlapping, chances are that no pixel will fall inside the overlapping region and be misclassified. The upper (or lower) bound of a range do not imply the existence, in the image, of any spectral signature having the maximum (or minimum) range values for all the bands, for instance pixel  $p_1$  of Figure 2.24 could not exist (Congedo, 2012).

One of the main benefit of the land cover signature classification is that it is possible to select pixels and include the signature thereof in a spectral range; therefore, the classification should be the direct representation of the class expected for every spectral signature. This is very suitable for the classification of a single land cover class (defined by specific spectral thresholds), and leave unclassified the rest of the image that is of no interest for the purpose of the classification (Congedo, 2012).

## 6. Algorithm Raster

An algorithm raster represents the “distance” (according to the definition of the classification algorithm) of an image pixel to a specific spectral signature. In general, an algorithm raster is produced for every spectral signature used as training input. The value of every pixel is the result of the algorithm calculation for a specific spectral signature. Therefore, a pixel belongs to class X if the value of the algorithm raster corresponding to class X is the lowest in case of minimum distance or spectral angle mapping, or highest in case of maximum likelihood (Congedo, 2012).

Given a classification, a combination of algorithm rasters can be produced, in order to create a raster with the lowest “distances” (i.e. pixels have the value of the algorithm raster corresponding to the class they belong in the classification). Therefore, this raster can be useful to identify pixels that require the collection of more similar spectral signatures (Congedo, 2012)

### **2.7 Participatory Mapping of Disaster Imagination Game (DIG)**

Participatory mapping is a powerful tool for providing a visual representation of how local communities perceive their physical environment and the significant features within it, based on culturally distinct ideas, concepts, and norms. By conducting this activity, a comparison can be made between the existing hazard maps with the local perception and cultural meanings of sensitive environments. Based on a holistic approach, the use of hazard map data not only showed local perceptions of disaster vulnerability, but also what kind of prevention should be done in order to face the disaster. The participatory disaster mapping has three different and interlinked phases or steps based on different objectives in each phase (IFAD, 2009).

Participatory risk mapping had been proved in initiating the process of disaster risk reduction in the area. For the first time, a base map was developed along with relevant base information in the context of spatial risks and its nature and characteristics. It will help in a great extent to reduce the data gap. Building up networks and interaction between all the stakeholders was a major outcome of the workshop (Warner, 2015). Disaster Imagination Game (DIG) is a map-based participatory workshop that was invented in 1997 in Mie Prefecture, Japan. It is an easy and cost-effective methodology of Table Top Exercises for disaster management. Through DIG a major platform was created for implementation of Integrated Community based Action Plan (Komura, 2002). It is important that communities build their own coping strategies to minimize the impacts of disaster and for quick recovery from a disaster. This activity can be a very empowering tool in disaster risk reduction. In the context of disaster risk reduction, participatory risk mapping such as this enables an assessment of the people’s perception of risks and coping strategies and triggers network-building between stakeholders (Warner, 2015).

In a DIG workshop, participants surround a large map. They are asked to mark symbols and color some areas on the map while they have enjoyable discussions. In the process, aspects of damage due to disasters will be portrayed in detail and “strengths” and “weaknesses” pertaining to the disasters in the region will also be made clear. As a result, possibilities and limitations of the local disaster prevention capability will become apparent, as will the direction of the community activities for disaster prevention and mitigation. Fundamentally, there are three main purposes of DIG, such as “know the disaster”, “know the area”, and “know the people”.

There is a variety of information that can be obtained from a DIG map. Participants will reconsider the geography and nature of the area and be able to understand their area, such as the structure of the area, dangerous places and facilities that they must be careful with. The strengths and weaknesses against the disaster of their area will become more familiar to them. Therefore, DIG is also called “rediscovery of the town”. Moreover, participants in DIG write some information, for instance about their dependable people in case of emergency. They write these elements results in a list of assets of human resources in the area. Through enjoyable talking, solidarity is formed in the area and relationships of trust are nurtured among neighbors (Komura, 2002).

## **2.8 Multi-Criteria Assessment**

The theoretical background for the multi-criteria evaluation is based on the Analytical Hierarchical Process (AHP). The AHP has been extensively applied on decision-making problems, and extensive research has been carried out to apply AHP to risk assessment. The input of spatial multi-criteria analysis is a set of maps that are the spatial representation of the criteria, which are grouped, standardized and weighted in a “criteria tree”. The output is one or more “composite index maps”, which indicates the realization of the model implemented (Saaty and Vargas 2001).

The AHP is essentially an interactive one where a decision-maker or group of decision-makers relay their preferences to the analyst and can debate or discuss opinions and outcomes (Proctor, 2000). The AHP is based upon the construction of a series of Pair-Wise Comparison Matrices (PCM), which compare all the criteria to one another. In the procedure for multi-criteria analysis using weighted linear combination, it is necessary that the weight sum to be 1. In Saaty’s technique of AHP, weight of the nature can be derived by taking the principal eigenvector of a square reciprocal matrix of pairwise comparisons between the criteria (Proctor, 2000).

The comparison concerns the relative importance of the two criteria involved in determining suitability for the state objective. Ratings are provided on a nine-point continuous scale (Figure 2.30). For instance, if one felt that elevation was very strongly more important than coastal proximity in determining a vulnerability area due to tsunami, one

would enter a 5 or 7 on the scale. If the inverse were the case (coastal proximity was very strongly more important than elevation), one would enter 1/5 or 1/7. Saaty (1980) suggests a scale of 1 to 9 for PCM elements, wherein the value of 1 suggests that the criteria are equally important and a value of 9 leads one to infer that the criterion under consideration is extremely important in relation to the other criterion with which the comparison is made (Saaty and Vargas 2001). Schematic procedures for spatial multi-criteria analysis on the AHP is described in Figure 2.31.

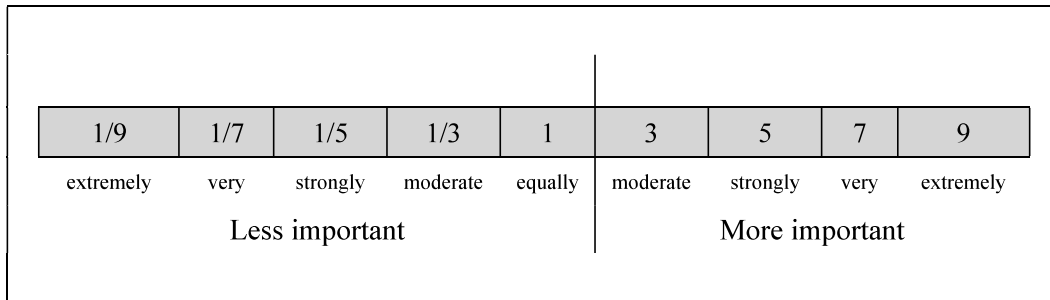


Figure 2.30 The continuous rating scale used for the pairwise comparison of factors in multi-criteria analysis  
(Source: Saaty and Vargas 2001)

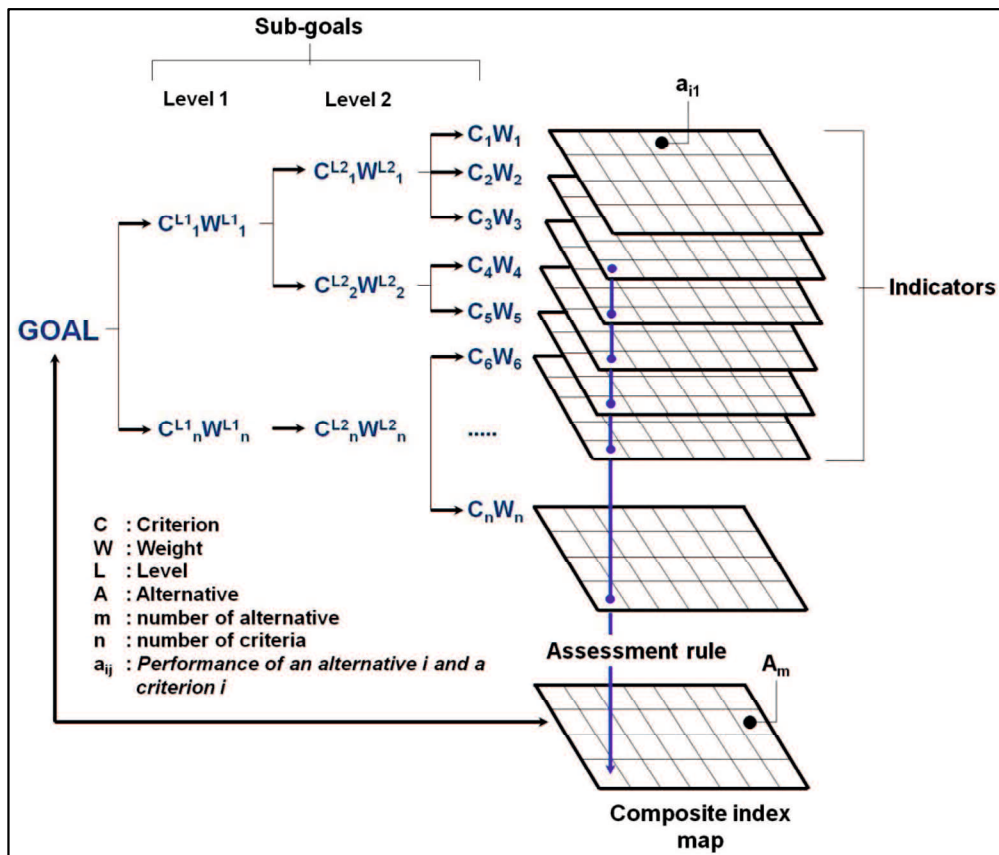


Figure 2.31 Schematic procedures for spatial multi-criteria analysis on the AHP  
(Source: Saaty and Vargas 2001)

According to mathematical expression in AHP, if there are n criteria, then PCM of order  $n \times n$  can be written as follows (Saaty and Vargas 2001):

$$\begin{bmatrix} w_1/w_1 & w_1/w_2 & \dots & w_1/w_n \\ w_2/w_1 & w_2/w_2 & \dots & w_2/w_n \\ w_3/w_1 & w_3/w_2 & \dots & w_3/w_n \\ \dots & \dots & \dots & \dots \\ w_n/w_1 & w_n/w_2 & \dots & w_n/w_n \end{bmatrix} \times \begin{bmatrix} w_1 \\ w_2 \\ w_3 \\ \dots \\ w_n \end{bmatrix} = \begin{bmatrix} n w_1 \\ n w_2 \\ n w_3 \\ \dots \\ n w_n \end{bmatrix}$$

i.e.

$$[A_{(j,j)}] \times [W_{(1,j)}] \times [n W_{(1,j)}] \tag{Equation 2.44}$$

where A is an  $n \times n$  PCM in terms of ratio of ratings/weights, W is the ratings or weights (priority rankings/weights) of criteria and n is the order of the PCM matrix. The input matrix is “A” and the solution for Equation 2.44 is the common eigen-value problem. Raise the PCM to powers that are successively squared each time. The rows of the PCM and the squared PCM are normalized (i.e. each row element is divided by the sum of the elements in that row) to give the eigenvectors of the PCM and the raised PCM. The difference between these eigenvectors is checked against a threshold value (i.e. in this study, a value of 0.0001 is used) and if the difference is less than the threshold value, the eigenvector of the raised PCM is the estimated rating/weight vector (Thirumalaivasan et al., 2003).

From a decision-making perspective, multi-criteria evaluation can be expressed in a matrix as shown in Table 2.12. The matrix A contains the criteria in one axis ( $C_1$  to  $C_n$ ), and a list of possible alternatives, from which a decision has to be taken on the other axis ( $A_1$  to  $A_m$ ). Each cell in the matrix ( $a_{ij}$ ) indicates the performance of a particular alternative in terms of a particular criterion. The value of each cell in the matrix is composed of the multiplication of the standardized value (between 0 and 1) of the criterion for the particular alternative, multiplied by the weight ( $W_1$  to  $W_n$ ) related to the criterion. Once the matrix has been filled, the final value can be obtained by adding up all cell values of the different criteria for the particular alternative.

Table 2.12 Multi-criteria decision matrix

	$C_1$	$C_2$	$C_3$	$C_4$	$C_5$	...	$C_n$
	$(W_1$	$W_2$	$W_3$	$W_4$	$W_5$	...	$W_n)$
$A_1$	$a_{11}$	$a_{12}$	$a_{13}$	$a_{14}$	$a_{15}$	...	$a_{1n}$
$A_2$	$a_{21}$	$a_{22}$	$a_{23}$	$a_{24}$	$a_{25}$	...	$a_{2n}$
.	.	.	.	.	.	.	.
.	.	.	.	.	.	.	.
.	$a_{21}$	$a_{22}$	$a_{23}$	$a_{24}$	$a_{25}$		$a_{2n}$
$A_m$	$a_{m1}$	$a_{m2}$	$a_{m3}$	$a_{m4}$	$a_{m5}$		$a_{mn}$

(Source: Saaty and Vargas 2001)

For implementing this matrix according to the AHP, three principle steps need to be considered. The first one decomposes the problem (and the weights) into a hierarchical structure. The second one considers the weighting process, employing the pairwise comparisons of the criteria, and the synthesis is related to the multiplications among the hierarchical levels. Additionally, in the spatial implementation of this procedure, every criterion ( $C_j$ ) becomes a raster layer, and every pixel (or set of pixels) of the final composite index map eventually becomes an alternative  $A_j$ . The goal (risk index) has been decomposed into criteria levels  $C_{L1}$  and  $C_{L2}$ . The intermediate levels are often indicated as sub-goals or objectives (e.g. in level 1, the sub-goals are a ‘hazard index’ and a ‘vulnerability index’). Each criterion of each level will also have an assigned weight (Saaty and Vargas 2001).

Therefore, the values for the layers of the intermediate levels are obtained through the summation of the performance for the alternative at lower levels. As the criteria consist of raster maps, their spatial performance ( $a_{ij}$ ) and the alternative ( $A_i$ ) will be identified for particular raster cells. The composite risk index map (e.g. tsunami risk) is obtained by an assessment rule, which is calculated by adding up the performance of all cell values of the different criteria ( $a_{ij}$ ) for the particular alternative. The performance of every element in the matrix ( $a_{ij}$ ) is applying by the following equation (Thirumalaivasan et al, 2003):

$$a_{ij} v_{ij} \prod_{L=0}^h w_j^L \tag{Equation 2.45}$$

In this equation,  $v_{ij}$  refers to the standardized value of criterion ( $C_j$ ) for alternative ( $A_i$ ), and weight  $w_{Lj}$  refers to the weight of criterion ( $C_j$ ) for level L (0–h levels). During the analysis, it could be desirable to produce the intermediate criteria maps. In this case, Equation 2.45 should not be applied because weights need to be multiplied with the standardized values only up to the specific level of the intermediate maps. The intermediate maps might also be combined using different methods. When designing vulnerability indicators, it is necessary to take into account the socio-economic conditions, which may vary from country to country (Abella, 2008, Thirumalaivasan et al., 2003).

## **CHAPTER III**

### **RESEARCH METHOD**

#### **3.1 Framework of Research**

Concerning the essential of risk assessment to reduce disaster loss, the research is devoted to introduce geospatial application through multi-criteria analysis for identifying risks, particularly for water-related hazards. There are two cases discussed in this study, i.e. groundwater depletion and tsunami inundation. A research framework (Figure 3.1) described the general analysis procedure for both cases represented as water related hazard. Criteria used for application are mainly damages due to the water-extreme events, including land-associated damages, i.e. land subsidence and land cover, considering the important of the hazard-damage relationship to identify disaster risks. The criteria are combined with other key criteria extracted from on-site data collection.

The land subsidence and land cover criteria are obtained from remote sensing technique. Therefore, the main input for the research is remote sensing data, such as SAR data and other satellite optical data. A technique called time-series InSAR is applied to process SAR data that is multi-temporal data. The result generated from the processing is cumulative displacement time series and mean velocity. It further compared with related information as reference. The comparison indicates a confirmed land subsidence distribution. Eventually, a map of land subsidence vulnerability can be produced that representing subsided and non-subsided areas. An optional analysis utilizing subsidence information and in situ information can be performed to evaluate or model the InSAR data processing result.



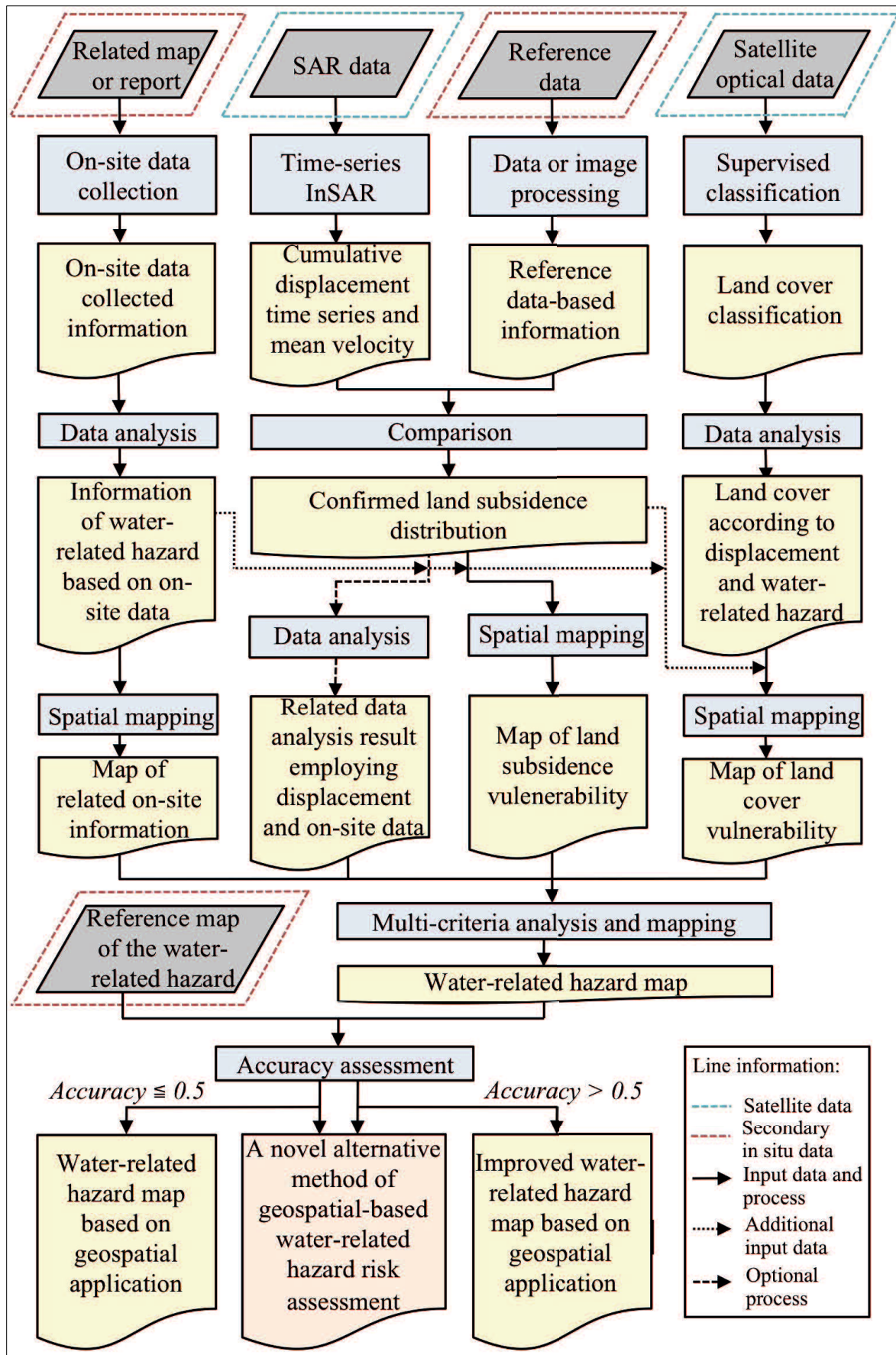


Figure 3.1 General framework of the research

Moreover, satellite optical data are processed based on a supervised classification for land cover mapping. Land cover classification derived from the processing is further analyzed to determine land cover according to displacement and water-related hazard information. A map of land cover vulnerability is eventually resulted through spatial mapping. In regard to collect in situ information, on-site data collection is conducted by employing maps or reports published by related agencies or institutions. The collected information is further analyzed and mapped.

The map results of the land subsidence vulnerability, land cover vulnerability, and related on-site information are integrated through multi-criteria analysis and mapping to produce water-related hazard map. A reference map of water-related hazard that is available for both groundwater depletion and tsunami inundation cases is utilized to assess the accuracy of the mapping result. Maps with accuracies below or equal to 0.5 are categorized having low accuracies. Despite low, the result is considered able to provide water-related hazards map based on geospatial application. On the other hand, a high accuracy map signified an improved water-related hazard map based on geospatial application. Regardless the accuracy, the mapping procedure as risks assessment of water-related hazards indicating a novel alternative method of geospatial-based water-related hazard risk assessment.

### **3.2 Research Scheme**

According to the general research framework, the data, analysis, processing, and mapping area described in research scheme for each case of groundwater depletion in Bali Island, Indonesia and tsunami inundation in Talcahuano City, Chile.

#### **1. Groundwater Depletion in Bali Island, Indonesia**

Groundwater conservation zonation as risk assessment for groundwater depletion case in Bali Island, Indonesia is determined through multi-criteria analysis based on geospatial application by utilizing land subsidence, land cover, groundwater level change, and groundwater usage criteria.

##### **a. Groundwater level**

Report of groundwater level data measurement is provided by the Ministry of Mining and Natural Resource at eighteen monitoring wells available in the study area. A recent data is collected at the monitoring wells through field observation of groundwater level measurement by utilizing a water-level measurement tool. The collected data are analyzed to estimate groundwater level change data. The groundwater level changes that signify depletion is further classified into three conditions, i.e. groundwater depletion below 10%, 10% - 25%, and above 25%. As a final result, a map of groundwater depletion is produced through spatial mapping.

#### b. Groundwater usage

The groundwater usage data is provided by several agencies, i.e. Drinking Water Agency, River Basin Agency of Bali-Penida, and Ministry of Public Work. There is no exact information of the groundwater usage. In case of wells for drinking water supply, the information consists of location, capacity, and the percentage of water supply using the wells. Data for the irrigation wells comprise of location and capacity. The data is analyzed to estimate groundwater usage and mapped through spatial mapping to produce a map of groundwater usage representing high, medium, and low water usage.

#### c. Land subsidence

Remote sensing SAR data is the input for the extraction of land subsidence information. Multi-temporal SAR data are processed through time-series InSAR analysis to generate cumulative displacement time series and mean velocity in the entire study area. The InSAR result is evaluated with available GNSS-CORS data available in the study area. The GNSS-CORS stations obtained in subsided areas based on the InSAR result are measured as references. The subsidence distribution estimated from InSAR displacement result is confirmed if the measured GNSS-CORS stations in the subsided areas show lowering in height or elevation. The confirmed subsidence distribution further mapped through spatial mapping to produce map of land subsidence vulnerability to groundwater depletion. The map is the representation of the land subsidence criteria.

Moreover, taking the inter-correlation of groundwater level change and subsidence, these parameters are used to estimate groundwater level. The groundwater level change data collected from monitoring wells and the land subsidence data extracted from InSAR are employed to calculate a coefficient of mean deformation module of soil that further used to scale subsidence information into groundwater level. Recent groundwater level is evaluated using this method by firstly calculate the coefficient using previous well data of groundwater level and corresponded subsidence data. The estimation is used to provide groundwater level information with higher temporal and spatial resolution.

#### d. Land cover

The land cover classification is classified based on supervised classification for land cover mapping by mainly utilizing optical data. The land cover classification is determined according to the land use classification of Bali Province published by Spatial Information Agency of Indonesia. There are five classifications, i.e. water area, built-up area, vegetation, paddy field, wetland, and bare land. Vulnerability of the land cover is analyzed by integrating land cover classification, confirmed land subsidence distribution, groundwater level change, and groundwater usage data. Eventually, a map of land cover vulnerability to subsidence and groundwater depletion can be produced through spatial mapping.

e. Risk assessment according to groundwater conservation map

Risks assessment for the groundwater depletion case in Bali Island is determined through geospatial application of multi-criteria analysis. A multi-criteria method of AHP is applied for calculating the weight of land subsidence, land cover, groundwater level, and groundwater usage criteria. The criteria assessment is estimated based on interview results with experts. As a result, a groundwater conservation map is produced representing risk assessment of groundwater depletion, i.e. safety, vulnerable, critical, and damage zones. Moreover accuracy assessment is performed using institutional groundwater conservation map. An improvement is signified by accuracy above 0.5. Regardless the accuracy, the produced map represents an alternative method of geospatial-based risk assessment of groundwater depletion. The research scheme of the groundwater depletion case is described in Figure 3.2 below.

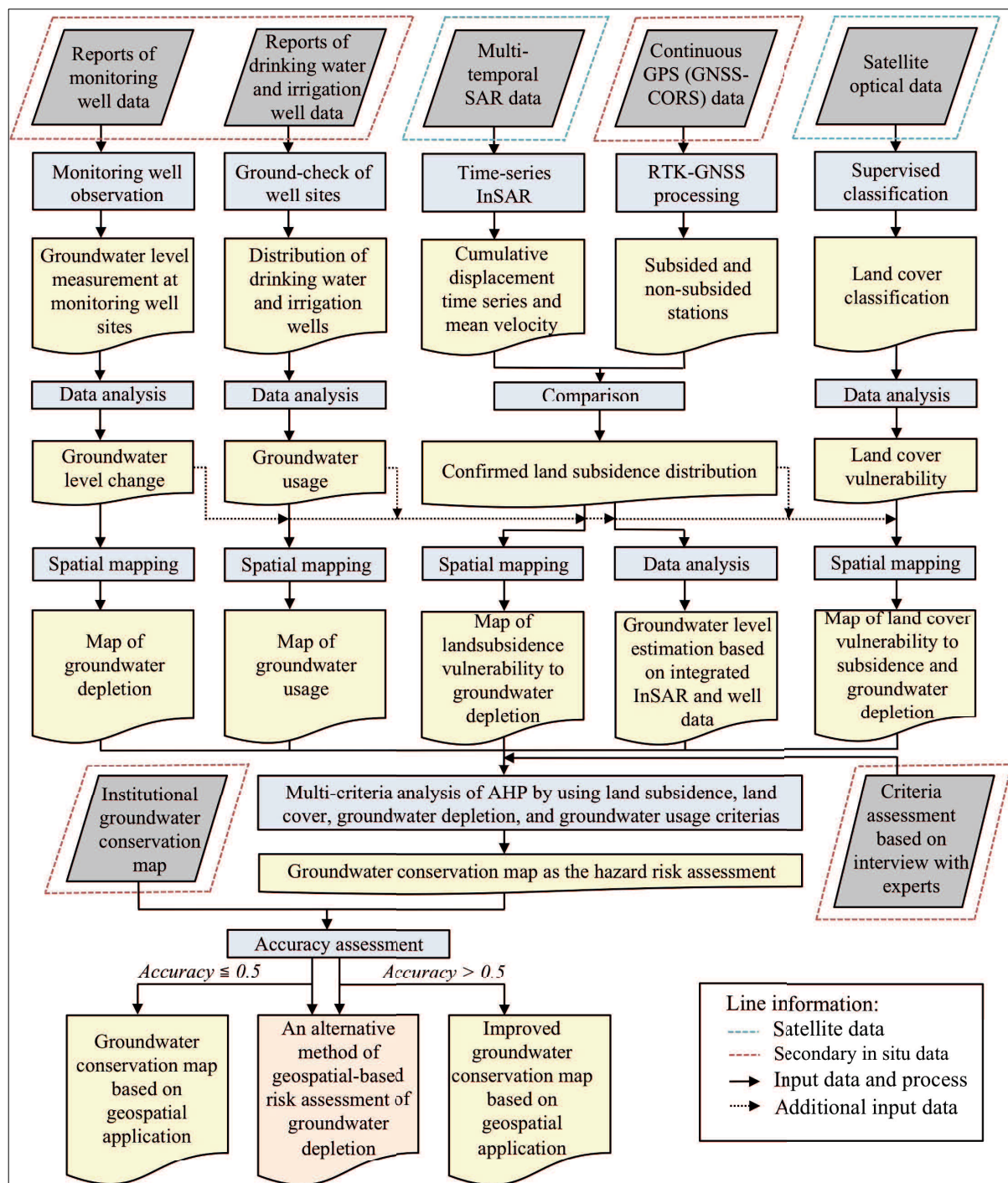


Figure 3.2 Research scheme of risk assessment of groundwater depletion case

## 2. Tsunami Inundation in Talcahuano, Chile

Risk assessment of tsunami inundation level zonation for tsunami inundation case in Talcahuano City, Chile is determined by employing geospatial application of multi-criteria analysis that consist of geospatial and local knowledge of tsunami inundation, land subsidence, and land cover criteria.

a. Geospatial knowledge of tsunami inundation

The extraction of spatial information of tsunami inundation involving remote sensing and in situ data, i.e. satellite optical data, satellite SAR data, and report of tsunami inundation from field observation. In this study, the tsunami inundation information is due to the tsunami event triggered by earthquake on February 27<sup>th</sup>, 2010. Pre- and post-disaster data are mainly employed for the analysis. Firstly, pre- and post-disaster VHR optical data are processed through panchromatic sharpening and color composite image processing to extract tsunami damaged locations in Talcahuano City. Moreover, pre- and post-disaster moderate resolution optical data is utilized to generate information of water and non-water area based on NDVI values due to the tsunami event. The distribution of tsunami damaged areas is eventually extracted by estimating backscatter values from SAR data. The damage locations from VHR optical data, water and non-water area from optical data, and damage distribution results from SAR data are compared with observed inundation sites analyzed from report of tsunami inundation to confirm the tsunami damaged areas. The result of the damage distribution extracted from SAR data processing is further use to produce map of tsunami inundation through spatial mapping application.

b. Local knowledge of tsunami inundation

A participatory mapping workshop of DIG is carried out to collect historical information of tsunami inundation from the community in the hazard vulnerable area. The information represents local-knowledge of tsunami inundation. In the DIG workshop, the participants are asked to draw tsunami-related information on a base map. Information of tsunami inundation line is analyzed to be able to extract a DIG-based map of tsunami inundation line. A map of tsunami inundation line based on local community information is eventually established by performing GIS spatial mapping of the DIG-based map drawn by the participants.

c. Land subsidence

Land subsidence information related to tsunami inundation is derived from multi-temporal SAR data processing of time-series InSAR. The cumulative displacement time series and mean velocity in the study area before, during, and after the inundation are generated from the time-series InSAR technique. The InSAR result is compared with the observed inundation sites and confirmed tsunami damaged areas that is the SAR data of distributed damages due to tsunami inundation. Inundated area whereby subsidence is obtained from InSAR result is confirmed as subsided areas. The confirmed map indicates that subsidence distribution obtained from InSAR data is corresponded to inundation areas due to the tsunami event. The evaluation emphasizes the correlation between subsidence and inundation, particularly the impact of subsidence associated with tsunami that triggered by earthquake. Furthermore, spatial mapping is conducted to produce a map of land subsidence

vulnerability to tsunami inundation.

d. Land cover

Satellite optical data is mainly employed as input for the land cover classification through the application of supervised classification for land cover mapping. According to the fundamental land use classification utilized in Chile, the land cover for this case is categorized into five classifications, i.e. water area, built-up area, vegetation, wetland, and bare land. Vulnerability of the land cover is analyzed by integrating land cover classification, confirmed land subsidence distribution, groundwater level change, and groundwater usage data. Eventually, a map of land cover vulnerability to subsidence and groundwater depletion can be produced through spatial mapping. Both pre- and post-disaster images of satellite optical data are classified and analyzed to obtain the changing of the land cover before and after the disaster. Vulnerability of land cover is further map by carrying out spatial mapping using the land cover change information. Areas with land cover changes indicate vulnerability due to tsunami inundation.

e. Risk assessment corresponding to tsunami inundation level map

Tsunami inundation level map represents risk assessment of the tsunami inundation hazard in Talcahuano City. The map is established through geospatial application processed based on multi-criteria analysis of AHP. The criteria weight of geospatial knowledge of tsunami inundation, local knowledge of tsunami inundation line, land subsidence vulnerability, and land cover change due to inundation are calculated based on the AHP method. Interview results with experts are used to estimate the criteria assessment. Figure 3.3 outlined the research scheme of the tsunami inundation case.

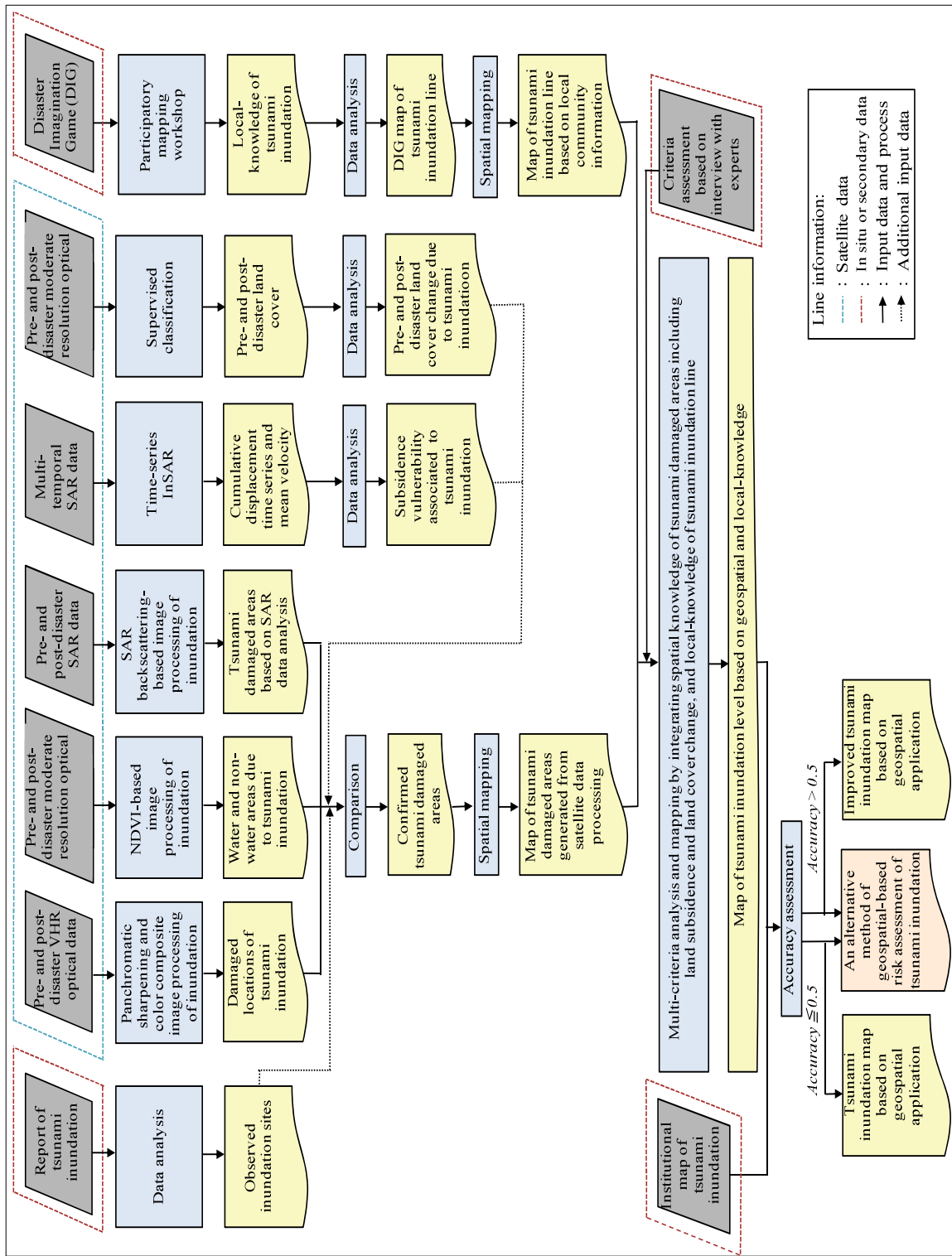


Figure 3.3 Research scheme of risk assessment of tsunami inundation case



A tsunami inundation level map is produced as a spatial mapping result indicating risk assessment of tsunami inundation, i.e. high, medium, and low inundation level zones. The map is further evaluated through accuracy assessment by employing institutional tsunami inundation level map. The map result represents an alternative method of geospatial-based risk assessment of tsunami inundation regardless the accuracy.

### **3.3 Research Area**

The study is performed in two study areas representing two study cases of water-related hazards, i.e. groundwater depletion in Bali Island, Indonesia and tsunami inundation in Talcahuano City, Chile.

#### **1. Groundwater Depletion Case in Bali Island, Indonesia**

The island of Bali extends from 80° 03' 140" to 80° 50' 48" South latitude and 114° 25' 53" to 115° 20' 2" East longitude (Figure 3.4). Administratively, Bali Island and surrounding smaller islands, i.e. Nusa Penida, Nusa Lembongan, Nusa Ceningan, Serangan, and Menjangan, are part of Bali Province of Indonesia. In this study, the area of Bali Province is represented as Bali Island that also including the other peripheral islands. The total area of the island covers an area of 5,632 km<sup>2</sup> equal to 0.29 % of total Indonesian archipelago. The area consists of eight regencies, i.e. Badung Regency, Bangli Regency, Buleleng Regency, Gianyar Regency, Jembrana Regency, Klungkung Regency, Karangasem Regency, and Tabanan Regency, and one capital city that is Denpasar City (BPS, 2017). The map of Bali Island in Figure 3.4 is extracted from natural color composite image of Landsat 7 ETM+ acquired in 2016.

The central part of Bali island composed by mountainous system with 2 volcanic mountain, Batur Mountain and Agung Mountain at elevation above sea level 1,717 m and 3,140 m, respectively. This high elevation range divides Bali to Southern and Northern development area. As the mountains system is closer to the North, the northern coastal area is narrower and has a steeper slope compare to the southern coastal area. The monsoon influence to Bali tropical climate makes an average rainfall over the latest 5 years around 2,082 mm with a lower rainfall occurred in the northern area at 1,455 mm. This condition forms a more perennial river flows to the south than to the northern coast (ESDM, 2013).

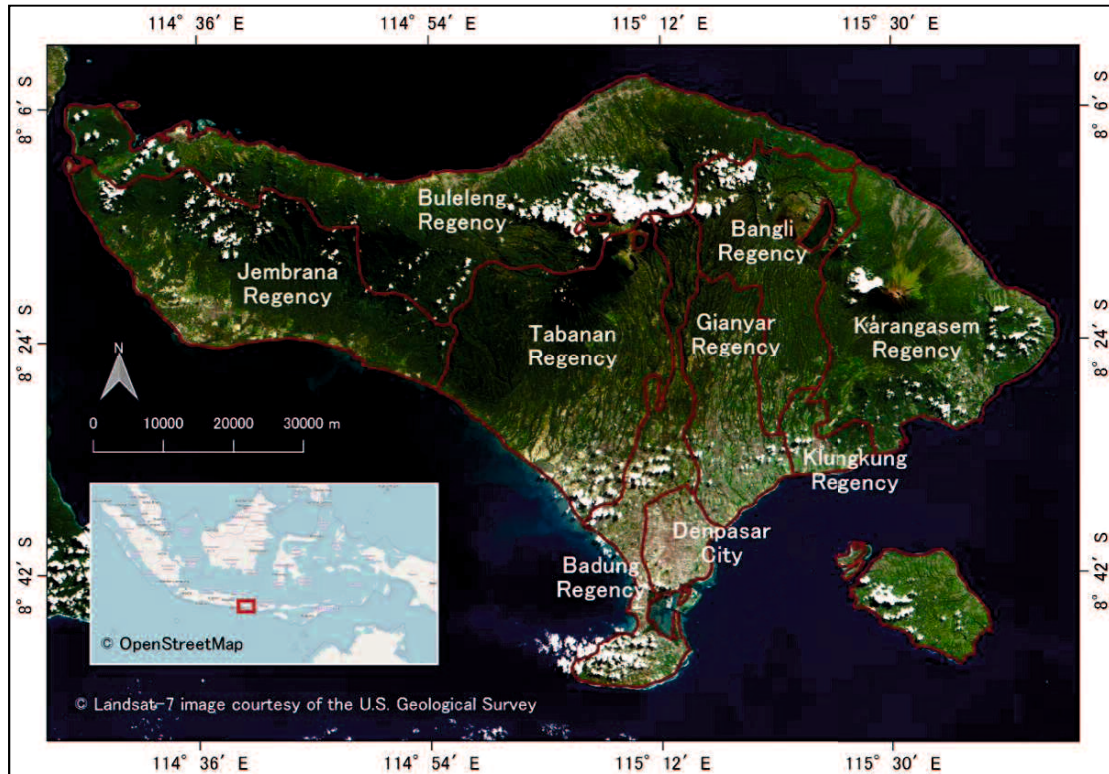


Figure 3.4 Study area of the groundwater depletion case in Bali Island, Indonesia

Various type of soil of Bali constitutes from latosol, regosol, andosol, alluvial, and mediteran soils. Latosol soils are low solum soils, unsuitable for major crops, and prone to erosion that occupies most of dry areas in the north, particularly in northern ridges of Buleleng Regency including some areas in Karangasem Regency. Regosol is less fertile sandy soils located in Karangasem Regency, Buleleng Regency, and southern coastal area of Badung Regency. A volcanic formation of fertile andosol soil occupies most of highland area in Tabanan Regency and Bangli Regency that are suitable for horticultures and major crops. Alluvial soils are suitable for food crops or annual crops distributed in the lower land of Tabanan Regency and Gianyar Regency. Mediteran soils are karstic influenced soils that are unsuitable for food crops and mainly located in in Nusa Penida Island and Nusa Dua Peninsula (ESDM, 2013).

Larger part of Bali land use is absorbed by dry land agriculture including settlement approximately covers 61.3% of the island total area. Other 23.4% is forest land-use with more than half use as forest reserves, which are protected as natural water sources. The reserves include coastal forest to sustain the valuable mangrove habitat. Wetland rice (14.3% of total area) are playing important role in agriculture production areas. Raw water use for irrigation is collected from perennial rivers or springs in most of the south and central area, i.e. Tabanan, Gianyar, Badung and Buleleng (BPS, 2017).

The number of population in Bali are in total 4,200,100 people based on projected

population figures in year 2016, with 1.23% annual growth since year 2010 to 2015. From average Bali density of 745 people/km<sup>2</sup>, Denpasar city is the highest at 7,022 people/km<sup>2</sup> with Jembrana district as the lowest (325 people/km<sup>2</sup>) since part of the district belong to West Bali National Park. As more water are available and better soils are suitable, large population are concentrated in southern areas with its economic activities are drive by agriculture, industries and services including tourism (BPS, 2017).

The area of Bali has been experienced a massive development particularly on tourism since 1925. In correlation with the utilization of groundwater, the water resource has been used largely to supply domestic water demand for the tourism accommodation, such as, housing, hotels, resorts, etc. (BWS of Bali Penida, 2017). Moreover, groundwater has been widely used as water resource for agriculture in the area that has a high potential of the water resource. Over-usage of groundwater in Bali area has resulted in several problems, such as the risk of land subsidence as well as saline water intrusion (Sukearsana, et al., 2015). The following graph of Figure 3.6 shows the groundwater level in the South Bali area from 2001 to 2015 based on a recent research based on well observation.

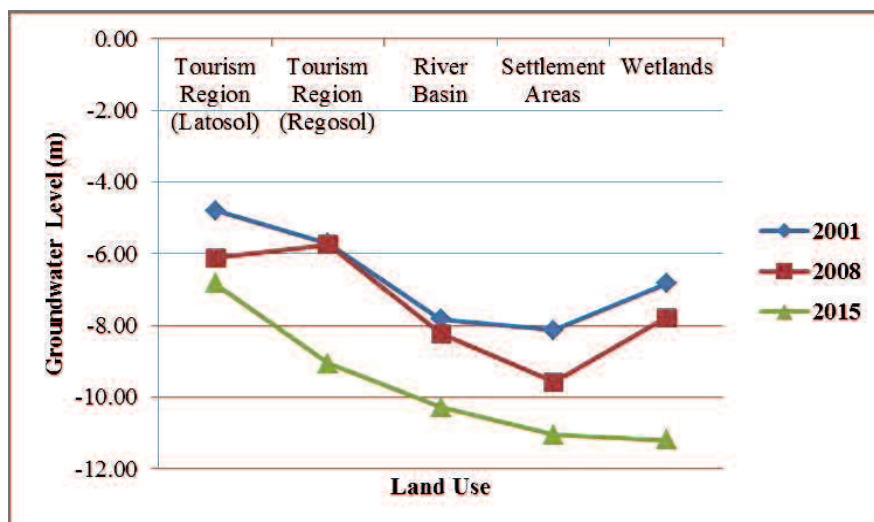


Figure 3.5 Groundwater level monitoring in the South Bali Area  
(Source: Sukearsana, et al., 2015)

## 2. Tsunami Inundation Case in Talcahuano City, Chile

The study of tsunami inundation case is performed in Talcahuano, Chile (Figure 3.6). Geographically, this settlement lies at latitude 36°43'29.22" South latitude and longitude 73°7'1.13" West longitude. The area is located within the boundary of the Greater Concepcion area. It is the port city in Biobio Region, which contains a naval base and has a population of around 250,000 inhabitants, based on the 2002 census. It was also one of the main regions affected by the 2010 tsunami (IOC, 2009).

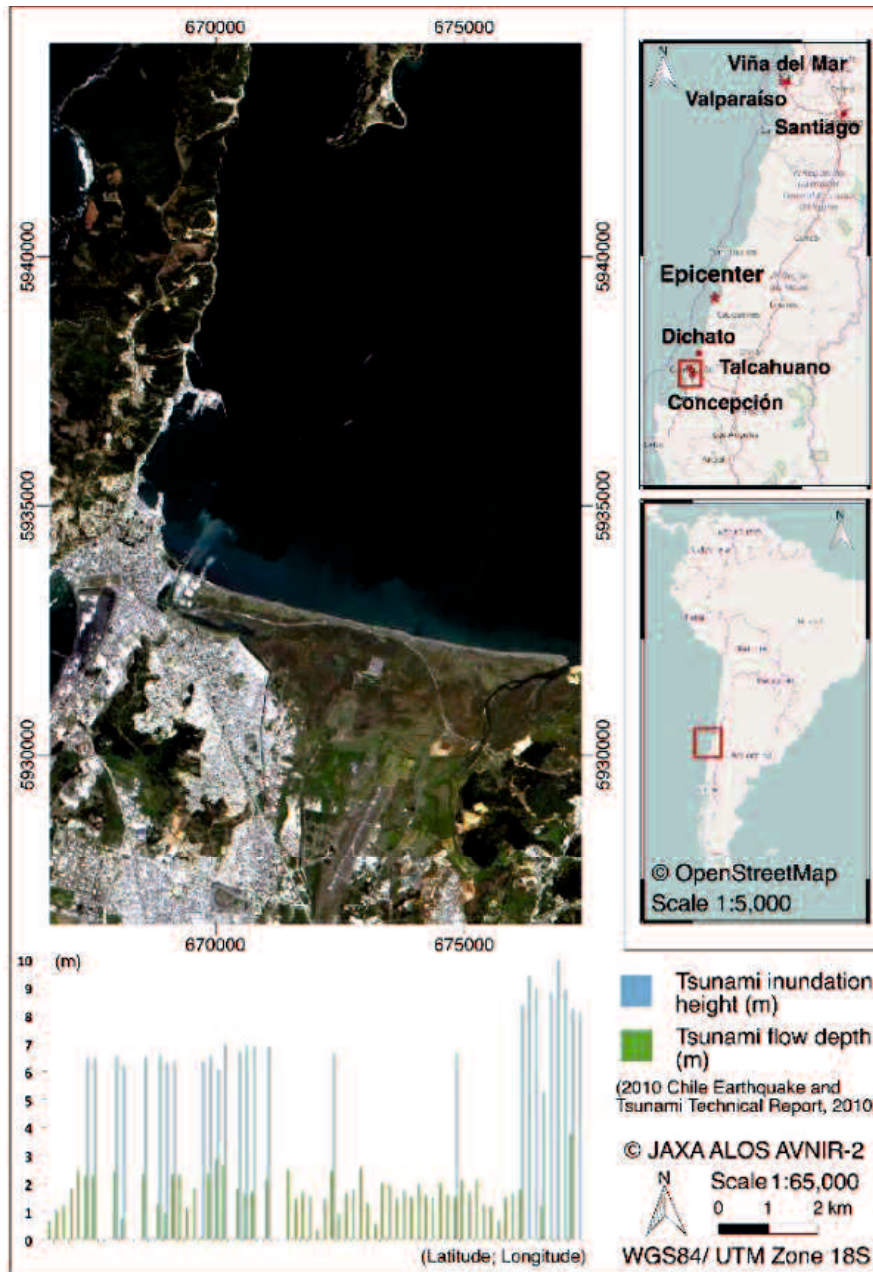


Figure 3.6 Study area of tsunami inundation case in Talcahuano City, Chile

The area of Concepcion is considered to be highly vulnerable to earthquakes and tsunamis (IOC, 2009). A mega-thrust earthquake of M8.8 took place on the coast of the Maule Region of Chile on 27 February 2010 at 03:34 local time (06:34 UTC). The earthquake generated a destructive tsunami, which is considered to be the biggest tsunami disaster in South America since 1979, and which propagated all the way to Japan (Siembieda and Guillermo, 2010). The map of Talcahuano in Figure 3.6 is generated using the natural color of the optical satellite imagery of ALOS AVNIR-2. It is also showed a map of the regions damaged by the 2010 Chile earthquake and a graph of tsunami inundation height and flows depth in the study area. This data are based on field survey reports.

### 3.4 Research Material

The data source consists of remote sensing data and in situ data based on reports and maps related to the groundwater depletion case and tsunami inundation case. The satellite data comprises SAR data of ALOS PALSAR and Sentinel 1A and optical data of Landsat. GNSS-CORS data provided by Geospatial Information Agency (BIG) and Ministry of Land and Spatial Planning (BPN) are also utilized for the study. Secondary data is used as reference for on-site data collection of groundwater level and groundwater usage and accuracy assessment. Information of monitoring wells are provided by Ministry of Mining and Natural Resource (ESDM) in Bali Province. Moreover, well locations, capacities, and supply percentage data are collected from River Basin Agency of Bali Penida (BWS-BP), Public Works Service (DPU) in Bali Province, Regional Public Works Service (DPU) and Regional Drinking Water Agency (PDAM) in each regency and the capital city of Denpasar. Besides, groundwater conservation map from Final Report of Project on Planning of Zonation Map of Groundwater Utilization in Bali Province Fiscal Year of 2014 published by Public Works Service of Bali Province is used as reference for evaluating the geospatial-based mapping result of groundwater conservation map.

In particular for the groundwater database information, authority of well data provision related to well locations for irrigation is belong to the BWS-BP. Nevertheless, the usage of the wells in provincial administration area is recorded by the DPU in Bali Province. Location and well usage data for irrigation in regional administration area are authorized by Regional DPU in each regency and the capital city of Denpasar. Wells for drinking water are entirely managed by Regional PDAM in each regency and the capital city of Denpasar. Table 3.1 describes remote sensing data used for conducting risk assessment of groundwater depletion in Bali Island, Indonesia. Moreover, the secondary data are listed in Table 3.2.

Table 3.1 Satellite-based data used for groundwater depletion case

<b>Satellite product</b>	<b>Data type</b>	<b>Period</b>	<b>Quantity</b>
ALOS PALSAR	L-band SAR	2007 – 2010	63 scenes
Sentinel 1A	C-band SAR	2014 – 2017	42 scenes
Landsat 7 +ETM	Moderate-resolution	2001 – 2003	6 scenes
Landsat 8 OLI-TIRS	optical	2013 – 2016	8 scenes
SRTM1	DEM	2000	1 scene
GNSS-CORS	Continuous GNSS/GPS	2008 – 2016	7 stations

Table 3.2 Secondary data used for groundwater depletion case

Source	Product	Type	Period	Quantity
Ministry of Mining and Mineral Resource (ESDM) in Bali Province	Groundwater level at report monitoring wells	Annual	2008 – 2013	18 wells
ESDM and Public Works Service (DPU) in Bali Province	Planning of Final project zonation map of report groundwater utilization in Bali Province	Final project report	2013 – 2014	1 map
DPU in Bali Province	Well location, Groundwater capacity, and database	Groundwater	1980 – 2016	351 wells
River Basin Agency of Bali-Penida (BWS-BP)	percentage of (built year water supply data)	of (built year water supply data)		365 wells
Regional DPU and Drinking Water Agency (PDAM) in Denpasar City	(service coverage)			15 wells
Regional DPU and PDAM in Badung Regency				10 wells
Regional DPU and PDAM in Bangli Regency				13 wells
Regional DPU and PDAM in Buleleng Regency				95 wells
Regional DPU and PDAM in Gianyar Regency				25 wells
Regional DPU and PDAM in Jembrana Regency				111 wells
Regional DPU and PDAM in Klungkung Regency				14 wells
Regional DPU and PDAM in Karangasem Regency				76 wells
Regional DPU and PDAM in Tabanan Regency				21 wells

In regard to the wells for drinking water, some wells that are built and recorded for irrigation wells by the BWS-BP and DPU of Bali Province are changed to be drinking water wells due to the local community requests. Therefore, data of the wells with usage changes are re-recorded by the regional PDAM in each regency and city. In order to collectively provide coordinate and usage of wells distributed throughout Bali area, on-site data collection is carried out based on groundwater database information from the BWS-BP, DPU of Bali Province, regional DPU and PDAM in each regency and city. Moreover, groundwater level at each monitoring well is measured to assign recent groundwater level information.

In case of tsunami inundation in Talcahuano City, the primary data for the study are satellite imageries. The satellite data comprise of VHR and moderate resolution of optical, SAR, and DEM data. The satellite data processing results are validated using secondary data that consist of reports and maps related to the tsunami inundation events in Chile. The tsunami inundation maps are of *carta de inundación por tsunami referida al evento del 27 de Febrero 2010* published by *comuna de Talcahuano* in 2010 and *histórico tsunami* published by *sistema de informacion comunal* which can be accessed from <http://riesgo.talcahuano.cl>. The reports are field survey of the 2010 tsunami in Chile that is part of Chile earthquake and tsunami technical report and damage investigation of the 2010 Chile earthquake and tsunami provided by JST, JICA, and SATREPS Peru Project in 2010.

Moreover, community-based participatory mapping workshop of DIG is carried out to collect local-knowledge information related to the tsunami inundation in Talcahuano. Materials necessary for the workshop are administration map and mapping and evaluation guideline. List of satellite data and secondary data used for the study are listed in Table 3.3 and Table 3.4, respectively.

Table 3.3 List of satellite-based data used for tsunami inundation case

<b>Satellite product</b>	<b>Data type</b>	<b>Period</b>	<b>Quantity</b>
GeoEye-1	VHR optical	2009	1 scene
QuickBird	VHR optical	2010	1 scene
ALOS AVNIR-2	High-resolution optical	2007 and 2010	2 scenes
ALOS PALSAR	L-band SAR	2009 – 2010	4 scenes
ASTER-GDEM	DEM	2007	1 scene

Table 3.4 List of secondary data used for tsunami inundation case

Source	Product	Data type	Period	Quantity
<i>Comuna de Talcahuano</i>	<i>Carta de inundación por tsunami referida al evento del 27 de Febrero 2010</i>	Tsunami inundation map	2010	1 map
<i>Sistema de informacion comunal</i>	<i>Histórico tsunami</i>			1 map
JST, JICA, and SATREPS Peru project	Field survey of the 2010 tsunami in Chile Damage investigation of the 2010 Chile earthquake and tsunami	Technical report	2010	1 report 1 report
<i>Universidad de Valparaiso Chile</i>	Administration map of Talcahuano City, Chile	Base map	2015	1 map
JICA and Yamaguchi University	DIG mapping and evaluation guideline in Talcahuano City, Chile	Guideline	2015	1 guideline

The mapping and evaluation guideline are distributed as a workshop handout for the DIG workshop in Talcahuano City. The handout is distributed to the participants before conducting the activity. The content of the handout should be briefly explained the fundamental of DIG, the disaster event that is tsunami, the mapping activity, and the evaluation that should be done before and after the mapping activity. Moreover, a map representing administration area of Chile is provided for the DIG mapping as base map. The map scale used as the base map should have a scale of 1:25,000. The printed map is distributed to each group of the participant by attaching a transparent sheet on the map.

### 3.5 Instrument of Research

Data analysis, processing, and mapping are performed using open-source software, i.e. Quantum GIS (QGIS), Generic Mapping Tools (GMT) for InSAR processing version 5.5 (GMT5SAR), and Real-Time Kinematic Library (RTKLIB). The software is run through computer hardware. The GMT5SAR requires UNIX operating system (OS). On the other hand, Windows OS is required for the RTKLIB. QGIS can be run both on UNIX and Windows OS. Besides the software, other instruments are utilized for on-site data collection, i.e. camera and drone for documentation, hands-on GPS and water-level meter for groundwater monitoring, mapping colored markers and evaluation form for DIG participatory mapping workshop, and multi-criteria analysis of AHP questionnaire for



interview with experts. Instruments used for the groundwater depletion and tsunami inundation cases are listed in Table 3.5.

Table 3.5 Instrument list for groundwater depletion and tsunami inundation cases

<b>Instrument</b>	<b>Function</b>	<b>Groundwater depletion case</b>	<b>Tsunami inundation case</b>
Computer hardware with Windows and UNIX operating system (OS)	Running data analysis, processing, and mapping software	√	√
GMT5SAR	InSAR processing	√	√
Q-GIS	Image processing and mapping	√	√
RTK-LIB	RTK GNSS/GPS	√	
Camera	On-site	√	√
Drone	documentation	√	
Hands-on GPS	Coordinate recorder	√	
Water level meter	Water level measurement	√	
Colored markers	DIG mapping		√
Evaluation sheets	DIG evaluation		√
AHP questionnaire	Interview with experts	√	√

1. Quantum GIS (QGIS).

QGIS is an open source image processing software with function to process and extract geospatial information of the satellite data as well as perform spatial mapping.

2. Generic Mapping Tools (GMT) SAR version 5.5 (GMTSAR)

GMT5SAR is an open source (GNU General Public License) InSAR processing system. The code is written in C and will compile on any computer where GMT and NETCDF are installed. The system has three main components as follow:

- a. A pre-processor for each satellite data type to convert the native format and orbital information into a generic format;
- b. An InSAR processor to focus and align stacks of images, map topography into phase, and form the complex interferogram;

- c. A post-processor, mostly based on GMT, to filter the interferogram and construct interferometric products of phase, coherence, phase gradient, and line-of-sight displacement in both radar and geographic coordinates. GMT is used to display all the products as postscript files and kml-images for Google Earth.

A set of C- shell scripts has been developed for standard 2-pass processing as well as image alignment for stacking and time series.

### 3. Real-Time Kinematic Library (RTKLIB)

RTKLIB is an open source program package for standard and precise positioning with GNSS (global navigation satellite system). RTKLIB consists of a portable program library and several APs (application programs) utilizing the library. The software is utilized to process the GNSS-CORS data in RINEX data format. The executable binary GUI and CUI APs included in the package require Microsoft Windows environment. All of the library functions and APIs were written in ANSI C (C89). Figure 3.7 described RTK RTKLAUNCH window and launcher icons for APs.

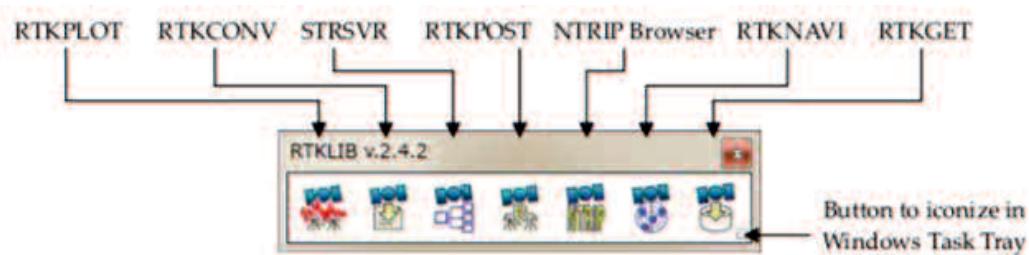


Figure 3.7 RTK RTKLAUNCH window and launcher icons for APs.

### 4. Camera and drone for documentation

Camera is utilized for documenting on-site data collection for the study that are groundwater monitoring and DIG mapping workshop. In particular, for the groundwater monitoring, aerial photos and videos are taken to be able to capture wider area coverage that represent the area condition related to groundwater conservation zones. Camera of Olympus Tough Tracker and DJI Phantom 4 UAV Quad-copter drone used for the documentation of the study are described in Figure 3.8 (a) and (b), respectively.

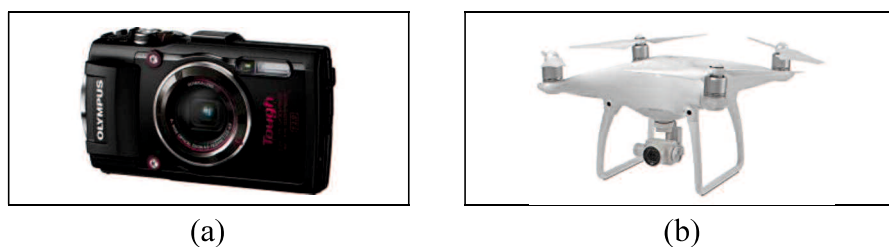


Figure 3.8 Documentation instruments: (a) Camera; (b) Drone

## 5. Hands-on GPS and water level meter for groundwater monitoring

Hands-on GPS and water level meter are employed for on-site data collection of groundwater monitoring. The hands-on GPS of Garmin and Soil flat-tape water level meter instruments used for in situ observation of groundwater in this study are described in Figure 3.9 (a) and (b), respectively.



Figure 3.9 Groundwater monitoring instruments: (a) Hands-on GPS; (b) Water level meter

### a. Hands-on GPS

Hands-on GPS is used to record well coordinates based on the data of well location provided by related agencies, i.e. BWS-BP, DPU of Bali Province, regional DPU and PDAM. The collected well coordinates are used to present information of well distribution by conducting spatial mapping. Water usage in the area whereby wells are distributed can be further calculated to provide geospatial information of groundwater utilization.

### b. Water level meter

Recent groundwater level at monitoring wells in Bali Island is measured using water level meter. Water level meter is a common tool used for measuring the depth to water in wells, boreholes, standpipes, and tanks. The type of water level meter employed for the groundwater level measurement in this study is flat-tape water level meter. This type of water level meter usually has a 3/4-inch wide rape marked in engineering, standard, or metric scale. Determining the number of tape that enters the well requires reading the tape which is similar to reading a ruler.

## 6. Mapping colored markers and evaluation sheets for DIG workshop

In regard to conduct DIG workshop in Talcahuano City, several instruments are needed, such as mapping colored markers and evaluation sheets. The marks for mapping activity and questions for evaluation before and after mapping activity are explained in Table 3.6.

a. Mapping colored markers

Colored markers are used to draw base map of Talcahuano city administration area in the participatory mapping activity. Designated shapes and colors are determined that represent information related to the disaster.

b. Evaluation sheets

Evaluation is arranged by considering five items according to the DIG guideline. The items that evaluated for the DIG workshop in Talcahuano City are hazard scenario knowledge, lifelines, transportation and other facilities conditions knowledge, knowledge of buildings conditions, knowledge of human suffering, and the knowledge about the earthquake and tsunami disaster in the area.

Table 3.6 Mapping mark and evaluation according to the item and process step of DIG in Talcahuano City, Chile






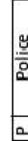
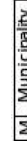








Item	Process step	Legend	Mark	Evaluation
A. Hazard scenario knowledge	1. Discuss and draw the shore line	Continuous black		How good is your general knowledge
	2. Discuss and draw the inundation line	Continuous blue		about tsunami hazard?
	3. Discuss and draw the inundation sequence	Blue arrows + number		a) Very bad b) Bad c) Medium d) Good e) Very good
B. Liveliness, transportation and the other facilities conditions knowledge	1. Discuss and draw the important facilities	Red "B" + ID: Firefighter	 B   Firefighter	How good is your general knowledge about urban facilities situation?
		Red cross + ID: Hospital	 Hospital	
		Black "p" + ID: Police	 P   Police	
		Black "M" + ID: Municipality	 M   Municipality	
		Black "G" + ID: Regional government	 G   Government	
		Black "JV" + ID: Community offices	 JV   Community off.	
		Blue cross + ID: Shelters	 Shelters	
		Blue star + ID: Schools	 Schools	
		Yellow triangle + ID: Industries	 Industries	
		Red triangle + ID: Fuel deposits	 Fuel deposits	
		Black triangle + ID: Military sites	 Military sites	
		Green triangle + ID: Cultural sites	 Cultural sites	

Table 3.6 (Continued)





















Item	Process step	Legend	Mark	Evaluation
	2. Discuss and draw the liveliness facilities	Blue "E" + ID: Electricity supply		
		Blue "AP" + ID: Water supply		
		Blue "AS" + ID: Sewage collection		
		Blue "C" + ID: Communication serv.		
	3. Discuss and draw the transportation facilities	Yellow lines: Main roads		
		Red envelope + ID: Bridges		
		Red envelope + ID: Railways		
		Red envelope + ID: Tunnels		
		Blue "X" + ID: Bus stations		
		Black dot + ID: Airports		
		Blue dot + ID: Ports		
		Green lines: Bicycle ways		
C. Buildings conditions knowledge	1. Discuss and draw the vulnerable earthquake buildings	Red hatch		How good is your general knowledge about buildings condition? a) Very bad b) Bad c) Medium d) Good e) Very good
		Blue hatch		
	2. Discuss and draw the vulnerable tsunami buildings	Red-yellow hatch		
		Green-yellow hatch		
3. Discuss and draw the vulnerable fire buildings	4. Discuss and draw the landslides vulnerable buildings			

Table 3.6 (Continued)

Item	Process step	Legend	Mark	Evaluation
D. Human suffering knowledge	1. Discuss and draw the human suffering due to building collapse	Black flag		How good is your general knowledge about human suffering due to
	2. Discuss and draw the human suffering due to lack of assistance	Red flag		earthquake and tsunami? a) Very bad
	3. Discuss and draw the human suffering due to trapping by debris	Green flag		b) Bad c) Medium
	4. Discuss and draw the human suffering due to sweeping away by tsunami	Blue flag		d) Good e) Very good
E. How good is your general knowledge about the earthquake and tsunami disaster in your city?				
				a) Very bad
				b) Bad
				c) Medium
				d) Good
				e) Very good

## 7. Multi-criteria analysis of AHP questionnaire for interview with experts

In regard to obtain information from experts for multi-criteria analysis of AHP, interview is conducted using questionnaire. The questionnaire indicating assessment of the criteria utilized for the analysis, i.e. groundwater level, groundwater usage, land subsidence, and land cover. In case of determining zonation for groundwater conservation as risk assessment of groundwater depletion in Bali Island, experts in the field of water resource management and land-associated damages are considered representative for achieving the purpose. Likewise, interview with experts was also conducted for the tsunami inundation level zonation as risk assessment of the tsunami inundation. The interview was able to be performed during the DIG workshop whereby experts in the field of disaster mitigation, particularly tsunami hazards, are invited to deliver explanation of the DIG as well as being tutor and evaluator for the mapping activity. Criteria used for determining zonation of tsunami inundation level are geospatial knowledge including land subsidence and land cover change of tsunami inundation, and local knowledge of tsunami inundation.

The experts are requested to assess the importance of a criteria compare to the other criteria. The importance values consist of absolute important, extremely important, quite important, slightly important, and equally important. The values range from one to nine. For instance, comparison of two criteria with values of 9:1 indicating the criteria on the left is absolutely more important than the criteria on the right. In particular for the groundwater conservation zonation. The results are employed as input to estimate rank of the criteria. Questionnaire for the groundwater conservation and tsunami inundation level mapping are described in Figure 3.10.



**Questionnaire**

Topic : Groundwater Conservation Zonation as Risk Assessment of Groundwater Depletion Based on Multi-Criteria Analysis of AHP

Place and date :

Name :

Affiliation :

---

More important on the left					More important on the right				
Extent					Extent				
Absolutely important	Extremely important	Quite important	Slightly important	Equally important	Slightly important	Quite important	Extremely important	Absolutely important	
9:01	8:01	7:01	6:01	5:01	4:01	3:01	2:01	1:01	
1:02	1:03	1:04	1:05	1:06	1:07	1:08	1:09		
Groundwater level					Groundwater usage				

---

More important on the left					More important on the right				
Extent					Extent				
Absolutely important	Extremely important	Quite important	Slightly important	Equally important	Slightly important	Quite important	Extremely important	Absolutely important	
9:01	8:01	7:01	6:01	5:01	4:01	3:01	2:01	1:01	
1:02	1:03	1:04	1:05	1:06	1:07	1:08	1:09		
Groundwater level					Land subsidence				

---

More important on the left					More important on the right				
Extent					Extent				
Absolutely important	Extremely important	Quite important	Slightly important	Equally important	Slightly important	Quite important	Extremely important	Absolutely important	
9:01	8:01	7:01	6:01	5:01	4:01	3:01	2:01	1:01	
1:02	1:03	1:04	1:05	1:06	1:07	1:08	1:09		
Groundwater level					Land cover				

---

More important on the left					More important on the right				
Extent					Extent				
Absolutely important	Extremely important	Quite important	Slightly important	Equally important	Slightly important	Quite important	Extremely important	Absolutely important	
9:01	8:01	7:01	6:01	5:01	4:01	3:01	2:01	1:01	
1:02	1:03	1:04	1:05	1:06	1:07	1:08	1:09		
Groundwater usage					Land subsidence				

---

More important on the left					More important on the right				
Extent					Extent				
Absolutely important	Extremely important	Quite important	Slightly important	Equally important	Slightly important	Quite important	Extremely important	Absolutely important	
9:01	8:01	7:01	6:01	5:01	4:01	3:01	2:01	1:01	
1:02	1:03	1:04	1:05	1:06	1:07	1:08	1:09		
Groundwater usage					Land cover				

---

More important on the left					More important on the right				
Extent					Extent				
Absolutely important	Extremely important	Quite important	Slightly important	Equally important	Slightly important	Quite important	Extremely important	Absolutely important	
9:01	8:01	7:01	6:01	5:01	4:01	3:01	2:01	1:01	
1:02	1:03	1:04	1:05	1:06	1:07	1:08	1:09		
Land subsidence					Land cover				

Sign :

---

Figure 3.10 Questionnaire for groundwater conservation zonation based on multi-criteria analysis of AHP

## 3.6 Data Analysis

### 3.6.1 Image Processing and Spatial Mapping

Fundamentally, there are three points in image processing, i.e., image rectification and restoration, image enhancement, and information extraction. However, variation and modification can be applied depending on the data quality and available methods.

#### 1. Optical Image Processing

Optical image processing in this study consists of panchromatic sharpened and natural color composite image, image calibration from Digital Number (DN) into radiance, radiometric image correction by converting reflectance values into top-of-atmosphere (TOA) reflectance values, and generating Normalized Difference Vegetation Index (NDVI) image. The process is able to be performed using QGIS software.

##### a. Pansharpening

A panchromatic sharpened image represents a sensor fusion between the high spectral resolution of the multispectral and panchromatic images. In general, Gram-Schmidt method based on a general algorithm vector orthogonalization is used for the panchromatic sharpening. The process is necessary for optical data processing to generate a high spatial and spectral resolution image (Maurer, 2013). Panchromatic image can be produced through “Pansharpening” tool from “Preprocessing” menu of “Semi-Automatic Classification Plugin – SCP” plugin on QGIS software.

In this study, pre-disaster image of GeoEye-1 and post-disaster image of QuickBird that are VHR optical data representing area before and after tsunami event in Talcahuano, Chile are processed through panchromatic sharpened image processing. The panchromatic sharpened image results are used as input for color composite process. Moreover, moderate resolution imageries of Landsat are also processed through pan-sharpening after performing radiometric calibration and atmospheric correction.

##### b. Color Compositing

Color composite can be performed by integrating multi band color. Fundamentally, true and false color composite are able to be displayed from optical data. True or natural color composite produces colors which would resemble those that would be observed by the human eye. On the other hand, false color composite image does not have any resemblance to its actual color. It is used to distinctly observe a certain surface material or object on the image. The color channels are displayed in red, green, and blue (RGB) by combining three different wavelength regions (band) of the data (Liew, 2001). In QGIS, the color composite can be arranged from band “Rendering Tool” in “Properties” menu of the image layer by using “Singleband Pseudocolor” option.

In this study, color compositing is conducted for optical data processing of tsunami inundation case. The natural color composite of the GeoEye-1 (pre-disaster) and QuickBird (post-disaster) are created using the combination of band 3-2-1 (red-green-blue) for these type of data. Moreover, true color and false color composite are applied to ALOS AVNIR imageries using combination of band 3-2-1 (red-green-blue) and band 4-3-2 (near infrared-red-green), respectively. The color composites images are obtained to see the difference of water and non-water area that indicating inundated and non-inundated areas.

c. Conversion of Digital Number (DN) to Physical Unit

A quantitative analysis can be performed based on the calculation of the measured values from the satellite data. In the case of the optical imagery, the data values are recorded by a passive sensor, which functions similarly to a human eye, by recording non-polarized sunlight reflectance of the surface materials with a large range of different wavelengths (Liew, 2001). A raw image is derived through conversion of at-sensor radiance measured in the wavelength region to Digital Numbers (DN) using a quantification system. It contains the effects of the light source, sensor, atmosphere, and surface material without any unit or physical connotation. Therefore, the raw image needs to be corrected by calibrating the DN into radiance. The following equation describes the algorithm for the conversion of DN to radiance (Chander et al., 2009):

$$L_{\lambda} = G_{rescale} \times Q_{CAL} + B_{rescale} \quad (\text{Equation 3.1})$$

Where,  $L_{\lambda}$  is the spectral radiance at the sensor's aperture ( $W/(m^2 \text{ sr } \mu m)$ ),  $G_{rescale}$  is the rescaled gain,  $Q_{CAL}$  is the DN, and  $B_{rescale}$  is the rescaled bias. The re-scaled gains and biases for ALOS AVNIR-2 are described in Table 3.7.

The radiance was then corrected to obtain the top-of-atmosphere (TOA) reflectance. It provides acceptable information of surface materials, e.g. vegetation, water, and other areas. Equation (3.2) describes the algorithm for the conversion of radiance to reflectance (Sah et al., 2012).

$$\rho_{\lambda} = \pi \times L_{\lambda} \times d^2 / ESUN_{\lambda} \times \cos\theta_s \quad (\text{Equation 3.2})$$

Where,  $\rho_{\lambda}$  is the unit less planetary reflectance,  $L_{\lambda}$  is the spectral radiance at the sensor's aperture,  $d^2$  is the Earth-sun distance in astronomical units from a nautical handbook,  $ESUN_{\lambda}$  is the mean solar exoatmospheric irradiances, and  $\theta_s$  is the solar zenith angle in degrees.

Table 3.7 Calibration factors of spectral reflectance for the ALOS AVNIR-2

<b>Bands</b>	<b>Spectral range (<math>\mu\text{m}</math>)**</b>	<b><math>G_{rescale}</math>*</b>	<b><math>B_{rescale}</math>*</b>	<b><math>ESUN</math>**</b>
Band 1	0.42 – 0.50 (blue)	0.5888	0	1943.3
Band 2	0.52 – 0.60 (green)	0.5730	0	1813.7
Band 3	0.61 – 0.69 (red)	0.5020	0	1562.3
Band 4	0.76 – 0.89 (NIR)	0.8350	0	1076.5

(Source: \*Bouvet et al., 2007; \*\*Sah et al., 2012)

In particular, conversion of DN to radiance for Landsat 7 ETM+ according to the described general equation can be expressed as follow (USGS, 2018a):

$$L_{\lambda} = \left( \frac{L_{MAX_{\lambda}} - L_{MIN_{\lambda}}}{Q_{CAL_{MAX}} - Q_{CAL_{MIN}}} \right) \cdot (Q_{CAL} - Q_{CAL_{MIN}}) + L_{MIN_{\lambda}} \quad (\text{Equation 3.3})$$

Where  $L_{MIN_{\lambda}}$  is the spectral radiance scaled to  $Q_{CAL_{MIN}}$  in  $W/(m^2 \text{ sr } \mu\text{m})$ ,  $L_{MAX_{\lambda}}$  is the spectral radiance scaled to  $Q_{CAL_{MAX}}$  in  $W/(m^2 \text{ sr } \mu\text{m})$ ,  $Q_{CAL_{MIN}}$  is the minimum quantized calibrated pixel value in DN, and  $Q_{CAL_{MAX}}$  is the maximum quantized calibrated pixel value in DN. These values can be found in the metadata file of the Landsat product. The calibration values for Landsat 7 ETM+ used in this study are described in Table 3.8. For relatively clear Landsat 7 ETM+ scenes, a reduction in between-scene variability can be achieved by normalizing solar irradiance by converting spectral radiance, as calculated using Equation (3.3), to planetary reflectance or albedo. This combined surface and atmospheric reflectance of the Earth is computed with formula of radiance to reflectance described in Equation (3.2).

Table 3.8 Calibration factors of spectral reflectance for the Landsat 7 ETM+

$Q_{CAL_{MIN}} = 1$ and $Q_{CAL_{MAX}} = 255$						
<b>Band</b>	<b>Spectral range</b>	<b><math>L_{MIN_{\lambda}}</math></b>	<b><math>L_{MAX_{\lambda}}</math></b>	<b><math>G_{rescale}</math></b>	<b><math>B_{rescale}</math></b>	<b><math>ESUN_{\lambda}</math></b>
<b>Units</b>	<b>(<math>\mu\text{m}</math>)</b>	<b>(<math>W/(m^2 \text{ sr } \mu\text{m})</math>)</b>	<b>(<math>W/(m^2 \text{ sr } \mu\text{m})/DN</math>)</b>	<b>(<math>W/(m^2 \text{ sr } \mu\text{m})</math>)</b>	<b>(<math>W/(m^2 \text{ sr } \mu\text{m})</math>)</b>	<b>(<math>W/(m^2 \text{ sr } \mu\text{m})</math>)</b>
<i>Low gain (LPGS)</i>						
Band 1	0.45 – 0.52 (Blue)	-6.2	293.7	1.180709	-7.38	1997
Band 2	0.52 – 0.60 (Green)	-6.4	300.9	1.209843	-7.61	1812
Band 3	0.63 – 0.69 (Red)	-5.0	234.4	0.94252	-5.94	1533
Band 4	0.77 – 0.90 (NIR)	-5.1	241.1	0.969291	-6.07	1039
Band 5	1.57 – 1.75 (SWIR)	-1.0	47.57	0.19122	-1.19	230.8
Band 6	10.40 – 12.50 (TIR)	0	17.04	0.067087	-0.07	N/A
Band 7	2.09 – 2.35 (SWIR)	-0.35	16.54	0.066496	-0.42	84.9
Band 8	0.52 – 0.90 (Panchromatic)	-4.7	243.1	0.975591	-5.68	1362
<i>High gain (LPGS)</i>						
Band 1	0.45 – 0.52 (Blue)	-6.2	191.6	0.77874	-6.98	1997
Band 2	0.52 – 0.60 (Green)	-6.4	196.5	0.798819	-7.20	1812
Band 3	0.63 – 0.69 (Red)	-5.0	152.9	0.621654	-5.62	1533
Band 4	0.77 – 0.90 (NIR)	-5.1	157.4	0.639764	-5.74	1039
Band 5	1.57 – 1.75 (SWIR)	-1.0	31.06	0.12622	-1.13	230.8
Band 6	10.40 – 12.50 (TIR)	3.2	12.65	0.037205	3.16	N/A
Band 7	2.09 – 2.35 (SWIR)	-0.35	10.8	0.043898	-0.39	84.9
Band 8	0.52 – 0.90 (Panchromatic)	-4.7	158.3	0.641732	-5.34	1362

(Source: Chander et al., 2009)

According to the Data User Handbook of Landsat 8, DN values of Level-1 product can be converted to spectral radiance using the radiance scaling factors provided in the metadata file (USGS, 2018b):

$$L_{\lambda} = M_L * Q_{CAL} + A_L \quad (\text{Equation 3.4})$$

Where  $M_L$  is radiance multiplicative scaling factor for the band (“RADIANCE\_MULT\_BAND\_n” from the metadata) and  $A_L$  is radiance additive scaling factor for the band (“RADIANCE\_ADD\_BAND\_n” from the metadata). In accordance to the general equation,  $M_L$  represents the  $G_{rescale}$  value while  $A_L$  represents  $B_{rescale}$  value.

Similar to the conversion to radiance, the 16-bit integer values in the L1 product of Landsat 8 data can also be converted to TOA reflectance. In correspondence to the general formula for converting radiance to reflectance mentioned in Equation (3.2), the following equation is used to convert Level-1 DN values to TOA reflectance of Landsat 8 (USGS, 2018b):

$$\rho_{\lambda} = \frac{\rho_{\lambda}'}{\sin(\theta)} \quad (\text{Equation 3.5})$$

Where  $\rho_{\lambda}'$  is the TOA planetary spectral reflectance without correction for solar angle and  $\theta$  is solar elevation angle. The  $\theta$  can be derived from the metadata or calculated. The calculation of the  $\rho_{\lambda}'$  is calculated using reflectance multiplicative scaling factor for the band ( $M_{\rho}$ ) and reflectance additive scaling factor for the band ( $A_{\rho}$ ) available on the metadata file as follow (USGS, 2018b):

$$\rho_{\lambda}' = M_{\rho} * Q_{CAL} + A_{\rho} \quad (\text{Equation 3.6})$$

Where  $M_{\rho}$  and  $A_{\rho}$  are metadata values of “REFLECTANCE\_MULT\_BAND\_n” and “REFLECTANCE\_ADD\_BAND\_n”, respectively. The  $M_L$ ,  $A_L$ ,  $M_{\rho}$ ,  $A_{\rho}$  values are different according to the product. Table 3.9 described values for the Landsat 8 data used in this study.

Table 3.9 Calibration factors of spectral reflectance for the Landsat 8 OLI-TIRS in Bali Island for the groundwater depletion case

Bands	Spectral range (µm)*	Mρ	Aρ	2013/11/03		2014/11/06		2015/10/24		2016/07/06		2017/04/20	
				M <sub>L</sub>	A <sub>L</sub>	M <sub>L</sub>	A <sub>L</sub>	M <sub>L</sub>	A <sub>L</sub>	M <sub>L</sub>	A <sub>L</sub>	M <sub>L</sub>	A <sub>L</sub>
Path 116; Row 66													
Band 1	0.435 - 0.451 (Coastal aerosol)	0.00002	0.10000	0.0128	-63.7877	0.0128	-63.8808	0.0127	-63.4379	0.0121	-60.7280	0.0124	-62.2000
Band 2	0.452 - 0.512 (Blue)	0.00002	0.10000	0.0131	-65.3194	0.0131	-65.4147	0.0129	-64.9612	0.0124	-62.1862	0.0127	-63.6936
Band 3	0.533 - 0.590 (Green)	0.00002	0.10000	0.0121	-60.1913	0.0121	-60.2791	0.0119	-59.8612	0.0115	-57.3041	0.0117	-58.6931
Band 4	0.636 - 0.673 (Red)	0.00002	0.10000	0.0102	-50.7567	0.0102	-50.8308	0.0101	-50.4783	0.0097	-48.3220	0.0098	-49.4934
Band 5	0.851 - 0.879 (NIR)	0.00002	0.10000	0.0062	-31.0605	0.0062	-31.1059	0.0062	-30.8902	0.0059	-29.5707	0.0061	-30.2875
Band 6	1.566 - 1.651 (SWIR 1)	0.00002	0.10000	0.0015	-7.7245	0.0015	-7.7358	0.0015	-7.6821	0.0015	-7.3539	0.0015	-7.5322
Band 7	2.107 - 2.294 (SWIR 2)	0.00002	0.10000	0.0005	-2.6036	0.0005	-2.6074	0.0005	-2.5893	0.0005	-2.4787	0.0005	-2.3388
Band 8	0.503 - 0.676 (Panchromatic)	0.00002	0.10000	0.0115	-57.4426	0.0115	-57.5264	0.0114	-57.1276	0.0109	-54.6872	0.0112	-56.0129
Band 9	1.363 - 1.384 (Cirrus)	0.00002	0.10000	0.0024	-12.1392	0.0024	-12.1569	0.0024	-12.0726	0.0023	-11.5569	0.0024	-11.8370
Band 10	10.60 - 11.19 (TIRS 1)	-	-	0.0003	0.1000	0.0003	0.1000	0.0003	0.1000	0.0003	0.1000	0.0003	0.1000
Band 11	11.50 - 12.51 (TIRS 2)	-	-	0.0003	0.1000	0.0003	0.1000	0.0003	0.1000	0.0003	0.1000	0.0003	0.1000
Path 117; Row 66													
Band 1	0.435 - 0.451 (Coastal aerosol)	0.00002	0.10000	0.0128	-64.0131	0.0124	-61.7268	0.0124	-61.9869	0.0122	-61.1686	0.0124	-62.1723
Band 2	0.452 - 0.512 (Blue)	0.00002	0.10000	0.0131	-65.5502	0.0126	-63.2089	0.0127	-63.4753	0.0125	-62.6374	0.0127	-63.6650
Band 3	0.533 - 0.590 (Green)	0.00002	0.10000	0.0121	-60.4039	0.0116	-58.2465	0.0117	-58.4919	0.0115	-57.7198	0.0117	-58.6669
Band 4	0.636 - 0.673 (Red)	0.00002	0.10000	0.0102	-50.9360	0.0098	-49.1167	0.0098	-49.3237	0.0097	-48.6726	0.0098	-49.4713
Band 5	0.851 - 0.879 (NIR)	0.00002	0.10000	0.0062	-31.1703	0.0060	-30.0569	0.0060	-30.1836	0.0059	-29.7852	0.0061	-30.2739
Band 6	1.566 - 1.651 (SWIR 1)	0.00002	0.10000	0.0015	-7.7518	0.0015	-7.4749	0.0015	-7.5064	0.0015	-7.4073	0.0015	-7.5289
Band 7	2.107 - 2.294 (SWIR 2)	0.00002	0.10000	0.0005	-2.6128	0.0005	-2.5194	0.0005	-2.5301	0.0005	-2.4967	0.0005	-2.5376
Band 8	0.503 - 0.676 (Panchromatic)	0.00002	0.10000	0.0115	-57.6456	0.0111	-55.5866	0.0111	-55.8208	0.0110	-55.0840	0.0112	-55.9878
Band 9	1.363 - 1.384 (Cirrus)	0.00002	0.10000	0.0024	-12.1821	0.0022	-11.7469	0.0022	-11.7965	0.0023	-11.6407	0.0024	-11.8317
Band 10	10.60 - 11.19 (TIRS 1)	-	-	0.0003	0.1000	0.0003	0.1000	0.0003	0.1000	0.0003	0.1000	0.0003	0.1000
Band 11	11.50 - 12.51 (TIRS 2)	-	-	0.0003	0.1000	0.0003	0.1000	0.0003	0.1000	0.0003	0.1000	0.0003	0.1000

(Source: \*Barsi et al., 2014)

The conversion calculation from DN of the optical images to reflectance can be performed by using “Raster Calculator” tool from “Raster” menu in QGIS software. The equation has to be written first accordingly prior to the image calculation. The other method to carry out the conversion in QGIS is through “SCP” plugin. An automatic calculation of DOS1 atmospheric correction can be utilized to convert DN to radiance and radiance to reflectance by choosing the “Apply DOS1 atmospheric correction” option in the “Preprocessing” menu of the SCP plugin. The other input is necessary for running the process, i.e. directory containing the data and metadata file of the data. Nevertheless, the tool can be applied for limited satellite optical data, i.e. Landsat, Sentinel-1, ASTER, and MODIS.

d. Normalized Difference Vegetation Index (NDVI) Image

Normalized Difference Vegetation Index (NDVI) is one of the common methods used to identify changes on land or water surfaces (Liew, 2001). NDVI essentially measures the reflectance difference between two certain wavelength ranges from -1 to 1 as explained in Equation 3.7 (Hansen et al., 2000):

$$NDVI = \frac{(NIR - VIS)}{(NIR + VIS)} \quad \text{(Equation 3.7)}$$

Where *NIR* is the reflectance of near infrared band and *VIS* is that the visible band. The equation can be applied to an image of optical data by writing the formula and adding necessary band from the image layer in “Raster Calculator” tool. The unit of band for NIR and VIS is different according to the data type.

In regard to the study, NDVI is applied for the pre- and post-disaster images of ALOS AVNIR-2 and multi-temporal Landsat data. The VIS band of ALOS AVNIR-2 is red band while the NIR band is band 4, as can be seen in Table 3.9. In the tsunami inundation case, high-resolution satellite optical data of ALOS AVNIR-2 before and after the disaster are employed to identify the changes that represent tsunami damaged areas. The NDVI for pre- and post-disaster images are calculated after performing calibration and atmospheric correction of the raw images. Besides observing changes in pre- and post-disaster images, both of the NDVI values are subtracted to determine a boundary value that can be used to divide the post-disaster image into inundated areas and those that are not. Furthermore, the information of vegetated and non- vegetated areas extracted from the NDVI images can be employed as reference to determine Region of Interest (ROI) for land cover classification mapping.

In case of Landsat, the VIS and NIR for Landsat 7 ETM+ corresponding to Table 3.10 are band 3 and band 4, respectively. Land 8 OLI-TIRS has a different spectral range as described in Table 3.11, the VIS band is band 4 and the NIR band is band 5. NDVI is processed to the available Landsat data in Bali Island before land cover classification mapping to define vegetated and non-vegetated areas (built-up and water areas).

## 2. SAR Image Processing

The radar backscatter per unit area or  $\sigma^{\circ}$  (*sigma-naught*) represents the radar image brightness, which has a unit of  $[m^2/m^2]$ , expressed in decibel (dB). The  $\sigma^{\circ}$  varies even for homogeneous targets depending on the incidence angle, and the angle between the ground and the sensor. In this case, normalization of the  $\sigma^{\circ}$  on the incidence angle can remove the range dependency to eventually obtain a normalized  $\sigma^{\circ}$  or  $\gamma^{\circ}$  (*gamma-naught*) (Lillesand and Kiefer, 1993). The backscatter values are useful to obtain difference of surface materials displayed on images. In regard to the tsunami case in this study, SAR data of ALOS PALSAR is utilized for analyzing tsunami-damaged areas due to the tsunami inundation.

The DN on raw images acquired particularly from ALOS PALSAR data can be converted to backscatter values ( $\gamma^{\circ}$ ), as described in Equation 3.8. A calibration factor (K) of -83.0 dB provided by JAXA is used for the calculation as follow (Matsuoka and Yamazaki, 2000):

$$\gamma^{\circ} = 10 * \log_{10}(DN^2) - 83 \quad \text{(Equation 3.8)}$$

In QGIS software, the equation can be performed to SAR imageries by writing the formula and adding single band of the SAR data in “Raster Calculator” tool.

## 3. Spatial Mapping

GIS application allows users to open digital maps, create new spatial information to be added to a map, create printed maps customized to the user needs, and perform spatial analysis. In particular, spatial analysis of spatial mapping is the process of manipulating spatial information to extract new information and meaning from the original data. Spatial mapping in this study is performed based on GIS application that comprises vector and raster data processing, coordinate reference system (CRS), and spatial analysis of buffering, interpolating, overlaying, and map production. These spatial analysis tools are mainly utilized in producing map of each criteria as well as AHP mapping for both groundwater depletion and tsunami inundation cases.

### a. Vector and raster data processing

Vector data provide a way to represent real world features within the GIS environment. The vector data has two key concepts, i.e. geometry and attributes. The geometry of a vector feature describes its shape and position, while the attributes of a vector feature describe its properties such as color, size, age etc. While vector features use geometry (points, polylines and polygons) to represent the real world, raster data takes a different approach. Raster images are made up of a matrix of pixels (also called cells), each containing a value that represents the conditions for the area covered by that cell. Creation and analysis of vector and raster data in QGIS software are able to be performed from “Vector” and “Raster” menu, respectively.



In this study, satellite data are input and processed as raster data. The satellite data are VHR optical data of GeoEye-1 and Quickbird, high-resolution optical data of ALOS AVNIR, moderate resolution optical data of Landsat, SAR data of ALOS PALSAR and Sentinel 1A, and DEM data of SRTM and ASTER-GDEM. The other raster data are map of groundwater conservation in Bali Island and map of tsunami inundation level in Talcahuano City. In regard to the groundwater depletion case, input data in vector format consist of point and polygon features. Vector data with point feature are wells for drinking water and irrigation, monitoring wells, and GNSS-CORS stations. Vector data with polygon features are administration area of Bali Province, administration area of regencies and city of Bali Province, administration area of district and sub-district of each regency and city in Bali Province, and groundwater basin areas. Likewise, in the case of tsunami inundation, input data in vector format comprises of point and polygon features. Vector data with point feature is tsunami damage sites based on VHR data result. Vector data with polygon feature are administration area of Talcahuano City, tsunami inundated areas based on field observation report, and tsunami inundation based on DIG mapping. The vector data that are used as input for the AHP need to be converted into raster data before the mapping.

#### b. Coordinate Reference System (CRS)

Prior to data processing, map projections need to be set appropriately. Map projection is used to portray the surface of the earth or a portion of the earth on a flat piece of paper or computer screen. In a Lay man's term, map projections are devoted to transform the earth from its spherical shape (3D) to a planar shape (2D) so that maps can be made on flat layers, e.g. maps. A coordinate reference system (CRS) particularly defines the two-dimensional, projected map in the GIS project related to real places on the earth, with the help of coordinates. The decision as to which map projection and coordinate reference system to use, depends on the regional extent of the project area, on the analysis and often on the availability of data.

The general setting for the CRS in QGIS working project is "WGS 84" or "EPSG:4326". The CRS can be arranged from the "CRS" tab of the "Project Properties" according to the location of study areas. In this study, the locations are in Bali Island for the groundwater depletion case and Talcahuano City for the tsunami inundation case. The proper CRS for the Bali Island is "WGS 84/UTM Zone 50N" or "EPSG:32650". Whereas, the CRS for the Talcahuano City is "WGS 84/UTM Zone 18S" or "EPSG:32718". In regard to the CRS, WGS 84 is the datum and ellipsoid and UTM is the map projection. The UTM is divided into several specific zones represented by numbers with orientation of north (N) or south (S) direction.

### c. Spatial Buffering

Buffering usually creates two areas, i.e. one area that is within a specified distance to selected real world features and the other area that is beyond. The area that is within the specified distance is called the buffer zone. A buffer zone is any area that serves the intended features distant from one another. In QGIS application, buffer zones are always represented as vector polygons enclosing other polygon, line or point features. There are several variations in buffering. The buffer distance or buffer size can vary according to numerical values provided in the vector layer attribute table for each feature. The numerical values have to be defined in map units according to the CRS used with the data. A feature can also have more than one buffer zone. The buffer zones that overlapping one another can have dissolved or intact boundary. It can also be extended outward or inward a polygon boundary. Figure 3.11 depicts a buffer zone with dissolved boundary that mainly applied for buffering in the study.

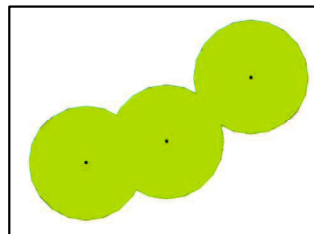


Figure 3.11 Buffer zones of overlapping areas with dissolved boundary  
(Source: QGIS, 2018)

### d. Spatial Overlay

Moreover, spatial overlay is also important in conducting spatial analysis using GIS application. Spatial overlay is a process that allows identification of relationship between two polygon features that share part of the same area. Overlaying is applied for spatial analysis that required combination of two or more data layers in this study. Output vector layer of overlaying is a combination of the input features information. Typical spatial overlay examples are intersection, union, symmetrical difference, and difference, as shown in Figure 3.12. The output layer of intersection contains all areas where both layers overlap (intersect). Union resulted in an output layer that contains all areas of the two input layers combined. Output layer of symmetrical difference contains all areas of the input layers except those areas where the two layers overlap (intersect). Lastly, difference output layer presents all areas of the first input layer that do not overlap (intersect) with the second input layer.

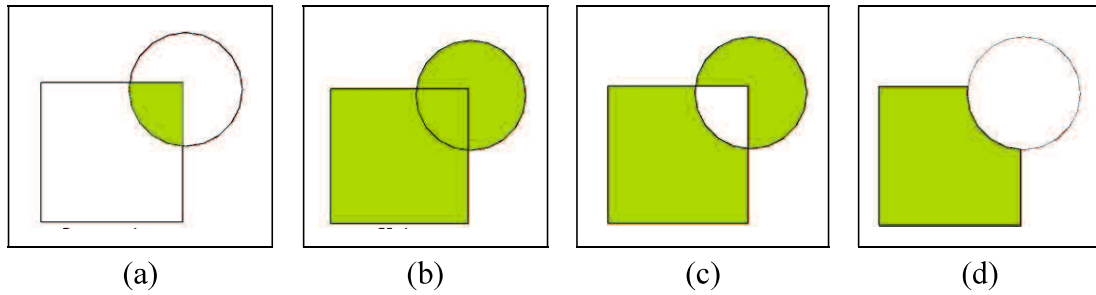


Figure 3.12 Spatial overlay using two input vectors, i.e. input is rectangle and input is circle) with vector layer result displayed in green color:

(a) Intersection; (b) Union; (c) Symmetrical difference; (d) Difference

(Source: QGIS, 2018)

e. Spatial Interpolation

Spatial interpolation is the process of using points with known values to estimate values at other unknown points. This type of interpolated surface is often called a statistical surface. Because of high cost and limited resources, data collection is usually conducted only in a limited number of selected point locations. In GIS, spatial interpolation of these points can be applied to create a raster surface with estimates made for all raster cells. The results of the interpolation analysis can then be used for analyses that cover the whole area and for modeling. There are many interpolation methods. In this study, a method of Triangulated Irregular Networks (TIN) that available in QGIS is utilized for the study mainly in conducting groundwater usage and groundwater level mapping of the groundwater depletion case.

A common TIN algorithm is called Delaunay triangulation. It tries to create a surface formed by triangles of nearest neighbor points. To do this, circumstances around selected sample points are created and their intersections are connected to a network of non-overlapping and as compact as possible triangles. An example of Delaunay triangulation is described in Figure 3.13.

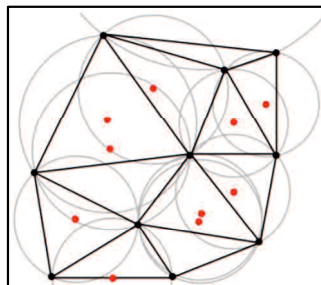


Figure 3.13 Delaunay triangulation with circumferences around the red sample data

(Source: QGIS, 2018)

The main disadvantage of the TIN interpolation is that the surfaces are not smooth and may give a jagged appearance. The reason is due to discontinuous slopes at the triangle edges and sample data points. In addition, triangulation is generally not suitable for extrapolation beyond the area with collected sample data points.

#### f. Map Production

A map has to be effective in communicating spatial information. Map production is the process of arranging map elements. Common elements of a map are the title, map body, legend, north arrow, scale bar, acknowledgement, and map border. Other elements that might be added are e.g. a graticule, or name of the map projection (CRS). These elements provide interpretation of the information shown on the map. The map body is, of course, the most important part of the map because it contains the map information. The other elements support the communication process and orientate map readers to understand the map topic. For example, the title describes the subject matter and the legend relates to map symbols to the mapped data.

In QGIS software, map production is processed through a creation of a working space by using “New Print Composer” option from “Project” menu. A map, label (text), image, scale bar, legend, arrow, and attribute table can be added from “Layout” menu in the “Composer” window by choosing the option of the intended added elements. For instance, a tool of “Add Map” will add map to the composer that represents image processed in “Project” window. Figure 3.14 describes an example of a blank working window of composer in QGIS.

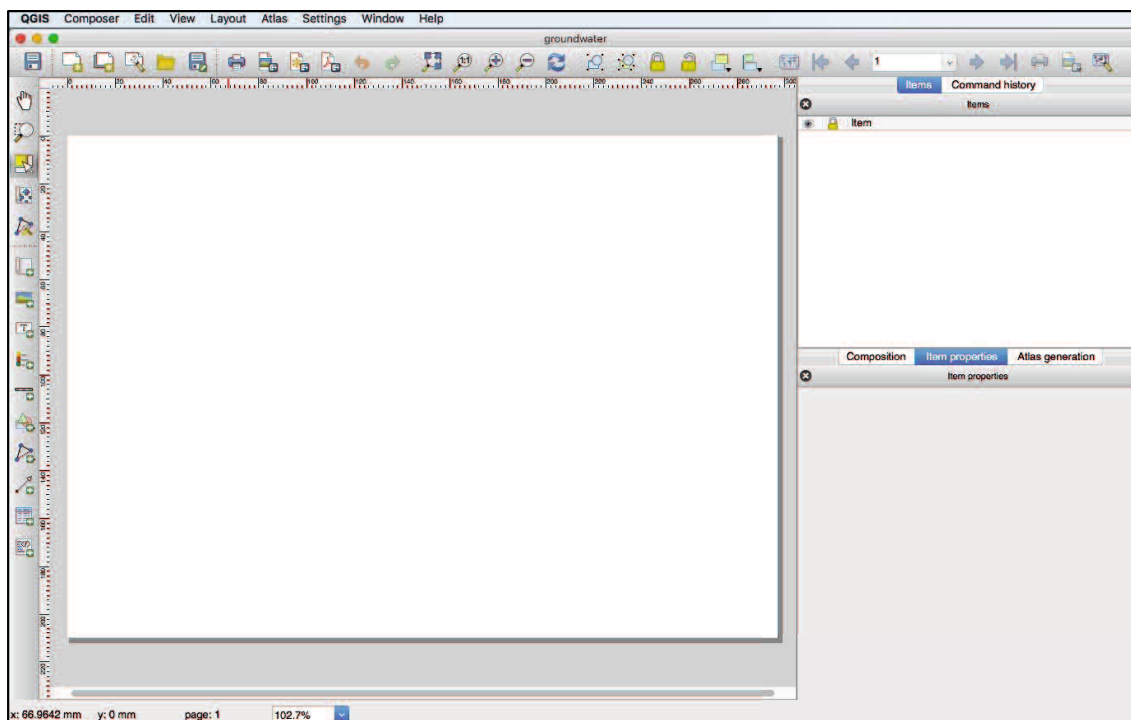


Figure 3.14 Map production window in QGIS

#### 4. Land Cover Mapping

Land cover classification is conducted using “Semi-Automatic Classification Plugin–SCP” plugin in QGIS software. In regard to the groundwater depletion case in this study, the purpose of performing land cover classification is to identify land cover classes that comprise water area, built-up area, vegetation, paddy field, wetland, and bare soil. Whereas, the classes of land cover in Talcahuano City for the tsunami inundation case are wetland, water area, vegetation area, built-up area, and bare land. Fundamentally, the procedure of using SCP for the classification of a multi-spectral image consists of download data, set input image, create training input file, create Region of Interest (ROIs), create a classification preview, and create the classification output.

##### a. Data Downloading

SCP plugin provides a tool for downloading open source satellite optical data, i.e. Landsat, Sentinel 2, ASTER, and MODIS. In groundwater depletion case, Landsat 7 ETM+ from 2001 to 2003 and Landsat 8 OLI-TIRS from 2013 to 2017 are used for the land cover classification in Bali Island. Since the area is constructed by two different paths, i.e. path 166 row 66 and path 167 row 66, there are 16 scenes needed to be downloaded from the “Download images” tool in “SCP” plugin of QGIS software. On the other hand, ALOS AVNIR-2 data is a commercial data that should be ordered from JAXA or the other authorized institution.

##### b. Input Image Setting

Prior to set input images, the necessary image is input using “Open a file” tool from the “SCP input” menu. After inputting the image, color composite of bands NIR, red, and green are selected from the “Working toolbar”. The color composite can be arranged through choosing the list RGB and selecting combination of false color with NIR-red-green bands that correspond to the band numbers in “Band set”. The image colors in the map will be changed according to the selected bands, and vegetation is highlighted in red. In contrast, if a combination of red-green-blue bands is selected, true or natural colors will be displayed.

The input image setting is mainly arranging color composite of the image. The band combination for the true and false color of Landsat ETM+ data used in this study are 3-2-1 and 4-3-2, respectively. Landsat 8 has different band combinations with the Landsat 7. The band combination of 4-3-2 is used to produce true color composite and band combination of 5-4-3 is employed to generate false color composite for Landsat 8 data. The Landsat data are utilized for land classification of groundwater depletion case. Moreover, true color and false color composite are applied to ALOS AVNIR imageries for the tsunami inundation case using combination of band 3-2-1 and band 4-3-2, respectively.

#### c. Creation of Training Input File

After the input image setting, training input is created in order to collect training areas (ROIs) and calculate spectral signature thereof. The training areas and spectral signature are used in classification. In the “SCP dock” of the “SCP” plugin, training input can be created by selecting “Create a new training input” option and define a name. The path of the file is displayed in “Training input” tab. A vector is added to QGIS layers with the same name as the training input for the purpose to prevent data loss.

#### d. Creation of ROIs

ROIs are created to define the “Classes and Macro-classes”. Each ROI identifies a land cover class through a “Class ID”. The Class ID codes used for the study are outlined in the Table 3.10. There are six classes (macro-classes) for the groundwater depletion case and five classes (macro-classes) in regard to the tsunami inundation case. ROI can be created by manually drawing a polygon or by using an automatic region-growing algorithm.

A tool “Create a ROI polygon” in the working toolbar is used to create ROI manually. Left click on the map to define the ROI vertices and right click to define the last vertex closing the polygon. An orange semi-transparent polygon will be displayed over the image that is a temporary polygon. If the shape of the temporary polygon is good then it can be saved to the “Training input”. Open the “Classification dock” to define the “Classes and Macro-classes”. For instance, in the “ROI creation”, set the “MC ID” as 1 and “MC Info” is water, besides “C ID” need to be set as 1 and “C Info” is Lake. After saving the set information, the ROI will be listed in the “ROI Signature list” and the spectral signature will be also calculated if the “Calculation sig.” option is checked. Moreover, the “C ID” in “ROI creation” will be automatically increased by 1. The saved ROI will be displayed a dark polygon changed from the temporary color which is removed after the ROI is saved. In the “ROI Signature list” there will be information of the ROI type that is B. The B type means that the ROI spectral signature was calculated and saved in the “Training input”.

Besides the manual method, ROI can be created using the automatic region-growing algorithm. As an example, built-up ROI is created for the built-up class. In working toolbar, set the “Dist. value” to 0.08. Click the button of “Activate ROI pointer” in the working toolbar and click over blue area that representing buildings on the image. In the “ROI creation” tab, “MC ID” and “MC Info” as well as “C ID”, and “C Info” should be set, i.e. 2 for the “MC ID”, Built-up for the “MC Info”, 2 for the “C ID”, and Buildings for the “C Info”. The other classes can also be created through this method. In regard to the available SAR data, surface material information extracted for SAR data are also used to supervise determination of ROI areas. Image displayed from SAR can assist to distinguish built-up and non-built up areas.

Table 3.10 Land cover macro-classes of ROIs in Bali Island and Talcahuano City

<b>Groundwater depletion</b>		<b>Tsunami inundation</b>	
<b>Class name</b>	<b>Class ID</b>	<b>Class name</b>	<b>Class ID</b>
Water	1	Water	1
Wetland	2	Wetland	2
Bare land	3	Bare land	3
Built-up	4	Built-up	4
Vegetation	5	Vegetation	5
Paddy field	6		

e. Creation of a Classification Preview

The classification is further processed based on the collected ROIs (and spectral signature thereof). In regard to assess the results that influenced by spectral signatures, it is useful to create a “Classification preview” before the final classification. In case the result are not good enough, more ROIs can be collected to classify the land cover more accurate. Prior to running a classification, the color of land cover classes that will be displayed in the classification raster are need to be set. The process can be conducted in the “ROI Signature list” by clicking the color of each ROI to choose a representative color of each class.

After setting the color, classification algorithm need to be selected. There are several algorithms available for the classification, i.e. minimum distance, maximum likelihood, spectral angle mapping, parallelepiped classification, land cover signature classification, and algorithm raster. In this study, the Spectral Angle Mapping algorithm is used for the land cover classification. In order to apply the algorithm, in “Classification algorithm” selects the “Spectral Angle Mapping” algorithm. In “Classification preview”, set the intended size of area whereby the classification will be applied, for instance 500. The classification process will be carried out rapidly and the result is a classified square centered with the set size.

Preview is temporary raster that will be deleted after QGIS is closed and placed in a group named “Class\_temp\_group” in the QGIS panel layers. In general, it is good to perform a classification preview every time a ROI (or spectral signature) is added to the “ROI signature list”. Therefore, the phases “Create the ROIs” and “Create a Classification Preview” should be iterative and concurrent processes.

f. Creation of the Classification Output

Assuming that the results of classification previews are acceptable, i.e. pixels are assigned to the correct class define in the “ROI Signature list”, actual land cover classification can be performed to the whole image. The process can be run through clicking “Run” in the “Classification output”. The classes of land cover classification, i.e. water, wetland, bare land, built-up area, vegetation, and paddy field, can be identified after

performing the classification output process. The result of the classification is a raster file. Classification errors are commonly appeared on the classified result, such as bare land classified as built-up and vice versa. In most cases, errors of classification are occurred due to insufficient number of ROIs (spectral signatures). In order to minimize such errors, surface reflectance is calculated to the bands used for creating color composite image. Moreover, information from other sufficient data such as SAR data is considered useful to in assisting ROI creation.

### **3.6.2 Time-Series InSAR Processing Using GMTSAR**

SAR satellites collect swaths of side-looking echoes at a sufficiently high range resolution and along-track sampling rate to form high-resolution imagery. The range resolution of the raw radar data is determined from the pulse length (or  $1/\text{bandwidth}$ ) and the incidence angle with a typical range resolution is 20 m. For real aperture radar, the along-track or azimuth resolution of the outgoing microwave pulse is diffraction limited to an angle corresponding to the wavelength of the radar (e.g. 0.05 m) divided by the length of the aperture (e.g. 10 m). When this beam pattern is projected onto the surface of the earth at a range of say 850 km, it illuminates 4250 m in the along-track dimension so the raw radar data are horribly out of focus in azimuth. Using the synthetic aperture method, the image can be focused on a point reflector on the ground by coherently summing thousands of consecutive echoes thus creating a synthetic aperture perhaps 4250 m long. Proper focus is achieved by summing the complex numbers along a constant range. The focused image contains both amplitude (backscatter) and phase (range) information for each pixel (Sandwell et al., 2016).

A complex radar interferogram (InSAR) is created through multiplying the reference image by the complex conjugate of the repeat image. For the ideal case where the trajectories of the reference and repeat images are exactly coincident, the phase difference between the two images will reflect differences in range between the antenna and a target pixel. This could be due to line-of-sight (LOS) motion of the target pixel or a travel time change due to the atmosphere or ionosphere. Normally there is an offset between the trajectories of the reference and repeat orbits. In this case the phase of the complex interferogram has an additional component due to the shape of the earth. The corrections for the topography of the earth can be removed from the interferogram if independent topography information is available, e.g. SRTM (Farr et al., 2007). An accurate orbit is needed to project the topography model from a latitude, longitude, and ellipsoidal height coordinate system into the range and azimuth coordinates of the radar image. An accurate orbit is also needed to correct the phase of the repeat image for the non-zero interferometric baseline since orbital error maps directly into interferometric phase (Sandwell et al., 2016).

In regard to InSAR processing, Generic Mapping Tools (GMT) SAR version 5.5 or GMT5SAR is utilized for the entire generation of InSAR products. In GMTSAR, the SAR



processor computer code is called *esarp*. Proper focus relies on having an accurate orbital trajectory for the satellite. For instance, the image will be out of focus if the range between the antenna and reflector has an error greater than about 1/4 wavelength, e.g. 0.01 m, over a distance of the synthetic aperture (4250 m). GMTSAR relies on sub-meter orbital accuracy to greatly simplify the SAR and InSAR processing algorithms. Moreover, large batches of SAR images can be automatically processed with no human intervention. The down side of this approach is that SAR satellites having less accurate orbits (>10m, e.g., RADARSAT-1 and JERS-1) cannot be easily processed using GMTSAR.

Creating SAR images and interferograms (InSAR) from satellite radar measurements requires specialized front-end computer codes for focusing imagery and computing interferometric phase. However, much of the back-end processing and display can be accomplished with existing generic codes. SAR/InSAR processing in GMTSAR system is initiated with raw (or SLC) SAR data in radar coordinates, along with precise orbital information, and eventually computes interferometric products in geographic coordinates. The system relies on precise orbital information, as discussed below, and a consistent geometric model to achieve proper focus and image alignment. The SAR processor code was originally derived from the Stanford/JPL FORTRAN and re-written in the C programming language ensuring compilation on many platforms using the standard *gcc* compiler (Sandwell et al., 2016).

GMT is used for the back-end processing. It is an open source collection of programs designed for manipulating and displaying geographic data sets. GMT includes efficient and robust programs for re-gridding, filtering, and trend removal, which make it highly useful for some aspects of InSAR processing. GMT uses the NETCDF file format that allows the exchange of files among computers having different architectures. The combined front- and back-end processing is done using the c-shell scripting language which is available on all UNIX platforms. GMTSAR package also includes the capability for ScanSAR processing and is flexible enough for performing time series analysis on stacks of interferograms (Sandwell et al., 2016).

Before introducing the main software components, it is useful to describe the standard products created by the GMTSAR system using the script *p2p\_SAT.csh* as follow (Sandwell et al., 2016):

1. *name.PRM*

Ascii file generated by the *pre\_processing* software. It contains all the information needed to focus and align a single look complex (SLC) image with a master image. This file contains all the important SAR and InSAR processing parameters.

2. *name.LED*

Ascii file generated by the *pre\_processing* software to contain the orbital information as a state vector.

3. *name.raw*  
File contains the raw signal data. Each row of signal data has a 412 byte header record containing timing and other information followed by the radar echo stored as unsigned 2-byte complex numbers (1 byte real and 1 byte imaginary).
4. *name.SLC*  
File contains the focused single look complex (SLC) image. The signed 4- byte complex numbers are stored as unsigned short integers (2-bytes real and 2-bytes imaginary). The numbers are scaled to utilize the full dynamic range of a short integer.
5. *trans.dat*  
File contains the mapping between range, azimuth coordinates and longitude, latitude, topography coordinates. The topography is calculated with respect to a local spherical approximation to the earth and therefore large negative and positive numbers are possible. The following is the file format:  
range azimuth topography longitude latitude and numbers are stored as double precision floating point.  
11301.587587 18451.999997 -272.883315 -115.156667 32.373333  
11308.909450 18451.999997 -273.413527 -115.156111 32.373333
6. *topo\_ra.grd*  
NetCDF format grid of range, azimuth, and topography.
7. *real.grd* or *imag.grd*  
NetCDF grids of range, azimuth, and the real or imaginary part of the complex interferogram (files are deleted when no longer needed).
8. *phase.grd*  
NetCDF grid of range, azimuth, and interferometric phase modulus  $2\pi$ .
9. *corr.grd*  
NetCDF grid of range, azimuth, and interferometric coherence (0-1).
10. *xphase.grd*  
NetCDF grid of range, azimuth, and phase gradient in the range direction in units of radians per pixel (optional).
11. *yphase.grd*  
NetCDF grid of range, azimuth, and phase gradient in the azimuth direction in units of radians per pixel (optional).
12. *mask.grd*  
NetCDF grid of range, azimuth, and NaN or 1. NaN signifies data should be masked.
13. *unwrap.grd*  
NetCDF grid of unwrapped interferometric phase in radians (optional).

When the interferometric products have been transformed back to geographic coordinates the file names include a “\_ll”. For example *phase\_ll.grd* is a netcdf file of longitude, latitude, and interferometric phase modulus  $2\pi$ . Files having a *.ps* suffix are postscript plots of the quantity. For instance, *phase\_mask\_ll.ps* is a postscript plot of masked phase in geographic coordinates. Files having a *.kml/png* suffix are Google Earth images. For instance, *phase\_mask\_ll.kml/png* is a Google Earth image of masked phase in geographic coordinates.

The overall design of the software is illustrated in Figure 3.15. There is a set of preprocessing code for each of the satellites including ALOS PALSAR and Sentinel 1A that are used in this study. Data, leader, and orbit files provided by the space agency are normally in CEOS format and are converted into generic *\*.raw* and *\*.PRM* files. The pre-processing code checks for missing lines in the CEOS data file and aligns the radar echoes on a common near range or sample window start time (SWST). The output is a raw file (*\*.raw*) that is ready to be focused in the SAR processor. The relevant parameters are extracted from the various leader and orbit files and used to prepare a parameter file (*\*.PRM*). After selecting the master image, a user-supplied topography grid of the area (*dem.grd*) is projected into radar coordinates to create a transformation file (*trans.dat*).

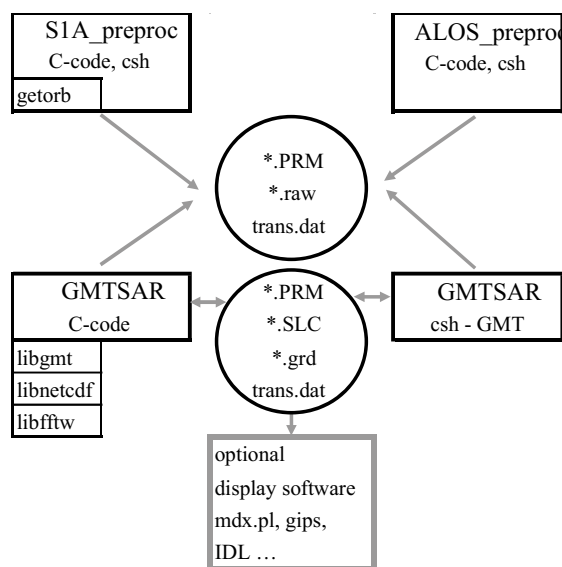


Figure 3.15 Design of GMTSAR and preprocessors

The GMTSAR code is the same for all the satellite data types. There are 4 essential programs written in C called *esarp*, *xcorr*, *phasediff*, and *conv*. The programs *esarp* and *xcorr* make extensive use of a 1-dimensional FFT routine built into GMT. In the original GMTSAR codes, the user needed to select the most appropriate FFT code for optimal performance. That task is now done automatically during the installation of GMT5. The three options are, i.e. the default option uses FFT routines from *fftpack.c* code (Swarztrauber, 1982), the fastest

option uses the Accelerate Framework included in the Mac OS X system, and the third option uses the fftw code that is distributed by <http://www.fftw.org/>. The optimized FFT codes will reduce the runtime of these programs by about 20-40%. The programs *phasediff*, and *conv* read/write GMT *grd*-files in netcdf format and therefore require that the user link with the libraries *libgmt.a* and *libnetcdf.a*. These programs, as well as many standard GMT routines, are called from shell scripts. A list of the current scripts is found by executing the command *gmtsar.csh*.

A second common approach to InSAR processing is to form a time series of land deformation from a stack of images. There are a variety of methods ranging from averaging to small baseline subsets to time series to persistent scattering. The practical, and sometimes most challenging issue related to these approaches is to geometrically align a large stack of images and align this stack with a topographic phase model. To achieve interferometric phase coherence, the alignment must have sub pixel accuracy in the radar coordinates of range and azimuth. In regard to GMTSAR terminology, many “slave” images are geometrically aligned with one “master” image. Once the alignment is done, an interferogram can be constructed from any pair of images in the stack. The terminologies related to the process are “reference” and “repeat” images for the first and second acquisition of the interferometric pair, respectively

Image alignment is problematic if the perpendicular baseline between the master image and one of the slave images is greater than about 3/4 of the critical baseline because the images will be baseline de-correlated. Temporal de-correlation can also occur when the scattering surface of the earth changes between the master and slave acquisitions because of vegetation, snow, or other small-scale surface disturbances. In regard to the image alignment algorithm in GMTSAR, the process begins with a guess at the range and azimuth shift based on the precise orbit and then uses 2-dimensional cross correlation on small patches. If there are no areas in the images that correlate one another then this cross-correlation approach can fail to achieve sub pixel correlation.

An overview of the seven main processing steps of time-series InSAR processing in this study is described in Figure 3.16 and the modules are provided in Table 3.11. The time-series technique in GMTSAR is processed through layer stacking whereby the interferograms are generated through batch processing. The characteristics the data type effect the processing parameters. The characteristics of two data types of SAR used in this study, i.e. L-band ALOS PALSAR and C-band Sentinel 1A, are presented in Table 3.12 and Table 3.13, respectively. Characteristics of SAR data related to the selection of processing parameters, e.g. mode, polarization, processing level, center frequency, wavelength, orbital revisit period, ascending/ descending, incident angle, critical baseline, range resolution, observation swath, data rate, and noise equivalent (NE).

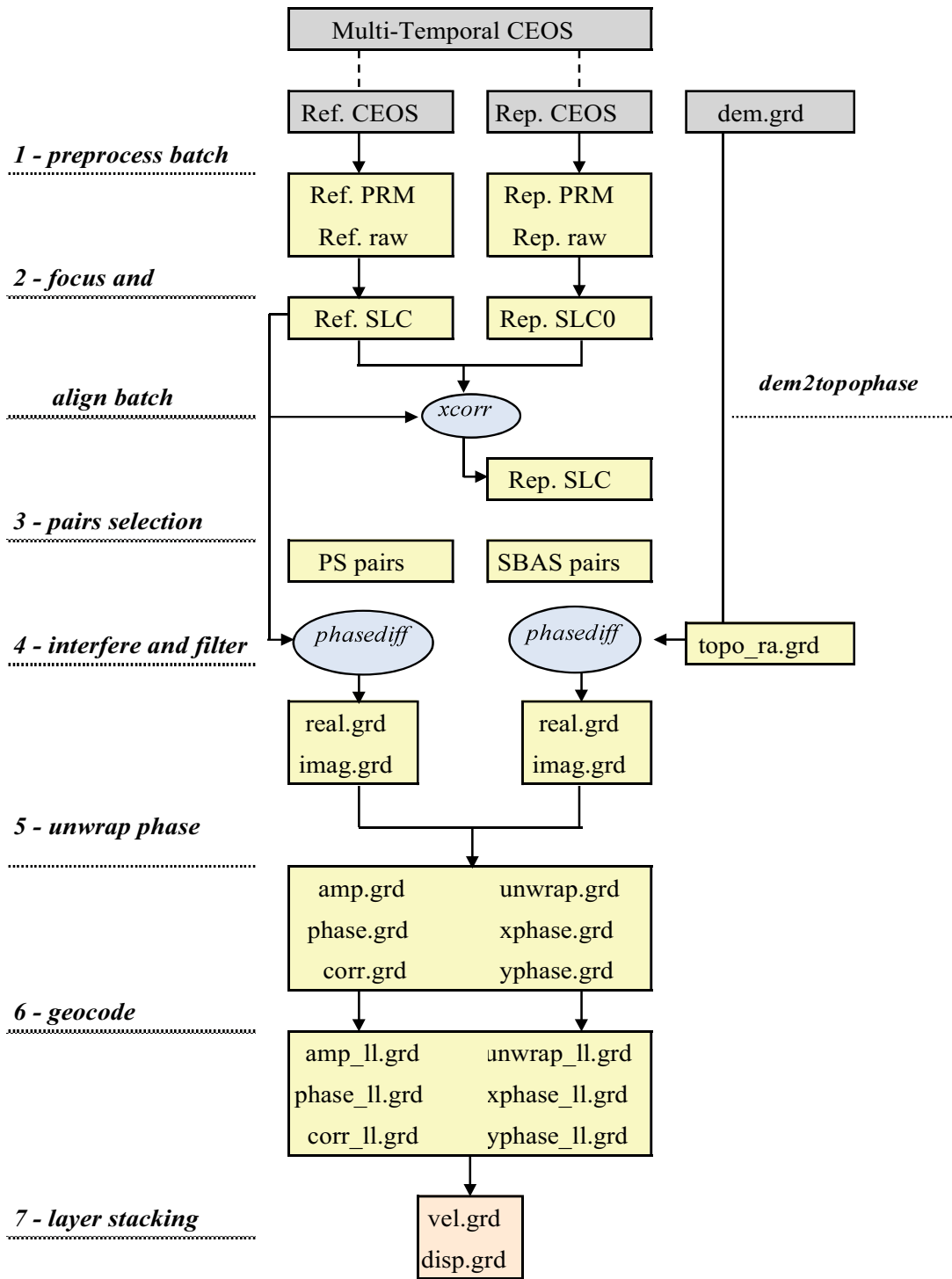


Figure 3.16 Overview of the main processing steps of time-series InSAR using GMTSAR processing in the study

Table 3.11 Modules of GMTSAR for time-series InSAR processing in the study

No.	Process	Command			
		ALOS PALSAR		Sentinel 1A	
1 - preprocess batch		<i>preproc_batch.csh</i>		<i>preproc_batch_tops.csh</i> (mode 1)	
		<i>update_PRM.csh</i>		<i>update_PRM.csh</i>	
		<i>ALOS_pre_process.c</i>		<i>make_S1_tops.c</i>	
		<i>ALOS_fbd2fbs.c</i>		<i>ext_orb_s1a.c</i>	
		<i>ALOS_fbs2fbd.c</i>			
2 - focus and align batch		<i>align_batch.csh</i>		<i>preproc_batch_tops.csh</i> (mode 2)	
		<i>sarp.csh</i>	<i>esarp.c</i>	<i>align_tops.csh</i>	
		<i>SAT_baseline.c</i>		<i>sarp.csh</i>	<i>esarp.c</i>
		<i>xcorr.c</i>		<i>SAT_baseline.c</i>	
		<i>fitoffset.csh</i>	<i>trend2d.c</i>	<i>xcorr.c</i>	
			<i>fitoffset.csh</i>	<i>trend2d.c</i>	
3 - topo_ra		<i>dem2topo_ra.csh</i>		<i>dem2topo_ra.csh</i>	
		<i>grd2xyz.c</i>		<i>grd2xyz.c</i>	
		<i>grdfilter.c</i>		<i>grdfilter.c</i>	
		<i>SAT_llt2rat.c</i>		<i>SAT_llt2rat.c</i>	
		<i>blockmedian.c</i>		<i>blockmedian.c</i>	
		<i>surface.c</i>		<i>surface.c</i>	
		<i>topo2phase.c</i>		<i>topo2phase.c</i>	
		<i>grdimage.c</i>		<i>grdimage.c</i>	
4 - pairs selection		<i>select_sbass_pairs.csh</i>		<i>select_sbass_pairs.csh</i>	
5 - interfere and filter/ snaphu		<i>intf_batch.csh</i>		<i>intf_tops.csh</i>	
		<i>filter.csh</i>		<i>filter.csh</i>	
		<i>SAT_baseline.c</i>		<i>SAT_baseline.c</i>	
		<i>phasediff.c</i>		<i>phasediff.c</i>	
		<i>conv.c</i>		<i>conv.c</i>	
		<i>grdmath.c</i>		<i>grdmath.c</i>	
		<i>grdimage.c</i>		<i>grdimage.c</i>	
		<i>phasefilt.c</i>		<i>phasefilt.c</i>	
		<i>snaphu.csh</i>		<i>snaphu.csh</i>	
		<i>grdcut.c</i>		<i>grdcut.c</i>	
		<i>grdmath.c</i>		<i>grdmath.c</i>	
		<i>grd2xyz.c</i>		<i>grd2xyz.c</i>	
		<i>snaphu.c</i>		<i>snaphu.c</i>	
	<i>xyz2grd.c</i>		<i>xyz2grd.c</i>		
	<i>grdimage.c</i>		<i>grdimage.c</i>		
7 - geocode		<i>geocode.csh</i>		<i>geocode.csh</i>	
		<i>grdmath.c</i>	<i>grd2xyz.c</i>	<i>grdmath.c</i>	<i>grd2xyz.c</i>
		<i>proj_ra2ll.csh</i>	<i>gmtconvert.c</i>	<i>proj_ra2ll.csh</i>	<i>gmtconvert.c</i>
			<i>blockmedian.c</i>		<i>blockmedian.c</i>
			<i>surface.c</i>		<i>surface.c</i>
			<i>grdtrack.c</i>		<i>grdtrack.c</i>
		<i>grd2kml.csh</i>	<i>grdimage.c</i>	<i>grd2kml.csh</i>	<i>grdimage.c</i>
			<i>ps2raster.c</i>		<i>ps2raster.c</i>
8 - layer stacking		<i>layer_stack.csh</i>		<i>layer_stack.csh</i>	
		<i>sbass</i>		<i>sbass</i>	

GMTSAR commands are italic; black – c-shell script; red – GMTSAR C-code, blue – GMT C-code, green – snaphu phase unwrapper.

(Source: Chen and Zebker, 2000)

Table 3.12 Characteristics of ALOS PALSAR data used in the study

Mode	Fine
Polarization	Single Polarization (HH)
Processing level	1.0
Center frequency	1270 MHz (L-band)
Wavelength	236 mm
Orbital revisit period	46 days
Ascending/ Descending	Ascending
Chirp bandwidth	28 MHz
Incident angle	34.3°
Critical baseline	13.1 km
Range resolution	10 m
Observation Swath	70 km
Bit length	5 bits
Data rate	240 Mbps
Noise Equivalent (NE) Sigma-0	-25dB
Signal-to-Ambiguity (S/A) ratio	25dB
Radiometric accuracy	scene: 1dB / orbit: 1.5 dB

(Source: Sandwell et al., 2016; Furuta et al., 2005; Rosenqvist et al, 2004)

Table 3.13 Characteristics of Sentinel 1A data used in this study

Item	Characteristics
Mode	Interferometric Wide Swath
Polarization	Single Polarization (VV)
Processing level	1.0
Center frequency	5404 MHz (C-band)
Wavelength	55 mm
Orbital revisit period	12 days
Ascending/ Descending	Ascending
Chirp bandwidth	
Incident angle	30.0°
Critical baseline	5 km
Range resolution	20 m
Observation Swath	250 km
Bit length	5 bits
Data rate	600 Mbps
Noise Equivalent (NE) Sigma-0	-22dB

(Source: ESA, 2000; Amitrano et al., 2014)

### 1. Preprocess Batch

The first step of the InSAR process is to *preprocess* raw SAR data and orbital information, generally in L1.0 CEOS format, to create an ascii parameter file and a raw data

file. An explanation of common parameter obtained from ascii parameter file is given in Table 3.14. This preprocessing involves specialized code to extract orbital position and velocity information from the leader files, align the raw radar echoes on a common near range, and estimate the Doppler centroid of the raw data. Preprocess is conducted using GMTSAR c-shell script called *pre\_proc\_batch.csh* for ALOS PALSAR processing. The script require input that are *data.in* and *batch.config*. In case of Sentinel 1A processing, TOPSAR data processing is conducted using GMT c-shell script called *preproc\_batch\_tops.csh*.

The input required for running the script are *data.in*, *dem.grd*, and *mode*. A configuration file of *batch\_tops.config* is not necessary for this step, nevertheless it can be prepared in advance since it will be used for the next process. Parameters for the configuration file are *proc\_stage*, *master\_image*, *threshold\_snavhu*, *filter\_wavelength*, *range\_dec*, *azimuth\_dec*, *dec\_factor*, *switch\_land*, and *defomax*. Similar parameters are used for ALOS PALSAR and Sentinel-1A in this study.

The parameter related to the pre-process on the configuration file is mainly the *master\_image*. The other related parameter including *num\_pathes*, *earth\_radius*, *near range*, and *Doppler centroid* can be left blank, so that the default setting of the common ALOS PALSAR mode data value will be used as the parameters. It can be also filled following the information obtainable from .PRM file of the SAR scene. The PRM file is possible to be generated by running GMT c-shell scripts or GMT c-code of preprocess for ALOS PALSAR. The configuration scripts of *batch.config* for ALOS PALSAR processing and *batch\_tops.config* for Sentinel 1A processing are outlined in Appendix A. In this study, the default parameter setting is used for the preprocessing.

## 2. Focus and Align Batch

The second step is to *focus* each image to create two single look complex images and *align* the repeat image to the reference image. The align process is accomplished by first using the orbital information to estimate the shift in range and azimuth needed to align the upper left corner of the images. Then many small patches (e.g., 64 x 64) are extracted from each image and cross-correlated to determine 6 affine parameters needed to warp the repeat image to match the second image. The repeat image is refocused using these 6 parameters resulting in sub-pixel alignment between the reference and repeat images. Smaller scale pixel shifts due to large amplitude surface topography are corrected at the *interfere* step.

## 3. DEM Generation for Topography Removal

The DEM generation for topography removal (*dem2topo\_ra.csh*) is a process to transform the DEM from longitude, latitude, and topography into range, azimuth, and topography. This is done using the precise orbital information of the reference image. In case



of a -1 pixel range shift, i.e., derived from a cross correlation between the amplitude image of the master and the range gradient of the topographic phase, *offset\_topo* is needed to improve the alignment.

#### 4. Pairs Selection

The fourth step of the process is to select interferogram pairs based on PS and SBAS method. In regard to PS method, one scene is selected as a super master or reference and the other scenes are used as slave or repeat. A good master image has to cover area of interest and minimizes perpendicular baselines between interferometric pairs. It is generally positioned in the middle with value close to 0 according to the baseline distribution table (*baseline.ps*).

In case of the SBAS method, pair selection is conducted by running a GMTSAR code called *select\_sbas\_pairs.csh*. The interferogram pairs are selected according to the perpendicular baseline and temporal baseline. Scenes pairs having the given perpendicular baseline and temporal baseline will be written on the result of the pairs selection process that is *intf.in*. The result is used as input for the next process by adding the baseline value for each master and slave pairs. Baseline values differ for each data type that are affected by the several parameters, e.g. wavelength, orbital revisit period, and critical baseline. The GMT c-shell script of *select\_sbas\_pairs.csh* is described in Appendix A. The baseline parameter for SBAS in the study is described in Table 3.16.

#### 5. Interfere and Filter

The fifth step is to interfere the reference and repeat SLCs using the *topo\_shift.grd* to both refine the image alignment of the repeat image due to topography parallax, and to remove the baseline-dependent topographic phase from the repeat image prior to cross multiplication (*phasediff*). Thus, the entire position and phase corrections are applied at the full resolution of the SLCs. The sixth step following the interfere process is *filter/ snaphu* which has a function to low-pass filter (*conv*) and decimate (4 in azimuth and 1 or 2 in range) the real and imaginary components of the interferogram and compute standard products of amplitude, phase, and coherence. The Gaussian filter wavelength need to be set in the *config.txt* file. A second set of filtered interferograms is also created using a modified Goldstein filter algorithm (*phasefilt*) (Goldstein and Werner, 1997; Baran et al., 2003).

Optionally one can compute unwrapped phase using the *snaphu* program of Chen and Zebker (2002) as well as phase gradients (Sandwell and Price, 1998) in the range (*xphase*) and azimuth (*yphase*) directions. To this point all the processing is done in the radar coordinates where the spacing of the range pixels before decimation is  $c\tau/2$  and the spacing of the azimuth pixels before decimation is  $V/PRF$ . The parameters used in this study can be found in Table 3.16.

## 6. Geocode

The further step after interfere and filter is to *geocode* all the products by transforming from the range/azimuth coordinate system of the master image to longitude and latitude. The c-shell scripts also produce postscript images and kml-images of relevant products using the capabilities of GMT.

## 7. Layer stacking

Layer stacking is the stacking process of multi-temporal inteferograms generated from the previous process based on PS and SBAS pairs selection. A GNT PS-based interferograms are combined can be used to calculate The further step after interfere and filter is to *geocode* all the products by transforming from the range/azimuth coordinate system of the master image to longitude and latitude. The c-shell scripts also produce postscript images and kml-images of relevant products using the capabilities of GMT.

Table 3.14 Configuration parameters for the InSAR processing using GMTSAR

Process	Parameter	Value	
		ALOS PALSAR	Sentinel-1A
Pairs selection for SBAS	Perpendicular baseline	1000	100
	Temporal baseline	2500	250
Interfere and filter	Method	Gauss 300	Gauss 300
Land mask	Perform land mask	1	1
Unwrapped	Threshold	0.45	0.45
Geocode	Threshold	0.45	0.45
SBAS	Smoothing factor	1	1
	Wavelength	0.2362 m	0.055 m
	Incidence angle	34.3 degree	30 degree
	Range	850014 - 848965	6377598
	Atmospheric correction	1	1

### 3.6.3 GNSS Data Processing Using RTKLIB

RTKLIB contains a post processing analysis AP RTKPOST. RTKPOST inputs the standard RINEX 2.10, 2.11, 2.12, 3.00, 3.01, 3.02 (draft) observation data and navigation message files (GPS, GLONASS, Galileo, QZSS, BeiDou and SBAS) and can computes the positioning solutions by various positioning modes including Single-point, DGPS/DGNSS, Kinematic, Static, PPP-Kinematic and PPP-Static.

1. Execute the binary AP file `<install dir>\rtklib_<ver>\bin\rtkpost.exe`. The main window of RTKPOST will be shown. After that, the binary AP file `<install`

`dir>Yrtklib_<ver>YbinYrtkpost_mkl.exe` can be executed instead, which is a version of RTKPOST linking the Intel MKL library for fast matrix computation. Main Window of RTKPOST is described in Figure 3.17.

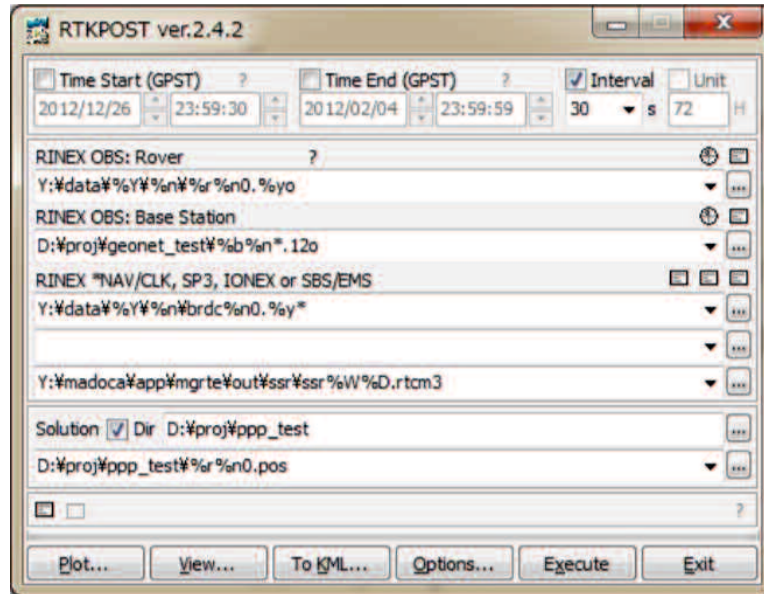


Figure 3.17 Main Window of RTKPOST  
(Source: Takasu, 2013)

2. Input the RINEX observation data file path of the rover receiver in the text field “RINEX OBS(:Rover)”. Fill in the file path or select a file using the file selection dialog shown by pushing button. Several compressed files can be used for the RINEX observation data, i.e. GZIP (**.gz**), COMPRESS (**.z**) or Hatanaka-Compression (**.yyd**). If the compression file or not is recognized by the file extension. If a wild-card (\*) is included in the file path, the wild-card is expanded and the multiple files are read.
3. If the RINEX data is processed in the relative positioning modes as: DGPS/DGNSS, Kinematic, Static, Moving-Base or Fixed, the second file path of the base-station receiver in the “RINEX OBS: Base Station” field has to be input in addition to the rover observation data file.
4. Furthermore, input the path of RINEX navigation message files of GPS, GLONASS, Galileo, QZSS and SBAS in the “RINEX \*NAV/CLK, SP3, IONEX or SBS/ EMS” field. If you leave first and second field blank, the observation data file path with the extension replaced by **.\*nav (.obs)** or **.yyN,.yyG,.yyH,.yyQ** and **.yyP (.yyO)** is used for the navigation message files of GPS, GLONASS, Galileo, QZSS, BeiDou and SBAS. If a wild-card (\*) is included in the file path, the wild-card is expanded and the multiple files are used like observation data files. To use precise ephemeris and clock for PPP-Kinematic, PPP-Static or PPP-Fixed mode, input a SP3-c (for precise satellite ephemeris

and clock) or RINEX CLK (for precise satellite clock) file path in the field. Input an IONEX 1.0 file path for ionospheric VTEC grid corrections. For SBAS corrections, input a SBAS message log file path as RTKLIB format or EMS (EGNOS message server) 2.0 format file. Wild-cards (\*) can also be included in these file paths. The wild-cards are expanded and multiple files are used. Input SSR (state space representation) corrections as RTCM 3 messages in a input file field. The formats of these input files are recognized by their extensions as follows (Takasu, 2013):

- a. **.sp3, .SP3, .eph, .EPH** : SP3-c precise ephemeris file;
- b. **.sbs, .SBS, .ems, .EMS** : SBAS message log file;
- c. **.rtcm3, .RTCM3** : RTCM 3 SSR correction message file;
- d. **.\*i, .\*I** : IONEX VTEC grid data file;
- e. **others** : RINEX OBS, NAV or CLK.

5. Input the output file path in the text field “Solution”. The field is automatically set as the first input file path with the extension replaced by **.pos** or **.nmea**. If the “Dir” is checked and fill in the field, the output directory is set to the specified directory. Modify the output file path manually by editing the field content.
6. Push “Options” button to set the processing options. For the detailed options for RTKPOST. The start time or end time can be set by checking and setting Time Start (GPST) or Time End (GPST) field in the main window. Moreover, the <sup>[ ]</sup>time interval can be set by checking and setting the “Interval” field. With the “?” button, the input time in GPS time can be converted to UTC, GPS Week/TOW, Day of Year, Day of Week, Time of Day and Leap Seconds (Figure 3.18). <sup>[ ]</sup>



Figure 3.18 Time Dialog of RTKPOST  
(Source: Takasu, 2013)

7. In case that both “Time Start” and “Time End” fields are checked, “Unit” for multiple session analysis can also be checked. If it is set then the “Unit” time in hours should be set, the analysis session is separated to multiple sessions for the unit time. To avoid overwriting the previous output file, the output file path has to contain the keyword replaced according to the session time. For the details of the keyword replacement in the input or output file paths.

8. Push button to start the analysis. The processing status is shown in the status message field lower center in the main window. When a “done” message appears, the analysis is completed. The processing can be stopped on the way, push “Abort” button.
9. After completing the analysis, by pushing button, the content of the output file can be displayed by “Text Viewer” (Figure 3.19). The output file can be reloaded by pushing button in the “Text Viewer” window. To close the window, push “Close” button. “Text Viewer” options can be configured by pushing “Options” button. Strings in the text by using button are also available.

```

D:\proj\ppp_test\GRAZ0010.pos
Find Read... Option... Close
% program : RTKPOST ver.2.4.2
% inp file : Y:\data\2012\001\GRAZ0010.12o
% inp file : Y:\data\2012\001\brdc0010.12n
% inp file : Y:\data\2012\002\brdc0020.12n
% inp file : Y:\product\1669\igs16690.sp3
% inp file : Y:\product\1669\igs16691.sp3
% inp file : Y:\product\1669\igs16690.clk_30s
% obs start : 2012/01/01 00:00:00.0 GPST (week1669 0.0s)
% obs end : 2012/01/01 23:59:30.0 GPST (week1669 86370.0s)
% pos mode : ppp-kinematic
% solution : forward
% elev mask : 10.0 deg
% dynamics : off
% tidecorr : on
% tropo opt : est ztd+grad
% ephemeris : precise
% antennal : ( 0.0000 0.0000 0.0000)
%
% (lat/lon/height=WGS84/ellipsoidal,Q=1:fix,2:float,3:sbas,4:dgps,5:single,6:ppp,ns=#
% GPST latitude(deg) longitude(deg) height(m) Q ns sdn(m) sde(m) sc
1669 0.000 47.067127520 15.493490558 542.3593 6 9 4.7698 4.0608 7.
1669 30.000 47.067126801 15.493488482 541.7852 6 9 3.0014 2.7802 5.
1669 60.000 47.067127193 15.493487416 542.0154 6 9 2.1736 2.1561 3.
1669 90.000 47.067128990 15.493484322 541.5252 6 9 1.7014 1.7704 3.
1669 120.000 47.067130185 15.493481111 540.8669 6 9 1.4004 1.5096 2.

```

Figure 3.19 Text Viewer showing Solutions by RTKPOST  
(Source: Takasu, 2013)

10. By pushing “Plot” button, the plot of the result with RTKPLOT can be shown. An example of RTKPLOT result is showed in Figure 3.20.

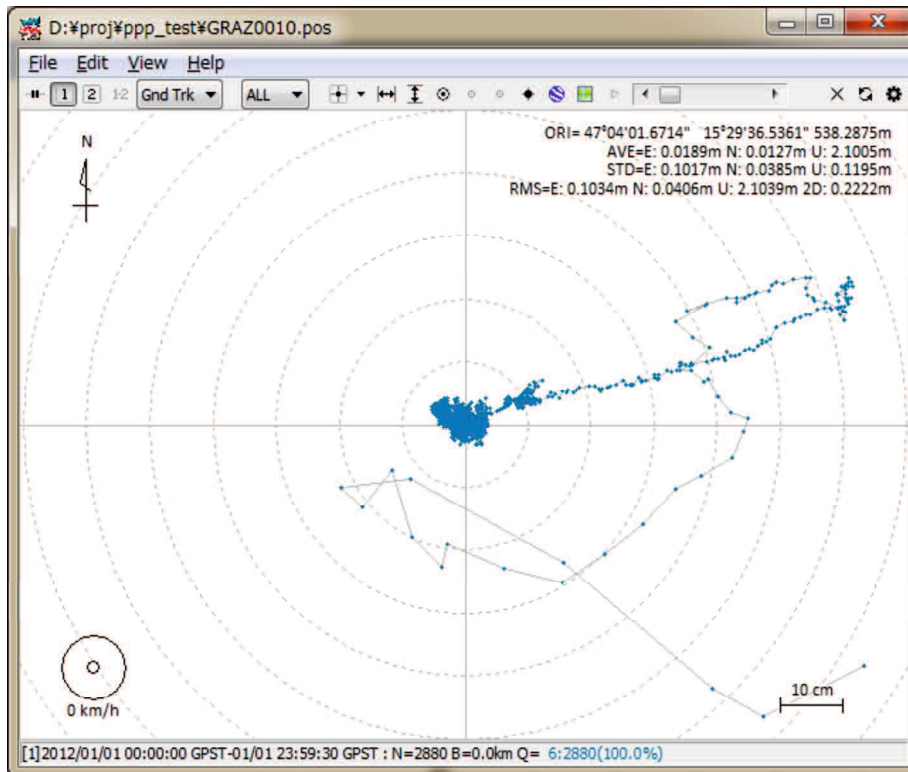


Figure 3.20 RTKPlot window executed by RTKPOST  
(Source: Takasu, 2013)

11. By pushing “To KML” button, the output file can be converted to Google Earth KML file with the “Google Earth Converter” dialog (Figure 2.21). Set or select the options and push “Convert” button in the dialog. Google Earth can also be launched with the generated KML/KMZ file by pushing “Google Earth” button. To specify the Google Earth execution file, configure “Options” - “Files” - “Google Earth Exe File”.

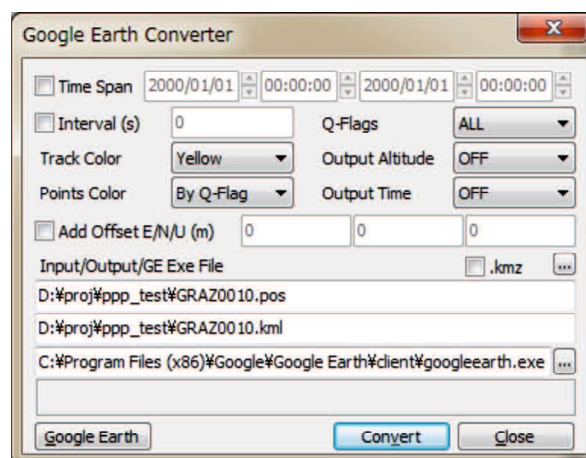





Figure 3.21 Google Earth converter dialog of RTKPOST  
(Source: Takasu, 2013)

12. With  button in the main window, the input observation data RTKPLOT can be viewed and plotted. The contents of the input files can also be displayed with “Text Viewer” by pushing  button.
13. In case of output solution statistics or debug trace as the processing options, push  buttons lower left of the window to view the solution statistics file or the debug trace file. To check processing error or warning in case of improper results, set Debug Trace in “Options” - “Output” dialog to “Level 2” (trace ERROR and WARNING) and see the output debug trace file.

Positioning options can be set through pushing “Options” button in the main windows of RTKPOST. Selectable or changeable positioning options are as follows. These options can be saved to the configuration file by pushing “Save” button on the dialog and select the file path. The options can be loaded from a configuration file by pushing “Load” button and selecting a configuration file.

### 3.6.4 Groundwater Depletion and Usage Analysis Using Groundwater Monitoring Data

Groundwater monitoring data collected from secondary data and field observation consists of information regarding groundwater level at monitoring wells and distribution of wells for drinking water and irrigation.

#### 1. Groundwater Depletion

Groundwater depletion is calculated using the collected secondary data of groundwater level measurement below the ground surface from 2008 to 2013 and field observation data in 2017. The percentage of depletion from two years data is determined based on the groundwater depletion ( $\Delta h$ ) that can be calculated as follow:

$$\Delta h = \frac{h_2 - h_1}{h_1} \quad (\text{Equation 3.9})$$

Where  $h_1$  is the groundwater level in the initial year and  $h_2$  is the groundwater level in the following year.

Furthermore, the groundwater depletion from the observation period of 2008 to 2012 is obtained by calculating the average of the depletion percentage in 2008 – 2009, 2009 – 2010, 2010 – 2011, 2011 – 2012, 2012 – 2013, and 2013 to 2017. The percentage of the groundwater depletion is calculated for each monitoring well. The values are input into the monitoring well points as vector data. The information is further interpolated to create a map of groundwater depletion distribution throughout the study area.

Interpolation uses vector points with known values to estimate values at unknown locations to create a raster surface covering an entire area. The interpolation result is typically a raster layer. It is important to find a suitable interpolation method to optimally estimate values for unknown locations. In case of the groundwater depletion distribution, the interpolation is carried out in QGIS application using Inverse Distance Weighting (IDW) method. In the IDW interpolation method, the sample points are weighted during interpolation such that the influence of one point relative to another declines with distance from the unknown point that will be created. Weighting is assigned to sample points through the use of a weighting coefficient that controls how the weighting influence will drop off as the distance from new point increases. The greater the weighting coefficient, the less the effect points will have if they are far from the unknown point during the interpolation process. As the coefficient increases, the value of the unknown point approaches the value of the nearest observational point (Mitasova, 1999).

## 2. Groundwater Usage Analysis

In general, groundwater usage for drinking water is determined based on percentage of water supply, population, and water needs in l/day/person of each sub-district region in the administration area of Bali Province. Since updated information of parameters necessary for the drinking water groundwater usage calculation is available for wells in the entire sub-district areas, the groundwater usage is estimated based on the percentage of service coverage of the groundwater supply at a well, population in service coverage area, and the water needs in l/day/person as follow:

$$\text{Groundwater usage} = \% \text{ of groundwater supply} \times \text{population} \times \text{water needs} \quad (\text{Equation 3.10})$$

In particular for the wells for drinking water, the usage of wells for drinking water managed by the local drinking water agency is differentiated with wells for drinking water maintained by local community organization according to the well capacity. The community-based wells for drinking water have a lower capacity compare to the wells managed by the local drinking water agency. Moreover, the usage of wells for irrigation is calculated based on the capacity of the wells according to the area of the irrigated paddy field. The coordinate (location) of the wells is further used to produce a distribution map of wells. The data is also utilized to show distribution of the groundwater usage corresponding to the distribution of the wells.

### 3.6.5 Local Knowledge Tsunami Analysis Based on DIG Workshop

Local knowledge of tsunami inundation represents information collected from local community living in the tsunami-prone area. Participatory mapping workshop is considered challenging yet effective to improve community understanding of a certain disaster (Warner, 2005). A Disaster Imagination Game (DIG) is an easy and cost-effective participatory



mapping methodology invented in 1997 in Japan (Komura, 2002). The workshop can be very empowering at the community level corresponding to disaster risk reduction, since it enables an assessment based on people's perception of risks and coping strategies (Samaddar et al., 2011).

In this study, DIG workshop is conducted to obtain historical information of tsunami inundation. Participants that are representative for the workshop are people who have been living for at least 20 years in the area. According to the DIG guidance, the first step of the workshop is initial evaluation that is a self-evaluation. The evaluation sheet used for the activity is explained in Table 3.6, particularly in the "Evaluation" column. The organizer will be able to comprehend local community understanding of the disaster through the initial evaluation. The following step is introduction to theme of the workshop. The introduction is a lecture related to the disaster delivered by experts. A handout with instructions for players is also distributed in this step.

After the introduction of the theme, the work group can be conducted by dividing the participants into several groups. The work group results are then collected and analyzed by the participants in guidance of the organizers. The participants are then asked to present the results by using the created map. As the final step, final self-evaluation is carried out to assess the understanding of the participants after the workshop. The knowledge is supposed to be improved so that the created map is considerable risk assessment input.

### **3.6.6 Geospatial-Based Multi-Criteria Analysis**

Maps of groundwater conservation and tsunami inundation level are indicating risk assessment of water-related hazards of groundwater depletion and tsunami inundation, respectively. In the conceptual framework of Davidson, adopted by Bollin et al. (2003), risk is explained as the sum of hazard, exposure, vulnerability and capacity measures. Hazard is characterized by probability and severity; exposure elements are structures, population and economy; capacity and measures is concerned with physical planning, management, social and economic capacity. Moreover, a risk-hazard (RH) model introduced by Turner and Kasperson (2003) describes that the impact of a hazard is seen as a function of exposure of a system to the hazard event and the response of the system. Therefore, the mapping results describe level of vulnerabilities according to the risk-hazard assessment of several essential parameters.

In case of groundwater depletion, the parameters consist of groundwater level, groundwater usage, land subsidence, and land cover. Parameters for the tsunami inundation level mapping are spatial knowledge of tsunami inundation, local knowledge of tsunami inundation, land subsidence, and land cover. procedure of multi-criteria analysis using AHP consists of decompose the decision-making problem into hierarchy, make pair wise comparisons and establish priorities among the elements in the hierarchy, synthesize

judgments to obtain the set of overall or weights for achieving the goal, and evaluate and check the consistency of judgments.

According to the AHP procedure, the decision-making problem has to be decomposed into a hierarchy of criteria and alternatives. Figure 3.22 describes a hierarchy of criteria and alternatives that comprise four criteria and four alternatives. Level 1 is the goal of the analysis. Level 2 is multi-criteria that consist of several criterions. Several other levels of sub-criteria can also be added for the criteria. The last level is the alternative choices.

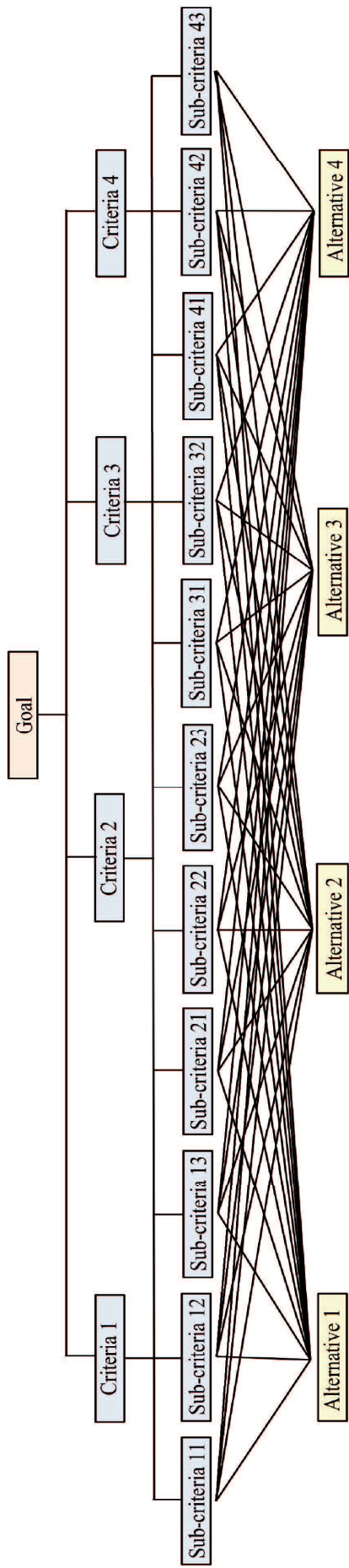


Figure 3.22 Hierarchy of criteria and alternatives

The following step is to make pair wise comparisons between each criteria. Results of the comparison (for each factors pairs) are described in term of integer values from 1 (equal value) to 9 (extreme different) where higher number means the chosen factor is considered more important in greater degree than other factor being compared with. In the pair wise comparison, the criteria in the row are being compared to the criteria in the column. After having a complete comparison matrix, the next step is to normalize the matrix. The normalization process is conducted by totaling the numbers in each column. Each entry in the column is then divided by the column sum to yield its normalized score. The sum of each column is 1.

Furthermore, the process is continued with the calculation of consistency ratio and checking the value. The purpose of conducting this step is to confirm that the original preference ratings were consistent. There are three steps to obtain the consistency ratio, i.e. calculate the consistency measure, calculate the consistency index (CI), and calculate the consistency ratio (CI/RI, where RI is a random index). The consistency measure can be calculated by taking the advantage of Excel's matrix multiplication function "`=MMULT()`".

The design and construction phases for a geospatial model in integration with AHP are described in Figure 3.23. Creation of spatial data are necessary to run a model in multi-criteria analysis. In this regard, Weighted Overlay tool is one of the most used approaches for overlay analysis to solve multi-criteria problems, such as site selection and suitability models. In a weighted overlay analysis, each of the general overlay analysis steps is followed. The tool combines several steps, i.e. reclassifies values in the input raster into a common evaluation scale of suitability or preference, risk, or some similarly unifying scale; multiplies the cell values of each input raster by the raster weight of importance; and adds the resulting cell values together to produce the output raster.

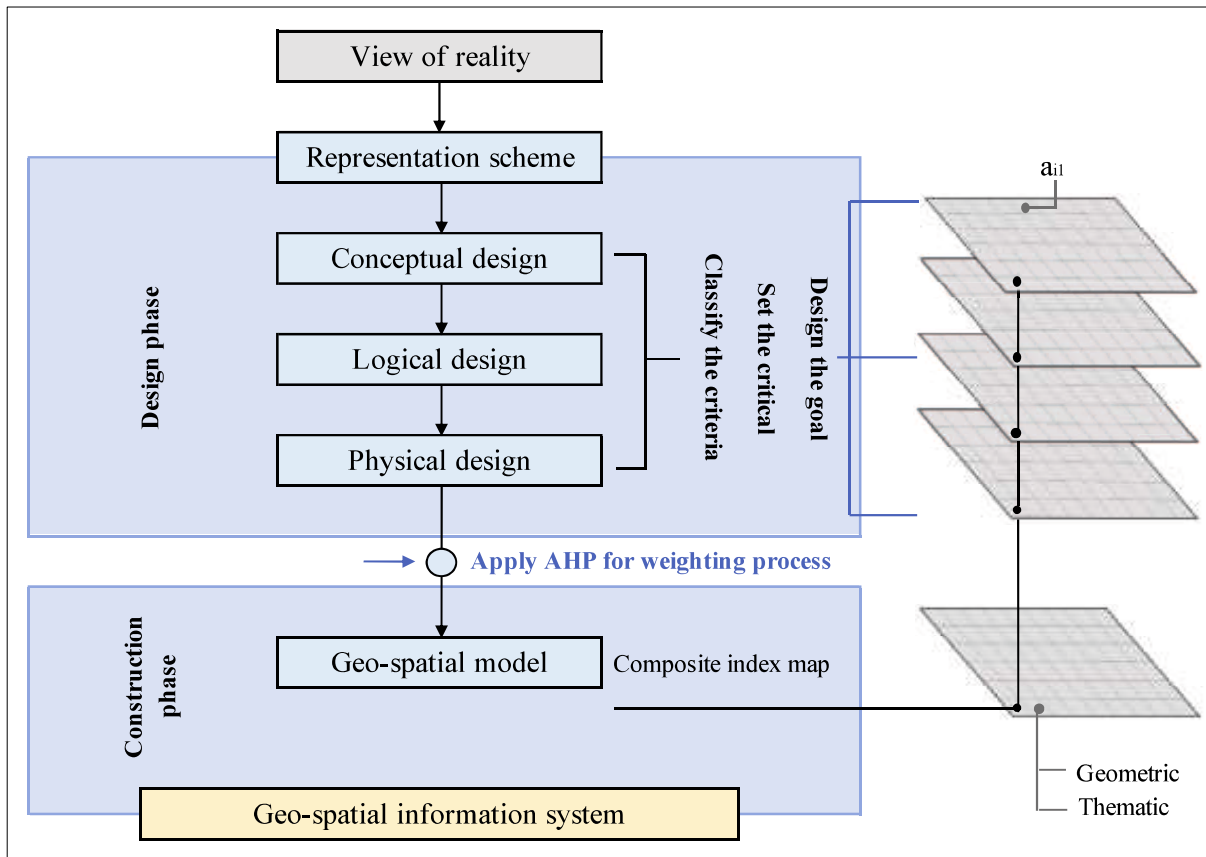


Figure 3.23 Design and construction phases for a geo-spatial model

### 3.6.7 Mapping Accuracy Assessment Using Confusion Matrix

In the field of machine learning and specifically the problem of statistical classification, a confusion matrix, also known as an error matrix (Stehman, 1997), is a specific table layout that allows visualization of the performance of an algorithm, typically a supervised learning one (in unsupervised learning it is usually called a matching matrix). Each row of the matrix represents the instances in a predicted class while each column represents the instances in an actual class (or vice versa) (Powers, 2011) The name stems from the fact that it makes it easy to see if the system is confusing two classes (i.e. commonly mislabeling one as another). It is a special kind of contingency table, with two dimensions (“actual” and “predicted”), and identical sets of "classes" in both dimensions (each combination of dimension and class is a variable in the contingency table).

If a classification system has been trained to distinguish between high, moderate and low risks due to hazard vulnerability in an area, a confusion matrix will summarize the results of testing the algorithm for further inspection. Assuming a sample of 27 points, i.e. eight high risks, six moderate risks, and 13 low risks, the resulting confusion matrix could look like Table 3.15.

Table 3.15 Example of confusion matrix of a classification result

		Actual class		
		High risk	Moderate risk	Low risks
Predicted class	High risk	5	2	0
	Moderate risk	3	3	2
	Low risk	0	1	<i>11</i>

In this confusion matrix, of the eight actual high risks, the system predicted that three were high risks, and of the six moderate risks, it predicted that one was a low risk and two were high risks. We can see from the matrix that the system in question has trouble distinguishing between high risk and moderate risk, but can make the distinction between low risk and other types of animals pretty well. All correct predictions are located in the diagonal of the table (highlighted in *italic*), so that it is easy to visually inspect the table for prediction errors, as they will be represented by values outside the diagonal.

In predictive analytics, a confusion matrix or table of confusion is a table with two rows and two columns that reports the number of *false positives*, *false negatives*, *true positives*, and *true negatives*. This allows more detailed analysis than mere proportion of correct classifications (accuracy). Accuracy is not a reliable metric for the real performance of a classifier because it will yield misleading results if the data set is unbalanced (that is, when the numbers of observations in different classes vary greatly).

For example, if there were 95 high risks and only 5 moderate risks in the data, a particular classifier might classify all the observations as high risk. The overall accuracy would be 95%, but in more detail the classifier would have a 100% recognition rate (sensitivity) for the cat class but a 0% recognition rate for the moderate risk class. F1 score is even more unreliable in such cases, and here would yield over 97.4%, whereas informedness removes such bias and yields 0 as the probability of an informed decision for any form of guessing (here always guessing high risk). Assuming the confusion matrix above, its corresponding table of confusion for the high-risk class is described in Table 3.16. The final table of confusion would contain the average values for all classes combined.

Table 3.16 Example of table of confusion for high risk class

		Actual class	
		High risk	Non-high risk
Predicted class	High risk	5 True positives	2 False positives
	Non-high risk	3 False negatives	17 True negatives

**CHAPTER IV**  
**RISK ASSESSMENT OF GROUNDWATER DEPLETION HAZARD ACCORDING**  
**TO GEOSPATIAL-BASED MULTI-CRITERIA ANALYSIS OF GROUNDWATER**  
**CONSERVATION MAP**

**4.1 Groundwater Conservation in Bali Island**

In accordance with Article 1, Government Regulation Number 43 of 2008 concerning groundwater, groundwater conservation is an effort to maintain the existence and sustainability of the condition, nature and function of groundwater so that it is always available in adequate quantity and quality to meet the needs of living things, both at the present and future. Groundwater conservation zones are presented in the form of classified maps (Article 24, paragraph 4):

1. Groundwater protection zone covering groundwater recharge area;
2. Groundwater utilization zone covering safe, vulnerable, critical, and damaged zones.

The preparation of groundwater conservation zones is carried out through several stages of activities, namely the activities of collecting, evaluating data and information as outlined in the form of groundwater conservation zone maps (DPU, 2014).

**1. Primary Data**

The collection of groundwater primary data is done through measurement, monitoring, investigation, and field research. Groundwater data primarily include:

- a. Groundwater;
- b. Drilling wells, peg wells, dug wells and springs;
- c. Total groundwater use;
- d. Groundwater quality;
- e. Groundwater pollution;
- f. Landfill area;
- g. Negative impacts of groundwater usage.

**2. Secondary Data**

Groundwater secondary data is obtained primarily through data collection from various related agencies including:

- a. Hydroclimatology data;
- b. Land use;
- c. Number and population growth;
- d. General spatial plan;
- e. Data on the need for water;
- f. Data on groundwater use;

- g. Horizontal and vertical limits of groundwater basins;
- h. Configuration and parameters of aquifer systems;
- i. Lithology section and well construction;
- j. Distribution of groundwater production wells, monitoring wells and springs;
- k. Aquifer test data and pumping test for dug wells, stake wells and boreholes;
- l. Groundwater surface, especially changes;
- m. Drilling wells, stake wells, dug wells and springs;
- n. Amount of groundwater usage;
- o. Groundwater quality, especially changes;
- p. Location and condition of groundwater recharge areas; q. Negative impacts due to groundwater use.

Water resources in the province of Bali are quite abundant (Table 4.1) consisting of ground water, river water, lakes/ reservoirs, and springs. Groundwater in groundwater basins (CAT) has a potential of around 1,598 million m<sup>3</sup>/year, river water has a potential of around 6,195 m<sup>3</sup>/year, lakes/ reservoirs have a potential of around 1,021 m<sup>3</sup>/year, and springs have a potential of around 913 m<sup>3</sup>/year (DPU Bali, 2014).

Table 4.1 Potency of freshwater resource in Bali Province

<b>Water resource</b>	<b>Potency (million m<sup>3</sup>/year)</b>
Groundwater	1,598
Surface water	6,195
Lake/reservoirs	1,021
Springs	913
Total	9,727

(Source: DPU Bali, 2014)

Utilization of these water resources for household, commercial (industrial, hotel, tourism, etc.), agriculture, and PDAM. The use of river water, lakes/ reservoirs and springs is mostly still for agricultural purposes. Whereas groundwater utilization is mostly for household, commercial purposes (industry, hotels, tourism, etc.). Besides that, ground water is also used for the needs of PDAMs as drinking water agency and agricultural needs for areas that are not irrigated by rivers or lakes/ reservoirs. At present, clean water services through PDAM in Bali Province only cover around 38%, so that around 62% of the community and commercial use of ground water for their clean water/ raw water needs. high dependence on ground water, so that the amount of groundwater extraction in Bali Province is currently around 134 million m<sup>3</sup>/year through 188 pantek wells and 441 drilled wells.

Based on the groundwater conservation map, it is known that the area of groundwater



basin is around 4,383.91 km<sup>2</sup> or around 77.77% of the area of Bali Province and the other area of about 22.23% is the area of non-groundwater basin. The area of groundwater recharge zones is around 2,142.53 km<sup>2</sup> (48.87% of the area of groundwater basin), safety zone of groundwater utilization covering 1,945.54 km<sup>2</sup> (44.38% of the area of groundwater basin), and critical zone for utilization of groundwater covering 295.84 km<sup>2</sup> (6.75% of groundwater basin area). Groundwater conservation zones in Bali Province are described in Table 4.2. Moreover, the modified map of groundwater conservation is shown in Figure 4.1.

Table 4.2 Groundwater conservation zones in Bali Province

Groundwater basin	Area (km <sup>2</sup> )	Conservation Zone					
		Recharge zone		Safety zone		Critical zone	
		km <sup>2</sup>	%	km <sup>2</sup>	%	km <sup>2</sup>	%
Denpasar-Tabanan	2,075.40	634.20	30.56	1,286.83		154.37	7.44
Singaraja	495.60	360.60	72.76	135.00	62.00	-	-
Gilimanuk	120.27	104.44	86.84	15.83	27.24	-	-
Negara	436.30	201.80	46.25	206.88	13.16	27.62	6.33
Tejakula	745.50	691.40	92.74	39.23	47.42	14.87	1.99
Amlapura	213.60	150.09	70.27	63.51	29.73	-	-
Nusapenida	198.25	-	-	198.25	100.00	-	-
Nusadua	98.99	-	-	-	-	98.99	100.00
<b>Total</b>	<b>4,383.91</b>	<b>2,142.53</b>	<b>48.87</b>	<b>1,945.54</b>	<b>44.38</b>	<b>295.84</b>	<b>6.75</b>

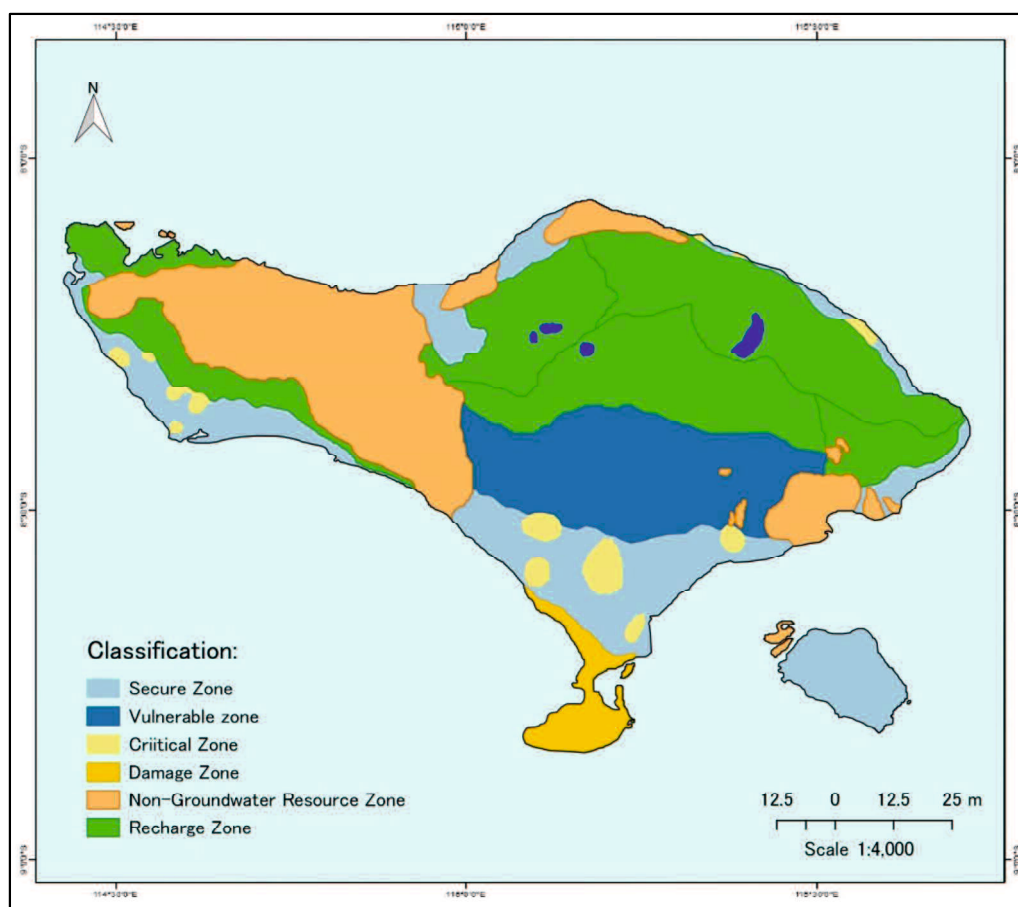


Figure 4.1 Modified Map of the Latest Groundwater Conservation Map of Bali in 2014

## **4.2 Monitoring of Groundwater Level and Groundwater Usage**

Report of groundwater level data measurement is provided by the Ministry of Mining and Natural Resource at eighteen monitoring wells available in the study area. A recent data was collected at the monitoring wells through field observation of groundwater level measurement by utilizing a water-level measurement tool as shown in Figure 4.2. The observation schedule conducted in 2017 is described in Table 4.3. Distribution of monitoring wells in Bali according to the boundary of the groundwater basin is described in Figure 4.3

Table 4.3 Field observation schedule of groundwater level measurement in Bali

Number of well	Monitoring well ID	Groundwater basin	Well location	Field observation schedule						
				2017/03/23	2017/03/24	2017/03/25	2017/03/26	2017/03/27	2017/03/29	2017/03/30
1	MW01-BD01	Denpasar-Tabanan	Wisma Bim Cottage II (Jalan Raya Kuta, Kuta, Badung)							
2	MW02-BD02		Dhyana Pura Hotel (Jalan Dhyana Pura, Kuta, Badung)							
3	MW03-BD03		Hospital (RSU) Kapal (Jalan Raya Kapal, Badung)							
4	MW04-BD04	Nusa Dua	BTDC Nusa Dua (Nusa Dua, Badung)							
5	MW05-BD05		Beraban (B) Villas (Kerobokan, Badung)							
6	MW06-DP01		Werdha Pura Hotel (Jalan Danau Tamblingan)							
7	MW07-DP02	Denpasar-Tabanan	Sport Center (GOR) Ngurah Rai (Jalan Melati, Denpasar)							
8	MW08-DP03		Grand Bali Beach (Jalan Hang Tuah, Sanur, Denpasar)							
9	MW09-DP04		Office of UPT Balai Pengujian, Dinas PU Ubung, Denpasar							
10	MW10-GR01		Cahaya Dewata Hotel (Jalan Raya Kedewatan, Ubud, Gianyar)							
11	MW11-GR02		Arma Museum (Pengosekan, Ubud Gianyar)							
12	MW12-BL01	Singaraja	Banyu Alit Inn (Jalan Pantai Lovina, Kalibukbuk, Buleleng)							
13	MW13-BL02	Tejakula	Tembok Villa & SPA (Tejakula, Buleleng)							
14	MW14-JB01	Negara	Regent's Office (Kantor Bupati) Park (Jalan Denpasar-Gilimanuk)							
15	MW15-JB02		Bale Tempek/ TK (Desa Tegal Badeng, Jembrana)							
16	MW16-TB01	Denpasar-Tabanan	Bali Nirwana Resort (BNR) (Kediri, Tabanan)							
17	MW17-TB02	Tabanan	Local Water Agency (PDAM) Office of Tabanan (Kediri, Tabanan)							
18	MW18-KR01	Amlapura	Sub-District Office (Kantor Camat) of Manggis (Karangasem)							



Figure 4.2 Documentation of groundwater level measurement using water level in Bali Island

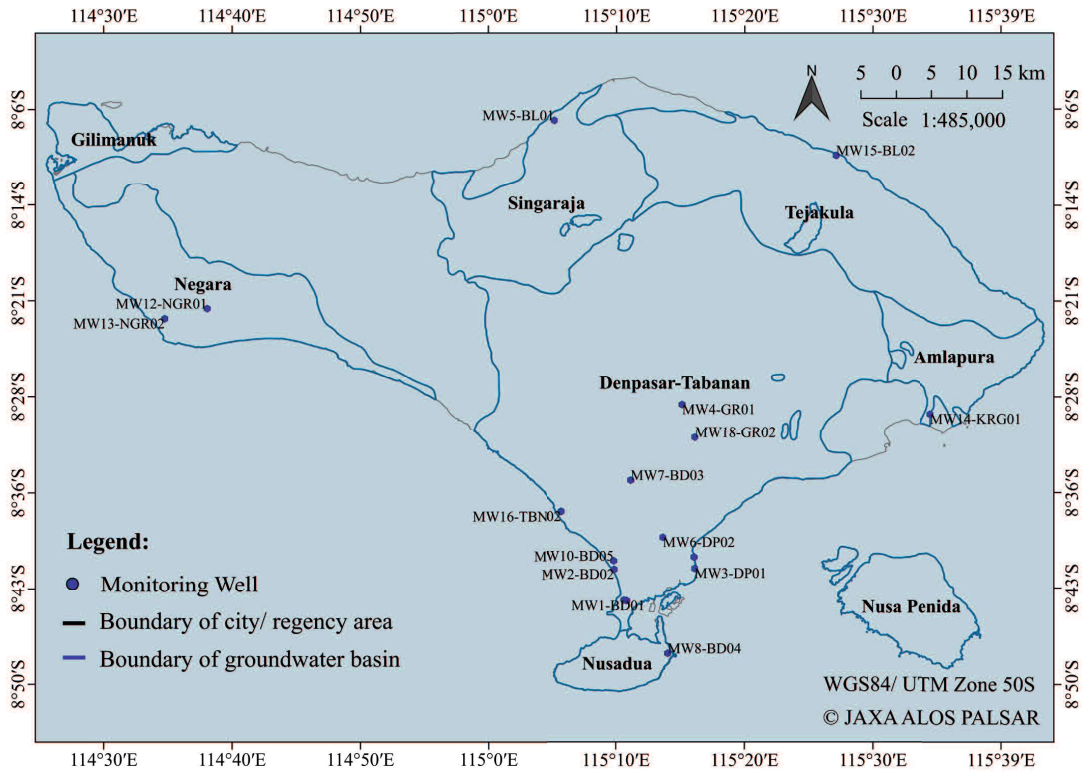


Figure 4.3 Distribution of monitoring wells in Bali area

Data of the collected groundwater level is described in Table 4.3. The collected data are analyzed to estimate groundwater level change data. Analysis result of the groundwater depletion is explained in Table 4.4. The groundwater level changes that signify depletion was further classified into three conditions, i.e. groundwater depletion below 10%, 10% - 25%, and above 25%. Figure 4.4 describes the groundwater depletion in Bali from 2008 to 2012 and 2017.

Table 4.4 Groundwater level data in Bali area from 2008 to 2012 and 2017

Number of well	Monitoring well ID	Built year	Groundwater level below the ground surface (m)						
			2008*	2009*	2010*	2011*	2012*	2013*	2017**
1	MW01-BD01	1996	6.25	6.40	6.00	6.35	6.50	6.00	6.10
2	MW02-BD02	1997	6.30	6.86	6.70	6.80	7.82	6.35	7.74
3	MW03-BD03	2002	2.15	2.20	1.75	1.84	3.01	3.50	1.63
4	MW04-BD04	2003	3.60	3.80	4.05	4.38	3.78	3.70	4.58
5	MW05-BD05	2004	15.75	16.57	16.20	16.75	15.05	18.20	17.66
6	MW06-DP01	1997	2.85	2.67	3.25	3.37	3.87	3.20	3.18
7	MW07-DP02	2001	8.45	8.45	6.25	6.38	8.45	7.00	6.30
8	MW08-DP03	2004	2.55	2.66	3.16	3.25	2.85	3.20	3.63
9	MW09-DP04	2008	6.25	6.25	9.01	9.21	7.69	8.70	10.39
10	MW10-GR01	1998	39.15	39.40	39.15	39.40	40.08	39.30	39.20
11	MW11-GR02	2009	7.85	7.85	7.85	7.85	7.16	12.10	12.00
12	MW12-BL01	1998	0.55	0.55	0.50	0.58	0.75	0.50	0.48
13	MW13-BL02	2007	7.35	7.10	6.75	7.00	7.66	7.12	7.08
14	MW14-JB01	2006	10.35	10.27	9.82	9.95	10.74	9.50	9.44
15	MW15-JB02	2006	17.26	17.50	17.20	16.00	16.83	16.00	17.53
16	MW16-TB01	2005	8.47	8.55	7.85	7.90	8.26	8.00	8.20
17	MW17-TB02	2008	7.82	7.82	8.25	8.34	7.87	8.50	8.55
18	MW18-KR01	2007	4.68	6.87	4.25	7.60	4.82	7.25	7.32

(Source: \*ESDM of Bali Province, 2014; \*\*Field observation in 2017)

Table 4.5 Groundwater depletion in Bali area from 2008 to 2012 and 2017

Number of well	Monitoring well ID	Groundwater depletion (%)						Average groundwater depletion (%)
		2008 -2009	2009 - 2010	2010 - 2011	2011 - 2012	2012 - 2013	2013 - 2017	
1	MW01-BD01	2.40%	-6.25%	5.83%	2.36%	-7.69%	1.67%	-0.48%
2	MW02-BD02	8.89%	-2.33%	1.49%	15.00%	-18.80%	21.89%	7.47%
3	MW03-BD03	2.33%	-20.45%	5.14%	63.59%	16.28%	-53.57%	3.80%
4	MW04-BD04	5.56%	6.58%	8.15%	-13.70%	-2.12%	23.65%	8.03%
5	MW05-BD05	5.21%	-2.23%	3.40%	-10.15%	20.93%	-2.99%	4.04%
6	MW06-DP01	-6.32%	21.72%	3.69%	14.84%	-17.31%	-0.63%	4.57%
7	MW08-DP03	4.31%	18.80%	2.85%	-12.31%	12.28%	13.44%	11.25%
8	MW09-DP04	0.00%	44.16%	2.22%	-16.50%	13.13%	19.43%	17.84%
9	MW12-BL01	0.00%	-9.09%	16.00%	29.31%	-33.33%	-5.00%	-0.60%
10	MW14-JB01	-0.77%	-4.38%	1.32%	7.94%	-11.55%	-0.68%	-2.32%
11	MW15-JB02	1.39%	-1.71%	-6.98%	5.19%	-4.93%	9.56%	0.72%
12	MW18-KR01	46.79%	-38.14%	78.82%	-36.58%	50.41%	0.97%	29.22%
13	MW07-DP02	0.00%	-26.04%	2.08%	32.45%	-17.16%	-10.00%	-5.33%
14	MW10-GR01	0.64%	-0.63%	0.64%	1.73%	-1.95%	-0.25%	0.05%
15	MW11-GR02	0.00%	0.00%	0.00%	-8.79%	68.99%	-0.83%	16.97%
16	MW13-BL02	-3.40%	-4.93%	3.70%	9.43%	-7.05%	-0.56%	-0.80%
17	MW16-TB01	0.94%	-8.19%	0.64%	4.56%	-3.15%	2.50%	-0.77%
18	MW17-TB02	0.00%	5.50%	1.09%	-5.64%	8.01%	0.59%	2.73%

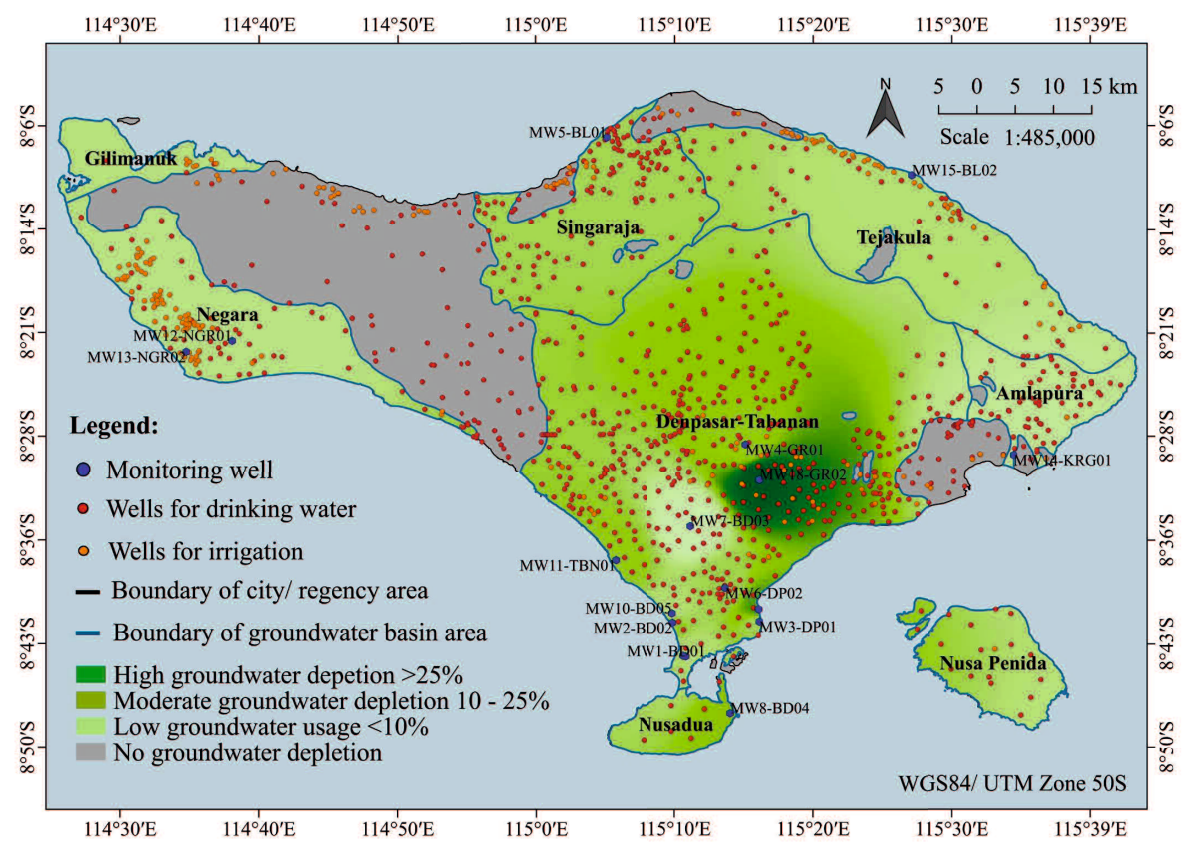
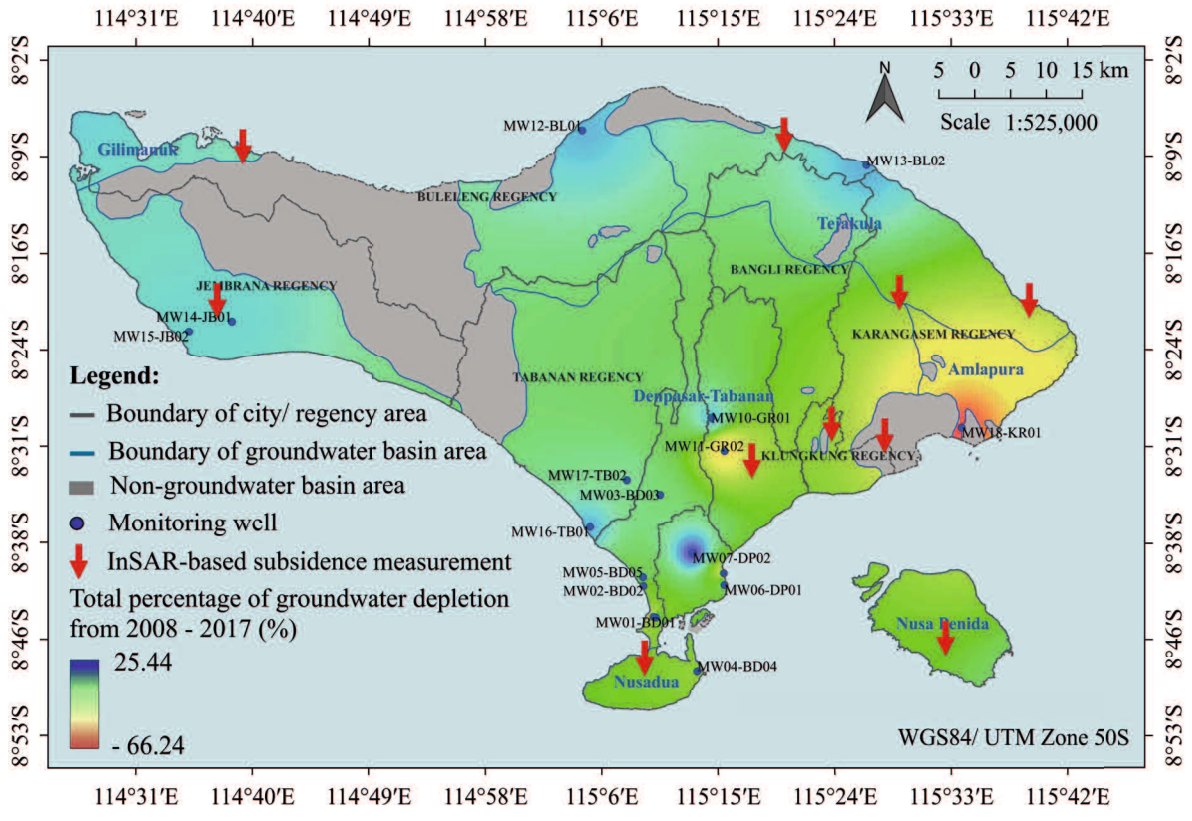


Figure 4.4 Groundwater depletion map in Bali area

The groundwater usage data is provided by several agencies, i.e. Drinking Water Agency, River Basin Agency of Bali-Penida, and Ministry of Public Works. There is no exact information of the groundwater usage. In case of wells for drinking water supply, the information consists of location, capacity, and the percentage of water supply using the wells. Data for the irrigation wells comprise of location and capacity. The data was analyzed to estimate groundwater usage and mapped through spatial mapping to produce a map of groundwater usage representing high, medium, and low water usage.

The field observation of the wells location is conducted in 2017 (Figure 4.5). The observation was conducted in three different period, i.e. March 23<sup>rd</sup> to 30<sup>th</sup>, 2017; October 30<sup>th</sup> to November 12<sup>th</sup>, 2017; and January 13<sup>th</sup> to 30<sup>th</sup>, 2018. Schedule of the well check observation is described in Table 4.6. The coordinate of wells based on the secondary data were collected to confirm the distribution and function of the wells. The collected information was further used to map wells distribution and calculate the usage of the wells based on the function, i.e. drinking water or irrigation. Moreover, Figure 4.6 describes groundwater level depletion based on secondary data of groundwater level and observation data in 2017.



Figure 4.5 Field observation documentation of wells location check

Table 4.6 Schedule of well check observation in Bali area

Reported well data	Number of well	Field observation schedule		
		2017/03/23 - 2017/03/30	2017/10/30 - 2017/11/12	2018/01/13 - 2018/01/30
DPU in Bali Province	351 wells			
River Basin Agency of Bali-Penida (BWS-BP)	365 wells			
Regional DPU and Drinking Water Agency (PDAM) in Denpasar City	15 wells			
Regional DPU and PDAM in Badung Regency	10 wells			
Regional DPU and PDAM in Bangli Regency	13 wells			
Regional DPU and PDAM in Buleleng Regency	95 wells			
Regional DPU and PDAM in Gianyar Regency	25 wells			
Regional DPU and PDAM in Jembrana Regency	111 wells			
Regional DPU and PDAM in Klungkung Regency	14 wells			
Regional DPU and PDAM in Karangasem Regency	76 wells			
Regional DPU and PDAM in Tabanan Regency	21 wells			

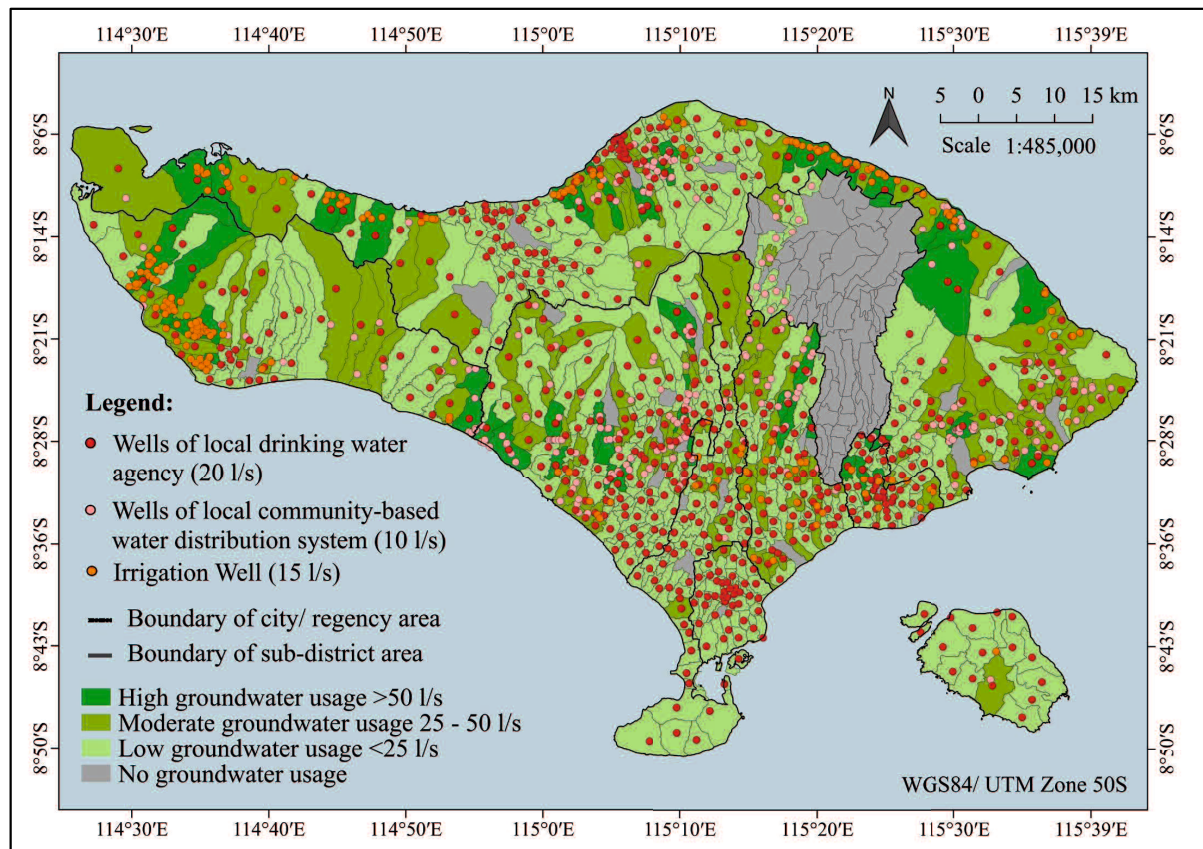


Figure 4.6 Groundwater usage map in Bali area

### 4.3 Land Subsidence Related to Groundwater Level Depletion

The land subsidence information was mainly based on the result of time series InSAR processing. The generated downlift vertical displacement is proportional to subsidence, so that the value is used to represent land subsidence. Moreover, the horizontal displacement is considered equal to zero. Evaluation of the result was conducted using RTK GNSS measurement. Furthermore, an intergrated analysis of land subsidence and groundwater level data was carried out to estimate groundwater level with higher temporal resolution.

#### 4.3.1 Application of Time Series InSAR Processing for Measuring Land Subsidence

Synthetic Aperture Radar (SAR), a microwave imaging system, uses a radar antenna mounted on an airborne or satellite-based platform to transmit and receive electromagnetic (EM) waves. In general, interferometric SAR (InSAR) processing techniques combine two SAR scenes that acquired at different times in the same area. The process of calculating the difference in the phase component ( $\Delta\phi$ ) of the reflected signals is known as radar interferometry, and the image of  $\Delta\phi$  for all pixels is known as an interferogram. Data used for the interferometry process are collected along the line-of-sight (LOS) direction, from the antenna to Earth's surface. The angle between the LOS and the normal to Earth's surface is determined as the look angle (Zebker et al., 1994). A schematic of the phase change



associated with the land subsidence modified from Chen and Zebker (2002) is outlined in Figure 4.7.

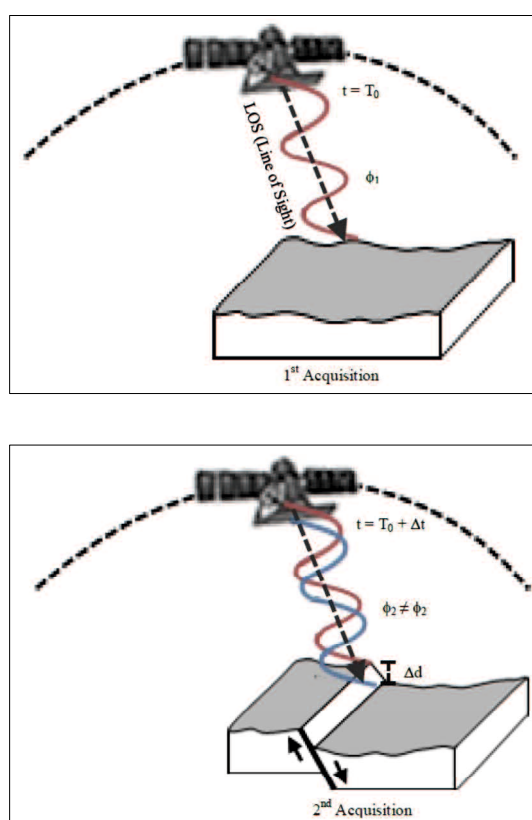


Figure 4.7 Schematic of the phase change of the EM wave associated with the land subsidence

An accurate measure of the change in the elevation of the land surface can be extracted through the processing if the effects to topography are removed. In order to increase the signal-to-noise ratio of the observed interferometric phase, pixels are often spatially averaged to correspond to a 50 m by 50 m resolution cell. In this regard,  $\Delta\phi$  can only be obtained within radian due to the cyclic nature of phase which is called wrapped phase. Furthermore, the estimation and summation of the unknown correct integer multiple of  $2\pi t_0$   $\Delta\phi$  is called phase unwrapping (Chen and Zebker, 2002).

The estimated difference in the phase of the two signals  $\Delta\phi$  is the summation of six parts (Zebker et al., 1994; Ferretti et al., 2000):

$$\Delta\phi = \Delta\phi_{def} + \Delta\phi_{topo} + \Delta\phi_{orb} + \Delta\phi_{ip} + \Delta\phi_{atm} + \Delta\phi_n \quad (\text{Equation 4.1})$$

Where  $\Delta\phi_{def}$  is the phase change due to the deformation of the ground surface,  $\Delta\phi_{topo}$  is the phase change due to topography,  $\Delta\phi_{ip}$  is the phase change due to integer phase ambiguities,  $\Delta\phi_{orb}$  is the phase change due to orbital errors,  $\Delta\phi_{atm}$  is the phase change due to atmospheric phase effects, and  $\Delta\phi_n$  is the phase change due to random phase noise. In this study, the phase

change is due to the deformation of the ground surface. Therefore  $\Delta\phi_{def}$  is related to the deformation ( $\Delta d$ ) by:

$$\Delta\phi_{def} = \frac{2\pi}{\lambda} (2\Delta d) = \frac{4\pi}{\lambda} \Delta d \quad (\text{Equation 4.2})$$

Where  $\lambda$  is the wavelength of the radar system. The noise components  $\Delta\phi_{topo}$  and  $\Delta\phi_{orb}$  must be eliminated. Moreover, the noise components  $\Delta\phi_{ip}$ ,  $\Delta\phi_{atm}$ , and  $\Delta\phi_n$  must be mitigated in order to accurately calculate  $\Delta\phi_{def}$ .

The scheme of time series InSAR in the study is shown in Figure 4.8.

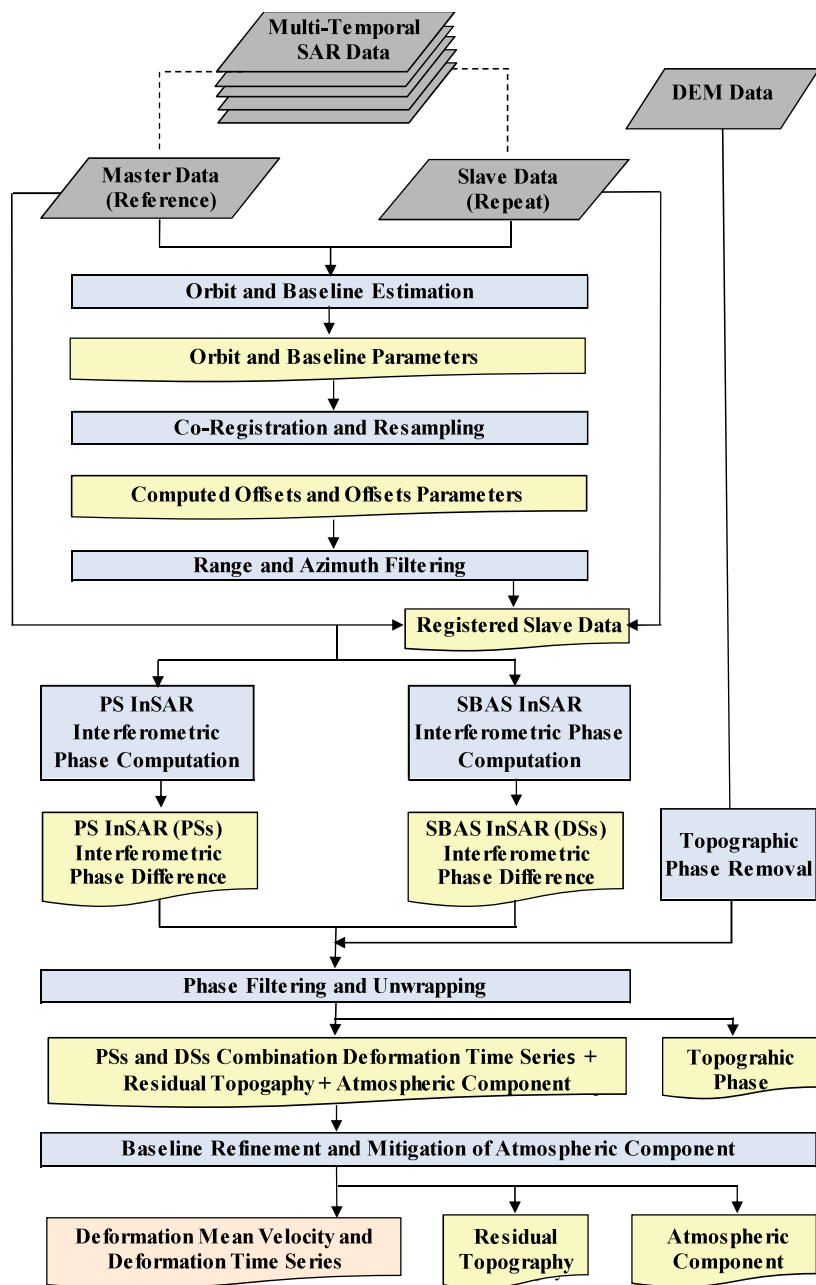


Figure 4.8 Land subsidence estimation by combining time series InSAR and GNSS-CORS measurements in Bali Island

Advanced time-series InSAR has been developed to overcome some of the limitations of conventional InSAR. The techniques use multi-temporal imageries to remove the atmospheric effects by stacking various interferograms. The most common technique to derive PSs is PS-InSAR (Crosetto et al, 2016; Ferretti et al, 2001; Kampes, 2005; Hooper et al, 2004). Moreover, one of the most common techniques to derive DSs is SBAS (Van der Kooij et al, 2006; Berardino et al, 2002). These methods allow millimeter precision in deformation mapping (Bouraoui, 2013). The time series InSAR methods of PS and SBAS are combined in this study, as described in Figure 4.8, to obtain deformation both in urban and agricultural regions.

The characteristics of stacking or multi-temporal or time-series InSAR technique of PS and SBAS used in the study are presented in Table 4.7. The PS algorithms are able to resolve double scatterers inside a resolution cell. Moreover, the SBAS method exploits only small temporal and spatial baseline to unwrap differential interferograms, to limit the effects of uncompensated geometric decorrelation and temporal decorrelation on the DSs.

Table 4.7 Characteristics of time-series InSAR technique of PS and SBAS

<b>Methods</b>	<b>Baseline configuration</b>	<b>Pixel Selection Criterion</b>	<b>Deformation Mode</b>
PS*	Single master	Amplitude dispersion	Linear deformation in time
SBAS**	Small baseline	Coherence	Spatial smoothness

(Source: \*Crosetto et al, 2016; Ferretti et al, 2001; Kampes, 2005; Hooper et al, 2004; \*\* Van der Kooij et al, 2006; Berardino et al, 2002)

An integrated monitoring of the land deformation and groundwater is crucial for the sustainability of water supplies, especially in the small island developing areas such as Bali. In this study, the L-band ALOS PALSAR along with Sentinel 1-A SAR data, acquired between February 2007 and January 2017, were utilised for the analysis. The dataset for the analysis consists of 63 scenes of L-band ALOS PALSAR acquired between February 2007 to December 2010 and 21 scenes of C-band Sentinel 1A over the Bali Island acquired from October 2014 to January 2017 from Alaska Satellite Facility. The data processing of all of the SAR scenes was conducted using InSAR processing system of GMTSAR. SAR data of ALOS PALSAR and Sentinel-1A in Bali Island is outlined in Figure 4.9.

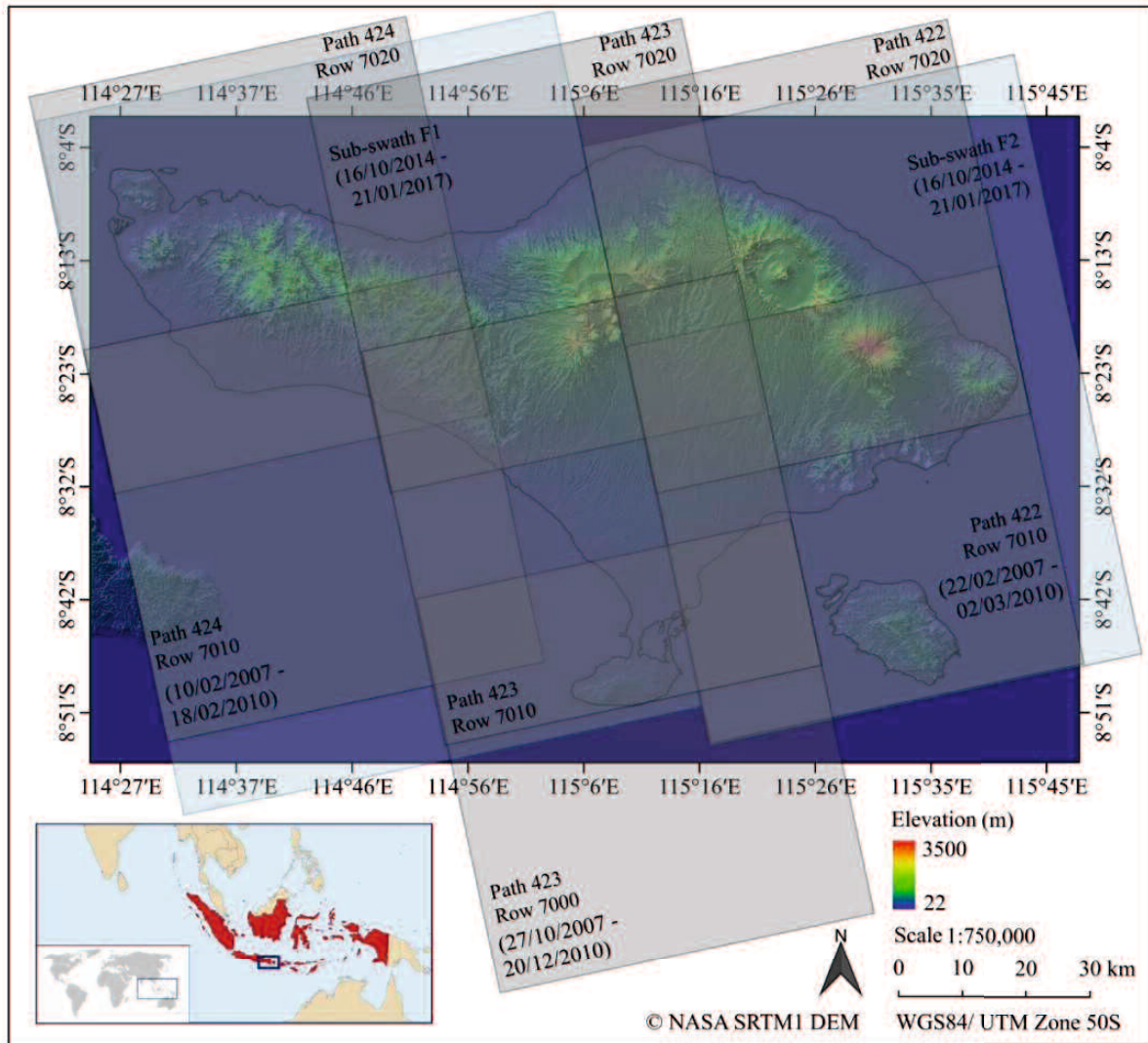


Figure 4.9 SAR Data of ALOS PALSAR and Sentinel-1A in Bali Island

The ALOS PALSAR and Sentinel-1A data was utilized to analyze time-series land deformation for from 2007 to 2017. The ALOS PALSAR data consist of 63 scenes with nine scenes for every path. Sentinel-1A data comprises two sub-swaths cover the entire study area. Scenes located at the same path were acquired at the same date. Scenes represent the same path were merged and processed for extracting the displacement information. The entire data were processed with GMT5SAR processing through several functions, i.e. preprocess, focus, align, pairs selection, interfere, filter or SNAPHU, geocode, and layer stacking (Sandwell et al, 2008). In particular, the PS and SBAS interferogram pairs process were processed based on coherence-based time-series analysis. The final results were displacement and the rate of displacement. Processing parameters for ALOS PALSAR are described in Table 4.8.

Table 4.8 InSAR processing parameters for ALOS PALSAR and Sentinel-1A

Process	Parameter	Value	
		ALOS PALSAR	Sentinel-1A
Pairs selection for SBAS	Perpendicular baseline	1000	100
	Temporal baseline	2500	250
Interfere and filter	Method	Gauss 300	Gauss 300
Land mask	Perform land mask	1	1
Unwrapped	Threshold	0.45	0.45
Geocode	Threshold	0.45	0.45
SBAS	Smoothing factor	1	1
	Wavelength	0.2362 m	0.055 m
	Incidence angle	34.3 degree	30 degree
	Range	850014 - 848965	6377598
	Atmospheric correction	1	1

The threshold value for the unwrapping was determined based on the coherence value of the SAR data. Both ALOS PALSAR and Sentinel-1A signified similar distribution of coherence values which can be obtained from the correlation image result of GMTSAR InSAR processing. The brighter the color (Figure 4.10) indicates the higher coherence values. In the area of Bali, high coherence can be inferred from built-up area. In general, the threshold value in ranging between 0.3 to 0.6. In this area, the value of 0.45 was determined to be able to detect surface movement in agricultural areas such as paddy field. Considering that the area development is also involving agricultural sector that mainly utilized groundwater as water resource.

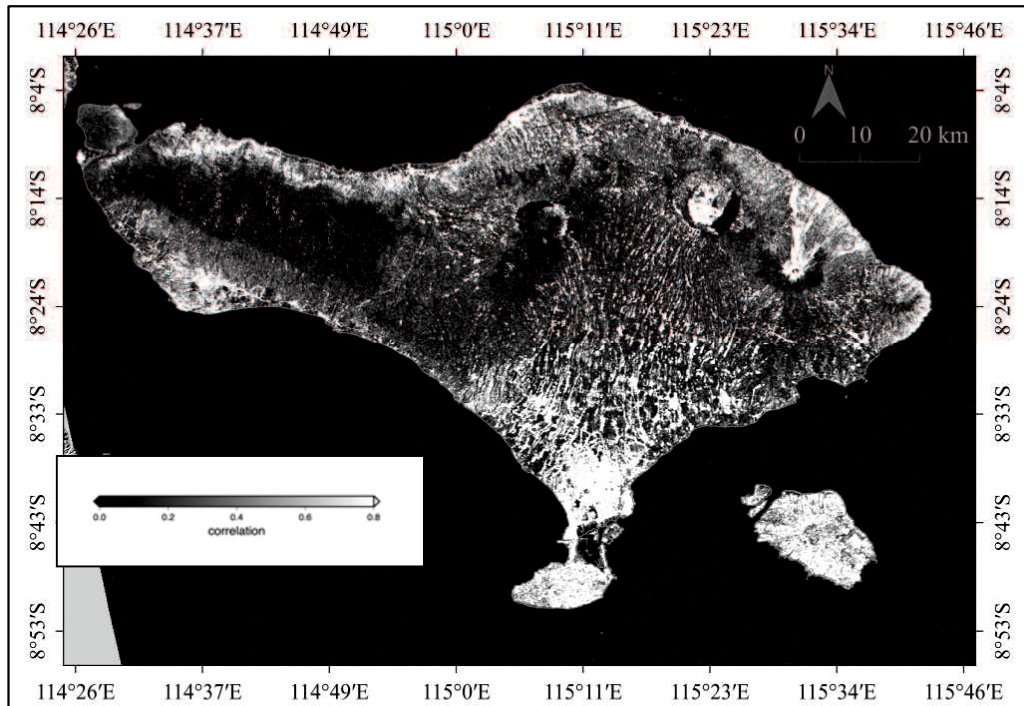


Figure 4.10 Coherence map in Bali Island

1. Displacement from 2007 to 2010

List of ALOS PALSAR data used in this study are described in Table 4.9. The satellite SAR data of ALOS PALSAR are Fine Beam Single Polarization (FBS) mode as described in Chapter III. The entire study area is formed by seven track acquisitions of ALOS PALSAR with a different path and raw. There are three different paths, i.e., 422, 423, and 424 (Figure 4.9). The first and second paths consist of two different rows, and the second path comprises of three different rows. Therefore, there were 63 scenes of ALOS PALSAR used to cover analysis throughout the study area.

Table 4.9 List of ALOS PALSAR data covering the entire study area in Bali

Path	Scene ID	Acquisition Date	Number of Days	Perpendicular Baseline (m)		
				Row 7000	Row 7010	Row 7020
422	05740	2007/02/22	417	-	(Super Master)	(Super Master)
	09766	2007/11/25	693	-	-280.159414	-261.965355
	11108	2008/02/25	785	-	-566.082561	-535.276776
	11779	2008/04/10	831	-	-579.321254	-543.448521
	15134	2008/11/27	1061	-	622.995138	597.259933
	16476	2009/02/27	1152	-	120.871632	107.375214
	20502	2009/11/30	1428	-	25.964374	29.963401
	21173	2010/01/15	1474	-	-208.649298	-199.001696
	21844	2010/03/02	1520	-	-247.445740	-230.944792
423	09343	2007/10/27	664	(Super Master)	(Super Master)	(Super Master)
	10014	2007/12/12	710	-273.874062	-271.096790	-268.912134
	10685	2008/01/27	756	-481.596607	-472.345306	-463.616308
	14711	2008/10/29	1032	769.627863	725.057614	680.827274
	15382	2008/12/14	1078	731.639111	691.291677	651.456039
	16053	2009/01/29	1123	426.681992	392.503573	358.437429
	20079	2009/11/01	1399	102.974247	87.717368	72.147166
	21421	2010/02/01	1491	-62.176939	-66.447985	-71.035465
	26118	2010/12/20	1813	-961.917072	-943.428413	-926.045642
424	05565	2007/02/10	405	-	(Super Master)	(Super Master)
	09591	2007/11/13	681	-	-154.443018	-133.910388
	11604	2008/03/30	819	-	-992.090931	-955.833850
	14959	2008/11/15	1049	-	838.266848	814.378031
	15630	2008/12/31	1095	-	279.200032	259.936381
	16301	2009/02/15	1140	-	279.200032	442.624606
	20327	2009/11/18	1416	-	-75.758321	-70.677559
	20998	2010/01/03	1462	-	-181.412780	-170.711935
	21669	2010/02/18	1508	-	-300.679701	-283.339000

Besides SAR data, 1 scene of Shuttle Radar Topography Mission (SRTM) Digital Elevation Model (DEM) data covering the entire study area is is utilized for topographic phase removal in interferometry processing. Taking a large baseline due to a long wavelength of ALOS PALSAR data, the SBAS was carried out using perpendicular baseline of 1000 and temporal baseline is limited to 2500 days. In case of PS processing, one scene was selected as super master to generate interferograms with the other scenes (Sandwell et al, 2008) for each track of ALOS PALSAR. A super master was selected with criteria able to minimize baseline with the others scenes (Rosenqvist et al, 2014). Pairs of interferograms in path 422, 423, and 424 (Figure 4.11 to Figure 4.17) were plotted as lines on the scatter chart of perpendicular and temporal baselines.

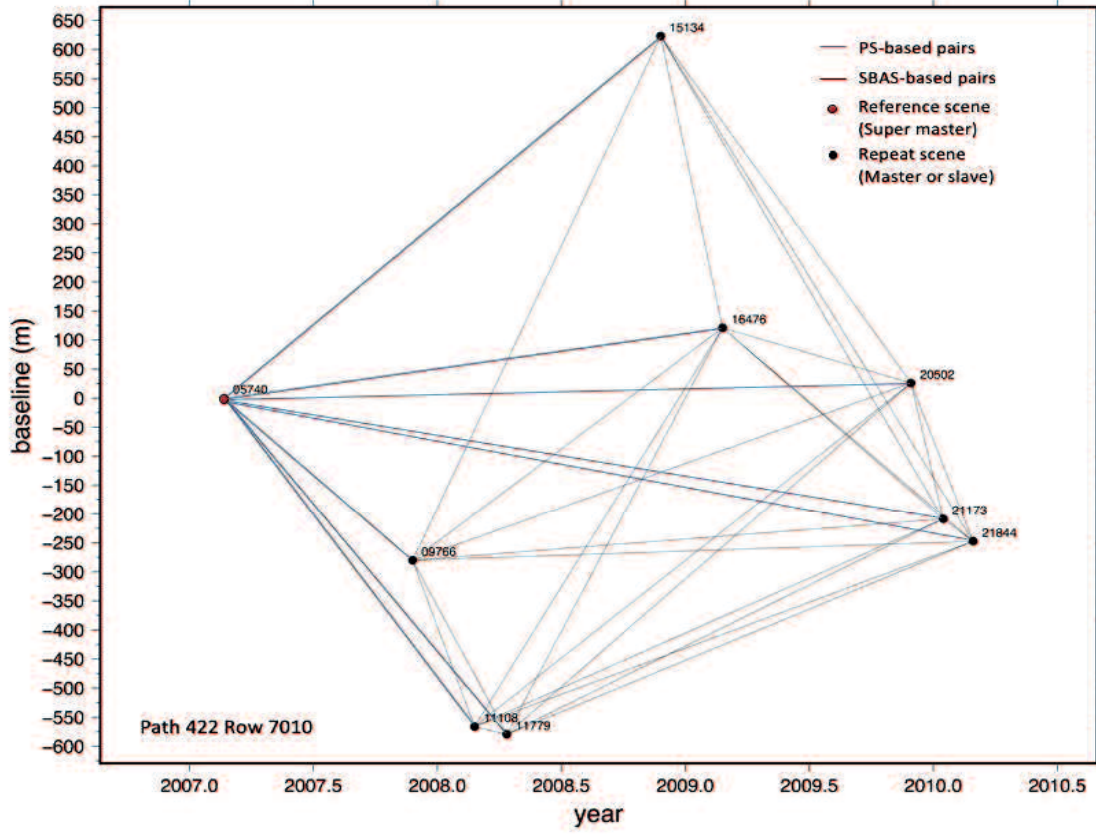


Figure 4.11 Pair selection of ALOS PALSAR for path 422 row 7010

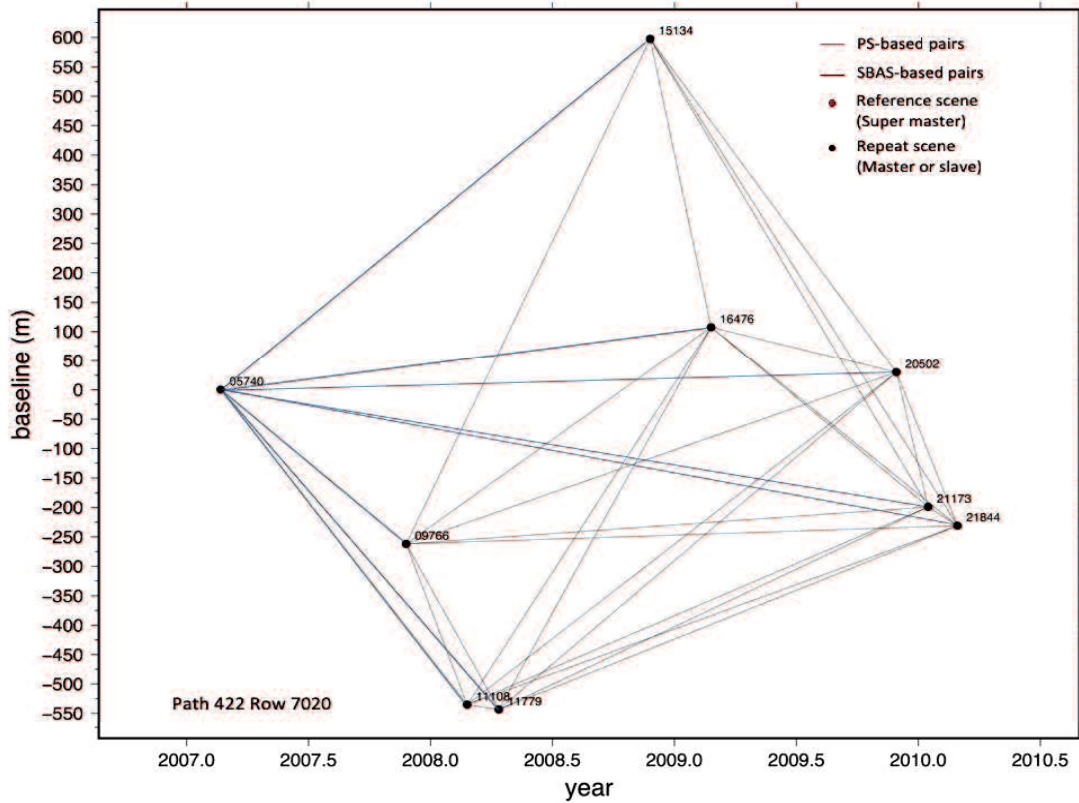


Figure 4.12 Pair selection of ALOS PALSAR for path 422 row 7020



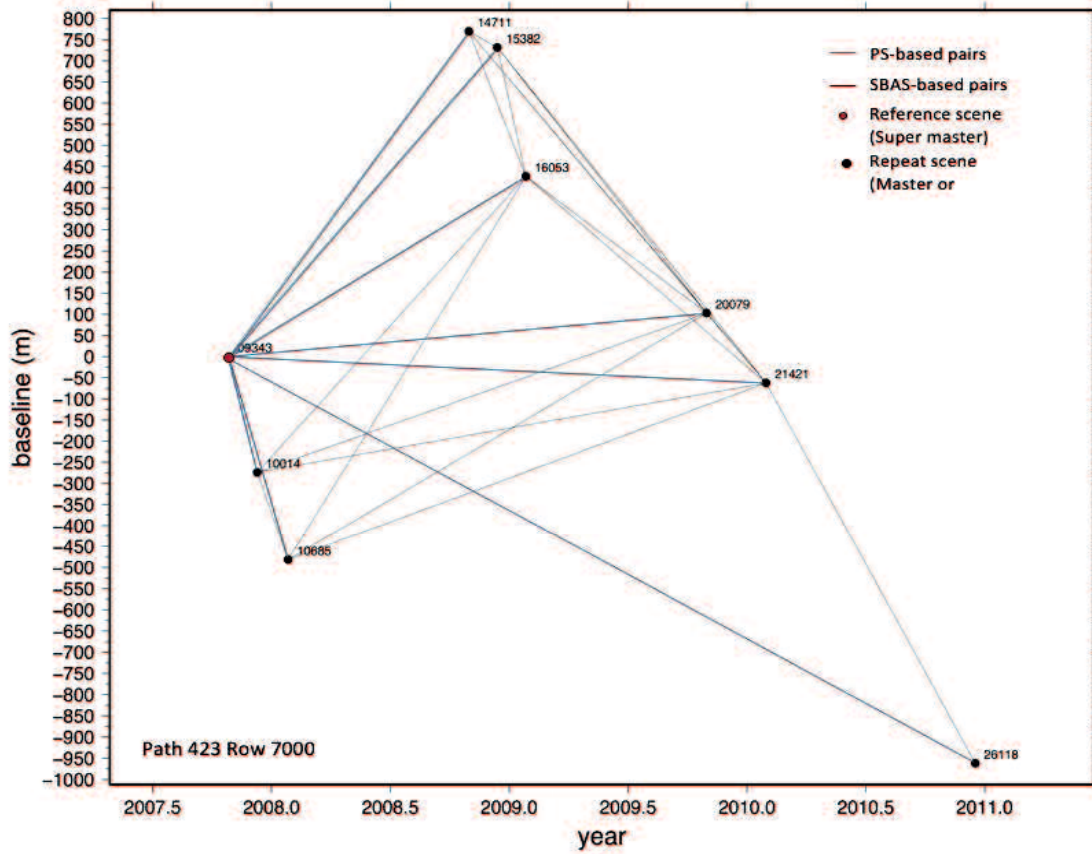


Figure 4.13 Pair selection of ALOS PALSAR for path 423 row 7000

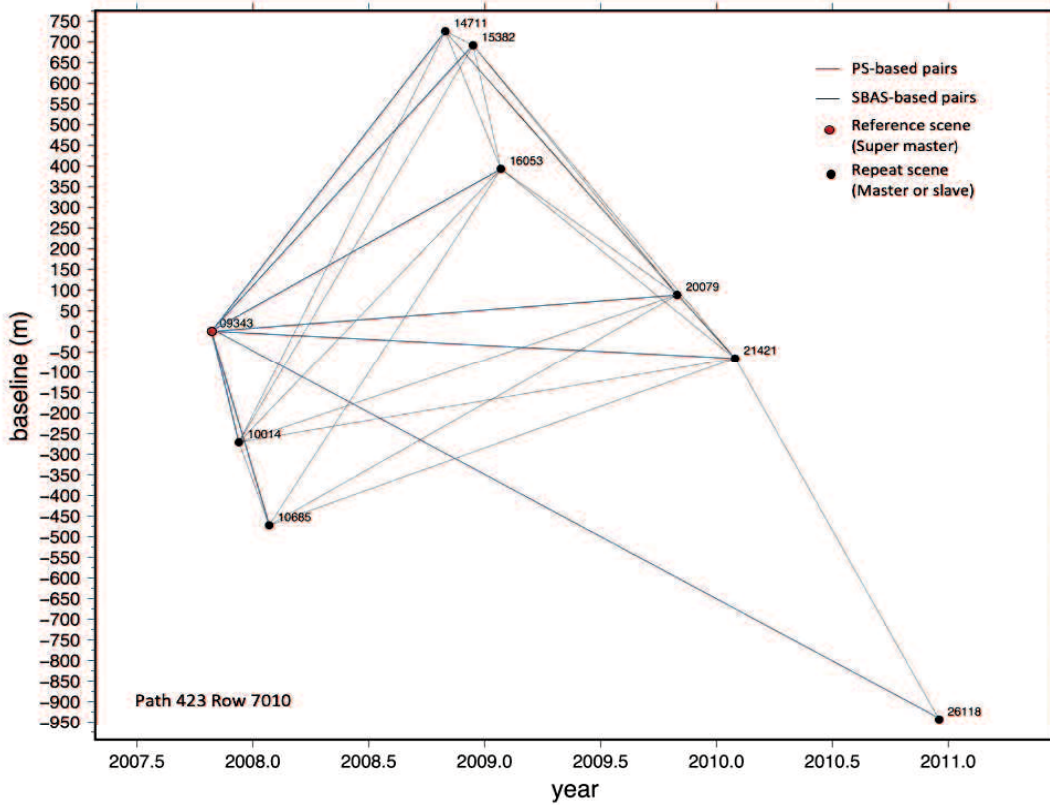


Figure 4.14 Pair selection of ALOS PALSAR for path 423 row 7010

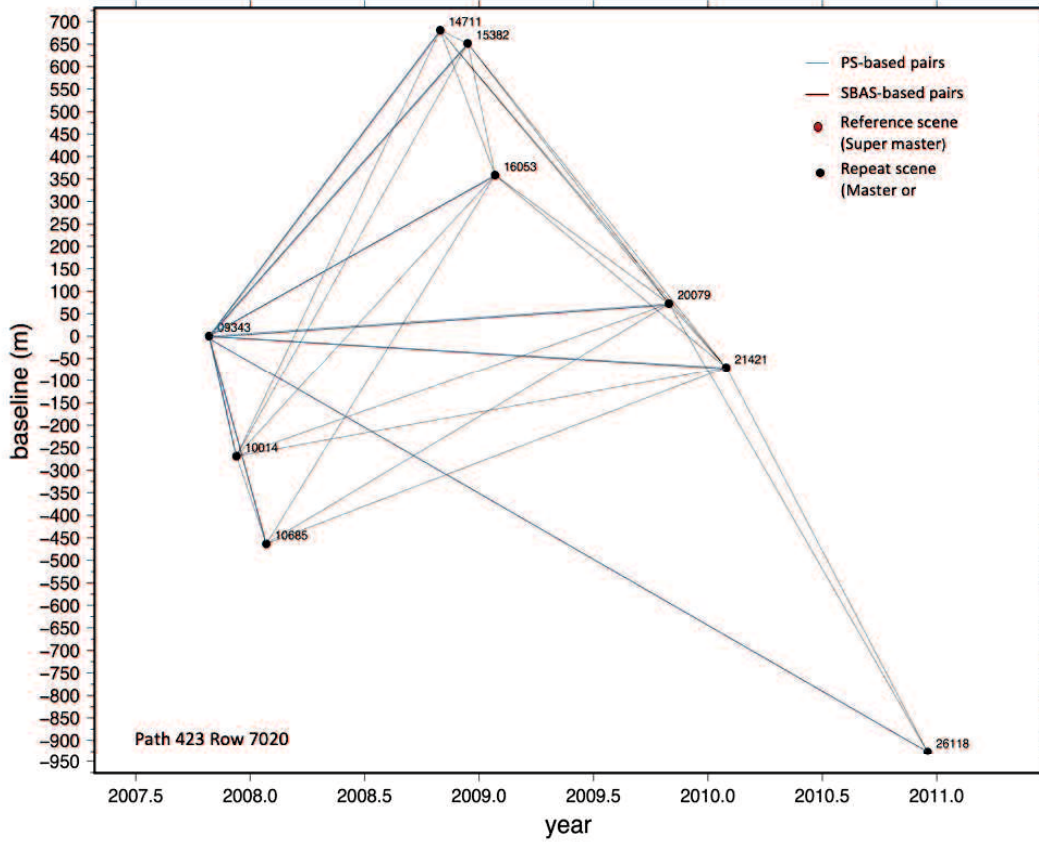


Figure 4.15 Pair selection of ALOS PALSAR for path 423 row 7020

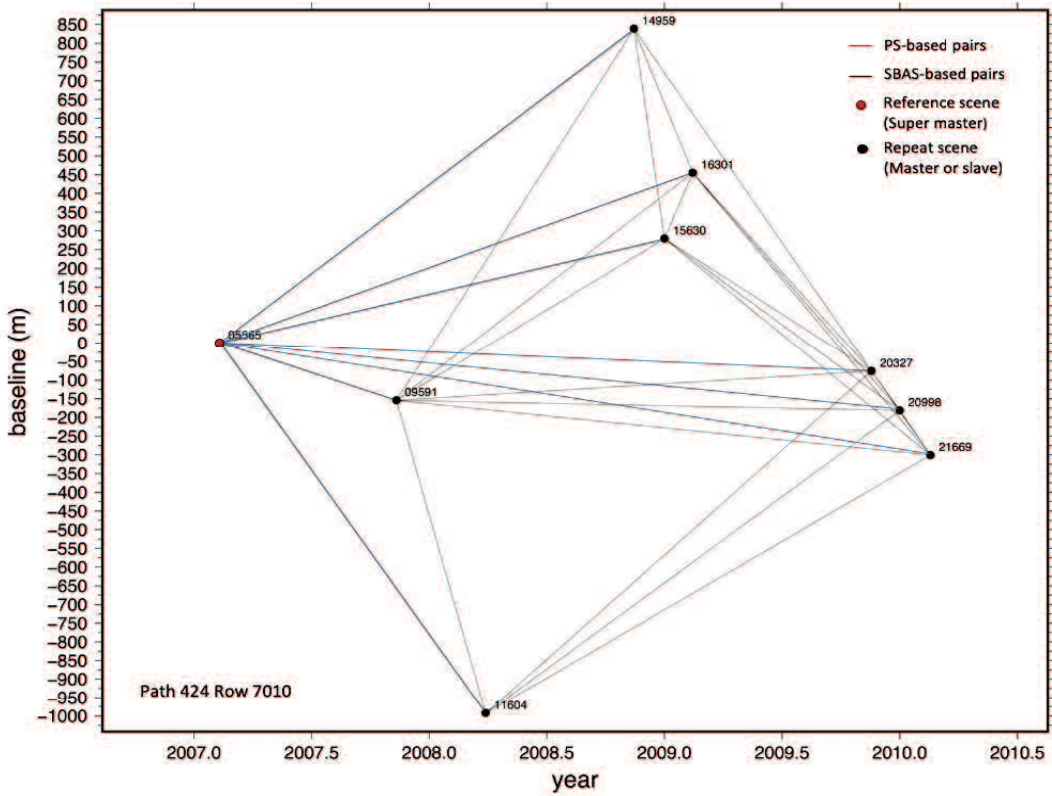


Figure 4.16 Pair selection of ALOS PALSAR for path 424 row 7010

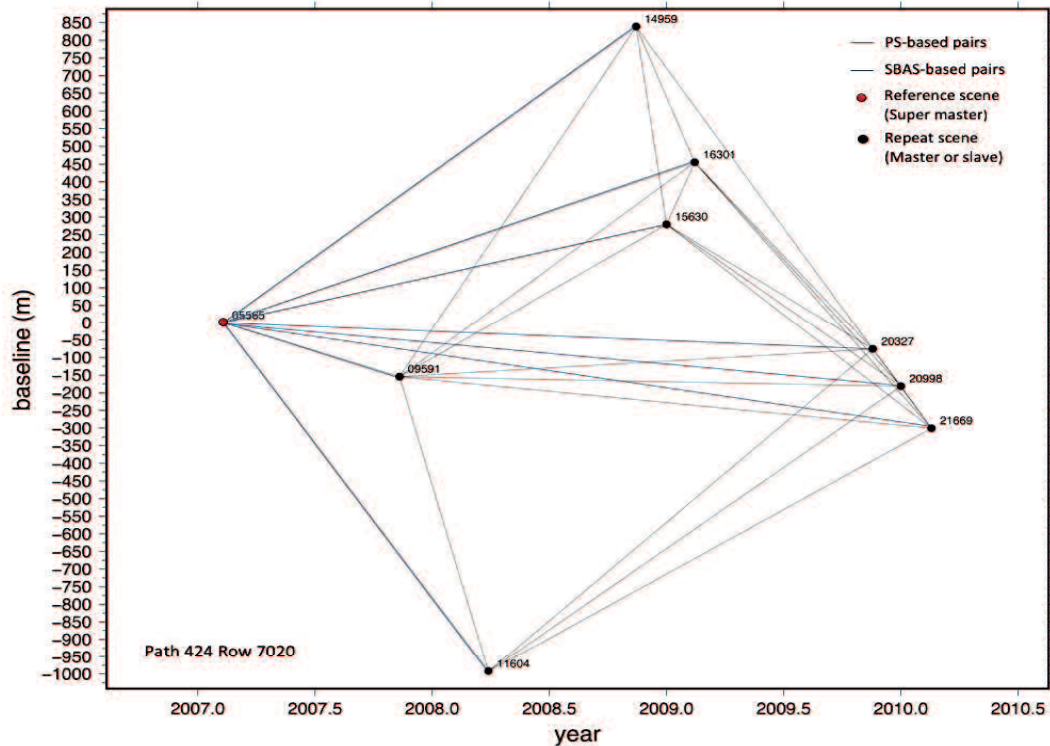


Figure 4.17 Pair selection of ALOS PALSAR for path 424 row 7020

Image results from a master and slave interferogram sequentially consists of amplitude, correlation, phase, phase-filtered, and unwrapped image results. Correlation image result is used to see the correlation between master and slave, the range is 0-1 value. The better the coherence between master and slave, the brighter the image (the value is close to 1). In contrast, the phase result of differential interferometry showed the different condition surface between master and slave SAR images. The phase and filtered-phase image results are results of interferometry which are unwrapped using SNAPHU. However, the unit of measurement is still in radian unit. Unwrapped phase is a deformation measurement from satellite viewed. Therefore, the (-) negative value means uplift (toward to radar sensor or range decrease) and the (+) value means down-lift (away to radar sensor or range increase). Finally, the cumulative displacement time series results from 2007 to 2010 are obtained by merging the entire processing results of the data as described in Figure 4.18. The results are explained more detail in Table 4.10. Moreover, the mean velocity is described in Figure 4.19.

According to the equation of LOS displacement, the value is proportional to vertical displacement. The vertical displacement is calculated by dividing the value of LOS with the incidence angle. Therefore, the down-lift cumulative displacement was used to represent subsidence in the area. The initial subsidence was obtained at -25.71 mm that is in November/ December 2007. The displacement fluctuated with decreasing trend until the end of observation period in February/ December 2010 at -31.91 mm. The mean velocity of the displacement was -8.35 mm/year.

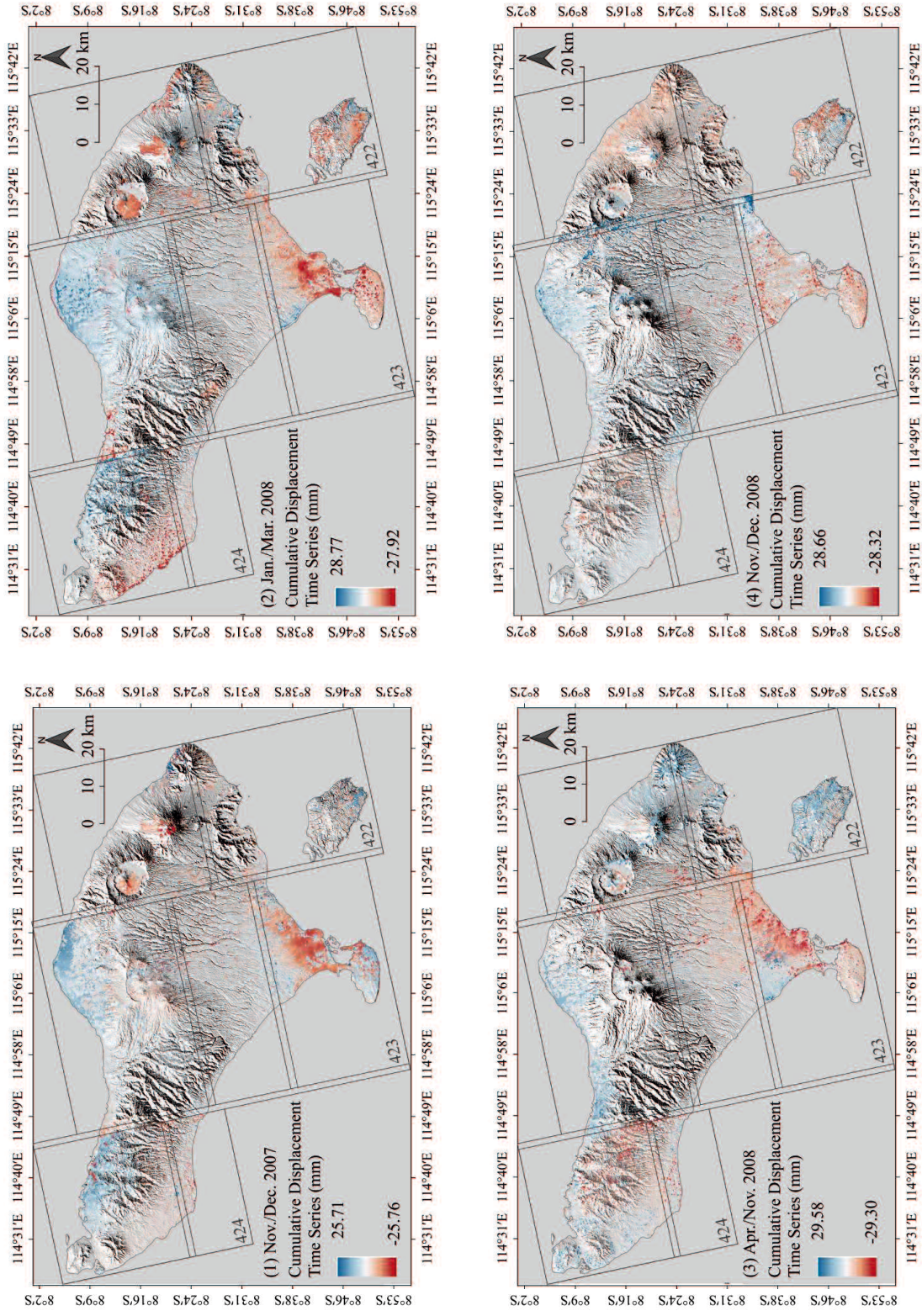


Figure 4.18 Time series cumulative displacement of ALOS PALSAR in Bali

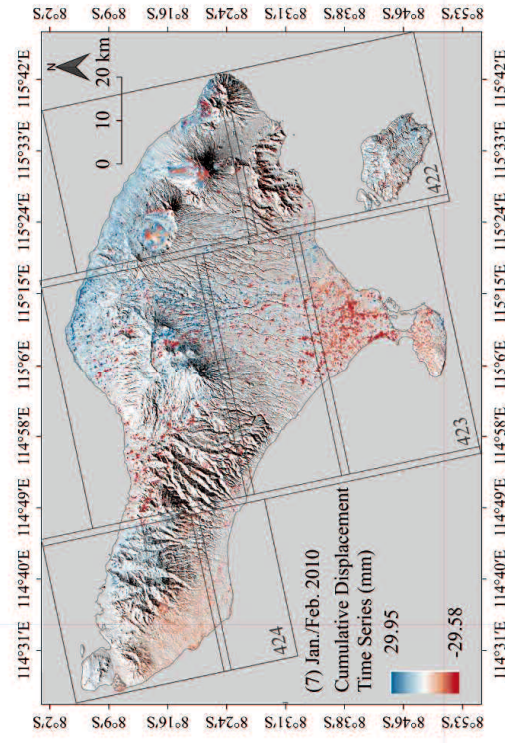
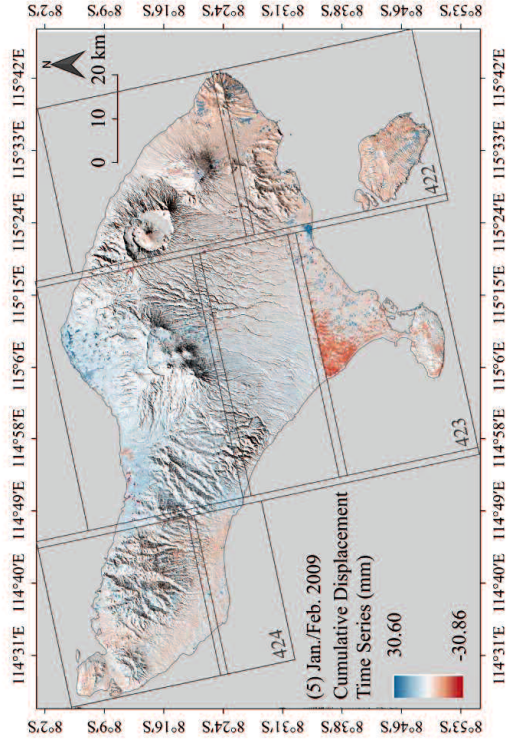
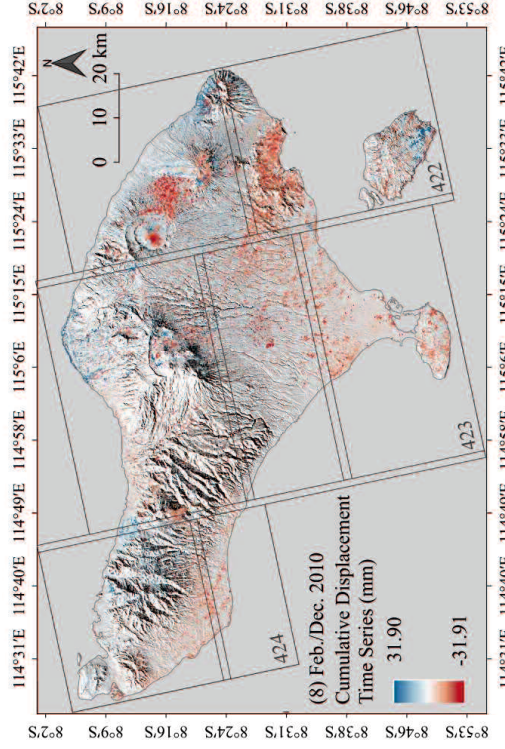
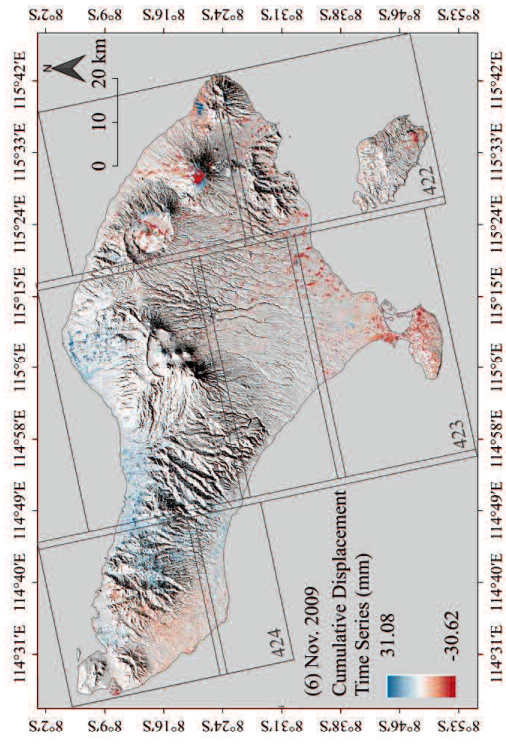


Figure 4.18 (Continued)

Table 4.10 Time series cumulative displacement and mean velocity of ALOS PALSAR in Bali from 2007 to 2010

Path	Raw	Direction	Time series cumulative displacement (mm)												Mean velocity (mm/year)	
			2007/02/22	2007/11/25	2008/02/25	2008/04/10	2008/11/27	2009/02/27	2009/11/30	2010/01/15	2010/03/02	2010/03/02	2010/03/02			
422	7010	Downlift (-)	-	-22,54	-25,75	-28,98	-26,05	-24,52	-28,25	-24,74	-27,99	-9,33				
		Uplift (+)	-	23,89	28,38	32,54	30,53	34,06	32,15	29,29	27,98	9,33				
422	7020	Downlift (-)	-	-29,36	-26,54	-30,15	-26,36	-29,84	-27,85	-31,13	-35,20	-11,73				
		Uplift (+)	-	28,25	31,64	29,86	28,29	32,40	36,37	32,67	35,20	11,73				
423	7000	Downlift (-)	-	-20,32	-23,26	-26,27	-24,16	-27,32	-24,33	-21,26	-24,32	-8,11				
		Uplift (+)	-	20,23	22,15	24,44	21,33	23,32	20,84	22,13	24,32	8,11				
423	7010	Downlift (-)	-	-32,47	-35,89	-39,24	-36,15	-39,07	-41,05	-37,60	-40,06	-13,35				
		Uplift (+)	-	32,79	37,42	42,03	39,11	36,35	33,56	36,23	40,04	13,35				
423	7020	Downlift (-)	-	-28,89	-31,81	-28,67	-32,35	-36,04	-37,95	-33,94	-37,45	-12,48				
		Uplift (+)	-	27,57	28,88	30,53	31,97	33,39	34,73	35,99	37,43	12,48				
424	7010	Downlift (-)	-	-19,59	-21,68	-23,89	-21,65	-24,02	-22,13	-23,11	-25,34	-8,45				
		Uplift (+)	-	20,02	23,14	21,77	20,17	22,83	25,40	22,91	25,36	8,45				
424	7020	Downlift (-)	-	-27,14	-30,52	-27,93	-31,48	-35,23	-32,79	-35,30	-32,99	-11,00				
		Uplift (+)	-	27,19	29,82	26,56	29,20	31,88	34,54	30,48	32,99	11,00				
422;	7000;	Downlift (-)	-	-25,76	-27,92	-29,30	-28,32	-30,86	-30,62	-29,58	-31,91	-8,35				
423; 424	7010; 7020	Uplift (+)	-	25,71	28,77	29,68	28,66	30,60	31,09	29,96	31,90	8,35				

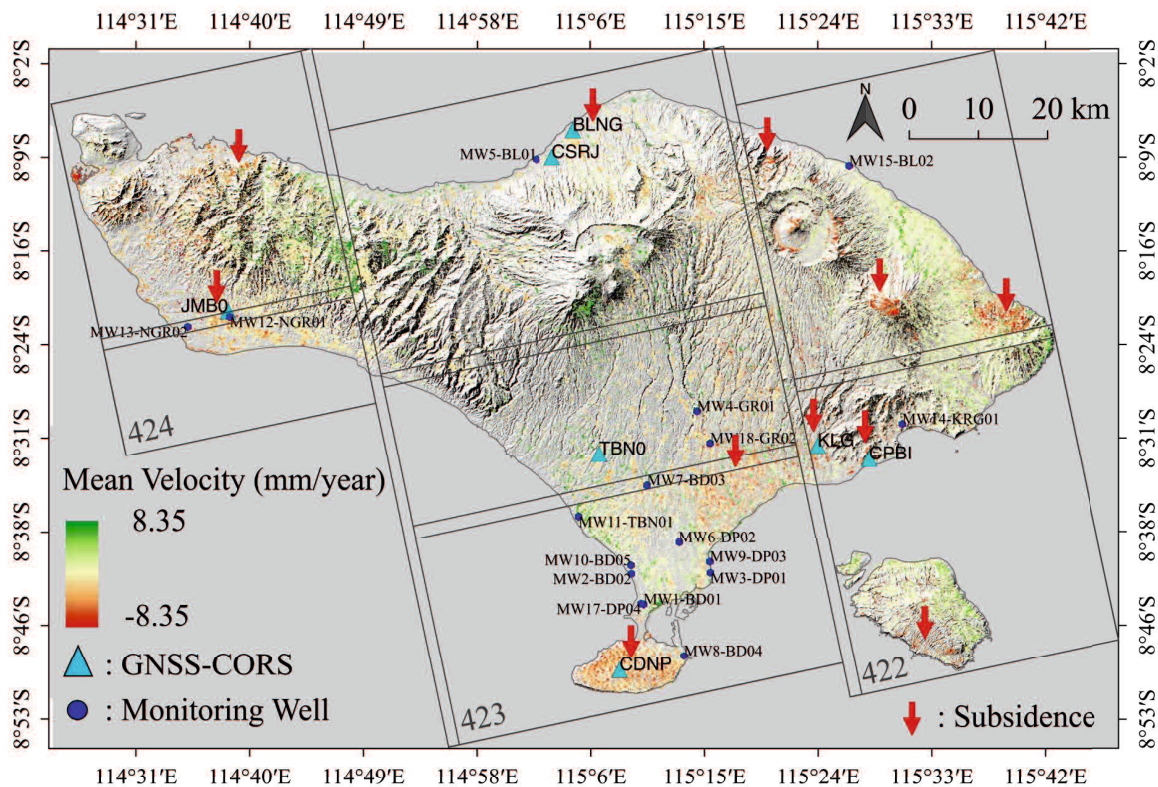


Figure 4.19 Mean velocity of displacement using ALOS PALSAR data from 2007 to 2010

## 2. Subsidence from 2014 to 2016

Based on the image results of the Sentinel 1-A data, the correlation as well as the phase difference which is related to land deformation among paired time series scenes showed consistency from 2014 to 2016. Areas with high changes can be observed in coastal area in the Southern part of Bali that is the area of Denpasar City and Badung Regency. The areas are the center of the activity in the island, such as residential, industries, and services including tourism accommodation. The extraction of the groundwater has been extensively used to accommodate the water supply of the domestic needs. Moreover, several small changes of land subsidence were observed in the west, east, as well as northern part of the coast of the island. These areas have been developed as irrigated paddy field areas in the island. The main source for the irrigation is the groundwater. Sentinel-1A data used for the study is listed in Table 4.11. Orbit data for the Sentinel-1A processing according to the acquisition date is described in Table 4.12.

Table 4.11 List of Sentinel-1A Data

<b>Sub-Swath</b>	<b>Scene ID</b>	<b>Acquisition date</b>	<b>Number of days</b>	<b>Perpendicular baseline (m)</b>
F1	S1A20141016	2014/10/16	288	(Super Master)
	S1A20141028	2014/10/28	300	-25,794993
	S1A20141121	2014/11/21	324	-68,52959
	S1A20150225	2015/02/25	420	128,258588
	S1A20150321	2015/03/21	444	-42,940559
	S1A20150508	2015/05/08	492	-28,30777
	S1A20150601	2015/06/01	516	-100,980561
	S1A20150625	2015/06/25	540	-58,143115
	S1A20150719	2015/07/19	564	-16,648726
	S1A20150812	2015/08/12	588	23,609184
	S1A20150929	2015/09/29	636	16,250752
	S1A20151023	2015/10/23	660	58,032623
	S1A20151116	2015/11/16	684	-42,183869
	S1A20160103	2016/01/03	732	-2,754282
	S1A20160127	2016/01/27	756	113,41497
	S1A20160220	2016/02/20	780	-34,933552
	S1A20160408	2016/04/08	828	-59,874454
	S1A20160502	2016/05/02	852	-18,556871
	S1A20160526	2016/05/26	876	28,857464
	S1A20160713	2016/07/13	924	61,600292
S1A20170121	2017/01/21	1115	61,635328	
F2	S1A20141016	2014/10/16	288	(Super Master)
	S1A20141028	2014/10/28	300	-23,573447
	S1A20141121	2014/11/21	324	-64,924527
	S1A20150225	2015/02/25	420	117,497141
	S1A20150321	2015/03/21	444	-40,262032
	S1A20150508	2015/05/08	492	-27,947519
	S1A20150601	2015/06/01	516	-96,237064
	S1A20150625	2015/06/25	540	-54,96647
	S1A20150719	2015/07/19	564	-16,190551
	S1A20150812	2015/08/12	588	23,743795
	S1A20150929	2015/09/29	636	14,714526
	S1A20151023	2015/10/23	660	52,766967
	S1A20151116	2015/11/16	684	-43,077072
	S1A20160103	2016/01/03	732	-5,131032
	S1A20160127	2016/01/27	756	103,616339
	S1A20160220	2016/02/20	780	-33,981451
	S1A20160408	2016/04/08	828	-57,001825
	S1A20160502	2016/05/02	852	-17,833709
	S1A20160526	2016/05/26	876	27,028632
	S1A20160713	2016/07/13	924	57,406903
S1A20170121	2017/01/21	1115	55,978231	



Table 4.12 Orbit data for Sentinel-1A InSAR processing

Scene ID	Acquisition date	Orbit data
S1A20141016	2014/10/16	S1A_OPER_AUX_POEORB_OPOD_20141106T123612_V20141015T225944_20141017T005944.EOF
S1A20141028	2014/10/28	S1A_OPER_AUX_POEORB_OPOD_20141118T123725_V20141027T225944_20141029T005944.EOF
S1A20141121	2014/11/21	S1A_OPER_AUX_POEORB_OPOD_20141212T123749_V20141120T225944_20141122T005944.EOF
S1A20150225	2015/02/25	S1A_OPER_AUX_POEORB_OPOD_20150318T123036_V20150224T225944_20150226T005944.EOF
S1A20150321	2015/03/21	S1A_OPER_AUX_POEORB_OPOD_20150411T123045_V20150320T225944_20150322T005944.EOF
S1A20150508	2015/05/08	S1A_OPER_AUX_POEORB_OPOD_20150529T122517_V20150507T225944_20150509T005944.EOF
S1A20150601	2015/06/01	S1A_OPER_AUX_POEORB_OPOD_20150621T122558_V20150531T225944_20150602T005944.EOF
S1A20150625	2015/06/25	S1A_OPER_AUX_POEORB_OPOD_20150715T122234_V20150624T225944_20150626T005944.EOF
S1A20150719	2015/07/19	S1A_OPER_AUX_POEORB_OPOD_20150808T122256_V20150718T225943_20150720T005943.EOF
S1A20150812	2015/08/12	S1A_OPER_AUX_POEORB_OPOD_20150901T122301_V20150811T225943_20150813T005943.EOF
S1A20150929	2015/09/29	S1A_OPER_AUX_POEORB_OPOD_20151019T122431_V20150928T225943_20150930T005943.EOF
S1A20151023	2015/10/23	S1A_OPER_AUX_POEORB_OPOD_20151112T122405_V20151022T225943_20151024T005943.EOF
S1A20151116	2015/11/16	S1A_OPER_AUX_POEORB_OPOD_20151206T122632_V20151115T225943_20151117T005943.EOF
S1A20160103	2016/01/03	S1A_OPER_AUX_POEORB_OPOD_20160123T121722_V20160102T225943_20160104T005943.EOF
S1A20160127	2016/01/27	S1A_OPER_AUX_POEORB_OPOD_20160216T121630_V20160126T225943_20160128T005943.EOF
S1A20160220	2016/02/20	S1A_OPER_AUX_POEORB_OPOD_20160311T121452_V20160219T225943_20160221T005943.EOF
S1A20160408	2016/04/08	S1A_OPER_AUX_POEORB_OPOD_20160428T121507_V20160407T225943_20160409T005943.EOF
S1A20160502	2016/05/02	S1A_OPER_AUX_POEORB_OPOD_20160522T121449_V20160501T225943_20160503T005943.EOF
S1A20160526	2016/05/26	S1A_OPER_AUX_POEORB_OPOD_20160615T121532_V20160525T225943_20160527T005943.EOF
S1A20160713	2016/07/13	S1A_OPER_AUX_POEORB_OPOD_20160802T121647_V20160712T225943_20160714T005943.EOF
S1A20170121	2017/01/21	S1A_OPER_AUX_POEORB_OPOD_20170210T121453_V20170120T225942_20170122T005942.EOF

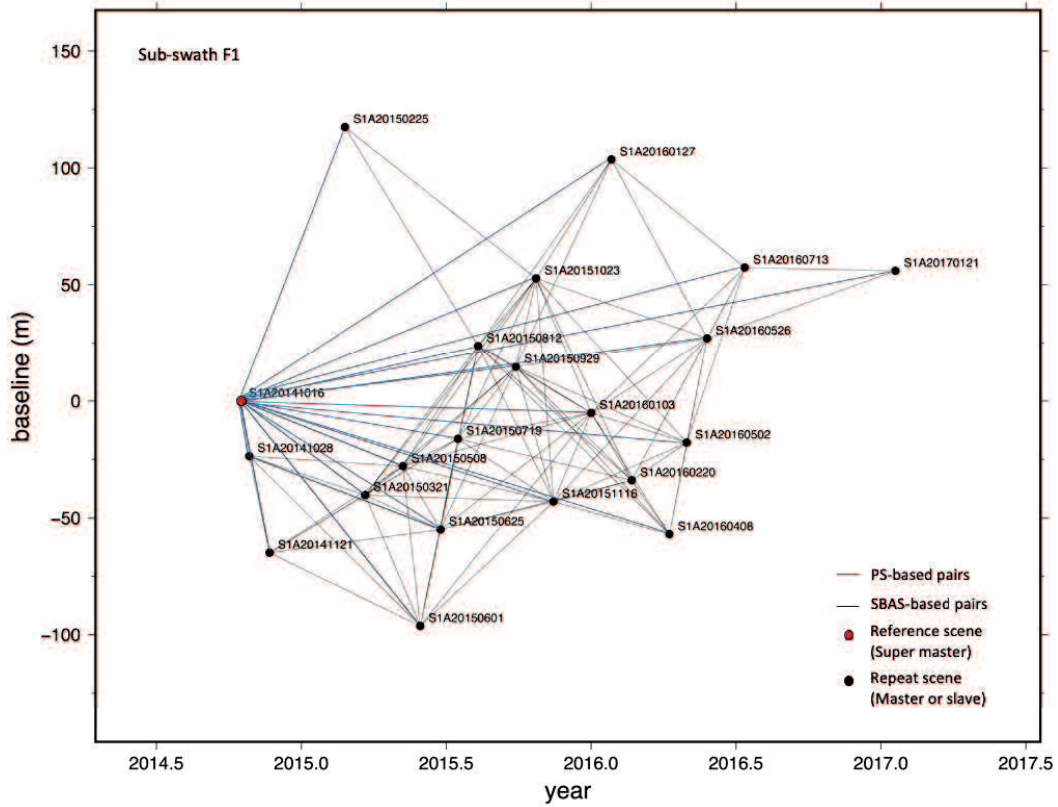


Figure 4.20 Pair selection of SENTINEL-1A data for sub-swath F1

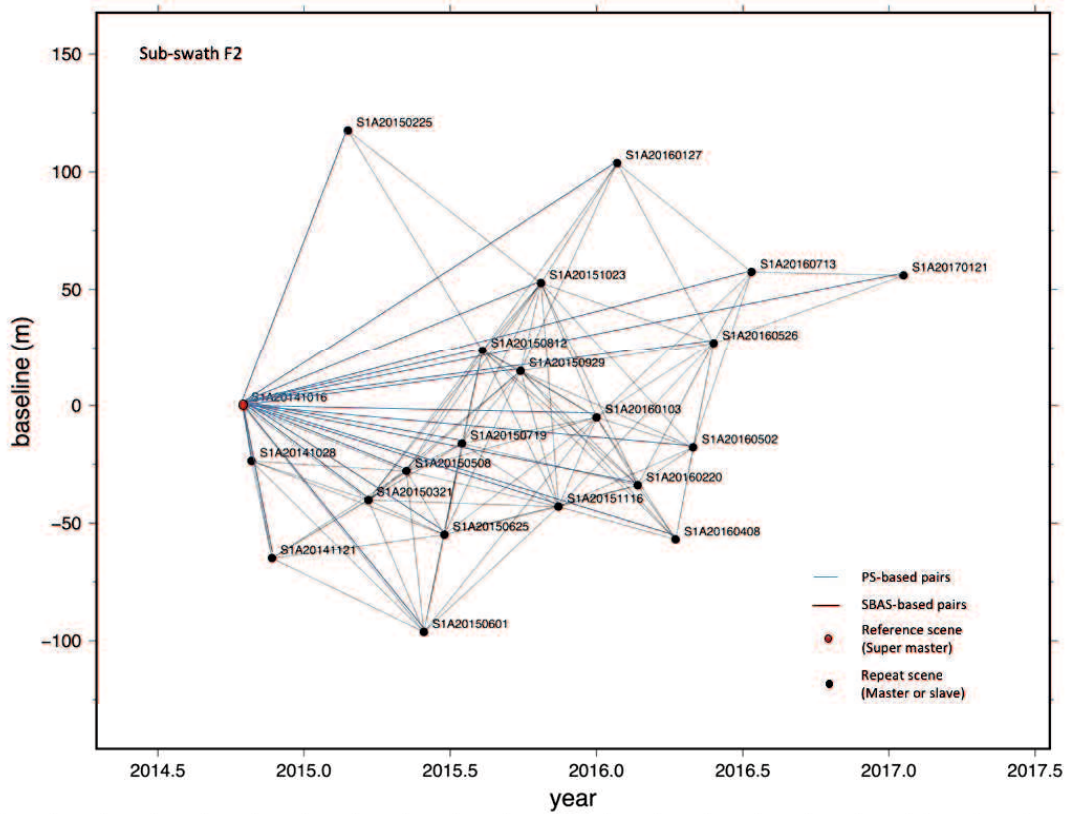


Figure 4.21 Pair selection of SENTINEL-1A data for sub-swath F2

As for Sentinel-1A, the SBAS was performed using perpendicular baseline of 100 and temporal baseline is limited to 250 days. The process is the same with ALOS PALSAR. In case of PS processing, one scene was selected as super master to generate interferograms with the other scenes (Sandwell et al, 2008) for each track of Sentinel-1A. A super master was selected with criteria able to minimize baseline with the other scenes (Rosenqvist et al, 2014). Pairs of interferograms in sub-swath F1 (Figure 4.20) and sub-swath F2 (Figure 4.21) were plotted as lines on the scatter chart of perpendicular and temporal baselines.

Changing of the elevation related to the land subsidence can be obtained from the correlation and phase difference image results. In the correlation image result, brighter color represents area that experiences low to high changes. The brighter the color is the higher the changes in the area. On the other hand, darker color denotes area with very low to no changes. Moreover, phase image result describes image result of interferometry which is unwrapped using SNAPHU. However, the unit of measurement is still in radian unit. Unwrapped phase is a deformation measurement from satellite viewed. Therefore, the (-) negative value means uplift (toward to radar sensor or range decrease) and the (+) value means down-lift (away to radar sensor or range increase). Finally, the cumulative displacement time series results from 2014 to 2017 are obtained by merging the entire processing results of the data as described in Figure 4.22. The results are explained more detail in Table 4.13. Moreover, the mean velocity is described in Figure 4.23.

According to the equation of LOS displacement, the value is proportional to vertical displacement. The vertical displacement is calculated by dividing the value of LOS with the incidence angle. Therefore, the down-lift cumulative displacement was used to represent subsidence in the area. The initial subsidence was obtained at -34.86 mm that is on October 28, 2014. The displacement fluctuated with decreasing trend until the end of observation period on January 21, 2017 at -47.41 mm. The mean velocity of the displacement was -15.80 mm/year.

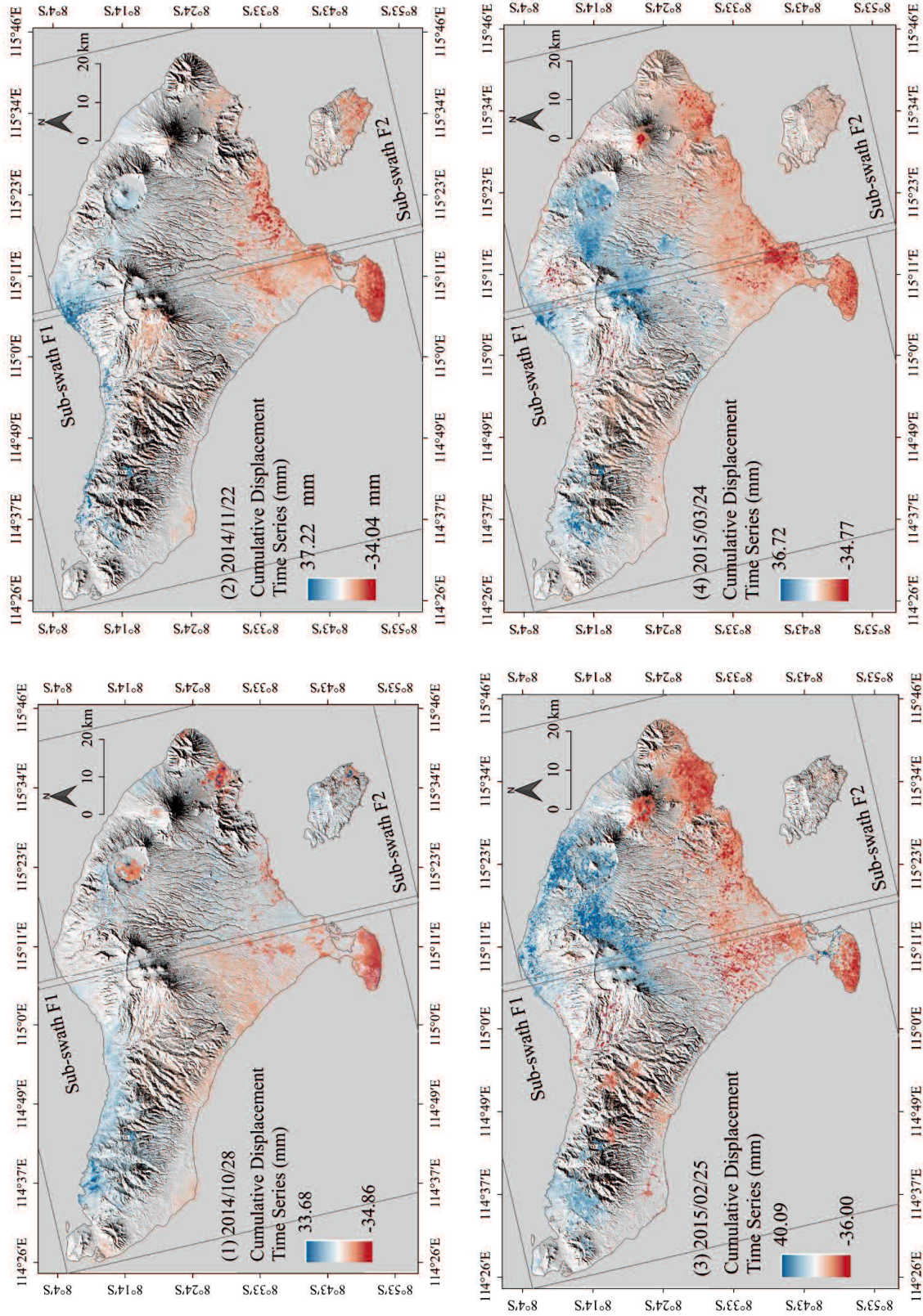


Figure 4.22 Time series cumulative displacement of Sentinel-1A in Bali from 2014 to 2016

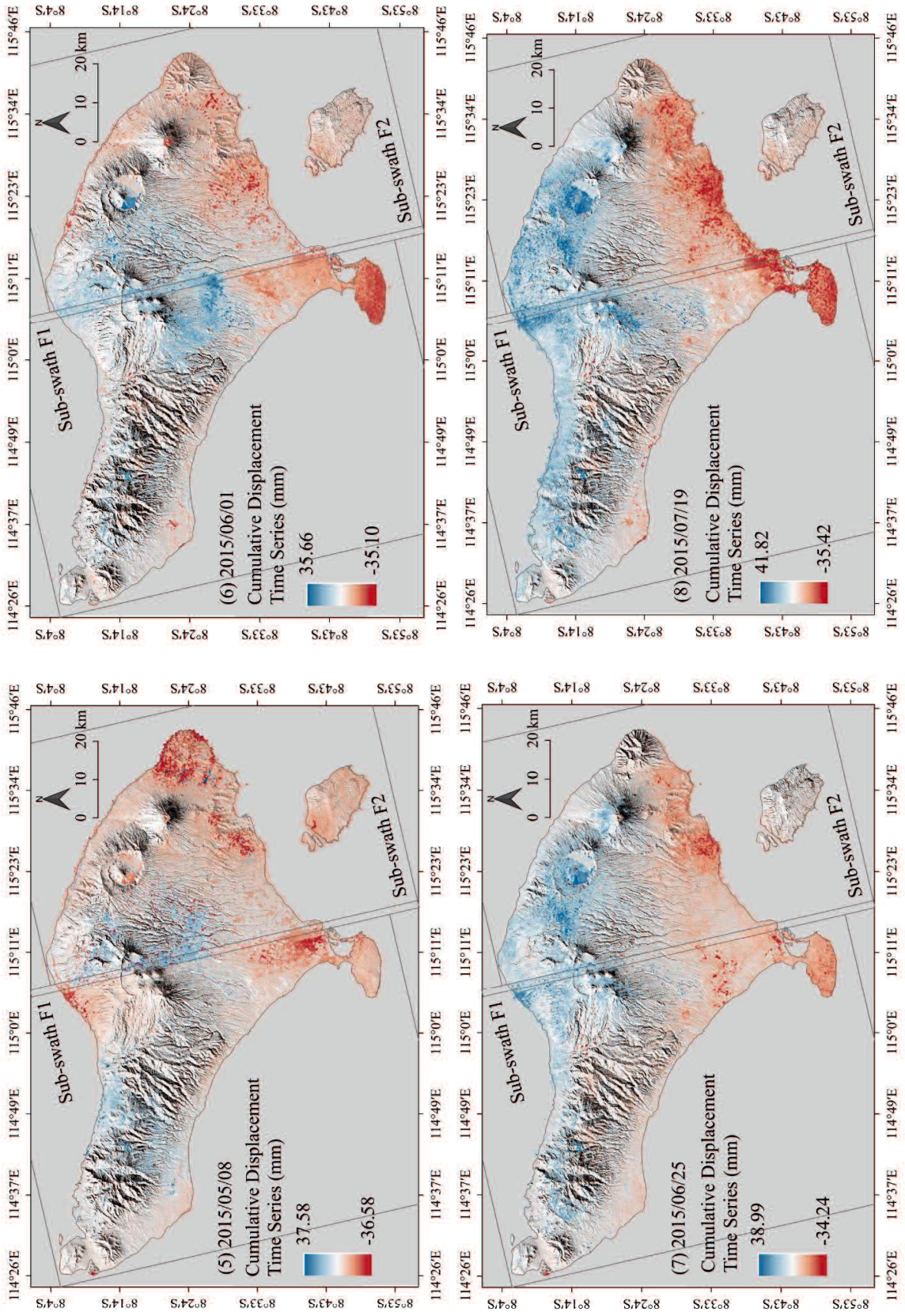


Figure 4.22 (Continued)

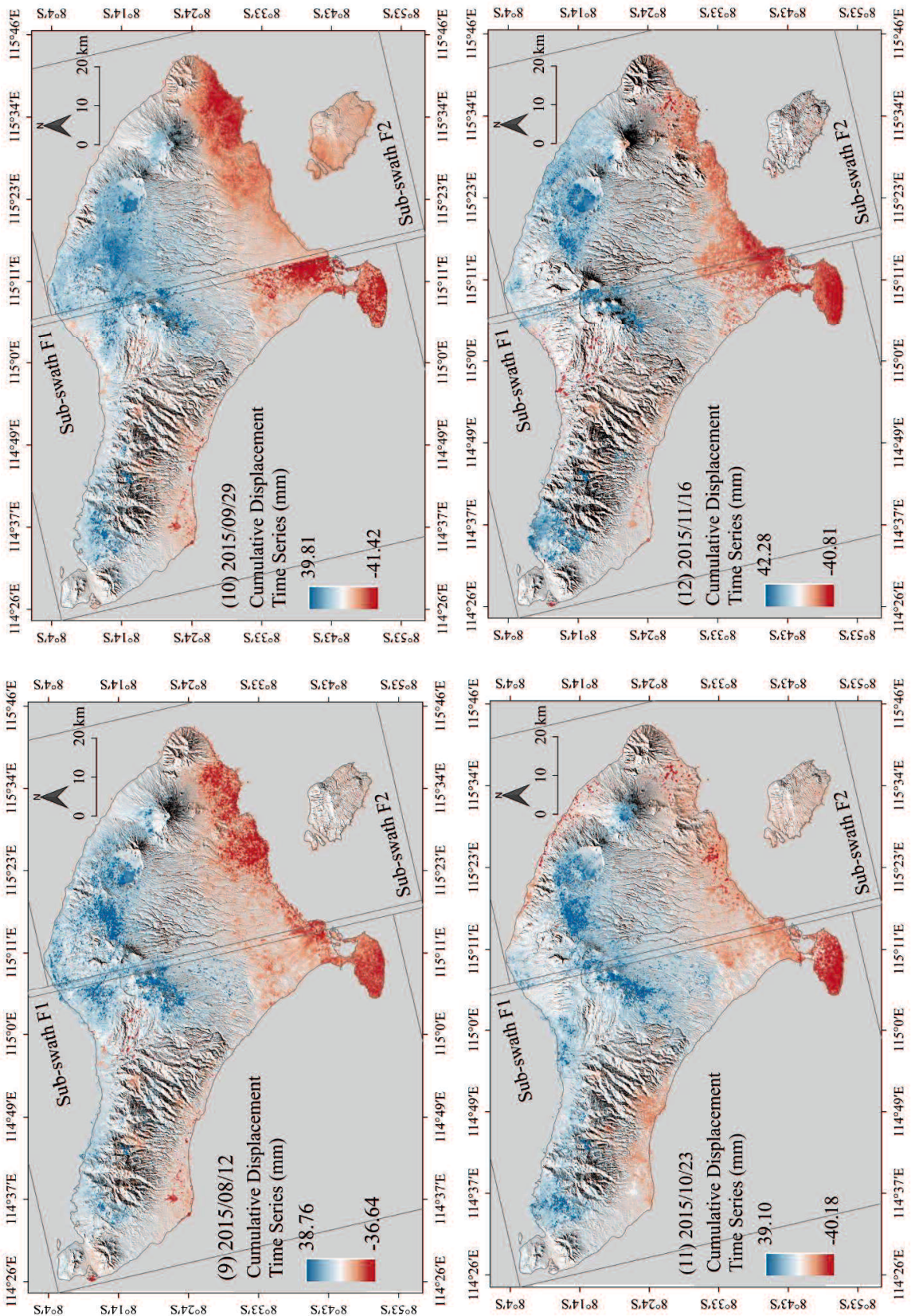


Figure 4.22 (Continued)

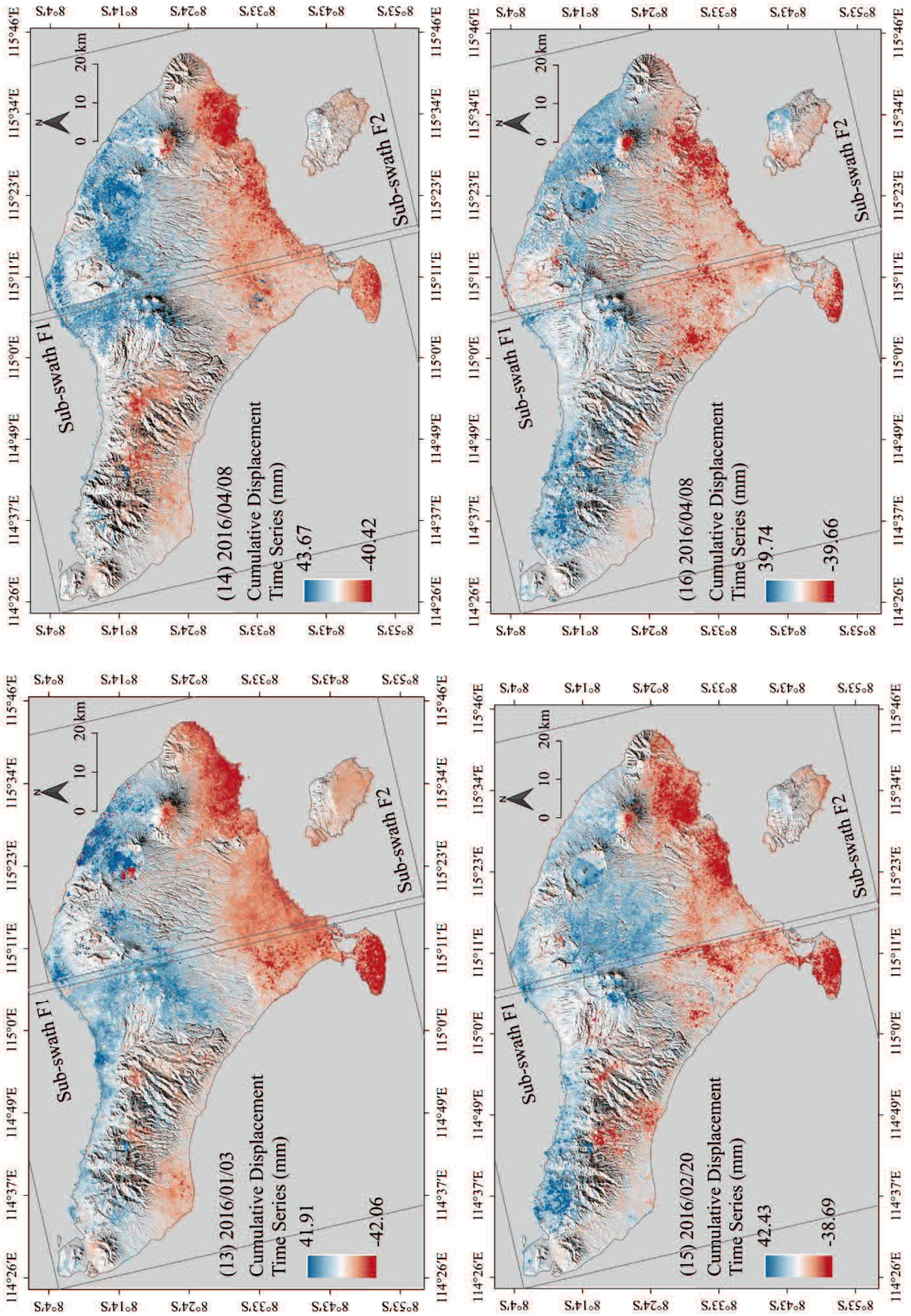


Figure 4.22 (Continued)

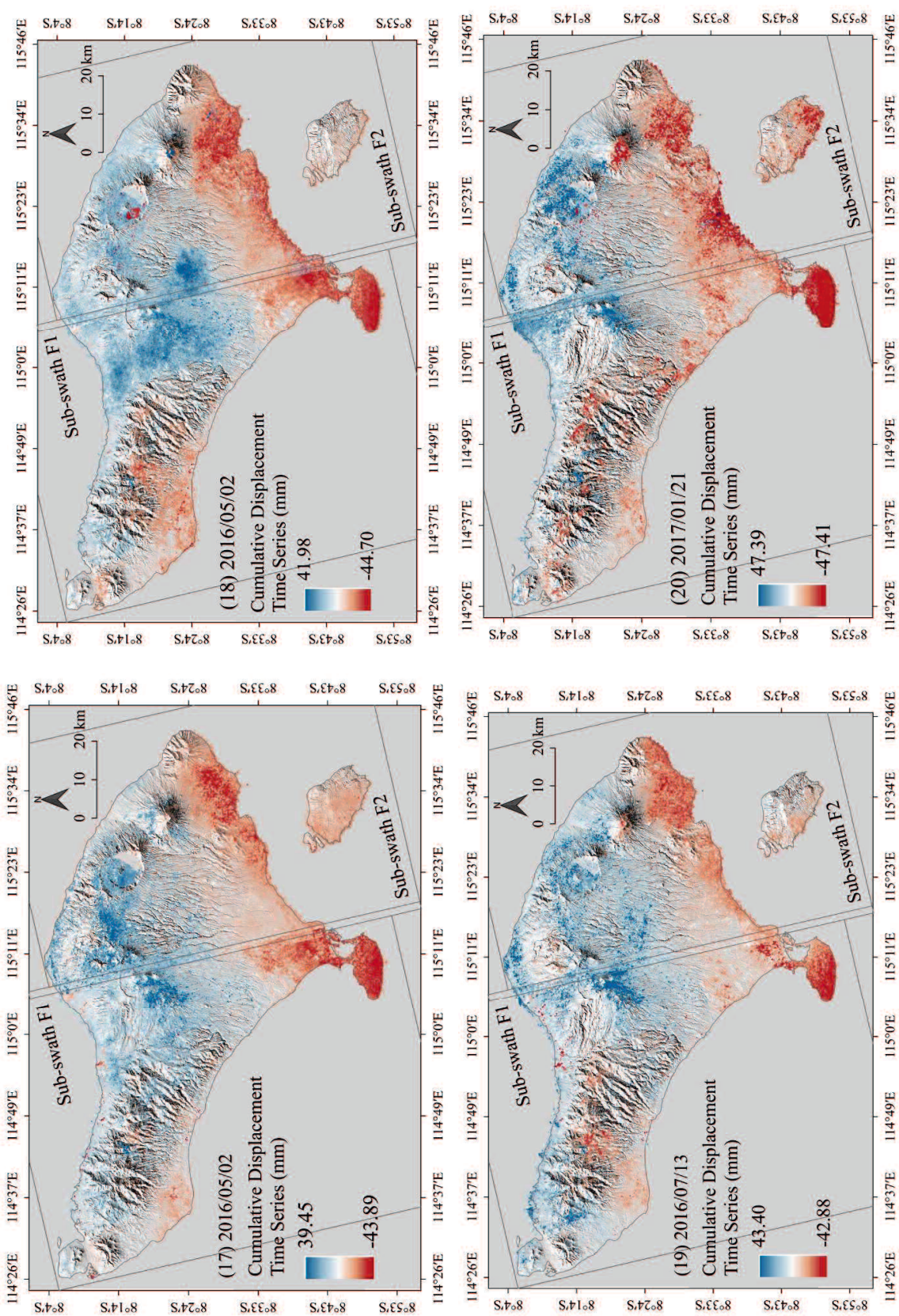


Figure 4.22 (Continued)



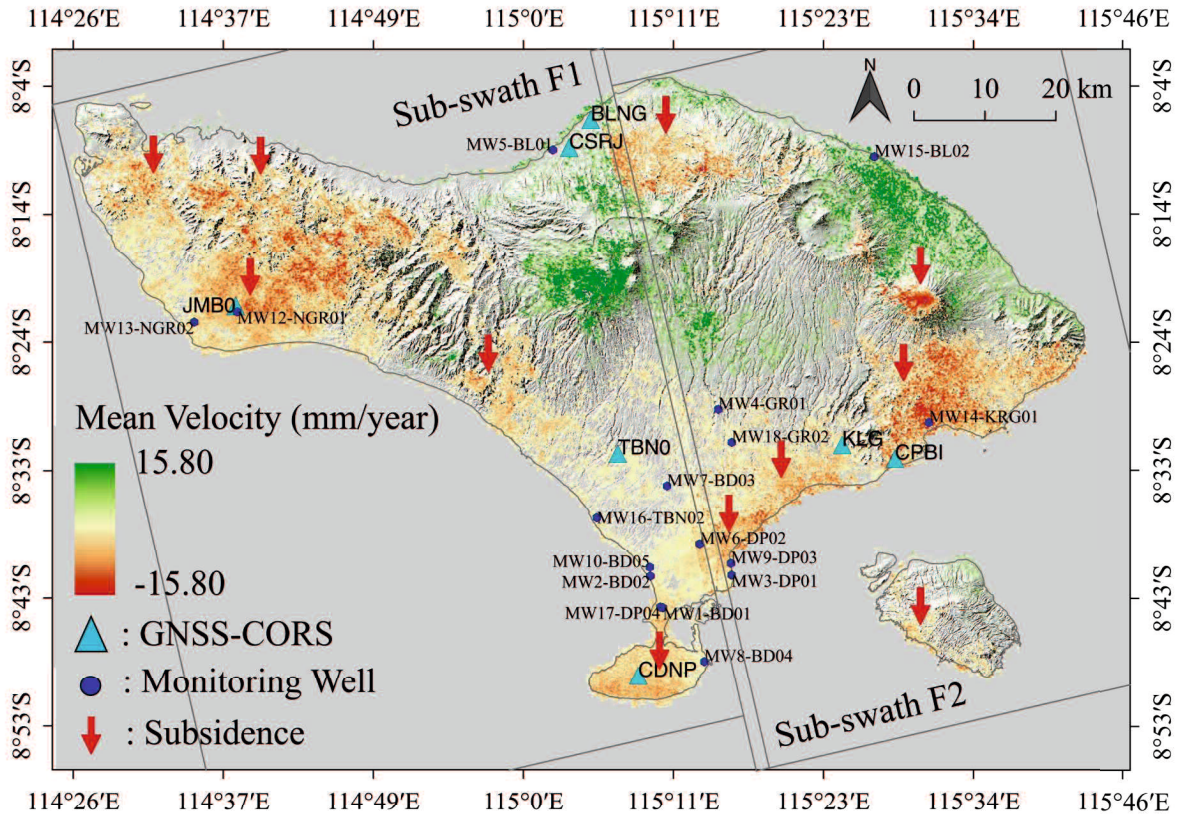


Figure 4.23 Mean velocity of displacement using Sentinel-1A data from 2014 to 2016

Determination of the land subsidence based on the InSAR processing result refers to several related conditions. According to the equation of LOS displacement, the value is proportional to vertical displacement. The vertical displacement is calculated by dividing the value of LOS with the incidence angle. Therefore, the down-lift cumulative displacement was used to represent subsidence in the area. Moreover, the horizontal displacement is considered as 0 or no horizontal displacement so that the vertical displacement with down-lift direction indicated from cumulative displacement time series as well as mean velocity result of InSAR processing can be considered as subsidence phenomenon.

Table 4.13 Time series cumulative displacement and mean velocity of Sentinel-1A in Bali from 2014 to 2017

Sub-Swath	Direction	Time series cumulative displacement (mm)													Mean velocity (mm/year)
		2014/10/16	2014/10/28	2014/11/21	2015/02/25	2015/03/21	2015/05/08	2015/06/01	2015/06/25	2015/07/19	2015/08/12	2015/09/29			
F1	Downlift (-)	-	-41,28	-39,92	-44,16	-42,11	-46,19	-43,78	-42,51	-41,00	-45,16	-49,22			
	Uplift (+)	-	41,59	44,68	46,28	42,75	41,25	39,37	42,32	44,68	42,43	40,94			
F2	Downlift (-)	-	-28,44	-28,17	-27,85	-27,43	-26,97	-26,42	-25,97	-29,83	-28,12	-33,62			
	Uplift (+)	-	25,77	29,76	33,89	30,68	33,92	31,94	35,65	38,97	35,08	38,68			
F1; F2	Downlift (-)	-	-34,86	-34,04	-36,00	-34,77	-36,58	-35,10	-34,24	-35,42	-36,64	-41,42			
	Uplift (+)	-	33,68	37,22	40,09	36,72	37,58	35,66	38,99	41,82	38,76	39,81			

Sub-swath	Direction	Time series cumulative displacement (mm)										Mean velocity (mm/year)
		2015/10/23	2015/11/16	2016/01/03	2016/01/27	2016/02/20	2016/04/08	2016/05/02	2016/05/26	2016/07/13	2017/01/21	
F1	Downlift (-)	-47,75	-51,56	-49,31	-47,24	-44,94	-49,05	-53,00	-50,62	-48,35	-52,66	-17,55
	Uplift (+)	43,72	46,44	43,70	45,61	47,02	44,50	46,76	48,15	49,45	52,65	17,55
F2	Downlift (-)	-32,61	-30,07	-34,81	-33,61	-32,44	-30,28	-34,78	-38,79	-37,41	-42,16	-14,05
	Uplift (+)	34,48	38,11	40,12	41,72	37,83	34,97	32,15	35,80	37,34	42,14	14,05
F1; F2	Downlift (-)	-40,18	-40,81	-42,06	-40,42	-38,69	-39,66	-43,89	-44,70	-42,88	-47,41	-15,80
	Uplift (+)	39,10	42,28	41,91	43,67	42,43	39,74	39,45	41,98	43,40	47,39	15,80

### 4.3.2 Comparison Between InSAR and GNSS-CORS Measurements

The processing result of the InSAR was evaluated using GNSS-CORS data. There are three stations of CORS in Bali maintained by the Geospatial Information Agency of Indonesia and five station maintained by the Ministry of Land and Spatial Planning. The data is available from the year the station was built until 2017. In this analysis, the position and elevation of the station when it was built is considered as the initial data. The data was estimated using Real Time Kinematics (RTK) processing system. Considering that the area in the Southern part of Bali showed the occurrence of land deformation. The station located in the area was estimated by comparing the elevation of the station with the elevation of another station. In this regard, a station with distance less than 70 km is utilized as references (Table 4.14). The station is located in the area with no subsidence based on the InSAR measurement. The graph of the GNSS-CORS measurement s in 2010 and 2011 can be seen in Figure 4.24 and Figure 4.29.

Table 4.14 List of the GNSS-CORS data in Bali Island used for the study

Station ID	Location	Latitude	Longitude	Height (m)	Data Period
CDNP <sup>a)</sup>	Denpasar	-8.8181	115.1456	234.5200	2008 - 2017
CPBI <sup>a)</sup>	Bukit Tengah	-8.5433	115.4708	278.7500	2008 - 2011
CSRJ <sup>a)</sup>	Singaraja	-8.1497	115.0580	60.3300	2008 - 2017
BLNG <sup>b)</sup>	Buleleng	-8.1144	115.0855	55.1439	2017
KLK <sup>b)</sup>	Klungkung	-8.5259	115.4038	172.9219	2016 - 2017
TBN <sup>b)</sup>	Tabanan	-8.5369	114.6357	60.6014	2016 - 2017
JMB <sup>b)</sup>	Jembrana	-8.3565	115.1195	159.558	2016 - 2017

a) Geospatial Information Agency (BIG)

b) Ministry of Land and Spatial Planning of Indonesia (BPN)

Based on the GNSS-CORS observation result, the elevation of the land in the area detected as area with land deformation showed the occurrence of subsidence on land. The trend is similar with the result of the InSAR data processing result. In this regards, the information of land deformation in the area is confirmed and further utilized as the spatial input for the groundwater conservation mapping. Table 4.15 describes data input and parameter setting for RTKLIB processing.

Table 4.15 Data input and parameter setting for RTKLIB processing

<b>Data/ Parameter</b>	<b>Input/ Setting</b>
Rover data	Observation data at station in subsided area (.o)
Base station data	Observation data at station in non-subsided area (.o)
Navigation data	IGS-NAV (.n)
Precise clock data	IGS-EPH (.sp3) IGS-CLK-30S (.clk_30s)
EOP data	IGS-ERP (.erp)
Positioning mode	Static
Frequencies/ filter type	L1+2 (Combined)
Elevation mask ( <sup>0</sup> )/ SNR mask (dEHzz)	15
Ionosphere correction	Estimate STEC
Troposphere correction	Estimate ZTD
Satellite ephemeris/ clock	Precise

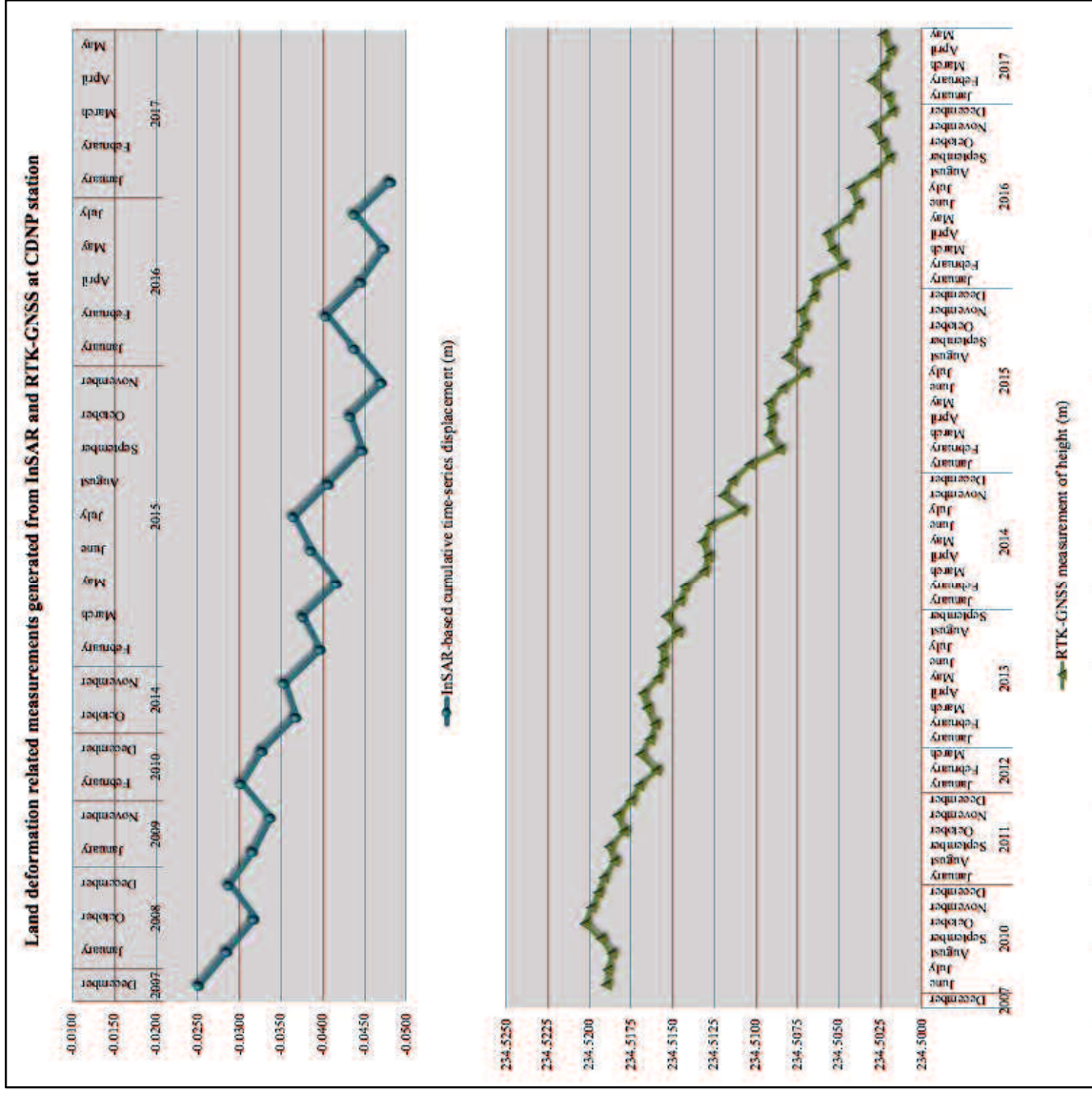


Figure 4.24 Changes of vertical deformation from InSAR and GNSS-CORS measurements at CDNP station

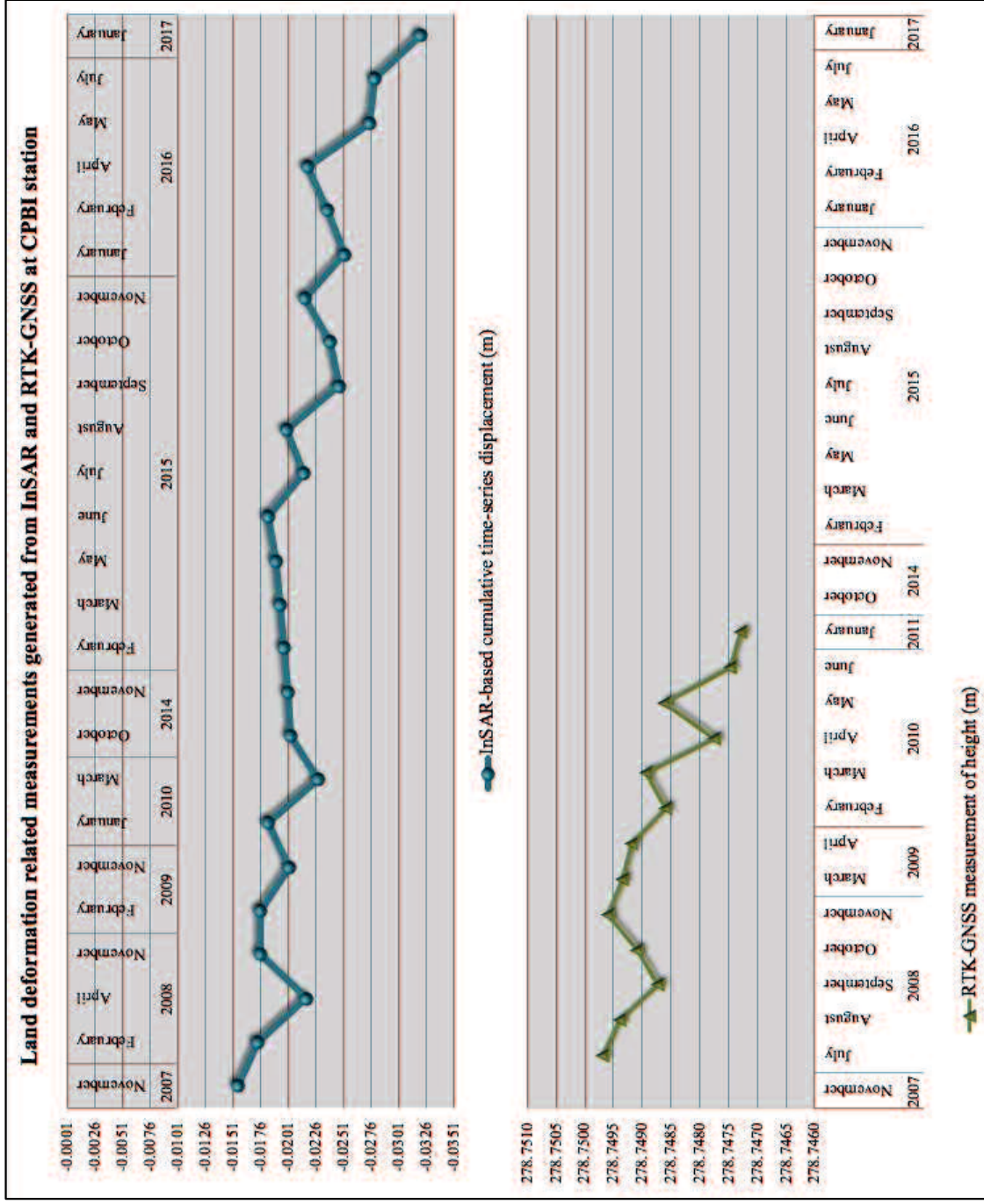


Figure 4.25 Changes of vertical deformation from InSAR and GNSS-CORS measurements at CPBI station

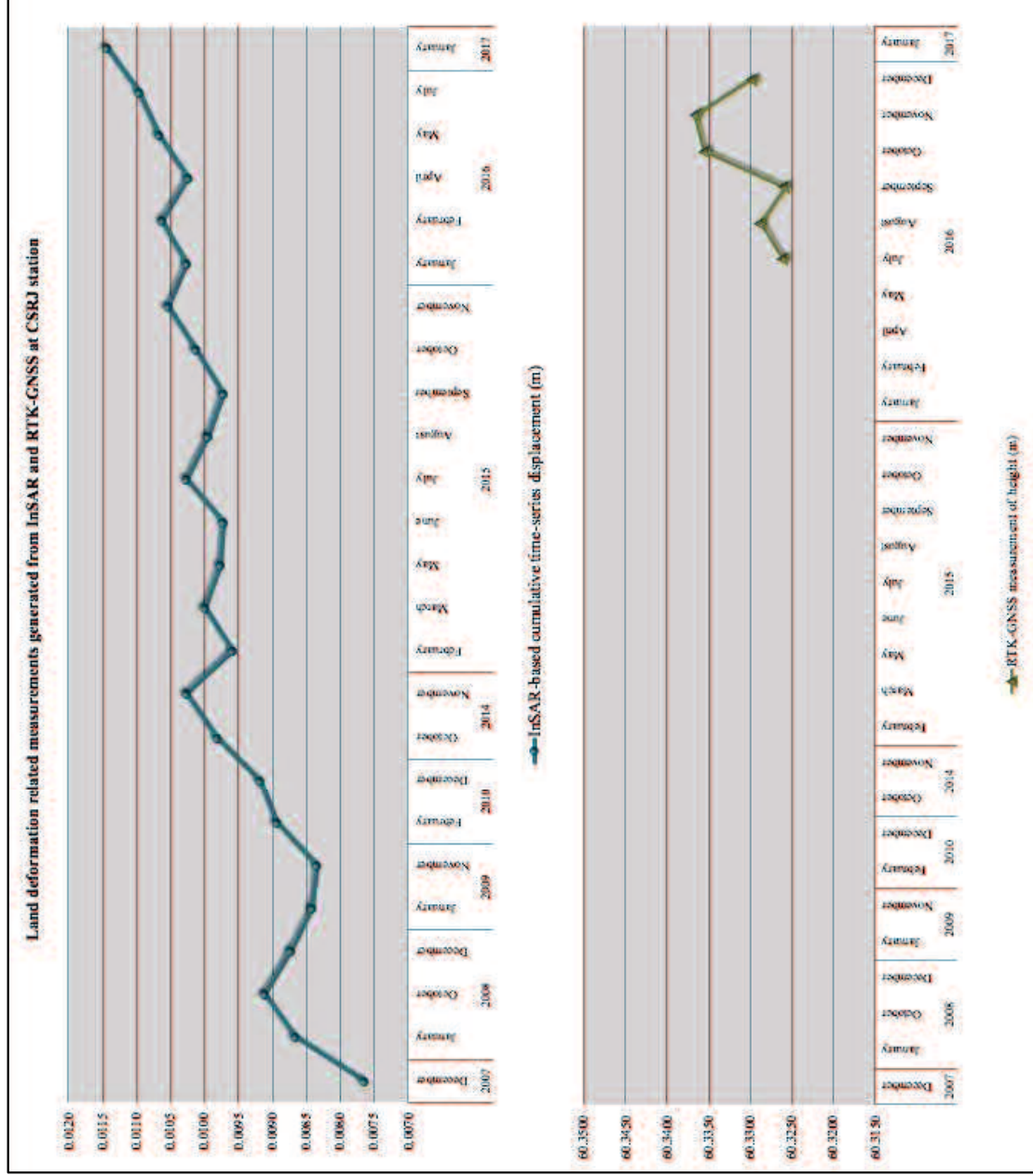


Figure 4.26 Changes of vertical deformation from InSAR and GNSS-CORS measurements at CSRJ station

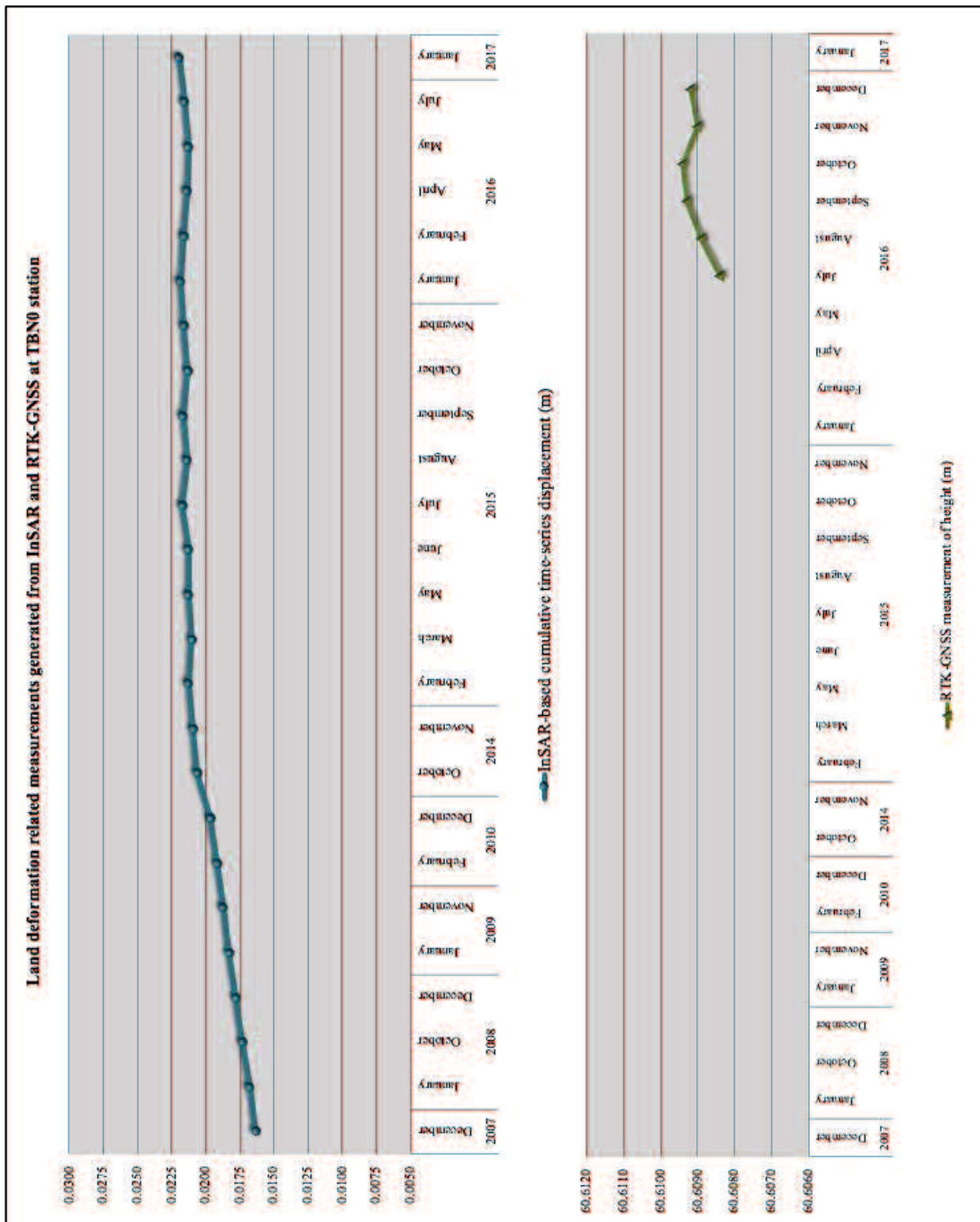


Figure 4.27 Changes of vertical deformation from InSAR and GNSS-CORS measurements at TBN0 station



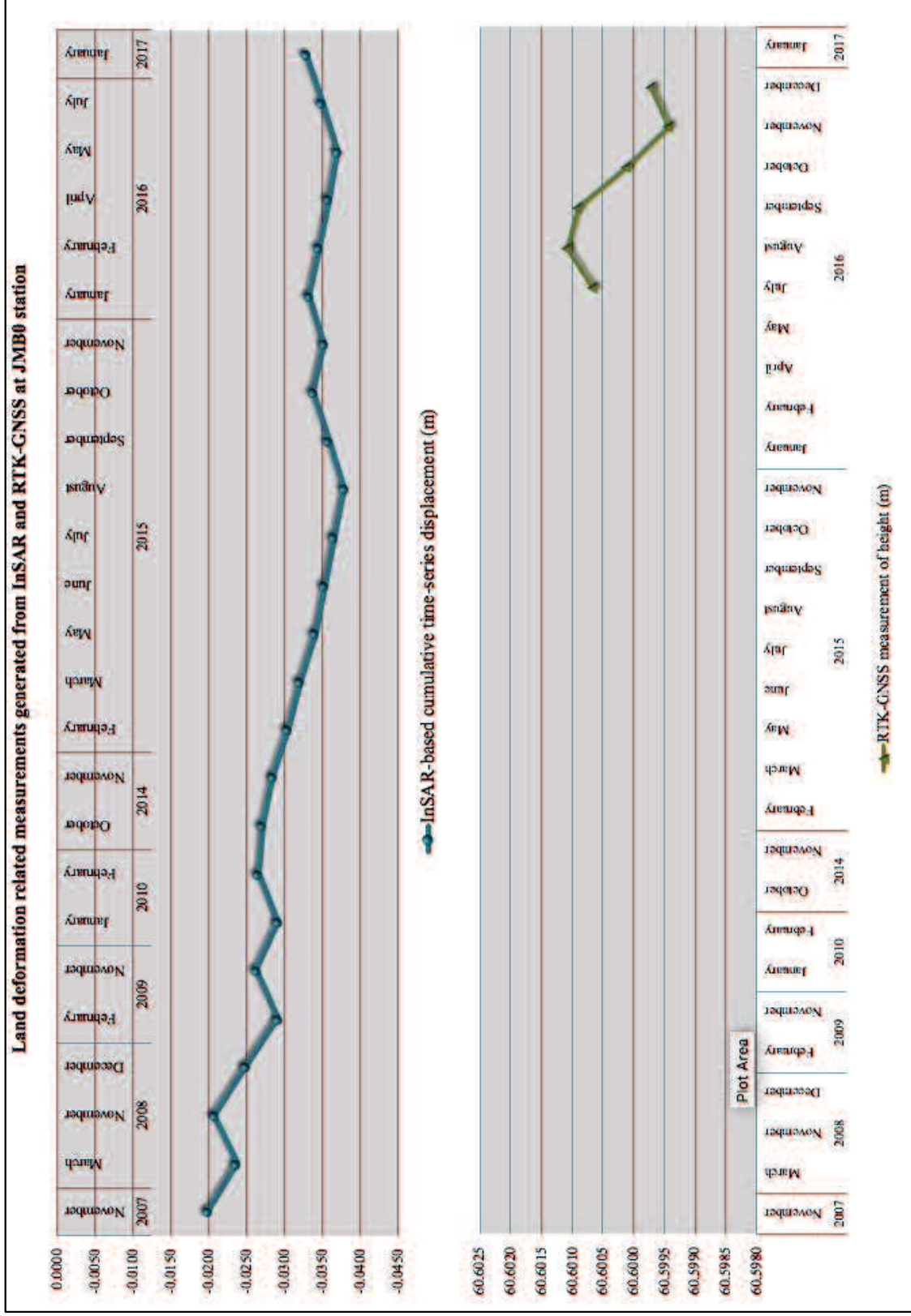


Figure 4.28 Changes of vertical deformation from InSAR and GNSS-CORS measurements at JMB0 station

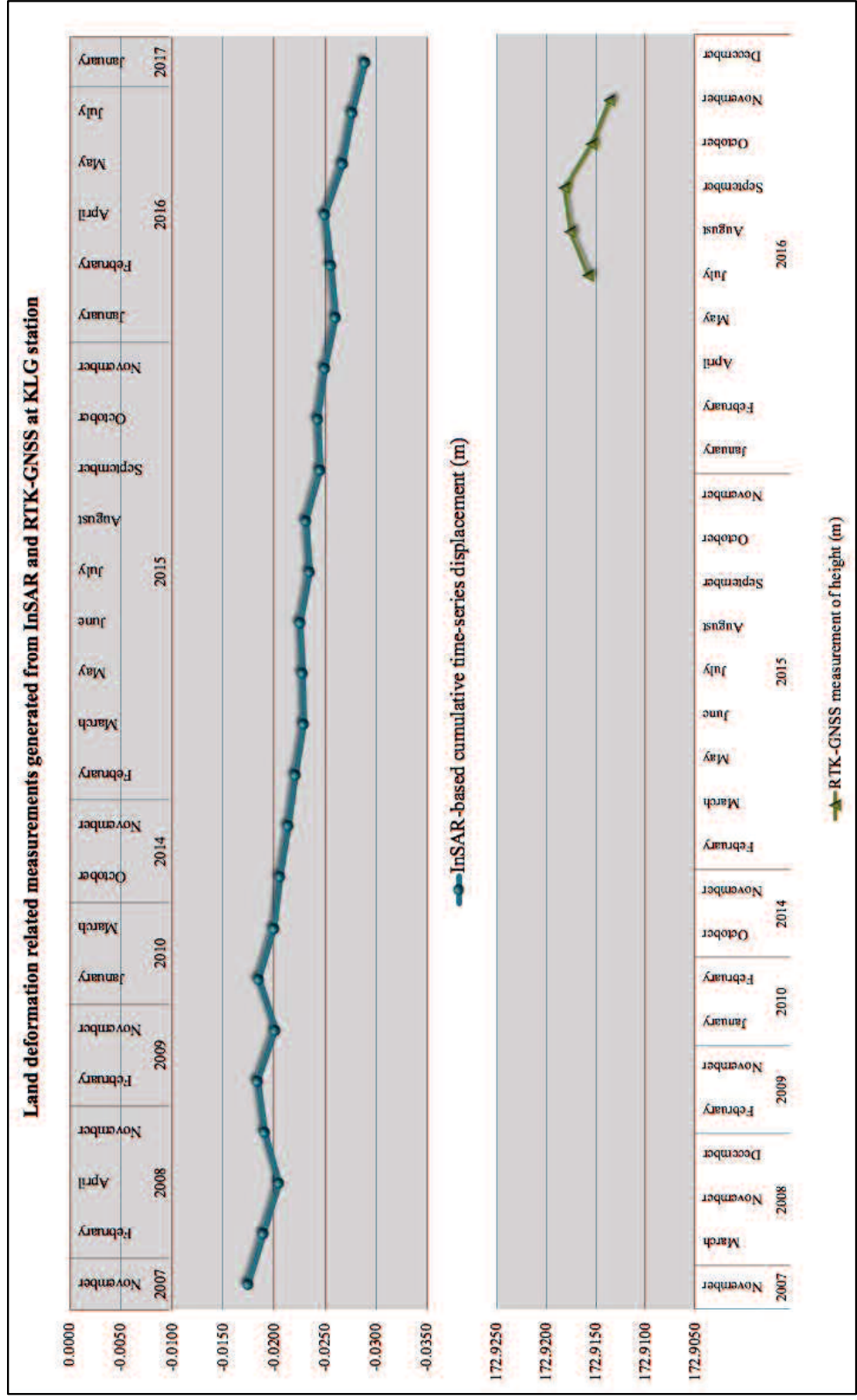


Figure 4.29 Changes of vertical deformation from InSAR and GNSS-CORS measurements at KLG station

### 4.3.3 Relationship Between Displacement and Rainfall

The InSAR measurements were then evaluated with the rainfall data. The evaluation points were selected based on available GNSS-CORS station locations. The GNSS-CORS data refer to the publication of the Central Agency on Statistics in the regions. There are two stations obtained in the subsided areas, i.e., CDNP and CPBI stations (Figure 4.30).

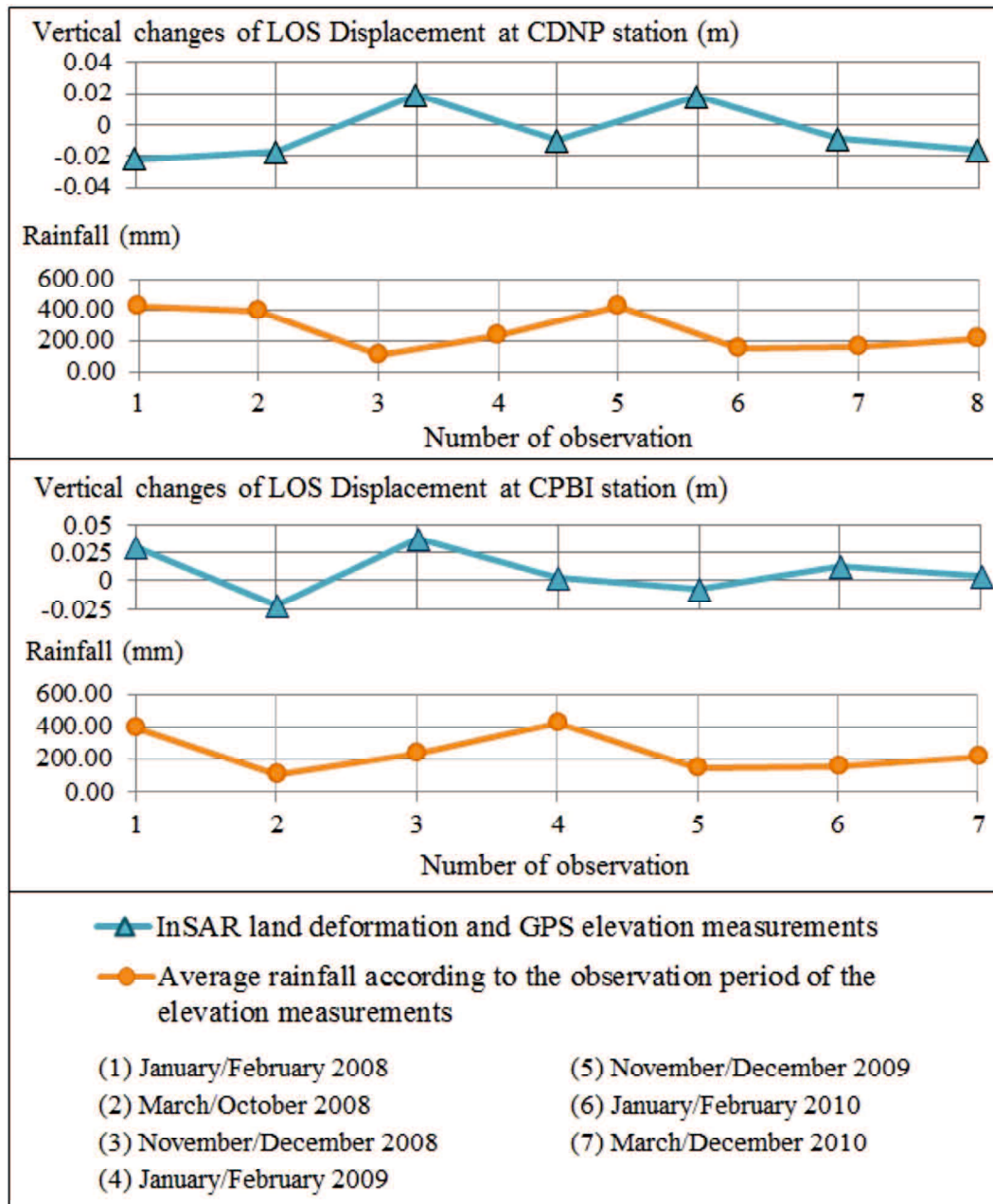


Figure 4.30 GNSS-CORS measurements using CDNP and CSRJ point from 2008 to 2010

There are two conditions can be inferred by referring to the correlation coefficient of the rainfall data with displacement. In the case of CDNP station, the overall records signified that the changing of rainfall during dry and wet seasons eventually resulted in a lowering trend of the land. In contrast, the land deformation fluctuated in opposite with the rainfall at most of the observation periods at the CPBI station. The trend of time-series land deformation was also decreasing from 2007 to 2010.

#### 4.3.4 Estimation of Groundwater Level by Using InSAR Result

Land deformation indicates a linear relationship with groundwater levels in confined aquifers (Sällfors, 2001). An extraction of groundwater generates a change in groundwater level  $\Delta h$  that results in changes in the pore water pressure  $\Delta p$  and the effective stress  $\sigma'_o$  (Chen et al, 2016; Ghiglia and Pritt, 1998). In this circumstance, the effective stress of the consolidation is considered equal to the total stress, as follow (Chen et al, 2016):

$$\sigma'_o = -\Delta p = -\rho g \Delta h \quad (\text{Equation 4.1})$$

The value of  $g$  is gravitational acceleration and  $\rho$  is the density of water.

Land deformation at a surface is measured as integrated compaction over the entire depth of the aquifer system. In general, deformation generated from pumping activities subjects to elastic deformation. The subsidence of land  $\Delta S$  relates with the changes in groundwater level  $\Delta h$ , and inversely proportional to the mean deformation module of the soil  $M$ . In this regard, clay thickness  $\Delta H$  is also involved concerning a difference in the timing of deformation (Riley, 1969), particularly relative to the timing of changes of groundwater level (Chen et al, 2016, Sällfors, 2001). Considering the ability to utilize the time-series InSAR and monitoring well data, the parameters are integrated to find an average  $M$  to estimate  $\Delta h$ , as follow (Sällfors, 2001):

$$\Delta h = \frac{\Delta S * M}{-\rho g \Delta H} \quad (\text{Equation 4.2})$$

The value of the mean deformation module between the groundwater level change and the corresponding deformation was estimated at each monitoring well obtained in subsided areas based on the InSAR land deformation result. Furthermore, the temporal resolution of existing well data was improved by interpolating the InSAR data measurement to groundwater level estimation.

Ratios between the groundwater level change and the corresponding deformation for monitoring wells dataset from 2008 to 2010 were subtracted to estimate the average value of  $M$ . The coefficient was applied to estimate groundwater level change in the subsided areas within the same observation period of the land deformation measurements. The clay thickness was 0.6 m based on soil investigation report of Soil Mechanic Laboratory of Udayana University conducted in the area represents the well site as shown in Figure 4.31 (Udayana Univeristy, 2014). The result denoted that 12 wells out of 18 monitoring wells in

the study area (Table 4.16) encountered groundwater depletion from 2% to 92%. The other six wells were obtained in the area with an absence of subsidence.

Table 4.16 Groundwater level in subsided and non-subsided areas

Number of well	Monitoring well ID	Groundwater depletion (%)						Average groundwater depletion (%)
		2008 -2009	2009 - 2010	2010 - 2011	2011 - 2012	2012 - 2013	2013 - 2017	
1	MW01-BD01	2.40%	-6.25%	5.83%	2.36%	-7.69%	1.67%	-0.48%
2	MW02-BD02	8.89%	-2.33%	1.49%	15.00%	-18.80%	21.89%	7.47%
3	MW03-BD03	2.33%	-20.45%	5.14%	63.59%	16.28%	-53.57%	3.80%
4	MW04-BD04	5.56%	6.58%	8.15%	-13.70%	-2.12%	23.65%	8.03%
5	MW05-BD05	5.21%	-2.23%	3.40%	-10.15%	20.93%	-2.99%	4.04%
6	MW06-DP01	-6.32%	21.72%	3.69%	14.84%	-17.31%	-0.63%	4.57%
7	MW08-DP03	4.31%	18.80%	2.85%	-12.31%	12.28%	13.44%	11.25%
8	MW09-DP04	0.00%	44.16%	2.22%	-16.50%	13.13%	19.43%	17.84%
9	MW12-BL01	0.00%	-9.09%	16.00%	29.31%	-33.33%	-5.00%	-0.60%
10	MW14-JB01	-0.77%	-4.38%	1.32%	7.94%	-11.55%	-0.68%	-2.32%
11	MW15-JB02	1.39%	-1.71%	-6.98%	5.19%	-4.93%	9.56%	0.72%
12	MW18-KR01	46.79%	-38.14%	78.82%	-36.58%	50.41%	0.97%	29.22%
13	MW07-DP02	0.00%	-26.04%	2.08%	32.45%	-17.16%	-10.00%	-5.33%
14	MW10-GR01	0.64%	-0.63%	0.64%	1.73%	-1.95%	-0.25%	0.05%
15	MW11-GR02	0.00%	0.00%	0.00%	-8.79%	68.99%	-0.83%	16.97%
16	MW13-BL02	-3.40%	-4.93%	3.70%	9.43%	-7.05%	-0.56%	-0.80%
17	MW16-TB01	0.94%	-8.19%	0.64%	4.56%	-3.15%	2.50%	-0.77%
18	MW17-TB02	0.00%	5.50%	1.09%	-5.64%	8.01%	0.59%	2.73%

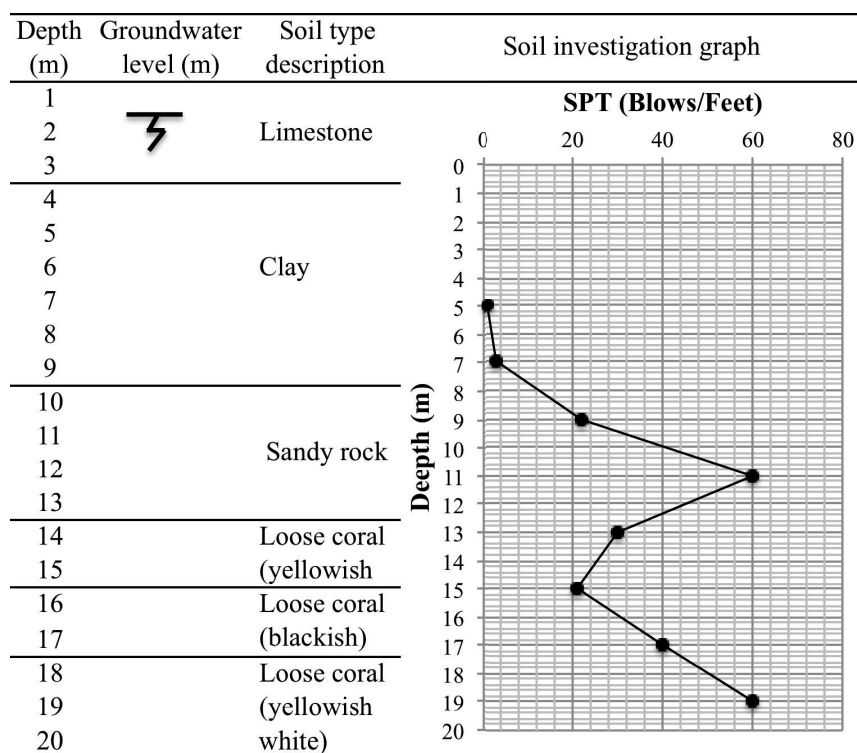


Figure 4.31 Modified soil investigation result at Estuary DAM of Badung region (Source: Udayana Univeristy, 2014)

Moreover, the temporal change according to the inter-correlation of the integrated InSAR and well data analysis was assessed from the monitoring well MW-BD04. The groundwater level change in correspondence with subsidence at the area of monitoring well during the period of 2008 to 2010. Besides the temporal change, the spatial distribution of the groundwater level depletion throughout the study area (Figure 4.31) was extracted based on the land deformation and well data of the groundwater level. The groundwater depletion was assessed based on the average groundwater level changes at the monitoring wells located in subsided areas.

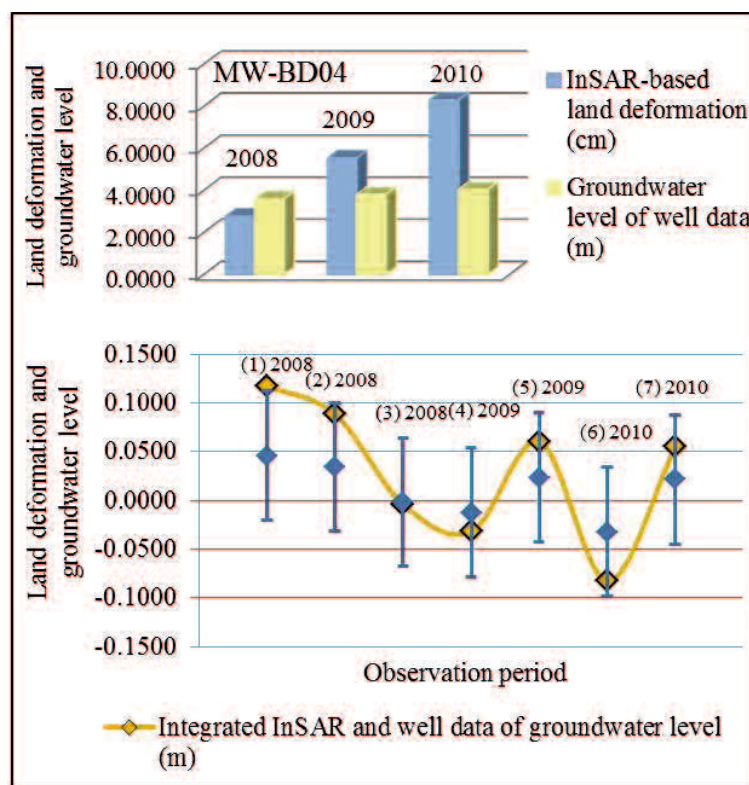


Figure 4.32 Temporal groundwater level changes of integrated InSAR and well data analysis at MW-BD04 monitoring well

In this study, an integrated approach was proposed to analyze the relation of groundwater level and land deformation. Artificial factors such as groundwater pumping may change the natural fluctuation of groundwater (Engdahl and Cecilia, 2013). Firstly, the land deformation was extracted from the time-series InSAR processing of PS and SBAS. The technique is an advanced and wide-spread method of measuring land subsidence by using satellite imageries (Crosetto et al, 2010). The result represented the advantages of the technique in the wide area which also allows information acquisition from areas where manually measurements are not available.

Furthermore, the InSAR analysis result was integrated with well data to analyze temporal changes of groundwater level according to the InSAR observation period. The result was correlated with the monitoring well. The average of  $M$  coefficient was calculated for the 12 monitoring wells located in the subsided areas. There were ten wells inferred consistency between the groundwater level changes with the land deformation. The other four wells with a small change indicated no groundwater depletion despite located in the subsided areas.

Fundamentally, InSAR generates a measurement of the object directions and the vertical movement by recording distances to different objects on the earth surface with an angle (Engdahl and Cecilia, 2013). In this regard, the inconsistency result indicated the shortcoming of the InSAR technique which may deficient compared to the actual land subsidence since it also measures the movement of the object itself (Crosetto et al, 2010). Dredging and dumping of soil that frequently conducted in the area (Putra et al, 2014) possibly resulted in displacement. In correspondence with the land subsidence result presented in Bali from 2007 to 2010, continuous GPS data measurement signified negative deformation in the northern and southern part of Bali, while a positive trend was shown in the central part. CSRJ station was also used as a reference considering that the point is clean from earthquake effect and bias (Sarsito et al, 2018).

Development in the urban area allows external load from buildings on the ground as well as groundwater lowering. As the result of massive development in Bali, subsidence that occurred in some part of Bali area was expected due to the over-usage of groundwater. According to the analysis result of MW04-BD04 monitoring well in southern Bali region, the groundwater depleted at about 2.5 cm per 1 cm of land subsidence. A comparable analysis of land subsidence was conducted due to groundwater leakage into a tunnel. The subsidence was measured to 0.3 – 0.5 m with a head dropped about 10 m (Hansbo, 1981).

Moreover, there is another environmental problem of groundwater resulted from land subsidence in combination with average global sea level rise of 2 mm/year (Hansbo, 1981), that is seawater intrusion. Regarding this problem, the groundwater condition in the southern part of Bali reported encountering seawater intrusion due to high salinity of the water (Sukearsana et al, 2015; BWS Bali-Penida, 2017). The area is located at around CDNP station with average groundwater depletion of 32.67%. A similar condition was also observed in the east part of Bali at around CPBI station. The groundwater depletion in the area was obtained about 22.17%. Seawater intrusion has resulted in the increasing of the groundwater salinity (BWS Bali-Penida, 2017; Hansbo, 1981).

#### **4.4 Classification of Land Coverage Using Optical Data in Combination with Interferometry Coherence**

Taking the inter-correlation between land use changes and the occurrence of land deformation, the changes of land use can be employed to determine the level of vulnerability

of the groundwater damage. In this regard, the land use in Bali Island in 2000, 2003, 2014, and 2016 were classified into six classes, i.e. water area, built-up area, vegetation, paddy field, wetland, and bare land (Figure 4.33 to Figure 4.36). A combination of two difference index of NDVI and NDWI as well as SAR data to distinguish vegetated and non-vegetated areas were applied to the moderate resolution of satellite optical image of Landsat-7 ETM to determine water and non-water area, and vegetation and non-vegetation area, respectively.

Furthermore, the result was processed through a supervised classification method were utilized to create the land use classification with reference to the institutional land use classification provided by the Geospatial Information Agency of Indonesia. According to the reference, water areas are freshwater and fish pond. Vegetation consists of Bushes, forest, grass, plantation, unirigated paddy field. Bare land class refers to the bare land, dry land, sand, and salt field. Wetland area comprises of mangrove and swamp. Paddy field is classification of irrigated paddy field). The land classification is built-up area which denotes residential area and building (including industries, hotel and resorts).



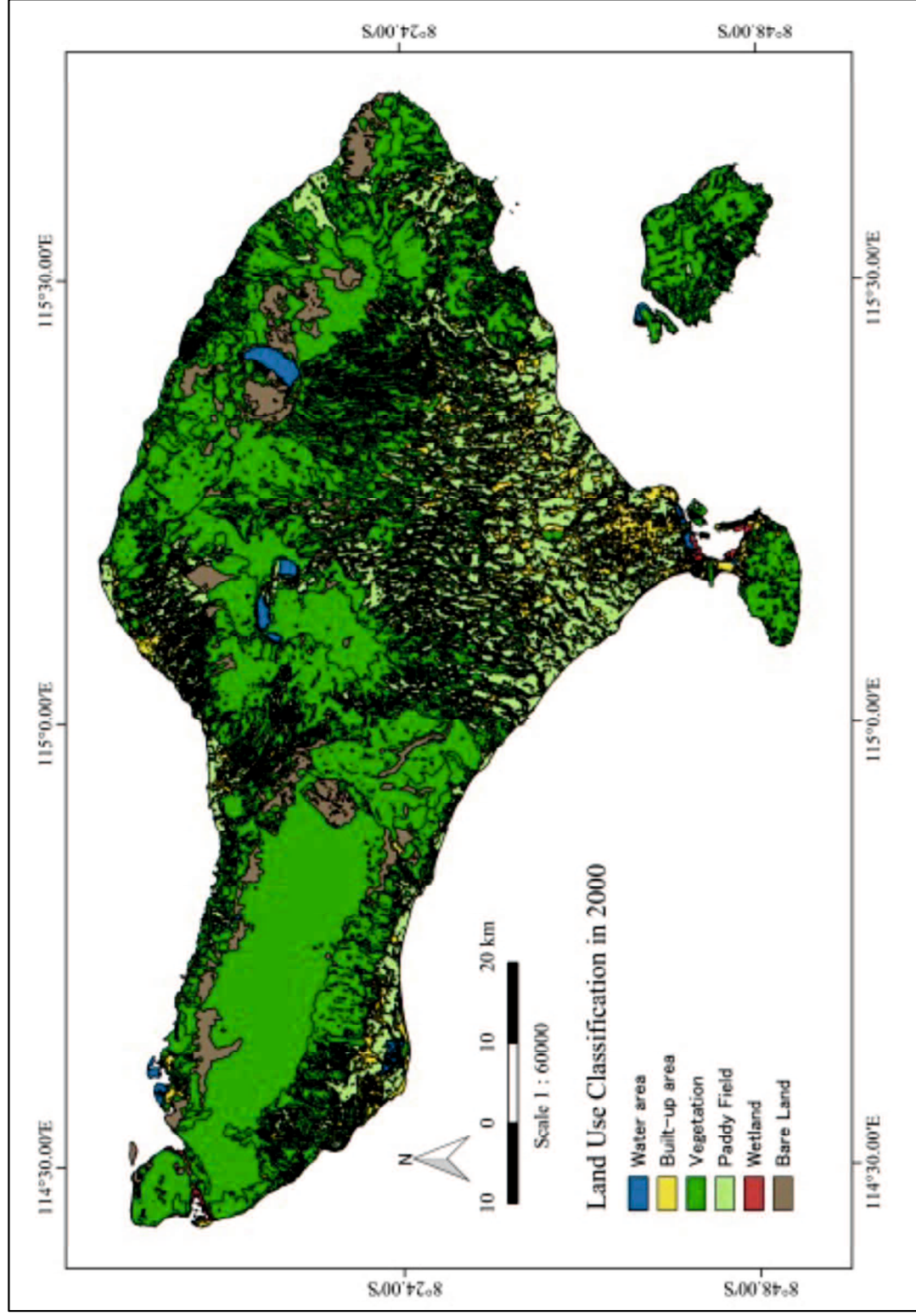


Figure 4.33 Land use classification in Bali Island in 2000

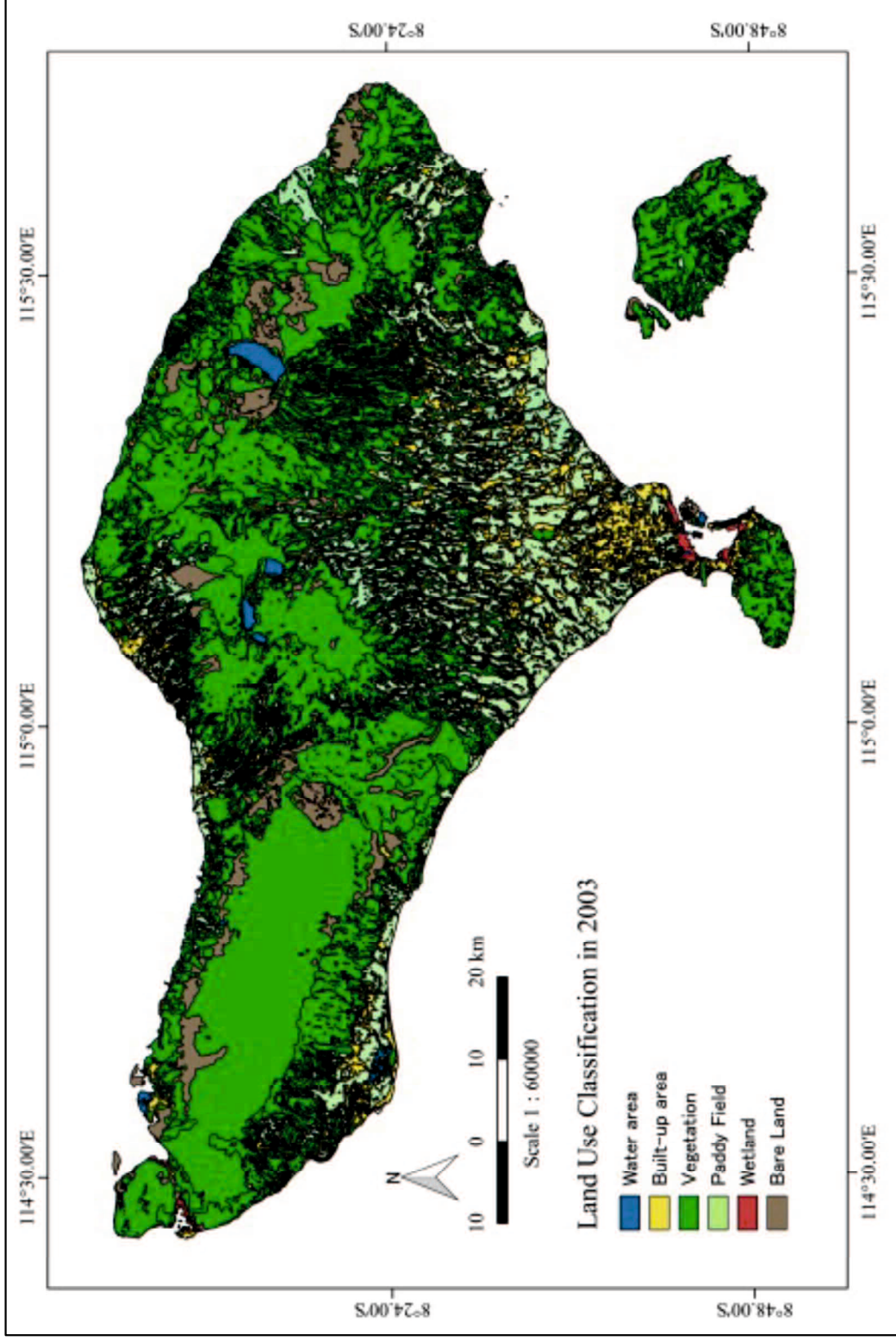


Figure 4.34 Land use classification in Bali Island in 2003

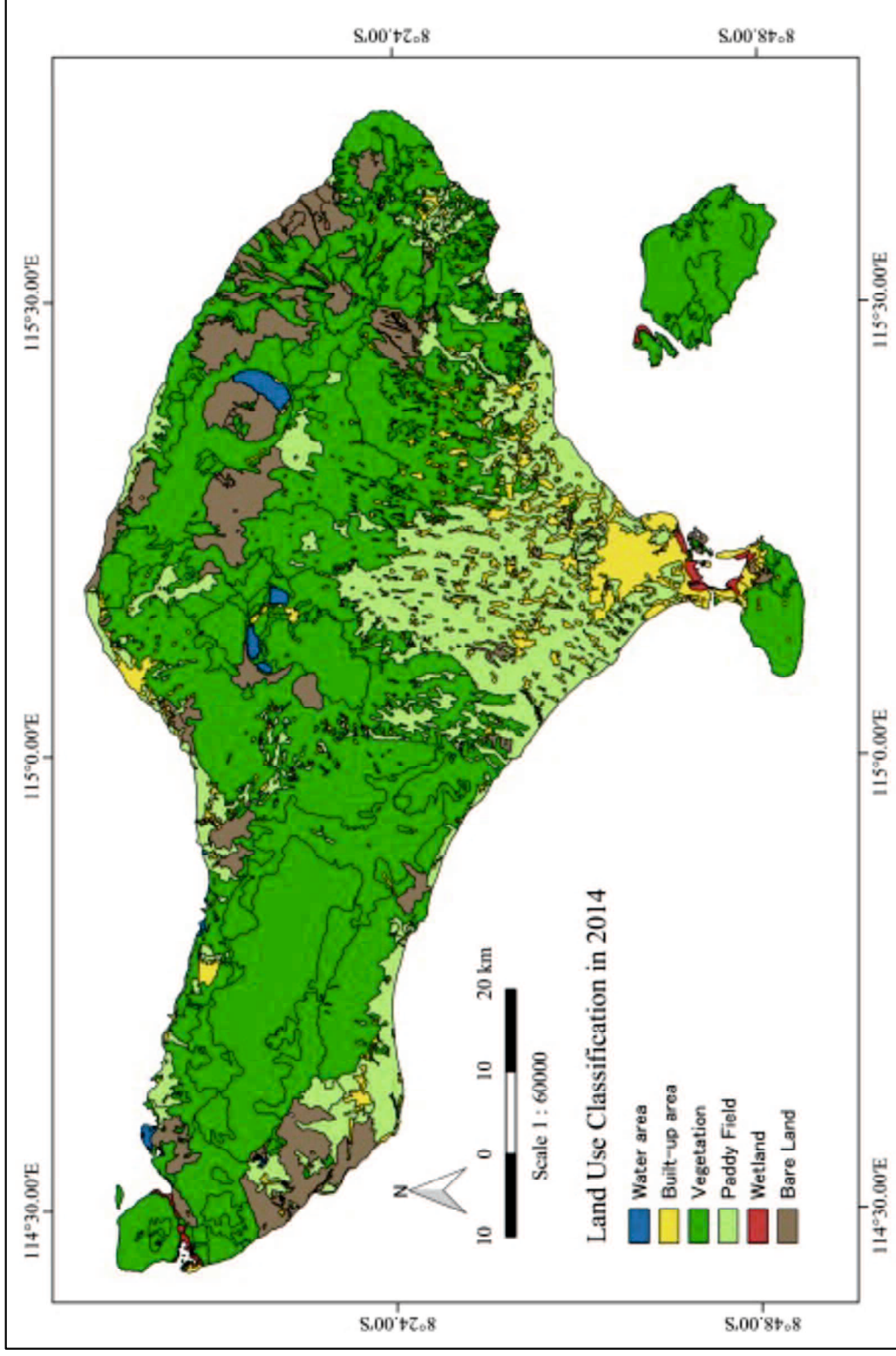


Figure 4.35 Land use classification in Bali Island in 2014

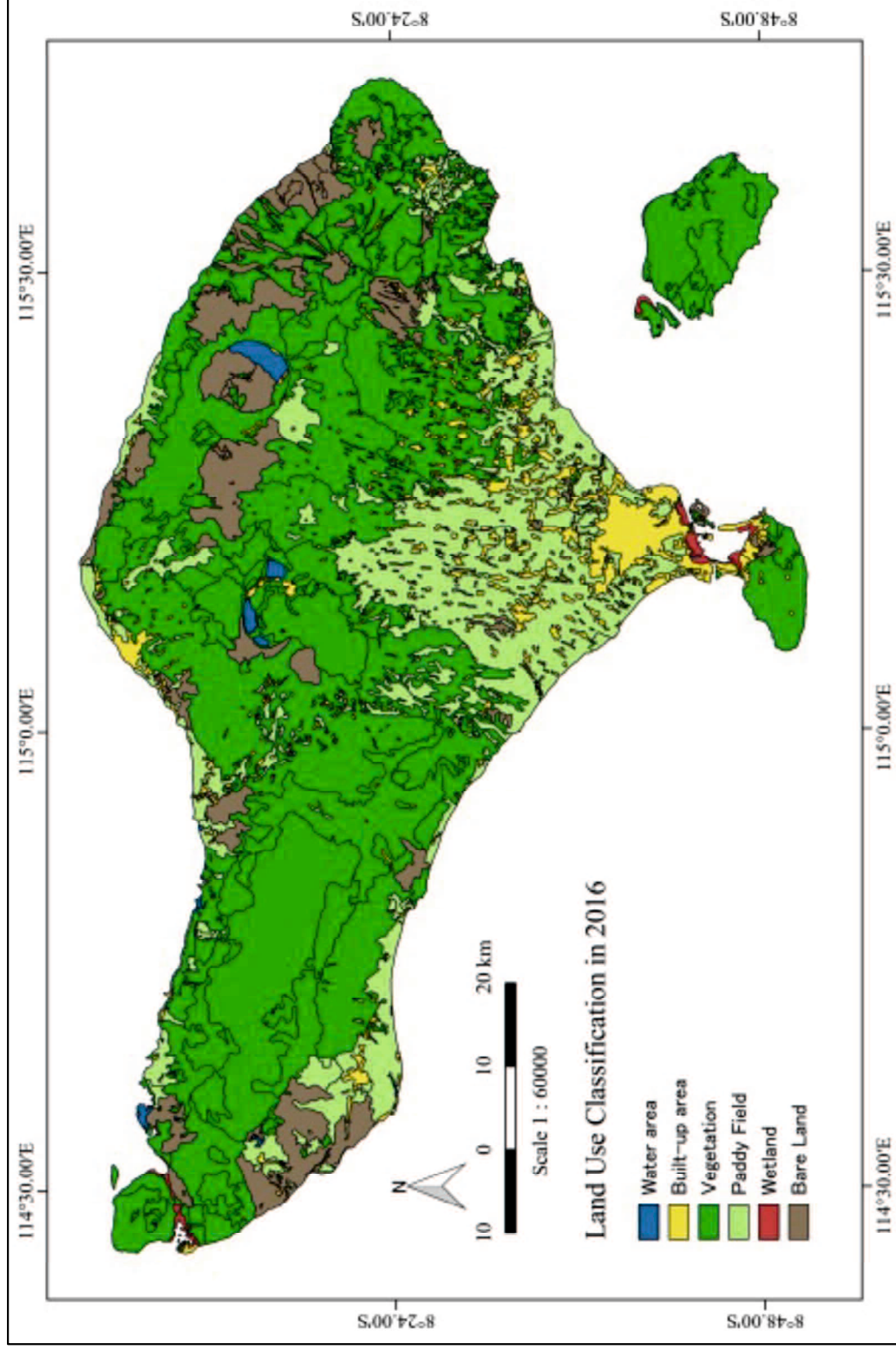


Figure 4.36 Land use classification in Bali Island in 2016

The land use was classified by conducting a semi-automatic supervised classification processing of satellite optical data, to obtain the changes related to the decreasing of the groundwater level. The entire information was integrated to produce the groundwater map in the study area through a spatial multi-criteria analysis of Analytic Hierarchy Process (AHP) and Geographical Information System (GIS). The study area is located in the area of Bali, one of the small island developing sites (SIDS) in Indonesia. The study attempts to propose a method that can be applied to other areas, in particular SIDS.

The land use classification was categorized into vulnerability levels associated with groundwater usage and groundwater level (Figure 4.37). In correlation with the damage level of the groundwater (Figure 4.38), the land use classification of bare land is considered having a low vulnerability. On the other hand, built-up area and paddy field are classified as a moderate to a high vulnerability area whereby the groundwater use has resulted in damages related to groundwater level depression. The moderate vulnerability is given to the land use classification of residential area. Moreover, the high vulnerability is denoted by the land use classification of hotels, resorts, restaurant, and other industrial and services areas as well as paddy field.

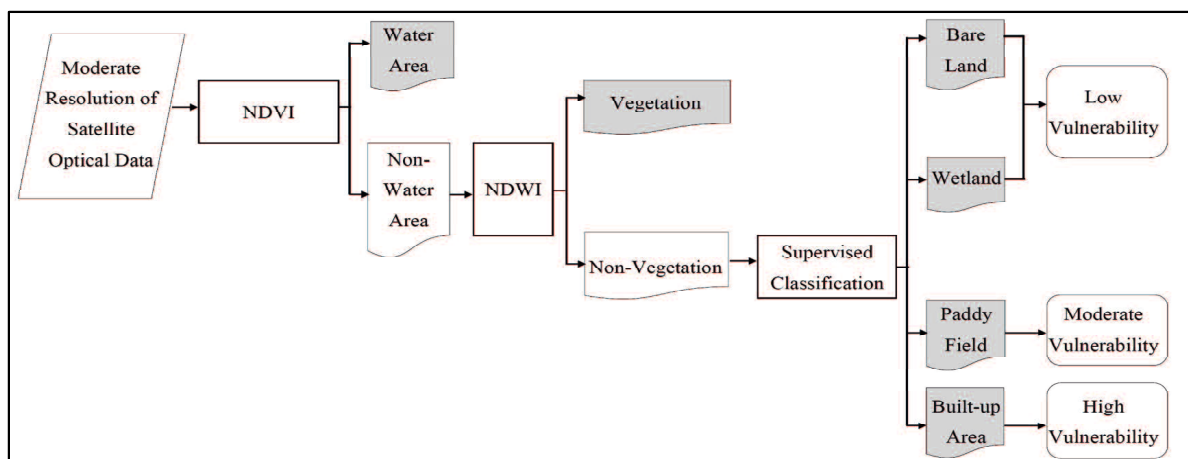


Figure 4.37 Land use classification for the groundwater vulnerability assessment

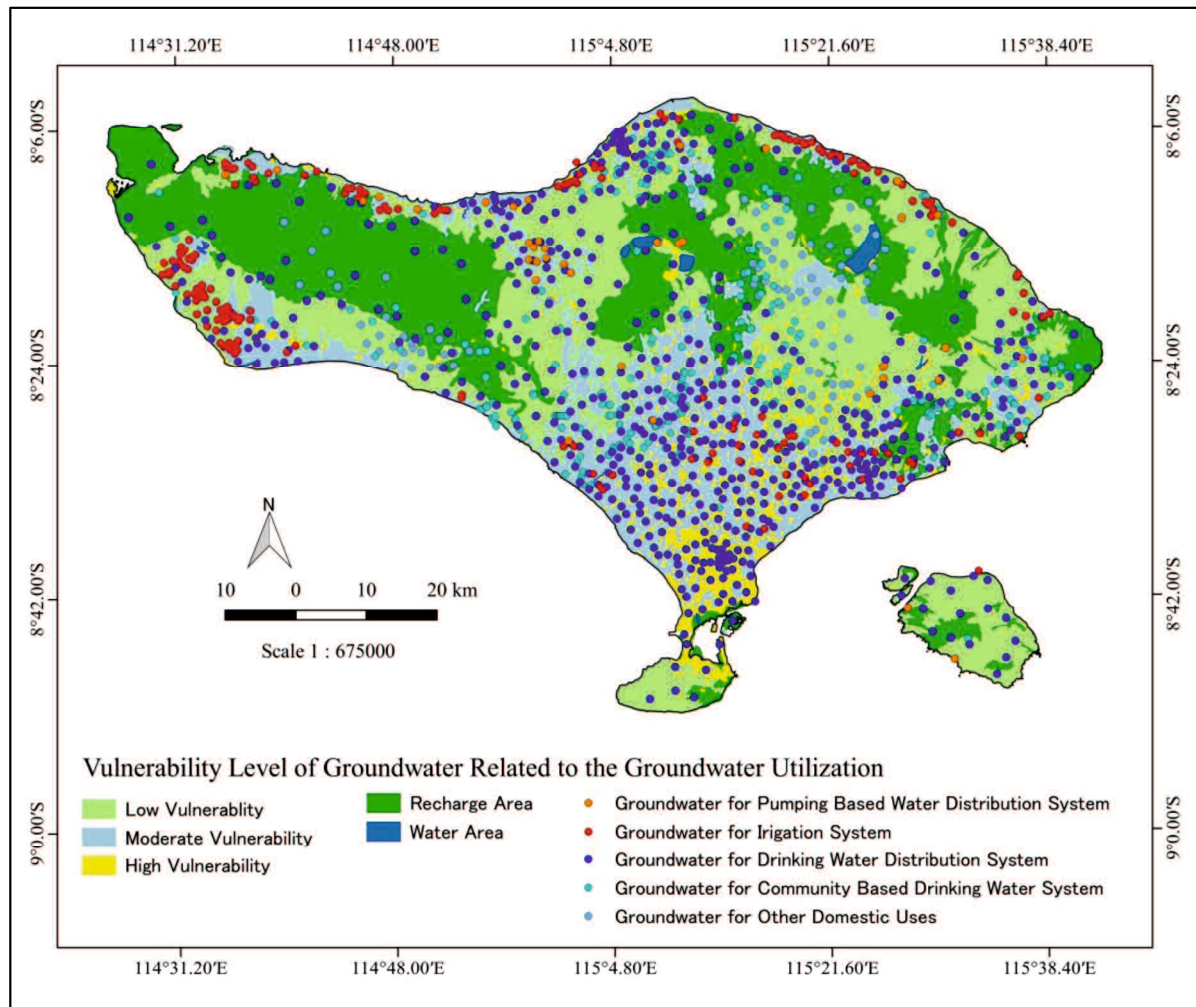


Figure 4.38 Vulnerability level of groundwater related to the groundwater utilization

#### 4.5 Groundwater Conservation Mapping in Bali Island

Scopes of the groundwater conservation are related to the study area, period of the assessment, and criterias, and methods of the data analysis, as follow:

1. The study area is located in Bali Province, Indonesia which includes Bali Islands, and several smaller islands, i.e. Nusa Penida, Nusa Lembongan, Nusa Ceningan, Serangan, and Menjangan. The province area is divided into eight regencies and one municipality, i.e. Jembrana, Tabanan, Badung, Gianyar, Klungkung, Bangli, Karangasem, Buleleng regencies, and Denpasar city.
2. The assessment is carried out for a period of 10 years by utilizing satellite data and data provided by related agencies or intitutions from the year of 2007 to 2017.
3. An integrated assessment of the groundwater level depression associated with land deformation is assessed to comprehend the intercorrelation between these factors by utilizing secondary historical data of groundwater level and differential InSAR of land deformation.

4. Estimation of land deformation is performed comprehensively through Persistent Scatterer (PS) and Small Baseline Subset (SBAS) methods in multitemporal InSAR using L-band SAR data of ALOS PALSAR and ALOS-2 PALSAR-2, and C-band SAR data of Sentinel 1A on an open-source C/C++ codes based Generic Mapping Tools of SAR (GMTSAR) processing system, with a further evaluation using Real Time Kinematic (RTK) positioning technique of GPS.
5. Estimation of groundwater level based on the InSAR-derived land deformation is carried out by employing intercorrelation equations of aquifer properties of groundwater and surface deformation.
6. Assessment of the groundwater level depression due to land use change is conducted by applying semi-automatic supervised classification method using satellite optical data of Landsat 7 on an open-source GIS application of QGIS, that supports viewing, editing, and analysis of geospatial data based on Python code.
7. An improved groundwater conservation mapping is produced through multi-criteria analysis of AHP and GIS by utilizing five decisive parameters, i.e. groundwater level, land deformation, and land use generated from satellite data processing, in compilation with water supply and water quality parameters from data provided by the Regional Bureau of Statistics (BPS) and Regional Drinking Water Agency (PDAM) in Bali.

#### **4.5.1 Zoning of Groundwater Conservation Through Multi-Criteria AHP Scheme**

In general, a GIS can be considered to have several components such as spatial, graphical, numerical, and textual components (Worboys, 1995; Abdul-rahman and Pilouk, 2007). These system components have several important building blocks such as data modeling, data structures, and types of applications. Principally, there is three spatial data component that need to be stored in GIS format; geometric data, thematic data, and a link identification or ID. Geometric component deals with the location of the data by means, for instance, of a reference coordinate system and the thematic component provides the attribute value of the data (Abdul-rahman and Pilouk, 2007). Design and construction phases for a geo-spatial model in integration with AHP is described in Figure 4.39. Furthermore, hierarchical decomposition of criteria, sub criteria, and alternatives of the groundwater conservation mapping is outlined in Figure 4.40.

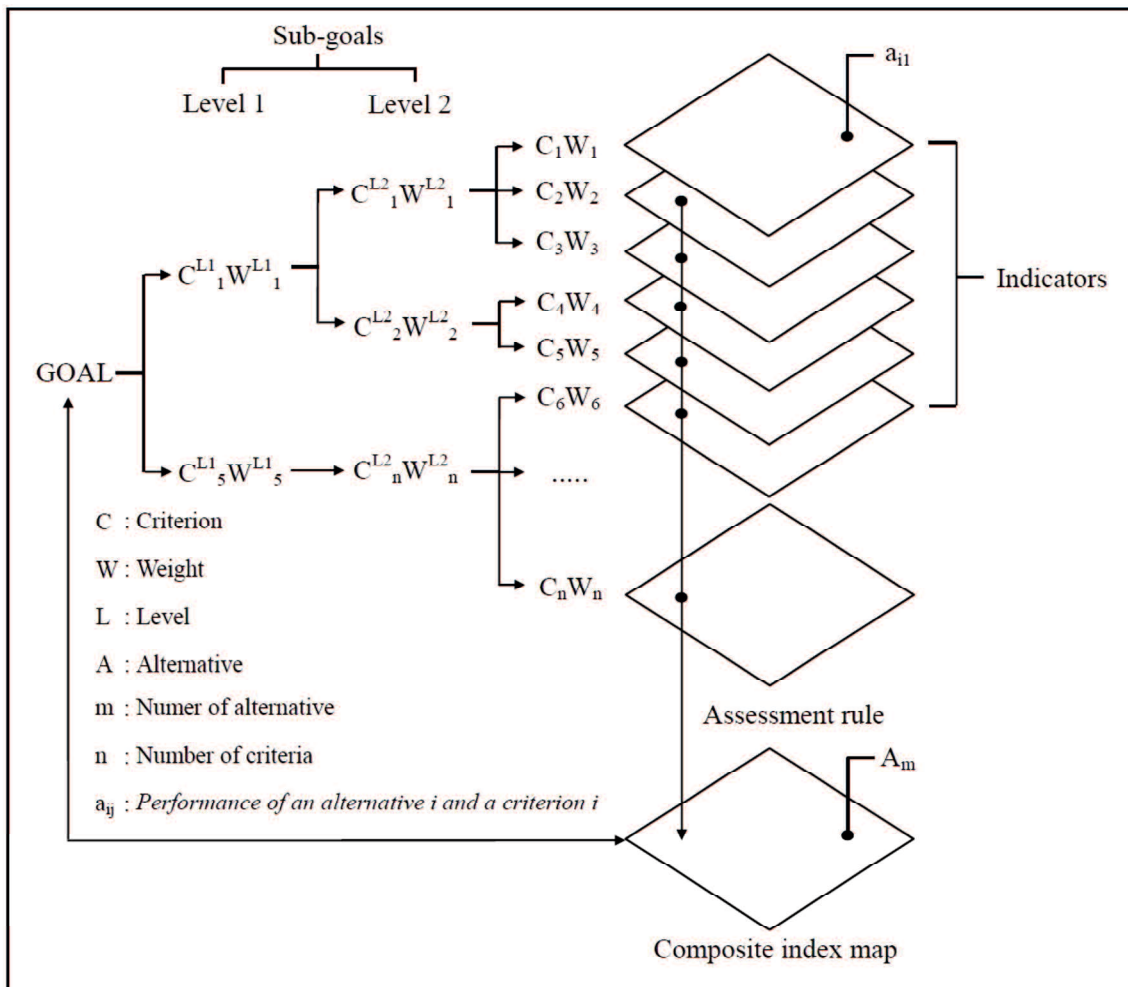


Figure 4.39 Design and construction phases for a geo-spatial model in integration with AHP



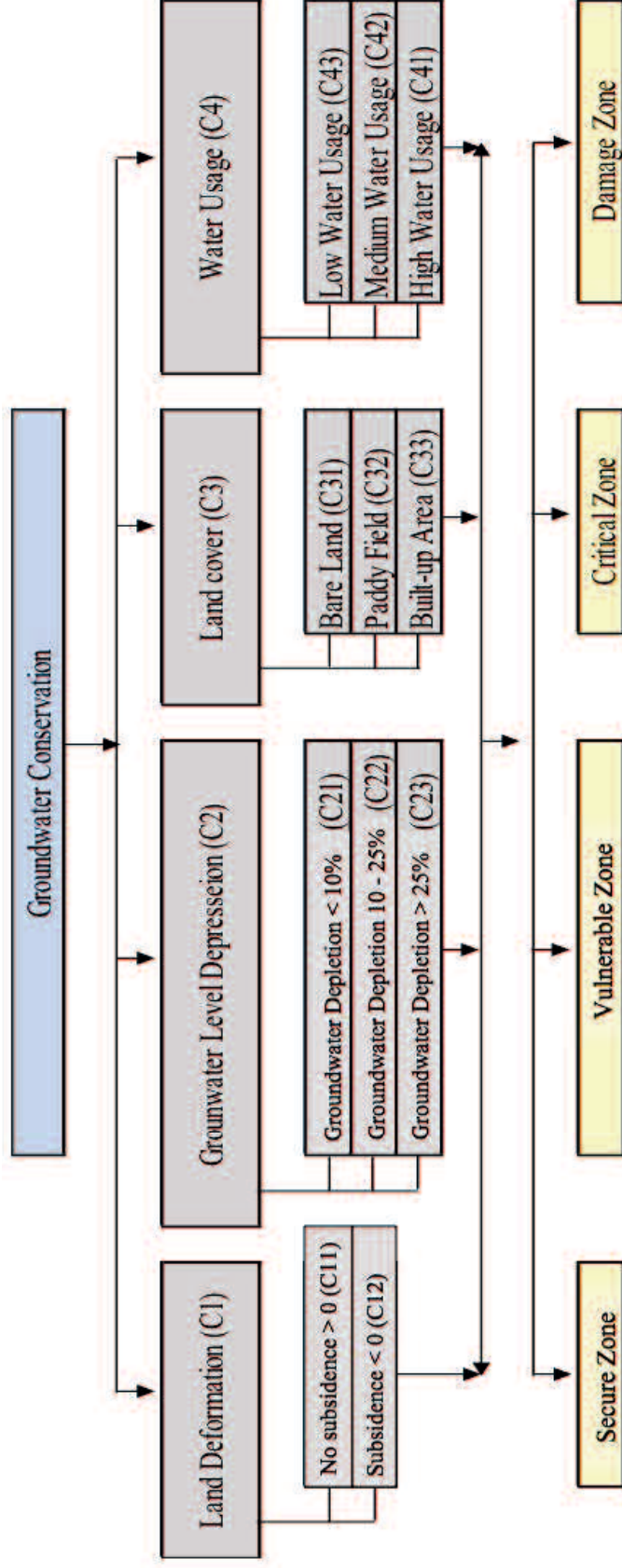


Figure 4.40 Hierarchical decomposition of criteria, sub criteria, and alternatives of the groundwater conservation mapping

Interview was conducted using questionnaire to collect various perception regarding the comparison of the criteria, i.e. land deformation, groundwater level depression, land coverage, and water usage. Experts for the interview are from Database Division of Ministry of Land and Spatial Planning, Engineering Faculty of Udayana University, Ministry of Mineral and Mining Resource in Bali Province, and Water River Basin Agency of Bali-Penida (Figure 4.41). The interview results are utilized as references to determine pairwise comparison matrix (Table 4.17) and further calculate rank of alternatives (Figure 4.42).



Figure 4.41 Interview with experts (a) Database Division of Ministry of Land and Spatial Planning, (b) Engineering Faculty of Udayana University, (c) Ministry of Mineral and Mining Resource in Bali Province, and (d) Water River Basin Agency of Bali-Penida

Table 4.17 Pairwise comparison matrix of groundwater conservation zoning

	Land Deformation	Groundwater Level Depression	Land Coverage	Water Usage
Land Deformation	1	2	3	3
Groundwater Level Depression	1/2	1	2	2 1/2
Land Coverage	1/3	1/2	1	3
Water Usage	1/3	2/5	1/3	1

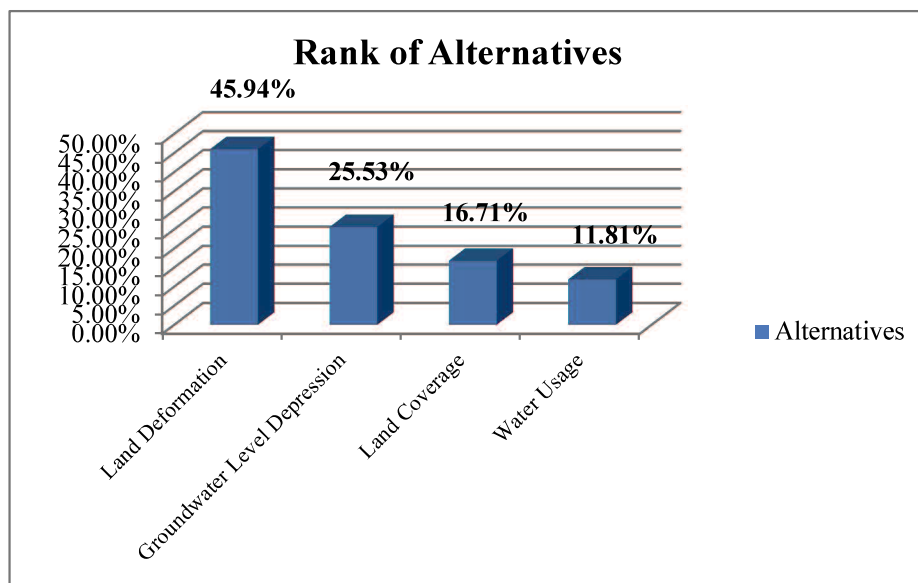


Figure 4.42 Rank of alternatives for groundwater conservation zoning

#### 4.5.2 GIS Mapping of Groundwater Conservation in Bali Island

Groundwater conservation map can be produced by taking into account decisive parameters for assessing the groundwater damage level, such as water quality and the risks of the groundwater resource. Regarding this matter, this study is devoted to providing the decisive parameters by utilizing open-source satellite remote sensing and GIS application to improve the conservation map. The study area is located on Bali Island, Indonesia. An integrated measurement of the groundwater level associated with Interferometric Synthetic Aperture Radar (InSAR) derived land deformation was carried out to obtain sufficient data.

The land deformation is the effect of the decreasing of the groundwater level which is essential in assessing the level of damage related to the groundwater utilization. Despite essentials, the factors have been neglected due to the insufficiency of the data. Therefore, this study is devoted to providing the decisive parameters by utilizing open-source satellite remote sensing and GIS application to improve the conservation map. The study area is located on Bali Island, Indonesia. An integrated measurement of the groundwater level

associated with Interferometric Synthetic Aperture Radar (InSAR) derived land deformation was carried out to obtain sufficient data.

A multi-temporal InSAR technique was applied to estimate land deformation. The L-band of ALOS PALSAR scenes in the year of 2007 to 2010 compiled with the Sentinel 1A scenes in the year of 2014 to 2016 were used for the processing. Based on the time-series InSAR method which was evaluated with Real-Time Kinematic (RTK) positioning measurement of Continuously Operating Reference Station (CORS) data, the land subsidence in Bali was detected in the average of 12.08 mm/year. The correlation between groundwater level in the subsided and non-subsided area are signified on Table 4.18. Groundwater level was observed depleted in the subsided area interpreted from InSAR result. On the other hand, absence of groundwater depletion was obtained in the area without subsidence indication.

Table 4.18 Groundwater depletion and subsidence monitoring results

Number of well	Monitoring well ID	Groundwater depletion		Subsidence rate (cm/y)
		Average (m)	Total (%)	
1	MW01-BD01	0.03	2.40%	0.61
2	MW02-BD02	-0.24	-22.86%	-0.39
3	MW03-BD03	-0.18	-48.84%	-0.17
4	MW04-BD04	-0.16	-27.08%	-0.29
5	MW05-BD05	-0.32	-12.10%	-0.32
6	MW06-DP01	-0.05	-11.58%	-0.27
7	MW07-DP02	0.36	25.44%	0.39
8	MW08-DP03	-0.18	-42.35%	-0.38
9	MW09-DP04	-0.69	-66.24%	-0.66
10	MW10-GR01	-0.01	-0.13%	0.00
11	MW11-GR02	-0.69	-52.87%	-0.17
12	MW12-BL01	0.01	13.64%	0.17
13	MW13-BL02	0.04	3.67%	0.55
14	MW14-JB01	-0.04	-2.51%	-0.95
15	MW15-JB02	-0.04	-1.56%	-0.51
16	MW16-TB01	0.05	3.19%	0.36
17	MW17-TB02	-0.12	-9.34%	-0.40
18	MW18-KR01	-0.44	-56.41%	-0.58

The information was further used to predict the groundwater level through inter-correlation equations. The result showed consistency with the existing well data. The groundwater level depression and land deformation parameters were compiled with other essential parameters, such as water quality, water supply, and land use. In particular, for the land use, satellite optical data processing of supervised classification performed an adequate result for the analysis of land use change. Moreover the other related parameters, i.e. groundwater level and water usage, used for the groundwater conservation map were provided by the related agencies and can be checked by conducting field observation in

representative sites. The entire parameters were employed as input for improving groundwater conservation mapping.

According to the condition of groundwater level, there are various related factors that should be considered for the assessment. In this study, the parameters are limited into four parameter, i.e. land deformation, land cover, groundwater level, and water usage, considering the ability for a continuous provision of the information using satellite data. Nevertheless, available data of rainfall (Table 4.43), morphology (Table 4.44), and groundwater basin (Table 4.45) were also taken into account for the mapping of groundwater conservation zone. These information were collected from related local agencies in Bali. The rainfall map was modified according to map published by Geospatial Agency of Indonesia. Moreover, the modified morphology map signified three classification comprised of lowland, undulating mountains, and volcanic cone. The groundwater basin map was modified referring to the Presidential Law Number 26 Year 2011 regarding the Delineation of Groundwater Basin. An overlay analysis was conducted with the produced map of groundwater level, groundwater usage, subsidence distribution, and land use.

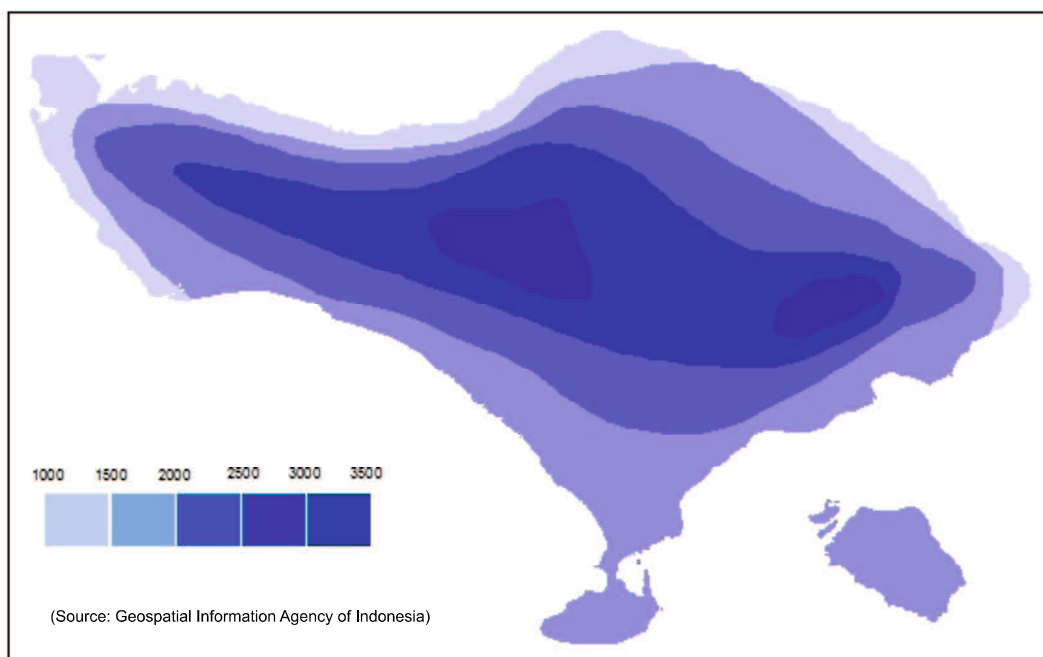


Figure 4.43 Modified rainfall map in Bali

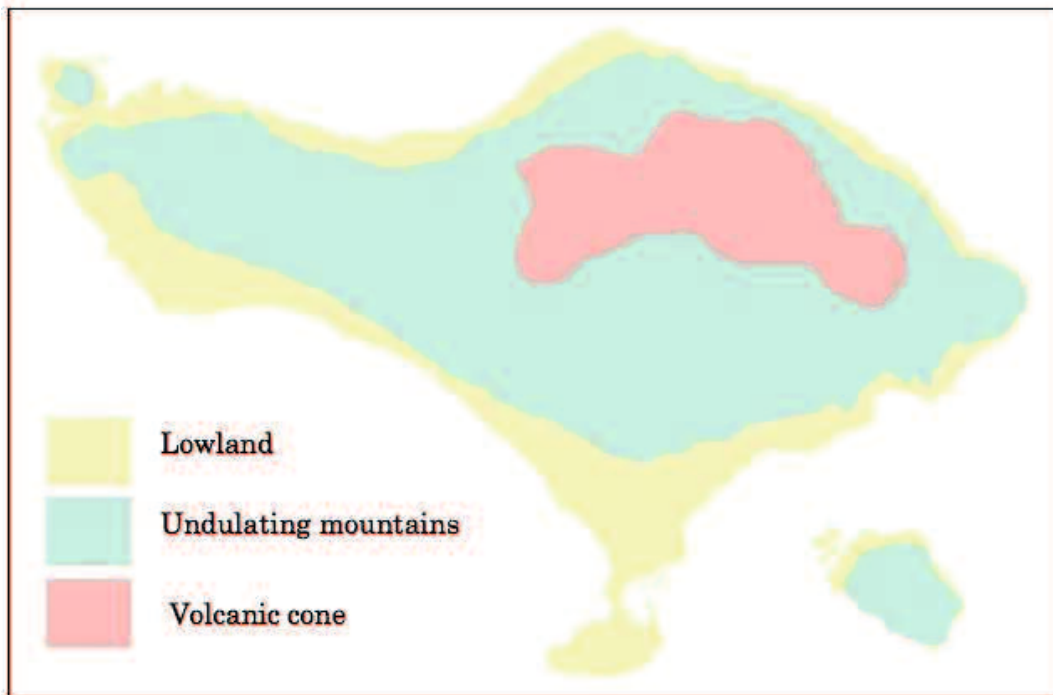


Figure 4.43 Modified morphology map in Bali

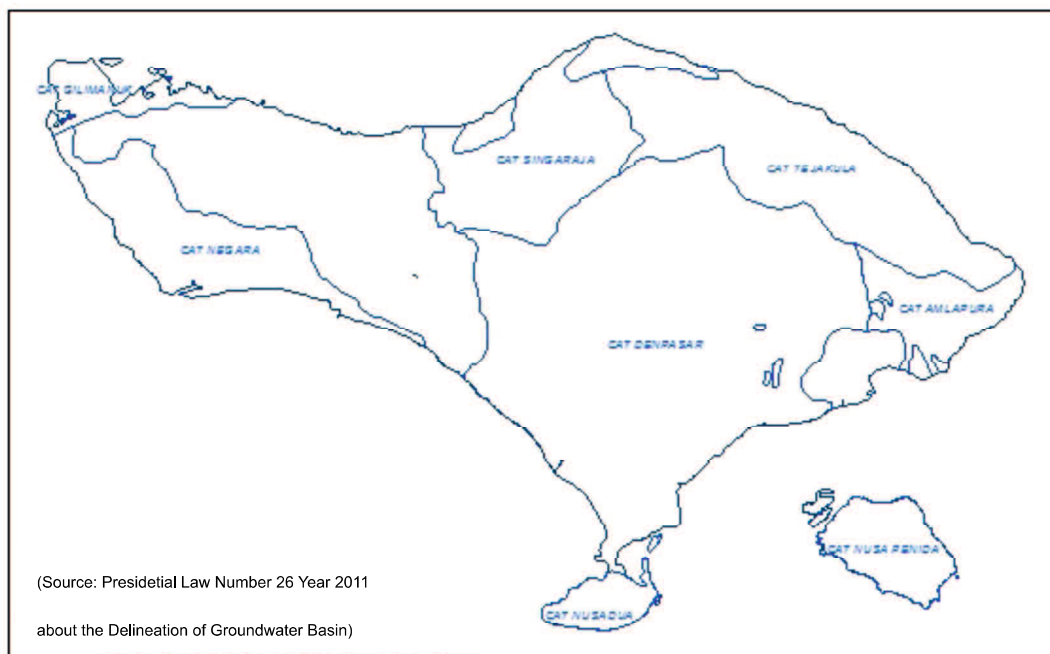


Figure 4.44 Modified groundwater basin map in Bali

In order to run a model in multi-criteria analysis, the creating of spatial data are necessary. The creation of spatial data should follow the design phase and construction phase (Figure 4.39) as well as the Hierarchical decomposition of criteria, sub criteria, and alternatives of the groundwater conservation mapping. Modified map of rainfall, morphology, and groundwater basin described in Figure 4.43, Figure 4.44, and Figure 4.45, respectively,

were used as references for the analysis, such as distribution of rainfall, soil types, and boundary of groundwater basin. Regardless the importance of the data, the information was not utilized as input for the groundwater conservation mapping. Spatial data that used as the input parameter for multi-criteria analysis of the groundwater conservation, were land subsidence, groundwater level, land use, water quality, and water supply. The information of the water usage and groundwater level depression can be seen in Figure 4.4 and Figure 4.6, respectively. The information of the water usage is collected based on field observation. As for the groundwater level depression, the map is created based on data in 2009 and 2011 of the related agency data, and field observation data in 2017. As the final result, the groundwater conservation map can be seen in the Figure 4.46.

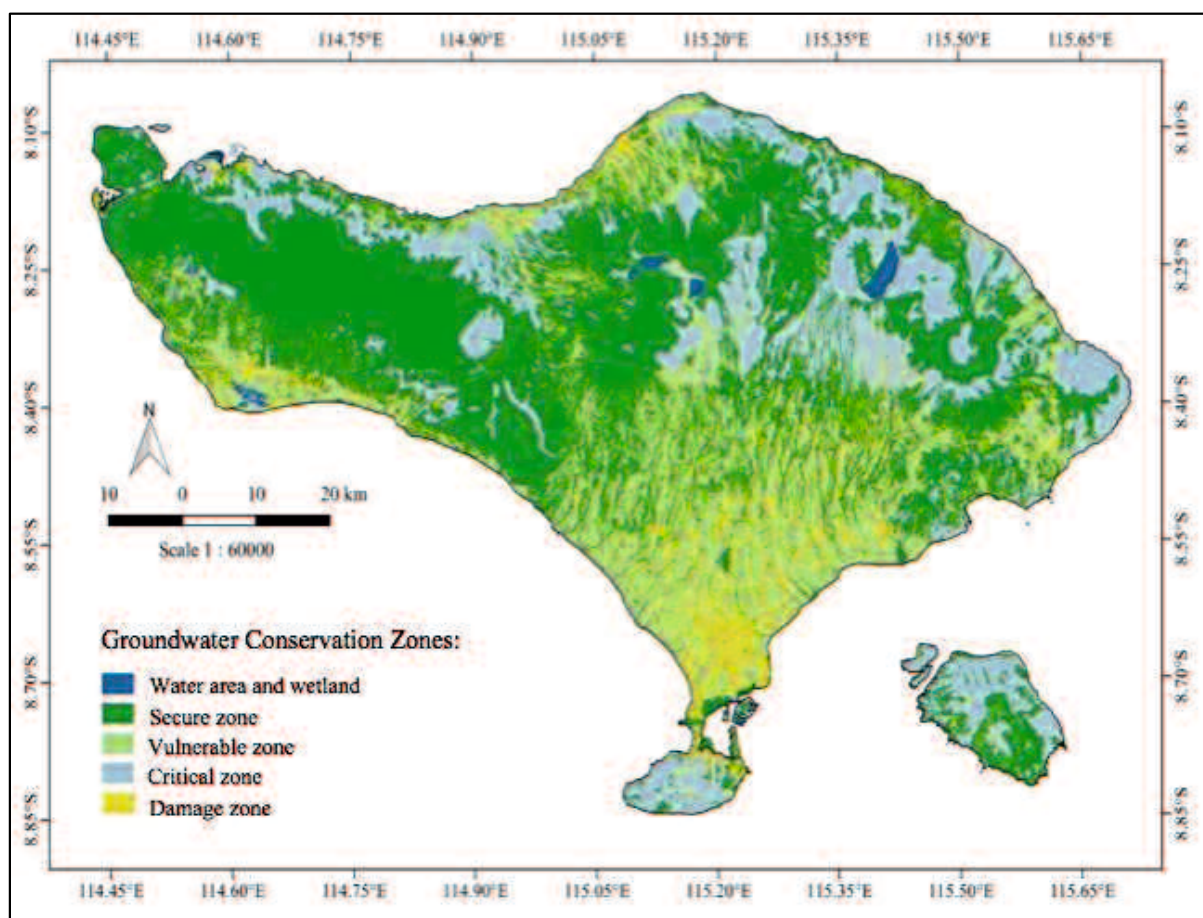


Figure 4.46 Groundwater conservation map in Bali Island

The groundwater conservation map represents safety, vulnerable, critical, and damage zones in the term of the discharge limit of the groundwater, i.e., 150m<sup>3</sup>/day for the safety zone, 72m<sup>3</sup>/day for the vulnerable zone, and restricted use for the critical and damage zones. It can also be used to determine permit of well utilization according to zones. The limit is determined based on the national regulation in the area. The map has a good agreement

compare with the previous map produced by related agency. Field condition in the areas classified as safety, vulnerable, critical, and damage zones are described in Figure 4.47 to Figure 4.50, respectively. Taking the low operational cost and prompt processing time of satellite remote sensing and GIS, the advanced application of the groundwater conservation mapping is supposed to be a potential tool in managing the groundwater resource for sustainable development.



Figure 4.47 Field condition in the areas classified as safety zone of groundwater conservation without subsidence



Figure 4.48 Field condition in the areas classified as vulnerable zone of groundwater conservation with subsidence

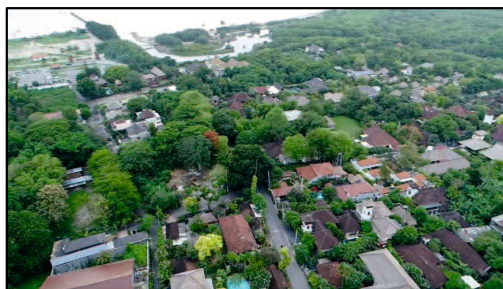


Figure 4.49 Field condition in the areas classified as critical zone of groundwater conservation with subsidence





Figure 4.50 Field condition in the areas classified as damage zone of groundwater conservation with subsidence

Aerial photos taken in the study area showed differences in the areas without subsidence and groundwater depletion (Figure 4.47) and areas with subsidence and groundwater depletion (Figure 4.48 to Figure 4.50) related to groundwater conservation zones. Areas with subsidence are dominated with land cover of built-up area as well as paddy field. Otherwise, areas without subsidence are dominated with vegetation coverage. The map has accuracy of more than 50% compare with existing groundwater conservation related map published in 2014 by the local government. The result indicated an alternative method of geospatial-based hazard risk assessment that able to produce an improved map water-related hazard map.

**CHAPTER V**  
**RISK ASSESSMENT OF TSUNAMI INUNDATION HAZARD CORRESPONDING**  
**TO GEOSPATIAL-BASED MULTI-CRITERIA ANALYSIS OF TSUNAMI**  
**INUNDATION LEVEL MAP**

**5.1 Tsunami Inundation in Chile**

Coastal Chile has a history of very large earthquakes. Since 1973, there have been 13 events of magnitude 7.0 or greater. The February 27th earthquake produced a tsunami that caused major damage locally over 500 km of coastline. The local tsunami water height and arrival times were influenced by bathymetry, coastal topography, aspect, fault slips, and localized subsidence and uplift due to the earthquake (Carderaz- Jiron, 2013).

In Talcahuano, the tsunami arrived 30 minutes after the earthquake with water flooding around the town coastline. Nonstructural damage was widespread; almost all exterior enclosures and contents of commercial buildings and industrial warehouses along the shorefront were damaged by the hydrodynamic loading of the flooding and debris field, and the commercial fishing facilities along the wharf were also rendered inoperable. Debris impact, particularly in the form of fishing vessels, shipping containers, and trucks, caused damage to masonry and steel-framed harbor buildings, though reinforced concrete structures were generally able to with-stand the battering. The piers at the Naval Base at Talcahuano were also damaged due to up-lifted large naval ships and barges (ITIC, 2015).

Scouring of shallow foundations caused a number of buildings to collapse. Sheet pile wharfs in Talcahuano Harbor collapsed or were damaged by soil failure induced by tsunami inundation and drawdown. Elevated pore pressures led to fluidization of backfill during tsunami inundation and drawdown, causing severe scour that damaged sheet pile wharf structures, machinery with shallow foundations, and soil-supported pavements. Eyewitness reports from dock-workers indicated that the majority of damage was caused by the tsunami. In addition, Chilean community had not been properly educated with signs for safety that caused hundred people live were lost.

An event report of the earthquake and tsunami event on February 27th, 2010 has been written by Impact Forecasting LLC. It reported the area of tsunami inundation in some regions of Chile including the area of Talcahuano (AON Benfield, 2010). There is also an inundation map provided by the government institution of Chile that is *Secretaria Comunal de Panicacion, I. Municipalidad*. According to the map, areas along the coast also showed as the tsunami inundation area in Talcahuano (*Secretaria Comunal de PanicacionI*, 2010).

Moreover, according to the historical tsunami events in Chile, the government has made hazard map of tsunami vulnerable areas. The map was created based on research results on tsunami analysis in the area. The latest map of the tsunami hazard map in the area of Talcahuano can be seen in Figure 5.1. The map shows areas of Talcahuano which are

observed as tsunami vulnerable area. The areas consist of housing and public building areas, the port of the city and vegetated areas.

A conspicuous feature of the Chilean tsunami was its extreme variability in height, destructiveness, and wave arrival times as described in Table 5.1. Local tsunami water height and arrival times were influenced by bathymetry, coastal topography, aspect, fault slips, and localized subsidence and uplift due to the earthquake. It was occurred on the February 27<sup>th</sup>, 2010 at 3:34 hours, local time in Chile (06:34 hours UTC). The first tsunami surges generally arrived less than 30 minutes after the earthquake. There were three or four distinct surges. The third or the fourth were typically the largest, arriving between 90 minutes and four hours after the earthquake.

Table 5.1 Water heights and wave arrival times of tsunami in Chile

Community	Water Height (meters)	Approximate Wave Arrival Time			
		1 <sup>st</sup>	2 <sup>nd</sup>	3 <sup>rd</sup>	4 <sup>th</sup>
Curanipe	6 - 9				
Constitución	6.9 - 11.2, 26*	3:50	4:17	4:50	5:20
Dichato	3.6 - 9.4	4:00	5:00		7:30
Iloca	4 - 8.2	4:00	4:25		
Juan Fernandez	5	4:25	4:40		
Pellehue	7.2 - 9.3	4:15			7:30
Pichilemu	4	3:50	4:20		
San Antonio	2.5 - 3.4	3:50	4:20		
Talcahuano	3.3 - 6.3	3:54	5:30	6:00	6:40
Valparaiso	2.6	4:00	4:50	5:20	6:00

(Source: NGDC, 2010)



Figure 5.1 Tsunami inundation level map due to the 2010 tsunami event in Talcahuano, Chile  
 (Source: Creixell, et.al, 2010)

## 5.2 Tsunami Damage Assessment Based on Satellite Data Processing

Damage assessment of the tsunami inundation was conducted due to the 2010 Chile tsunami event. Satellite optical and SAR data were utilized for the analysis to obtain damage location, damage distribution, and the area of damage particularly in Talcahuano City.

### 5.2.1 Monitoring of Tsunami Damaged Locations Using VHR Optical Data

A qualitative observation through visual interpretation of damaged locations was carried out using VHR optical data. Based on research conducted using VHR satellite optical data in three different areas, visual interpretation of the pre- and post-disaster images has produced excellent results for tsunami damage assessment (Ramírez-Herrera and Navarrete-Pacheco, 2012). In this study, the VHR satellite optical imageries were visualized through the natural color composite of a panchromatic sharpened image.

A panchromatic sharpened image represents a sensor fusion between the high spectral resolution of the multispectral and panchromatic images (Sah et al, 2012). The Gram-Schmidt method, based on a general algorithm vector orthogonalization, was used for the panchromatic sharpening, which is necessary for the VHR optical data processing to generate a high spatial and spectral resolution image. Band composite represented the natural color, which was applied afterward to produce colors which would resemble those that would be observed by the human eye. The color channels were displayed in red, green, and blue (RGB) by combining three different wavelength regions (band) of the data (Liew, 2001). The natural color composite of the GeoEye-1 (pre-disaster) and QuickBird (post-disaster) were created using the combination of band 3, 2, and 1, which has the spectral range of red, green, and blue, respectively (Figure 5.2). The results were compared to identify the initial tsunami-damaged areas.

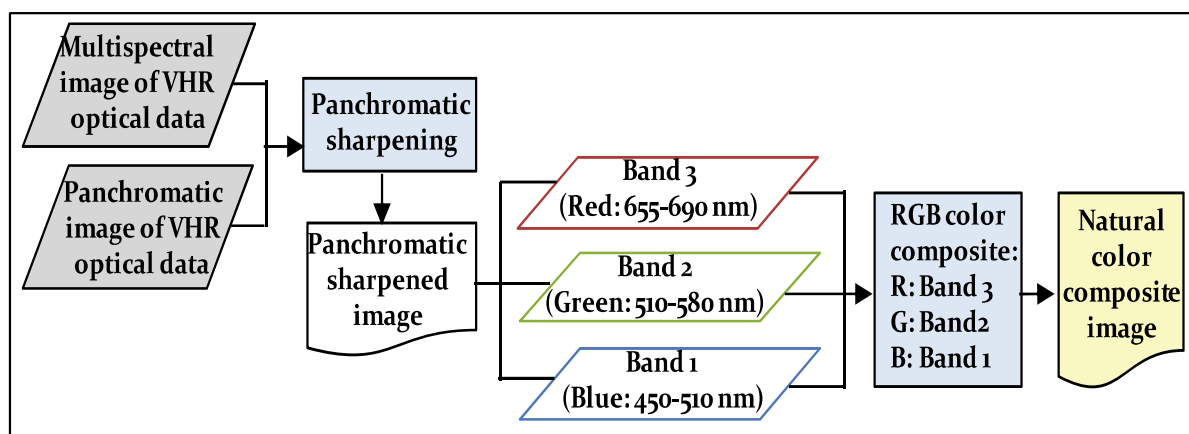


Figure 5.2 Image processing of the VHR satellite optical imageries

The locations that were damaged due to the 2010 tsunami inundation generated by earthquake in Talcahuano area was able to be observed from the visual interpretation of the

pre- and post-disaster images of VHR optical data. Objects could be recognized in detail from the panchromatic sharpened images, with resolutions ranging from 1.65 to 2.44 m. The natural color composite of the images appropriately represented the colors of the surface materials. The extension of the damage was obtained by comparing the condition of several points before and after the disaster. Based on this identification, the damaged (Figure 5.3) areas encompassed the shoreline, the port area, and housing areas, which has a good correlation with field survey reports.

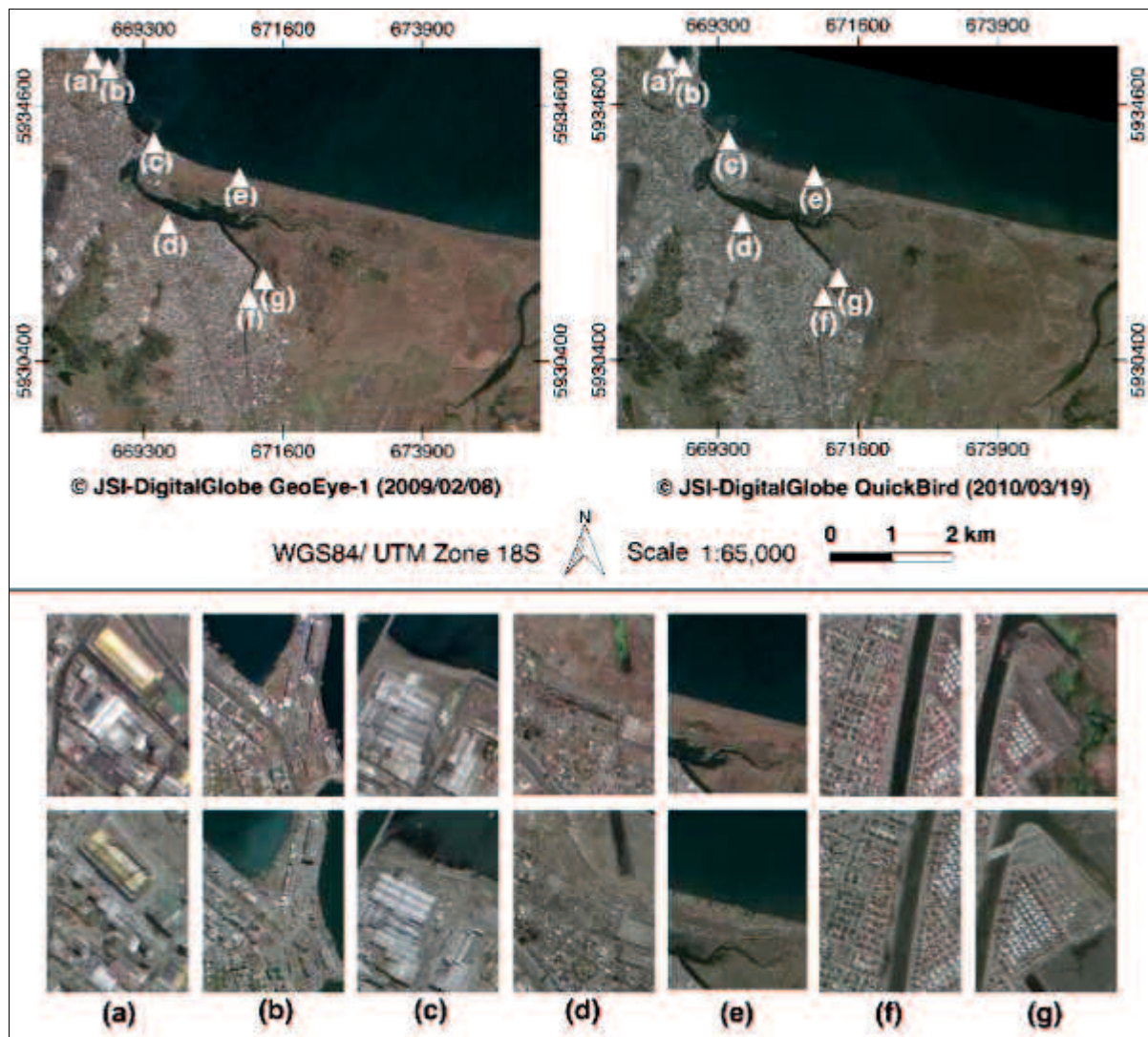


Figure 5.3 Visual interpretation of damage locations due to tsunami inundation from pre-and post-disaster images of VHR satellite optical data

## 5.2.2 Extraction of Tsunami Damaged Areas by Integrating Satellite Optical and SAR Data

A quantitative analysis can be performed by calculating the measured values of the satellite data. ALOS have concerned both high-resolution optical images and Synthetic Aperture Radar (SAR) data. The on-board ALOS AVNIR-2 is the optical imagery of ALOS which has a high-resolution imaging spectrometer operating in the visible and near-infrared (NIR) spectrum. The detection of tsunami damaged areas can be obtained from Normalized Difference Vegetation Index (NDVI) from the post-event imagery (Suppasri, 2012). Furthermore, the ALOS PALSAR is attempted to extract the tsunami disaster area by integrating the data with a Digital Elevation Model (DEM) data as an elevation mask and AVNIR-2 data as a water mask (Iseki, 2013). ALOS data both optical (ALOS AVNIR-2) and SAR (ALOS PALSAR) were utilized for extracting tsunami damage areas. The extraction results were compared with in situ damage map of the disaster. The extraction of tsunami damage areas is very important as a form of mitigation where the areas are generally remote areas which are difficult to observe directly.

### 1. Satellite Optical Data Processing

In the case of the optical imagery, the data values are recorded by a passive sensor, which functions similarly to a human eye, by recording non-polarized sunlight reflectance of the surface materials with a large range of different wavelengths (Liew, 2001). A raw image was produced by converting at-sensor radiance measured in the wavelength region to Digital Numbers (DN) using a quantification system. It contains the effects of the light source, sensor, atmosphere, and surface material without any unit or physical connotation. Therefore, the raw image needs to be corrected by calibrating the DN into radiance. The following equation describes the algorithm for the conversion of DN to radiance (Bouvet et al, 2007).

$$L_{\lambda} = G_{rescale} \times QCAL + B_{rescale} \quad (\text{Equation 5.1})$$

Where,  $L_{\lambda}$  is the spectral radiance at the sensor's aperture ( $W/m^2/sr/\mu m$ ),  $G_{rescale}$  is the rescaled gain,  $QCAL$  is the DN, and  $B_{rescale}$  is the rescaled bias. The rescaled gains and biases for ALOS/AVNIR-2 are shown in Table 5.2.

Table 5.2 Calibration factors of spectral reflectance for the ALOS AVNIR-2

Bands	Wavelength regions ( $\mu m$ ) *	$G_{rescale}$ **	$B_{rescale}$ **	$ESUN$ *
Band 1	0.42-0.50 (blue)	0.5888	0	1943.3
Band 2	0.52-0.60 (green)	0.5730	0	1813.7
Band 3	0.61-0.69 (red)	0.5020	0	1562.3
Band 4	0.76-0.89 (NIR)	0.8350	0	1076.5

(Source: \* Sah et al, 2013; \*\* Bouvet et al, 2007)

The radiance was then corrected to obtain the top-of-atmosphere (TOA) reflectance. It provides acceptable information of surface materials, e.g. vegetation, water, and other areas. Equation 5.2 describes the algorithm for the conversion of radiance to reflectance (Sah et al, 2013).

$$\rho_{\lambda} = \pi \times L_{\lambda} \times d^2 / ESUN_{\lambda} \times \cos \theta_s \quad (\text{Equation 5.2})$$

Where,  $\rho_{\lambda}$  is the unitless planetary reflectance,  $L_{\lambda}$  is the spectral radiance at the sensor's aperture,  $d^2$  is the Earth-sun distance in astronomical units from a nautical handbook,  $ESUN$  is the mean solar exoatmospheric irradiances, and  $\theta_s$  is the solar zenith angle in degrees.

An analytical process to identify changes on land or water surfaces was conducted after quantitatively interpreting an image from the satellite data. In this regard, the difference in the vegetation index, or Normalized Difference Vegetation Index (NDVI), is one of the common methods used. A study after the 2004 Indian Ocean tsunami, using various moderate- to high-resolution optical satellite imageries before and after the event, demonstrated that the tsunami-affected areas were able to be identified from the NDVI (Yamazaki et al, 2006). Therefore, in the present work, high-resolution satellite optical data of ALOS AVNIR-2 before and after the disaster was employed to identify the damaged areas. The NDVI pre- and post-disaster were calculated after performing calibration and atmospheric correction of the raw images. NDVI, as explained in Equation 5.3, essentially measures the reflectance difference between two certain wavelength ranges from  $-1$  to  $1$  (Hansen et al, 2000).

$$NDVI = \frac{(NIR - VIS)}{(NIR + VIS)} \quad (\text{Equation 5.3})$$

Where  $NIR$  is the reflectance of near infrared band and  $VIS$  is that the visible band of red band of ALOS AVNIR-2. In particular, band 4 is NIR, and band 3 is red (Table 5.2). Besides observing changes in pre- and post-disaster images, both of the NDVI values were subtracted to determine a boundary value that could be used to divide the post-disaster image into inundated areas and those that were not. Areas damaged as the result of tsunami inundation lie in the water areas of the image. The inundated area can be calculated by subtracting the pre-disaster water areas from the post-disaster water areas. Figure 5.4 describes the flowchart of the image processing of ALOS AVNIR-2 imageries.



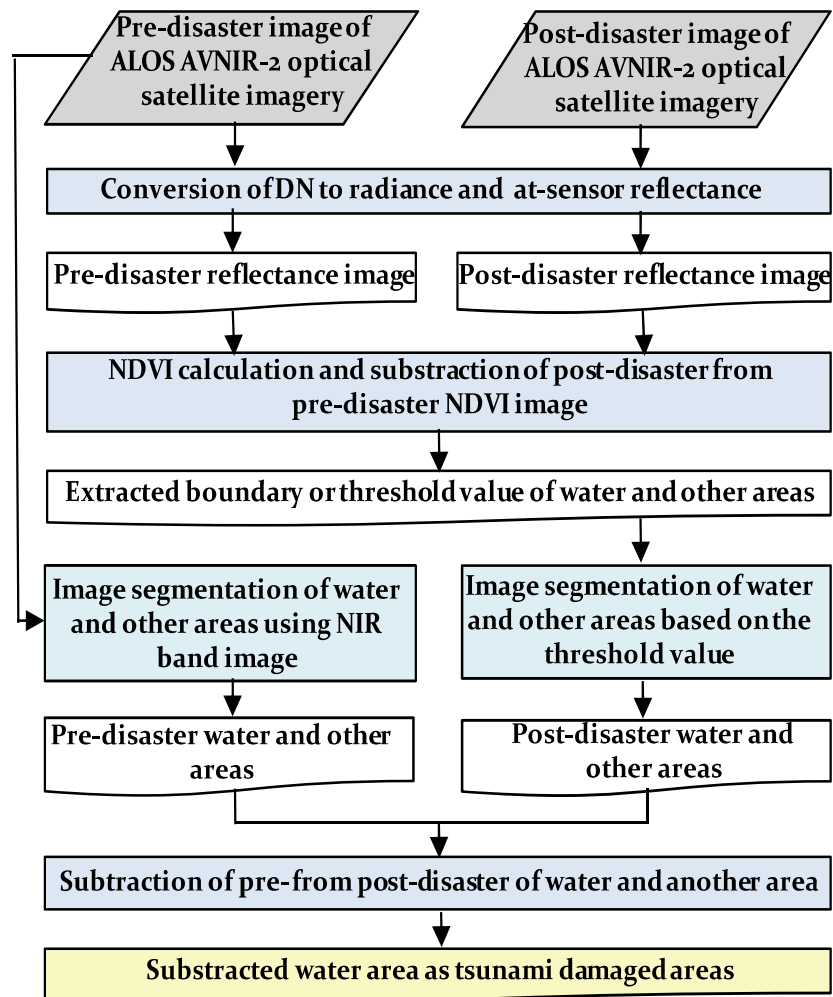


Figure 5.4 Image processing of the extraction of tsunami-damaged areas using ALOS AVNIR-2 imageries

The first step is done by applying color-composites of the optical image of ALOS AVNIR-2 images. The differences between pre- and post-disaster images can be observed visually through the color-composites images. Nevertheless, an integrated image processing is necessary to extract the area of inundation. The color-compositing of the data was conducted after performing a geometric correction process. There 10 Ground Control Point (GCP) utilized for the geometric correction. It is necessary to get corresponding images for the next processes. After the correction process, images were resized according to the research area. Then, the tsunami inundation area was observed by obtaining the true-color (Figure 5.5) and false-color (Figure 5.6) of the images. The true-color composite was used to represent the image close to its natural shades. On the other hand, the false-color composite images represented a red color that indicated areas with strong activity of vegetations or plants.

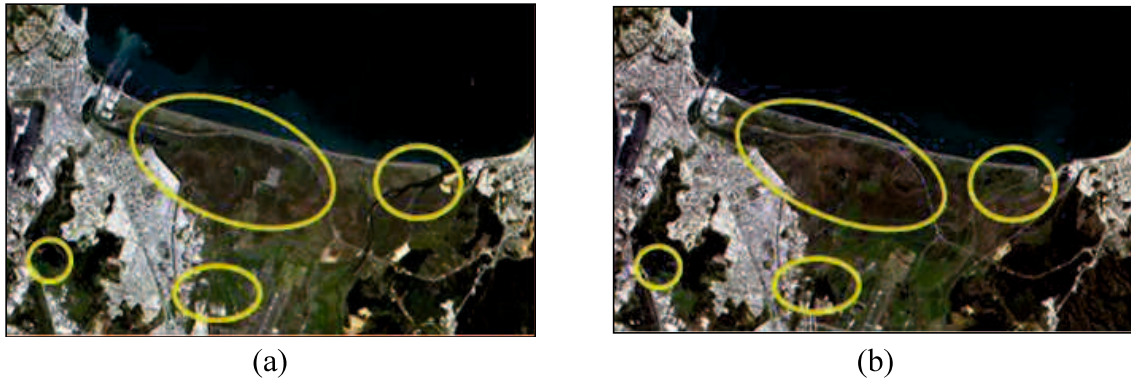


Figure 5.5 ALOS AVNIR-2 true-color composite images: (a) Pre-disaster (2007/2/24); and (b) Post-disaster (2010/9/4)

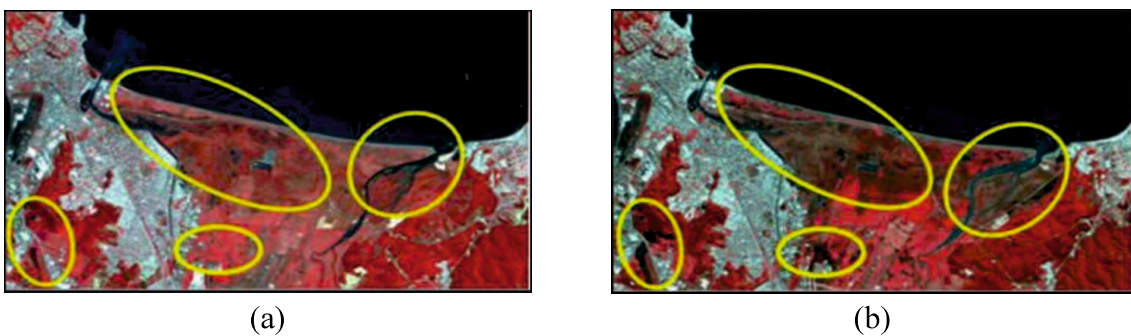


Figure 5.6 ALOS AVNIR-2 false-color composite images: (a) Pre-disaster (2007/2/24); and (b) Post-disaster (2010/9/4)

Figure 5.5 describes the tsunami-damaged areas that were quantitatively assessed based on the NDVI difference before and after the event. The NDVI ratio makes use of the NIR and visible band of red acquired by the optical sensor. The image which is calculated in grey scale can be obtained easily to understand the value of the NDVI. The value which shows the color close to the white color has a high activity of the plant, while a low activity in contrast has the value close to the -1 or shows the color of black. Figure 5.7 below showed the NDVI calculation and classification result of the image. Technically, the sensor forms images of targets on the ground, which reflect and absorb the solar radiation detected by the sensor at a different wavelength. Thus, surface materials such as water or inundated areas can be differentiated by their spectral reflectance signatures.

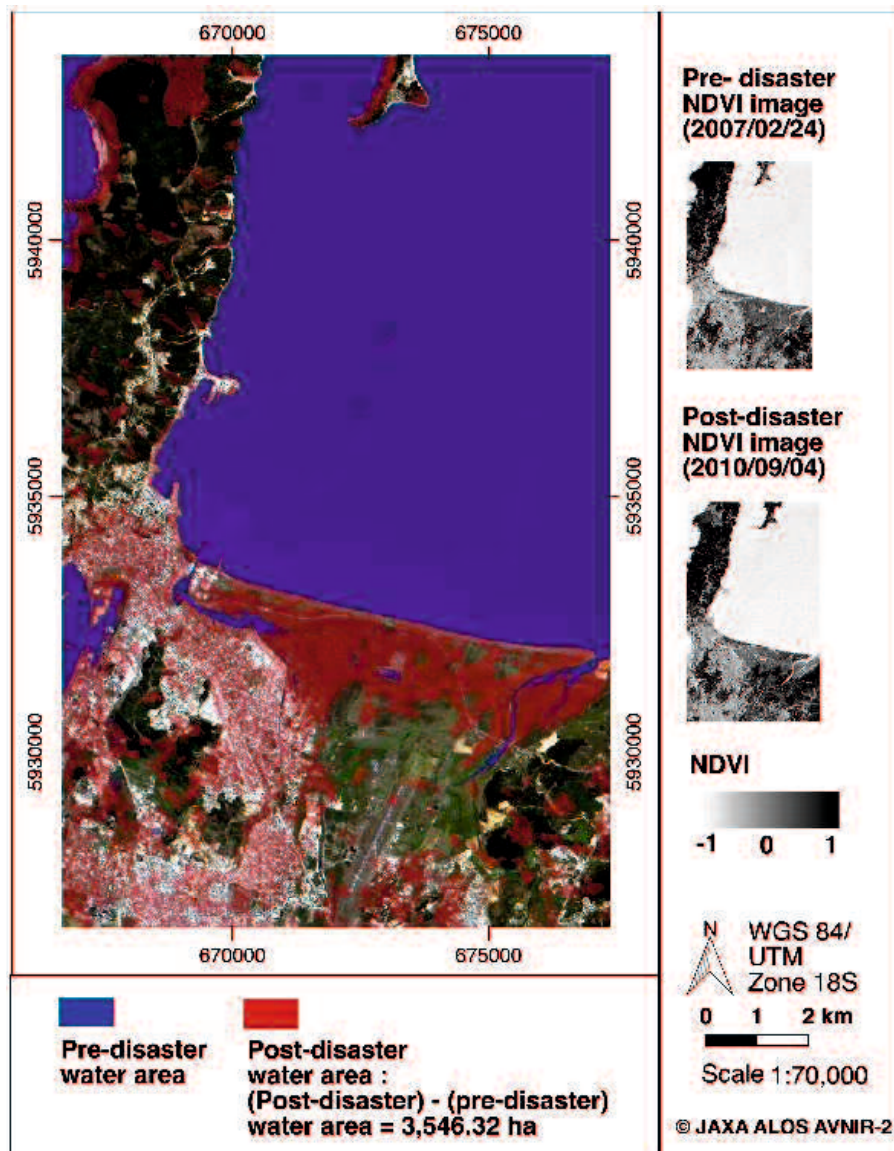


Figure 5.7 Water area changes based on NDVI difference of pre- and post-disaster images of ALOS AVNIR-2 optical data

It is also important to calculate the NDVI based on the converted reflectance values from the DN of the raw image. The values express the reflection from objects recorded by the optical sensor of the satellite. Based on third processing, the NDVI difference in values between the post and pre-disaster images range from 1 to -1. Fundamentally, the NDVI values of water areas are expressed in negative values below 0, while dense vegetation has values of more than 0.5 (Hansen et al, 2000). By subtracting the pre- and post-disaster image, the areas which still had NDVI water values on the post-disaster image represented the tsunami inundation areas. Such areas were observed around the coastal area, housing area, built-up areas such as housing and airport, and water basins alongside rivers, representing a total area of 3,546.32 ha.

## 2. Satellite SAR Data Processing

Additionally, the SAR data of ALOS PALSAR were processed to extract tsunami-damaged areas. Figure 5.8 describes the flowchart of the image processing. One of the advantages of using radar is that the sensor is not affected by the weather and day and night cycles (McCandless and Jackson, 2004). Unlike the optical imagery, the SAR imagery is generated by an active or radar sensor. It emits a light pulse and records the part of the pulse, which is reflected, or scattered, back to the sensor, referred to as backscatter. The radar is a laser, which operates within a narrow and well-defined wavelength band at a specific polarization. It technically works as a flash camera in a dark room (Lillesand and Kiefer, 1993). The wavelength band strongly affects the sensitivity of the radar to the size of objects. It recognizes objects, which have the same and larger spatial magnitude than the radar wavelength. On the other hand, objects smaller than the radar wavelengths have less influence or become transparent on the backscatter (Curlander, J. C. and McDonough, 1991).

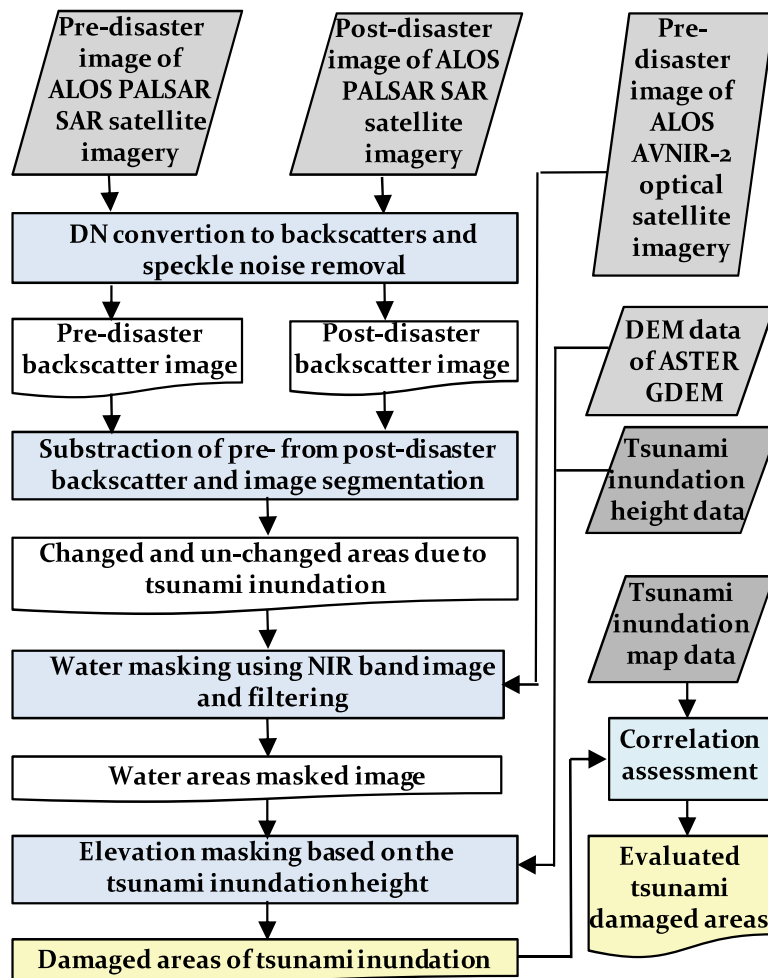


Figure 5.8 Image processing of the extraction of tsunami-damaged areas using ALOS PALSAR imageries

In case of ALOS PALSAR, it operates within the L-band, which has a long wavelength radar signal of 23.5 cm. Therefore, it penetrates through the forest canopy and interacts with the larger structures, such as the trunks and the larger branches of trees. Systems operated at shorter wavelengths are more sensitive to sparse and low vegetation (Matsuoka and Yamazaki, 2000). Moreover, the strength of the backscatter is affected by the radar polarization. Currently, the radar signal of spaceborne radar systems operates with linear polarization. It is transmitted and received at horizontal (H) and vertical (V) polarization (Liew, 2001).

The SAR raw images of ALOS/PALSAR before and after the tsunami disaster are displayed as black and white images, where the image brightness corresponds to the backscattered radar brightness. The brightness of the radar image is dependent on many properties of the objects that are scattering the radiation. There are three primary ways that radar waves scatter off the ground, i.e., rough surface scatter, diffuse scatter, and double bounce scatter. These different scattering mechanisms result in three vary different brightness in the imagery, from dark (rough surface), to medium brightness (diffuse), to bright (double bounce). The scattering mechanism depends also on the orientation angles and incidence angles, as well as the transmitted polarization of the radar. Factors that affect the dielectric constant can also affect the radar image brightness (Comer and Harrower, 2013). The raw images of ALOS PALSAR used in the study are shown in Figure 5.9.

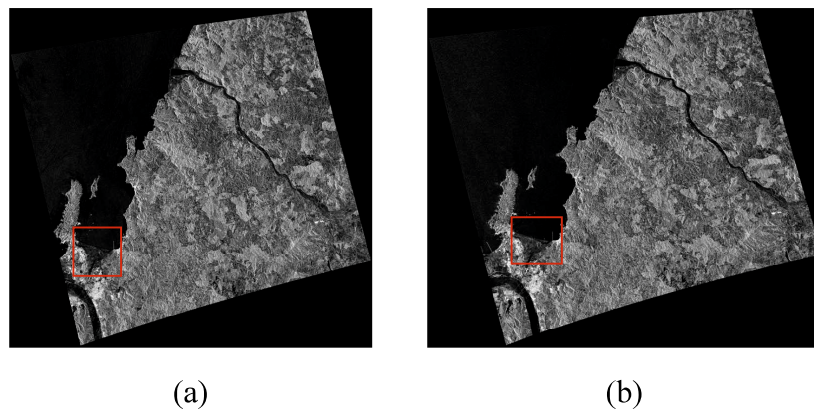


Figure 5.9 ALOS PALSAR raw images: (a) Pre-disaster (2009/3/11); and (b) Post-disaster (2010/3/14)

Firstly, a correction is necessary to get a corresponding image for the next processes. The image is not geometrically corrected due to the shapefile of Chile area. Therefore, it was performed image to image registration using 10 Ground Control Point (GCP). In the image to image registration needs a base image as a correct image and a warp image that is the image which is going to be corrected. In this process, the high-resolution image of ALOS/AVNIR-2 was used as the base image because the image is already corresponded to the shapefile of Chile. The method of the wrapping process is 1<sup>st</sup> degree Polynomial with the resampling

method of Nearest Neighbour. Based on the reference, this method required minimum 6 GCP with the RMS (Root Mean Square) below than 1. The correction process for images before and after the disaster was done by using the method with 10 GCP and the RMS was below than 1. After that, images were resized according to the research area as shown in Figure 5.10 below.

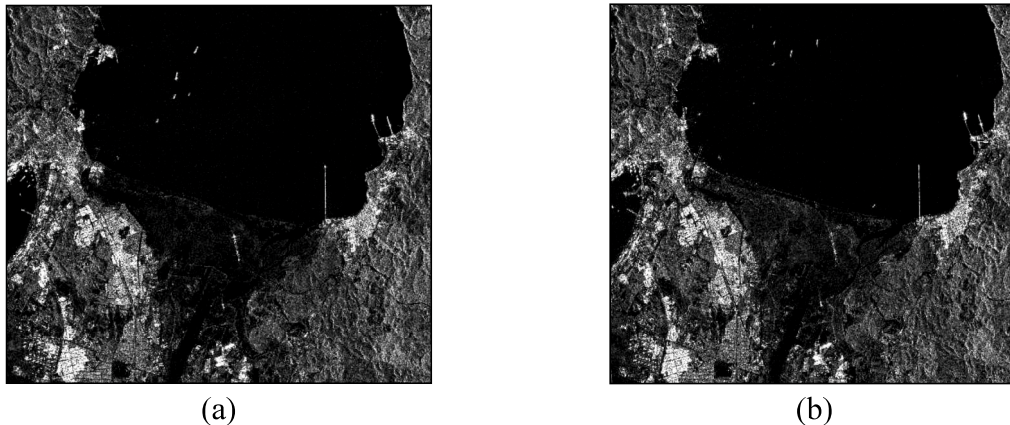


Figure 5.10 Image results of the registration and resize process: (a) Pre- disaster; and (b) Post- disaster

Regarding tsunami disaster monitoring, the backscatter difference between pre- and post-disaster images generated from SAR data in different wavelengths have been successfully utilized to detect damage or inundation areas (Chen and Motoyuki, 2013; Xhang et al, 2014; Gokon et al, 2016). In the present work, the backscatter value was applied for the pre-processing, considering its ability for this purpose.

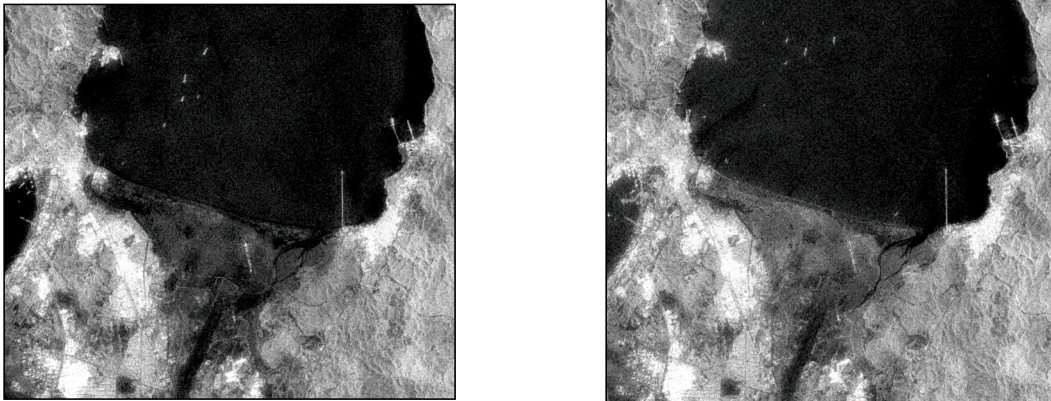
A process of removing speckle noise from the backscattered image results was carried out before the backscatter calibration. The speckle noises were removed using a Lee filtering method to reduce the interferences on the image acquired by the radar image, as well as soften the image. Figure 5.11 shows the result images after removed speckle noise through filtration process. The following is the equation for the speckle noise removal (Dewantoro and Nur, 2012):

$$(|X_a - X_b|^2) \tag{Equation 5.4}$$

where:

$X_a$  : Estimate of the filtered image

$X_b$  : The intensity of the image that does not exist speckle (un-speckle).



(a)

(b)

Figure 5.11 Image results after speckle noise removal: (a) Pre-disaster; and (b) Post- disaster

After carried out the speckle noise removal, images became darker, yet it showed the detail of the image clearer. Then, the calibration process made images became brighter or looked the same as the colour of the raw images. Images also had some values below and above 1 indicated the backscatter value. Darker areas contained value below 1 or minus which can be interpreted as water areas, such as sea water, river, or prospective inundation. While brighter areas contained value above 1 or positive which can be interpreted as vegetation, land or other areas. According to the pre-processing, images were corrected geometrically, filtered from noises and calibrated to get images with appropriate and clear appearance contained backscatter value. The images were then used for the analysis processing.

The radar backscatter per unit area or  $\sigma^{\circ}$  (*sigma-naught*) represents the radar image brightness, which has a unit of  $[m^2/m^2]$ , expressed in decibel (dB). The  $\sigma^{\circ}$  varies even for homogeneous targets depending on the incidence angle, and the angle between the ground and the sensor. In this case, normalization of the  $\sigma^{\circ}$  on the incidence angle can remove the range dependency to eventually obtain a normalized  $\sigma^{\circ}$  or  $\gamma^{\circ}$  (*gamma-naught*) (Lillesand and Kiefer, 1993). The DN on raw images acquired particularly from ALOS PALSAR data can be converted to  $\gamma^{\circ}$ , as described in Equation 5.4, using a calibration factor (K) of -83.0 dB, as provided by JAXA (Matsuoka and Yamazaki, 2000). The result of normalized images by applying the backscatter equation of ALOS PALSAR images can be seen in Figure 5.12.

$$\gamma^{\circ} = 10 * \log_{10}(DN^2) - CF \quad \text{(Equation 5.5)}$$

where:

DN : Value of Converted Brightness

CF : Calibration Factor, that is -83 dB

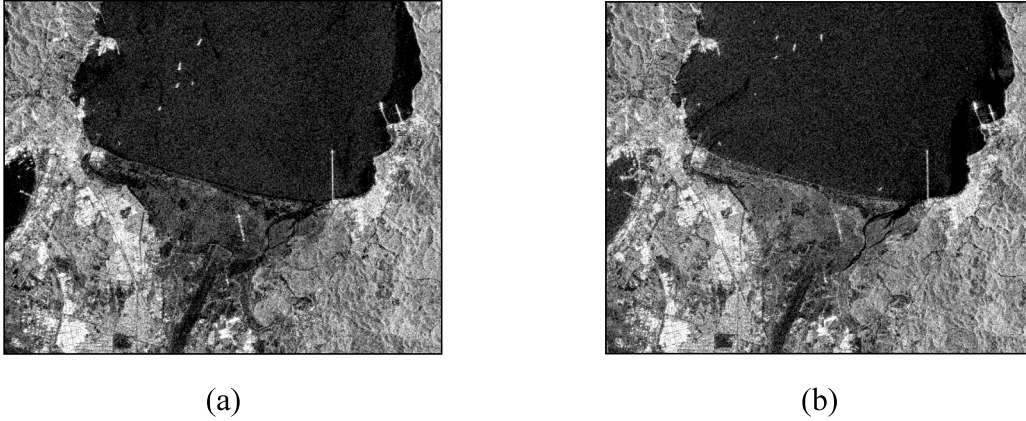


Figure 5.12 Result images after backscattering processing: (a) Pre-disaster; and (b) Post-disaster

Further stage is the analysis processing to find the absolute difference between images before and after the tsunami disaster. The image is obtained by subtracting the pre-processed image after and before the disaster as can be seen in Figure 5.13. In the image, the rubble area shows positive value otherwise the inundation area shows negative value, and the others are non-affected area.



Figure 5.13 The absolute difference of pre- and post-disaster images

A histogram can be derived from the image result. It is created from the statistics calculation of the image values. The pre- and post-disaster images have some differences because of some changes due to the disaster. The pre-processed image signifies many changing values, so that there are some changing points that might be refer as a threshold value. This value is applied to an image in order to classify or segment images into two different areas. However, the threshold value is observed clearly in the absolute difference image. It is used for the segmentation process. A segmentation threshold value of changed and unchanged area values was obtained based on the subtraction results of the post-disaster from the pre-disaster backscatter. The changed area values were obtained initially as tsunami



damage areas.

Afterward, the damage analysis was conducted more thoroughly on the analysis processing. Masking is the main process of this step, which was undertaken through the use of other satellite data. Fundamentally, a mask is a raster image that consists of the values of 1 and 0, which denote the active pixels and the masked pixels, respectively. By multiplying the mask onto an actual image, masked pixels are screened out from the image, so that the image only has the desired pixels (Liew, 2001). In this case, a water mask from the NIR band images of ALOS AVNIR-2 and an elevation mask of the tsunami inundation height from the DEM data of ASTER GDEM were created for the analysis processing.

Water areas can be observed adequately through the NIR wavelength of the optical imageries, such as ALOS AVNIR-2. The water mask is used to eliminate the water areas, e.g., sea water, river, lake, pond, and so forth, obtained by the optical sensor on the post-disaster image of ALOS PALSAR. Therefore, the resulting image only contains values of inundation water, and not actual water areas, and thus represent the extent of the tsunami-damaged areas. A median filtering method was then applied to the result to reduce disturbances in the image.

The water mask processing in this analysis was conducted to omit water areas, i.e. sea water and river. Therefore the image values which indicate water areas might be the inundation areas. The pre-disaster image of AVNIR-2 band 4 (Near Infrared band) was used as a mask of water area. The first step of mask processing was created a range value of water areas. In general, the value of water areas is ranging among the percentage of cumulative frequency of 20% to 60%. Thus, some range values which lied at those percentages were used. The best range was given by the value of the percentage of 45% which ranged among 1-41. The value of percentages below it showed small areas of water. In the other hand, the bigger percentage values gave too large water areas. The water mask was created by using the range value of water areas. The mask of water body has value only of 1 (white area) and 0 (black area). The area which has values among the range values of water areas will turned into black colour with the value of 0. These areas are the area of sea water and river which will not be included in the inundation area calculation.

The mask of water body that has been built was then applied to the ALOS/PALSAR image to deplete the value of the water areas. It is necessary to adjust the resolution of the mask image and the image which will be masked. By applying the mask, areas which have value of 1 are left with the original raster value of the original image, but areas which have the mask value of 0 will also have the value of 0. The mask and the image result after the masking process are shown in Figure 5.14.

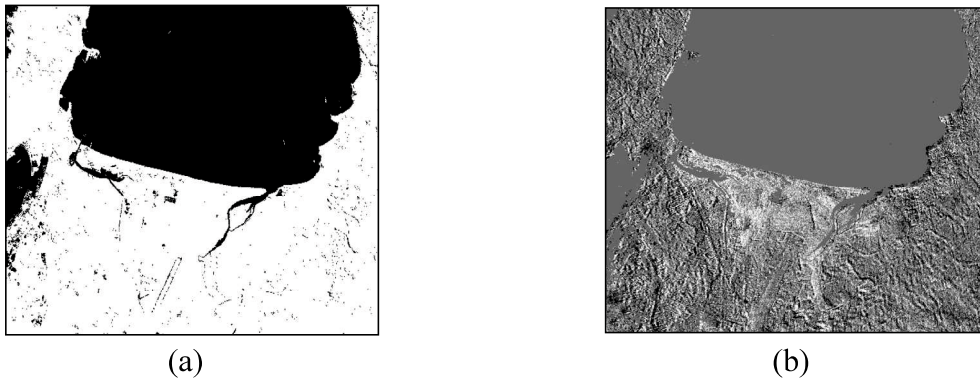


Figure 5.14 The water mask processing: (a) Water mask; and (b) Image result after the water mask processing

Median filter processing was then conducted in order to highlight the edge of the extraction target. The object was filtered in the  $N \times N$  pixels with the filter size of  $21 \times 21$  in this study ( $N=21$ ). It was carried out to the image result after the mask processing. This filter size is used because it gave the best appearance of the image. The edge of the extraction target areas which might represent inundation areas can be observed visually from the image. All of the small parts which represent same areas or have same interpretation are gathered. Therefore, generally this process makes images easier to be segmented into two or three areas, i.e., water and another area.

The segmentation process was performed using the threshold value obtained from the image histogram after the median filter processing. This process is conducted to extract the region of interest in the image. In order to accurately extract a target region, the determination of the threshold which separates the target area and the background area is important. Based on the statistics calculation data of the image, the segmentation result by using the threshold value of 1.99 at the percentage of 50% was given a good segmentation result. While other percentage values were not giving appropriate image results. The segmentation image result is showed in Figure 5.15 below.

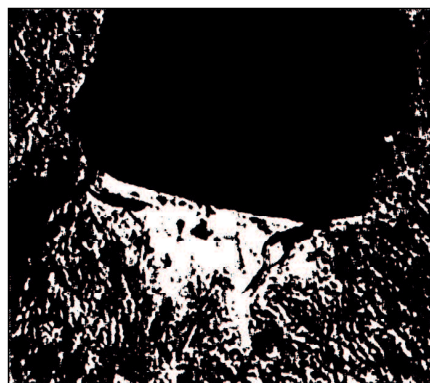


Figure 5.15 The binary image result of water and other areas

In the case where information regarding the tsunami inundation height is available, this information can be used to build an elevation mask covering the areas with the range of the inundation height. Based on the field survey data, the tsunami inundation due the 2010 event reached 0-10 m in the area of Talcahuano (Koshimura et al, 2010, Khew et al, 2016). The elevation mask was applied to the filtered water masked image to create a so-called active area which denotes tsunami-damaged areas. These areas are water areas with an elevation range similar to the tsunami inundation height.

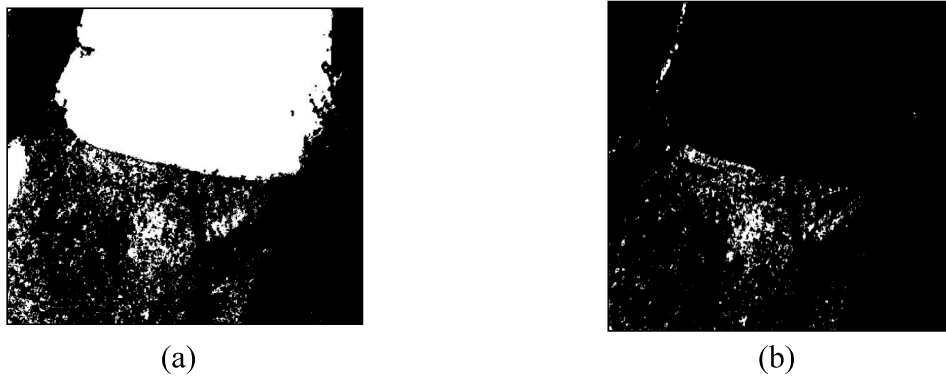


Figure 5.16 The elevation mask processing: (a) Elevation mask and (b) Image result after the elevation mask processing

The ASTER GDEM was used to create the elevation mask. Firstly, the DEM image was resized according to the research area. Based on the data of Table 2, the water height in Talcahuano was among 3.3-6.3 m (NGDC, 2010). By obtaining the horizontal profile of the DEM image, the elevation range of 1-7 m was created to represent the area elevations which are considered damaged as tsunami inundation areas. In this mask processing, the mask areas which have values among the elevation range were set to have the original raster value of the original image or the value of 1. Otherwise areas which were not at the elevation range will have the value of 0. It is necessary to adjust the resolution too before the mask image will be applying to an image. The image result after the mask was applied will showed the areas at the elevation range in white colour with the original raster value of the original image. In the other hand, other areas were in black colour with the value of 0.

Masking is the most important process to extract the damage area. A mask in image mask is a way to mask out pixel from image. Those pixels are might not need to induce or visualize in the analysis. In this case, to obtain the damage area of inundation, water area and elevation have to represent clearly in the image. Therefore, masking process is necessary for water and elevation. The area of water which does not water area based on the water mask can be considered as inundation area. Likewise for the elevation mask, areas which are located on the elevation below the range of the inundation height can be considered as the inundated area. Those two masks give a good image result of inundation areas.

In this processing, a process called resampled should have to conduct before applying a mask into an image. The resample process is done by the function of layer stacking in ENVI in order to adjust the resolution of the mask and the image which will be masked. The range for creating the mask also has to determine exactly. For the water mask, the threshold can be obtained from the histogram of the image where the threshold value can be considered as the point where there is a significant change of the image. On the other hand, the range for DEM mask refers to the inundation height in Talcahuano.

The post-processing was initiated by the morphological transformation and followed with the area calculation. The morphological processing was conducted to diminish or expand certain pixels on the image. Lastly, the two main segmented areas of the image, i.e., damaged and undamaged areas were calculated, to measure the total dimensions of the inundated and non-inundated. These areas were evaluated according to the land classification generated from the optical data of ALOS AVNIR-2 and the inundation map produced by the related institution in Talcahuano, Chile.

Unlike optical data image, a more comprehensive image processing for obtaining damaged areas using images regards the use of ALOS PALSAR data. The backscatter was calibrated from the DN of the SAR data to obtain the actual values of reflected light pulses recorded by the SAR sensor. The frequency distribution of the backscatter absolute values from pre- and post-disaster was used to determine a segmentation threshold value. An image without water areas was produced afterward by applying a water mask on the segmented image. Areas inundated by the tsunami were extracted after masking out areas with elevation beyond the tsunami inundation height of 0-10 m (Figure 5.17). The inundated areas encompassed a total of 3,554.54 ha.

Despite the fact that damaged areas were distributed in a disordered manner and covered an extensive terrain, the changes in surface reflection values generated from the pre- and post-disaster satellite data appeared to be good. The map produced by the local government indicated a similar distribution of tsunami inundated areas, which represents a total area of 3,521.57 ha (Comuna de Talcahuano, 2010). Thus, a good agreement was attained, with the percentage of error difference between the satellite data extraction results and the observation results being around 0.70% for the ALOS AVNIR-2 and 0.93% for the ALOS PALSAR-2. Hence, it was possible to conclude that satellite imageries are adequate for estimating inundation areas after a tsunami.

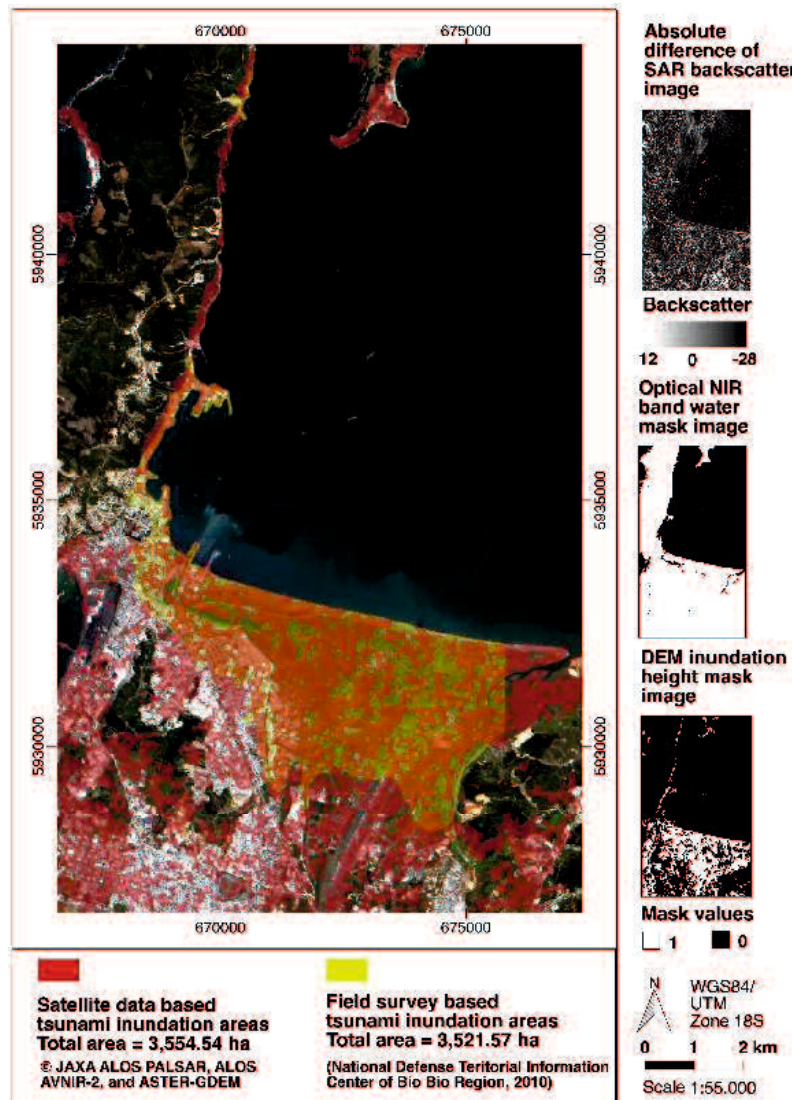


Figure 5.17 Inundated area according to the satellite data extraction and field survey reports

### 5.3 Land Subsidence Vulnerability Due to Tsunami Inundation

Time series InSAR analysis was conducted using five datasets of the images before, during, and after the 2010 Chile Earthquake and Tsunami Disaster. The list of data set of ALOS PALSAR used for the analysis is described in Table 5.3. There are five L-band ALOS PALSAR dataset acquired before, during, and after the tsunami disaster in Talcahuano, Chile on February 27<sup>th</sup>, 2010 used for the InSAR processing. The entire data are in Fine mode that is Fine Beam Single-Polarization (FBS) with ascending direction. The polarization is HH with off nadir angle at 34.3°. SAR data before the disaster is data acquired on March 3<sup>rd</sup>, 2009. The data during the disaster is scenes obtained in the period of the tsunami inundation in Talcahuano city from the time of the earthquake that triggered tsunami until three months after the event, i.e. ALPSRP220276440 on March 14<sup>th</sup>, 2010 and ALPSRP226986440 on April 4<sup>th</sup>, 2010. SAR data used to represent condition after the tsunami are data observed on January 1<sup>st</sup>, 2011 and March 17<sup>th</sup>, 2011.

Table 5.3 List of time series SAR interferometry in Talcahuano due to the 2010 Chile earthquake and tsunami event

Scene ID	Acquisition date	Beam mode	Ascending/ descending	Polarization	Off nadir angle	Frequency
ALPSRP273956440	2011/03/17	FBS	Ascending	HH	34.3°	L-Band
ALPSRP267246440	2011/01/30	FBS	Ascending	HH	34.3°	L-Band
ALPSRP226986440	2010/04/29	FBS	Ascending	HH	34.4°	L-Band
ALPSRP220276440	2010/03/14	FBS	Ascending	HH	34.3°	L-Band
ALPSRP166596440	2009/03/11	FBS	Ascending	HH	34.5°	L-Band

The threshold value for the unwrapping was determined based on the coherence value of the SAR data. The distribution of the coherence values were obtained from the correlation image result of GMTSAR InSAR processing. The brighter the color (Figure 5.18) indicates the higher coherence values. In the area of Talcahuano, high coherence can be inferred from built-up area. In this area, the value of 0.16 was determined to be able to detect displacement before, during, and after tsunami disaster in the damaged areas regardless the land cover.

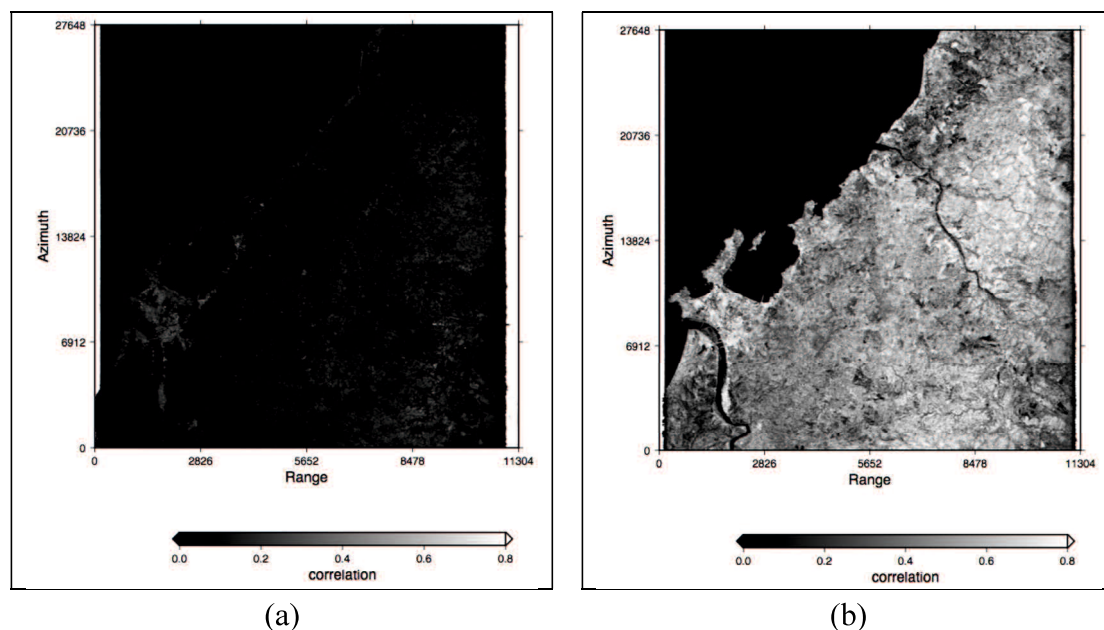


Figure 5.18 Coherence values based on correlation image result in Talcahuano City: (a) pre-disaster and (b) post-disaster

Besides SAR data, 1 scene of Shuttle Radar Topography Mission (SRTM) Digital Elevation Model (DEM) data covering the entire study area is is utilized for topographic phase removal in interferometry processing. Taking a large baseline due to a long wavelength of ALOS PALSAR data, the SBAS was carried out using perpendicular baseline of 1000 and temporal baseline is limited to 2059 days. In case of PS processing, one scene was selected as

super master to generate interferograms with the other scenes (Sandwell et al, 2008). A super master was selected with criteria able to minimize baseline with the others scenes (Rosenqvist et al, 2014). The super master scene was scene acquired during the tsunami event on March 14th, 2010. Temporal and perpendicular baseline of SAR data used for the analysis are listed in Table 5.4. Pairs of interferograms (Figure 5.19) were plotted as lines on the scatter chart of perpendicular and temporal baselines. Image results from 2010/03/14 (master) and 2011/01/30 (slave) are described in Figure 5.20.

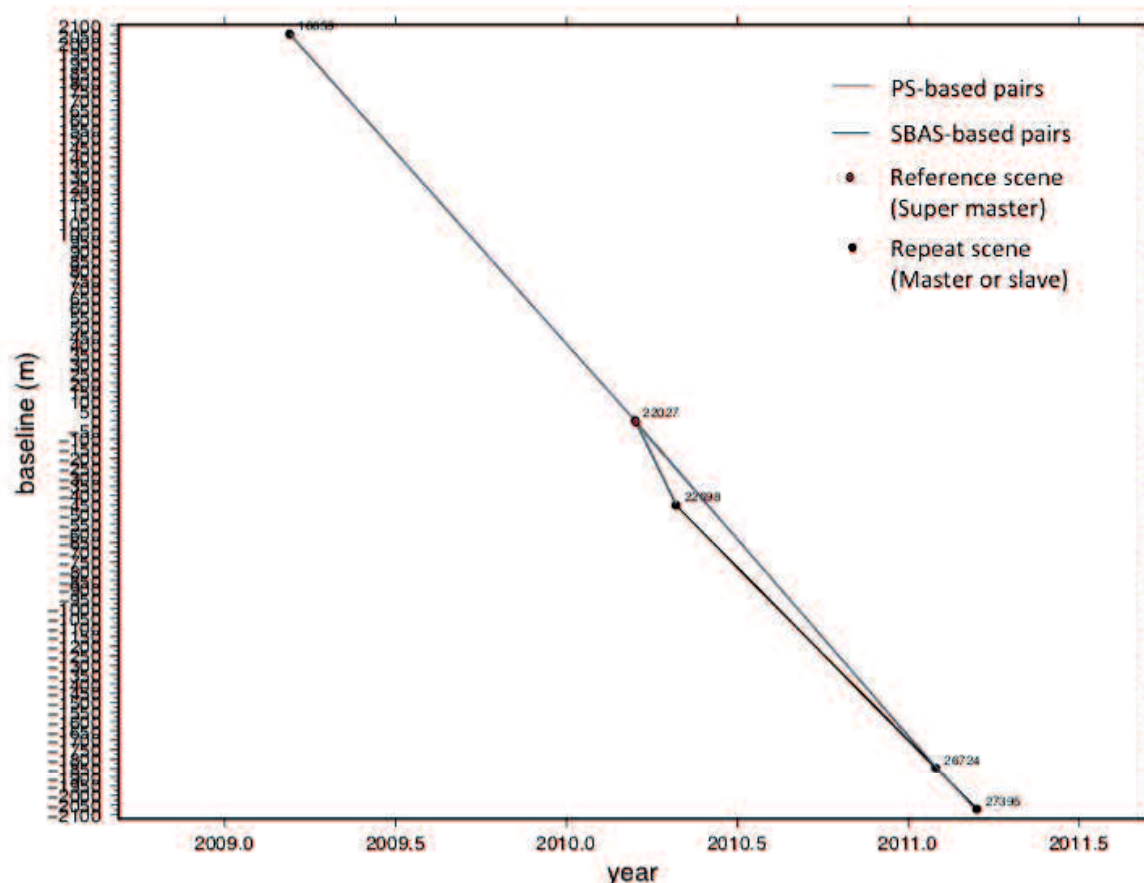
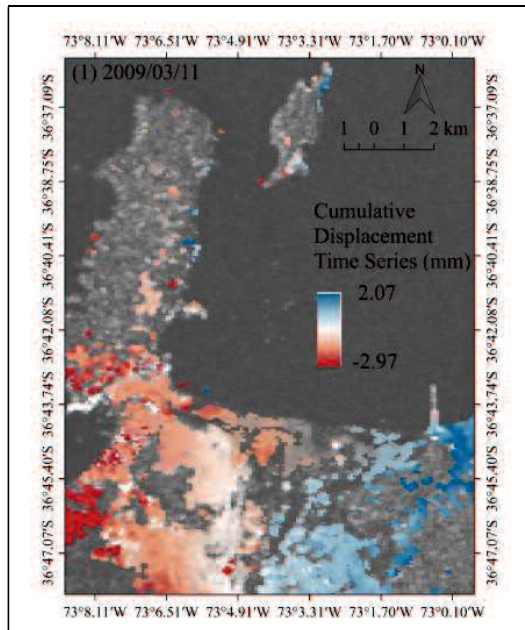


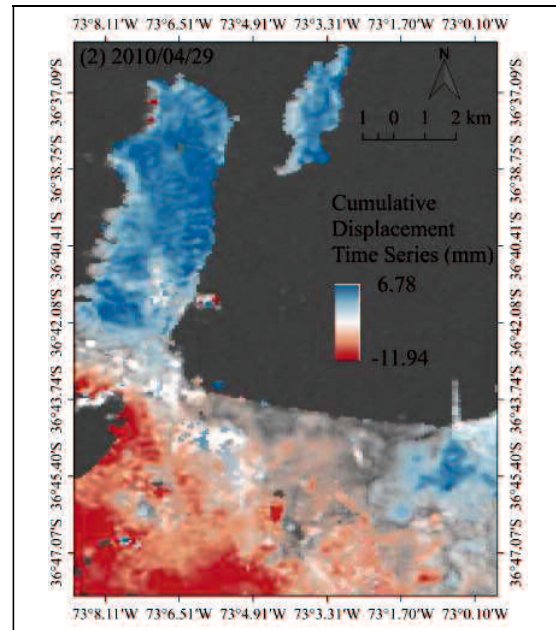
Figure 5.19 Plot of interferogram pairs based on PS and SBAS method

Table 5.4 Temporal and perpendicular baseline of the ALOS PALSAR data for tsunami inundation case in Talcahuano City, Chile

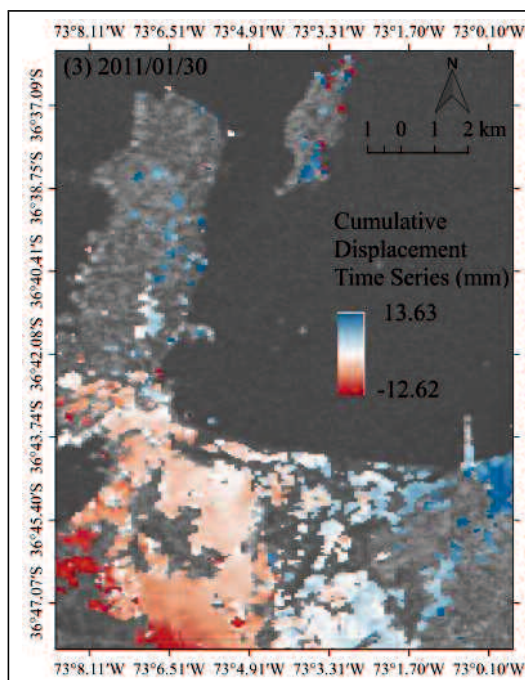
Scene ID	Acquisition date	Number of days	Perpendicular baseline (m)
ALPSRP220276440	2010/03/14	1533	(Super Master)
ALPSRP166596440	2009/03/11	1165	2053.815036
ALPSRP226986440	2010/04/29	1579	-450.437285
ALPSRP267246440	2011/01/30	1855	-1847.689031
ALPSRP273956440	2011/03/17	1901	-2071.893898



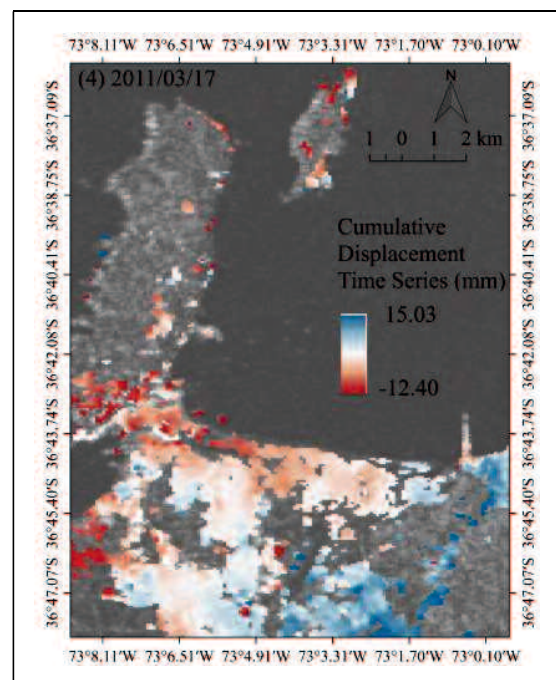
(a) 2009/03/11 Pre-disaster



(b) 2010/03/14 During-disaster



(c) 2010/04/29 Post-disaster



(d) 2011/01/30 Post-disaster

Figure 5.20 Time series cumulative displacement in Talcahuano City, Chile

Image results from a master and slave interferogram sequentially consists of amplitude, correlation, phase, phase-filtered, and unwrapped image results. Correlation image result is used to see the correlation between master and slave, the range is 0-1 value. The better the coherence between master and slave, the brighter the image (the value is close to 1). In contrast, the phase result of differential interferometry showed the different condition surface



between master and slave SAR images. The phase and filtered-phase image results are results of interferometry which are unwrapped using SNAPHU. However the unit of measurement is still in radian unit. Unwrapped phase is a deformation measurement from satellite viewed. Therefore, the (-) negative value means uplift (toward to radar sensor or range decrease) and the (+) value means down-lift (away to radar sensor or range increase). Finally, the cumulative displacement time series results from 2009 to 2011 were obtained by merging the entire processing results of the data as described in Figure 5.20. Moreover, the mean velocity is described in Figure 5.21.

The result showed that a small land subsidence has been occurred in the area inundated by tsunami. The initial values before the tsunami event indicated displacement in down-lift direction as subsidence at -2.97 mm (Figure 5.10 (a)). The subsidence was significantly increased during the tsunami event at -11.94 mm (Figure 5.10 (b)) to -12.62 mm (Figure 5.10 (c)). After the tsunami in 2011, a very small subsidence was observed and the number is slightly decreased to -12.40 mm (Figure 5.10 (d)). The mean velocity of the down-lift displacement or the average rate of the subsidence is -2.32 mm/year (Figure 5.11). The result can be an adequate input for assessing risk of tsunami inundation.

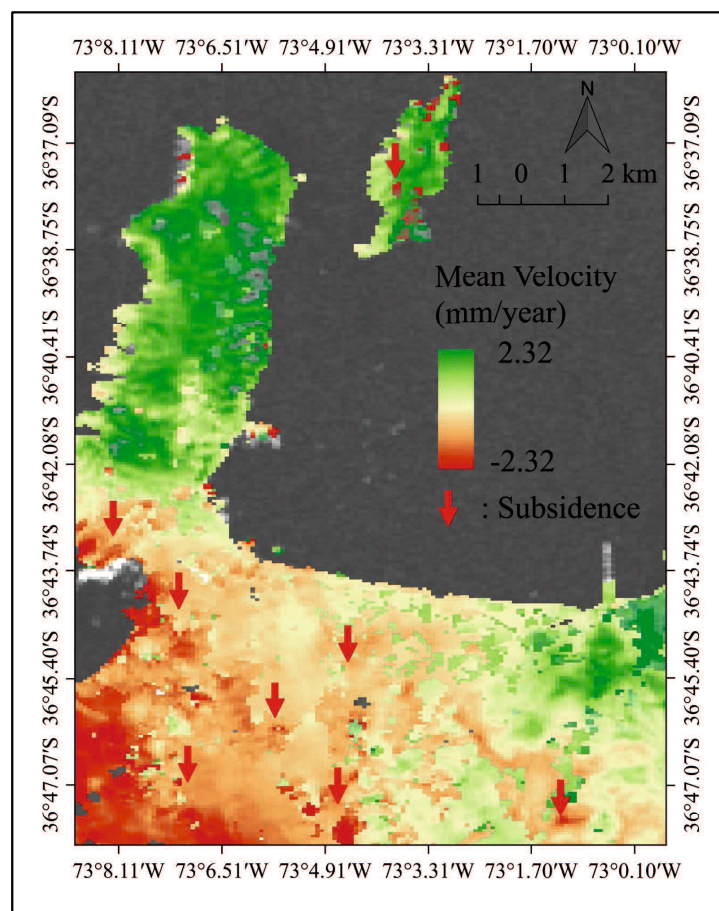


Figure 5.21 Mean velocity of displacement in Talcahuano City before, during, and after the 2010 tsunami event

Differences before, during, and after the tsunami inundation were able to be obtained based on the interferogram results of land displacements. There was no displacement obtained before the event which was resulted from the interferometry of data before and during the disaster. On the other hand, down-lift displacements were observed on the images generated during and a month after the tsunami inundation. Moreover, the result a year after the disaster showed the same condition with the image before the disaster. The displacement indicated an uplift condition.

#### **5.4 Land Cover Changes of Pre- and Post-Earthquake and Tsunami Disaster**

Land cover change results from a variety of natural and anthropogenic sources, such as tsunami disaster. The conversion of vegetation can further affect the hydrological cycle in an area. Eventually, the changes will contribute to reduce evapotranspiration and increase the long-term discharge. Therefore, there is a great deal of concern regarding the effects of tsunami inundation to land use changes. Geographic Information System (GIS) and remote sensing techniques is considered effective in providing more efficient detection of land cover changes. The paired techniques have been widely used in land cover change detection as they are both accessible at decreased cost and allow for efficient and quantitative resource mapping (Kabanda and Palamuleni, 2013). In this case study, the land use of the area before and after the disaster was classified and compared to assess land cover changes according to tsunami inundation.

The areas damaged by the tsunami inundation and the other areas, which encompass 68% of the total area of Talcahuano city, were evaluated according to land classification maps (Figure 5.22). The Chilean land classification system was used, which consists of five different general classes, i.e., wetland, water area, vegetation area, built-up area, and bare land (Sistema de Informacion Comunal, 2017). A maximum likelihood method for supervised classification was applied to the ALOS AVNIR-2 optical data. The process was assisted with the panchromatic sharpened image of the pre-disaster GeoEye-1 VHR optical data as a reference.

Land classification result before and after the 2010 Earthquake and Tsunami in Chile demonstrated that the areas classified as water area and wetland expanded in the post-disaster images compare with the pre-disaster, by about 2% and 6%, respectively. Otherwise, the bare land, built-up, and vegetation area diminished by more than 5%. In agreement with the results, the satellite optical sensor detected that the earthquake and tsunami resulted in changes to the bare land, built-up area, and vegetation areas, which turned into wetland and water areas.

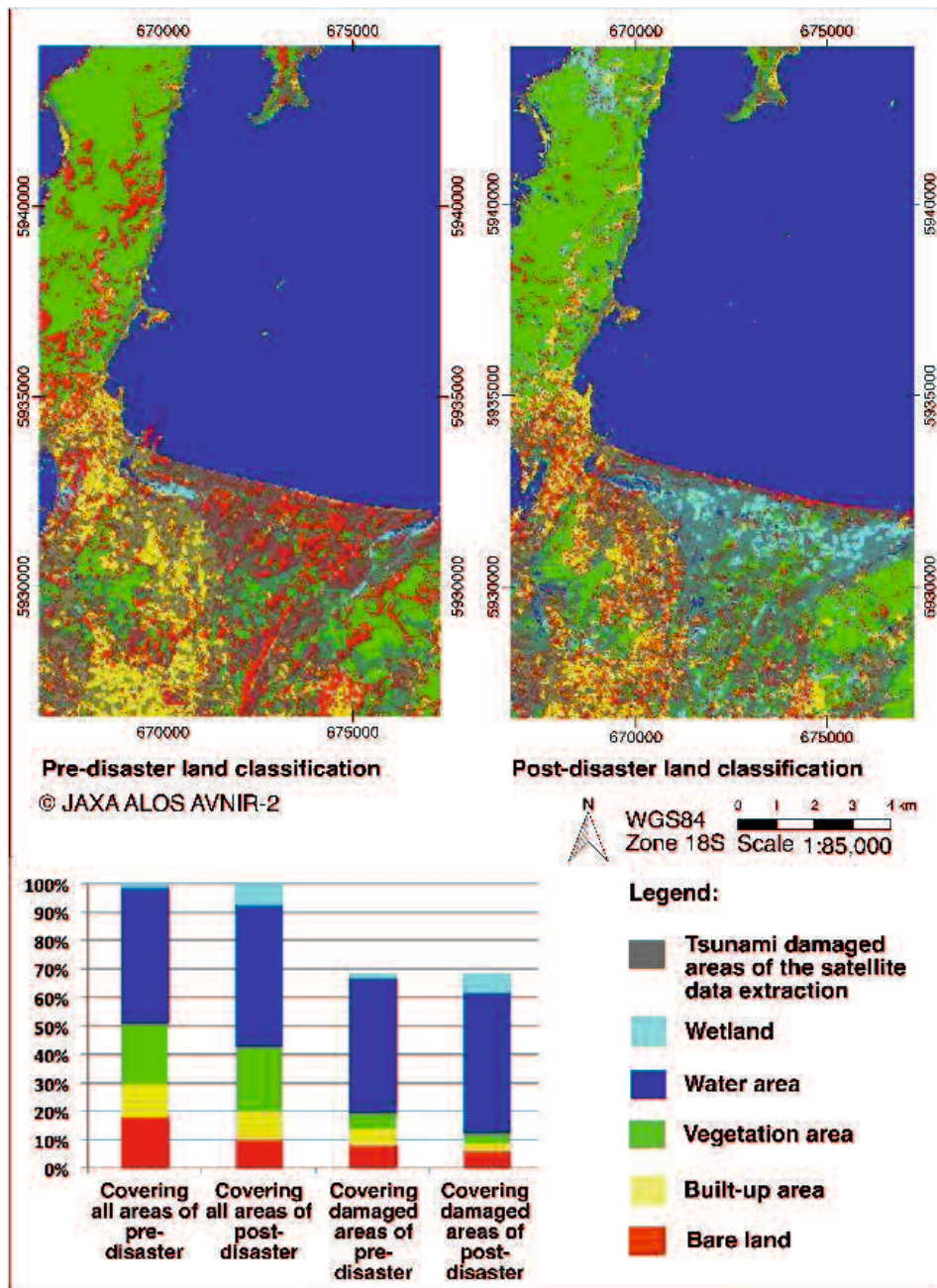


Figure 5.22 Comparison of the Pre- and Post-Disaster Land Classification in the Area of Talcahuano, Chile

### 5.5 Local Knowledge of Tsunami Inundation

Despite the challenges associated with it, participatory mapping is valuable for improving community understanding of a certain disaster (Warner, 2015). A Disaster Imagination Game (DIG) is an easy and cost-effective participatory mapping methodology invented in 1997 in Japan (Komura, 2002). In the context of disaster risk reduction, it can be very empowering at the community level, since it enables an assessment based on people's perception of risks and coping strategies (Samaddar et al, 2011).

DIG was invented in 1997 in Mie Prefecture, Japan. It is an easy and cost-effective methodology of Table Top Exercises for disaster management (Komura, 2002). Two stages should be considered when performing DIG (Figure 5.23), i.e., the pre-event or preparation stage and the event stage. The DIG was performed as part of the training on Communitarian Management of Disaster Risks in Talcahuano and was organized as a cooperation exercise between Chilean and Japanese institutions, i.e., Ingenieria Civil Oceanica of the Universidad de Valparaiso Chile, JICA, and Yamaguchi University.

A lecture was provided as an introduction to the theme of the study. Then, a handout with instructions for participants was provided for the mapping exercise, as well as the evaluation. Items, process steps, legends, and the instruction used for the handout (Table 5.5) were translated into the local language that is Spanish. Participants were grouped into teams, and each team was requested to draw the information mentioned on the handout onto a base map of the area and present the results afterward. In the last step of the workshop, the participants assessed the initial and final evaluation of the exercise through a self-evaluation activity.

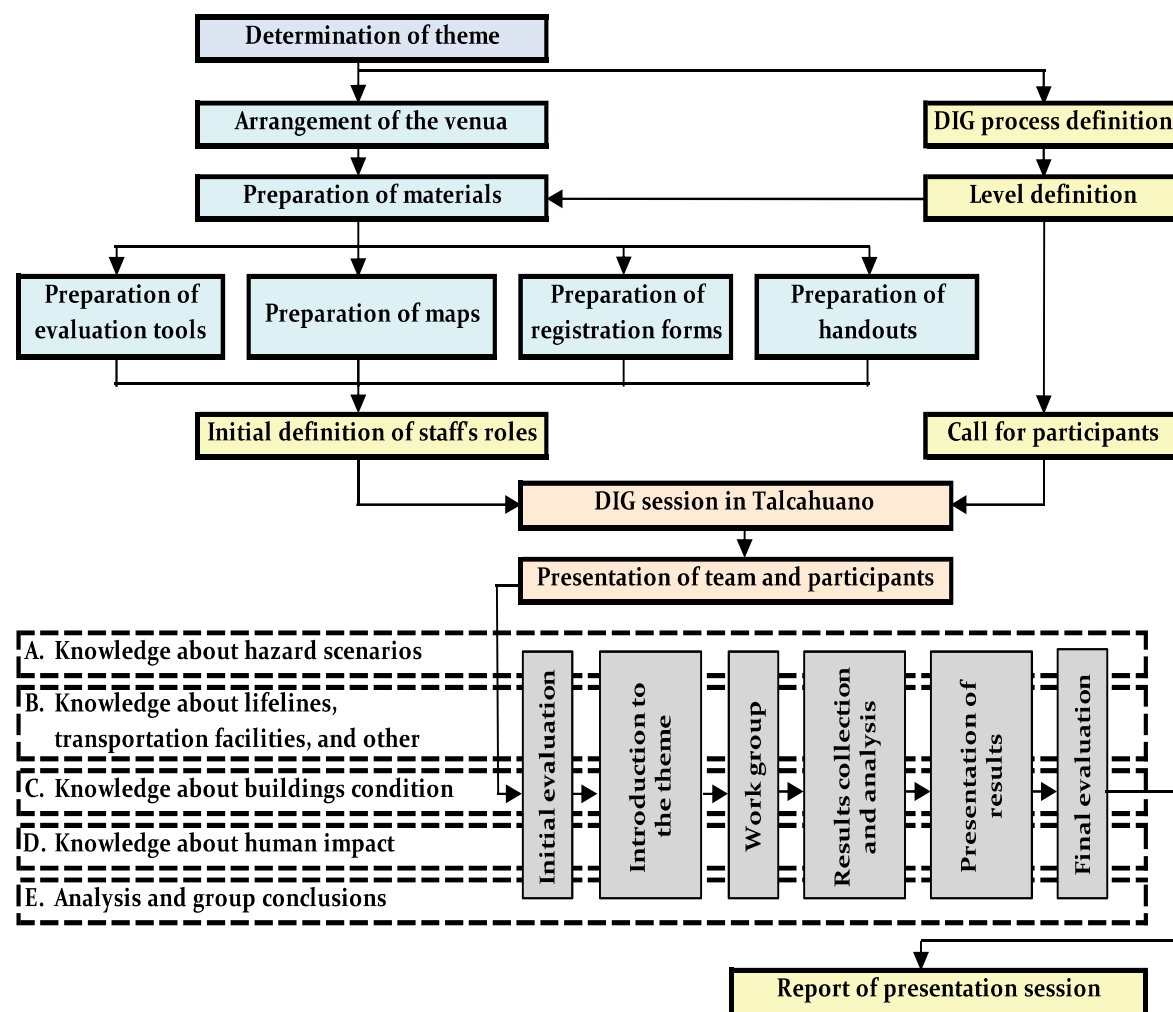


Figure 5.23 DIG flowchart, which comprises pre-event and event stages

There are five items which were evaluated by the DIG, i.e., knowledge about hazard scenarios, knowledge about lifelines, transportation facilities, and other, knowledge about the condition of buildings, knowledge about human impacts, and analysis and group discussion. According to the process of the hazard scenario item on the DIG handout, this step evaluates the community's understanding of the shoreline, inundation line, and inundation sequence. Further, such information was also utilized as the input for mapping the tsunami inundation zone.

The DIG session was held in Talcahuano city on April 20<sup>th</sup>, 2015. There were 70 participants, consisting of professional and non-professional, who had been living and working in the area for at least 20 years. Participants were requested to divide themselves into seven groups. Each team wrote down information on a 1:25,000 scale map of the Talcahuano administrative area, which was covered with a transparent sheet. The information comprised the present location of strategic roads and bridges, rivers, and open places. Other important facilities and buildings were also confirmed on the map, such as a hospital, communication center, airport or churches. In particular, information regarding the tsunami inundation was also gained, based on the knowledge of the participants of the disaster event. Figure 5.24 shows how these participatory mapping activities were conducted.



Figure 5.24 The DIG mapping activities in Talcahuano City

After participating in the DIG, an evaluation of the exercise was made by requesting participants to describe their knowledge of the disaster and other related aspects before and after the DIG activity, on a scale of 0-5. The DIG evaluation is shown in Figure 5.25, which indicates a high knowledge about the hazard scenario, human impacts, and the earthquake and tsunami hazard. On the contrary, the knowledge about lifelines, transportation, and other facilities, as well as the knowledge about building conditions, were not as good. Moreover, the assessment was able to detect issues for future improvements in the DIG method.

Knowledge about the hazard scenarios increased, and it thus seems that the DIG map is useful for improving knowledge, particularly of the shoreline, tsunami inundation, and tsunami sequence of events.

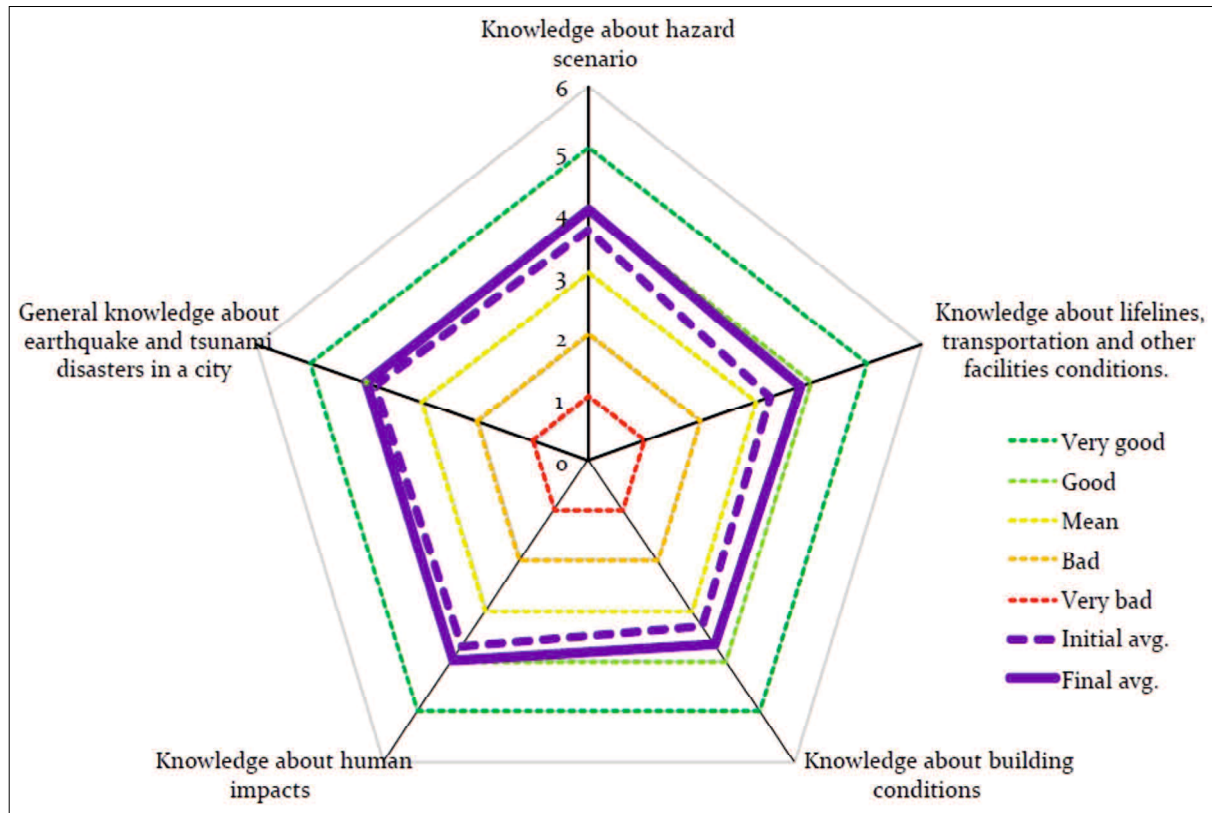


Figure 5.25 The evaluation result of DIG in Talcahuano city

The map drawn by the participants of the DIG was modified and transformed into a tsunami inundation map, as shown in Figure 5.26. The information obtained from the community about the area was presented on the map, i.e., vegetation and built-up areas. The main information is related to the tsunami inundation, i.e., the primer or index curve and secondary curve of the inundation line. There are three levels of danger highlighted in this map, i.e., a high level for ground elevations between 0 to 0.5 m, a medium level between 1 to 2 m, and the low level for higher grounds above 2 m. Moreover, the inundation level indicates the flow speeds. A high level indicates high flow speed, whereas a medium and low inundation level denotes lower flow speeds.

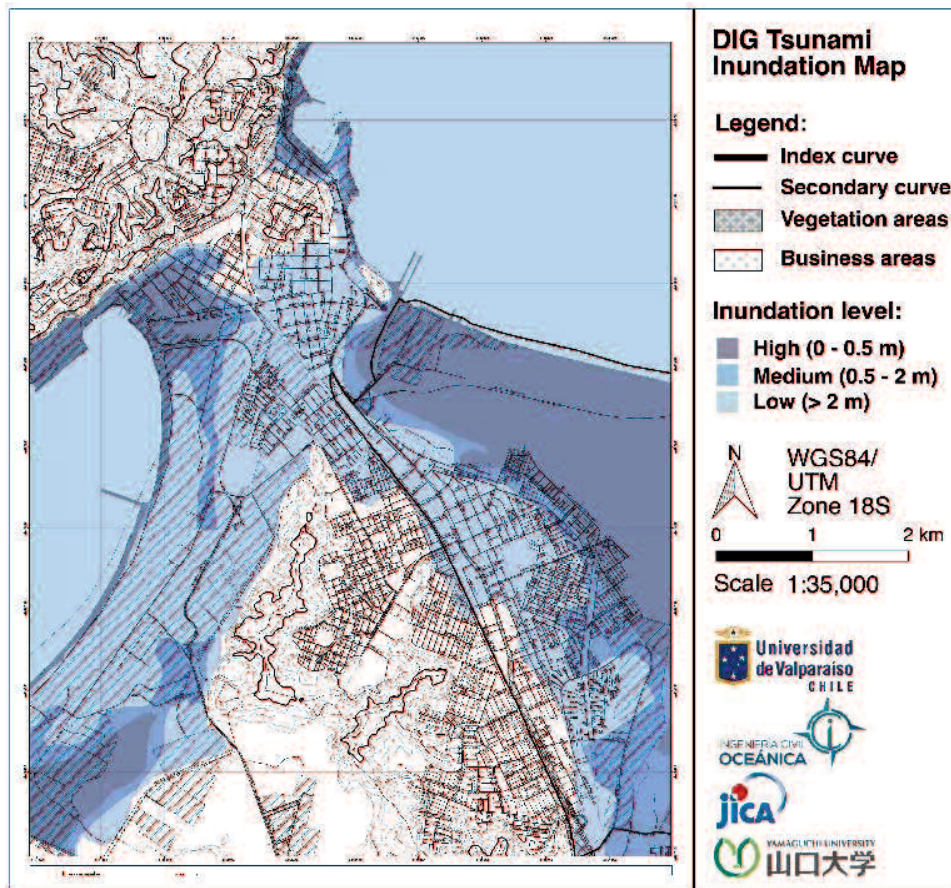


Figure 5.26 Modified map of tsunami inundation zone based on the DIG

## 5.6 Geospatial-Based Multi-Criteria Analysis by Integrating Spatial and Local Knowledge of Tsunami Inundation Zone in Talcahuano City

The number of recorded natural disasters has risen globally in the past decades, and their impact on human society has also increased, affecting several hundred million people annually (Debarati et al, 2012). A single disaster event can sometimes destroy a considerable proportion of the Gross Domestic Product (GDP) in many countries (ADRC, 2005). In 2011, the losses caused by natural disasters reached a record of US\$ 371 billion [1]. Tsunamis are one of the main types of disaster hazards (IOC, 2009). Since the 2004 Indian Ocean Tsunami, the awareness of tsunami risks has been increasing worldwide (Esteban et al, 2013). Although having a relatively low frequency (compared to other disaster events), tsunamis have the power to cause massive loss of life, significant economic losses, and cascading effects from the destruction of critical facilities (UNISDR, 2015).

The February 27<sup>th</sup> Chile's Maule M8.8 Earthquake, which triggered a tsunami, produced the largest insured losses of 2010 (Alarcon J. E. and Guillermo, 2010). This earthquake was the fifth largest earthquake measured in history (Koshimura et al, 2010). As Chile is located on the so-called "Pacific Ring of Fire," it has been affected by thirteen earthquakes with magnitudes equal to or greater than 7.0 since 1973 (UNISDR, 2015). The tsunami generated

by the 2010 Maule earthquake was also the most intense in this period, with 2 to 11-meters waves hitting coastal towns for periods of up to four hours (Siembieda W. and Guillermo, 2010). It caused severe damage to 45 coastal towns, with total economic damage of US\$ 30 billion (EM-DAT, 2015). The government reported casualties due to the earthquake and tsunami totaled 521, with a fourth of them being tsunami-related (Siembieda W. and Guillermo, 2010).

When attempting to reduce disaster losses, as stated on Sendai Framework for Disaster Risk Reduction (DRR) 2015-2030, the first of the four priorities of DRR is the understanding of disaster risk (UNISDR, 2015). It is an essential requisite for the sustainable development of disaster-prone areas (UNISDR, 2016). The improvement of risk assessments deals with the provision of adequate disaster-related information that can contribute to the DRR (OOSA, 2013). Regarding this matter, there is a need to address existing challenges and prepare for future ones by focusing on risk assessment based on damage identification, as well as the dissemination of such information to the community.

According to the Integrated Coastal Area Management (ICAM) guidelines, the utilization of satellite remote sensing imageries through GIS technology is appropriate for estimating damage due to hazards, such as inundation areas (Arthurton, 2007). Satellite data can be used for assessing risks promptly, as well as assisting rehabilitation plans (Joyce et al, 2009). Visual interpretation of inundated areas can be performed using Very-High-Resolution (VHR) optical satellite imageries (Ramírez-Herrera and Navarrete-Pacheco, 2011), which can provide high accuracy in the identification of affected areas (Yamazaki et al, 2006). Various types of Synthetic Aperture Radar (SAR) satellite imageries have also demonstrated a powerful ability to identify tsunami damage, i.e., L-band Advanced Land Observing Satellite (ALOS) Polarimetric SAR (PolSAR) (Chen et al, 2013), C-band ENVISAT Advanced SAR (ASAR) (Xhang et al, 2014), and C-band TerraSAR-X imageries (Gokon, 2016). Particularly in Chile, tsunami-damaged areas have been detected by employing ALOS Phased-Array L-band SAR (PALSAR) imageries (Matsuoka and Koshimura, 2010). These identifications were carried out by obtaining the backscattering intensity of SAR data before and after the disaster.

Considering the possibility of damage detection by integrating two or more different types satellite data, research has been performed using optical, SAR, and DEM data. The optical data of the Advanced Spaceborne Thermal Emission Reflectance Radiometer (ASTER) and the DEM data was used to delineate the inundation line on SAR data of ENVISAT in tsunami-damaged areas (Chini et al, 2013). Satellite missions, such as ALOS operated by Japan Aerospace Exploration Agency (JAXA), have developed the capability of satellite-derived imageries.

In addition to providing a damage assessment, satellite-based analysis results can be used as an input for creating disaster-related risk maps, together with other historical data. Based



on a global stakeholder assessment, end-users attributed a high operational benefit of inundation maps to design and operate critical infrastructure and provide humanitarian aid (OOSA, 2013). Therefore, an inundation map can be an important tool to support the dissemination of disaster-related information to the community. This sort of disaster knowledge represents one of the eight fundamental elements of coastal community resilience, as identified by the United States Agency for International Development (USAID) guide to reduce risk from coastal hazards, accelerate recoveries, and adapt to changes (Hettiarachchi et al, 2011). Despite the challenges associated with it, participatory mapping is valuable for improving community understanding of a certain disaster (Warner, 2015). A Disaster Imagination Game (DIG) is an easy and cost-effective participatory mapping methodology invented in 1997 in Japan (Komura, 2002). In the context of disaster risk reduction, it can be very empowering at the community level, since it enables an assessment based on people's perception of risks and coping strategies (Samaddar et al, 2011).

Regarding the achievements of sustainable development that associated with DRR, this study concerns itself with the improvement of risk assessments through geospatial and local knowledge. Concerning the functionality and performance of satellite data on damage assessment, satellite optical and SAR imageries were utilized to identify inundation areas due to the 2010 Chile tsunami event. These damaged areas were extracted using the pre- and post-disaster images of the DigitalGlobe VHR optical data, ALOS AVNIR-2, ALOS PALSAR, and DEM data. The result was verified using land classification and field observation data, showing good agreement with the analysis of the satellite data. Moreover, on the part of generating local knowledge amongst coastal resident, a local community's understanding on tsunami damage was assessed through a map-based DIG participatory workshop. The results of the exercise indicate that the integration of the geospatial and local knowledge for assessing tsunami inundation zones can be a valuable tool to ensure sustainable development by reducing local risks and improving the resilience of the local population.

### **5.6.1 Framework of Integrated Spatial and Local Knowledge Analysis for Tsunami Inundation Level Mapping**

An assessment of hazard risks is necessary to accomplish the sustainable development of an area (UNISDR, 2003). A short-term assessment of a major natural hazard is a difficult task, considering that the impacts may vary according to the spatial scale. Nevertheless, recent studies have highlighted a variety of ways in which geospatial information systems can contribute to risk reduction practices (Maurer, 2013). Based on a global stakeholder assessment, in the case of tsunami hazards, it appears that the inundation zone is one of the most important geospatial information criteria for assessing the risk. A tsunami inundation hazard map can be created by combining the results of satellite data analysis with other tsunami inundation related information from the local community. Aside for constituting a

tool for investigating community knowledge on disasters, a participatory mapping exercise can extensively contribute to the collection of information. Therefore, the general framework of the integrated spatial and local knowledge analysis (Figure 5.27) aims to achieve a holistic understanding of the risks to a given community through satellite data processing and community-based participatory mapping for improving the resilience of the community to tsunami hazards.

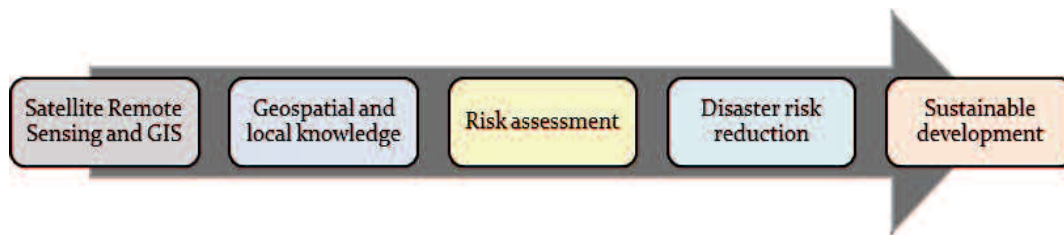


Figure 5.27 General framework of the integrated spatial and local knowledge analysis for tsunami inundation level mapping

According to the framework of the study, the scheme used for the analysis (as described in the flowchart below, see Figure 5.28) consists of two main processes, i.e., satellite data analysis and map-based DIG participatory mapping. The evaluation, using observation data, is the subprocess for both of the main processes. A map of tsunami inundation zone was finally produced through an integrated assessment of the tsunami hazard risk through the analysis of satellite imageries and the information obtained from the community.

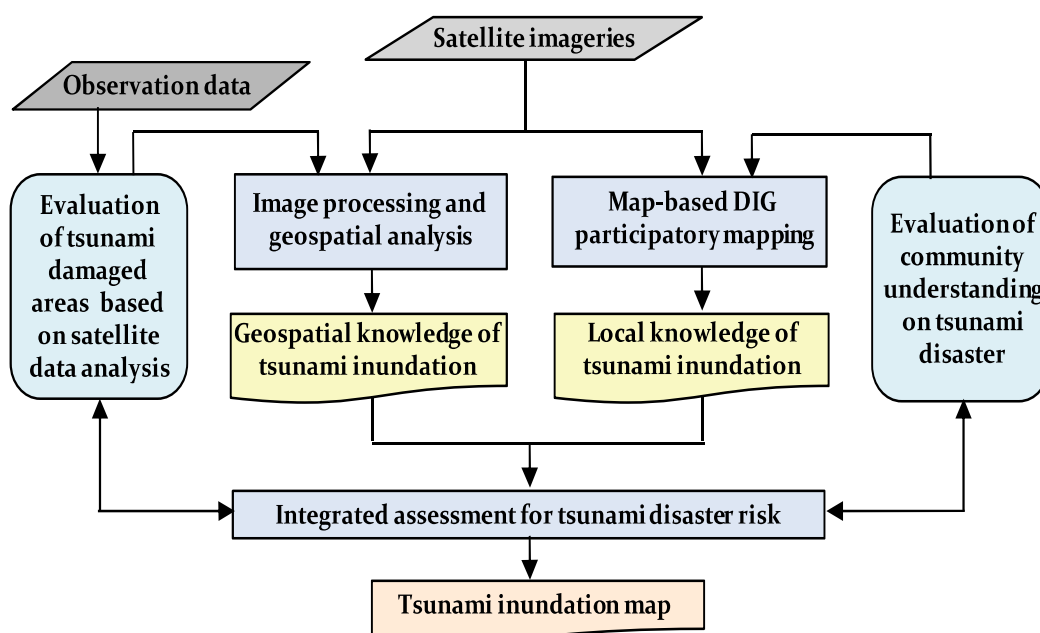


Figure 5.28 Process scheme according to the framework of the integrated spatial and local knowledge analysis of tsunami risk assessment

### **5.6.2 Integrated Risk Assessment of Tsunami Inundation Zone**

Tsunamis are considered to be one of the main types of hazards that can affect coastal areas (IOC, 2009). Regarding sustainable development, disaster prevention measures are essential to reduce the disaster risk along coastal areas. Experiences over recent years regarding the impacts of tsunamis have shown that inadequate preparation for, and response to, emergency situations have contributed to widespread damage and the avoidable loss of lives and livelihoods (Siembieda W. and Guillermo, 2010). In some instances, these shortcomings have been due to a poor regional identification of the risk as well as its dissemination to the community (Alarcon J. E. and Guillermo, 2010). In this regard, it is crucial to identify and quantify tsunami disaster risks, particularly the potential extent of tsunami inundation (Arthurton, 2007).

Satellite remote sensing and GIS analysis are an advanced tool that can be used to carry out an identification of damaged areas after an event, which can serve as the foundation of risk assessment methodologies. A major reason for the adoption of remote sensing by risk management methodologies is that it is one of the fastest means of acquiring data for pre- and post-disaster studies, which can also assist rehabilitation plans (Joyce et al, 2009). The extraction result of damaged areas due to the 2010 tsunami and earthquake disaster in Chile using satellite data demonstrated a good agreement when compared with the results of field survey observations. The processed images of optical data were qualitatively and quantitatively sufficient to be utilized as an initial rapid damage assessment. Moreover, the processing result using SAR, optical, and DEM data generated an adequate identification of tsunami inundation. Both the vegetation index of NDVI calculated from the image of ALOS AVNIR and the backscatter of the ALOS PALSAR were applicable for detecting the damage due to the tsunami's inundation.

Due to high condensation during certain periods, optical data sometimes results in images which consist mostly of clouds, and in this case, the use of SAR data can prove to be effective. In the last two decades, SAR has become the premier sensor to observe some phenomena due to its sensitivity to small surface roughness changes, and given that it is also independent of solar illumination and is unaffected by cloud cover (McCandless and Jackson, 2004). In this regard, the SAR surfaces reflected light pulses and were able to extract changed and unchanged areas. Subsequently, the inundated areas were determined using the optical and DEM data to delineate the water and elevation of inundation, respectively.

However, when attempting to compute the extent of the damage, it is important to consider the difference in time between the event and the time when the satellite images are taken (Joyce et al, 2009). The identification of areas damaged by the 2010 Chile event was generated using the ALOS PALSAR data, acquired two weeks after the disaster. The ALOS AVNIR-2 data, acquired six months after the event, was also used. The image processing result using these data still showed damages in the affected area. This information indirectly

conveys that post-disaster recovery was very slow in the Talcahuano area.

Community-based information is essential for disaster risk assessment, and participatory mapping activities such as DIG can cover the breadth of local spatial knowledge around a given area, including both quantitative and qualitative pieces of information (Bretschneider and Wybro, 1976). Through this exercise, it was possible to comprehend that the community had well understood the general knowledge regarding the tsunami disaster. This result is reasonable considering the frequency with which communities in Chile have been affected by tsunami events.

Regarding the 2010 field survey report, it is estimated that at least a fourth of the total deaths was among the tourist population, who were in the coastal area for holidays. The local coastal communities, who experienced the 1960 earthquake and tsunami event, evacuated right after noticing the ground shaking (Khew et al, 2015). It indicates that education and lesson from past events are highly valuable to mitigate tsunami fatalities. Nevertheless, tsunami countermeasures, including prevention systems, have not been developed adequately in Chile (Khew et al, 2015). Additionally, there was a lack of emergency response staff in the field and lack of proper communication between the government and the population (Siembieda and Guillermo, 2010). Therefore, it is necessary to constantly disseminate disaster-related information through community-based activities, such as DIG.

Fundamentally, it is appropriate to extensively use qualitative data, such as local knowledge, to complement the use of quantitative data (Warner, 2015). Regarding the improvement of the risk assessment, it is important to combine geospatial knowledge with the local knowledge when assessing the risks of the tsunami inundation, which can then be combined to create a tsunami inundation zone map. Such a map can comprehensively communicate the risk of tsunami inundation. In the case of Talcahuano, tsunami inundation zones encompass high, medium, and low inundation level, which were delineated according to the DIG classification and the results of the satellite data analysis.

The quantitative data from the satellite data analysis was complemented with the qualitative data from the community DIG activity. The integration of such information can be considered an important tool to improve risk assessment of tsunami inundation. A tsunami inundation zone map was produced as the integrated risk assessment result (Figure 5.19). The map provides information regarding the level of tsunami inundation, which identifies the vulnerability of Talcahuano to tsunami events.

The map comprises three levels of inundation, following the DIG map. This classification further compiled and interpreted using the coastal proximity algorithm (Equation 5.1) into the distances from the shoreline, i.e., high (0 to 0.5 km), medium (0.5 to 2 km), and high (above 2 km).

$$\text{Log}X_{max} = \text{log}1400 + \frac{3}{4} \text{log} \left( \frac{Y_0}{10} \right) \quad (\text{Equation 5.5})$$

Where  $X_{max}$  is the maximum reach of the tsunami over land, and  $Y_0$  is the height of the tsunami at the coast (Bretschneider and Wybro, 1976).

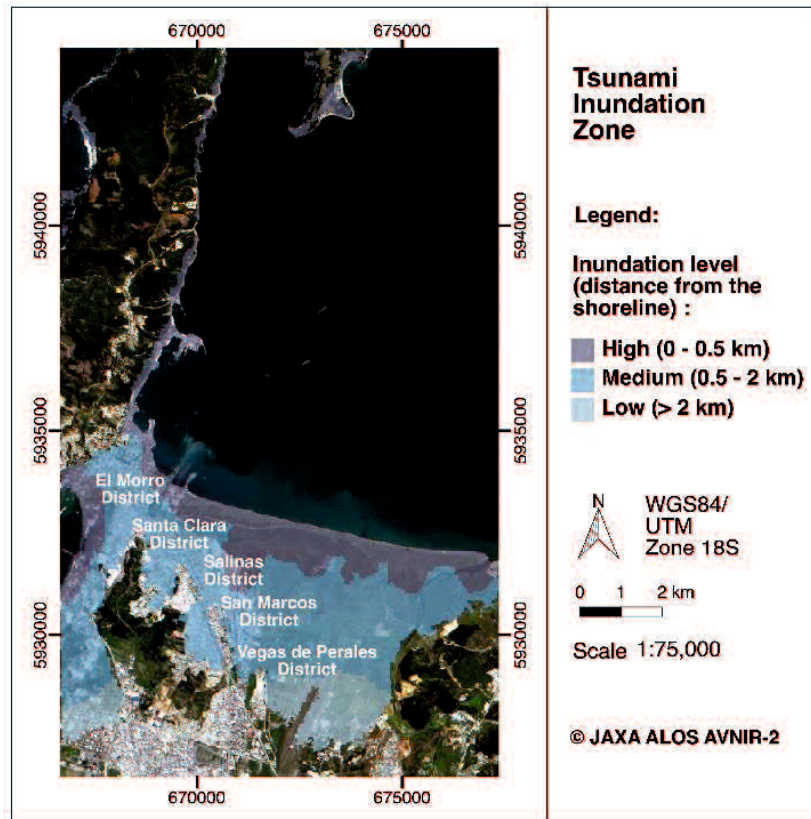


Figure 5.29 Tsunami inundation zone map based on the integrated geospatial and local knowledge assessment

According to the classification of the land, vegetation area and bare land along the coast are mostly classified as having a high level of inundation. The built-up area nearby the coast in El Morro District also has a high potential level of tsunami inundation. In the other districts, most of the built-up areas are on medium inundation level. The airport area is also within the tsunami inundation zone, with a low inundation level.

In regard to the result of the integrated tsunami risk assessment in Talcahuano area (Figure 5.29), the areas within the tsunami inundation zone, particularly the built-up area, are supposed to be developed by carefully taking into account DRR. The field observation report of the 2010 Chile event revealed that numerous houses at coastal locations (made of adobe, wood, and concrete) were built well enough to survive the earthquake, although the houses were destroyed by the tsunami that followed (Shoji et al, 2010).

According to the visual interpretation of the VHR optical data (Figure 5.3), a housing area that was being constructed in the Salinas District on the pre-disaster image was damaged on the post-disaster image. A bridge in the area was also damaged, as shown in a field survey

report (Koshimura et. al., 2010). In agreement with the tsunami inundation zone map (Figure 5.29), this area was located within the high inundation zone, highlighting the need for proper zoning laws.

This result points out the necessity to continuously improve the provision and dissemination of risk assessment information in the future. In this regard, satellite-based tsunami-damaged areas can be utilized as the reference for the future DIG activities. Further, the result of the DIG can be a useful input for improving satellite data analysis. Such a framework should allow for continuous improvement of tsunami risk mitigation strategies, contributing to the sustainable development of disaster-prone areas.

Concerning the risk reduction for achieving sustainable development in such a disaster-prone area, an integrated risk assessment was carried out by compiling the disaster-related information based on the geospatial data and local knowledge. The result was represented as a map of the potential tsunami inundation zones (showing high, medium, and low inundation levels), that supposed to be beneficial to disaster risk management efforts in the area, and improve the resilience of local communities to future tsunami events (for example by improving evacuation routes and sites).

## CHAPTER VI

### CONCLUSION

#### 6.1 Conclusions

The conclusions of the research are:

1. An alternative risk assessment of geospatial-based multi-criteria analysis was applied using groundwater monitoring data and satellite data processing of land subsidence and land cover for groundwater conservation mapping.

Groundwater in Bali is mainly use for drinking water and irrigation. The usage can be divided into high ( $>50$  l/s), moderate (25 - 50 l/s), and low ( $<25$  l/s). Moreover, the groundwater level were classified into three levels, i.e groundwater depletion  $<10\%$ ,  $10\%$  -  $25\%$ , and  $>25\%$ .

In regard to the satellite data processing, area with value below 0 (-) according to the InSAR time series processing is considered as subsided area. The mean velocity of the subsidence is  $-8.35$  mm/year from 2007 to 2010 and  $-15.80$  mm/year from 2014. The result was confirmed with available GNSS-CORS data. Land cover are further classified into three categories, i.e. low vulnerability (bare land), moderate vulnerability (paddy field), and high vulnerability (industrial and residential areas).

A multi-criteria analysis of AHP was applied to classify the study area into secure, vulnerable, critical, and damage zones. The secure area is concentrated in vegetated areas without subsidence. The vulnerable area is obtained in paddy field. Critical and damage zones are dominated in residential and industrial (tourism) area, respectively. The map has a good agreement with available map of the related agency in Bali.

2. A risk assessment of tsunami inundation level was proposed by integrating spatial and local-based tsunami damaged areas with land subsidence and land cover as land-associated damage parameters.

The geospatial information on the damaged areas was effectively extracted by interpreting pre- and post-disaster of the VHR and ALOS AVNIR-2 optical data. The total inundation area was extracted by subtracting pre- and post-disaster backscatter images of ALOS PALSAR. The total damaged area correlated well with field observation result, with an error of  $0.93\%$ .

Moreover, the initial value of subsidence was obtained before the disaster at  $-2.97$  mm, the subsidence was significantly increased during the tsunami event at  $-11.94$  mm to  $-12.62$  mm, and slightly decreased to  $-12.40$  mm after the disaster. In regard to land cover, the areas classified as water area and wetland expanded in the post-disaster images compare with the pre-disaster, by about  $2\%$  and  $6\%$ , respectively. Otherwise, the bare land, built-up, and vegetation area diminished by more than  $5\%$ .

In addition to spatial-based information, local-based information of tsunami inundation was collected by conducting a DIG. The inundation lines and levels were obtained through the map created from the DIG.

The produced tsunami inundation level map consists of high, medium, and low vulnerability zones. Built-up area with distance 0 to 0.5 km from the shoreline has a high potential level of tsunami inundation. Besides, built-up area nearby the coast in distance 0.5 to 2 km from the shoreline are in medium inundation level. Area located more than 2 km from the shoreline was obtained having a low vulnerability of tsunami inundation.

## **6.2 Suggestions**

Development of the study can be carried out by applying the proposed technique to other water-related hazards. Moreover, a further policy based on the mapping result is supposed to be useful for the vulnerable area development in the future.



## REFERENCES

- Aggarwal, S. 2005. *Principles of Remote Sensing*. Dehra Dun: Indian Institute of Remote Sensing. p. 23-38.
- AON Benfield. 2010. *Event Recap Report: 02/27/10 Chile Earthquake*. Chicago: Impact Forecasting LLC.
- Amelung, F., Galloway, D. L., Bell, J. W., Zebker, H. A., and Lacznia, R. J. 1999. "Sensing the Ups and Downs of Las Vegas: InSAR Reveals Structural Control of Land Subsidence and Aquifer-System Deformation." *Geology* 27 (6): 483–486.
- Bali Post. 2013a. "Bali Selatan Makin Cepat Tenggelam, Intrusi Air Laut Sampai Sanglah Bali is Sinking Faster, Sea Water Intrusion Has Reached Sanglah Region." *Bali Post*, January 13.
- Bali Post. 2013b. "Bali akan Alami Krisis Air Hebat, Intrusi Air Laut Kian Parah - Bali is Predicted Encountering Severe Water Crisis, Sea Water Intrusion is Getting Worse." *Bali Post*, January 15.
- Baumann, P. R. 2010. *Introduction to Remote Sensing*. New York: State University of New York.
- Bell, J. W., Amelung, F., Ferretti, A., Bianchi, M., and Novali, F. 2008. "Permanent Scatterer InSAR Reveals Seasonal and Long-Term Aquifer-System Response to Groundwater Pumping and Artificial Recharge." *Water Resources Research* 44 (2):1-18.
- Berardino, P., Fornaro G., Lanari, R., and Sansosti, E. 2002. A New Algorithm for Surface Deformation Monitoring Based on Small Baseline Differential Sar Interferograms. *IEEE Transactions on Geoscience and Remote Sensing* 40 (11): 2375–2383.
- BKPM-JICA (2006), *Investment Opportunities Study for Bali Province*, Investment Coordinating Board (BKPM) - Japan International Cooperation Agency (JICA), Bali, Indonesia,1-8.
- BPS (Statistics Indonesia) of Badung Regency. 2011. *Badung Regency in Figures 2011*. BPS of Badung Regency.
- BPS (Statistics Indonesia) of Klungkung Regency. 2011. *Klungkung Regency in Figures 2011*. BPS of Klungkung Regency.
- BPS (Statistics Indonesia) of Bali Province. 2017. *Bali Province in Figures*. Bali: BPS of Bali Province.
- Bouraoui, S. 2013. "Time Series Analysis of SAR Images Using Persistent Scatterer (PS), Small Baseline (SB) and Merged Approaches in Regions With Small Surface Deformation." Doctoral thesis, Universite de Strasbourg.
- BWS (River Basin Agency) of Bali-Penida. 2017. *Planning of the Improvement And Rehabilitation of Freshwater and Groundwater Supply Networks in Bali Province*. Preliminary Report of the Ministry of Public Works of Indonesia.

- Campbell, J. B., and Wynne R.H. 2011. *Introduction to Remote Sensing*. 5<sup>th</sup> Edition. New York: Guilford. 667 p.
- Cardenaz-Jiron, L A. 2013. *The Chilean Earthquake and Tsunami 2010, A Multidisciplinary Study of  $M_w$  8.8, Maule*. United Kingdom: WIT Press. 41 p.
- CCPO. 2003. *Sensor Systems*. [Cited on June 20, 2015]. Available from: URL: <http://www.ccpo.odu.edu>.
- Chaussard, E., B€urgmann, R. Shirzaei, M. Fielding, E. J., and Baker, B. 2014. “Predictability of Hydraulic Head Changes and Characterization of Aquifer-System and Fault Properties From InSAR-Derived Ground Deformation.” *Journal of Geophysical Research* 119 (8): 6572–6590.
- Chen, J., Knight, R., Zebker, H. A., and Schreuder, W. A. 2016. “Confined Aquifer Head Measurements and Storage Properties in the San Luis Valley, Colorado, From Spaceborne InSAR Observations.” *Water Resources Research* 2016 (52): 3623-3636.
- Chini, M., Alessandro P., Francesca R. C., Stefania A., Rosa N., and Paolo M. D. M.. 2013. *The 2011 Tohoku (Japan) Tsunami Inundation and Liquefaction Investigated Through Optical, Thermal, and SAR Data*. IEEE Geoscience and Remote Sensing Letters, 10 (2): 347-351.
- Chini, M. 2015. *Earthquake Damage Mapping Techniques Using SAR and Optical Remote Sensing Satellite Data*. Italy: Istituto Nazionale di Geofisica e Vulcanologia.
- Crosetto M., Monserrat, O., Cuevas-González, M., Devanthéry, N., Crippa. B. “Persistent Scatterer Interferometry: A Review.” *ISPRS Journal of Photogrammetry and Remote Sensing* 115 (2016): 78–89.
- Crosetto, M., Monserrat, O., Iglesias, R., Crippa, B., 2010. “Persistent Scatterer Interferometry: Potential, Limits and Initial C- and X-Band Comparison.” *Photogrammetric Engineering & Remote Sensing* 76 (9): 1061–1069.
- Curlander, J. C. and R. N. McDonough. 1991. *Synthetic Aperture Radar: System and Signal Processing*. New York: John Wiley and Sons.
- Danaryanto, H. (1991), *Groundwater Quantification for Four Urban Development Areas in Denpasar, Bali*, DEG-Bandung-BGR-Hannover, Bandung, 30-36.
- Department of Public Works (2014), *Project on Mapping of the Utilization of the Groundwater Utilization*, Working Group of Groundwater Utilization – Regional Department of Public Works of Bali Province, Bali, Indonesia, 71-75.
- Dewantoro, M. D. R. and Nur M. F. 2012. *ALOS PALSAR Image for Landcover Classification Using Pulse Coupled Neural Network (PCNN)*. International Journal of Advanced Research in Computer and Communication Engineering, 1 (5): 289-294.
- Doocy S., Daniels A., Dick A., and Kirsch T. D. 2013. *The Human Impact of Tsunamis: a Historical Review of Events 1900-2009 and Systematic Literature Review*. 1<sup>st</sup> Edition. California: PLOS Currents Disasters.

- Engdahl, M. and Cecilia, J. 2013. *Geohazard Description for Göteborg, Version 1*. Seattle: PanGeo.
- ESA. 2007. *Information on ALOS AVNIR-2/PRISM Products for ADEN Users*. Italy: European Space Agency.
- Fetter, C.W. 2001. *Applied Hydrogeology*. New Jersey: Prentice Hall.
- Ferretti A., Prati, C., and Rocca, F. 2001. Permanent Scatterers in SAR Interferometry. *IEEE Transactions on Geoscience and Remote Sensing* 39 (1): 8-20.
- Furuta, R., Shimada, M., Tadono, T., and Watanabe, M.. *Interferometric Capabilities of ALOS PALSAR and Its Utilization*. Tokyo: EORC, JAXA.
- Galloway, D. L., and Burbey, T. J. 2011. “Review: Regional Land Subsidence Accompanying Groundwater Extraction.” *Hydrogeology Journal* 19 (8): 1459–1486.
- Galloway, D. and Hoffmann, J. 2007. “The Application of Satellite Differential SAR Interferometry-Derived Ground Displacements in Hydrogeology.” *Hydrogeology Journal* 15 (1): 133–154.
- Geist, E. 2010. *The 2010 Chilean Tsunami and Uncertainty in Tsunami Modeling*. United States of America: United States Geological Survey (USGS).
- Ghiglia, D. C. and Pritt, M. D. 1998. *Two-Dimensional Phase Unwrapping: Theory, Algorithms, and Software*. New York: Wiley.
- GMTSAR. 2010. “Generate DEM files for use with GMTSAR.” Accessed May 10, 2018. <http://topex.ucsd.edu/gmtsar/demgen/>.
- Graham, S. 1999. *Remote Sensing*. [Cited on June 20, 2015]. Available from: URL: <http://earthobservatory.nasa.gov>.
- Hansbo, S. 1981. “Consolidation of Fine-Grained Soils by Prefabricated Drains,” In *Proceedings of 10th International Conference on Soil Mechanics and Foundation Engineering* 3 (1981): 677-682.
- Hanssen, R. F. 2001. *Radar Interferometry: Data Interpretation and Error Analysis, Remote Sensing Digital Image Process*. Netherlands: Springer.
- Harbaugh, A. W. (2005), MODFLOW-2005, U.S. Geological Survey Modular Groundwater Model - The Groundwater Flow Process, *U.S. Geol. Surv. Tech. Methods, 6-A16*.
- Hoang, B. and Ashley C. 2012. *Remote Sensing*. United States of America: IEEE Emerging Technology Portal.
- Haryadi, T. and Schmidt, G. (1991), *Groundwater Quantification for Four Urban Development Areas - Groundwater Flow Simulation Model, Denpasar*. Bundesanstalt fuer Geowissenschaften und Rohstoffe (BGR), Hannover, 101-111.
- Hoffmann, J., Zebker, H. A., Galloway, D. L., and Amelung, F. 2001. “Seasonal Subsidence and Rebound in Las Vegas Valley, Nevada, Observed by Synthetic Aperture Radar Interferometry.” *Water Resources Research.*, 37 (6), 1551–1566.

- Hooper, A., Zebker, H., Segall, P., and Kampes, B. 2004. "A New Method for Measuring Deformation on Volcanoes and Other Natural Terrains Using InSAR Persistent Scatterers." *Geophysical Research Letter* 31 (2004): 1-5.
- Hoper, A. 2009. *StaMPS/MTI Manual Version 3.1*. Delft: Delft Institute of Earth Observation and Space Systems, Delft University of Technology.
- Iseki, S. 2013. *Extraction of Disaster Domain Caused by the 2011 Tohoku Earthquake Tsunami Disaster Using the ALOS/PALSAR Images* (thesis). Yamaguchi: Yamaguchi University.
- ITIC. 2010. *27 February 2010, MW 8.8, Off Central Chile*. [Cited on June 20, 2015]. Available from: URL: <http://193.191.134.38/itic/index>.
- ITT. 2006. *ENVI Tutorial: Basic SAR Processing and Analysis*. Pearl East Circle: ITT Visual Information Solutions.
- JSI. 2010. *QuickBird Image of Chile (March 9<sup>th</sup>, 2010)*. Japan: Japan Space Imaging.
- Kampes, B. M. 2005. "Displacement Parameter Estimation Using Permanent Scatterer Interferometry." Doctoral thesis, Technische Universiteit Delft.
- Keller, E and Blodgett R. 2008. *Natural Hazards: Earth's Processes as Hazards, Disasters, and Catastrophes*. New Jersey: Pearson Education.
- Knutsson, G. and Torbjörn, F. 1977. *Groundwater Resources in Sweden*. Uppsala: SGU (Geological Survey of Sweden).
- IDRISI. 2009. *Segmentation and Segment-Based Classification* (paper). Massachusetts: Clark Labs, Clark University.
- Liew, S. C. 2001. *Principles of Remote Sensing*. Singapore: Center for Remote Imaging, Sensing, and Processing (CRISP), National University of Singapore.
- Lillesand, T. M. and Kiefer R. 1993. *Remote Sensing and Image Interpretation*. 3<sup>rd</sup> Edition. New York: John Wiley.
- Ljungdahi, J. (2015), *Analysis of groundwater level changes and land subsidence in Gothenburg, SW Sweden*, University of Gothenburg, Sweden, 3-6.
- Lu, Z., and W. R. Danskin (2001), InSAR analysis of natural recharge to define structure of a ground-water basin, San Bernardino, California, *Geophys. Res. Lett.*, 28(13), 2661–2664.
- Matsuoka, M. and Yamazaki F. 2000. *Use of Interferometric Satellite SAR for Earthquake Damage Detection*. Proceedings of the 6<sup>th</sup> International Conference on Seismic Zonation. California, November 12-15.
- McCandless, S. W. Jr. and C. R. Jackson, 2004. *Principles of Synthetic Aperture Radar*. United States of America: Radar Imaging Resources. p. 1-23.
- Meijde, M. V. D.. 2006. *Characteristics of Tsunamis*. Netherlands: International Institute for Geo-Information Science and Earth Observation (ITC).

- Mulligan, K.B.; Brown, C.; Yang, Y.C.E.; Ahlfeld, D.P. 2014. "Assessing Groundwater Policy with Coupled Economic-Groundwater Hydrologic Modeling." *Water Resources Research* 2014 (50): 2257–2275.
- NGDC. 2010. *NOAA/WDC Historical Tsunami Data Base*. United States of America: National Geophysical Data Center.
- PU (Public Work Agency) of Bali Province. 2014. Zonation Map of Groundwater Usage in Bali Province, 2014 Fiscal Year. Final Report.
- Putra, A. A. G. P., Handayani, C. I. M., Mustafa, F., Jasmini, M., Rahmaeni, N.K. D., Sukarji, M. A., Amer, L. 2014. SLHE (Status of Ecoregion Environment) in Bali and Nusa Tenggara. Annual Report of the Center for Ecoregion Management in Bali and Nusa Tenggara.
- Rosen, P. A., Hensley, S., Joughin I. R., Li, F. K., Madsen S. N., Rodríguez E., Goldstein, R. M. 2000. "Synthetic Aperture Radar Interferometry." In *Proceedings of the IEEE* 88 (3), 333-382.
- Reeves, J. A., Knight, R., Zebker, H. A., Kitanidis, P. K., and Schre€uder, W. A. 2014. "Estimating Temporal Changes in Hydraulic Head Using InSAR Data in the San Luis Valley, Colorado." *Water Resources Research* 50 (5), 4459–4473.
- Reeves, J. A., Knight, R., Zebker, H. A., Schre€uder, W. A., Shanker A. P., and Lauknes, T. R. 2011. "High quality InSAR Data Linked to Seasonal Change in Hydraulic Head for an Agricultural Area in the San Luis Valley, Colorado." *Water Resources Research* 47 (12): 1029-1039.
- Riley, F. S. 1969. Analysis of Borehole Extensometer Data from Central California. (IAHS). International Association of Hydrological Sciences Publication.
- Rosenqvist A., Shimada, M., and Watanabe, M. 2004. "ALOS PALSAR: Technical Outline and Mission Concepts." Presented at the 4th International Symposium on Retrieval of Bio- and Geophysical Parameters from SAR Data for Land Applications, Innsbruck, Austria.
- Sällfors, G. 2001. *Geoteknik, Jordmateriallära-Jordmekanik*. Sweden: Göteborg.
- Sandwell, D. T., Myer, D., Mellors, R., Shimada, M., Brooks, B., and Foster, J. 2008. "Accuracy and Resolution of ALOS Interferometry: Vector Deformation Maps of the Father's Day Intrusion at Kilauea." *IEEE Transactions on Geoscience and Remote Sensing* 46 (11): 3524 – 3534.
- Sarsito, D. A., Susilo, Andreas, H., Pradipta, D., and Gumilar, I. "Regional Phenomena of Vertical Deformation in Southern Part of Indonesia." In 2nd Geoplanning-International Conference on Geomatics and Planning. *IOP Conference Series: Earth and Environmental Science* 123 (2018): 1-7.

- Schmidt, D. A., and Brügmann, R. 2003. "Time-Dependent Land Uplift and Subsidence in the Santa Clara Valley, California, From a Large Interferometric Synthetic Aperture Radar Data Set, *Journal of Geophysical Research* 108(B9): 2416.
- Secretaria Comunal de Panicacion*. 2010. *Inundation Map of Talcahuano*. Chile: *I. Municipalidad*.
- Shimada, M. 2007. *ALOS User Handbook*. Japan: Earth Observation Center, Japan Aerospace Agency.
- Stramondo, S., C. Bignami, M. Chini, N. Pierdicca. 2008. *Space-Based Tools Supporting Earthquake Damage Detection and Mapping: SAR and Optical Data*. 6<sup>th</sup> International Workshop on Remote Sensing for Disaster Applications. Italy, September 11-12.
- Sukearsana, I M., Dharma; I G. B. S., Nuarsa, I W. 2015. "Kajian Daerah Terintrusi Air Laut di Wilayah Pesisir Kecamatan Kuta Utara, Kabupaten Badung - Regional Study on Sea Water Intrusion in the Coastal Area in North Kuta District of Badung Regency." *ECOTROPHIC: Jurnal Ilmu Lingkungan (Journal of Environmental Science)* 9 (2): 72-78.
- Suppasri, A., Koshimura S., Matsuoka M. 2012. *Application of Remote Sensing for Tsunami Disaster*. Japan: Remote Sensing of Planet Earth. p. 143-166.
- Taylor, C. J. and Alley, W. M. 2001. *Ground-Water-Level Monitoring and the Importance of Long-Term Water-Level Data*. Colorado: U.S. Geological Survey.
- Udayana Univeristy. 2014. *Soil Investigation Report: Project on Planning of Estuary Reservoir, Suwung, Denpasar, Bali*. 2014. Project Report of Soil Mechanics Laboratory, Civil Faculty, Udayana Univeristy.
- UN (United Nations). 2017. "World Population Prospects: The 2017 Revision". United Nation Population Database. Accessed May 15, 2018. <http://www.un.org/en/development/>.
- UNEP (2014), *Emerging issues for Small Island Developing States (SISD) emerging issues for small Island developing states*, United Nations Environment Programme (UNEP), Kenya, 23-24.
- USGS. 2010. *Shake Map*. U.S. Geological Survey. Cited on June 20, 2015]. Available from: URL: <http://earthquake.usgs.gov>.
- USGS (United States Geological Survey). 2015. "Shuttle Radar Topography Mission (SRTM) 1 Arc-Second Global." Accessed May 10, 2018. <http://lta.cr.usgs.gov/SRTM1Arc>.
- Van der Kooij, M., Hughes, W., Sato, S. and Poncos, V. 2006. *Coherent Target Monitoring at High Spatial Density: Examples of Validation Results*. European Space Agency Special Publication.
- Wijayantari, I. A. M. 2017. "Studi Intrusi Air Laut di Kawasan Candidasa Karangasem – Study on Sewa Water Intrusion in Candidasa Region of Karangasem." Accessed in May 15, 2018. <https://ft.unud.ac.id>.

- Yamazaki, F. and Matsuoka M., 2007. *Remote Sensing Technologies in Post-Disaster Damage Assessment*. Japan: National Institute of Advanced Industrial Science and Technology (AIST). 17 p.
- Zebker, H. A., Hensley, S., Shanker, P., and Wortham, C. 2010. “Geodetically Accurate InSAR Data Processor.” *IEEE Transactions on Geoscience and Remote Sensing* 48 (12): 4309–4321.
- Zebker, H. A., Rosen, P. A., and Hensley, S. 1997. “Atmospheric Effects in Interferometric Synthetic Aperture Radar Surface Deformation and Topographic Maps.” *Journal of Geophysical Research* 102 (B4): 7547–7563.
- Zhou, Q., Chen, Chong., Zhang, Gaofeng., Chen, H., Chen, D., Yan, Y., Shen, J., and Zhou, R. 2018. “Real-Time Management of Groundwater Resources Based on Wireless Sensors Networks.” *Journal of Sensor and Actuator Networks* 7 (4): 3-11.

# APPENDIX A. GMT5SAR PROCESSING

## A.1 ALOS PALSAR (Path 422 Row 7010) in Bali, Indonesia

```
data.in
IMG-HH-ALPSRP057407010-H1.0__A
IMG-HH-ALPSRP097667010-H1.0__A
IMG-HH-ALPSRP111087010-H1.0__A
IMG-HH-ALPSRP117797010-H1.0__A
IMG-HH-ALPSRP151347010-H1.0__A
IMG-HH-ALPSRP164767010-H1.0__A
IMG-HH-ALPSRP205027010-H1.0__A
IMG-HH-ALPSRP211737010-H1.0__A
IMG-HH-ALPSRP218447010-H1.0__A

pre_proc_batch.csh ALOS data.in batch.config

START PREPROCESS A STACK OF IMAGES

preprocess master image
ledflag 1
.... swapping bytes
writing generic LED file: IMG-HH-ALPSRP057407010-H1.0__A.LED
.... calculating doppler for IMG-HH-ALPSRP057407010-H1.0__A.raw
Working on line 2000
Working on line 4000
Working on line 6000
Working on line 8000
Working on line 10000
Working on line 12000
Working on line 14000
Working on line 16000
Working on line 18000
Working on line 20000
Working on line 22000
Working on line 24000
Working on line 26000
Working on line 28000
Working on line 30000
Working on line 32000
Working on line 34000
pre_proc_batch.csh
preprocess slave images
setting fd1 to 51.897064
setting near_range to 849115.00
setting radius to 6377562.801111
setting npatches to 3
ledflag 1
.... swapping bytes
writing generic LED file: IMG-HH-ALPSRP097667010-H1.0__A.LED
near_range, shift = 849714 256
near_range, shift = 848815 -128
The range sampling rate for master and slave images are: 32000000
pre_proc_batch.csh
preprocess slave images
setting fd1 to 51.897064
setting near_range to 849115.00
setting radius to 6377562.801111
setting npatches to 3
ledflag 1
.... swapping bytes
writing generic LED file: IMG-HH-ALPSRP111087010-H1.0__A.LED
near_range, shift = 849415 128
near_range, shift = 848815 -128
The range sampling rate for master and slave images are: 32000000
pre_proc_batch.csh
preprocess slave images
setting fd1 to 51.897064
setting near_range to 849115.00
setting radius to 6377562.801111
setting npatches to 3
ledflag 1
.... swapping bytes
writing generic LED file: IMG-HH-ALPSRP117797010-H1.0__A.LED
The range sampling rate for master and slave images are: 32000000
pre_proc_batch.csh
preprocess slave images
setting fd1 to 51.897064
setting near_range to 849115.00
setting radius to 6377562.801111
setting npatches to 3
ledflag 1
.... swapping bytes
writing generic LED file: IMG-HH-ALPSRP151347010-H1.0__A.LED
near_range, shift = 848965 -64
The range sampling rate for master and slave images are: 32000000
pre_proc_batch.csh
preprocess slave images
setting fd1 to 51.897064
setting near_range to 849115.00
setting radius to 6377562.801111
setting npatches to 3
ledflag 1
.... swapping bytes
writing generic LED file: IMG-HH-ALPSRP164767010-H1.0__A.LED
near_range, shift = 849565 192
near_range, shift = 848815 -128
The range sampling rate for master and slave images are: 32000000
pre_proc_batch.csh
preprocess slave images
setting fd1 to 51.897064
setting near_range to 849115.00
setting radius to 6377562.801111
setting npatches to 3
ledflag 1
.... swapping bytes
writing generic LED file: IMG-HH-ALPSRP205027010-H1.0__A.LED
The range sampling rate for master and slave images are: 32000000
pre_proc_batch.csh
preprocess slave images
setting fd1 to 51.897064
setting near_range to 849115.00
setting radius to 6377562.801111
setting npatches to 3
```



```
ledflag 1
... swapping bytes
writing generic LED file: IMG-HH-ALPSRP211737010-H1.0_A.LED
near_range, shift = 849265 64
near_range, shift = 848665 -192
The range sampling rate for master and slave images are: 32000000
pre_proc_batch.csh
preprocess slave images
setting fd1 to 51.897064
setting near_range to 849115.00
setting radius to 6377562.801111
setting npatches to 3
ledflag 1
... swapping bytes
writing generic LED file: IMG-HH-ALPSRP218447010-H1.0_A.LED
near_range, shift = 848965 -64
The range sampling rate for master and slave images are: 32000000
```

END PREPROCESS A STACK OF IMAGES

baseline\_table.dat

```
05740 2007052.6322886334 417 0.000000 0.000000
09766 2007328.6318059019 693 -228.908004 -280.159414
11108 2008055.6311110638 785 -364.922815 -566.082561
11779 2008101.6306031356 831 -433.069790 -579.321254
15134 2008331.6315637375 1061 496.755333 622.995138
16476 2009057.6324624296 1152 74.726216 120.871632
20502 2009333.6334803810 1428 118.300496 25.964374
21173 2010014.6334367814 1474 -63.414077 -208.649298
21844 2010060.6332845823 1520 -137.084695 -247.445740
```

intf.in

```
IMG-HH-ALPSRP057407010-H1.0_A:IMG-HH-ALPSRP097667010-H1.0_A
IMG-HH-ALPSRP057407010-H1.0_A:IMG-HH-ALPSRP111087010-H1.0_A
IMG-HH-ALPSRP057407010-H1.0_A:IMG-HH-ALPSRP117797010-H1.0_A
IMG-HH-ALPSRP057407010-H1.0_A:IMG-HH-ALPSRP151347010-H1.0_A
IMG-HH-ALPSRP057407010-H1.0_A:IMG-HH-ALPSRP164767010-H1.0_A
IMG-HH-ALPSRP057407010-H1.0_A:IMG-HH-ALPSRP205027010-H1.0_A
IMG-HH-ALPSRP057407010-H1.0_A:IMG-HH-ALPSRP211737010-H1.0_A
IMG-HH-ALPSRP057407010-H1.0_A:IMG-HH-ALPSRP218447010-H1.0_A
IMG-HH-ALPSRP097667010-H1.0_A:IMG-HH-ALPSRP111087010-H1.0_A
IMG-HH-ALPSRP097667010-H1.0_A:IMG-HH-ALPSRP117797010-H1.0_A
IMG-HH-ALPSRP097667010-H1.0_A:IMG-HH-ALPSRP151347010-H1.0_A
IMG-HH-ALPSRP097667010-H1.0_A:IMG-HH-ALPSRP164767010-H1.0_A
IMG-HH-ALPSRP097667010-H1.0_A:IMG-HH-ALPSRP205027010-H1.0_A
IMG-HH-ALPSRP097667010-H1.0_A:IMG-HH-ALPSRP211737010-H1.0_A
IMG-HH-ALPSRP097667010-H1.0_A:IMG-HH-ALPSRP218447010-H1.0_A
IMG-HH-ALPSRP111087010-H1.0_A:IMG-HH-ALPSRP117797010-H1.0_A
IMG-HH-ALPSRP111087010-H1.0_A:IMG-HH-ALPSRP151347010-H1.0_A
IMG-HH-ALPSRP111087010-H1.0_A:IMG-HH-ALPSRP164767010-H1.0_A
IMG-HH-ALPSRP111087010-H1.0_A:IMG-HH-ALPSRP205027010-H1.0_A
IMG-HH-ALPSRP111087010-H1.0_A:IMG-HH-ALPSRP211737010-H1.0_A
IMG-HH-ALPSRP111087010-H1.0_A:IMG-HH-ALPSRP218447010-H1.0_A
IMG-HH-ALPSRP117797010-H1.0_A:IMG-HH-ALPSRP164767010-H1.0_A
IMG-HH-ALPSRP117797010-H1.0_A:IMG-HH-ALPSRP205027010-H1.0_A
IMG-HH-ALPSRP117797010-H1.0_A:IMG-HH-ALPSRP211737010-H1.0_A
IMG-HH-ALPSRP117797010-H1.0_A:IMG-HH-ALPSRP218447010-H1.0_A
IMG-HH-ALPSRP151347010-H1.0_A:IMG-HH-ALPSRP164767010-H1.0_A
IMG-HH-ALPSRP151347010-H1.0_A:IMG-HH-ALPSRP205027010-H1.0_A
IMG-HH-ALPSRP151347010-H1.0_A:IMG-HH-ALPSRP211737010-H1.0_A
IMG-HH-ALPSRP151347010-H1.0_A:IMG-HH-ALPSRP218447010-H1.0_A
IMG-HH-ALPSRP164767010-H1.0_A:IMG-HH-ALPSRP205027010-H1.0_A
IMG-HH-ALPSRP164767010-H1.0_A:IMG-HH-ALPSRP211737010-H1.0_A
IMG-HH-ALPSRP164767010-H1.0_A:IMG-HH-ALPSRP218447010-H1.0_A
IMG-HH-ALPSRP205027010-H1.0_A:IMG-HH-ALPSRP211737010-H1.0_A
IMG-HH-ALPSRP205027010-H1.0_A:IMG-HH-ALPSRP218447010-H1.0_A
IMG-HH-ALPSRP211737010-H1.0_A:IMG-HH-ALPSRP218447010-H1.0_A
```

align.in

```
IMG-HH-ALPSRP057407010-H1.0_A:IMG-HH-ALPSRP097667010-H1.0_A:IMG-HH-ALPSRP057407010-H1.0_A
IMG-HH-ALPSRP057407010-H1.0_A:IMG-HH-ALPSRP111087010-H1.0_A:IMG-HH-ALPSRP057407010-H1.0_A
IMG-HH-ALPSRP057407010-H1.0_A:IMG-HH-ALPSRP117797010-H1.0_A:IMG-HH-ALPSRP057407010-H1.0_A
IMG-HH-ALPSRP057407010-H1.0_A:IMG-HH-ALPSRP151347010-H1.0_A:IMG-HH-ALPSRP057407010-H1.0_A
IMG-HH-ALPSRP057407010-H1.0_A:IMG-HH-ALPSRP164767010-H1.0_A:IMG-HH-ALPSRP057407010-H1.0_A
IMG-HH-ALPSRP057407010-H1.0_A:IMG-HH-ALPSRP205027010-H1.0_A:IMG-HH-ALPSRP057407010-H1.0_A
IMG-HH-ALPSRP057407010-H1.0_A:IMG-HH-ALPSRP211737010-H1.0_A:IMG-HH-ALPSRP057407010-H1.0_A
IMG-HH-ALPSRP057407010-H1.0_A:IMG-HH-ALPSRP218447010-H1.0_A:IMG-HH-ALPSRP057407010-H1.0_A
IMG-HH-ALPSRP097667010-H1.0_A:IMG-HH-ALPSRP111087010-H1.0_A:IMG-HH-ALPSRP057407010-H1.0_A
IMG-HH-ALPSRP097667010-H1.0_A:IMG-HH-ALPSRP117797010-H1.0_A:IMG-HH-ALPSRP057407010-H1.0_A
IMG-HH-ALPSRP097667010-H1.0_A:IMG-HH-ALPSRP151347010-H1.0_A:IMG-HH-ALPSRP057407010-H1.0_A
IMG-HH-ALPSRP097667010-H1.0_A:IMG-HH-ALPSRP164767010-H1.0_A:IMG-HH-ALPSRP057407010-H1.0_A
IMG-HH-ALPSRP097667010-H1.0_A:IMG-HH-ALPSRP205027010-H1.0_A:IMG-HH-ALPSRP057407010-H1.0_A
IMG-HH-ALPSRP097667010-H1.0_A:IMG-HH-ALPSRP211737010-H1.0_A:IMG-HH-ALPSRP057407010-H1.0_A
IMG-HH-ALPSRP097667010-H1.0_A:IMG-HH-ALPSRP218447010-H1.0_A:IMG-HH-ALPSRP057407010-H1.0_A
IMG-HH-ALPSRP111087010-H1.0_A:IMG-HH-ALPSRP117797010-H1.0_A:IMG-HH-ALPSRP057407010-H1.0_A
IMG-HH-ALPSRP111087010-H1.0_A:IMG-HH-ALPSRP164767010-H1.0_A:IMG-HH-ALPSRP057407010-H1.0_A
IMG-HH-ALPSRP111087010-H1.0_A:IMG-HH-ALPSRP205027010-H1.0_A:IMG-HH-ALPSRP057407010-H1.0_A
IMG-HH-ALPSRP111087010-H1.0_A:IMG-HH-ALPSRP211737010-H1.0_A:IMG-HH-ALPSRP057407010-H1.0_A
IMG-HH-ALPSRP111087010-H1.0_A:IMG-HH-ALPSRP218447010-H1.0_A:IMG-HH-ALPSRP057407010-H1.0_A
IMG-HH-ALPSRP117797010-H1.0_A:IMG-HH-ALPSRP164767010-H1.0_A:IMG-HH-ALPSRP057407010-H1.0_A
IMG-HH-ALPSRP117797010-H1.0_A:IMG-HH-ALPSRP205027010-H1.0_A:IMG-HH-ALPSRP057407010-H1.0_A
IMG-HH-ALPSRP117797010-H1.0_A:IMG-HH-ALPSRP211737010-H1.0_A:IMG-HH-ALPSRP057407010-H1.0_A
IMG-HH-ALPSRP117797010-H1.0_A:IMG-HH-ALPSRP218447010-H1.0_A:IMG-HH-ALPSRP057407010-H1.0_A
IMG-HH-ALPSRP151347010-H1.0_A:IMG-HH-ALPSRP164767010-H1.0_A:IMG-HH-ALPSRP057407010-H1.0_A
IMG-HH-ALPSRP151347010-H1.0_A:IMG-HH-ALPSRP205027010-H1.0_A:IMG-HH-ALPSRP057407010-H1.0_A
IMG-HH-ALPSRP151347010-H1.0_A:IMG-HH-ALPSRP211737010-H1.0_A:IMG-HH-ALPSRP057407010-H1.0_A
IMG-HH-ALPSRP151347010-H1.0_A:IMG-HH-ALPSRP218447010-H1.0_A:IMG-HH-ALPSRP057407010-H1.0_A
IMG-HH-ALPSRP164767010-H1.0_A:IMG-HH-ALPSRP205027010-H1.0_A:IMG-HH-ALPSRP057407010-H1.0_A
IMG-HH-ALPSRP164767010-H1.0_A:IMG-HH-ALPSRP211737010-H1.0_A:IMG-HH-ALPSRP057407010-H1.0_A
IMG-HH-ALPSRP164767010-H1.0_A:IMG-HH-ALPSRP218447010-H1.0_A:IMG-HH-ALPSRP057407010-H1.0_A
IMG-HH-ALPSRP205027010-H1.0_A:IMG-HH-ALPSRP211737010-H1.0_A:IMG-HH-ALPSRP057407010-H1.0_A
IMG-HH-ALPSRP205027010-H1.0_A:IMG-HH-ALPSRP218447010-H1.0_A:IMG-HH-ALPSRP057407010-H1.0_A
IMG-HH-ALPSRP211737010-H1.0_A:IMG-HH-ALPSRP218447010-H1.0_A:IMG-HH-ALPSRP057407010-H1.0_A
```

align\_batch.csh AL05 align.in

ALIGN.CSH - START

```
focussing master
Computing range reference function.
Processing patch 1
Processing Elapsed Time: 0 min 0.04 sec
Range Compression
Processing Elapsed Time: 0 min 5.69 sec
Azimuthal Transform
Processing Elapsed Time: 0 min 13.58 sec
Range Migration
Processing Elapsed Time: 0 min 23.50 sec
Azimuthal Compression
Processing Elapsed Time: 0 min 45.94 sec
Writing Data
```

```

Processing patch 2
Processing Elapsed Time: 0 min 47.45 sec
Range Compression
Processing Elapsed Time: 0 min 52.11 sec
Azimuthal Transform
Processing Elapsed Time: 0 min 59.99 sec
Range Migration
Processing Elapsed Time: 1 min 9.89 sec
Azimuthal Compression
Processing Elapsed Time: 1 min 33.02 sec
Writing Data
Processing patch 3
Processing Elapsed Time: 1 min 34.59 sec
Range Compression
Processing Elapsed Time: 1 min 39.19 sec
Azimuthal Transform
Processing Elapsed Time: 1 min 47.28 sec
Range Migration
Processing Elapsed Time: 1 min 57.19 sec
Azimuthal Compression
Processing Elapsed Time: 2 min 19.92 sec
Writing Data
Processing Elapsed Time: 2 min 21.44 sec
number of points clipped to short int 53
align.csh
focusing slave
Computing range reference function.
Processing patch 1
Processing Elapsed Time: 0 min 0.03 sec
Range Compression
Processing Elapsed Time: 0 min 5.57 sec
Azimuthal Transform
Processing Elapsed Time: 0 min 13.87 sec
Range Migration
Processing Elapsed Time: 0 min 23.93 sec
Azimuthal Compression
Processing Elapsed Time: 0 min 47.04 sec
Writing Data
Processing patch 2
Processing Elapsed Time: 0 min 48.58 sec
Range Compression
Processing Elapsed Time: 0 min 53.18 sec
Azimuthal Transform
Processing Elapsed Time: 1 min 1.26 sec
Range Migration
Processing Elapsed Time: 1 min 11.19 sec
Azimuthal Compression
Processing Elapsed Time: 1 min 35.27 sec
Writing Data
Processing patch 3
Processing Elapsed Time: 1 min 36.80 sec
Range Compression
Processing Elapsed Time: 1 min 41.44 sec
Azimuthal Transform
Processing Elapsed Time: 1 min 49.63 sec
Range Migration
Processing Elapsed Time: 1 min 59.54 sec
Azimuthal Compression
Processing Elapsed Time: 2 min 23.60 sec
Writing Data
Processing Elapsed Time: 2 min 25.14 sec
number of points clipped to short int 175
align.csh
correlate master and slave to find offset parameters
  setting xsearch to 64
  setting nx_corr to 128
  setting ysearch to 64
  setting ny_corr to 128
11304 27648 11304 27648 104 68 -0.002141
locations n 512 nx 11304 nyl 32 nxl 16 x_inc 574 y_inc 826
elapsed time: 19.338003
align.csh
refocus slave
Computing range reference function.
Processing patch 1
Processing Elapsed Time: 0 min 0.03 sec
Range Compression
Processing Elapsed Time: 0 min 5.83 sec
Azimuthal Transform
Processing Elapsed Time: 0 min 20.32 sec
Range Migration
Processing Elapsed Time: 0 min 30.42 sec
Azimuthal Compression
Processing Elapsed Time: 1 min 3.81 sec
apply azimuth-dependent azimuth shift
Processing Elapsed Time: 1 min 28.67 sec
Writing Data
Processing patch 2
Processing Elapsed Time: 1 min 35.16 sec
Range Compression
Processing Elapsed Time: 1 min 39.93 sec
Azimuthal Transform
Processing Elapsed Time: 1 min 49.27 sec
Range Migration
Processing Elapsed Time: 1 min 59.38 sec
Azimuthal Compression
Processing Elapsed Time: 2 min 29.37 sec
apply azimuth-dependent azimuth shift
Processing Elapsed Time: 2 min 56.98 sec
Writing Data
Processing patch 3
Processing Elapsed Time: 3 min 3.89 sec
Range Compression
Processing Elapsed Time: 3 min 8.54 sec
Azimuthal Transform
Processing Elapsed Time: 3 min 18.00 sec
Range Migration
Processing Elapsed Time: 3 min 28.25 sec
Azimuthal Compression
Processing Elapsed Time: 4 min 2.25 sec
apply azimuth-dependent azimuth shift
Processing Elapsed Time: 4 min 28.31 sec
Writing Data
Processing Elapsed Time: 4 min 35.06 sec
number of points clipped to short int 187
rm: No match.
ALIGN.CSH - END

intf_batch.csh ALOS batch.config

```

clean up topo/ folder

```
DEM2TOPO_RA.CSH - START
USER SHOULD PROVIDE DEM FILE
  range decimation is: 2
blockmedian: Provides 3, expects 3-column binary data
blockmedian: Processing input table data
blockmedian: W: 0 E: 11304 S: 0 N: 27648 n_columns: 5652 n_rows: 6912
blockmedian: Input 3 columns via binary records using format ddd
blockmedian: Output 3 columns via binary records using format ddd
blockmedian: N read: 880412 N used: 877562 outside_area: 2850 N cells filled: 877534
surface: Provides 3, expects 3-column binary data
surface: Grid domain: W: 0 E: 11304 S: 0 N: 27648 n_columns: 5652 n_rows: 6912 [pixel registration]
surface: Processing input table data
surface: Input 3 columns via binary records using format ddd
surface: Minimum value of your dataset x,y,z at: surface: 9.47925853729 20.111221313 79.1265945435
surface: Maximum value of your dataset x,y,z at: surface: 4982.25195312 19988.2792969 3152.45239258
surface: LS plane determined: z = 203.081 + (-0.085365 * col) + (0.111885 * row)
surface:


| Grid | Mode | Iteration | Max Change        | Conv Limit       | Total Iterations |
|------|------|-----------|-------------------|------------------|------------------|
| 36   | D    | 22        | 0.000546255543946 | 0.00086758828296 | 22               |
| 12   | I    | 28        | 0.00218929156934  | 0.0026027648489  | 50               |
| 12   | D    | 20        | 0.00178716015478  | 0.0026027648489  | 70               |
| 4    | I    | 25        | 0.00575992186722  | 0.0078082945467  | 95               |
| 4    | D    | 42        | 0.00697227533129  | 0.0078082945467  | 137              |
| 2    | I    | 18        | 0.0144953689828   | 0.0156165890934  | 155              |
| 2    | D    | 92        | 0.0155055815236   | 0.0156165890934  | 247              |
| 1    | I    | 16        | 0.0282327391979   | 0.0312331781868  | 263              |
| 1    | D    | 245       | 0.0309639238689   | 0.0312331781868  | 508              |


surface: Fit info: N data points N nodes mean error rms error curvature
surface: 877534 39079189 -3.16770048757e-06 0.0062199362068 22227.5479258
grd2cpt: Processing input grid(s)
grd2cpt: Mean and S.D. of data are 349.387377152 406.116523212
grdimage: Allocates memory and read data file topo_ra.grd
grdimage: Evaluate image pixel colors
grdimage: Creating 8-bit grayscale image
DEM2TOPO_RA.CSH - END
NO TOPO_RA SHIFT
```

START FORM A STACK OF INTERFEROGRAMS

```
INTF.CSH, FILTER.CSH - START
intf.csh
  running phasediff...
  reading topo topo_ra.grd
  xdim 11304, ydim 27648
filter.csh
  gauss 300 4 2 (4 2)
  making amplitudes...
  filtering interferogram...
  making amplitude...
  making correlation...
  making phase...
  filtering phase...
INTF.CSH, FILTER.CSH - END
```

MAKE LANDMASK -- START

REQUIRE FULL RESOLUTION COASTLINE FROM GMT

```
grdlandmask: GSHHG version 2.3.7
Derived from World Vector Shoreline, CIA WDB-II, and Atlas of the Cryosphere
Processed by Paul Wessel and Walter H. F. Smith, 1994-2017
grdlandmask: Nodes in water will be set to NaN
grdlandmask: Nodes on land will be set to 1
grdlandmask: Level 0 contained 8112640 nodes
grdlandmask: Level 1 contained 2478081 nodes
grdlandmask: Done!
surface: Provides 3, expects 3-column binary data
surface: Grid domain: W: 113.833333329 E: 117.416666662 S: -9.166666663 N: -7.416666663 n_columns: 4300 n_rows: 2100 [gridline registration]
surface: Processing input table data
surface: Input 3 columns via binary records using format fff
surface: Minimum value of your dataset x,y,z at: surface: 115.220001221 -8.85499954224 -9.99483108521
surface: Maximum value of your dataset x,y,z at: surface: 115.945831299 -8.5683267212 11313.9638672
surface: LS plane determined: z = -21214.5 + (12.0682 * col) + (2.5925 * row)
surface:


| Grid | Mode | Iteration | Max Change        | Conv Limit       | Total Iterations |
|------|------|-----------|-------------------|------------------|------------------|
| 100  | D    | 6384      | 7.54209935596e-05 | 7.63795351882e-0 | 6384             |
| 20   | I    | 88        | 0.00034390910789  | 0.00038189767594 | 6472             |
| 20   | D    | 10000     | 0.00127684555265  | 0.00038189767594 | 16472            |
| 4    | I    | 63        | 0.00180797931012  | 0.00190948837971 | 16535            |
| 4    | D    | 1552      | 0.00190942585768  | 0.00190948837971 | 18087            |
| 2    | I    | 17        | 0.00351663660741  | 0.00381897675941 | 18104            |
| 2    | D    | 392       | 0.00381115027586  | 0.00381897675941 | 18496            |
| 1    | I    | 15        | 0.005502280015928 | 0.00763795351882 | 18511            |
| 1    | D    | 133       | 0.00763743786382  | 0.00763795351882 | 18644            |


surface: Fit info: N data points N nodes mean error rms error curvature
surface: 880412 9036401 0 0 6703.59290537
surface: Provides 3, expects 3-column binary data
surface: Grid domain: W: 113.833333329 E: 117.416666662 S: -9.166666663 N: -7.416666663 n_columns: 4300 n_rows: 2100 [gridline registration]
surface: Processing input table data
surface: Input 3 columns via binary records using format fff
surface: Minimum value of your dataset x,y,z at: surface: 115.785835266 -8.86583328247 -19.9908485413
surface: Maximum value of your dataset x,y,z at: surface: 115.442497253 -8.12583255768 27667.9804688
surface: LS plane determined: z = 4765.3 + (-6.38892 * col) + (28.2121 * row)
surface:


| Grid | Mode | Iteration | Max Change        | Conv Limit       | Total Iterations |
|------|------|-----------|-------------------|------------------|------------------|
| 100  | D    | 7005      | 2.69743062392e-06 | 2.73171285111e-0 | 7005             |
| 20   | I    | 103       | 1.34681571328e-05 | 1.36585642556e-0 | 7108             |
| 20   | D    | 10000     | 0.000305607492168 | 1.36585642556e-0 | 17108            |
| 4    | I    | 77        | 6.17369685184e-05 | 6.82928212778e-0 | 17185            |
| 4    | D    | 2000      | 0.000463692123562 | 6.82928212778e-0 | 19185            |
| 2    | I    | 18        | 0.000106690979598 | 0.00013658564255 | 19203            |
| 2    | D    | 973       | 0.000136448198424 | 0.00013658564255 | 20176            |
| 1    | I    | 16        | 0.000247783697653 | 0.00027317128511 | 20192            |
| 1    | D    | 500       | 0.000301086446475 | 0.00027317128511 | 20692            |


surface: Fit info: N data points N nodes mean error rms error curvature
surface: 880412 9036401 0 0 548605.402922
MAKE LANDMASK -- END
```

SNAPHU.CSH - START

```
threshold_snaphu: .45
grdmath: Perform reverse Polish notation calculations on grids
grdmath: phase_patch.grd landmask_ra_patch.grd MUL = phase_patch.grd
unwrapping phase with snaphu - higher threshold for faster unwrapping
```

snaphu v1.4.2

```
32 parameters input from file snaphu.conf.brief (297 lines total)
Reading wrapped phase from file phase.in
No weight file specified. Assuming uniform weights
Reading correlation data from file corr.in
```

```

Calculating deformation-mode cost parameters
Building range cost arrays
Building azimuth cost arrays
Initializing flows with MST algorithm
Running approximate minimum spanning tree solver
Running nonlinear network flow optimizer
Maximum flow on network: 5
Number of nodes in network: 4878776
Flow increment: 1 (Total improvements: 0)
Treesize: 4878776 Pivots: 54505 Improvements: 983
Maximum flow on network: 5
Flow increment: 2 (Total improvements: 983)
Treesize: 4878776 Pivots: 353 Improvements: 26
Maximum flow on network: 5
Flow increment: 3 (Total improvements: 1009)
Treesize: 4878776 Pivots: 30 Improvements: 7
Maximum flow on network: 5
Flow increment: 4 (Total improvements: 1016)
Treesize: 4878776 Pivots: 19 Improvements: 3
Maximum flow on network: 3
Total solution cost: 1886110
Integrating phase
Writing output to file unwrap.out
Program snaphu done
Elapsed processor time: 0:02:01.68
Elapsed wall clock time: 0:02:02
grdmath: Perform reverse Polish notation calculations on grids
grdmath: unwrap.grd landmask_ra_patch.grd MUL = tmp.grd
SNAPHU.CSH - END

GEOCODE.CSH - START
threshold_geocode: .45
grdmath: Perform reverse Polish notation calculations on grids
grdmath: corr.grd 0.45 GE 0 NAN mask.grd MUL = mask2.grd
psscale: Warning: The -E option is deprecated but is accepted.
psscale: For the current -D syntax you should use -D modifier +e instead.
psscale: Note you cannot mix new-style modifiers (+e) with the old-style -D option.
psscale: Warning: The -E option is deprecated but is accepted.
psscale: For the current -D syntax you should use -D modifier +e instead.
psscale: Note you cannot mix new-style modifiers (+e) with the old-style -D option.
geocode.csh
project correlation, phase, unwrapped and amplitude back to lon lat coordinates
remarked is by root on Wed May 23 19:26:21 JST 2018 with geocode.csh
proj_ra2ll.csh
surface: Provides 3, expects 3-column binary data
surface: Grid domain: W: 48 E: 11248 S: 0 N: 27648 n_columns: 700 n_rows: 864 [gridline registration]
surface: Processing input table data
surface: Input 3 columns via binary records using format fff
surface: Minimum value of your dataset x,y,z at: surface: 47.1167106628 27644.0820312 115.090835571
surface: Maximum value of your dataset x,y,z at: surface: 11254.5410156 59.4462890625 116.002582441
surface: 268953 unusable points were supplied; these will be ignored.
surface: You should have pre-processed the data with block-mean, -median, or -mode.
surface: Check that previous processing steps write results with enough decimals.
surface: LS plane determined: z = 115.263 + (0.00105249 * col) + (-0.000193897 * row)
surface: Grid Mode IterationMax Change Conv Limit Total Iterations
surface: 4 D 18 9.29664558309e-08 1.23550245428e-0 18
surface: 2 I 18 1.7133228938e-07 2.47100490855e-0 36
surface: 2 D 16 2.32558109563e-07 2.47100490855e-0 52
surface: 1 I 17 2.86991464972e-07 4.94200981711e-0 69
surface: 1 D 19 4.13126227982e-07 4.94200981711e-0 88
surface: Fit info: N data points N nodes mean error rms error curvature
surface: 602775 606365 -2.83816215768e-06 0.00615192647878 7119.33530528
surface: Provides 3, expects 3-column binary data
surface: Grid domain: W: 48 E: 11248 S: 0 N: 27648 n_columns: 700 n_rows: 864 [gridline registration]
surface: Processing input table data
surface: Input 3 columns via binary records using format fff
surface: Minimum value of your dataset x,y,z at: surface: 43.218296051 2.08512806892 -8.98583316803
surface: Maximum value of your dataset x,y,z at: surface: 11191.7929688 27663.4941406 -8.04083347321
surface: 268953 unusable points were supplied; these will be ignored.
surface: You should have pre-processed the data with block-mean, -median, or -mode.
surface: Check that previous processing steps write results with enough decimals.
surface: LS plane determined: z = -8.9837 + (0.000238355 * col) + (0.000901305 * row)
surface: Grid Mode IterationMax Change Conv Limit Total Iterations
surface: 4 D 18 2.07556780564e-08 2.76283641929e-0 18
surface: 2 I 18 3.84978466417e-08 5.52567283858e-0 36
surface: 2 D 17 3.25372203106e-08 5.52567283858e-0 53
surface: 1 I 17 6.58793872319e-08 1.10513456772e-0 70
surface: 1 D 19 9.6406783006e-08 1.10513456772e-0 89
surface: Fit info: N data points N nodes mean error rms error curvature
surface: 602775 606365 -1.36029670003e-06 0.0089474772787 8448.30765751
blockmedian: Provides 3, expects 3-column binary data
blockmedian: Processing input table data
blockmedian: W: 115.088888889 E: 116.011111111 S: -8.98611111111 N: -8.04166666667 n_columns: 830 n_rows: 1360
blockmedian: Input 3 columns via binary records using format fff
blockmedian: Output 3 columns via binary records using format fff
blockmedian: N read: 4776703 N used: 4776703 outside_area: 0 N cells filled: 773895
proj_ra2ll.csh
blockmedian: Provides 3, expects 3-column binary data
blockmedian: Processing input table data
blockmedian: W: 115.088888889 E: 116.011111111 S: -8.98611111111 N: -8.04166666667 n_columns: 830 n_rows: 1360
blockmedian: Input 3 columns via binary records using format fff
blockmedian: Output 3 columns via binary records using format fff
blockmedian: N read: 4781665 N used: 4781665 outside_area: 0 N cells filled: 774703
proj_ra2ll.csh
blockmedian: Provides 3, expects 3-column binary data
blockmedian: Processing input table data
blockmedian: W: 115.133333333 E: 115.922222222 S: -8.80555555556 N: -8.15277777778 n_columns: 710 n_rows: 940
blockmedian: Input 3 columns via binary records using format fff
blockmedian: Output 3 columns via binary records using format fff
blockmedian: N read: 9253 N used: 9253 outside_area: 0 N cells filled: 2817
proj_ra2ll.csh
blockmedian: Provides 3, expects 3-column binary data
blockmedian: Processing input table data
blockmedian: W: 115.088888889 E: 116.011111111 S: -8.98611111111 N: -8.03472222222 n_columns: 830 n_rows: 1370
blockmedian: Input 3 columns via binary records using format fff
blockmedian: Output 3 columns via binary records using format fff
blockmedian: N read: 4838400 N used: 4838400 outside_area: 0 N cells filled: 783792
proj_ra2ll.csh
blockmedian: Provides 3, expects 3-column binary data
blockmedian: Processing input table data
blockmedian: W: 115.133333333 E: 115.922222222 S: -8.80555555556 N: -8.15277777778 n_columns: 710 n_rows: 940
blockmedian: Input 3 columns via binary records using format fff
blockmedian: Output 3 columns via binary records using format fff
blockmedian: N read: 9228 N used: 9228 outside_area: 0 N cells filled: 2810
proj_ra2ll.csh
blockmedian: Provides 3, expects 3-column binary data
blockmedian: Processing input table data
blockmedian: W: 115.088888889 E: 116.011111111 S: -8.84722222222 N: -8.13194444444 n_columns: 830 n_rows: 1030
blockmedian: Input 3 columns via binary records using format fff

```

```

blockmedian: Output 3 columns via binary records using format fff
blockmedian: N read: 1936109 N used: 1936109 outside_area: 0 N cells filled: 317695
proj_ra2ll.csh
blockmedian: Provides 3, expects 3-column binary data
blockmedian: Processing input table data
blockmedian: W: 115.133333333 E: 115.922222222 S: -8.805555555556 N: -8.15277777778 n_columns: 710 n_rows: 940
blockmedian: Input 3 columns via binary records using format fff
blockmedian: Output 3 columns via binary records using format fff
blockmedian: N read: 9253 N used: 9253 outside_area: 0 N cells filled: 2817
geocode.csh
make the KML files for Google Earth
grdimage: Allocates memory and read data file display_amp_ll.grd
grdimage: Evaluate image pixel colors
grdimage: Creating 24-bit color image
Make display_amp_ll.kml and display_amp_ll.png
psconvert: Processing display_amp_ll.ps...
psconvert: Figure dimensions: Width: 66.42 points [0.9225 inch] Height: 68.52 points [0.951666 inch]
psconvert: gs -q -dSAFER -dNOPAUSE -dBATCH -dPDFSETTINGS=/prepress -dDownsampleColorImages=false -dDownsampleGrayImages=false -
dDownsampleMonoImages=false -dUseFlateCompression=true -dEmbedAllFonts=true -dSubsetFonts=true -dMonoImageFilter=/FlateEncode -
dAutoFilterGrayImages=false -dGrayImageFilter=/FlateEncode -dAutoFilterColorImages=false -dColorImageFilter=/FlateEncode -dSCANCONVERTERTYPE=2 -
dMaxBitmap=2147483647 -dUseFastColor=true -sDEVICE=pngalpha -g831x857 -r900 -sOutputFile='display_amp_ll.png' -f'./psconvert_64919d.eps'
psconvert: Done.
grdimage: Allocates memory and read data file corr_ll.grd
grdimage: Evaluate image pixel colors
grdimage: Creating 24-bit color image
PSL: Colormap of 224 colors created
Make corr_ll.kml and corr_ll.png
psconvert: Processing corr_ll.ps...
psconvert: Figure dimensions: Width: 66.42 points [0.9225 inch] Height: 67.986 points [0.94425 inch]
psconvert: gs -q -dSAFER -dNOPAUSE -dBATCH -dPDFSETTINGS=/prepress -dDownsampleColorImages=false -dDownsampleGrayImages=false -
dDownsampleMonoImages=false -dUseFlateCompression=true -dEmbedAllFonts=true -dSubsetFonts=true -dMonoImageFilter=/FlateEncode -
dAutoFilterGrayImages=false -dGrayImageFilter=/FlateEncode -dAutoFilterColorImages=false -dColorImageFilter=/FlateEncode -dSCANCONVERTERTYPE=2 -
dMaxBitmap=2147483647 -dUseFastColor=true -sDEVICE=pngalpha -g831x850 -r900 -sOutputFile='corr_ll.png' -f'./psconvert_64933d.eps'
psconvert: Done.
grdimage: Allocates memory and read data file phase_mask_ll.grd
grdimage: Evaluate image pixel colors
grdimage: Creating 24-bit color image
Make phase_mask_ll.kml and phase_mask_ll.png
psconvert: Processing phase_mask_ll.ps...
psconvert: Figure dimensions: Width: 56.82 points [0.789166 inch] Height: 46.98 points [0.6525 inch]
psconvert: gs -q -dSAFER -dNOPAUSE -dBATCH -dPDFSETTINGS=/prepress -dDownsampleColorImages=false -dDownsampleGrayImages=false -
dDownsampleMonoImages=false -dUseFlateCompression=true -dEmbedAllFonts=true -dSubsetFonts=true -dMonoImageFilter=/FlateEncode -
dAutoFilterGrayImages=false -dGrayImageFilter=/FlateEncode -dAutoFilterColorImages=false -dColorImageFilter=/FlateEncode -dSCANCONVERTERTYPE=2 -
dMaxBitmap=2147483647 -dUseFastColor=true -sDEVICE=pngalpha -g711x588 -r900 -sOutputFile='phase_mask_ll.png' -f'./psconvert_64947d.eps'
psconvert: Done.
grdimage: Allocates memory and read data file phasefilt_mask_ll.grd
grdimage: Evaluate image pixel colors
grdimage: Creating 24-bit color image
Make phasefilt_mask_ll.kml and phasefilt_mask_ll.png
psconvert: Processing phasefilt_mask_ll.ps...
psconvert: Figure dimensions: Width: 56.82 points [0.789166 inch] Height: 46.98 points [0.6525 inch]
psconvert: gs -q -dSAFER -dNOPAUSE -dBATCH -dPDFSETTINGS=/prepress -dDownsampleColorImages=false -dDownsampleGrayImages=false -
dDownsampleMonoImages=false -dUseFlateCompression=true -dEmbedAllFonts=true -dSubsetFonts=true -dMonoImageFilter=/FlateEncode -
dAutoFilterGrayImages=false -dGrayImageFilter=/FlateEncode -dAutoFilterColorImages=false -dColorImageFilter=/FlateEncode -dSCANCONVERTERTYPE=2 -
dMaxBitmap=2147483647 -dUseFastColor=true -sDEVICE=pngalpha -g711x588 -r900 -sOutputFile='phasefilt_mask_ll.png' -f'./psconvert_64965d.eps'
psconvert: Done.
grdimage: Allocates memory and read data file unwrap_mask_ll.grd
grdimage: Evaluate image pixel colors
grdimage: Creating 24-bit color image
Make unwrap_mask_ll.kml and unwrap_mask_ll.png
psconvert: Processing unwrap_mask_ll.ps...
psconvert: Figure dimensions: Width: 56.82 points [0.789166 inch] Height: 46.98 points [0.6525 inch]
psconvert: gs -q -dSAFER -dNOPAUSE -dBATCH -dPDFSETTINGS=/prepress -dDownsampleColorImages=false -dDownsampleGrayImages=false -
dDownsampleMonoImages=false -dUseFlateCompression=true -dEmbedAllFonts=true -dSubsetFonts=true -dMonoImageFilter=/FlateEncode -
dAutoFilterGrayImages=false -dGrayImageFilter=/FlateEncode -dAutoFilterColorImages=false -dColorImageFilter=/FlateEncode -dSCANCONVERTERTYPE=2 -
dMaxBitmap=2147483647 -dUseFastColor=true -sDEVICE=pngalpha -g711x588 -r900 -sOutputFile='unwrap_mask_ll.png' -f'./psconvert_64980d.eps'
psconvert: Done.
grdimage: Allocates memory and read data file phasefilt_mask_ll.grd
grdimage: Evaluate image pixel colors
grdimage: Creating 24-bit color image
Make phasefilt_mask_ll.kml and phasefilt_mask_ll.png
psconvert: Processing phasefilt_mask_ll.ps...
psconvert: Figure dimensions: Width: 56.82 points [0.789166 inch] Height: 46.98 points [0.6525 inch]
psconvert: gs -q -dSAFER -dNOPAUSE -dBATCH -dPDFSETTINGS=/prepress -dDownsampleColorImages=false -dDownsampleGrayImages=false -
dDownsampleMonoImages=false -dUseFlateCompression=true -dEmbedAllFonts=true -dSubsetFonts=true -dMonoImageFilter=/FlateEncode -
dAutoFilterGrayImages=false -dGrayImageFilter=/FlateEncode -dAutoFilterColorImages=false -dColorImageFilter=/FlateEncode -dSCANCONVERTERTYPE=2 -
dMaxBitmap=2147483647 -dUseFastColor=true -sDEVICE=pngalpha -g711x588 -r900 -sOutputFile='phasefilt_mask_ll.png' -f'./psconvert_64994d.eps'
psconvert: Done.
grdimage: Allocates memory and read data file los_ll.grd
grdimage: Evaluate image pixel colors
grdimage: Creating 24-bit color image
Make los_ll.kml and los_ll.png
psconvert: Processing los_ll.ps...
psconvert: Figure dimensions: Width: 56.82 points [0.789166 inch] Height: 46.98 points [0.6525 inch]
psconvert: gs -q -dSAFER -dNOPAUSE -dBATCH -dPDFSETTINGS=/prepress -dDownsampleColorImages=false -dDownsampleGrayImages=false -
dDownsampleMonoImages=false -dUseFlateCompression=true -dEmbedAllFonts=true -dSubsetFonts=true -dMonoImageFilter=/FlateEncode -
dAutoFilterGrayImages=false -dGrayImageFilter=/FlateEncode -dAutoFilterColorImages=false -dColorImageFilter=/FlateEncode -dSCANCONVERTERTYPE=2 -
dMaxBitmap=2147483647 -dUseFastColor=true -sDEVICE=pngalpha -g711x588 -r900 -sOutputFile='los_ll.png' -f'./psconvert_65011d.eps'
psconvert: Done.
GEOCODE.CSH - END

```

```

stack.list
cut_2007052_2007328.grd IMG-HH-ALPSRP057407010-H1.0_A.PRM IMG-HH-ALPSRP097667010-H1.0_A.PRM
cut_2007052_2008055.grd IMG-HH-ALPSRP057407010-H1.0_A.PRM IMG-HH-ALPSRP111087010-H1.0_A.PRM
cut_2007052_2008101.grd IMG-HH-ALPSRP057407010-H1.0_A.PRM IMG-HH-ALPSRP11797010-H1.0_A.PRM
cut_2007052_2008331.grd IMG-HH-ALPSRP057407010-H1.0_A.PRM IMG-HH-ALPSRP151347010-H1.0_A.PRM
cut_2007052_2009057.grd IMG-HH-ALPSRP057407010-H1.0_A.PRM IMG-HH-ALPSRP164767010-H1.0_A.PRM
cut_2007052_2009333.grd IMG-HH-ALPSRP057407010-H1.0_A.PRM IMG-HH-ALPSRP20507010-H1.0_A.PRM
cut_2007052_2010014.grd IMG-HH-ALPSRP057407010-H1.0_A.PRM IMG-HH-ALPSRP211737010-H1.0_A.PRM
cut_2007052_2010060.grd IMG-HH-ALPSRP057407010-H1.0_A.PRM IMG-HH-ALPSRP218447010-H1.0_A.PRM

```

```
bash stack_phase.bash stack.list mean.grd std.grd
```

```
compute the mean LOS velocity ..
```

```

time span (days) of cut_2007052_2007328.grd: 276
accumulative days in the stack: 276
time span (days) of cut_2007052_2008055.grd: 368
accumulative days in the stack: 644
time span (days) of cut_2007052_2008101.grd: 414
accumulative days in the stack: 1058
time span (days) of cut_2007052_2008331.grd: 644
accumulative days in the stack: 1702
time span (days) of cut_2007052_2009057.grd: 735
accumulative days in the stack: 2437
time span (days) of cut_2007052_2009333.grd: 1011
accumulative days in the stack: 3448
time span (days) of cut_2007052_2010014.grd: 1057
accumulative days in the stack: 4505

```

time span (days) of cut\_2007052\_2010060.grd: 1103  
accumulative days in the stack: 5608

compute the standard deviations ..

mean\_ll.grd  
std\_ll.grd  
los\_ll\_2007328.grd  
los\_ll\_2008055.grd  
los\_ll\_2008101.grd  
los\_ll\_2008331.grd  
los\_ll\_2009057.grd  
los\_ll\_2009333.grd  
los\_ll\_2010014.grd  
los\_ll\_2010060.grd

csh select\_pairs.csh baseline\_table.dat 950 1000

intf.tab

cut_2007052_2007328.grd	corcut_2007052_2007328.grd	2007052	2007328	-280.159414
cut_2007052_2008055.grd	corcut_2007052_2008055.grd	2007052	2008055	-566.082561
cut_2007052_2008101.grd	corcut_2007052_2008101.grd	2007052	2008101	-579.321254
cut_2007052_2008331.grd	corcut_2007052_2008331.grd	2007052	2008331	622.995138
cut_2007052_2009057.grd	corcut_2007052_2009057.grd	2007052	2009057	120.871632
cut_2007328_2008055.grd	corcut_2007328_2008055.grd	2007328	2008055	-285.922485
cut_2007328_2008101.grd	corcut_2007328_2008101.grd	2007328	2008101	-299.156890
cut_2007328_2008331.grd	corcut_2007328_2008331.grd	2007328	2008331	903.143820
cut_2007328_2009057.grd	corcut_2007328_2009057.grd	2007328	2009057	401.011845
cut_2007328_2009333.grd	corcut_2007328_2009333.grd	2007328	2009333	306.119329
cut_2007328_2010014.grd	corcut_2007328_2010014.grd	2007328	2010014	71.493396
cut_2007328_2010060.grd	corcut_2007328_2010060.grd	2007328	2010060	32.696168
cut_2008055_2008101.grd	corcut_2008055_2008101.grd	2008055	2008101	-13.220521
cut_2008055_2009057.grd	corcut_2008055_2009057.grd	2008055	2009057	686.849965
cut_2008055_2009333.grd	corcut_2008055_2009333.grd	2008055	2009333	591.960684
cut_2008055_2010014.grd	corcut_2008055_2010014.grd	2008055	2010014	357.355385
cut_2008055_2010060.grd	corcut_2008055_2010060.grd	2008055	2010060	318.569452
cut_2008101_2009057.grd	corcut_2008101_2009057.grd	2008101	2009057	700.111097
cut_2008101_2009333.grd	corcut_2008101_2009333.grd	2008101	2009333	605.230000
cut_2008101_2010014.grd	corcut_2008101_2010014.grd	2008101	2010014	370.604326
cut_2008101_2010060.grd	corcut_2008101_2010060.grd	2008101	2010060	331.811303
cut_2008331_2009057.grd	corcut_2008331_2009057.grd	2008331	2009057	-502.137049
cut_2008331_2009333.grd	corcut_2008331_2009333.grd	2008331	2009333	-597.062518
cut_2008331_2010014.grd	corcut_2008331_2010014.grd	2008331	2010014	-831.669751
cut_2008331_2010060.grd	corcut_2008331_2010060.grd	2008331	2010060	-870.469570
cut_2009057_2009333.grd	corcut_2009057_2009333.grd	2009057	2009333	-94.917429
cut_2009057_2010014.grd	corcut_2009057_2010014.grd	2009057	2010014	-329.525554
cut_2009057_2010060.grd	corcut_2009057_2010060.grd	2009057	2010060	-368.322928
cut_2009333_2010014.grd	corcut_2009333_2010014.grd	2009333	2010014	-234.593314
cut_2009333_2010060.grd	corcut_2009333_2010060.grd	2009333	2010060	-273.380590
cut_2010014_2010060.grd	corcut_2010014_2010060.grd	2010014	2010060	-38.784519

scene.tab

2007052 417  
2007328 693  
2008055 785  
2008101 831  
2008331 1061  
2009057 1152  
2009333 1428  
2010014 1474  
2010060 1520

sbas intf.tab scene.tab 31 9 2826 1728 -smooth 1.0 -wavelength 0.2362 -incidence 34.3 -range 849115 -rms -dem -atm 1

compute RMS misfit  
compute DEM error

setting smoothing to 1.000  
setting radar wavelength to 0.236 m  
setting radar incidence angle to 34.300 degree  
setting range to 849115.000 m  
Memory Allocation Successful...  
read table file ...  
number of SAR scenes is 9  
number of interferograms is 31  
read phase and correlation grids ...  
fill the G matrix ...

Applying atmospheric correction by common point stacking...

Hit Matrix:

2007052	0	1	1	1	1	1	0	0	0
2007328	0	0	1	1	1	1	1	1	1
2008055	0	0	0	1	0	1	1	1	1
2008101	0	0	0	0	0	1	1	1	1
2008331	0	0	0	0	0	1	1	1	1
2009057	0	0	0	0	0	0	1	1	1
2009333	0	0	0	0	0	0	0	1	1
2010014	0	0	0	0	0	0	0	0	1
2010060	0	0	0	0	0	0	0	0	0

Applying exponential relaxation on smoothing parameters

Setting smoothing parameter to 1000.000000...  
fill the G matrix ...  
Computing deformation time-series...  
run least-squares problem over 2826 by 1728 pixel (0) ...  
matrix is full rank: 9

Removing deformation time-series from original unwrapped phase...  
Computing atmospheric phase screen by common-point stacking...

Initial estimate of APS...  
atm\_noise(NO.5) = 5.307827  
atm\_noise(NO.2) = 2.339757  
atm\_noise(NO.7) = 1.881590  
atm\_noise(NO.4) = 1.636672  
atm\_noise(NO.0) = 0.000000  
atm\_noise(NO.1) = 0.000000  
atm\_noise(NO.3) = 0.000000  
atm\_noise(NO.6) = 0.000000  
atm\_noise(NO.8) = 0.000000

atm\_noise(NO.5) = 5.216019

```
atm_noise(N0.2) = 2.245731
atm_noise(N0.7) = 1.841071
atm_noise(N0.4) = 1.706226
atm_noise(N0.0) = 0.000000
atm_noise(N0.1) = 0.000000
atm_noise(N0.3) = 0.000000
atm_noise(N0.6) = 0.000000
atm_noise(N0.8) = 0.000000
```

```
Applying atmospheric phase screen to original unwrapped phase...
Setting smoothing parameter to 1.000000...
fill the G matrix ...
run least-squares problem over 2826 by 1728 pixel (3) ...
matrix is rank-deficient: 8
```

```
write output ...
```

```
raln.grd
ralt.grd
rms_ll.grd
dem.grd
vel_ll.grd
disp_2007052_ll.grd
disp_2007328_ll.grd
disp_2008055_ll.grd
disp_2008101_ll.grd
disp_2008331_ll.grd
disp_2009057_ll.grd
disp_2009333_ll.grd
disp_2010014_ll.grd
disp_2010060_ll.grd
aps_2007052.grd
aps_2007328.grd
aps_2008055.grd
aps_2008101.grd
aps_2008331.grd
aps_2009057.grd
aps_2009333.grd
aps_2010014.grd
aps_2010060.grd
```

## A.2 ALOS PALSAR (Path 422 Row 7020) in Bali, Indonesia

```
data.in
IMG-HH-ALPSRP057407020-H1.0__A
IMG-HH-ALPSRP097667020-H1.0__A
IMG-HH-ALPSRP111087020-H1.0__A
IMG-HH-ALPSRP117797020-H1.0__A
IMG-HH-ALPSRP151347020-H1.0__A
IMG-HH-ALPSRP164767020-H1.0__A
IMG-HH-ALPSRP205027020-H1.0__A
IMG-HH-ALPSRP211737020-H1.0__A
IMG-HH-ALPSRP218447020-H1.0__A

pre_proc_batch.csh ALOS data.in batch.config

START PREPROCESS A STACK OF IMAGES

preprocess master image
ledflag 1
... swapping bytes
writing generic LED file: IMG-HH-ALPSRP057407020-H1.0__A.LED
near_range, shift = 848515 -256
... calculating doppler for IMG-HH-ALPSRP057407020-H1.0__A.raw
Working on line 2000
Working on line 4000
Working on line 6000
Working on line 8000
Working on line 10000
Working on line 12000
Working on line 14000
Working on line 16000
Working on line 18000
Working on line 20000
Working on line 22000
Working on line 24000
Working on line 26000
Working on line 28000
Working on line 30000
Working on line 32000
Working on line 34000
pre_proc_batch.csh
preprocess slave images
setting fd1 to 7.990594
setting near_range to 849115.00
setting radius to 6377621.128533
setting npatches to 3
ledflag 1
... swapping bytes
writing generic LED file: IMG-HH-ALPSRP097667020-H1.0__A.LED
near_range, shift = 849714 256
near_range, shift = 848815 -128
The range sampling rate for master and slave images are: 32000000
pre_proc_batch.csh
preprocess slave images
setting fd1 to 7.990594
setting near_range to 849115.00
setting radius to 6377621.128533
setting npatches to 3
ledflag 1
... swapping bytes
writing generic LED file: IMG-HH-ALPSRP111087020-H1.0__A.LED
near_range, shift = 848815 -128
The range sampling rate for master and slave images are: 32000000
pre_proc_batch.csh
preprocess slave images
setting fd1 to 7.990594
setting near_range to 849115.00
setting radius to 6377621.128533
setting npatches to 3
ledflag 1
... swapping bytes
writing generic LED file: IMG-HH-ALPSRP117797020-H1.0__A.LED
near_range, shift = 848665 -192
```

```
The range sampling rate for master and slave images are: 32000000
pre_proc_batch.csh
preprocess slave images
  setting fd1 to 7.990594
  setting near_range to 849115.00
  setting radius to 6377621.128533
  setting npatches to 3
ledflag 1
.... swapping bytes
writing generic LED file: IMG-HH-ALPSRP151347020-H1.0_A.LED
  near_range, shift = 848965 -64
The range sampling rate for master and slave images are: 32000000
pre_proc_batch.csh
preprocess slave images
  setting fd1 to 7.990594
  setting near_range to 849115.00
  setting radius to 6377621.128533
  setting npatches to 3
ledflag 1
.... swapping bytes
writing generic LED file: IMG-HH-ALPSRP164767020-H1.0_A.LED
  near_range, shift = 848815 -128
The range sampling rate for master and slave images are: 32000000
pre_proc_batch.csh
preprocess slave images
  setting fd1 to 7.990594
  setting near_range to 849115.00
  setting radius to 6377621.128533
  setting npatches to 3
ledflag 1
.... swapping bytes
writing generic LED file: IMG-HH-ALPSRP205027020-H1.0_A.LED
  near_range, shift = 848515 -256
The range sampling rate for master and slave images are: 32000000
pre_proc_batch.csh
preprocess slave images
  setting fd1 to 7.990594
  setting near_range to 849115.00
  setting radius to 6377621.128533
  setting npatches to 3
ledflag 1
.... swapping bytes
writing generic LED file: IMG-HH-ALPSRP211737020-H1.0_A.LED
  near_range, shift = 849265 64
  near_range, shift = 848665 -192
The range sampling rate for master and slave images are: 32000000
pre_proc_batch.csh
preprocess slave images
  setting fd1 to 7.990594
  setting near_range to 849115.00
  setting radius to 6377621.128533
  setting npatches to 3
ledflag 1
.... swapping bytes
writing generic LED file: IMG-HH-ALPSRP218447020-H1.0_A.LED
  near_range, shift = 848965 -64
The range sampling rate for master and slave images are: 32000000
```

END PREPROCESS A STACK OF IMAGES

```
baseline_table.dat
05740 2007052.6323838762 417 0.000000 0.000000
09766 2007328.6319011450 693 -215.071089 -261.965355
11108 2008055.6312063069 785 -340.875861 -535.276776
11779 2008011.6306983787 831 -403.144053 -543.448521
15134 2008331.6316589806 1061 475.929613 597.259933
16476 2009057.6325576610 1152 63.631337 107.375214
20502 2009333.6335756124 1428 121.744740 29.963401
21173 2010014.6335320128 1474 -56.467333 -199.001696
21844 2010060.6333798254 1520 -123.650314 -230.944792
```

intf.in

```
IMG-HH-ALPSRP057407020-H1.0_A:IMG-HH-ALPSRP097667020-H1.0_A
IMG-HH-ALPSRP057407020-H1.0_A:IMG-HH-ALPSRP111087020-H1.0_A
IMG-HH-ALPSRP057407020-H1.0_A:IMG-HH-ALPSRP117797020-H1.0_A
IMG-HH-ALPSRP057407020-H1.0_A:IMG-HH-ALPSRP151347020-H1.0_A
IMG-HH-ALPSRP057407020-H1.0_A:IMG-HH-ALPSRP164767020-H1.0_A
IMG-HH-ALPSRP057407020-H1.0_A:IMG-HH-ALPSRP205027020-H1.0_A
IMG-HH-ALPSRP057407020-H1.0_A:IMG-HH-ALPSRP211737020-H1.0_A
IMG-HH-ALPSRP057407020-H1.0_A:IMG-HH-ALPSRP218447020-H1.0_A
IMG-HH-ALPSRP097667020-H1.0_A:IMG-HH-ALPSRP111087020-H1.0_A
IMG-HH-ALPSRP097667020-H1.0_A:IMG-HH-ALPSRP117797020-H1.0_A
IMG-HH-ALPSRP097667020-H1.0_A:IMG-HH-ALPSRP151347020-H1.0_A
IMG-HH-ALPSRP097667020-H1.0_A:IMG-HH-ALPSRP164767020-H1.0_A
IMG-HH-ALPSRP097667020-H1.0_A:IMG-HH-ALPSRP205027020-H1.0_A
IMG-HH-ALPSRP097667020-H1.0_A:IMG-HH-ALPSRP211737020-H1.0_A
IMG-HH-ALPSRP097667020-H1.0_A:IMG-HH-ALPSRP218447020-H1.0_A
IMG-HH-ALPSRP111087020-H1.0_A:IMG-HH-ALPSRP117797020-H1.0_A
IMG-HH-ALPSRP111087020-H1.0_A:IMG-HH-ALPSRP164767020-H1.0_A
IMG-HH-ALPSRP111087020-H1.0_A:IMG-HH-ALPSRP205027020-H1.0_A
IMG-HH-ALPSRP111087020-H1.0_A:IMG-HH-ALPSRP211737020-H1.0_A
IMG-HH-ALPSRP111087020-H1.0_A:IMG-HH-ALPSRP218447020-H1.0_A
IMG-HH-ALPSRP117797020-H1.0_A:IMG-HH-ALPSRP164767020-H1.0_A
IMG-HH-ALPSRP117797020-H1.0_A:IMG-HH-ALPSRP205027020-H1.0_A
IMG-HH-ALPSRP117797020-H1.0_A:IMG-HH-ALPSRP211737020-H1.0_A
IMG-HH-ALPSRP117797020-H1.0_A:IMG-HH-ALPSRP218447020-H1.0_A
IMG-HH-ALPSRP151347020-H1.0_A:IMG-HH-ALPSRP164767020-H1.0_A
IMG-HH-ALPSRP151347020-H1.0_A:IMG-HH-ALPSRP205027020-H1.0_A
IMG-HH-ALPSRP151347020-H1.0_A:IMG-HH-ALPSRP211737020-H1.0_A
IMG-HH-ALPSRP151347020-H1.0_A:IMG-HH-ALPSRP218447020-H1.0_A
IMG-HH-ALPSRP164767020-H1.0_A:IMG-HH-ALPSRP205027020-H1.0_A
IMG-HH-ALPSRP164767020-H1.0_A:IMG-HH-ALPSRP211737020-H1.0_A
IMG-HH-ALPSRP164767020-H1.0_A:IMG-HH-ALPSRP218447020-H1.0_A
IMG-HH-ALPSRP205027020-H1.0_A:IMG-HH-ALPSRP211737020-H1.0_A
IMG-HH-ALPSRP205027020-H1.0_A:IMG-HH-ALPSRP218447020-H1.0_A
IMG-HH-ALPSRP211737020-H1.0_A:IMG-HH-ALPSRP218447020-H1.0_A
```

align.in

```
IMG-HH-ALPSRP057407020-H1.0_A:IMG-HH-ALPSRP097667020-H1.0_A:IMG-HH-ALPSRP057407020-H1.0_A
IMG-HH-ALPSRP057407020-H1.0_A:IMG-HH-ALPSRP111087020-H1.0_A:IMG-HH-ALPSRP057407020-H1.0_A
IMG-HH-ALPSRP057407020-H1.0_A:IMG-HH-ALPSRP117797020-H1.0_A:IMG-HH-ALPSRP057407020-H1.0_A
IMG-HH-ALPSRP057407020-H1.0_A:IMG-HH-ALPSRP151347020-H1.0_A:IMG-HH-ALPSRP057407020-H1.0_A
IMG-HH-ALPSRP057407020-H1.0_A:IMG-HH-ALPSRP164767020-H1.0_A:IMG-HH-ALPSRP057407020-H1.0_A
IMG-HH-ALPSRP057407020-H1.0_A:IMG-HH-ALPSRP205027020-H1.0_A:IMG-HH-ALPSRP057407020-H1.0_A
IMG-HH-ALPSRP057407020-H1.0_A:IMG-HH-ALPSRP211737020-H1.0_A:IMG-HH-ALPSRP057407020-H1.0_A
IMG-HH-ALPSRP057407020-H1.0_A:IMG-HH-ALPSRP218447020-H1.0_A:IMG-HH-ALPSRP057407020-H1.0_A
IMG-HH-ALPSRP097667020-H1.0_A:IMG-HH-ALPSRP111087020-H1.0_A:IMG-HH-ALPSRP057407020-H1.0_A
IMG-HH-ALPSRP097667020-H1.0_A:IMG-HH-ALPSRP117797020-H1.0_A:IMG-HH-ALPSRP057407020-H1.0_A
IMG-HH-ALPSRP097667020-H1.0_A:IMG-HH-ALPSRP151347020-H1.0_A:IMG-HH-ALPSRP057407020-H1.0_A
```



IMG-HH-ALPSRP097667020-H1.0\_A:IMG-HH-ALPSRP164767020-H1.0\_A:IMG-HH-ALPSRP057407020-H1.0\_A  
IMG-HH-ALPSRP097667020-H1.0\_A:IMG-HH-ALPSRP205027020-H1.0\_A:IMG-HH-ALPSRP057407020-H1.0\_A  
IMG-HH-ALPSRP097667020-H1.0\_A:IMG-HH-ALPSRP211737020-H1.0\_A:IMG-HH-ALPSRP057407020-H1.0\_A  
IMG-HH-ALPSRP097667020-H1.0\_A:IMG-HH-ALPSRP218447020-H1.0\_A:IMG-HH-ALPSRP057407020-H1.0\_A  
IMG-HH-ALPSRP11087020-H1.0\_A:IMG-HH-ALPSRP117797020-H1.0\_A:IMG-HH-ALPSRP057407020-H1.0\_A  
IMG-HH-ALPSRP11087020-H1.0\_A:IMG-HH-ALPSRP164767020-H1.0\_A:IMG-HH-ALPSRP057407020-H1.0\_A  
IMG-HH-ALPSRP11087020-H1.0\_A:IMG-HH-ALPSRP205027020-H1.0\_A:IMG-HH-ALPSRP057407020-H1.0\_A  
IMG-HH-ALPSRP11087020-H1.0\_A:IMG-HH-ALPSRP211737020-H1.0\_A:IMG-HH-ALPSRP057407020-H1.0\_A  
IMG-HH-ALPSRP11087020-H1.0\_A:IMG-HH-ALPSRP218447020-H1.0\_A:IMG-HH-ALPSRP057407020-H1.0\_A  
IMG-HH-ALPSRP117797020-H1.0\_A:IMG-HH-ALPSRP164767020-H1.0\_A:IMG-HH-ALPSRP057407020-H1.0\_A  
IMG-HH-ALPSRP117797020-H1.0\_A:IMG-HH-ALPSRP205027020-H1.0\_A:IMG-HH-ALPSRP057407020-H1.0\_A  
IMG-HH-ALPSRP117797020-H1.0\_A:IMG-HH-ALPSRP211737020-H1.0\_A:IMG-HH-ALPSRP057407020-H1.0\_A  
IMG-HH-ALPSRP117797020-H1.0\_A:IMG-HH-ALPSRP218447020-H1.0\_A:IMG-HH-ALPSRP057407020-H1.0\_A  
IMG-HH-ALPSRP151347020-H1.0\_A:IMG-HH-ALPSRP164767020-H1.0\_A:IMG-HH-ALPSRP057407020-H1.0\_A  
IMG-HH-ALPSRP151347020-H1.0\_A:IMG-HH-ALPSRP205027020-H1.0\_A:IMG-HH-ALPSRP057407020-H1.0\_A  
IMG-HH-ALPSRP151347020-H1.0\_A:IMG-HH-ALPSRP211737020-H1.0\_A:IMG-HH-ALPSRP057407020-H1.0\_A  
IMG-HH-ALPSRP151347020-H1.0\_A:IMG-HH-ALPSRP218447020-H1.0\_A:IMG-HH-ALPSRP057407020-H1.0\_A  
IMG-HH-ALPSRP164767020-H1.0\_A:IMG-HH-ALPSRP205027020-H1.0\_A:IMG-HH-ALPSRP057407020-H1.0\_A  
IMG-HH-ALPSRP164767020-H1.0\_A:IMG-HH-ALPSRP211737020-H1.0\_A:IMG-HH-ALPSRP057407020-H1.0\_A  
IMG-HH-ALPSRP164767020-H1.0\_A:IMG-HH-ALPSRP218447020-H1.0\_A:IMG-HH-ALPSRP057407020-H1.0\_A  
IMG-HH-ALPSRP205027020-H1.0\_A:IMG-HH-ALPSRP211737020-H1.0\_A:IMG-HH-ALPSRP057407020-H1.0\_A  
IMG-HH-ALPSRP205027020-H1.0\_A:IMG-HH-ALPSRP218447020-H1.0\_A:IMG-HH-ALPSRP057407020-H1.0\_A  
IMG-HH-ALPSRP211737020-H1.0\_A:IMG-HH-ALPSRP218447020-H1.0\_A:IMG-HH-ALPSRP057407020-H1.0\_A

align\_batch.csh ALOS align.in

```
ALIGN.CSH - START
focussing master
Computing range reference function.
Processing patch 1
Processing Elapsed Time: 0 min 0.04 sec
Range Compression
Processing Elapsed Time: 0 min 5.69 sec
Azimuthal Transform
Processing Elapsed Time: 0 min 13.58 sec
Range Migration
Processing Elapsed Time: 0 min 23.50 sec
Azimuthal Compression
Processing Elapsed Time: 0 min 45.94 sec
Writing Data
Processing patch 2
Processing Elapsed Time: 0 min 47.45 sec
Range Compression
Processing Elapsed Time: 0 min 52.11 sec
Azimuthal Transform
Processing Elapsed Time: 0 min 59.99 sec
Range Migration
Processing Elapsed Time: 1 min 9.89 sec
Azimuthal Compression
Processing Elapsed Time: 1 min 33.02 sec
Writing Data
Processing patch 3
Processing Elapsed Time: 1 min 34.59 sec
Range Compression
Processing Elapsed Time: 1 min 39.19 sec
Azimuthal Transform
Processing Elapsed Time: 1 min 47.28 sec
Range Migration
Processing Elapsed Time: 1 min 57.19 sec
Azimuthal Compression
Processing Elapsed Time: 2 min 19.92 sec
Writing Data
Processing Elapsed Time: 2 min 21.44 sec
number of points clipped to short int 53
align.csh
focusing slave
Computing range reference function.
Processing patch 1
Processing Elapsed Time: 0 min 0.03 sec
Range Compression
Processing Elapsed Time: 0 min 5.57 sec
Azimuthal Transform
Processing Elapsed Time: 0 min 13.87 sec
Range Migration
Processing Elapsed Time: 0 min 23.93 sec
Azimuthal Compression
Processing Elapsed Time: 0 min 47.04 sec
Writing Data
Processing patch 2
Processing Elapsed Time: 0 min 48.58 sec
Range Compression
Processing Elapsed Time: 0 min 53.18 sec
Azimuthal Transform
Processing Elapsed Time: 1 min 1.26 sec
Range Migration
Processing Elapsed Time: 1 min 11.19 sec
Azimuthal Compression
Processing Elapsed Time: 1 min 35.27 sec
Writing Data
Processing patch 3
Processing Elapsed Time: 1 min 36.80 sec
Range Compression
Processing Elapsed Time: 1 min 41.44 sec
Azimuthal Transform
Processing Elapsed Time: 1 min 49.63 sec
Range Migration
Processing Elapsed Time: 1 min 59.54 sec
Azimuthal Compression
Processing Elapsed Time: 2 min 23.60 sec
Writing Data
Processing Elapsed Time: 2 min 25.14 sec
number of points clipped to short int 175
align.csh
correlate master and slave to find offset parameters
setting xsearch to 64
setting nx_corr to 128
setting ysearch to 64
setting ny_corr to 128
11304 27648 11304 27648 104 68 -0.002141
locations n 512 nx 11304 nyl 32 nxl 16 x_inc 574 y_inc 826
elapsed time: 19.338003
align.csh
refocus slave
Computing range reference function.
Processing patch 1
Processing Elapsed Time: 0 min 0.03 sec
Range Compression
Processing Elapsed Time: 0 min 5.83 sec
Azimuthal Transform
```

Processing Elapsed Time: 0 min 20.32 sec  
Range Migration  
Processing Elapsed Time: 0 min 30.42 sec  
Azimuthal Compression  
Processing Elapsed Time: 1 min 3.81 sec  
apply azimuth-dependent azimuth shift  
Processing Elapsed Time: 1 min 28.67 sec  
Writing Data  
Processing patch 2  
Processing Elapsed Time: 1 min 35.16 sec  
Range Compression  
Processing Elapsed Time: 1 min 39.93 sec  
Azimuthal Transform  
Processing Elapsed Time: 1 min 49.27 sec  
Range Migration  
Processing Elapsed Time: 1 min 59.38 sec  
Azimuthal Compression  
Processing Elapsed Time: 2 min 29.37 sec  
apply azimuth-dependent azimuth shift  
Processing Elapsed Time: 2 min 56.98 sec  
Writing Data  
Processing patch 3  
Processing Elapsed Time: 3 min 3.89 sec  
Range Compression  
Processing Elapsed Time: 3 min 8.54 sec  
Azimuthal Transform  
Processing Elapsed Time: 3 min 18.00 sec  
Range Migration  
Processing Elapsed Time: 3 min 28.25 sec  
Azimuthal Compression  
Processing Elapsed Time: 4 min 2.25 sec  
apply azimuth-dependent azimuth shift  
Processing Elapsed Time: 4 min 28.31 sec  
Writing Data  
Processing Elapsed Time: 4 min 35.06 sec  
number of points clipped to short int 187  
rm: No match.  
ALIGN.CSH - END

intf\_batch.csh ALOS batch.config  
clean up topo/ folder

DEM2TOPO\_RA.CSH - START  
USER SHOULD PROVIDE DEM FILE  
range decimation is: 2  
blockmedian: Provides 3, expects 3-column binary data  
blockmedian: Processing input table data  
blockmedian: W: 0 E: 11304 S: 0 N: 27648 n\_columns: 5652 n\_rows: 6912  
blockmedian: Input 3 columns via binary records using format ddd  
blockmedian: Output 3 columns via binary records using format ddd  
blockmedian: N read: 880412 N used: 877562 outside\_area: 2850 N cells filled: 877534  
surface: Provides 3, expects 3-column binary data  
surface: Grid domain: W: 0 E: 11304 S: 0 N: 27648 n\_columns: 5652 n\_rows: 6912 [pixel registration]  
surface: Processing input table data  
surface: Input 3 columns via binary records using format ddd  
surface: Minimum value of your dataset x,y,z at: surface: 9.47925853729 20.1111221313 79.1265945435  
surface: Maximum value of your dataset x,y,z at: surface: 4982.25195312 19988.2792969 3152.45239258  
surface: LS plane determined: z = 203.081 + (-0.085365 \* col) + (0.111885 \* row)  
surface: Grid Mode IterationMax Change Conv Limit Total Iterations  
surface: 36 D 22 0.000546255543946 0.00086758828296 22  
surface: 12 I 28 0.00218929156934 0.0026027648489 50  
surface: 12 D 20 0.00178716015478 0.0026027648489 70  
surface: 4 I 25 0.00575992186722 0.0078082945467 95  
surface: 4 D 42 0.00697227533129 0.0078082945467 137  
surface: 2 I 18 0.0144953689828 0.0156165890934 155  
surface: 2 D 92 0.0155055815236 0.0156165890934 247  
surface: 1 I 16 0.0282327391979 0.0312331781868 263  
surface: 1 D 245 0.0309639238689 0.0312331781868 508  
surface: Fit info: N data points N nodes mean error rms errorcurvature  
surface: 877534 39079189 -3.16770048757e-06 0.0062199362068 22227.5479258  
grd2cpt: Processing input grid(s)  
grd2cpt: Mean and S.D. of data are 349.387377152 406.116523212  
grdimage: Allocates memory and read data file topo\_ra.grd  
grdimage: Evaluate image pixel colors  
grdimage: Creating 8-bit grayscale image  
DEM2TOPO\_RA.CSH - END  
NO TOPO\_RA SHIFT

START FORM A STACK OF INTERFEROGRAMS

INTF.CSH, FILTER.CSH - START  
intf.csh  
running phasediff...  
reading topo topo\_ra.grd  
xdim 11304, ydim 27648  
filter.csh  
gauss\_300 4 2 (4 2)  
making amplitudes...  
filtering interferogram...  
making amplitude...  
making correlation...  
making phase...  
filtering phase...  
INTF.CSH, FILTER.CSH - END

MAKE LANDMASK -- START  
REQUIRE FULL RESOLUTION COASTLINE FROM GMT

grdlandmask: GSHHG version 2.3.7  
Derived from World Vector Shoreline, CIA WDB-II, and Atlas of the Cryosphere  
Processed by Paul Wessel and Walter H. F. Smith, 1994-2017  
grdlandmask: Nodes in water will be set to NaN  
grdlandmask: Nodes on land will be set to 1  
grdlandmask: Level 0 contained 8112640 nodes  
grdlandmask: Level 1 contained 2478081 nodes  
grdlandmask: Done!  
surface: Provides 3, expects 3-column binary data  
surface: Grid domain: W: 113.83333329 E: 117.416666662 S: -9.166666663 N: -7.4166666637 n\_columns: 4300 n\_rows: 2100 [gridline registration]  
surface: Processing input table data  
surface: Input 3 columns via binary records using format fff  
surface: Minimum value of your dataset x,y,z at: surface: 115.220001221 -8.85499954224 -9.99483108521  
surface: Maximum value of your dataset x,y,z at: surface: 115.945831299 -8.56833267212 11313.9638672  
surface: LS plane determined: z = -21214.5 + (12.0682 \* col) + (2.5925 \* row)  
surface: Grid Mode IterationMax Change Conv Limit Total Iterations  
surface: 100 D 6384 7.54209935596e-05 7.63795351882e-0 6384  
surface: 20 I 88 0.00034390910789 0.00038189767594 6472  
surface: 20 D 10000 0.00127684555265 0.00038189767594 16472

```

surface: 4 I 63 0.00180797931012 0.00190948837971 16535
surface: 4 D 1552 0.00190942585768 0.00190948837971 18087
surface: 2 I 17 0.00351663660741 0.00381897675941 18104
surface: 2 D 392 0.00381115027586 0.00381897675941 18496
surface: 1 I 15 0.00550228015928 0.00763795351882 18511
surface: 1 D 133 0.00763743786382 0.00763795351882 18644
surface: Fit info: N data points N nodes mean error rms error curvature
surface: 880412 9036401 0 0 6703.59290537
surface: Provides 3, expects 3-column binary data
surface: Grid domain: W: 113.83333329 E: 117.416666662 S: -9.166666663 N: -7.4166666637 n_columns: 4300 n_rows: 2100 [gridline registration]
surface: Processing input table data
surface: Input 3 columns via binary records using format fff
surface: Minimum value of your dataset x,y,z at: surface: 115.785835266 -8.86583328247 -19.9908485413
surface: Maximum value of your dataset x,y,z at: surface: 115.442497253 -8.12583255768 27667.9804688
surface: LS plane determined: z = 4765.3 + (-6.38092 * col) + (28.2121 * row)
surface: Grid Mode IterationMax Change Conv Limit Total Iterations
surface: 100 D 7005 2.69743062392e-06 2.73171285111e-0 7005
surface: 20 I 103 1.34681571328e-05 1.36585642556e-0 7108
surface: 20 D 10000 0.000305607492168 1.36585642556e-0 17108
surface: 4 I 77 6.17369685184e-05 6.82928212778e-0 17185
surface: 4 D 2000 0.000463692123562 6.82928212778e-0 19185
surface: 2 I 18 0.000106690979598 0.00013658564255 19203
surface: 2 D 973 0.000136448198424 0.00013658564255 20176
surface: 1 I 16 0.000247783697653 0.00027317128511 20192
surface: 1 D 500 0.000301086446475 0.00027317128511 20692
surface: Fit info: N data points N nodes mean error rms error curvature
surface: 880412 9036401 0 0 548605.402922
MAKE LANDMASK -- END

```

```

SNAPHU.CSH - START
threshold_snaphu: .45
grdmath: Perform reverse Polish notation calculations on grids
grdmath: phase_patch.grd landmask_ra_patch.grd MUL = phase_patch.grd
unwrapping phase with snaphu - higher threshold for faster unwrapping

```

```

snaphu v1.4.2
32 parameters input from file snaphu.conf.brief (297 lines total)
Reading wrapped phase from file phase.in
No weight file specified. Assuming uniform weights
Reading correlation data from file corr.in
Calculating deformation-mode cost parameters
Building range cost arrays
Building azimuth cost arrays
Initializing flows with MST algorithm
Running approximate minimum spanning tree solver
Running nonlinear network flow optimizer
Maximum flow on network: 5
Number of nodes in network: 4878776
Flow increment: 1 (Total improvements: 0)
Treesize: 4878776 Pivots: 54505 Improvements: 983
Maximum flow on network: 5
Flow increment: 2 (Total improvements: 983)
Treesize: 4878776 Pivots: 353 Improvements: 26
Maximum flow on network: 5
Flow increment: 3 (Total improvements: 1009)
Treesize: 4878776 Pivots: 30 Improvements: 7
Maximum flow on network: 5
Flow increment: 4 (Total improvements: 1016)
Treesize: 4878776 Pivots: 19 Improvements: 3
Maximum flow on network: 3
Total solution cost: 1886110
Integrating phase
Writing output to file unwrap.out
Program snaphu done
Elapsed processor time: 0:02:01.68
Elapsed wall clock time: 0:02:02
grdmath: Perform reverse Polish notation calculations on grids
grdmath: unwrap.grd landmask_ra_patch.grd MUL = tmp.grd
SNAPHU.CSH - END

```

```

GEOCODE.CSH - START
threshold_geocode: .45
grdmath: Perform reverse Polish notation calculations on grids
grdmath: corr.grd 0.45 GE 0 NAN mask.grd MUL = mask2.grd
psscale: Warning: The -E option is deprecated but is accepted.
psscale: For the current -D syntax you should use -D modifier +e instead.
psscale: Note you cannot mix new-style modifiers (+e) with the old-style -D option.
psscale: Warning: The -E option is deprecated but is accepted.
psscale: For the current -D syntax you should use -D modifier +e instead.
psscale: Note you cannot mix new-style modifiers (+e) with the old-style -D option.
geocode.csh
project correlation, phase, unwrapped and amplitude back to lon lat coordinates
remarked is by root on Wed May 23 19:26:21 JST 2018 with geocode.csh
proj_ra2ll.csh
surface: Provides 3, expects 3-column binary data
surface: Grid domain: W: 48 E: 11248 S: 0 N: 27648 n_columns: 700 n_rows: 864 [gridline registration]
surface: Processing input table data
surface: Input 3 columns via binary records using format fff
surface: Minimum value of your dataset x,y,z at: surface: 47.1167106628 27644.0820312 115.090835571
surface: Maximum value of your dataset x,y,z at: surface: 11254.5410156 59.4462890625 116.002502441
surface: 268953 unusable points were supplied; these will be ignored.
surface: You should have pre-processed the data with block-mean, -median, or -mode.
surface: Check that previous processing steps write results with enough decimals.
surface: LS plane determined: z = 115.263 + (0.00105249 * col) + (-0.000193897 * row)
surface: Grid Mode IterationMax Change Conv Limit Total Iterations
surface: 4 D 18 9.29664558309e-08 1.23550245428e-0 18
surface: 2 I 18 1.7133228938e-07 2.47100490855e-0 36
surface: 2 D 16 2.32558109563e-07 2.47100490855e-0 52
surface: 1 I 17 2.86991464972e-07 4.94200981711e-0 69
surface: 1 D 19 4.13126227982e-07 4.94200981711e-0 88
surface: Fit info: N data points N nodes mean error rms error curvature
surface: 602775 606365 -2.83816215768e-06 0.00615192647878 7119.33530528
surface: Provides 3, expects 3-column binary data
surface: Grid domain: W: 48 E: 11248 S: 0 N: 27648 n_columns: 700 n_rows: 864 [gridline registration]
surface: Processing input table data
surface: Input 3 columns via binary records using format fff
surface: Minimum value of your dataset x,y,z at: surface: 43.218296051 2.00512806892 -8.98583316803
surface: Maximum value of your dataset x,y,z at: surface: 11191.7929688 27663.4941406 -8.04083347321
surface: 268953 unusable points were supplied; these will be ignored.
surface: You should have pre-processed the data with block-mean, -median, or -mode.
surface: Check that previous processing steps write results with enough decimals.
surface: LS plane determined: z = -8.9837 + (0.000238355 * col) + (0.000901305 * row)
surface: Grid Mode IterationMax Change Conv Limit Total Iterations
surface: 4 D 18 2.07556780564e-08 2.76283641929e-0 18
surface: 2 I 18 3.84978466417e-08 5.52567283858e-0 36
surface: 2 D 17 3.25372203106e-08 5.52567283858e-0 53
surface: 1 I 17 6.58793872319e-08 1.10513456772e-0 70
surface: 1 D 19 9.6406783006e-08 1.10513456772e-0 89
surface: Fit info: N data points N nodes mean error rms error curvature

```

```
surface: 602775 606365 -1.36029670003e-06 0.0089474772787 8448.30765751
blockmedian: Provides 3, expects 3-column binary data
blockmedian: Processing input table data
blockmedian: W: 115.088888889 E: 116.011111111 N: -8.98611111111 N: -8.04166666667 n_columns: 830 n_rows: 1360
blockmedian: Input 3 columns via binary records using format fff
blockmedian: Output 3 columns via binary records using format fff
blockmedian: N read: 4776703 N used: 4776703 outside_area: 0 N cells filled: 773895
proj_ra2ll.csh
blockmedian: Provides 3, expects 3-column binary data
blockmedian: Processing input table data
blockmedian: W: 115.088888889 E: 116.011111111 N: -8.98611111111 N: -8.04166666667 n_columns: 830 n_rows: 1360
blockmedian: Input 3 columns via binary records using format fff
blockmedian: Output 3 columns via binary records using format fff
blockmedian: N read: 4781665 N used: 4781665 outside_area: 0 N cells filled: 774703
proj_ra2ll.csh
blockmedian: Provides 3, expects 3-column binary data
blockmedian: Processing input table data
blockmedian: W: 115.133333333 E: 115.922222222 S: -8.80555555556 N: -8.15277777778 n_columns: 710 n_rows: 940
blockmedian: Input 3 columns via binary records using format fff
blockmedian: Output 3 columns via binary records using format fff
blockmedian: N read: 9253 N used: 9253 outside_area: 0 N cells filled: 2817
proj_ra2ll.csh
blockmedian: Provides 3, expects 3-column binary data
blockmedian: Processing input table data
blockmedian: W: 115.088888889 E: 116.011111111 S: -8.98611111111 N: -8.03472222222 n_columns: 830 n_rows: 1370
blockmedian: Input 3 columns via binary records using format fff
blockmedian: Output 3 columns via binary records using format fff
blockmedian: N read: 4838400 N used: 4838400 outside_area: 0 N cells filled: 783792
proj_ra2ll.csh
blockmedian: Provides 3, expects 3-column binary data
blockmedian: Processing input table data
blockmedian: W: 115.133333333 E: 115.922222222 S: -8.80555555556 N: -8.15277777778 n_columns: 710 n_rows: 940
blockmedian: Input 3 columns via binary records using format fff
blockmedian: Output 3 columns via binary records using format fff
blockmedian: N read: 9228 N used: 9228 outside_area: 0 N cells filled: 2810
proj_ra2ll.csh
blockmedian: Provides 3, expects 3-column binary data
blockmedian: Processing input table data
blockmedian: W: 115.088888889 E: 116.011111111 S: -8.84722222222 N: -8.13194444444 n_columns: 830 n_rows: 1030
blockmedian: Input 3 columns via binary records using format fff
blockmedian: Output 3 columns via binary records using format fff
blockmedian: N read: 1936109 N used: 1936109 outside_area: 0 N cells filled: 317695
proj_ra2ll.csh
blockmedian: Provides 3, expects 3-column binary data
blockmedian: Processing input table data
blockmedian: W: 115.133333333 E: 115.922222222 S: -8.80555555556 N: -8.15277777778 n_columns: 710 n_rows: 940
blockmedian: Input 3 columns via binary records using format fff
blockmedian: Output 3 columns via binary records using format fff
blockmedian: N read: 9253 N used: 9253 outside_area: 0 N cells filled: 2817
geocode.csh
make the KML files for Google Earth
grdimage: Allocates memory and read data file display_amp_ll.grd
grdimage: Evaluate image pixel colors
grdimage: Creating 24-bit color image
Make display_amp_ll.kml and display_amp_ll.png
psconvert: Processing display_amp_ll.ps...
psconvert: Figure dimensions: Width: 66.42 points [0.9225 inch] Height: 68.52 points [0.951666 inch]
psconvert: gs -q -dSAFER -dNOPAUSE -dBATCH -dPDFSETTINGS=/prepress -dDownsampleColorImages=false -dDownsampleGrayImages=false -
dDownsampleMonoImages=false -dUseFlateCompression=true -dEmbedAllFonts=true -dSubsetFonts=true -dMonoImageFilter=/FlateEncode -
dAutoFilterGrayImages=false -dGrayImageFilter=/FlateEncode -dAutoFilterColorImages=false -dColorImageFilter=/FlateEncode -dSCANCONVERTERTYPE=2 -
dMaxBitmap=2147483647 -dUseFastColor=true -sDEVICE=pngalpha -g831x857 -r900 -sOutputFile='display_amp_ll.png' -f'./psconvert_64919d.eps'
psconvert: Done.
grdimage: Allocates memory and read data file corr_ll.grd
grdimage: Evaluate image pixel colors
grdimage: Creating 24-bit color image
PSL: Colormap of 224 colors created
Make corr_ll.kml and corr_ll.png
psconvert: Processing corr_ll.ps...
psconvert: Figure dimensions: Width: 66.42 points [0.9225 inch] Height: 67.986 points [0.94425 inch]
psconvert: gs -q -dSAFER -dNOPAUSE -dBATCH -dPDFSETTINGS=/prepress -dDownsampleColorImages=false -dDownsampleGrayImages=false -
dDownsampleMonoImages=false -dUseFlateCompression=true -dEmbedAllFonts=true -dSubsetFonts=true -dMonoImageFilter=/FlateEncode -
dAutoFilterGrayImages=false -dGrayImageFilter=/FlateEncode -dAutoFilterColorImages=false -dColorImageFilter=/FlateEncode -dSCANCONVERTERTYPE=2 -
dMaxBitmap=2147483647 -dUseFastColor=true -sDEVICE=pngalpha -g831x850 -r900 -sOutputFile='corr_ll.png' -f'./psconvert_64933d.eps'
psconvert: Done.
grdimage: Allocates memory and read data file phase_mask_ll.grd
grdimage: Evaluate image pixel colors
grdimage: Creating 24-bit color image
Make phase_mask_ll.kml and phase_mask_ll.png
psconvert: Processing phase_mask_ll.ps...
psconvert: Figure dimensions: Width: 56.82 points [0.789166 inch] Height: 46.98 points [0.6525 inch]
psconvert: gs -q -dSAFER -dNOPAUSE -dBATCH -dPDFSETTINGS=/prepress -dDownsampleColorImages=false -dDownsampleGrayImages=false -
dDownsampleMonoImages=false -dUseFlateCompression=true -dEmbedAllFonts=true -dSubsetFonts=true -dMonoImageFilter=/FlateEncode -
dAutoFilterGrayImages=false -dGrayImageFilter=/FlateEncode -dAutoFilterColorImages=false -dColorImageFilter=/FlateEncode -dSCANCONVERTERTYPE=2 -
dMaxBitmap=2147483647 -dUseFastColor=true -sDEVICE=pngalpha -g711x588 -r900 -sOutputFile='phase_mask_ll.png' -f'./psconvert_64947d.eps'
psconvert: Done.
grdimage: Allocates memory and read data file phasefilt_mask_ll.grd
grdimage: Evaluate image pixel colors
grdimage: Creating 24-bit color image
Make phasefilt_mask_ll.kml and phasefilt_mask_ll.png
psconvert: Processing phasefilt_mask_ll.ps...
psconvert: Figure dimensions: Width: 56.82 points [0.789166 inch] Height: 46.98 points [0.6525 inch]
psconvert: gs -q -dSAFER -dNOPAUSE -dBATCH -dPDFSETTINGS=/prepress -dDownsampleColorImages=false -dDownsampleGrayImages=false -
dDownsampleMonoImages=false -dUseFlateCompression=true -dEmbedAllFonts=true -dSubsetFonts=true -dMonoImageFilter=/FlateEncode -
dAutoFilterGrayImages=false -dGrayImageFilter=/FlateEncode -dAutoFilterColorImages=false -dColorImageFilter=/FlateEncode -dSCANCONVERTERTYPE=2 -
dMaxBitmap=2147483647 -dUseFastColor=true -sDEVICE=pngalpha -g711x588 -r900 -sOutputFile='phasefilt_mask_ll.png' -f'./psconvert_64965d.eps'
psconvert: Done.
grdimage: Allocates memory and read data file unwrap_mask_ll.grd
grdimage: Evaluate image pixel colors
grdimage: Creating 24-bit color image
Make unwrap_mask_ll.kml and unwrap_mask_ll.png
psconvert: Processing unwrap_mask_ll.ps...
psconvert: Figure dimensions: Width: 56.82 points [0.789166 inch] Height: 46.98 points [0.6525 inch]
psconvert: gs -q -dSAFER -dNOPAUSE -dBATCH -dPDFSETTINGS=/prepress -dDownsampleColorImages=false -dDownsampleGrayImages=false -
dDownsampleMonoImages=false -dUseFlateCompression=true -dEmbedAllFonts=true -dSubsetFonts=true -dMonoImageFilter=/FlateEncode -
dAutoFilterGrayImages=false -dGrayImageFilter=/FlateEncode -dAutoFilterColorImages=false -dColorImageFilter=/FlateEncode -dSCANCONVERTERTYPE=2 -
dMaxBitmap=2147483647 -dUseFastColor=true -sDEVICE=pngalpha -g711x588 -r900 -sOutputFile='unwrap_mask_ll.png' -f'./psconvert_64980d.eps'
psconvert: Done.
grdimage: Allocates memory and read data file phasefilt_mask_ll.grd
grdimage: Evaluate image pixel colors
grdimage: Creating 24-bit color image
Make phasefilt_mask_ll.kml and phasefilt_mask_ll.png
psconvert: Processing phasefilt_mask_ll.ps...
psconvert: Figure dimensions: Width: 56.82 points [0.789166 inch] Height: 46.98 points [0.6525 inch]
psconvert: gs -q -dSAFER -dNOPAUSE -dBATCH -dPDFSETTINGS=/prepress -dDownsampleColorImages=false -dDownsampleGrayImages=false -
dDownsampleMonoImages=false -dUseFlateCompression=true -dEmbedAllFonts=true -dSubsetFonts=true -dMonoImageFilter=/FlateEncode -
dAutoFilterGrayImages=false -dGrayImageFilter=/FlateEncode -dAutoFilterColorImages=false -dColorImageFilter=/FlateEncode -dSCANCONVERTERTYPE=2 -
dMaxBitmap=2147483647 -dUseFastColor=true -sDEVICE=pngalpha -g711x588 -r900 -sOutputFile='phasefilt_mask_ll.png' -f'./psconvert_64994d.eps'
psconvert: Done.
grdimage: Allocates memory and read data file los_ll.grd
```

```
grdimage: Evaluate image pixel colors
grdimage: Creating 24-bit color image
Make los_ll.kml and los_ll.png
psconvert: Processing los_ll.ps...
psconvert: Figure dimensions: Width: 56.82 points [0.789166 inch] Height: 46.98 points [0.6525 inch]
psconvert: gs -q -dSAFER -dNOPAUSE -dBATCH -dPDFSETTINGS=/prepress -dDownsampleColorImages=false -dDownsampleMonoImages=false -dUseFlateCompression=true -dEmbedAllFonts=true -dSubsetFonts=true -dMonoImageFilter=/FlateEncode -dAutoFilterGrayImages=false -dGrayImageFilter=/FlateEncode -dAutoFilterColorImages=false -dColorImageFilter=/FlateEncode -dSCANCONVERTERTYPE=2 -dMaxBitmap=2147483647 -dUseFastColor=true -sDEVICE=pngalpha -g711x588 -r900 -sOutputFile='los_ll.png' -f'./psconvert_65011d.eps'
psconvert: Done.
GEOCODE.CSH - END
```

```
stack.list
cut_2007052_2007328.grd IMG-HH-ALPSRP057407020-H1.0_A.PRM IMG-HH-ALPSRP097667020-H1.0_A.PRM
cut_2007052_2008055.grd IMG-HH-ALPSRP057407020-H1.0_A.PRM IMG-HH-ALPSRP111067020-H1.0_A.PRM
cut_2007052_2008101.grd IMG-HH-ALPSRP057407020-H1.0_A.PRM IMG-HH-ALPSRP11797020-H1.0_A.PRM
cut_2007052_2008331.grd IMG-HH-ALPSRP057407020-H1.0_A.PRM IMG-HH-ALPSRP151347020-H1.0_A.PRM
cut_2007052_2009057.grd IMG-HH-ALPSRP057407020-H1.0_A.PRM IMG-HH-ALPSRP164767020-H1.0_A.PRM
cut_2007052_2009333.grd IMG-HH-ALPSRP057407020-H1.0_A.PRM IMG-HH-ALPSRP205027020-H1.0_A.PRM
cut_2007052_2010014.grd IMG-HH-ALPSRP057407020-H1.0_A.PRM IMG-HH-ALPSRP211737020-H1.0_A.PRM
cut_2007052_2010060.grd IMG-HH-ALPSRP057407020-H1.0_A.PRM IMG-HH-ALPSRP218447020-H1.0_A.PRM
```

```
bash stack_phase.bash stack.list mean.grd std.grd
```

```
compute the mean LOS velocity ..
```

```
time span (days) of cut_2007052_2007328.grd: 276
accumulative days in the stack: 276
time span (days) of cut_2007052_2008055.grd: 368
accumulative days in the stack: 644
time span (days) of cut_2007052_2008101.grd: 414
accumulative days in the stack: 1058
time span (days) of cut_2007052_2008331.grd: 644
accumulative days in the stack: 1702
time span (days) of cut_2007052_2009057.grd: 735
accumulative days in the stack: 2437
time span (days) of cut_2007052_2009333.grd: 1011
accumulative days in the stack: 3448
time span (days) of cut_2007052_2010014.grd: 1057
accumulative days in the stack: 4505
time span (days) of cut_2007052_2010060.grd: 1103
accumulative days in the stack: 5608
```

```
compute the standard deviations ..
```

```
mean_ll.grd
std_ll.grd
los_ll_2007328.grd
los_ll_2008055.grd
los_ll_2008101.grd
los_ll_2008331.grd
los_ll_2009057.grd
los_ll_2009333.grd
los_ll_2010014.grd
los_ll_2010060.grd
```

```
csf select_pairs.csf baseline_table.dat 950 1000
```

```
intf.tab
cut_2007052_2007328.grd corcut_2007052_2007328.grd 2007052 2007328 -261.965355
cut_2007052_2008055.grd corcut_2007052_2008055.grd 2007052 2008055 -535.276776
cut_2007052_2008101.grd corcut_2007052_2008101.grd 2007052 2008101 -543.448521
cut_2007052_2008331.grd corcut_2007052_2008331.grd 2007052 2008331 597.259933
cut_2007052_2009057.grd corcut_2007052_2009057.grd 2007052 2009057 107.375214
cut_2007328_2008055.grd corcut_2007328_2008055.grd 2007328 2008055 -273.311886
cut_2007328_2008101.grd corcut_2007328_2008101.grd 2007328 2008101 -281.479534
cut_2007328_2008331.grd corcut_2007328_2008331.grd 2007328 2008331 859.218355
cut_2007328_2009057.grd corcut_2007328_2009057.grd 2007328 2009057 369.325324
cut_2007328_2009333.grd corcut_2007328_2009333.grd 2007328 2009333 291.927829
cut_2007328_2010014.grd corcut_2007328_2010014.grd 2007328 2010014 62.949568
cut_2007328_2010060.grd corcut_2007328_2010060.grd 2007328 2010060 31.003199
cut_2008055_2008101.grd corcut_2008055_2008101.grd 2008055 2008101 -8.154786
cut_2008055_2009057.grd corcut_2008055_2009057.grd 2008055 2009057 642.561654
cut_2008055_2009333.grd corcut_2008055_2009333.grd 2008055 2009333 565.164722
cut_2008055_2010014.grd corcut_2008055_2010014.grd 2008055 2010014 336.260653
cut_2008055_2010060.grd corcut_2008055_2010060.grd 2008055 2010060 304.268270
cut_2008101_2009057.grd corcut_2008101_2009057.grd 2008101 2009057 650.753302
cut_2008101_2009333.grd corcut_2008101_2009333.grd 2008101 2009333 573.365615
cut_2008101_2010014.grd corcut_2008101_2010014.grd 2008101 2010014 344.387181
cut_2008101_2010060.grd corcut_2008101_2010060.grd 2008101 2010060 312.442422
cut_2008331_2009057.grd corcut_2008331_2009057.grd 2008331 2009057 -489.896673
cut_2008331_2009333.grd corcut_2008331_2009333.grd 2008331 2009333 -567.327123
cut_2008331_2010014.grd corcut_2008331_2010014.grd 2008331 2010014 -796.284619
cut_2008331_2010060.grd corcut_2008331_2010060.grd 2008331 2010060 -828.227313
cut_2009057_2009333.grd corcut_2009057_2009333.grd 2009057 2009333 -77.421374
cut_2009057_2010014.grd corcut_2009057_2010014.grd 2009057 2010014 -306.380321
cut_2009057_2010060.grd corcut_2009057_2010060.grd 2009057 2010060 -338.322448
cut_2009333_2010014.grd corcut_2009333_2010014.grd 2009333 2010014 -228.945299
cut_2009333_2010060.grd corcut_2009333_2010060.grd 2009333 2010060 -260.880573
cut_2010014_2010060.grd corcut_2010014_2010060.grd 2010014 2010060 -31.933626
```

```
scene.tab
2007052 417
2007328 693
2008055 785
2008101 831
2008331 1061
2009057 1152
2009333 1428
2010014 1474
2010060 1520
```

```
sbas intf.tab scene.tab 31 9 2826 1728 -smooth 1.0 -wavelength 0.2362 -incidence 34.3 -range 849115 -rms -dem -atm 1
```

```
compute RMS misfit
compute DEM error
```

```
setting smoothing to 1.000
setting radar wavelength to 0.236 m
setting radar incidence angle to 34.300 degree
setting range to 849115.000 m
Memory Allocation Successful...
read table file ...
number of SAR scenes is 9
number of interferograms is 31
read phase and correlation grids ...
fill the G matrix ...
```

Applying atmospheric correction by common point stacking...

```
Hit Matrix:
2007052 0 1 1 1 1 1 0 0 0
2007328 0 0 1 1 1 1 1 1 1
2008055 0 0 0 1 0 1 1 1 1
2008101 0 0 0 0 0 1 1 1 1
2008331 0 0 0 0 0 1 1 1 1
2009057 0 0 0 0 0 0 1 1 1
2009333 0 0 0 0 0 0 0 1 1
2010014 0 0 0 0 0 0 0 0 1
2010060 0 0 0 0 0 0 0 0 0
```

Applying exponential relaxation on smoothing parameters

```
Setting smoothing parameter to 1000.000000...
fill the G matrix ...
Computing deformation time-series...
run least-squares problem over 2826 by 1728 pixel (0) ...
matrix is full rank: 9
```

Removing deformation time-series from original unwrapped phase...
Computing atmospheric phase screen by common-point stacking...

```
Initial estimate of APS...
atm_noise(NO.5) = 5.691496
atm_noise(NO.2) = 2.581232
atm_noise(NO.7) = 1.638382
atm_noise(NO.4) = 1.586102
atm_noise(NO.0) = 0.000000
atm_noise(NO.1) = 0.000000
atm_noise(NO.3) = 0.000000
atm_noise(NO.6) = 0.000000
atm_noise(NO.8) = 0.000000
```

```
atm_noise(NO.5) = 5.604452
atm_noise(NO.7) = 1.625857
atm_noise(NO.4) = 1.609620
atm_noise(NO.2) = 1.565607
atm_noise(NO.0) = 0.000000
atm_noise(NO.1) = 0.000000
atm_noise(NO.3) = 0.000000
atm_noise(NO.6) = 0.000000
atm_noise(NO.8) = 0.000000
```

Applying atmospheric phase screen to original unwrapped phase...
Setting smoothing parameter to 1.000000...

```
fill the G matrix ...
run least-squares problem over 2826 by 1728 pixel (3) ...
matrix is rank-deficient: 8
```

write output ...

```
raln.grd
ralt.grd
rms_ll.grd
dem.grd
vel_ll.grd
disp_2007052_ll.grd
disp_2007328_ll.grd
disp_2008055_ll.grd
disp_2008101_ll.grd
disp_2008331_ll.grd
disp_2009057_ll.grd
disp_2009333_ll.grd
disp_2010014_ll.grd
disp_2010060_ll.grd
aps_2007052.grd
aps_2007328.grd
aps_2008055.grd
aps_2008101.grd
aps_2008331.grd
aps_2009057.grd
aps_2009333.grd
aps_2010014.grd
aps_2010060.grd
```

### A.3 ALOS PALSAR (Path 423 Row 7000) in Bali, Indonesia

```
data.in
IMG-HH-ALPSRP093437000-H1.0__A
IMG-HH-ALPSRP100147000-H1.0__A
IMG-HH-ALPSRP106857000-H1.0__A
IMG-HH-ALPSRP147117000-H1.0__A
IMG-HH-ALPSRP153827000-H1.0__A
IMG-HH-ALPSRP160537000-H1.0__A
IMG-HH-ALPSRP200797000-H1.0__A
IMG-HH-ALPSRP214217000-H1.0__A
IMG-HH-ALPSRP261187000-H1.0__A
```

pre\_proc\_batch.csh ALOS data.in batch.config

START PREPROCESS A STACK OF IMAGES

```
preprocess master image
ledflag 1
... swapping bytes
writing generic LED file: IMG-HH-ALPSRP093437000-H1.0__A.LED
near_range_shift = 848815 -384
... Calculating doppler for IMG-HH-ALPSRP093437000-H1.0__A.raw
Working on line 2000
Working on line 4000
Working on line 6000
Working on line 8000
Working on line 10000
Working on line 12000
Working on line 14000
Working on line 16000
Working on line 18000
Working on line 20000
```

```

Working on line 22000
Working on line 24000
Working on line 26000
Working on line 28000
Working on line 30000
Working on line 32000
Working on line 34000
pre_proc_batch.csh
preprocess slave images
setting fd1 to 121.625899
setting near_range to 849714.00
setting radius to 6377501.376673
setting npatches to 3
ledflag 1
.... swapping bytes
writing generic LED file: IMG-HH-ALPSRP100147000-H1.0__A.LED
near_range, shift = 849565 -64
near_range, shift = 848815 -384
The range sampling rate for master and slave images are: 32000000
pre_proc_batch.csh
preprocess slave images
setting fd1 to 121.625899
setting near_range to 849714.00
setting radius to 6377501.376673
setting npatches to 3
ledflag 1
.... swapping bytes
writing generic LED file: IMG-HH-ALPSRP106857000-H1.0__A.LED
near_range, shift = 848815 -384
The range sampling rate for master and slave images are: 32000000
pre_proc_batch.csh
preprocess slave images
setting fd1 to 121.625899
setting near_range to 849714.00
setting radius to 6377501.376673
setting npatches to 3
ledflag 1
.... swapping bytes
writing generic LED file: IMG-HH-ALPSRP147117000-H1.0__A.LED
near_range, shift = 850014 128
near_range, shift = 848965 -320
The range sampling rate for master and slave images are: 32000000
pre_proc_batch.csh
preprocess slave images
setting fd1 to 121.625899
setting near_range to 849714.00
setting radius to 6377501.376673
setting npatches to 3
ledflag 1
.... swapping bytes
writing generic LED file: IMG-HH-ALPSRP153827000-H1.0__A.LED
near_range, shift = 849115 -256
The range sampling rate for master and slave images are: 32000000
pre_proc_batch.csh
preprocess slave images
setting fd1 to 121.625899
setting near_range to 849714.00
setting radius to 6377501.376673
setting npatches to 3
ledflag 1
.... swapping bytes
writing generic LED file: IMG-HH-ALPSRP160537000-H1.0__A.LED
near_range, shift = 849265 -192
The range sampling rate for master and slave images are: 32000000
pre_proc_batch.csh
preprocess slave images
setting fd1 to 121.625899
setting near_range to 849714.00
setting radius to 6377501.376673
setting npatches to 3
ledflag 1
.... swapping bytes
writing generic LED file: IMG-HH-ALPSRP200797000-H1.0__A.LED
near_range, shift = 849565 -64
The range sampling rate for master and slave images are: 32000000
pre_proc_batch.csh
preprocess slave images
setting fd1 to 121.625899
setting near_range to 849714.00
setting radius to 6377501.376673
setting npatches to 3
ledflag 1
.... swapping bytes
writing generic LED file: IMG-HH-ALPSRP214217000-H1.0__A.LED
near_range, shift = 849864 64
near_range, shift = 848815 -384
The range sampling rate for master and slave images are: 32000000
pre_proc_batch.csh
preprocess slave images
setting fd1 to 121.625899
setting near_range to 849714.00
setting radius to 6377501.376673
setting npatches to 3
ledflag 1
.... swapping bytes
writing generic LED file: IMG-HH-ALPSRP261187000-H1.0__A.LED
near_range, shift = 849415 -128
near_range, shift = 848815 -384
The range sampling rate for master and slave images are: 32000000

```

END PREPROCESS A STACK OF IMAGES

```

baseline_table.dat
09343 2007299.6333463648 664 0.000000 0.000000
10014 2007345.6330960637 710 -418.245516 -273.874062
10685 2008026.6327651842 756 -390.513976 -481.596607
14711 2008302.6326072214 1032 318.148714 769.627063
15302 2008348.6331485524 1078 429.272412 751.639111
16053 2009028.6336109713 1123 141.523694 426.681992
20079 2009304.6348709827 1399 -189.025272 102.974247
21421 2010031.6347835406 1491 -212.667704 -62.176939
26118 2010353.6322258324 1813 -816.477288 -961.917072

```

```

intf.in
IMG-HH-ALPSRP093437000-H1.0__A:IMG-HH-ALPSRP100147000-H1.0__A
IMG-HH-ALPSRP093437000-H1.0__A:IMG-HH-ALPSRP106857000-H1.0__A
IMG-HH-ALPSRP093437000-H1.0__A:IMG-HH-ALPSRP147117000-H1.0__A
IMG-HH-ALPSRP093437000-H1.0__A:IMG-HH-ALPSRP153827000-H1.0__A
IMG-HH-ALPSRP093437000-H1.0__A:IMG-HH-ALPSRP160537000-H1.0__A

```

IMG-HH-ALPSRP093437000-H1.0\_A:IMG-HH-ALPSRP200797000-H1.0\_A  
IMG-HH-ALPSRP093437000-H1.0\_A:IMG-HH-ALPSRP214217000-H1.0\_A  
IMG-HH-ALPSRP093437000-H1.0\_A:IMG-HH-ALPSRP261187000-H1.0\_A  
IMG-HH-ALPSRP100147000-H1.0\_A:IMG-HH-ALPSRP106857000-H1.0\_A  
IMG-HH-ALPSRP100147000-H1.0\_A:IMG-HH-ALPSRP160537000-H1.0\_A  
IMG-HH-ALPSRP100147000-H1.0\_A:IMG-HH-ALPSRP200797000-H1.0\_A  
IMG-HH-ALPSRP100147000-H1.0\_A:IMG-HH-ALPSRP214217000-H1.0\_A  
IMG-HH-ALPSRP106857000-H1.0\_A:IMG-HH-ALPSRP160537000-H1.0\_A  
IMG-HH-ALPSRP106857000-H1.0\_A:IMG-HH-ALPSRP200797000-H1.0\_A  
IMG-HH-ALPSRP106857000-H1.0\_A:IMG-HH-ALPSRP214217000-H1.0\_A  
IMG-HH-ALPSRP147117000-H1.0\_A:IMG-HH-ALPSRP153827000-H1.0\_A  
IMG-HH-ALPSRP147117000-H1.0\_A:IMG-HH-ALPSRP160537000-H1.0\_A  
IMG-HH-ALPSRP147117000-H1.0\_A:IMG-HH-ALPSRP200797000-H1.0\_A  
IMG-HH-ALPSRP147117000-H1.0\_A:IMG-HH-ALPSRP214217000-H1.0\_A  
IMG-HH-ALPSRP153827000-H1.0\_A:IMG-HH-ALPSRP160537000-H1.0\_A  
IMG-HH-ALPSRP153827000-H1.0\_A:IMG-HH-ALPSRP200797000-H1.0\_A  
IMG-HH-ALPSRP153827000-H1.0\_A:IMG-HH-ALPSRP214217000-H1.0\_A  
IMG-HH-ALPSRP160537000-H1.0\_A:IMG-HH-ALPSRP200797000-H1.0\_A  
IMG-HH-ALPSRP160537000-H1.0\_A:IMG-HH-ALPSRP214217000-H1.0\_A  
IMG-HH-ALPSRP200797000-H1.0\_A:IMG-HH-ALPSRP214217000-H1.0\_A  
IMG-HH-ALPSRP214217000-H1.0\_A:IMG-HH-ALPSRP261187000-H1.0\_A

align.in

IMG-HH-ALPSRP093437000-H1.0\_A:IMG-HH-ALPSRP100147000-H1.0\_A:IMG-HH-ALPSRP093437000-H1.0\_A  
IMG-HH-ALPSRP093437000-H1.0\_A:IMG-HH-ALPSRP106857000-H1.0\_A:IMG-HH-ALPSRP093437000-H1.0\_A  
IMG-HH-ALPSRP093437000-H1.0\_A:IMG-HH-ALPSRP147117000-H1.0\_A:IMG-HH-ALPSRP093437000-H1.0\_A  
IMG-HH-ALPSRP093437000-H1.0\_A:IMG-HH-ALPSRP153827000-H1.0\_A:IMG-HH-ALPSRP093437000-H1.0\_A  
IMG-HH-ALPSRP093437000-H1.0\_A:IMG-HH-ALPSRP160537000-H1.0\_A:IMG-HH-ALPSRP093437000-H1.0\_A  
IMG-HH-ALPSRP093437000-H1.0\_A:IMG-HH-ALPSRP200797000-H1.0\_A:IMG-HH-ALPSRP093437000-H1.0\_A  
IMG-HH-ALPSRP093437000-H1.0\_A:IMG-HH-ALPSRP214217000-H1.0\_A:IMG-HH-ALPSRP093437000-H1.0\_A  
IMG-HH-ALPSRP093437000-H1.0\_A:IMG-HH-ALPSRP261187000-H1.0\_A:IMG-HH-ALPSRP093437000-H1.0\_A  
IMG-HH-ALPSRP100147000-H1.0\_A:IMG-HH-ALPSRP106857000-H1.0\_A:IMG-HH-ALPSRP093437000-H1.0\_A  
IMG-HH-ALPSRP100147000-H1.0\_A:IMG-HH-ALPSRP160537000-H1.0\_A:IMG-HH-ALPSRP093437000-H1.0\_A  
IMG-HH-ALPSRP100147000-H1.0\_A:IMG-HH-ALPSRP200797000-H1.0\_A:IMG-HH-ALPSRP093437000-H1.0\_A  
IMG-HH-ALPSRP100147000-H1.0\_A:IMG-HH-ALPSRP214217000-H1.0\_A:IMG-HH-ALPSRP093437000-H1.0\_A  
IMG-HH-ALPSRP106857000-H1.0\_A:IMG-HH-ALPSRP160537000-H1.0\_A:IMG-HH-ALPSRP093437000-H1.0\_A  
IMG-HH-ALPSRP106857000-H1.0\_A:IMG-HH-ALPSRP200797000-H1.0\_A:IMG-HH-ALPSRP093437000-H1.0\_A  
IMG-HH-ALPSRP106857000-H1.0\_A:IMG-HH-ALPSRP214217000-H1.0\_A:IMG-HH-ALPSRP093437000-H1.0\_A  
IMG-HH-ALPSRP147117000-H1.0\_A:IMG-HH-ALPSRP153827000-H1.0\_A:IMG-HH-ALPSRP093437000-H1.0\_A  
IMG-HH-ALPSRP147117000-H1.0\_A:IMG-HH-ALPSRP160537000-H1.0\_A:IMG-HH-ALPSRP093437000-H1.0\_A  
IMG-HH-ALPSRP147117000-H1.0\_A:IMG-HH-ALPSRP200797000-H1.0\_A:IMG-HH-ALPSRP093437000-H1.0\_A  
IMG-HH-ALPSRP147117000-H1.0\_A:IMG-HH-ALPSRP214217000-H1.0\_A:IMG-HH-ALPSRP093437000-H1.0\_A  
IMG-HH-ALPSRP153827000-H1.0\_A:IMG-HH-ALPSRP160537000-H1.0\_A:IMG-HH-ALPSRP093437000-H1.0\_A  
IMG-HH-ALPSRP153827000-H1.0\_A:IMG-HH-ALPSRP200797000-H1.0\_A:IMG-HH-ALPSRP093437000-H1.0\_A  
IMG-HH-ALPSRP153827000-H1.0\_A:IMG-HH-ALPSRP214217000-H1.0\_A:IMG-HH-ALPSRP093437000-H1.0\_A  
IMG-HH-ALPSRP160537000-H1.0\_A:IMG-HH-ALPSRP200797000-H1.0\_A:IMG-HH-ALPSRP093437000-H1.0\_A  
IMG-HH-ALPSRP160537000-H1.0\_A:IMG-HH-ALPSRP214217000-H1.0\_A:IMG-HH-ALPSRP093437000-H1.0\_A  
IMG-HH-ALPSRP200797000-H1.0\_A:IMG-HH-ALPSRP214217000-H1.0\_A:IMG-HH-ALPSRP093437000-H1.0\_A  
IMG-HH-ALPSRP214217000-H1.0\_A:IMG-HH-ALPSRP261187000-H1.0\_A:IMG-HH-ALPSRP093437000-H1.0\_A

align\_batch.csh ALOS align.in

ALIGN.CSH - START  
focussing master  
Computing range reference function.  
Processing patch 1  
Processing Elapsed Time: 0 min 0.04 sec  
Range Compression  
Processing Elapsed Time: 0 min 5.69 sec  
Azimuthal Transform  
Processing Elapsed Time: 0 min 13.58 sec  
Range Migration  
Processing Elapsed Time: 0 min 23.50 sec  
Azimuthal Compression  
Processing Elapsed Time: 0 min 45.94 sec  
Writing Data  
Processing patch 2  
Processing Elapsed Time: 0 min 47.45 sec  
Range Compression  
Processing Elapsed Time: 0 min 52.11 sec  
Azimuthal Transform  
Processing Elapsed Time: 0 min 59.99 sec  
Range Migration  
Processing Elapsed Time: 1 min 9.89 sec  
Azimuthal Compression  
Processing Elapsed Time: 1 min 33.02 sec  
Writing Data  
Processing patch 3  
Processing Elapsed Time: 1 min 34.59 sec  
Range Compression  
Processing Elapsed Time: 1 min 39.19 sec  
Azimuthal Transform  
Processing Elapsed Time: 1 min 47.28 sec  
Range Migration  
Processing Elapsed Time: 1 min 57.19 sec  
Azimuthal Compression  
Processing Elapsed Time: 2 min 19.92 sec  
Writing Data  
Processing Elapsed Time: 2 min 21.44 sec  
number of points clipped to short int 53  
align.csh  
focusing slave  
Computing range reference function.  
Processing patch 1  
Processing Elapsed Time: 0 min 0.03 sec  
Range Compression  
Processing Elapsed Time: 0 min 5.57 sec  
Azimuthal Transform  
Processing Elapsed Time: 0 min 13.87 sec  
Range Migration  
Processing Elapsed Time: 0 min 23.93 sec  
Azimuthal Compression  
Processing Elapsed Time: 0 min 47.04 sec  
Writing Data  
Processing patch 2  
Processing Elapsed Time: 0 min 48.58 sec  
Range Compression  
Processing Elapsed Time: 0 min 53.18 sec  
Azimuthal Transform  
Processing Elapsed Time: 1 min 1.26 sec  
Range Migration  
Processing Elapsed Time: 1 min 11.19 sec  
Azimuthal Compression  
Processing Elapsed Time: 1 min 35.27 sec  
Writing Data  
Processing patch 3  
Processing Elapsed Time: 1 min 36.80 sec  
Range Compression  
Processing Elapsed Time: 1 min 41.44 sec



```

Azimuthal Transform
Processing Elapsed Time: 1 min 49.63 sec
Range Migration
Processing Elapsed Time: 1 min 59.54 sec
Azimuthal Compression
Processing Elapsed Time: 2 min 23.60 sec
Writing Data
Processing Elapsed Time: 2 min 25.14 sec
number of points clipped to short int 175
align.csh
correlate master and slave to find offset parameters
  setting xsearch to 64
  setting nx_corr to 128
  setting ysearch to 64
  setting ny_corr to 128
11304 27648 11304 27648 104 68 -0.002141
locations n 512 nx 11304 nyl 32 nxl 16 x_inc 574 y_inc 826
elapsed time: 19.338003
align.csh
refocus slave
Computing range reference function.
Processing patch 1
Processing Elapsed Time: 0 min 0.03 sec
Range Compression
Processing Elapsed Time: 0 min 5.83 sec
Azimuthal Transform
Processing Elapsed Time: 0 min 20.32 sec
Range Migration
Processing Elapsed Time: 0 min 30.42 sec
Azimuthal Compression
Processing Elapsed Time: 1 min 3.81 sec
apply azimuth-dependent azimuth shift
Processing Elapsed Time: 1 min 28.67 sec
Writing Data
Processing patch 2
Processing Elapsed Time: 1 min 35.16 sec
Range Compression
Processing Elapsed Time: 1 min 39.93 sec
Azimuthal Transform
Processing Elapsed Time: 1 min 49.27 sec
Range Migration
Processing Elapsed Time: 1 min 59.38 sec
Azimuthal Compression
Processing Elapsed Time: 2 min 29.37 sec
apply azimuth-dependent azimuth shift
Processing Elapsed Time: 2 min 56.98 sec
Writing Data
Processing patch 3
Processing Elapsed Time: 3 min 3.89 sec
Range Compression
Processing Elapsed Time: 3 min 8.54 sec
Azimuthal Transform
Processing Elapsed Time: 3 min 18.00 sec
Range Migration
Processing Elapsed Time: 3 min 28.25 sec
Azimuthal Compression
Processing Elapsed Time: 4 min 2.25 sec
apply azimuth-dependent azimuth shift
Processing Elapsed Time: 4 min 28.31 sec
Writing Data
Processing Elapsed Time: 4 min 35.06 sec
number of points clipped to short int 187
rm: No match.
ALIGN.CSH - END

```

```

intf_batch.csh ALOS batch.config
clean up topo/ folder

```

```

DEM2TOPO_RA.CSH - START
USER SHOULD PROVIDE DEM FILE
  range decimation is: 2
blockmedian: Provides 3, expects 3-column binary data
blockmedian: Processing input table data
blockmedian: W: 0 E: 11304 S: 0 N: 27648 n_columns: 5652 n_rows: 6912
blockmedian: Input 3 columns via binary records using format ddd
blockmedian: Output 3 columns via binary records using format ddd
blockmedian: N read: 880412 N used: 877562 outside_area: 2850 N cells filled: 877534
surface: Provides 3, expects 3-column binary data
surface: Grid domain: W: 0 E: 11304 S: 0 N: 27648 n_columns: 5652 n_rows: 6912 [pixel registration]
surface: Processing input table data
surface: Input 3 columns via binary records using format ddd
surface: Minimum value of your dataset x,y,z at: surface: 9.47925853729 20.1111221313 79.1265945435
surface: Maximum value of your dataset x,y,z at: surface: 4982.25195312 19988.2792969 3152.45239258
surface: LS plane determined: z = 203.081 + (-0.085365 * col) + (0.111885 * row)
surface:


| surface: | Grid | Mode | Iteration | Max Change        | Conv Limit       | Total Iterations |
|----------|------|------|-----------|-------------------|------------------|------------------|
| surface: | 36   | D    | 22        | 0.000546255543946 | 0.00086758828296 | 22               |
| surface: | 12   | I    | 28        | 0.00218929156934  | 0.0026027648489  | 50               |
| surface: | 12   | D    | 20        | 0.00178716015478  | 0.0026027648489  | 70               |
| surface: | 4    | I    | 25        | 0.00575992186722  | 0.0078082945467  | 95               |
| surface: | 4    | D    | 42        | 0.00697227533129  | 0.0078082945467  | 137              |
| surface: | 2    | I    | 18        | 0.0144953689828   | 0.0156165890934  | 155              |
| surface: | 2    | D    | 92        | 0.0155055815236   | 0.0156165890934  | 247              |
| surface: | 1    | I    | 16        | 0.0282327391979   | 0.0312331781868  | 263              |
| surface: | 1    | D    | 245       | 0.0309639238689   | 0.0312331781868  | 508              |


surface: Fit info: N data points N nodes mean error rms error curvature
surface: 877534 39079189 -3.16770048757e-06 0.0062199362068 22227.5479258
grd2cpt: Processing input grid(s)
grd2cpt: Mean and S.D. of data are 349.387377152 406.116523212
grdimage: Allocates memory and read data file topo_ra.grd
grdimage: Evaluate image pixel colors
grdimage: Creating 8-bit grayshade image
DEM2TOPO_RA.CSH - END
NO TOPO_RA SHIFT

```

```
START FORM A STACK OF INTERFEROGRAMS
```

```

INTF.CSH, FILTER.CSH - START
intf.csh
running phasediff...
reading topo topo_ra.grd
  xdim 11304, ydim 27648
filter.csh
gauss_300 4 2 (4 2)
making amplitudes...
filtering interferogram...
making amplitude...
making correlation...

```

making phase...  
filtering phase...  
INTF.CSH, FILTER.CSH - END

SNAPHU.CSH - START  
threshold\_snaphu: .45  
grdmath: Perform reverse Polish notation calculations on grids  
grdmath: phase\_patch.grd landmask\_ra\_patch.grd MUL = phase\_patch.grd  
unwrapping phase with snaphu - higher threshold for faster unwrapping

snaphu v1.4.2  
32 parameters input from file snaphu.conf.brief (297 lines total)  
Reading wrapped phase from file phase.in  
No weight file specified. Assuming uniform weights  
Reading correlation data from file corr.in  
Calculating deformation-mode cost parameters  
Building range cost arrays  
Building azimuth cost arrays  
Initializing flows with MST algorithm  
Running approximate minimum spanning tree solver  
Running nonlinear network flow optimizer  
Maximum flow on network: 2  
Number of nodes in network: 4878776  
Flow increment: 1 (Total improvements: 0)  
Treesize: 4878776 Pivots: 134 Improvements: 19  
Maximum flow on network: 1  
Total solution cost: 97607  
Integrating phase  
Writing output to file unwrap.out  
Program snaphu done  
Elapsed processor time: 0:01:21.96  
Elapsed wall clock time: 0:01:26  
grdmath: Perform reverse Polish notation calculations on grids  
grdmath: unwrap.grd landmask\_ra\_patch.grd MUL = tmp.grd  
SNAPHU.CSH - END

GEOCODE.CSH - START  
threshold\_geocode: .45  
grdmath: Perform reverse Polish notation calculations on grids  
grdmath: corr.grd 0.45 GE 0 NAN mask.grd MUL = mask2.grd  
psscale: Warning: The -E option is deprecated but is accepted.  
psscale: For the current -D syntax you should use -D modifier +e instead.  
psscale: Note you cannot mix new-style modifiers (+e) with the old-style -D option.  
psscale: Warning: The -E option is deprecated but is accepted.  
psscale: For the current -D syntax you should use -D modifier +e instead.  
psscale: Note you cannot mix new-style modifiers (+e) with the old-style -D option.  
geocode.csh  
project correlation, phase, unwrapped and amplitude back to lon lat coordinates  
remarked in by root on Sun May 20 22:13:53 JST 2018 with geocode.csh  
proj\_ra2ll.csh  
surface: Provides 3, expects 3-column binary data  
surface: Grid domain: W: 128 E: 11168 S: 0 N: 27648 n\_columns: 690 n\_rows: 864 [gridline registration]  
surface: Processing input table data  
surface: Input 3 columns via binary records using format fff  
surface: Minimum value of your dataset x,y,z at: surface: 126.963264465 27647.2949219 114.666664124  
surface: Maximum value of your dataset x,y,z at: surface: 11174.9462891 82.5900421143 115.574165344  
surface: 260031 unusable points were supplied; these will be ignored.  
surface: You should have pre-processed the data with block-mean, -median, or -mode.  
surface: Check that previous processing steps write results with enough decimals.  
surface: LS plane determined: z = 114.849 + (0.00106011 \* col) + (-0.000202915 \* row)  
surface: Grid Mode IterationMax Change Conv Limit Total Iterations  
surface: 6 D 1565 4.96930443203e-08 4.97084985842e-08 1565  
surface: 2 I 18 1.14692209972e-07 1.49125495753e-07 1583  
surface: 2 D 485 1.4895469295e-07 1.49125495753e-07 2068  
surface: 1 I 13 2.74493923862e-07 2.98250991505e-07 2081  
surface: 1 D 63 2.95710945707e-07 2.98250991505e-07 2144  
surface: Fit info: N data points N nodes mean error rms errorcurvature  
surface: 586013 597715 -5.66513051953e-07 0.00132725814588 1317.88061672  
surface: Provides 3, expects 3-column binary data  
surface: Grid domain: W: 128 E: 11168 S: 0 N: 27648 n\_columns: 690 n\_rows: 864 [gridline registration]  
surface: Processing input table data  
surface: Input 3 columns via binary records using format fff  
surface: Minimum value of your dataset x,y,z at: surface: 120.510879517 2581.31201172 -9.39999961853  
surface: Maximum value of your dataset x,y,z at: surface: 11127.0439453 27662.7226562 -8.52916717529  
surface: 260031 unusable points were supplied; these will be ignored.  
surface: You should have pre-processed the data with block-mean, -median, or -mode.  
surface: Check that previous processing steps write results with enough decimals.  
surface: LS plane determined: z = -9.47075 + (0.000240623 \* col) + (0.00089931 \* row)  
surface: Grid Mode IterationMax Change Conv Limit Total Iterations  
surface: 6 D 1588 1.01943648707e-08 1.02660901213e-08 1588  
surface: 2 I 23 2.74648182992e-08 3.07982703639e-08 1611  
surface: 2 D 697 3.07673287111e-08 3.07982703639e-08 2308  
surface: 1 I 14 4.39899694215e-08 6.15965407277e-08 2322  
surface: 1 D 143 6.12775562358e-08 6.15965407277e-08 2465  
surface: Fit info: N data points N nodes mean error rms errorcurvature  
surface: 586013 597715 2.17544583827e-05 0.0115162382511 4950.65087718  
blockmedian: Provides 3, expects 3-column binary data  
blockmedian: Processing input table data  
blockmedian: W: 114.666666667 E: 115.577777778 S: -9.47222222222 N: -8.52777777778 n\_columns: 820 n\_rows: 1360  
blockmedian: Input 3 columns via binary records using format fff  
blockmedian: Output 3 columns via binary records using format fff  
blockmedian: N read: 4740409 N used: 4740409 outside\_area: 0 N cells filled: 771742  
proj\_ra2ll.csh  
blockmedian: Provides 3, expects 3-column binary data  
blockmedian: Processing input table data  
blockmedian: W: 114.666666667 E: 115.577777778 S: -9.47222222222 N: -8.52777777778 n\_columns: 820 n\_rows: 1360  
blockmedian: Input 3 columns via binary records using format fff  
blockmedian: Output 3 columns via binary records using format fff  
blockmedian: N read: 4745436 N used: 4745436 outside\_area: 0 N cells filled: 772591  
proj\_ra2ll.csh  
blockmedian: Provides 3, expects 3-column binary data  
blockmedian: Processing input table data  
blockmedian: W: 115.077777778 E: 115.4 S: -8.85416666667 N: -8.53472222222 n\_columns: 290 n\_rows: 460  
blockmedian: Input 3 columns via binary records using format fff  
blockmedian: Output 3 columns via binary records using format fff  
blockmedian: N read: 111353 N used: 111353 outside\_area: 0 N cells filled: 22116  
proj\_ra2ll.csh  
blockmedian: Provides 3, expects 3-column binary data  
blockmedian: Processing input table data  
blockmedian: W: 114.666666667 E: 115.577777778 S: -9.47222222222 N: -8.52777777778 n\_columns: 820 n\_rows: 1360  
blockmedian: Input 3 columns via binary records using format fff  
blockmedian: Output 3 columns via binary records using format fff  
blockmedian: N read: 4769280 N used: 4769280 outside\_area: 0 N cells filled: 776356  
proj\_ra2ll.csh  
blockmedian: Provides 3, expects 3-column binary data  
blockmedian: Processing input table data  
blockmedian: W: 115.077777778 E: 115.4 S: -8.85416666667 N: -8.53472222222 n\_columns: 290 n\_rows: 460  
blockmedian: Input 3 columns via binary records using format fff  
blockmedian: Output 3 columns via binary records using format fff

```
blockmedian: N read: 110984 N used: 110984 outside_area: 0 N cells filled: 22006
proj_ra2ll.csh
blockmedian: Provides 3, expects 3-column binary data
blockmedian: Processing input table data
blockmedian: W: 115.066666667 E: 115.444444444 S: -8.85416666667 N: -8.52777777778 n_columns: 340 n_rows: 470
blockmedian: Input 3 columns via binary records using format fff
blockmedian: Output 3 columns via binary records using format fff
blockmedian: N read: 336277 N used: 336277 outside_area: 0 N cells filled: 54037
proj_ra2ll.csh
blockmedian: Provides 3, expects 3-column binary data
blockmedian: Processing input table data
blockmedian: W: 115.077777778 E: 115.4 S: -8.85416666667 N: -8.53472222222 n_columns: 290 n_rows: 460
blockmedian: Input 3 columns via binary records using format fff
blockmedian: Output 3 columns via binary records using format fff
blockmedian: N read: 111353 N used: 111353 outside_area: 0 N cells filled: 22116
geocode.csh
make the KML files for Google Earth
grdimage: Allocates memory and read data file display_amp_ll.grd
grdimage: Evaluate image pixel colors
grdimage: Creating 24-bit color image
PSL: Colormap of 256 colors created
Make display_amp_ll.kml and display_amp_ll.png
psconvert: Processing display_amp_ll.ps...
psconvert: Figure dimensions: Width: 65.58 points [0.910833 inch] Height: 67.98 points [0.944166 inch]
psconvert: gs -q -dSAFER -dNOPAUSE -dBATCH -dPDFSETTINGS=/prepress -dDownsampleColorImages=false -dDownsampleGrayImages=false -dDownsampleMonoImages=false -dUseFlateCompression=true -dEmbedAllFonts=true -dSubsetFonts=true -dMonoImageFilter=/FlateEncode -dAutoFilterGrayImages=false -dGrayImageFilter=/FlateEncode -dAutoFilterColorImages=false -dColorImageFilter=/FlateEncode -dSCANVERTERTYPE=2 -dMaxBitmap=2147483647 -dUseFastColor=true -sDEVICE=pngalpha -g820x850 -r900 -sOutputFile='display_amp_ll.png' -f'./psconvert_18414d.eps'
psconvert: Done.
grdimage: Allocates memory and read data file corr_ll.grd
grdimage: Evaluate image pixel colors
grdimage: Creating 24-bit color image
PSL: Colormap of 256 colors created
Make corr_ll.kml and corr_ll.png
psconvert: Processing corr_ll.ps...
psconvert: Figure dimensions: Width: 65.58 points [0.910833 inch] Height: 67.98 points [0.944166 inch]
psconvert: gs -q -dSAFER -dNOPAUSE -dBATCH -dPDFSETTINGS=/prepress -dDownsampleColorImages=false -dDownsampleGrayImages=false -dDownsampleMonoImages=false -dUseFlateCompression=true -dEmbedAllFonts=true -dSubsetFonts=true -dMonoImageFilter=/FlateEncode -dAutoFilterGrayImages=false -dGrayImageFilter=/FlateEncode -dAutoFilterColorImages=false -dColorImageFilter=/FlateEncode -dSCANVERTERTYPE=2 -dMaxBitmap=2147483647 -dUseFastColor=true -sDEVICE=pngalpha -g820x850 -r900 -sOutputFile='corr_ll.png' -f'./psconvert_18514d.eps'
psconvert: Done.
grdimage: Allocates memory and read data file phase_mask_ll.grd
grdimage: Evaluate image pixel colors
grdimage: Creating 24-bit color image
Make phase_mask_ll.kml and phase_mask_ll.png
psconvert: Processing phase_mask_ll.ps...
psconvert: Figure dimensions: Width: 23.22 points [0.3225 inch] Height: 22.98 points [0.319166 inch]
psconvert: gs -q -dSAFER -dNOPAUSE -dBATCH -dPDFSETTINGS=/prepress -dDownsampleColorImages=false -dDownsampleGrayImages=false -dDownsampleMonoImages=false -dUseFlateCompression=true -dEmbedAllFonts=true -dSubsetFonts=true -dMonoImageFilter=/FlateEncode -dAutoFilterGrayImages=false -dGrayImageFilter=/FlateEncode -dAutoFilterColorImages=false -dColorImageFilter=/FlateEncode -dSCANVERTERTYPE=2 -dMaxBitmap=2147483647 -dUseFastColor=true -sDEVICE=pngalpha -g291x288 -r900 -sOutputFile='phase_mask_ll.png' -f'./psconvert_18614d.eps'
psconvert: Done.
grdimage: Allocates memory and read data file phasefilt_mask_ll.grd
grdimage: Evaluate image pixel colors
grdimage: Creating 24-bit color image
Make phasefilt_mask_ll.kml and phasefilt_mask_ll.png
psconvert: Processing phasefilt_mask_ll.ps...
psconvert: Figure dimensions: Width: 23.22 points [0.3225 inch] Height: 22.98 points [0.319166 inch]
psconvert: gs -q -dSAFER -dNOPAUSE -dBATCH -dPDFSETTINGS=/prepress -dDownsampleColorImages=false -dDownsampleGrayImages=false -dDownsampleMonoImages=false -dUseFlateCompression=true -dEmbedAllFonts=true -dSubsetFonts=true -dMonoImageFilter=/FlateEncode -dAutoFilterGrayImages=false -dGrayImageFilter=/FlateEncode -dAutoFilterColorImages=false -dColorImageFilter=/FlateEncode -dSCANVERTERTYPE=2 -dMaxBitmap=2147483647 -dUseFastColor=true -sDEVICE=pngalpha -g291x288 -r900 -sOutputFile='phasefilt_mask_ll.png' -f'./psconvert_18706d.eps'
psconvert: Done.
grdimage: Allocates memory and read data file unwrap_mask_ll.grd
grdimage: Evaluate image pixel colors
grdimage: Creating 24-bit color image
Make unwrap_mask_ll.kml and unwrap_mask_ll.png
psconvert: Processing unwrap_mask_ll.ps...
psconvert: Figure dimensions: Width: 23.22 points [0.3225 inch] Height: 22.98 points [0.319166 inch]
psconvert: gs -q -dSAFER -dNOPAUSE -dBATCH -dPDFSETTINGS=/prepress -dDownsampleColorImages=false -dDownsampleGrayImages=false -dDownsampleMonoImages=false -dUseFlateCompression=true -dEmbedAllFonts=true -dSubsetFonts=true -dMonoImageFilter=/FlateEncode -dAutoFilterGrayImages=false -dGrayImageFilter=/FlateEncode -dAutoFilterColorImages=false -dColorImageFilter=/FlateEncode -dSCANVERTERTYPE=2 -dMaxBitmap=2147483647 -dUseFastColor=true -sDEVICE=pngalpha -g291x288 -r900 -sOutputFile='unwrap_mask_ll.png' -f'./psconvert_18858d.eps'
psconvert: Done.
grdimage: Allocates memory and read data file phasefilt_mask_ll.grd
grdimage: Evaluate image pixel colors
grdimage: Creating 24-bit color image
Make phasefilt_mask_ll.kml and phasefilt_mask_ll.png
psconvert: Processing phasefilt_mask_ll.ps...
psconvert: Figure dimensions: Width: 23.22 points [0.3225 inch] Height: 22.98 points [0.319166 inch]
psconvert: gs -q -dSAFER -dNOPAUSE -dBATCH -dPDFSETTINGS=/prepress -dDownsampleColorImages=false -dDownsampleGrayImages=false -dDownsampleMonoImages=false -dUseFlateCompression=true -dEmbedAllFonts=true -dSubsetFonts=true -dMonoImageFilter=/FlateEncode -dAutoFilterGrayImages=false -dGrayImageFilter=/FlateEncode -dAutoFilterColorImages=false -dColorImageFilter=/FlateEncode -dSCANVERTERTYPE=2 -dMaxBitmap=2147483647 -dUseFastColor=true -sDEVICE=pngalpha -g291x288 -r900 -sOutputFile='phasefilt_mask_ll.png' -f'./psconvert_18997d.eps'
psconvert: Done.
grdimage: Allocates memory and read data file los_ll.grd
grdimage: Evaluate image pixel colors
grdimage: Creating 24-bit color image
Make los_ll.kml and los_ll.png
psconvert: Processing los_ll.ps...
psconvert: Figure dimensions: Width: 23.22 points [0.3225 inch] Height: 22.98 points [0.319166 inch]
psconvert: gs -q -dSAFER -dNOPAUSE -dBATCH -dPDFSETTINGS=/prepress -dDownsampleColorImages=false -dDownsampleGrayImages=false -dDownsampleMonoImages=false -dUseFlateCompression=true -dEmbedAllFonts=true -dSubsetFonts=true -dMonoImageFilter=/FlateEncode -dAutoFilterGrayImages=false -dGrayImageFilter=/FlateEncode -dAutoFilterColorImages=false -dColorImageFilter=/FlateEncode -dSCANVERTERTYPE=2 -dMaxBitmap=2147483647 -dUseFastColor=true -sDEVICE=pngalpha -g291x288 -r900 -sOutputFile='los_ll.png' -f'./psconvert_19174d.eps'
psconvert: Done.
GEOCODE.CSH - END
```

#### stack.list

```
cut_2007299_2007345.grd IMG-HH-ALPSRP093437000-H1.0_A.PRM IMG-HH-ALPSRP100147000-H1.0_A.PRM
cut_2007299_2008026.grd IMG-HH-ALPSRP093437000-H1.0_A.PRM IMG-HH-ALPSRP106857000-H1.0_A.PRM
cut_2007299_2008302.grd IMG-HH-ALPSRP093437000-H1.0_A.PRM IMG-HH-ALPSRP147117000-H1.0_A.PRM
cut_2007299_2008348.grd IMG-HH-ALPSRP093437000-H1.0_A.PRM IMG-HH-ALPSRP153827000-H1.0_A.PRM
cut_2007299_2009028.grd IMG-HH-ALPSRP093437000-H1.0_A.PRM IMG-HH-ALPSRP160537000-H1.0_A.PRM
cut_2007299_2009304.grd IMG-HH-ALPSRP093437000-H1.0_A.PRM IMG-HH-ALPSRP200797000-H1.0_A.PRM
cut_2007299_2010031.grd IMG-HH-ALPSRP093437000-H1.0_A.PRM IMG-HH-ALPSRP214217000-H1.0_A.PRM
cut_2007299_2010353.grd IMG-HH-ALPSRP093437000-H1.0_A.PRM IMG-HH-ALPSRP261187000-H1.0_A.PRM
```

```
bash stack_phase.bash stack.list mean.grd std.grd
```

```
compute the mean LOS velocity ..
```

```
time span (days) of cut_2007299_2007345.grd: 46
accumulative days in the stack: 46
time span (days) of cut_2007299_2008026.grd: 92
accumulative days in the stack: 138
time span (days) of cut_2007299_2008302.grd: 368
accumulative days in the stack: 506
time span (days) of cut_2007299_2008348.grd: 414
```

accumulative days in the stack: 920  
time span (days) of cut\_2007299\_2009028.grd: 459  
accumulative days in the stack: 1379  
time span (days) of cut\_2007299\_2009304.grd: 735  
accumulative days in the stack: 2114  
time span (days) of cut\_2007299\_2010031.grd: 827  
accumulative days in the stack: 2941  
time span (days) of cut\_2007299\_2010353.grd: 1149  
accumulative days in the stack: 4090

compute the standard deviations ..

mean\_ll.grd  
std\_ll.grd  
los\_ll\_2007345.grd  
los\_ll\_2008026.grd  
los\_ll\_2008302.grd  
los\_ll\_2008348.grd  
los\_ll\_2009028.grd  
los\_ll\_2009304.grd  
los\_ll\_2010031.grd  
los\_ll\_2010353.grd

csf select\_pairs.csf baseline\_table.dat 950 1000

intf.tab

cut_2007299_2007345.grd	corcut_2007299_2007345.grd	2007299	2007345	-273.874062
cut_2007299_2008026.grd	corcut_2007299_2008026.grd	2007299	2008026	-481.596607
cut_2007299_2008302.grd	corcut_2007299_2008302.grd	2007299	2008302	769.627863
cut_2007299_2008348.grd	corcut_2007299_2008348.grd	2007299	2008348	731.639111
cut_2007299_2009028.grd	corcut_2007299_2009028.grd	2007299	2009028	426.681992
cut_2007299_2009304.grd	corcut_2007299_2009304.grd	2007299	2009304	102.974247
cut_2007299_2010031.grd	corcut_2007299_2010031.grd	2007299	2010031	-62.176939
cut_2007345_2008026.grd	corcut_2007345_2008026.grd	2007345	2008026	-207.716456
cut_2007345_2009028.grd	corcut_2007345_2009028.grd	2007345	2009028	700.687984
cut_2007345_2009304.grd	corcut_2007345_2009304.grd	2007345	2009304	376.901681
cut_2007345_2010031.grd	corcut_2007345_2010031.grd	2007345	2010031	211.746483
cut_2008026_2009028.grd	corcut_2008026_2009028.grd	2008026	2009028	908.235979
cut_2008026_2009304.grd	corcut_2008026_2009304.grd	2008026	2009304	584.552338
cut_2008026_2010031.grd	corcut_2008026_2010031.grd	2008026	2010031	419.409339
cut_2008302_2008348.grd	corcut_2008302_2008348.grd	2008302	2008348	-37.941877
cut_2008302_2009028.grd	corcut_2008302_2009028.grd	2008302	2009028	-343.019743
cut_2008302_2009304.grd	corcut_2008302_2009304.grd	2008302	2009304	-666.887615
cut_2008302_2010031.grd	corcut_2008302_2010031.grd	2008302	2010031	-832.084093
cut_2008348_2009028.grd	corcut_2008348_2009028.grd	2008348	2009028	-305.020703
cut_2008348_2009304.grd	corcut_2008348_2009304.grd	2008348	2009304	-626.820943
cut_2008348_2010031.grd	corcut_2008348_2010031.grd	2008348	2010031	-794.009395
cut_2009028_2009304.grd	corcut_2009028_2009304.grd	2009028	2009304	-323.805524
cut_2009028_2010031.grd	corcut_2009028_2010031.grd	2009028	2010031	-488.989781
cut_2009304_2010031.grd	corcut_2009304_2010031.grd	2009304	2010031	-165.172048
cut_2010031_2010353.grd	corcut_2010031_2010353.grd	2010031	2010353	-899.865726

scene.tab

2007299 664  
2007345 710  
2008026 756  
2008302 1032  
2008348 1078  
2009028 1123  
2009304 1399  
2010031 1491  
2010353 1813

sbas intf.tab scene.tab 25 9 2826 1728 -smooth 1.0 -wavelength 0.2362 -incidence 34.3 -range 849714 -rms -dem -atm 1

compute RMS misfit  
compute DEM error

setting smoothing to 1.000  
setting radar wavelength to 0.236 m  
setting radar incidence angle to 34.300 degree  
setting range to 849714.000 m  
Memory Allocation Successful...  
read table file ...  
number of SAR scenes is 9  
number of interferograms is 25  
read phase and correlation grids ...  
fill the G matrix ...

Applying atmospheric correction by common point stacking...

Hit Matrix:

2007299	0	1	1	1	1	1	1	0
2007345	0	0	1	0	0	1	1	0
2008026	0	0	0	0	0	1	1	0
2008302	0	0	0	1	1	1	1	0
2008348	0	0	0	0	1	1	1	0
2009028	0	0	0	0	0	1	1	0
2009304	0	0	0	0	0	0	1	0
2010031	0	0	0	0	0	0	0	1
2010353	0	0	0	0	0	0	0	0

Applying exponential relaxation on smoothing parameters

Setting smoothing parameter to 1000.000000...  
fill the G matrix ...  
Computing deformation time-series...  
run least-squares problem over 2826 by 1728 pixel (0) ...  
matrix is full rank: 9

Removing deformation time-series from original unwrapped phase...  
Computing atmospheric phase screen by common-point stacking...

Initial estimate of APS...  
atm\_noise(NO.3) = 1.86583  
atm\_noise(NO.5) = 1.519463  
atm\_noise(NO.4) = 1.454082  
atm\_noise(NO.1) = 0.474738  
atm\_noise(NO.0) = 0.000000  
atm\_noise(NO.2) = 0.000000  
atm\_noise(NO.6) = 0.000000  
atm\_noise(NO.7) = 0.000000  
atm\_noise(NO.8) = 0.000000

```

atm_noise(NO.3) = 1.840013
atm_noise(NO.5) = 1.383736
atm_noise(NO.4) = 0.979039
atm_noise(NO.1) = 0.449513
atm_noise(NO.0) = 0.000000
atm_noise(NO.2) = 0.000000
atm_noise(NO.6) = 0.000000
atm_noise(NO.7) = 0.000000
atm_noise(NO.8) = 0.000000

```

```

Applying atmospheric phase screen to original unwrapped phase...
Setting smoothing parameter to 1.000000...
fill the G matrix ...
run least-squares problem over 2826 by 1728 pixel (3) ...
matrix is rank-deficient: 8

```

write output ...

```

raln.grd
ralt.grd
rms_ll.grd
dem.grd
vel_ll.grd
disp_2007299_ll.grd
disp_2007345_ll.grd
disp_2008026_ll.grd
disp_2008302_ll.grd
disp_2008348_ll.grd
disp_2009028_ll.grd
disp_2009304_ll.grd
disp_2010031_ll.grd
disp_2010353_ll.grd
aps_2007299.grd
aps_2007345.grd
aps_2008026.grd
aps_2008302.grd
aps_2008348.grd
aps_2009028.grd
aps_2009304.grd
aps_2010031.grd
aps_2010353.grd

```

## A.4 ALOS PALSAR (Path 423 Row 7010) in Bali, Indonesia

```

data.in
IMG-HH-ALPSRP093437010-H1.0__A
IMG-HH-ALPSRP100147010-H1.0__A
IMG-HH-ALPSRP106857010-H1.0__A
IMG-HH-ALPSRP147117010-H1.0__A
IMG-HH-ALPSRP153827010-H1.0__A
IMG-HH-ALPSRP160537010-H1.0__A
IMG-HH-ALPSRP200797010-H1.0__A
IMG-HH-ALPSRP214217010-H1.0__A
IMG-HH-ALPSRP261187010-H1.0__A

```

pre\_proc\_batch.csh ALOS data.in batch.config

START PREPROCESS A STACK OF IMAGES

```

preprocess master image
ledflag 1
... swapping bytes
writing generic LED file: IMG-HH-ALPSRP093437010-H1.0__A.LED
near_range, shift = 848815 -384
... calculating doppler for IMG-HH-ALPSRP093437010-H1.0__A.raw
Working on line 2000
Working on line 4000
Working on line 6000
Working on line 8000
Working on line 10000
Working on line 12000
Working on line 14000
Working on line 16000
Working on line 18000
Working on line 20000
Working on line 22000
Working on line 24000
Working on line 26000
Working on line 28000
Working on line 30000
Working on line 32000
Working on line 34000
pre_proc_batch.csh
preprocess slave images
setting fd1 to 30.113341
setting near_range to 849714.00
setting radius to 6377562.741418
setting npatches to 3
ledflag 1
... swapping bytes
writing generic LED file: IMG-HH-ALPSRP100147010-H1.0__A.LED
near_range, shift = 849565 -64
near_range, shift = 848815 -384
The range sampling rate for master and slave images are: 32000000
pre_proc_batch.csh
preprocess slave images
setting fd1 to 30.113341
setting near_range to 849714.00
setting radius to 6377562.741418
setting npatches to 3
ledflag 1
... swapping bytes
writing generic LED file: IMG-HH-ALPSRP106857010-H1.0__A.LED
near_range, shift = 848815 -384
The range sampling rate for master and slave images are: 32000000
pre_proc_batch.csh
preprocess slave images
setting fd1 to 30.113341
setting near_range to 849714.00
setting radius to 6377562.741418
setting npatches to 3
ledflag 1
... swapping bytes
writing generic LED file: IMG-HH-ALPSRP147117010-H1.0__A.LED

```

```
near_range, shift = 850014 128
near_range, shift = 848965 -320
The range sampling rate for master and slave images are: 32000000
pre_proc_batch.csh
preprocess slave images
setting fd1 to 30.113341
setting near_range to 849714.00
setting radius to 6377562.741418
setting npatches to 3
ledflag 1
.... swapping bytes
writing generic LED file: IMG-HH-ALPSRP153827010-H1.0_A.LED
near_range, shift = 849115 -256
The range sampling rate for master and slave images are: 32000000
pre_proc_batch.csh
preprocess slave images
setting fd1 to 30.113341
setting near_range to 849714.00
setting radius to 6377562.741418
setting npatches to 3
ledflag 1
.... swapping bytes
writing generic LED file: IMG-HH-ALPSRP160537010-H1.0_A.LED
near_range, shift = 849265 -192
The range sampling rate for master and slave images are: 32000000
pre_proc_batch.csh
preprocess slave images
setting fd1 to 30.113341
setting near_range to 849714.00
setting radius to 6377562.741418
setting npatches to 3
ledflag 1
.... swapping bytes
writing generic LED file: IMG-HH-ALPSRP200797010-H1.0_A.LED
near_range, shift = 849565 -64
near_range, shift = 848815 -384
The range sampling rate for master and slave images are: 32000000
pre_proc_batch.csh
preprocess slave images
setting fd1 to 30.113341
setting near_range to 849714.00
setting radius to 6377562.741418
setting npatches to 3
ledflag 1
.... swapping bytes
writing generic LED file: IMG-HH-ALPSRP214217010-H1.0_A.LED
near_range, shift = 848815 -384
The range sampling rate for master and slave images are: 32000000
pre_proc_batch.csh
preprocess slave images
setting fd1 to 30.113341
setting near_range to 849714.00
setting radius to 6377562.741418
setting npatches to 3
ledflag 1
.... swapping bytes
writing generic LED file: IMG-HH-ALPSRP261187010-H1.0_A.LED
near_range, shift = 849415 -128
near_range, shift = 848815 -384
The range sampling rate for master and slave images are: 32000000
```

END PREPROCESS A STACK OF IMAGES

```
baseline_table.dat
09343 2007299.6334416079 664 0.000000 0.000000
10014 2007345.6331913068 710 -414.654329 -271.096790
10685 2008026.6328604156 756 -382.085445 -472.345306
14711 2008302.6327024759 1032 282.848712 725.057614
15382 2008348.6332437953 1078 397.637262 691.291677
16053 2009028.6337062027 1123 114.328782 392.503573
20079 2009304.6349662258 1399 -200.138665 87.717368
21421 2010031.6348787837 1491 -215.356482 -66.447985
26118 2010353.6323210755 1813 -800.627986 -943.428413
```

```
intf.in
IMG-HH-ALPSRP093437010-H1.0_A:IMG-HH-ALPSRP100147010-H1.0_A
IMG-HH-ALPSRP093437010-H1.0_A:IMG-HH-ALPSRP106857010-H1.0_A
IMG-HH-ALPSRP093437010-H1.0_A:IMG-HH-ALPSRP147117010-H1.0_A
IMG-HH-ALPSRP093437010-H1.0_A:IMG-HH-ALPSRP153827010-H1.0_A
IMG-HH-ALPSRP093437010-H1.0_A:IMG-HH-ALPSRP160537010-H1.0_A
IMG-HH-ALPSRP093437010-H1.0_A:IMG-HH-ALPSRP200797010-H1.0_A
IMG-HH-ALPSRP093437010-H1.0_A:IMG-HH-ALPSRP214217010-H1.0_A
IMG-HH-ALPSRP093437010-H1.0_A:IMG-HH-ALPSRP261187010-H1.0_A
IMG-HH-ALPSRP100147010-H1.0_A:IMG-HH-ALPSRP106857010-H1.0_A
IMG-HH-ALPSRP100147010-H1.0_A:IMG-HH-ALPSRP147117010-H1.0_A
IMG-HH-ALPSRP100147010-H1.0_A:IMG-HH-ALPSRP153827010-H1.0_A
IMG-HH-ALPSRP100147010-H1.0_A:IMG-HH-ALPSRP160537010-H1.0_A
IMG-HH-ALPSRP100147010-H1.0_A:IMG-HH-ALPSRP200797010-H1.0_A
IMG-HH-ALPSRP100147010-H1.0_A:IMG-HH-ALPSRP214217010-H1.0_A
IMG-HH-ALPSRP100147010-H1.0_A:IMG-HH-ALPSRP261187010-H1.0_A
IMG-HH-ALPSRP106857010-H1.0_A:IMG-HH-ALPSRP147117010-H1.0_A
IMG-HH-ALPSRP106857010-H1.0_A:IMG-HH-ALPSRP153827010-H1.0_A
IMG-HH-ALPSRP106857010-H1.0_A:IMG-HH-ALPSRP160537010-H1.0_A
IMG-HH-ALPSRP106857010-H1.0_A:IMG-HH-ALPSRP200797010-H1.0_A
IMG-HH-ALPSRP106857010-H1.0_A:IMG-HH-ALPSRP214217010-H1.0_A
IMG-HH-ALPSRP147117010-H1.0_A:IMG-HH-ALPSRP153827010-H1.0_A
IMG-HH-ALPSRP147117010-H1.0_A:IMG-HH-ALPSRP160537010-H1.0_A
IMG-HH-ALPSRP147117010-H1.0_A:IMG-HH-ALPSRP200797010-H1.0_A
IMG-HH-ALPSRP147117010-H1.0_A:IMG-HH-ALPSRP214217010-H1.0_A
IMG-HH-ALPSRP147117010-H1.0_A:IMG-HH-ALPSRP261187010-H1.0_A
IMG-HH-ALPSRP153827010-H1.0_A:IMG-HH-ALPSRP160537010-H1.0_A
IMG-HH-ALPSRP153827010-H1.0_A:IMG-HH-ALPSRP200797010-H1.0_A
IMG-HH-ALPSRP153827010-H1.0_A:IMG-HH-ALPSRP214217010-H1.0_A
IMG-HH-ALPSRP153827010-H1.0_A:IMG-HH-ALPSRP261187010-H1.0_A
IMG-HH-ALPSRP160537010-H1.0_A:IMG-HH-ALPSRP200797010-H1.0_A
IMG-HH-ALPSRP160537010-H1.0_A:IMG-HH-ALPSRP214217010-H1.0_A
IMG-HH-ALPSRP200797010-H1.0_A:IMG-HH-ALPSRP214217010-H1.0_A
IMG-HH-ALPSRP214217010-H1.0_A:IMG-HH-ALPSRP261187010-H1.0_A
```

```
align.in
IMG-HH-ALPSRP093437010-H1.0_A:IMG-HH-ALPSRP100147010-H1.0_A:IMG-HH-ALPSRP093437010-H1.0_A
IMG-HH-ALPSRP093437010-H1.0_A:IMG-HH-ALPSRP106857010-H1.0_A:IMG-HH-ALPSRP093437010-H1.0_A
IMG-HH-ALPSRP093437010-H1.0_A:IMG-HH-ALPSRP147117010-H1.0_A:IMG-HH-ALPSRP093437010-H1.0_A
IMG-HH-ALPSRP093437010-H1.0_A:IMG-HH-ALPSRP153827010-H1.0_A:IMG-HH-ALPSRP093437010-H1.0_A
IMG-HH-ALPSRP093437010-H1.0_A:IMG-HH-ALPSRP160537010-H1.0_A:IMG-HH-ALPSRP093437010-H1.0_A
IMG-HH-ALPSRP093437010-H1.0_A:IMG-HH-ALPSRP200797010-H1.0_A:IMG-HH-ALPSRP093437010-H1.0_A
IMG-HH-ALPSRP093437010-H1.0_A:IMG-HH-ALPSRP214217010-H1.0_A:IMG-HH-ALPSRP093437010-H1.0_A
IMG-HH-ALPSRP093437010-H1.0_A:IMG-HH-ALPSRP261187010-H1.0_A:IMG-HH-ALPSRP093437010-H1.0_A
IMG-HH-ALPSRP100147010-H1.0_A:IMG-HH-ALPSRP106857010-H1.0_A:IMG-HH-ALPSRP093437010-H1.0_A
IMG-HH-ALPSRP100147010-H1.0_A:IMG-HH-ALPSRP147117010-H1.0_A:IMG-HH-ALPSRP093437010-H1.0_A
IMG-HH-ALPSRP100147010-H1.0_A:IMG-HH-ALPSRP153827010-H1.0_A:IMG-HH-ALPSRP093437010-H1.0_A
IMG-HH-ALPSRP100147010-H1.0_A:IMG-HH-ALPSRP160537010-H1.0_A:IMG-HH-ALPSRP093437010-H1.0_A
IMG-HH-ALPSRP100147010-H1.0_A:IMG-HH-ALPSRP200797010-H1.0_A:IMG-HH-ALPSRP093437010-H1.0_A
IMG-HH-ALPSRP100147010-H1.0_A:IMG-HH-ALPSRP214217010-H1.0_A:IMG-HH-ALPSRP093437010-H1.0_A
IMG-HH-ALPSRP100147010-H1.0_A:IMG-HH-ALPSRP261187010-H1.0_A:IMG-HH-ALPSRP093437010-H1.0_A
```

IMG-HH-ALPSRP106857010-H1.0\_A:IMG-HH-ALPSRP160537010-H1.0\_A:IMG-HH-ALPSRP093437010-H1.0\_A  
IMG-HH-ALPSRP106857010-H1.0\_A:IMG-HH-ALPSRP200797010-H1.0\_A:IMG-HH-ALPSRP093437010-H1.0\_A  
IMG-HH-ALPSRP106857010-H1.0\_A:IMG-HH-ALPSRP214217010-H1.0\_A:IMG-HH-ALPSRP093437010-H1.0\_A  
IMG-HH-ALPSRP147117010-H1.0\_A:IMG-HH-ALPSRP153827010-H1.0\_A:IMG-HH-ALPSRP093437010-H1.0\_A  
IMG-HH-ALPSRP147117010-H1.0\_A:IMG-HH-ALPSRP160537010-H1.0\_A:IMG-HH-ALPSRP093437010-H1.0\_A  
IMG-HH-ALPSRP147117010-H1.0\_A:IMG-HH-ALPSRP200797010-H1.0\_A:IMG-HH-ALPSRP093437010-H1.0\_A  
IMG-HH-ALPSRP147117010-H1.0\_A:IMG-HH-ALPSRP214217010-H1.0\_A:IMG-HH-ALPSRP093437010-H1.0\_A  
IMG-HH-ALPSRP153827010-H1.0\_A:IMG-HH-ALPSRP160537010-H1.0\_A:IMG-HH-ALPSRP093437010-H1.0\_A  
IMG-HH-ALPSRP153827010-H1.0\_A:IMG-HH-ALPSRP200797010-H1.0\_A:IMG-HH-ALPSRP093437010-H1.0\_A  
IMG-HH-ALPSRP153827010-H1.0\_A:IMG-HH-ALPSRP214217010-H1.0\_A:IMG-HH-ALPSRP093437010-H1.0\_A  
IMG-HH-ALPSRP160537010-H1.0\_A:IMG-HH-ALPSRP200797010-H1.0\_A:IMG-HH-ALPSRP093437010-H1.0\_A  
IMG-HH-ALPSRP160537010-H1.0\_A:IMG-HH-ALPSRP214217010-H1.0\_A:IMG-HH-ALPSRP093437010-H1.0\_A  
IMG-HH-ALPSRP200797010-H1.0\_A:IMG-HH-ALPSRP214217010-H1.0\_A:IMG-HH-ALPSRP093437010-H1.0\_A  
IMG-HH-ALPSRP214217010-H1.0\_A:IMG-HH-ALPSRP261187010-H1.0\_A:IMG-HH-ALPSRP093437010-H1.0\_A

align\_batch.csh ALOS align.in

```
ALIGN.CSH - START
focussing master
Computing range reference function.
Processing patch 1
Processing Elapsed Time: 0 min 0.04 sec
Range Compression
Processing Elapsed Time: 0 min 5.69 sec
Azimuthal Transform
Processing Elapsed Time: 0 min 13.58 sec
Range Migration
Processing Elapsed Time: 0 min 23.50 sec
Azimuthal Compression
Processing Elapsed Time: 0 min 45.94 sec
Writing Data
Processing patch 2
Processing Elapsed Time: 0 min 47.45 sec
Range Compression
Processing Elapsed Time: 0 min 52.11 sec
Azimuthal Transform
Processing Elapsed Time: 0 min 59.99 sec
Range Migration
Processing Elapsed Time: 1 min 9.89 sec
Azimuthal Compression
Processing Elapsed Time: 1 min 33.02 sec
Writing Data
Processing patch 3
Processing Elapsed Time: 1 min 34.59 sec
Range Compression
Processing Elapsed Time: 1 min 39.19 sec
Azimuthal Transform
Processing Elapsed Time: 1 min 47.28 sec
Range Migration
Processing Elapsed Time: 1 min 57.19 sec
Azimuthal Compression
Processing Elapsed Time: 2 min 19.92 sec
Writing Data
Processing Elapsed Time: 2 min 21.44 sec
number of points clipped to short int 53
align.csh
focussing slave
Computing range reference function.
Processing patch 1
Processing Elapsed Time: 0 min 0.03 sec
Range Compression
Processing Elapsed Time: 0 min 5.57 sec
Azimuthal Transform
Processing Elapsed Time: 0 min 13.87 sec
Range Migration
Processing Elapsed Time: 0 min 23.93 sec
Azimuthal Compression
Processing Elapsed Time: 0 min 47.04 sec
Writing Data
Processing patch 2
Processing Elapsed Time: 0 min 48.58 sec
Range Compression
Processing Elapsed Time: 0 min 53.18 sec
Azimuthal Transform
Processing Elapsed Time: 1 min 1.26 sec
Range Migration
Processing Elapsed Time: 1 min 11.19 sec
Azimuthal Compression
Processing Elapsed Time: 1 min 35.27 sec
Writing Data
Processing patch 3
Processing Elapsed Time: 1 min 36.80 sec
Range Compression
Processing Elapsed Time: 1 min 41.44 sec
Azimuthal Transform
Processing Elapsed Time: 1 min 49.63 sec
Range Migration
Processing Elapsed Time: 1 min 59.54 sec
Azimuthal Compression
Processing Elapsed Time: 2 min 23.60 sec
Writing Data
Processing Elapsed Time: 2 min 25.14 sec
number of points clipped to short int 175
align.csh
correlate master and slave to find offset parameters
setting xsearch to 64
setting nx_corr to 128
setting ysearch to 64
setting ny_corr to 128
11304 27648 11304 27648 104 68 -0.002141
locations n 512 nx 11304 nyl 32 nxl 16 x_inc 574 y_inc 826
elapsed time: 19.338003
align.csh
refocus slave
Computing range reference function.
Processing patch 1
Processing Elapsed Time: 0 min 0.03 sec
Range Compression
Processing Elapsed Time: 0 min 5.83 sec
Azimuthal Transform
Processing Elapsed Time: 0 min 20.32 sec
Range Migration
Processing Elapsed Time: 0 min 30.42 sec
Azimuthal Compression
Processing Elapsed Time: 1 min 3.81 sec
apply azimuth-dependent azimuth shift
Processing Elapsed Time: 1 min 28.67 sec
Writing Data
Processing patch 2
```

Processing Elapsed Time: 1 min 35.16 sec  
Range Compression  
Processing Elapsed Time: 1 min 39.93 sec  
Azimuthal Transform  
Processing Elapsed Time: 1 min 49.27 sec  
Range Migration  
Processing Elapsed Time: 1 min 59.38 sec  
Azimuthal Compression  
Processing Elapsed Time: 2 min 29.37 sec  
apply azimuth-dependent azimuth shift  
Processing Elapsed Time: 2 min 56.98 sec  
Writing Data  
Processing patch 3  
Processing Elapsed Time: 3 min 3.89 sec  
Range Compression  
Processing Elapsed Time: 3 min 8.54 sec  
Azimuthal Transform  
Processing Elapsed Time: 3 min 18.00 sec  
Range Migration  
Processing Elapsed Time: 3 min 28.25 sec  
Azimuthal Compression  
Processing Elapsed Time: 4 min 2.25 sec  
apply azimuth-dependent azimuth shift  
Processing Elapsed Time: 4 min 28.31 sec  
Writing Data  
Processing Elapsed Time: 4 min 35.06 sec  
number of points clipped to short int 187  
rm: No match.  
ALIGN.CSH - END

intf\_batch.csh ALOS batch.config  
clean up topo/ folder

DEM2TOPO\_RA.CSH - START  
USER SHOULD PROVIDE DEM FILE  
range decimation is: 2  
blockmedian: Provides 3, expects 3-column binary data  
blockmedian: Processing input table data  
blockmedian: W: 0 E: 11304 S: 0 N: 27648 n\_columns: 5652 n\_rows: 6912  
blockmedian: Input 3 columns via binary records using format ddd  
blockmedian: Output 3 columns via binary records using format ddd  
blockmedian: N read: 880412 N used: 877562 outside\_area: 2850 N cells filled: 877534  
surface: Provides 3, expects 3-column binary data  
surface: Grid domain: W: 0 E: 11304 S: 0 N: 27648 n\_columns: 5652 n\_rows: 6912 [pixel registration]  
surface: Processing input table data  
surface: Input 3 columns via binary records using format ddd  
surface: Minimum value of your dataset x,y,z at: surface: 9.47925853729 20.111221313 79.1265945435  
surface: Maximum value of your dataset x,y,z at: surface: 4982.25195312 19988.2792969 3152.45239258  
surface: LS plane determined: z = 203.081 + (-0.005365 \* col) + (0.111885 \* row)  
surface: Grid Mode IterationMax Change Conv Limit Total Iterations  
surface: 36 D 22 0.000546255543946 0.00086758828296 22  
surface: 12 I 28 0.00218929156934 0.0026027648489 50  
surface: 12 D 20 0.00178716015478 0.0026027648489 70  
surface: 4 I 25 0.00575992186722 0.0078082945467 95  
surface: 4 D 42 0.00697227533129 0.0078082945467 137  
surface: 2 I 18 0.0144953689828 0.0156165890934 155  
surface: 2 D 92 0.0155055815236 0.0156165890934 247  
surface: 1 I 16 0.0282327391979 0.0312331781868 263  
surface: 1 D 245 0.0309639238689 0.0312331781868 508  
surface: Fit info: N data points N nodes mean error rms errorcurvature  
surface: 877534 39079189 -3.16770048757e-06 0.0062199362068 22227.5479258  
grd2cpt: Processing input grid(s)  
grd2cpt: Mean and S.D. of data are 349.387377152 406.116523212  
grdimage: Allocates memory and read data file topo\_ra.grd  
grdimage: Evaluate image pixel colors  
grdimage: Creating 8-bit grayscale image  
DEM2TOPO\_RA.CSH - END  
NO TOPO\_RA SHIFT

START FORM A STACK OF INTERFEROGRAMS

INTF.CSH, FILTER.CSH - START  
intf.csh  
running phasediff...  
reading topo topo\_ra.grd  
xdim 11304, ydim 27648  
filter.csh  
gauss\_300 4 2 (4 2)  
making amplitudes...  
filtering interferogram...  
making amplitude...  
making correlation...  
making phase...  
filtering phase...  
INTF.CSH, FILTER.CSH - END

SNAPHU.CSH - START  
threshold\_snaphu: .45  
grdmath: Perform reverse Polish notation calculations on grids  
grdmath: phase\_patch.grd landmask\_ra\_patch.grd MUL = phase\_patch.grd  
unwrapping phase with snaphu - higher threshold for faster unwrapping

snaphu v1.4.2  
32 parameters input from file snaphu.conf.brief (297 lines total)  
Reading wrapped phase from file phase.in  
No weight file specified. Assuming uniform weights  
Reading correlation data from file corr.in  
Calculating deformation-mode cost parameters  
Building range cost arrays  
Building azimuth cost arrays  
Initializing flows with MST algorithm  
Running approximate minimum spanning tree solver  
Running nonlinear network flow optimizer  
Maximum flow on network: 3  
Number of nodes in network: 4878776  
Flow increment: 1 (Total improvements: 0)  
Treesize: 4878776 Pivots: 5720 Improvements: 120  
Maximum flow on network: 2  
Flow increment: 2 (Total improvements: 120)  
Treesize: 4878776 Pivots: 10 Improvements: 5  
Maximum flow on network: 2  
Total solution cost: 474662  
Integrating phase  
Writing output to file unwrap.out  
Program snaphu done  
Elapsed processor time: 0:01:03.42  
Elapsed wall clock time: 0:01:08



```
grdmath: Perform reverse Polish notation calculations on grids
grdmath: unwrap.grd landmask_ra_patch.grd MUL = tmp.grd
SNAPHU.CSH - END

GEOCODE.CSH - START
threshold_geocode: .45
grdmath: Perform reverse Polish notation calculations on grids
grdmath: corr.grd 0.45 GE 0 NAN mask.grd MUL = mask2.grd
psscale: Warning: The -E option is deprecated but is accepted.
psscale: For the current -D syntax you should use -D modifier +e instead.
psscale: Note you cannot mix new-style modifiers (+e) with the old-style -D option.
psscale: Warning: The -E option is deprecated but is accepted.
psscale: For the current -D syntax you should use -D modifier +e instead.
psscale: Note you cannot mix new-style modifiers (+e) with the old-style -D option.
geocode.csh
project correlation, phase, unwrapped and amplitude back to lon lat coordinates
remarked is by root on Sun May 20 18:18:26 JST 2018 with geocode.csh
proj_ra2ll.csh
surface: Provides 3, expects 3-column binary data
surface: Grid domain: W: 64 E: 11168 S: 0 N: 27648 n_columns: 694 n_rows: 864 [gridline registration]
surface: Processing input table data
surface: Input 3 columns via binary records using format fff
surface: Minimum value of your dataset x,y,z at: surface: 67.533164978 27658.8203125 114.555831909
surface: Maximum value of your dataset x,y,z at: surface: 11173.3945312 65.1778945923 115.464164734
surface: 275394 unusable points were supplied; these will be ignored.
surface: You should have pre-processed the data with block-mean, -median, or -mode.
surface: Check that previous processing steps write results with enough decimals.
surface: LS plane determined: z = 114.732 + (0.0010656 * col) + (-0.000193916 * row)
surface: Grid Mode IterationMax Change Conv Limit Total Iterations
surface: 2 D 21 1.18721530527e-07 2.11642910597e-07 21
surface: 1 I 17 3.20632926145e-07 4.23285821194e-07 38
surface: 1 D 19 3.20250274163e-07 4.23285821194e-07 57
surface: Fit info: N data points N nodes mean error rms error curvature
surface: 596815 601175 7.48553167841e-06 0.00723721464458 12923.6118694
surface: Provides 3, expects 3-column binary data
surface: Grid domain: W: 64 E: 11168 S: 0 N: 27648 n_columns: 694 n_rows: 864 [gridline registration]
surface: Processing input table data
surface: Input 3 columns via binary records using format fff
surface: Minimum value of your dataset x,y,z at: surface: 64.4236907959 2.82209205627 -8.98750019073
surface: Maximum value of your dataset x,y,z at: surface: 11159.8701172 27663.1875 -8.04416656494
surface: 275394 unusable points were supplied; these will be ignored.
surface: You should have pre-processed the data with block-mean, -median, or -mode.
surface: Check that previous processing steps write results with enough decimals.
surface: LS plane determined: z = -8.98658 + (0.000240361 * col) + (0.000901273 * row)
surface: Grid Mode IterationMax Change Conv Limit Total Iterations
surface: 2 D 21 2.70047037799e-08 4.57862044979e-08 21
surface: 1 I 17 7.44972555822e-08 9.15724089959e-08 38
surface: 1 D 19 7.32045858772e-08 9.15724089959e-08 57
surface: Fit info: N data points N nodes mean error rms error curvature
surface: 596815 601175 -3.2921637132e-07 0.0106658565621 15656.0536096
blockmedian: Provides 3, expects 3-column binary data
blockmedian: Processing input table data
blockmedian: W: 114.555555556 E: 115.466666667 S: -8.98611111111 N: -8.04166666667 n_columns: 820 n_rows: 1360
blockmedian: Input 3 columns via binary records using format fff
blockmedian: Output 3 columns via binary records using format fff
blockmedian: N read: 4730579 N used: 4730579 outside_area: 0 N cells filled: 773617
proj_ra2ll.csh
blockmedian: Provides 3, expects 3-column binary data
blockmedian: Processing input table data
blockmedian: W: 114.555555556 E: 115.466666667 S: -8.98611111111 N: -8.04166666667 n_columns: 820 n_rows: 1360
blockmedian: Input 3 columns via binary records using format fff
blockmedian: Output 3 columns via binary records using format fff
blockmedian: N read: 4735604 N used: 4735604 outside_area: 0 N cells filled: 774482
proj_ra2ll.csh
blockmedian: Provides 3, expects 3-column binary data
blockmedian: Processing input table data
blockmedian: W: 114.588888889 E: 115.4 S: -8.85416666667 N: -8.0625 n_columns: 730 n_rows: 1140
blockmedian: Input 3 columns via binary records using format fff
blockmedian: Output 3 columns via binary records using format fff
blockmedian: N read: 237698 N used: 237698 outside_area: 0 N cells filled: 53319
proj_ra2ll.csh
blockmedian: Provides 3, expects 3-column binary data
blockmedian: Processing input table data
blockmedian: W: 114.555555556 E: 115.466666667 S: -8.99305555556 N: -8.04166666667 n_columns: 820 n_rows: 1370
blockmedian: Input 3 columns via binary records using format fff
blockmedian: Output 3 columns via binary records using format fff
blockmedian: N read: 4796928 N used: 4796928 outside_area: 0 N cells filled: 784244
proj_ra2ll.csh
blockmedian: Provides 3, expects 3-column binary data
blockmedian: Processing input table data
blockmedian: W: 114.588888889 E: 115.4 S: -8.85416666667 N: -8.0625 n_columns: 730 n_rows: 1140
blockmedian: Input 3 columns via binary records using format fff
blockmedian: Output 3 columns via binary records using format fff
blockmedian: N read: 237269 N used: 237269 outside_area: 0 N cells filled: 53185
proj_ra2ll.csh
blockmedian: Provides 3, expects 3-column binary data
blockmedian: Processing input table data
blockmedian: W: 114.555555556 E: 115.444444444 S: -8.85416666667 N: -8.0625 n_columns: 800 n_rows: 1140
blockmedian: Input 3 columns via binary records using format fff
blockmedian: Output 3 columns via binary records using format fff
blockmedian: N read: 2514628 N used: 2514628 outside_area: 0 N cells filled: 409503
proj_ra2ll.csh
blockmedian: Provides 3, expects 3-column binary data
blockmedian: Processing input table data
blockmedian: W: 114.588888889 E: 115.4 S: -8.85416666667 N: -8.0625 n_columns: 730 n_rows: 1140
blockmedian: Input 3 columns via binary records using format fff
blockmedian: Output 3 columns via binary records using format fff
blockmedian: N read: 237698 N used: 237698 outside_area: 0 N cells filled: 53319
geocode.csh
make the KML files for Google Earth
grdimage: Allocates memory and read data file display_amp_ll.grd
grdimage: Evaluate image pixel colors
grdimage: Creating 24-bit color image
Make display_amp_ll.kml and display_amp_ll.png
psconvert: Processing display_amp_ll.ps...
psconvert: Figure dimensions: Width: 65.58 points [0.910833 inch] Height: 68.52 points [0.951666 inch]
psconvert: gs -q -dSAFER -dNOPAUSE -dBATCH -dPDFSETTINGS=/prepress -dDownsampleColorImages=false -dDownsampleGrayImages=false -
dDownsampleMonoImages=false -dUseFlateCompression=true -dEmbedAllFonts=true -dSubsetFonts=true -dMonoImageFilter=/FlateEncode -
dAutoFilterGrayImages=false -dGrayImageFilter=/FlateEncode -dAutoFilterColorImages=false -dColorImageFilter=/FlateEncode -dSCANCONVERTERTYPE=2 -
dMaxBitmap=2147483647 -dUseFastColor=true -dDEVICE=pngalpha -g820x857 -r900 -sOutputFile=display_amp_ll.png' -f'./psconvert_1496Id.eps'
psconvert: Done
grdimage: Allocates memory and read data file corr_ll.grd
grdimage: Evaluate image pixel colors
grdimage: Creating 24-bit color image
PSL: Colormap of 256 colors created
Make corr_ll.kml and corr_ll.png
psconvert: Processing corr_ll.ps...
psconvert: Figure dimensions: Width: 65.58 points [0.910833 inch] Height: 67.98 points [0.944166 inch]
```

```
psconvert: gs -q -dSAFER -dNOPAUSE -dBATCH -dPDFSETTINGS=/prepress -dDownsampleColorImages=false -dDownsampleGrayImages=false -dDownsampleMonoImages=false -dUseFastColor=true -dUseFlateCompression=true -dEmbedAllFonts=true -dSubsetFonts=true -dMonoImageFilter=/FlateEncode -dAutoFilterGrayImages=false -dGrayImageFilter=/FlateEncode -dAutoFilterColorImages=false -dColorImageFilter=/FlateEncode -dSCANCONVERTERTYPE=2 -dMaxBitmap=2147483647 -dUseFastColor=true -sDEVICE=pngalpha -g820x850 -r900 -sOutputFile='corr_ll.png' -f'./psconvert_15110d.eps'
psconvert: Done.
grdimage: Allocates memory and read data file phase_mask_ll.grd
grdimage: Evaluate image pixel colors
grdimage: Creating 24-bit color image
Make phase_mask_ll.kml and phase_mask_ll.png
psconvert: Processing phase_mask_ll.ps...
psconvert: Figure dimensions: Width: 58.38 points [0.810833 inch] Height: 57 points [0.791666 inch]
psconvert: gs -q -dSAFER -dNOPAUSE -dBATCH -dPDFSETTINGS=/prepress -dDownsampleColorImages=false -dDownsampleGrayImages=false -dDownsampleMonoImages=false -dUseFlateCompression=true -dEmbedAllFonts=true -dSubsetFonts=true -dMonoImageFilter=/FlateEncode -dAutoFilterGrayImages=false -dGrayImageFilter=/FlateEncode -dAutoFilterColorImages=false -dColorImageFilter=/FlateEncode -dSCANCONVERTERTYPE=2 -dMaxBitmap=2147483647 -dUseFastColor=true -sDEVICE=pngalpha -g730x713 -r900 -sOutputFile='phase_mask_ll.png' -f'./psconvert_15211d.eps'
psconvert: Done.
grdimage: Allocates memory and read data file phasefilt_mask_ll.grd
grdimage: Evaluate image pixel colors
grdimage: Creating 24-bit color image
Make phasefilt_mask_ll.kml and phasefilt_mask_ll.png
psconvert: Processing phasefilt_mask_ll.ps...
psconvert: Figure dimensions: Width: 58.38 points [0.810833 inch] Height: 57 points [0.791666 inch]
psconvert: gs -q -dSAFER -dNOPAUSE -dBATCH -dPDFSETTINGS=/prepress -dDownsampleColorImages=false -dDownsampleGrayImages=false -dDownsampleMonoImages=false -dUseFlateCompression=true -dEmbedAllFonts=true -dSubsetFonts=true -dMonoImageFilter=/FlateEncode -dAutoFilterGrayImages=false -dGrayImageFilter=/FlateEncode -dAutoFilterColorImages=false -dColorImageFilter=/FlateEncode -dSCANCONVERTERTYPE=2 -dMaxBitmap=2147483647 -dUseFastColor=true -sDEVICE=pngalpha -g730x713 -r900 -sOutputFile='phasefilt_mask_ll.png' -f'./psconvert_15288d.eps'
psconvert: Done.
grdimage: Allocates memory and read data file unwrap_mask_ll.grd
grdimage: Evaluate image pixel colors
grdimage: Creating 24-bit color image
Make unwrap_mask_ll.kml and unwrap_mask_ll.png
psconvert: Processing unwrap_mask_ll.ps...
psconvert: Figure dimensions: Width: 58.38 points [0.810833 inch] Height: 57 points [0.791666 inch]
psconvert: gs -q -dSAFER -dNOPAUSE -dBATCH -dPDFSETTINGS=/prepress -dDownsampleColorImages=false -dDownsampleGrayImages=false -dDownsampleMonoImages=false -dUseFlateCompression=true -dEmbedAllFonts=true -dSubsetFonts=true -dMonoImageFilter=/FlateEncode -dAutoFilterGrayImages=false -dGrayImageFilter=/FlateEncode -dAutoFilterColorImages=false -dColorImageFilter=/FlateEncode -dSCANCONVERTERTYPE=2 -dMaxBitmap=2147483647 -dUseFastColor=true -sDEVICE=pngalpha -g730x713 -r900 -sOutputFile='unwrap_mask_ll.png' -f'./psconvert_15350d.eps'
psconvert: Done.
grdimage: Allocates memory and read data file phasefilt_mask_ll.grd
grdimage: Evaluate image pixel colors
grdimage: Creating 24-bit color image
Make phasefilt_mask_ll.kml and phasefilt_mask_ll.png
psconvert: Processing phasefilt_mask_ll.ps...
psconvert: Figure dimensions: Width: 58.38 points [0.810833 inch] Height: 57 points [0.791666 inch]
psconvert: gs -q -dSAFER -dNOPAUSE -dBATCH -dPDFSETTINGS=/prepress -dDownsampleColorImages=false -dDownsampleGrayImages=false -dDownsampleMonoImages=false -dUseFlateCompression=true -dEmbedAllFonts=true -dSubsetFonts=true -dMonoImageFilter=/FlateEncode -dAutoFilterGrayImages=false -dGrayImageFilter=/FlateEncode -dAutoFilterColorImages=false -dColorImageFilter=/FlateEncode -dSCANCONVERTERTYPE=2 -dMaxBitmap=2147483647 -dUseFastColor=true -sDEVICE=pngalpha -g730x713 -r900 -sOutputFile='phasefilt_mask_ll.png' -f'./psconvert_15455d.eps'
psconvert: Done.
grdimage: Allocates memory and read data file los_ll.grd
grdimage: Evaluate image pixel colors
grdimage: Creating 24-bit color image
Make los_ll.kml and los_ll.png
psconvert: Processing los_ll.ps...
psconvert: Figure dimensions: Width: 58.38 points [0.810833 inch] Height: 57 points [0.791666 inch]
psconvert: gs -q -dSAFER -dNOPAUSE -dBATCH -dPDFSETTINGS=/prepress -dDownsampleColorImages=false -dDownsampleGrayImages=false -dDownsampleMonoImages=false -dUseFlateCompression=true -dEmbedAllFonts=true -dSubsetFonts=true -dMonoImageFilter=/FlateEncode -dAutoFilterGrayImages=false -dGrayImageFilter=/FlateEncode -dAutoFilterColorImages=false -dColorImageFilter=/FlateEncode -dSCANCONVERTERTYPE=2 -dMaxBitmap=2147483647 -dUseFastColor=true -sDEVICE=pngalpha -g730x713 -r900 -sOutputFile='los_ll.png' -f'./psconvert_15559d.eps'
psconvert: Done.
GEOCODE.CSH - END
```

```
stack.list
cut_2007299_2007345.grd IMG-HH-ALPSRP093437010-H1.0_A.PRM IMG-HH-ALPSRP100147010-H1.0_A.PRM
cut_2007299_2008026.grd IMG-HH-ALPSRP093437010-H1.0_A.PRM IMG-HH-ALPSRP106857010-H1.0_A.PRM
cut_2007299_2008302.grd IMG-HH-ALPSRP093437010-H1.0_A.PRM IMG-HH-ALPSRP147117010-H1.0_A.PRM
cut_2007299_2008348.grd IMG-HH-ALPSRP093437010-H1.0_A.PRM IMG-HH-ALPSRP153827010-H1.0_A.PRM
cut_2007299_2009028.grd IMG-HH-ALPSRP093437010-H1.0_A.PRM IMG-HH-ALPSRP160537010-H1.0_A.PRM
cut_2007299_2009304.grd IMG-HH-ALPSRP093437010-H1.0_A.PRM IMG-HH-ALPSRP200797010-H1.0_A.PRM
cut_2007299_2010031.grd IMG-HH-ALPSRP093437010-H1.0_A.PRM IMG-HH-ALPSRP214217010-H1.0_A.PRM
cut_2007299_2010353.grd IMG-HH-ALPSRP093437010-H1.0_A.PRM IMG-HH-ALPSRP261187010-H1.0_A.PRM
```

```
bash stack_phase.bash stack.list mean.grd std.grd
```

```
compute the mean LOS velocity ..
```

```
time span (days) of cut_2007299_2007345.grd: 46
accumulative days in the stack: 46
time span (days) of cut_2007299_2008026.grd: 92
accumulative days in the stack: 138
time span (days) of cut_2007299_2008302.grd: 368
accumulative days in the stack: 506
time span (days) of cut_2007299_2008348.grd: 414
accumulative days in the stack: 920
time span (days) of cut_2007299_2009028.grd: 459
accumulative days in the stack: 1379
time span (days) of cut_2007299_2009304.grd: 735
accumulative days in the stack: 2114
time span (days) of cut_2007299_2010031.grd: 827
accumulative days in the stack: 2941
time span (days) of cut_2007299_2010353.grd: 1149
accumulative days in the stack: 4090
```

```
compute the standard deviations ..
```

```
mean_ll.grd
std_ll.grd
los_ll_2007345.grd
los_ll_2008026.grd
los_ll_2008302.grd
los_ll_2008348.grd
los_ll_2009028.grd
los_ll_2009304.grd
los_ll_2010031.grd
los_ll_2010353.grd
```

```
csh select_pairs.csh baseline_table.dat 950 1000
```

```
intf.tab
cut_2007299_2007345.grd corcut_2007299_2007345.grd 2007299 2007345 -271.096790
cut_2007299_2008026.grd corcut_2007299_2008026.grd 2007299 2008026 -472.345306
cut_2007299_2008302.grd corcut_2007299_2008302.grd 2007299 2008302 725.057614
cut_2007299_2008348.grd corcut_2007299_2008348.grd 2007299 2008348 691.291677
cut_2007299_2009028.grd corcut_2007299_2009028.grd 2007299 2009028 392.503573
cut_2007299_2009304.grd corcut_2007299_2009304.grd 2007299 2009304 87.717368
cut_2007299_2010031.grd corcut_2007299_2010031.grd 2007299 2010031 -66.447985
cut_2007345_2008026.grd corcut_2007345_2008026.grd 2007345 2008026 -201.241131
cut_2007345_2008302.grd corcut_2007345_2008302.grd 2007345 2008302 996.318542
cut_2007345_2008348.grd corcut_2007345_2008348.grd 2007345 2008348 962.580536
```

```

cut_2007345_2009028.grd corcut_2007345_2009028.grd 2007345 2009028 663.724393
cut_2007345_2009304.grd corcut_2007345_2009304.grd 2007345 2009304 358.863575
cut_2007345_2010031.grd corcut_2007345_2010031.grd 2007345 2010031 204.696313
cut_2008026_2009028.grd corcut_2008026_2009028.grd 2008026 2009028 864.809514
cut_2008026_2009304.grd corcut_2008026_2009304.grd 2008026 2009304 560.044992
cut_2008026_2010031.grd corcut_2008026_2010031.grd 2008026 2010031 405.887107
cut_2008302_2008348.grd corcut_2008302_2008348.grd 2008302 2008348 -33.722313
cut_2008302_2009028.grd corcut_2008302_2009028.grd 2008302 2009028 -332.631933
cut_2008302_2009304.grd corcut_2008302_2009304.grd 2008302 2009304 -637.562282
cut_2008302_2010031.grd corcut_2008302_2010031.grd 2008302 2010031 -791.767313
cut_2008348_2009028.grd corcut_2008348_2009028.grd 2008348 2009028 -298.852998
cut_2008348_2009304.grd corcut_2008348_2009304.grd 2008348 2009304 -603.719689
cut_2008348_2010031.grd corcut_2008348_2010031.grd 2008348 2010031 -757.918547
cut_2009028_2009304.grd corcut_2009028_2009304.grd 2009028 2009304 -304.873018
cut_2009028_2010031.grd corcut_2009028_2010031.grd 2009028 2010031 -459.067734
cut_2009304_2010031.grd corcut_2009304_2010031.grd 2009304 2010031 -154.182362
cut_2010031_2010353.grd corcut_2010031_2010353.grd 2010031 2010353 -877.100652

```

```

scene.tab
2007299 664
2007345 710
2008026 756
2008302 1032
2008348 1078
2009028 1123
2009304 1399
2010031 1491
2010353 1813

```

```
sbas intf.tab scene.tab 27 9 2826 1728 -smooth 1.0 -wavelength 0.2362 -incidence 34.3 -range 849714 -rms -dem -atm 1
```

```

compute RMS misfit
compute DEM error

```

```

setting smoothing to 1.000
setting radar wavelength to 0.236 m
setting radar incidence angle to 34.300 degree
setting range to 849714.000 m
Memory Allocation Successful...
read table file ...
number of SAR scenes is 9
number of interferograms is 27
read phase and correlation grids ...
fill the G matrix ...

```

Applying atmospheric correction by common point stacking...

```

Hit Matrix:
2007299 0 1 1 1 1 1 1 0
2007345 0 0 1 1 1 1 1 0
2008026 0 0 0 0 1 1 1 0
2008302 0 0 0 0 1 1 1 0
2008348 0 0 0 0 1 1 1 0
2009028 0 0 0 0 0 1 1 0
2009304 0 0 0 0 0 0 1 0
2010031 0 0 0 0 0 0 0 1
2010353 0 0 0 0 0 0 0 0

```

Applying exponential relaxation on smoothing parameters

```

Setting smoothing parameter to 1000.000000...
fill the G matrix ...
Computing deformation time-series...
run least-squares problem over 2826 by 1728 pixel (0) ...
matrix is full rank: 9

```

Removing deformation time-series from original unwrapped phase...

```

Computing atmospheric phase screen by common-point stacking...
Initial estimate of APS...
atm_noise(NO.3) = 10.905028
atm_noise(NO.4) = 4.935258
atm_noise(NO.5) = 1.953275
atm_noise(NO.1) = 1.095303
atm_noise(NO.0) = 0.000000
atm_noise(NO.2) = 0.000000
atm_noise(NO.6) = 0.000000
atm_noise(NO.7) = 0.000000
atm_noise(NO.8) = 0.000000

```

```

atm_noise(NO.3) = 10.898907
atm_noise(NO.4) = 2.637189
atm_noise(NO.5) = 1.951638
atm_noise(NO.1) = 1.088181
atm_noise(NO.0) = 0.000000
atm_noise(NO.2) = 0.000000
atm_noise(NO.6) = 0.000000
atm_noise(NO.7) = 0.000000
atm_noise(NO.8) = 0.000000

```

Applying atmospheric phase screen to original unwrapped phase...

```

Setting smoothing parameter to 1.000000...
fill the G matrix ...
run least-squares problem over 2826 by 1728 pixel (3) ...
matrix is rank-deficient: 8

```

write output ...

```

raln.grd
ralt.grd
rms_ll.grd
dem.grd
vel_ll.grd
disp_2007299_ll.grd
disp_2007345_ll.grd
disp_2008026_ll.grd
disp_2008302_ll.grd
disp_2008348_ll.grd
disp_2009028_ll.grd
disp_2009304_ll.grd
disp_2010031_ll.grd
disp_2010353_ll.grd
aps_2007299.grd

```

aps\_2007345.grd  
aps\_2008026.grd  
aps\_2008302.grd  
aps\_2008348.grd  
aps\_2009028.grd  
aps\_2009304.grd  
aps\_2010031.grd  
aps\_2010353.grd

## A.5 ALOS PALSAR (Path 423 Row 7020) in Bali, Indonesia

```
data.in
IMG-HH-ALPSRP093437020-H1.0__A
IMG-HH-ALPSRP100147020-H1.0__A
IMG-HH-ALPSRP106857020-H1.0__A
IMG-HH-ALPSRP147117020-H1.0__A
IMG-HH-ALPSRP153827020-H1.0__A
IMG-HH-ALPSRP160537020-H1.0__A
IMG-HH-ALPSRP200797020-H1.0__A
IMG-HH-ALPSRP214217020-H1.0__A
IMG-HH-ALPSRP261187020-H1.0__A

pre_proc_batch.csh ALOS data.in batch.config

START PREPROCESS A STACK OF IMAGES

preprocess master image
ledflag 1
... swapping bytes
writing generic LED file: IMG-HH-ALPSRP093437020-H1.0__A.LED
... calculating doppler for IMG-HH-ALPSRP093437020-H1.0__A.raw
Working on line 2000
Working on line 4000
Working on line 6000
Working on line 8000
Working on line 10000
Working on line 12000
Working on line 14000
Working on line 16000
Working on line 18000
Working on line 20000
Working on line 22000
Working on line 24000
Working on line 26000
Working on line 28000
Working on line 30000
Working on line 32000
Working on line 34000
pre_proc_batch.csh
preprocess slave images
setting fd1 to -3.251612
setting near_range to 848815.00
setting radius to 6377621.077067
setting npatches to 3
ledflag 1
... swapping bytes
writing generic LED file: IMG-HH-ALPSRP100147020-H1.0__A.LED
The range sampling rate for master and slave images are: 32000000
pre_proc_batch.csh
preprocess slave images
setting fd1 to -3.251612
setting near_range to 848815.00
setting radius to 6377621.077067
setting npatches to 3
ledflag 1
... swapping bytes
writing generic LED file: IMG-HH-ALPSRP106857020-H1.0__A.LED
The range sampling rate for master and slave images are: 32000000
pre_proc_batch.csh
preprocess slave images
setting fd1 to -3.251612
setting near_range to 848815.00
setting radius to 6377621.077067
setting npatches to 3
ledflag 1
... swapping bytes
writing generic LED file: IMG-HH-ALPSRP147117020-H1.0__A.LED
near_range, shift = 848965 64
The range sampling rate for master and slave images are: 32000000
pre_proc_batch.csh
preprocess slave images
setting fd1 to -3.251612
setting near_range to 848815.00
setting radius to 6377621.077067
setting npatches to 3
ledflag 1
... swapping bytes
writing generic LED file: IMG-HH-ALPSRP153827020-H1.0__A.LED
near_range, shift = 849115 128
near_range, shift = 848665 -64
The range sampling rate for master and slave images are: 32000000
pre_proc_batch.csh
preprocess slave images
setting fd1 to -3.251612
setting near_range to 848815.00
setting radius to 6377621.077067
setting npatches to 3
ledflag 1
... swapping bytes
writing generic LED file: IMG-HH-ALPSRP160537020-H1.0__A.LED
near_range, shift = 849265 192
near_range, shift = 848665 -64
The range sampling rate for master and slave images are: 32000000
pre_proc_batch.csh
preprocess slave images
setting fd1 to -3.251612
setting near_range to 848815.00
setting radius to 6377621.077067
setting npatches to 3
ledflag 1
... swapping bytes
writing generic LED file: IMG-HH-ALPSRP200797020-H1.0__A.LED
near_range, shift = 849565 320
near_range, shift = 848815 0
The range sampling rate for master and slave images are: 32000000
```

```
pre_proc_batch.csh
preprocess slave images
  setting fd1 to -3.251612
  setting near_range to 848815.00
  setting radius to 6377621.077067
  setting npatches to 3
  ledflag 1
.... swapping bytes
writing generic LED file: IMG-HH-ALPSRP214217020-H1.0_A.LED
The range sampling rate for master and slave images are: 32000000
pre_proc_batch.csh
preprocess slave images
  setting fd1 to -3.251612
  setting near_range to 848815.00
  setting radius to 6377621.077067
  setting npatches to 3
  ledflag 1
.... swapping bytes
writing generic LED file: IMG-HH-ALPSRP261187020-H1.0_A.LED
The range sampling rate for master and slave images are: 32000000
```

END PREPROCESS A STACK OF IMAGES

```
baseline_table.dat
09343 2007299.6335368508 664 0.000000 0.000000
10014 2007345.6332865383 710 -410.630841 -268.912134
10685 2008026.6329556587 756 -372.932224 -463.616308
14711 2008302.6327977190 1032 246.492560 680.827274
15382 2008348.6333390384 1078 364.978691 651.456039
16053 2009028.6338014458 1123 86.568067 358.437429
20079 2009304.6350614689 1399 -211.353866 72.147166
21421 2010031.6349740268 1491 -217.926645 -71.035465
26118 2010353.6324163070 1813 -783.332397 -926.045642
```

```
intf.in
IMG-HH-ALPSRP093437020-H1.0_A:IMG-HH-ALPSRP100147020-H1.0_A
IMG-HH-ALPSRP093437020-H1.0_A:IMG-HH-ALPSRP106857020-H1.0_A
IMG-HH-ALPSRP093437020-H1.0_A:IMG-HH-ALPSRP147117020-H1.0_A
IMG-HH-ALPSRP093437020-H1.0_A:IMG-HH-ALPSRP153827020-H1.0_A
IMG-HH-ALPSRP093437020-H1.0_A:IMG-HH-ALPSRP160537020-H1.0_A
IMG-HH-ALPSRP093437020-H1.0_A:IMG-HH-ALPSRP200797020-H1.0_A
IMG-HH-ALPSRP093437020-H1.0_A:IMG-HH-ALPSRP214217020-H1.0_A
IMG-HH-ALPSRP093437020-H1.0_A:IMG-HH-ALPSRP261187020-H1.0_A
IMG-HH-ALPSRP100147020-H1.0_A:IMG-HH-ALPSRP106857020-H1.0_A
IMG-HH-ALPSRP100147020-H1.0_A:IMG-HH-ALPSRP147117020-H1.0_A
IMG-HH-ALPSRP100147020-H1.0_A:IMG-HH-ALPSRP153827020-H1.0_A
IMG-HH-ALPSRP100147020-H1.0_A:IMG-HH-ALPSRP160537020-H1.0_A
IMG-HH-ALPSRP100147020-H1.0_A:IMG-HH-ALPSRP200797020-H1.0_A
IMG-HH-ALPSRP100147020-H1.0_A:IMG-HH-ALPSRP214217020-H1.0_A
IMG-HH-ALPSRP106857020-H1.0_A:IMG-HH-ALPSRP160537020-H1.0_A
IMG-HH-ALPSRP106857020-H1.0_A:IMG-HH-ALPSRP200797020-H1.0_A
IMG-HH-ALPSRP106857020-H1.0_A:IMG-HH-ALPSRP214217020-H1.0_A
IMG-HH-ALPSRP147117020-H1.0_A:IMG-HH-ALPSRP153827020-H1.0_A
IMG-HH-ALPSRP147117020-H1.0_A:IMG-HH-ALPSRP160537020-H1.0_A
IMG-HH-ALPSRP147117020-H1.0_A:IMG-HH-ALPSRP200797020-H1.0_A
IMG-HH-ALPSRP147117020-H1.0_A:IMG-HH-ALPSRP214217020-H1.0_A
IMG-HH-ALPSRP147117020-H1.0_A:IMG-HH-ALPSRP261187020-H1.0_A
IMG-HH-ALPSRP153827020-H1.0_A:IMG-HH-ALPSRP160537020-H1.0_A
IMG-HH-ALPSRP153827020-H1.0_A:IMG-HH-ALPSRP200797020-H1.0_A
IMG-HH-ALPSRP153827020-H1.0_A:IMG-HH-ALPSRP214217020-H1.0_A
IMG-HH-ALPSRP160537020-H1.0_A:IMG-HH-ALPSRP200797020-H1.0_A
IMG-HH-ALPSRP160537020-H1.0_A:IMG-HH-ALPSRP214217020-H1.0_A
IMG-HH-ALPSRP200797020-H1.0_A:IMG-HH-ALPSRP214217020-H1.0_A
IMG-HH-ALPSRP200797020-H1.0_A:IMG-HH-ALPSRP261187020-H1.0_A
IMG-HH-ALPSRP214217020-H1.0_A:IMG-HH-ALPSRP261187020-H1.0_A
```

```
align.in
IMG-HH-ALPSRP093437020-H1.0_A:IMG-HH-ALPSRP100147020-H1.0_A:IMG-HH-ALPSRP093437020-H1.0_A
IMG-HH-ALPSRP093437020-H1.0_A:IMG-HH-ALPSRP106857020-H1.0_A:IMG-HH-ALPSRP093437020-H1.0_A
IMG-HH-ALPSRP093437020-H1.0_A:IMG-HH-ALPSRP147117020-H1.0_A:IMG-HH-ALPSRP093437020-H1.0_A
IMG-HH-ALPSRP093437020-H1.0_A:IMG-HH-ALPSRP153827020-H1.0_A:IMG-HH-ALPSRP093437020-H1.0_A
IMG-HH-ALPSRP093437020-H1.0_A:IMG-HH-ALPSRP160537020-H1.0_A:IMG-HH-ALPSRP093437020-H1.0_A
IMG-HH-ALPSRP093437020-H1.0_A:IMG-HH-ALPSRP200797020-H1.0_A:IMG-HH-ALPSRP093437020-H1.0_A
IMG-HH-ALPSRP093437020-H1.0_A:IMG-HH-ALPSRP214217020-H1.0_A:IMG-HH-ALPSRP093437020-H1.0_A
IMG-HH-ALPSRP093437020-H1.0_A:IMG-HH-ALPSRP261187020-H1.0_A:IMG-HH-ALPSRP093437020-H1.0_A
IMG-HH-ALPSRP100147020-H1.0_A:IMG-HH-ALPSRP106857020-H1.0_A:IMG-HH-ALPSRP093437020-H1.0_A
IMG-HH-ALPSRP100147020-H1.0_A:IMG-HH-ALPSRP147117020-H1.0_A:IMG-HH-ALPSRP093437020-H1.0_A
IMG-HH-ALPSRP100147020-H1.0_A:IMG-HH-ALPSRP153827020-H1.0_A:IMG-HH-ALPSRP093437020-H1.0_A
IMG-HH-ALPSRP100147020-H1.0_A:IMG-HH-ALPSRP160537020-H1.0_A:IMG-HH-ALPSRP093437020-H1.0_A
IMG-HH-ALPSRP100147020-H1.0_A:IMG-HH-ALPSRP200797020-H1.0_A:IMG-HH-ALPSRP093437020-H1.0_A
IMG-HH-ALPSRP100147020-H1.0_A:IMG-HH-ALPSRP214217020-H1.0_A:IMG-HH-ALPSRP093437020-H1.0_A
IMG-HH-ALPSRP106857020-H1.0_A:IMG-HH-ALPSRP160537020-H1.0_A:IMG-HH-ALPSRP093437020-H1.0_A
IMG-HH-ALPSRP106857020-H1.0_A:IMG-HH-ALPSRP200797020-H1.0_A:IMG-HH-ALPSRP093437020-H1.0_A
IMG-HH-ALPSRP106857020-H1.0_A:IMG-HH-ALPSRP214217020-H1.0_A:IMG-HH-ALPSRP093437020-H1.0_A
IMG-HH-ALPSRP147117020-H1.0_A:IMG-HH-ALPSRP153827020-H1.0_A:IMG-HH-ALPSRP093437020-H1.0_A
IMG-HH-ALPSRP147117020-H1.0_A:IMG-HH-ALPSRP160537020-H1.0_A:IMG-HH-ALPSRP093437020-H1.0_A
IMG-HH-ALPSRP147117020-H1.0_A:IMG-HH-ALPSRP200797020-H1.0_A:IMG-HH-ALPSRP093437020-H1.0_A
IMG-HH-ALPSRP147117020-H1.0_A:IMG-HH-ALPSRP214217020-H1.0_A:IMG-HH-ALPSRP093437020-H1.0_A
IMG-HH-ALPSRP147117020-H1.0_A:IMG-HH-ALPSRP261187020-H1.0_A:IMG-HH-ALPSRP093437020-H1.0_A
IMG-HH-ALPSRP153827020-H1.0_A:IMG-HH-ALPSRP160537020-H1.0_A:IMG-HH-ALPSRP093437020-H1.0_A
IMG-HH-ALPSRP153827020-H1.0_A:IMG-HH-ALPSRP200797020-H1.0_A:IMG-HH-ALPSRP093437020-H1.0_A
IMG-HH-ALPSRP153827020-H1.0_A:IMG-HH-ALPSRP214217020-H1.0_A:IMG-HH-ALPSRP093437020-H1.0_A
IMG-HH-ALPSRP160537020-H1.0_A:IMG-HH-ALPSRP200797020-H1.0_A:IMG-HH-ALPSRP093437020-H1.0_A
IMG-HH-ALPSRP160537020-H1.0_A:IMG-HH-ALPSRP214217020-H1.0_A:IMG-HH-ALPSRP093437020-H1.0_A
IMG-HH-ALPSRP200797020-H1.0_A:IMG-HH-ALPSRP214217020-H1.0_A:IMG-HH-ALPSRP093437020-H1.0_A
IMG-HH-ALPSRP200797020-H1.0_A:IMG-HH-ALPSRP261187020-H1.0_A:IMG-HH-ALPSRP093437020-H1.0_A
IMG-HH-ALPSRP214217020-H1.0_A:IMG-HH-ALPSRP261187020-H1.0_A:IMG-HH-ALPSRP093437020-H1.0_A
```

align\_batch.csh AL05 align.in

```
ALIGN.CSH - START
focussing master
Computing range reference function.
Processing patch 1
Processing Elapsed Time: 0 min 0.04 sec
Range Compression
Processing Elapsed Time: 0 min 5.69 sec
Azimuthal Transform
Processing Elapsed Time: 0 min 13.58 sec
Range Migration
Processing Elapsed Time: 0 min 23.50 sec
Azimuthal Compression
Processing Elapsed Time: 0 min 45.94 sec
Writing Data
Processing patch 2
Processing Elapsed Time: 0 min 47.45 sec
Range Compression
Processing Elapsed Time: 0 min 52.11 sec
Azimuthal Transform
Processing Elapsed Time: 0 min 59.99 sec
Range Migration
```

```
Processing Elapsed Time: 1 min 9.89 sec
Azimuthal Compression
Processing Elapsed Time: 1 min 33.02 sec
Writing Data
Processing patch 3
Processing Elapsed Time: 1 min 34.59 sec
Range Compression
Processing Elapsed Time: 1 min 39.19 sec
Azimuthal Transform
Processing Elapsed Time: 1 min 47.28 sec
Range Migration
Processing Elapsed Time: 1 min 57.19 sec
Azimuthal Compression
Processing Elapsed Time: 2 min 19.92 sec
Writing Data
Processing Elapsed Time: 2 min 21.44 sec
number of points clipped to short int 53
align.csh
focusing slave
Computing range reference function.
Processing patch 1
Processing Elapsed Time: 0 min 0.03 sec
Range Compression
Processing Elapsed Time: 0 min 5.57 sec
Azimuthal Transform
Processing Elapsed Time: 0 min 13.87 sec
Range Migration
Processing Elapsed Time: 0 min 23.93 sec
Azimuthal Compression
Processing Elapsed Time: 0 min 47.04 sec
Writing Data
Processing patch 2
Processing Elapsed Time: 0 min 48.58 sec
Range Compression
Processing Elapsed Time: 0 min 53.18 sec
Azimuthal Transform
Processing Elapsed Time: 1 min 1.26 sec
Range Migration
Processing Elapsed Time: 1 min 11.19 sec
Azimuthal Compression
Processing Elapsed Time: 1 min 35.27 sec
Writing Data
Processing patch 3
Processing Elapsed Time: 1 min 36.80 sec
Range Compression
Processing Elapsed Time: 1 min 41.44 sec
Azimuthal Transform
Processing Elapsed Time: 1 min 49.63 sec
Range Migration
Processing Elapsed Time: 1 min 59.54 sec
Azimuthal Compression
Processing Elapsed Time: 2 min 23.60 sec
Writing Data
Processing Elapsed Time: 2 min 25.14 sec
number of points clipped to short int 175
align.csh
correlate master and slave to find offset parameters
setting xsearch to 64
setting nx_corr to 128
setting ysearch to 64
setting ny_corr to 128
11304 27648 11304 27648 104 68 -0.002141
locations n 512 nx 11304 nyl 32 nxl 16 x_inc 574 y_inc 826
elapsed time: 19.338003
align.csh
refocus slave
Computing range reference function.
Processing patch 1
Processing Elapsed Time: 0 min 0.03 sec
Range Compression
Processing Elapsed Time: 0 min 5.83 sec
Azimuthal Transform
Processing Elapsed Time: 0 min 20.32 sec
Range Migration
Processing Elapsed Time: 0 min 30.42 sec
Azimuthal Compression
Processing Elapsed Time: 1 min 3.81 sec
apply azimuth-dependent azimuth shift
Processing Elapsed Time: 1 min 28.67 sec
Writing Data
Processing patch 2
Processing Elapsed Time: 1 min 35.16 sec
Range Compression
Processing Elapsed Time: 1 min 39.93 sec
Azimuthal Transform
Processing Elapsed Time: 1 min 49.27 sec
Range Migration
Processing Elapsed Time: 1 min 59.38 sec
Azimuthal Compression
Processing Elapsed Time: 2 min 29.37 sec
apply azimuth-dependent azimuth shift
Processing Elapsed Time: 2 min 56.98 sec
Writing Data
Processing patch 3
Processing Elapsed Time: 3 min 3.89 sec
Range Compression
Processing Elapsed Time: 3 min 8.54 sec
Azimuthal Transform
Processing Elapsed Time: 3 min 18.00 sec
Range Migration
Processing Elapsed Time: 3 min 28.25 sec
Azimuthal Compression
Processing Elapsed Time: 4 min 2.25 sec
apply azimuth-dependent azimuth shift
Processing Elapsed Time: 4 min 28.31 sec
Writing Data
Processing Elapsed Time: 4 min 35.06 sec
number of points clipped to short int 187
rm: No match.
ALIGN.CSH - END

intf_batch.csh ALOS batch.config
clean up topo/ folder

DEM2TOPO_RA.CSH - START
USER SHOULD PROVIDE DEM FILE
range decimation is: 2
blockmedian: Provides 3, expects 3-column binary data
blockmedian: Processing input table data
```

```

blockmedian: W: 0 E: 11304 S: 0 N: 27648 n_columns: 5652 n_rows: 6912
blockmedian: Input 3 columns via binary records using format ddd
blockmedian: Output 3 columns via binary records using format ddd
blockmedian: N read: 880412 N used: 877562 outside_area: 2850 N cells filled: 877534
surface: Provides 3, expects 3-column binary data
surface: Grid domain: W: 0 E: 11304 S: 0 N: 27648 n_columns: 5652 n_rows: 6912 [pixel registration]
surface: Processing input table data
surface: Input 3 columns via binary records using format ddd
surface: Minimum value of your dataset x,y,z at: surface: 9.47925853729 20.1111221313 79.1265945435
surface: Maximum value of your dataset x,y,z at: surface: 4982.25195312 19988.2792969 3152.45239258
surface: LS plane determined: z = 203.081 + (-0.085365 * col) + (0.111885 * row)
surface: Grid Mode IterationMax Change Conv Limit Total Iterations
surface: 36 D 22 0.000546255543946 0.00086758828296 22
surface: 12 I 28 0.00218929156934 0.0026027648489 50
surface: 12 D 20 0.00178716015478 0.0026027648489 70
surface: 4 I 25 0.00575992186722 0.0078082945467 95
surface: 4 D 42 0.00697227533129 0.0078082945467 137
surface: 2 I 18 0.0144953680828 0.0156165890934 155
surface: 2 D 92 0.0155055815236 0.0156165890934 247
surface: 1 I 16 0.0282327391979 0.0312331781868 263
surface: 1 D 245 0.0309639238689 0.0312331781868 508
surface: Fit info: N data points N nodes mean error rms errorcurvature
surface: 877534 39079189 -3.16770048757e-06 0.0062199362068 22227.5479258
grd2cpt: Processing input grid(s)
grd2cpt: Mean and S.D. of data are 349.387377152 406.116523212
grdimage: Allocates memory and read data file topo_ra.grd
grdimage: Evaluate image pixel colors
grdimage: Creating 8-bit grayscale image
DEM2TOPO_RA.CSH - END
NO TOPO_RA SHIFT

```

START FORM A STACK OF INTERFEROGRAMS

INTF.CSH, FILTER.CSH - START

```

intf.csh
running phasediff...
reading topo topo_ra.grd
  xdim 11304, ydim 27648
filter.csh
gauss_300 4 2 (4 2)
making amplitudes...
filtering interferogram...
making amplitude...
making correlation...
making phase...
filtering phase...
INTF.CSH, FILTER.CSH - END

```

SNAPHU.CSH - START

```

threshold_snaphu: .45
grdmath: Perform reverse Polish notation calculations on grids
grdmath: phase_patch.grd landmask_ra_patch.grd MUL = phase_patch.grd
unwrapping phase with snaphu - higher threshold for faster unwrapping

```

snaphu v1.4.2

```

32 parameters input from file snaphu.conf.brief (297 lines total)
Reading wrapped phase from file phase.in
No weight file specified. Assuming uniform weights
Reading correlation data from file corr.in
Calculating deformation-mode cost parameters
Building range cost arrays
Building azimuth cost arrays
Initializing flows with MST algorithm
Running approximate minimum spanning tree solver
Running nonlinear network flow optimizer
Maximum flow on network: 9
Number of nodes in network: 4878776
Flow increment: 1 (Total improvements: 0)
Treesize: 4878776 Pivots: 402760 Improvements: 2621
Maximum flow on network: 7
Flow increment: 2 (Total improvements: 2621)
Treesize: 4878776 Pivots: 2602 Improvements: 98
Maximum flow on network: 7
Flow increment: 3 (Total improvements: 2719)
Treesize: 4878776 Pivots: 90 Improvements: 26
Maximum flow on network: 7
Flow increment: 4 (Total improvements: 2745)
Treesize: 4878776 Pivots: 79 Improvements: 8
Maximum flow on network: 7
Flow increment: 1 (Total improvements: 2753)
Treesize: 4878776 Pivots: 15804 Improvements: 38
Maximum flow on network: 7
Total solution cost: 3727674
Integrating phase
Writing output to file unwrap.out
Program snaphu done
Elapsed processor time: 0:04:56.57
Elapsed wall clock time: 0:04:58
grdmath: Perform reverse Polish notation calculations on grids
grdmath: unwrap.grd landmask_ra_patch.grd MUL = tmp.grd
SNAPHU.CSH - END

```

GEOCODE.CSH - START

```

threshold_geocode: .45
grdmath: Perform reverse Polish notation calculations on grids
grdmath: corr.grd 0.45 GE 0 NAN mask.grd MUL = mask2.grd
pscale: Warning: The -E option is deprecated but is accepted.
pscale: For the current -D syntax you should use -D modifier +e instead.
pscale: Note you cannot mix new-style modifiers (+e) with the old-style -D option.
pscale: Warning: The -E option is deprecated but is accepted.
pscale: For the current -D syntax you should use -D modifier +e instead.
pscale: Note you cannot mix new-style modifiers (+e) with the old-style -D option.
geocode.csh
project correlation, phase, unwrapped and amplitude back to lon lat coordinates
remarked is by root on Thu May 24 02:28:50 JST 2018 with geocode.csh
proj_ra2ll.csh
surface: Provides 3, expects 3-column binary data
surface: Grid domain: W: 0 E: 11216 S: 0 N: 27648 n_columns: 701 n_rows: 864 [gridline registration]
surface: Warning: Your grid dimensions are mutually prime. Convergence is very unlikely.
surface: Hint: Choosing -R-144/11376/0/27648 [n_columns = 720, n_rows = 864] might cut run time by a factor of 315.10809
surface: Hint: Choosing -R-144/11376/-576/28224 [n_columns = 720, n_rows = 900] might cut run time by a factor of 297.73196
surface: Hint: Choosing -R-528/11760/0/27648 [n_columns = 768, n_rows = 864] might cut run time by a factor of 295.59004
surface: Hint: Choosing -R-144/11376/-1536/29184 [n_columns = 720, n_rows = 960] might cut run time by a factor of 283.52844
surface: Hint: Choosing -R-784/12016/0/27648 [n_columns = 800, n_rows = 864] might cut run time by a factor of 281.39743
surface: Hint: Choosing -R-144/11376/-1728/29376 [n_columns = 720, n_rows = 972] might cut run time by a factor of 273.97863
surface: Hint: Choosing -R-384/11616/-576/28224 [n_columns = 750, n_rows = 900] might cut run time by a factor of 267.81599
surface: Hint: Choosing -R-144/11376/-2176/29824 [n_columns = 720, n_rows = 1000] might cut run time by a factor of 267.32756

```

surface: Hint: Choosing -R-528/11760/-1536/29184 [n\_columns = 768, n\_rows = 960] might cut run time by a factor of 266.13928  
surface: Hint: Choosing -R-1296/12528/0/27648 [n\_columns = 864, n\_rows = 864] might cut run time by a factor of 262.80727  
surface: Hint: After completion you can recover the desired region via gmt grdcut  
surface: Processing input table data  
surface: Input 3 columns via binary records using format fff  
surface: Minimum value of your dataset x,y,z at: surface: -7.24586963654 27662.3886719 114.425834656  
surface: Maximum value of your dataset x,y,z at: surface: 11223.3798828 77.2237319946 115.354164124  
surface: 276688 unusable points were supplied; these will be ignored.  
surface: You should have pre-processed the data with block-mean, -median, or -mode.  
surface: Check that previous processing steps write results with enough decimals.  
surface: LS plane determined: z = 114.612 + (0.00106387 \* col) + (-0.000210292 \* row)  
surface: Grid Mode IterationMax Change Conv Limit Total Iterations  
surface: 1 0 24 3.24448393289e-07 4.32808274729e-07 24  
surface: Fit info: N data points N nodes mean error rms error curvature  
surface: 603076 607230 1.97797248687e-05 0.00721375272255 12084.2202472  
surface: Provides 3, expects 3-column binary data  
surface: Grid domain: W: 0 E: 11216 S: 0 N: 27648 n\_columns: 701 n\_rows: 864 [gridline registration]  
surface: Warning: Your grid dimensions are mutually prime. Convergence is very unlikely.  
surface: Hint: Choosing -R-144/11376/0/27648 [n\_columns = 720, n\_rows = 864] might cut run time by a factor of 315.10809  
surface: Hint: Choosing -R-144/11376/-576/28224 [n\_columns = 720, n\_rows = 900] might cut run time by a factor of 297.73196  
surface: Hint: Choosing -R-528/11760/0/27648 [n\_columns = 768, n\_rows = 864] might cut run time by a factor of 295.59004  
surface: Hint: Choosing -R-144/11376/-1536/29184 [n\_columns = 720, n\_rows = 960] might cut run time by a factor of 283.52844  
surface: Hint: Choosing -R-784/12016/0/27648 [n\_columns = 800, n\_rows = 864] might cut run time by a factor of 281.39743  
surface: Hint: Choosing -R-144/11376/-1728/29376 [n\_columns = 720, n\_rows = 972] might cut run time by a factor of 273.97863  
surface: Hint: Choosing -R-384/11616/-576/28224 [n\_columns = 750, n\_rows = 900] might cut run time by a factor of 267.81599  
surface: Hint: Choosing -R-144/11376/-2176/29824 [n\_columns = 720, n\_rows = 1000] might cut run time by a factor of 267.32756  
surface: Hint: Choosing -R-528/11760/-1536/29184 [n\_columns = 768, n\_rows = 960] might cut run time by a factor of 266.13928  
surface: Hint: Choosing -R-1296/12528/0/27648 [n\_columns = 864, n\_rows = 864] might cut run time by a factor of 262.80727  
surface: Hint: After completion you can recover the desired region via gmt grdcut  
surface: Processing input table data  
surface: Input 3 columns via binary records using format fff  
surface: Minimum value of your dataset x,y,z at: surface: -3.54017567635 -9.6104593277 -8.49916744232  
surface: Maximum value of your dataset x,y,z at: surface: 11211.8613281 27663.2226562 -7.55416679382  
surface: 276688 unusable points were supplied; these will be ignored.  
surface: You should have pre-processed the data with block-mean, -median, or -mode.  
surface: Check that previous processing steps write results with enough decimals.  
surface: LS plane determined: z = -8.49608 + (0.000239016 \* col) + (0.00089748 \* row)  
surface: Grid Mode IterationMax Change Conv Limit Total Iterations  
surface: 1 0 24 7.66480128108e-08 9.55342623429e-08 24  
surface: Fit info: N data points N nodes mean error rms error curvature  
surface: 603076 607230 -3.28008492206e-05 0.0102564813666 14142.1693428  
blockmedian: Provides 3, expects 3-column binary data  
blockmedian: Processing input table data  
blockmedian: W: 114.433333333 E: 115.355555556 S: -8.5 N: -7.55555555556 n\_columns: 830 n\_rows: 1360  
blockmedian: Input 3 columns via binary records using format fff  
blockmedian: Output 3 columns via binary records using format fff  
blockmedian: N read: 4772303 N used: 4772303 outside\_area: 0 N cells filled: 779162  
proj\_ra2ll.csh  
blockmedian: Provides 3, expects 3-column binary data  
blockmedian: Processing input table data  
blockmedian: W: 114.433333333 E: 115.355555556 S: -8.5 N: -7.55555555556 n\_columns: 830 n\_rows: 1360  
blockmedian: Input 3 columns via binary records using format fff  
blockmedian: Output 3 columns via binary records using format fff  
blockmedian: N read: 4777461 N used: 4777461 outside\_area: 0 N cells filled: 780054  
proj\_ra2ll.csh  
blockmedian: Provides 3, expects 3-column binary data  
blockmedian: Processing input table data  
blockmedian: W: 114.6 E: 115.266666667 S: -8.40277777778 N: -8.06944444444 n\_columns: 600 n\_rows: 480  
blockmedian: Input 3 columns via binary records using format fff  
blockmedian: Output 3 columns via binary records using format fff  
blockmedian: N read: 1094 N used: 1094 outside\_area: 0 N cells filled: 402  
proj\_ra2ll.csh  
blockmedian: Provides 3, expects 3-column binary data  
blockmedian: Processing input table data  
blockmedian: W: 114.422222222 E: 115.355555556 S: -8.5 N: -7.54861111111 n\_columns: 840 n\_rows: 1370  
blockmedian: Input 3 columns via binary records using format fff  
blockmedian: Output 3 columns via binary records using format fff  
blockmedian: N read: 4845312 N used: 4845312 outside\_area: 0 N cells filled: 791026  
proj\_ra2ll.csh  
blockmedian: Provides 3, expects 3-column binary data  
blockmedian: Processing input table data  
blockmedian: W: 114.6 E: 115.266666667 S: -8.40277777778 N: -8.06944444444 n\_columns: 600 n\_rows: 480  
blockmedian: Input 3 columns via binary records using format fff  
blockmedian: Output 3 columns via binary records using format fff  
blockmedian: N read: 1094 N used: 1094 outside\_area: 0 N cells filled: 402  
proj\_ra2ll.csh  
blockmedian: Provides 3, expects 3-column binary data  
blockmedian: Processing input table data  
blockmedian: W: 114.444444444 E: 115.355555556 S: -8.44444444444 N: -7.79861111111 n\_columns: 820 n\_rows: 930  
blockmedian: Input 3 columns via binary records using format fff  
blockmedian: Output 3 columns via binary records using format fff  
blockmedian: N read: 1607804 N used: 1607804 outside\_area: 0 N cells filled: 265411  
proj\_ra2ll.csh  
blockmedian: Provides 3, expects 3-column binary data  
blockmedian: Processing input table data  
blockmedian: W: 114.6 E: 115.266666667 S: -8.40277777778 N: -8.06944444444 n\_columns: 600 n\_rows: 480  
blockmedian: Input 3 columns via binary records using format fff  
blockmedian: Output 3 columns via binary records using format fff  
blockmedian: N read: 1094 N used: 1094 outside\_area: 0 N cells filled: 402  
geocode.csh  
make the KML files for Google Earth  
grdimage: Allocates memory and read data file display\_amp\_ll.grd  
grdimage: Evaluate image pixel colors  
grdimage: Creating 24-bit color image  
Make display\_amp\_ll.kml and display\_amp\_ll.png  
psconvert: Processing display\_amp\_ll.ps...  
psconvert: Figure dimensions: Width: 67.2 points [0.933333 inch] Height: 68.52 points [0.951666 inch]  
psconvert: gs -q -dSAFER -dNOPAUSE -dBATCH -dPDFSETTINGS=/prepress -dDownsampleColorImages=false -dDownsampleGrayImages=false -dDownsampleMonoImages=false -dUseFlateCompression=true -dEmbedAllFonts=true -dSubsetFonts=true -dMonoImageFilter=/FlateEncode -dAutoFilterGrayImages=false -dGrayImageFilter=/FlateEncode -dAutoFilterColorImages=false -dColorImageFilter=/FlateEncode -dSCANCONVERTERTYPE=2 -dMaxBitmap=2147483647 -dUseFastColor=true -sDEVICE=pngalpha -g840x857 -r900 -sOutputFile='display\_amp\_ll.png' -f./psconvert\_611d.eps'  
psconvert: Done.  
grdimage: Allocates memory and read data file corr\_ll.grd  
grdimage: Evaluate image pixel colors  
grdimage: Creating 24-bit color image  
PSL: Colormap of 206 colors created  
Make corr\_ll.kml and corr\_ll.png  
psconvert: Processing corr\_ll.ps...  
psconvert: Figure dimensions: Width: 66.42 points [0.9225 inch] Height: 67.986 points [0.94425 inch]  
psconvert: gs -q -dSAFER -dNOPAUSE -dBATCH -dPDFSETTINGS=/prepress -dDownsampleColorImages=false -dDownsampleGrayImages=false -dDownsampleMonoImages=false -dUseFlateCompression=true -dEmbedAllFonts=true -dSubsetFonts=true -dMonoImageFilter=/FlateEncode -dAutoFilterGrayImages=false -dGrayImageFilter=/FlateEncode -dAutoFilterColorImages=false -dColorImageFilter=/FlateEncode -dSCANCONVERTERTYPE=2 -dMaxBitmap=2147483647 -dUseFastColor=true -sDEVICE=pngalpha -g831x850 -r900 -sOutputFile='corr\_ll.png' -f./psconvert\_626d.eps'  
psconvert: Done.  
grdimage: Allocates memory and read data file phase\_mask\_ll.grd  
grdimage: Evaluate image pixel colors  
grdimage: Creating 24-bit color image  
Make phase\_mask\_ll.kml and phase\_mask\_ll.png  
psconvert: Processing phase\_mask\_ll.ps...



```
psconvert: Figure dimensions: Width: 48.006 points [0.66675 inch] Height: 24 points [0.333333 inch]
psconvert: gs -q -dSAFER -dNOPAUSE -dBATCH -dPDFSETTINGS=/prepress -dDownsampleColorImages=false -dDownsampleGrayImages=false -dDownsampleMonoImages=false -dUseFlateCompression=true -dEmbedAllFonts=true -dSubsetFonts=true -dMonoImageFilter=/FlateEncode -dAutoFilterGrayImages=false -dGrayImageFilter=/FlateEncode -dAutoFilterColorImages=false -dColorImageFilter=/FlateEncode -dSCANCONVERTERTYPE=2 -dMaxBitmap=2147483647 -dUseFastColor=true -sDEVICE=pngalpha -g601x300 -r900 -sOutputFile='phase_mask_ll.png' -f'./psconvert_640d.eps'
psconvert: Done.
grdimage: Allocates memory and read data file phasefilt_mask_ll.grd
grdimage: Evaluate image pixel colors
grdimage: Creating 24-bit color image
Make phasefilt_mask_ll.kml and phasefilt_mask_ll.png
psconvert: Processing phasefilt_mask_ll.ps...
psconvert: Figure dimensions: Width: 48.006 points [0.66675 inch] Height: 24 points [0.333333 inch]
psconvert: gs -q -dSAFER -dNOPAUSE -dBATCH -dPDFSETTINGS=/prepress -dDownsampleColorImages=false -dDownsampleGrayImages=false -dDownsampleMonoImages=false -dUseFlateCompression=true -dEmbedAllFonts=true -dSubsetFonts=true -dMonoImageFilter=/FlateEncode -dAutoFilterGrayImages=false -dGrayImageFilter=/FlateEncode -dAutoFilterColorImages=false -dColorImageFilter=/FlateEncode -dSCANCONVERTERTYPE=2 -dMaxBitmap=2147483647 -dUseFastColor=true -sDEVICE=pngalpha -g601x300 -r900 -sOutputFile='phasefilt_mask_ll.png' -f'./psconvert_654d.eps'
psconvert: Done.
grdimage: Allocates memory and read data file unwrap_mask_ll.grd
grdimage: Evaluate image pixel colors
grdimage: Creating 24-bit color image
PSL: Colormap of 96 colors created
Make unwrap_mask_ll.kml and unwrap_mask_ll.png
psconvert: Processing unwrap_mask_ll.ps...
psconvert: Figure dimensions: Width: 48.006 points [0.66675 inch] Height: 24 points [0.333333 inch]
psconvert: gs -q -dSAFER -dNOPAUSE -dBATCH -dPDFSETTINGS=/prepress -dDownsampleColorImages=false -dDownsampleGrayImages=false -dDownsampleMonoImages=false -dUseFlateCompression=true -dEmbedAllFonts=true -dSubsetFonts=true -dMonoImageFilter=/FlateEncode -dAutoFilterGrayImages=false -dGrayImageFilter=/FlateEncode -dAutoFilterColorImages=false -dColorImageFilter=/FlateEncode -dSCANCONVERTERTYPE=2 -dMaxBitmap=2147483647 -dUseFastColor=true -sDEVICE=pngalpha -g601x300 -r900 -sOutputFile='unwrap_mask_ll.png' -f'./psconvert_668d.eps'
psconvert: Done.
grdimage: Allocates memory and read data file phasefilt_mask_ll.grd
grdimage: Evaluate image pixel colors
grdimage: Creating 24-bit color image
Make phasefilt_mask_ll.kml and phasefilt_mask_ll.png
psconvert: Processing phasefilt_mask_ll.ps...
psconvert: Figure dimensions: Width: 48.006 points [0.66675 inch] Height: 24 points [0.333333 inch]
psconvert: gs -q -dSAFER -dNOPAUSE -dBATCH -dPDFSETTINGS=/prepress -dDownsampleColorImages=false -dDownsampleGrayImages=false -dDownsampleMonoImages=false -dUseFlateCompression=true -dEmbedAllFonts=true -dSubsetFonts=true -dMonoImageFilter=/FlateEncode -dAutoFilterGrayImages=false -dGrayImageFilter=/FlateEncode -dAutoFilterColorImages=false -dColorImageFilter=/FlateEncode -dSCANCONVERTERTYPE=2 -dMaxBitmap=2147483647 -dUseFastColor=true -sDEVICE=pngalpha -g601x300 -r900 -sOutputFile='phasefilt_mask_ll.png' -f'./psconvert_682d.eps'
psconvert: Done.
grdimage: Allocates memory and read data file los_ll.grd
grdimage: Evaluate image pixel colors
grdimage: Creating 24-bit color image
PSL: Colormap of 217 colors created
Make los_ll.kml and los_ll.png
psconvert: Processing los_ll.ps...
psconvert: Figure dimensions: Width: 48.006 points [0.66675 inch] Height: 24 points [0.333333 inch]
psconvert: gs -q -dSAFER -dNOPAUSE -dBATCH -dPDFSETTINGS=/prepress -dDownsampleColorImages=false -dDownsampleGrayImages=false -dDownsampleMonoImages=false -dUseFlateCompression=true -dEmbedAllFonts=true -dSubsetFonts=true -dMonoImageFilter=/FlateEncode -dAutoFilterGrayImages=false -dGrayImageFilter=/FlateEncode -dAutoFilterColorImages=false -dColorImageFilter=/FlateEncode -dSCANCONVERTERTYPE=2 -dMaxBitmap=2147483647 -dUseFastColor=true -sDEVICE=pngalpha -g601x300 -r900 -sOutputFile='los_ll.png' -f'./psconvert_698d.eps'
psconvert: Done.
GEOCODE.CSH - END
```

```
stack.list
cut_2007299_2007345.grd IMG-HH-ALPSRP093437020-H1.0_A.PRM IMG-HH-ALPSRP100147020-H1.0_A.PRM
cut_2007299_2008026.grd IMG-HH-ALPSRP093437020-H1.0_A.PRM IMG-HH-ALPSRP106857020-H1.0_A.PRM
cut_2007299_2008302.grd IMG-HH-ALPSRP093437020-H1.0_A.PRM IMG-HH-ALPSRP147117020-H1.0_A.PRM
cut_2007299_2008348.grd IMG-HH-ALPSRP093437020-H1.0_A.PRM IMG-HH-ALPSRP153827020-H1.0_A.PRM
cut_2007299_2009028.grd IMG-HH-ALPSRP093437020-H1.0_A.PRM IMG-HH-ALPSRP160537020-H1.0_A.PRM
cut_2007299_2009304.grd IMG-HH-ALPSRP093437020-H1.0_A.PRM IMG-HH-ALPSRP200797020-H1.0_A.PRM
cut_2007299_2010031.grd IMG-HH-ALPSRP093437020-H1.0_A.PRM IMG-HH-ALPSRP214217020-H1.0_A.PRM
cut_2007299_2010353.grd IMG-HH-ALPSRP093437020-H1.0_A.PRM IMG-HH-ALPSRP261187020-H1.0_A.PRM
```

```
bash stack_phase.bash stack.list mean.grd std.grd
```

```
compute the mean LOS velocity ..
```

```
time span (days) of cut_2007299_2007345.grd: 46
accumulative days in the stack: 46
time span (days) of cut_2007299_2008026.grd: 92
accumulative days in the stack: 138
time span (days) of cut_2007299_2008302.grd: 368
accumulative days in the stack: 506
time span (days) of cut_2007299_2008348.grd: 414
accumulative days in the stack: 920
time span (days) of cut_2007299_2009028.grd: 459
accumulative days in the stack: 1379
time span (days) of cut_2007299_2009304.grd: 735
accumulative days in the stack: 2114
time span (days) of cut_2007299_2010031.grd: 827
accumulative days in the stack: 2941
time span (days) of cut_2007299_2010353.grd: 1149
accumulative days in the stack: 4090
```

```
compute the standard deviations ..
```

```
mean_ll.grd
std_ll.grd
los_ll_2007345.grd
los_ll_2008026.grd
los_ll_2008302.grd
los_ll_2008348.grd
los_ll_2009028.grd
los_ll_2009304.grd
los_ll_2010031.grd
los_ll_2010353.grd
```

```
csk select_pairs.csh baseline_table.dat 950 1000
```

```
intf.tab
cut_2007299_2007345.grd corcut_2007299_2007345.grd 2007299 2007345 -268.912134
cut_2007299_2008026.grd corcut_2007299_2008026.grd 2007299 2008026 -463.616308
cut_2007299_2008302.grd corcut_2007299_2008302.grd 2007299 2008302 680.827274
cut_2007299_2008348.grd corcut_2007299_2008348.grd 2007299 2008348 651.456039
cut_2007299_2009028.grd corcut_2007299_2009028.grd 2007299 2009028 358.437429
cut_2007299_2009304.grd corcut_2007299_2009304.grd 2007299 2009304 72.147166
cut_2007299_2010031.grd corcut_2007299_2010031.grd 2007299 2010031 -71.035465
cut_2007345_2008026.grd corcut_2007345_2008026.grd 2007345 2008026 -194.696067
cut_2007345_2008302.grd corcut_2007345_2008302.grd 2007345 2008302 949.803193
cut_2007345_2008348.grd corcut_2007345_2008348.grd 2007345 2008348 920.550578
cut_2007345_2009028.grd corcut_2007345_2009028.grd 2007345 2009028 627.465340
cut_2007345_2009304.grd corcut_2007345_2009304.grd 2007345 2009304 341.104589
cut_2007345_2010031.grd corcut_2007345_2010031.grd 2007345 2010031 197.922110
cut_2008026_2009028.grd corcut_2008026_2009028.grd 2008026 2009028 822.017729
cut_2008026_2009304.grd corcut_2008026_2009304.grd 2008026 2009304 535.747862
cut_2008026_2010031.grd corcut_2008026_2010031.grd 2008026 2010031 392.571910
cut_2008302_2008348.grd corcut_2008302_2008348.grd 2008302 2008348 -29.325367
cut_2008302_2009028.grd corcut_2008302_2009028.grd 2008302 2009028 -322.461017
```

```
cut_2008302_2009304.grd corcut_2008302_2009304.grd 2008302 2009304 -608.885194
cut_2008302_2010031.grd corcut_2008302_2010031.grd 2008302 2010031 -752.102035
cut_2008348_2009028.grd corcut_2008348_2009028.grd 2008348 2009028 -293.080004
cut_2008348_2009304.grd corcut_2008348_2009304.grd 2008348 2009304 -579.443878
cut_2008348_2010031.grd corcut_2008348_2010031.grd 2008348 2010031 -722.656428
cut_2009028_2009304.grd corcut_2009028_2009304.grd 2009028 2009304 -286.370494
cut_2009028_2010031.grd corcut_2009028_2010031.grd 2009028 2010031 -429.578921
cut_2009304_2010031.grd corcut_2009304_2010031.grd 2009304 2010031 -143.195904
cut_2009304_2010353.grd corcut_2010031_2010353.grd 2010031 2010353 -998.403670
cut_2010031_2010353.grd corcut_2010031_2010353.grd 2010031 2010353 -855.125728
```

```
scene.tab
2007299 664
2007345 710
2008026 756
2008302 1032
2008348 1078
2009028 1123
2009304 1399
2010031 1491
2010353 1813
```

```
sbas intf.tab scene.tab 28 9 2826 1728 -smooth 1.0 -wavelength 0.2362 -incidence 34.3 -range 848815 -rms -dem -atm 1
```

```
compute RMS misfit
compute DEM error
```

```
setting smoothing to 1.000
setting radar wavelength to 0.236 m
setting radar incidence angle to 34.300 degree
setting range to 848815.000 m
Memory Allocation Successful...
read table file ...
number of SAR scenes is 9
number of interferograms is 28
read phase and correlation grids ...
fill the G matrix ...
```

```
Applying atmospheric correction by common point stacking...
```

```
Hit Matrix:
2007299 0 1 1 1 1 1 1 1 0
2007345 0 0 1 1 1 1 1 1 0
2008026 0 0 0 0 1 1 1 1 0
2008302 0 0 0 0 1 1 1 1 0
2008348 0 0 0 0 0 1 1 1 0
2009028 0 0 0 0 0 0 1 1 0
2009304 0 0 0 0 0 0 0 1 0
2010031 0 0 0 0 0 0 0 0 1
2010353 0 0 0 0 0 0 0 0 0
```

```
Applying exponential relaxation on smoothing parameters
```

```
Setting smoothing parameter to 1000.000000...
fill the G matrix ...
Computing deformation time-series...
run least-squares problem over 2826 by 1728 pixel (0) ...
matrix is full rank: 9
```

```
Removing deformation time-series from original unwrapped phase...
Computing atmospheric phase screen by common-point stacking...
```

```
Initial estimate of APS...
atm_noise(NO.3) = 10.526015
atm_noise(NO.4) = 4.061861
atm_noise(NO.5) = 2.296265
atm_noise(NO.1) = 1.077755
atm_noise(NO.0) = 0.000000
atm_noise(NO.2) = 0.000000
atm_noise(NO.6) = 0.000000
atm_noise(NO.7) = 0.000000
atm_noise(NO.8) = 0.000000
```

```
atm_noise(NO.3) = 10.477235
atm_noise(NO.4) = 2.499390
atm_noise(NO.5) = 2.310724
atm_noise(NO.1) = 1.076998
atm_noise(NO.0) = 0.000000
atm_noise(NO.2) = 0.000000
atm_noise(NO.6) = 0.000000
atm_noise(NO.7) = 0.000000
atm_noise(NO.8) = 0.000000
```

```
Applying atmospheric phase screen to original unwrapped phase...
Setting smoothing parameter to 1.000000...
```

```
fill the G matrix ...
run least-squares problem over 2826 by 1728 pixel (3) ...
matrix is full rank: 9
```

```
write output ...
```

```
raln.grd
ralt.grd
rms_ll.grd
dem.grd
vel_ll.grd
disp_2007299_ll.grd
disp_2007345_ll.grd
disp_2008026_ll.grd
disp_2008302_ll.grd
disp_2008348_ll.grd
disp_2009028_ll.grd
disp_2009304_ll.grd
disp_2010031_ll.grd
disp_2010353_ll.grd
aps_2007299.grd
aps_2007345.grd
aps_2008026.grd
aps_2008302.grd
aps_2008348.grd
aps_2009028.grd
aps_2009304.grd
aps_2010031.grd
```

aps\_2010353.grd

## A.6 ALOS PALSAR (Path 424 Row 7010) in Bali, Indonesia

```
data.in
IMG-HH-ALPSRP055657010-H1.0__A
IMG-HH-ALPSRP095917010-H1.0__A
IMG-HH-ALPSRP116047010-H1.0__A
IMG-HH-ALPSRP149597010-H1.0__A
IMG-HH-ALPSRP156307010-H1.0__A
IMG-HH-ALPSRP163017010-H1.0__A
IMG-HH-ALPSRP203277010-H1.0__A
IMG-HH-ALPSRP209987010-H1.0__A
IMG-HH-ALPSRP216697010-H1.0__A

pre_proc_batch.csh ALOS data.in batch.config

START PREPROCESS A STACK OF IMAGES

preprocess master image
ledflag 1
.... swapping bytes
writing generic LED file: IMG-HH-ALPSRP055657010-H1.0__A.LED
.... calculating doppler for IMG-HH-ALPSRP055657010-H1.0__A.raw
Working on line 2000
Working on line 4000
Working on line 6000
Working on line 8000
Working on line 10000
Working on line 12000
Working on line 14000
Working on line 16000
Working on line 18000
Working on line 20000
Working on line 22000
Working on line 24000
Working on line 26000
Working on line 28000
Working on line 30000
Working on line 32000
Working on line 34000
pre_proc_batch.csh
preprocess slave images
setting fd1 to 77.112301
setting near_range to 848965.00
setting radius to 6377562.807544
setting npatches to 3
ledflag 1
.... swapping bytes
writing generic LED file: IMG-HH-ALPSRP095917010-H1.0__A.LED
near_range, shift = 849265 128
The range sampling rate for master and slave images are: 32000000
pre_proc_batch.csh
preprocess slave images
setting fd1 to 77.112301
setting near_range to 848965.00
setting radius to 6377562.807544
setting npatches to 3
ledflag 1
.... swapping bytes
writing generic LED file: IMG-HH-ALPSRP116047010-H1.0__A.LED
near_range, shift = 849265 128
The range sampling rate for master and slave images are: 32000000
pre_proc_batch.csh
preprocess slave images
setting fd1 to 77.112301
setting near_range to 848965.00
setting radius to 6377562.807544
setting npatches to 3
ledflag 1
.... swapping bytes
writing generic LED file: IMG-HH-ALPSRP149597010-H1.0__A.LED
near_range, shift = 850014 448
near_range, shift = 848965 0
The range sampling rate for master and slave images are: 32000000
pre_proc_batch.csh
preprocess slave images
setting fd1 to 77.112301
setting near_range to 848965.00
setting radius to 6377562.807544
setting npatches to 3
ledflag 1
.... swapping bytes
writing generic LED file: IMG-HH-ALPSRP156307010-H1.0__A.LED
The range sampling rate for master and slave images are: 32000000
pre_proc_batch.csh
preprocess slave images
setting fd1 to 77.112301
setting near_range to 848965.00
setting radius to 6377562.807544
setting npatches to 3
ledflag 1
.... swapping bytes
writing generic LED file: IMG-HH-ALPSRP163017010-H1.0__A.LED
near_range, shift = 849115 64
The range sampling rate for master and slave images are: 32000000
pre_proc_batch.csh
preprocess slave images
setting fd1 to 77.112301
setting near_range to 848965.00
setting radius to 6377562.807544
setting npatches to 3
ledflag 1
.... swapping bytes
writing generic LED file: IMG-HH-ALPSRP203277010-H1.0__A.LED
near_range, shift = 849115 64
The range sampling rate for master and slave images are: 32000000
pre_proc_batch.csh
preprocess slave images
setting fd1 to 77.112301
setting near_range to 848965.00
setting radius to 6377562.807544
setting npatches to 3
ledflag 1
.... swapping bytes
```

```
writing generic LED file: IMG-HH-ALPSRP209987010-H1.0_A.LED
near_range, shift = 849415 192
near_range, shift = 848815 -64
The range sampling rate for master and slave images are: 32000000
pre_proc_batch.csh
preprocess slave images
setting fd1 to 77.112301
setting near_range to 848965.00
setting radius to 6377562.807544
setting npatches to 3
ledflag 1
.... swapping bytes
writing generic LED file: IMG-HH-ALPSRP216697010-H1.0_A.LED
near_range, shift = 849265 128
near_range, shift = 848815 -64
The range sampling rate for master and slave images are: 32000000
```

END PREPROCESS A STACK OF IMAGES

```
baseline table.dat
05565 2007040.6352353694 405 0.000000 0.000000
09591 2007316.6348459597 681 -64.141343 -154.443018
11604 2008089.6337344318 819 -765.325177 -992.090931
14959 2008319.6343932052 1049 653.428933 838.266848
15630 2008365.6349251843 1095 310.794113 279.200032
16301 2009045.6353371635 1140 350.283380 454.752539
20327 2009321.6364631124 1416 -18.167020 -75.758321
20998 2010002.6364338764 1462 -26.532355 -181.412780
21669 2010048.6363133439 1508 -169.717788 -300.679701
```

```
intf.in
IMG-HH-ALPSRP055657010-H1.0_A:IMG-HH-ALPSRP095917010-H1.0_A
IMG-HH-ALPSRP055657010-H1.0_A:IMG-HH-ALPSRP116047010-H1.0_A
IMG-HH-ALPSRP055657010-H1.0_A:IMG-HH-ALPSRP149597010-H1.0_A
IMG-HH-ALPSRP055657010-H1.0_A:IMG-HH-ALPSRP156307010-H1.0_A
IMG-HH-ALPSRP055657010-H1.0_A:IMG-HH-ALPSRP163017010-H1.0_A
IMG-HH-ALPSRP055657010-H1.0_A:IMG-HH-ALPSRP203277010-H1.0_A
IMG-HH-ALPSRP055657010-H1.0_A:IMG-HH-ALPSRP209987010-H1.0_A
IMG-HH-ALPSRP055657010-H1.0_A:IMG-HH-ALPSRP216697010-H1.0_A
IMG-HH-ALPSRP095917010-H1.0_A:IMG-HH-ALPSRP116047010-H1.0_A
IMG-HH-ALPSRP095917010-H1.0_A:IMG-HH-ALPSRP149597010-H1.0_A
IMG-HH-ALPSRP095917010-H1.0_A:IMG-HH-ALPSRP156307010-H1.0_A
IMG-HH-ALPSRP095917010-H1.0_A:IMG-HH-ALPSRP163017010-H1.0_A
IMG-HH-ALPSRP095917010-H1.0_A:IMG-HH-ALPSRP203277010-H1.0_A
IMG-HH-ALPSRP095917010-H1.0_A:IMG-HH-ALPSRP209987010-H1.0_A
IMG-HH-ALPSRP095917010-H1.0_A:IMG-HH-ALPSRP216697010-H1.0_A
IMG-HH-ALPSRP116047010-H1.0_A:IMG-HH-ALPSRP149597010-H1.0_A
IMG-HH-ALPSRP116047010-H1.0_A:IMG-HH-ALPSRP156307010-H1.0_A
IMG-HH-ALPSRP116047010-H1.0_A:IMG-HH-ALPSRP163017010-H1.0_A
IMG-HH-ALPSRP116047010-H1.0_A:IMG-HH-ALPSRP203277010-H1.0_A
IMG-HH-ALPSRP116047010-H1.0_A:IMG-HH-ALPSRP209987010-H1.0_A
IMG-HH-ALPSRP116047010-H1.0_A:IMG-HH-ALPSRP216697010-H1.0_A
IMG-HH-ALPSRP149597010-H1.0_A:IMG-HH-ALPSRP156307010-H1.0_A
IMG-HH-ALPSRP149597010-H1.0_A:IMG-HH-ALPSRP163017010-H1.0_A
IMG-HH-ALPSRP149597010-H1.0_A:IMG-HH-ALPSRP203277010-H1.0_A
IMG-HH-ALPSRP149597010-H1.0_A:IMG-HH-ALPSRP209987010-H1.0_A
IMG-HH-ALPSRP149597010-H1.0_A:IMG-HH-ALPSRP216697010-H1.0_A
IMG-HH-ALPSRP156307010-H1.0_A:IMG-HH-ALPSRP163017010-H1.0_A
IMG-HH-ALPSRP156307010-H1.0_A:IMG-HH-ALPSRP203277010-H1.0_A
IMG-HH-ALPSRP156307010-H1.0_A:IMG-HH-ALPSRP209987010-H1.0_A
IMG-HH-ALPSRP156307010-H1.0_A:IMG-HH-ALPSRP216697010-H1.0_A
IMG-HH-ALPSRP163017010-H1.0_A:IMG-HH-ALPSRP203277010-H1.0_A
IMG-HH-ALPSRP163017010-H1.0_A:IMG-HH-ALPSRP209987010-H1.0_A
IMG-HH-ALPSRP163017010-H1.0_A:IMG-HH-ALPSRP216697010-H1.0_A
IMG-HH-ALPSRP203277010-H1.0_A:IMG-HH-ALPSRP209987010-H1.0_A
IMG-HH-ALPSRP203277010-H1.0_A:IMG-HH-ALPSRP216697010-H1.0_A
IMG-HH-ALPSRP209987010-H1.0_A:IMG-HH-ALPSRP216697010-H1.0_A
```

```
align.in
IMG-HH-ALPSRP055657010-H1.0_A:IMG-HH-ALPSRP095917010-H1.0_A:IMG-HH-ALPSRP055657010-H1.0_A
IMG-HH-ALPSRP055657010-H1.0_A:IMG-HH-ALPSRP116047010-H1.0_A:IMG-HH-ALPSRP055657010-H1.0_A
IMG-HH-ALPSRP055657010-H1.0_A:IMG-HH-ALPSRP149597010-H1.0_A:IMG-HH-ALPSRP055657010-H1.0_A
IMG-HH-ALPSRP055657010-H1.0_A:IMG-HH-ALPSRP156307010-H1.0_A:IMG-HH-ALPSRP055657010-H1.0_A
IMG-HH-ALPSRP055657010-H1.0_A:IMG-HH-ALPSRP163017010-H1.0_A:IMG-HH-ALPSRP055657010-H1.0_A
IMG-HH-ALPSRP055657010-H1.0_A:IMG-HH-ALPSRP203277010-H1.0_A:IMG-HH-ALPSRP055657010-H1.0_A
IMG-HH-ALPSRP055657010-H1.0_A:IMG-HH-ALPSRP209987010-H1.0_A:IMG-HH-ALPSRP055657010-H1.0_A
IMG-HH-ALPSRP055657010-H1.0_A:IMG-HH-ALPSRP216697010-H1.0_A:IMG-HH-ALPSRP055657010-H1.0_A
IMG-HH-ALPSRP095917010-H1.0_A:IMG-HH-ALPSRP116047010-H1.0_A:IMG-HH-ALPSRP055657010-H1.0_A
IMG-HH-ALPSRP095917010-H1.0_A:IMG-HH-ALPSRP149597010-H1.0_A:IMG-HH-ALPSRP055657010-H1.0_A
IMG-HH-ALPSRP095917010-H1.0_A:IMG-HH-ALPSRP156307010-H1.0_A:IMG-HH-ALPSRP055657010-H1.0_A
IMG-HH-ALPSRP095917010-H1.0_A:IMG-HH-ALPSRP163017010-H1.0_A:IMG-HH-ALPSRP055657010-H1.0_A
IMG-HH-ALPSRP095917010-H1.0_A:IMG-HH-ALPSRP203277010-H1.0_A:IMG-HH-ALPSRP055657010-H1.0_A
IMG-HH-ALPSRP095917010-H1.0_A:IMG-HH-ALPSRP209987010-H1.0_A:IMG-HH-ALPSRP055657010-H1.0_A
IMG-HH-ALPSRP095917010-H1.0_A:IMG-HH-ALPSRP216697010-H1.0_A:IMG-HH-ALPSRP055657010-H1.0_A
IMG-HH-ALPSRP116047010-H1.0_A:IMG-HH-ALPSRP149597010-H1.0_A:IMG-HH-ALPSRP055657010-H1.0_A
IMG-HH-ALPSRP116047010-H1.0_A:IMG-HH-ALPSRP156307010-H1.0_A:IMG-HH-ALPSRP055657010-H1.0_A
IMG-HH-ALPSRP116047010-H1.0_A:IMG-HH-ALPSRP163017010-H1.0_A:IMG-HH-ALPSRP055657010-H1.0_A
IMG-HH-ALPSRP116047010-H1.0_A:IMG-HH-ALPSRP203277010-H1.0_A:IMG-HH-ALPSRP055657010-H1.0_A
IMG-HH-ALPSRP116047010-H1.0_A:IMG-HH-ALPSRP209987010-H1.0_A:IMG-HH-ALPSRP055657010-H1.0_A
IMG-HH-ALPSRP116047010-H1.0_A:IMG-HH-ALPSRP216697010-H1.0_A:IMG-HH-ALPSRP055657010-H1.0_A
IMG-HH-ALPSRP149597010-H1.0_A:IMG-HH-ALPSRP156307010-H1.0_A:IMG-HH-ALPSRP055657010-H1.0_A
IMG-HH-ALPSRP149597010-H1.0_A:IMG-HH-ALPSRP163017010-H1.0_A:IMG-HH-ALPSRP055657010-H1.0_A
IMG-HH-ALPSRP149597010-H1.0_A:IMG-HH-ALPSRP203277010-H1.0_A:IMG-HH-ALPSRP055657010-H1.0_A
IMG-HH-ALPSRP149597010-H1.0_A:IMG-HH-ALPSRP209987010-H1.0_A:IMG-HH-ALPSRP055657010-H1.0_A
IMG-HH-ALPSRP149597010-H1.0_A:IMG-HH-ALPSRP216697010-H1.0_A:IMG-HH-ALPSRP055657010-H1.0_A
IMG-HH-ALPSRP156307010-H1.0_A:IMG-HH-ALPSRP163017010-H1.0_A:IMG-HH-ALPSRP055657010-H1.0_A
IMG-HH-ALPSRP156307010-H1.0_A:IMG-HH-ALPSRP203277010-H1.0_A:IMG-HH-ALPSRP055657010-H1.0_A
IMG-HH-ALPSRP156307010-H1.0_A:IMG-HH-ALPSRP209987010-H1.0_A:IMG-HH-ALPSRP055657010-H1.0_A
IMG-HH-ALPSRP156307010-H1.0_A:IMG-HH-ALPSRP216697010-H1.0_A:IMG-HH-ALPSRP055657010-H1.0_A
IMG-HH-ALPSRP163017010-H1.0_A:IMG-HH-ALPSRP203277010-H1.0_A:IMG-HH-ALPSRP055657010-H1.0_A
IMG-HH-ALPSRP163017010-H1.0_A:IMG-HH-ALPSRP209987010-H1.0_A:IMG-HH-ALPSRP055657010-H1.0_A
IMG-HH-ALPSRP163017010-H1.0_A:IMG-HH-ALPSRP216697010-H1.0_A:IMG-HH-ALPSRP055657010-H1.0_A
IMG-HH-ALPSRP203277010-H1.0_A:IMG-HH-ALPSRP209987010-H1.0_A:IMG-HH-ALPSRP055657010-H1.0_A
IMG-HH-ALPSRP203277010-H1.0_A:IMG-HH-ALPSRP216697010-H1.0_A:IMG-HH-ALPSRP055657010-H1.0_A
IMG-HH-ALPSRP209987010-H1.0_A:IMG-HH-ALPSRP216697010-H1.0_A:IMG-HH-ALPSRP055657010-H1.0_A
```

align\_batch.csh AL05 align.in

```
ALIGN.CSH - START
focussing master
Computing range reference function.
Processing patch 1
Processing Elapsed Time: 0 min 0.05 sec
Range Compression
Processing Elapsed Time: 0 min 5.14 sec
Azimuthal Transform
Processing Elapsed Time: 0 min 12.01 sec
Range Migration
Processing Elapsed Time: 0 min 21.49 sec
Azimuthal Compression
Processing Elapsed Time: 0 min 40.82 sec
Writing Data
Processing patch 2
Processing Elapsed Time: 0 min 42.83 sec
Range Compression
Processing Elapsed Time: 0 min 47.10 sec
Azimuthal Transform
Processing Elapsed Time: 0 min 54.06 sec
Range Migration
```

```

Processing Elapsed Time: 1 min 3.68 sec
Azimuthal Compression
Processing Elapsed Time: 1 min 23.19 sec
Writing Data
Processing patch 3
Processing Elapsed Time: 1 min 24.70 sec
Range Compression
Processing Elapsed Time: 1 min 29.20 sec
Azimuthal Transform
Processing Elapsed Time: 1 min 36.84 sec
Range Migration
Processing Elapsed Time: 1 min 46.88 sec
Azimuthal Compression
Processing Elapsed Time: 2 min 8.20 sec
Writing Data
Processing Elapsed Time: 2 min 9.75 sec
number of points clipped to short int 64
align.csh
focusing slave
Computing range reference function.
Processing patch 1
Processing Elapsed Time: 0 min 0.04 sec
Range Compression
Processing Elapsed Time: 0 min 5.40 sec
Azimuthal Transform
Processing Elapsed Time: 0 min 12.92 sec
Range Migration
Processing Elapsed Time: 0 min 22.99 sec
Azimuthal Compression
Processing Elapsed Time: 0 min 44.84 sec
Writing Data
Processing patch 2
Processing Elapsed Time: 0 min 46.43 sec
Range Compression
Processing Elapsed Time: 0 min 51.66 sec
Azimuthal Transform
Processing Elapsed Time: 0 min 58.58 sec
Range Migration
Processing Elapsed Time: 1 min 8.08 sec
Azimuthal Compression
Processing Elapsed Time: 1 min 27.34 sec
Writing Data
Processing patch 3
Processing Elapsed Time: 1 min 29.45 sec
Range Compression
Processing Elapsed Time: 1 min 34.10 sec
Azimuthal Transform
Processing Elapsed Time: 1 min 41.05 sec
Range Migration
Processing Elapsed Time: 1 min 50.40 sec
Azimuthal Compression
Processing Elapsed Time: 2 min 9.62 sec
Writing Data
Processing Elapsed Time: 2 min 11.78 sec
number of points clipped to short int 29
align.csh
correlate master and slave to find offset parameters
setting xsearch to 64
setting nx_corr to 128
setting ysearch to 64
setting ny_corr to 128
11304 27648 11304 27648 10 91 0.002151
locations n 512 nx 11304 nyl 32 nxl 16 x_inc 574 y_inc 826
elapsed time: 19.355816
align.csh
refocus slave
Computing range reference function.
Processing patch 1
Processing Elapsed Time: 0 min 0.05 sec
Range Compression
Processing Elapsed Time: 0 min 6.34 sec
Azimuthal Transform
Processing Elapsed Time: 0 min 13.16 sec
Range Migration
Processing Elapsed Time: 0 min 22.64 sec
Azimuthal Compression
Processing Elapsed Time: 0 min 44.62 sec
apply azimuth-dependent azimuth shift
Processing Elapsed Time: 1 min 1.72 sec
Writing Data
Processing patch 2
Processing Elapsed Time: 1 min 7.93 sec
Range Compression
Processing Elapsed Time: 1 min 13.09 sec
Azimuthal Transform
Processing Elapsed Time: 1 min 20.02 sec
Range Migration
Processing Elapsed Time: 1 min 29.42 sec
Azimuthal Compression
Processing Elapsed Time: 1 min 51.58 sec
apply azimuth-dependent azimuth shift
Processing Elapsed Time: 2 min 8.93 sec
Writing Data
Processing patch 3
Processing Elapsed Time: 2 min 15.64 sec
Range Compression
Processing Elapsed Time: 2 min 20.75 sec
Azimuthal Transform
Processing Elapsed Time: 2 min 27.96 sec
Range Migration
Processing Elapsed Time: 2 min 37.35 sec
Azimuthal Compression
Processing Elapsed Time: 3 min 0.74 sec
apply azimuth-dependent azimuth shift
Processing Elapsed Time: 3 min 20.23 sec
Writing Data
Processing Elapsed Time: 3 min 26.96 sec
number of points clipped to short int 35
rm: No match.
ALIGN.CSH - END

intf_batch.csh ALOS batch.config
clean up topo/ folder

DEM2TOPO_RA.CSH - START
USER SHOULD PROVIDE DEM FILE
range decimation is: 2
blockmedian: Provides 3, expects 3-column binary data
blockmedian: Processing input table data

```

```

blockmedian: W: 0 E: 11304 S: 0 N: 27648 n_columns: 5652 n_rows: 6912
blockmedian: Input 3 columns via binary records using format ddd
blockmedian: Output 3 columns via binary records using format ddd
blockmedian: N read: 884645 N used: 881816 outside_area: 2829 N cells filled: 881811
surface: Provides 3, expects 3-column binary data
surface: Grid domain: W: 0 E: 11304 S: 0 N: 27648 n_columns: 5652 n_rows: 6912 [pixel registration]
surface: Processing input table data
surface: Input 3 columns via binary records using format ddd
surface: Minimum value of your dataset x,y,z at: surface: 10.7620668411 25.3873825073 75.5127410889
surface: Maximum value of your dataset x,y,z at: surface: 9031.2578125 21985.4921875 1537.36853027
surface: LS plane determined: z = 37.8542 + (-0.00195957 * col) + (0.055743 * row)
surface:


| surface: | Grid | Mode | Iteration | Max Change        | Conv Limit        | Total Iterations |
|----------|------|------|-----------|-------------------|-------------------|------------------|
| surface: | 36   | D    | 22        | 0.000210190902124 | 0.000451679175952 | 22               |
| surface: | 12   | I    | 30        | 0.00123702018121  | 0.0013550375278   | 52               |
| surface: | 12   | D    | 22        | 0.0008157291249   | 0.00135503752786  | 74               |
| surface: | 4    | I    | 25        | 0.00379925759496  | 0.0040651125835   | 99               |
| surface: | 4    | D    | 49        | 0.00365791616648  | 0.0040651125835   | 148              |
| surface: | 2    | I    | 18        | 0.00718692895031  | 0.0081302251671   | 166              |
| surface: | 2    | D    | 150       | 0.0079501726638   | 0.00813022516713  | 316              |
| surface: | 1    | I    | 17        | 0.0128335190144   | 0.0162604503343   | 333              |
| surface: | 1    | D    | 234       | 0.016173982333    | 0.0162604503343   | 567              |


surface: Fit info: N data points N nodes mean error rms errorcurvature
surface: 881811 39079189 1.27329464994e-06 0.00592835020284 48831.2714734
grd2cpt: Processing input grid(s)
grd2cpt: Mean and S.D. of data are 224.563997199 196.578984971
grdimage: Allocates memory and read data file topo_ra.grd
grdimage: Evaluate image pixel colors
grdimage: Creating 8-bit grayscale image
DEM2TOPO_RA.CSH - END
NO TOPO_RA SHIFT

```

START FORM A STACK OF INTERFEROGRAMS

```

INTF.CSH, FILTER.CSH - START
intf.csh
running phasediff...
reading topo topo_ra.grd
xdim 11304, ydim 27648
filter.csh
gauss_300 4 2 (4 2)
making amplitudes...
filtering interferogram...
making amplitude...
making correlation...
making phase...
filtering phase...
INTF.CSH, FILTER.CSH - END

```

MAKE LANDMASK -- START
REQUIRE FULL RESOLUTION COASTLINE FROM GMT

```

grdlandmask: GSHHG version 2.3.7
Derived from World Vector Shoreline, CIA MDB-II, and Atlas of the Cryosphere
Processed by Paul Wessel and Walter H. F. Smith, 1994-2017
grdlandmask: Nodes in water will be set to NaN
grdlandmask: Nodes on land will be set to 1
grdlandmask: Level 0 contained 8112640 nodes
grdlandmask: Level 1 contained 2478081 nodes
grdlandmask: Done!
surface: Provides 3, expects 3-column binary data
surface: Grid domain: W: 113.83333329 E: 117.416666662 S: -9.166666663 N: -7.4166666637 n_columns: 4300 n_rows: 2100 [gridline registration]
surface: Processing input table data
surface: Input 3 columns via binary records using format fff
surface: Minimum value of your dataset x,y,z at: surface: 114.131668091 -8.81166744232 -9.98584938049
surface: Maximum value of your dataset x,y,z at: surface: 114.752502441 -8.06000041962 11313.9794922
surface: LS plane determined: z = -5537.18 + (11.9718 * col) + (2.63785 * row)
surface:


| surface: | Grid | Mode | Iteration | Max Change        | Conv Limit        | Total Iterations |
|----------|------|------|-----------|-------------------|-------------------|------------------|
| surface: | 100  | D    | 15632     | 4.97881483045e-05 | 5.00683227883e-05 | 15632            |
| surface: | 20   | I    | 82        | 0.00023466581793  | 0.000250341613942 | 15714            |
| surface: | 20   | D    | 10000     | 0.000262519327484 | 0.000250341613942 | 25714            |
| surface: | 4    | I    | 58        | 0.00122450991342  | 0.0012517080697   | 25772            |
| surface: | 4    | D    | 2000      | 0.00162037791787  | 0.0012517080697   | 27772            |
| surface: | 2    | I    | 18        | 0.00189403864915  | 0.0025034161394   | 27790            |
| surface: | 2    | D    | 990       | 0.00249980896072  | 0.0025034161394   | 28780            |
| surface: | 1    | I    | 15        | 0.00343781941582  | 0.0050068322788   | 28795            |
| surface: | 1    | D    | 289       | 0.00500475341226  | 0.0050068322788   | 29084            |


surface: Fit info: N data points N nodes mean error rms errorcurvature
surface: 884645 9036401 0 10628.5901568
surface: Provides 3, expects 3-column binary data
surface: Grid domain: W: 113.83333329 E: 117.416666662 S: -9.166666663 N: -7.4166666637 n_columns: 4300 n_rows: 2100 [gridline registration]
surface: Processing input table data
surface: Input 3 columns via binary records using format fff
surface: Minimum value of your dataset x,y,z at: surface: 114.608329773 -8.88583278656 -19.9133529663
surface: Maximum value of your dataset x,y,z at: surface: 114.511665344 -8.09000015259 27667.96875
surface: LS plane determined: z = -3589.86 + (-6.38689 * col) + (28.2138 * row)
surface:


| surface: | Grid | Mode | Iteration | Max Change        | Conv Limit        | Total Iterations |
|----------|------|------|-----------|-------------------|-------------------|------------------|
| surface: | 100  | D    | 16620     | 2.72951310095e-06 | 2.76420307001e-06 | 16620            |
| surface: | 20   | I    | 99        | 1.27056912631e-05 | 1.38210153501e-05 | 16719            |
| surface: | 20   | D    | 10000     | 0.000144635361436 | 1.38210153501e-05 | 26719            |
| surface: | 4    | I    | 76        | 6.89682605929e-05 | 6.91050767503e-05 | 26795            |
| surface: | 4    | D    | 2000      | 0.000456770562002 | 6.91050767503e-05 | 28795            |
| surface: | 2    | I    | 18        | 0.000108709586896 | 0.000138210153501 | 28813            |
| surface: | 2    | D    | 911       | 0.000137974965032 | 0.000138210153501 | 29724            |
| surface: | 1    | I    | 16        | 0.000250151856504 | 0.000276420307001 | 29740            |
| surface: | 1    | D    | 500       | 0.000304191740787 | 0.000276420307001 | 30240            |


surface: Fit info: N data points N nodes mean error rms errorcurvature
surface: 884645 9036401 0 525087.416621
MAKE LANDMASK -- END

```

```

SNAPHU.CSH - START
threshold_snaphu: .45
grdmath: Perform reverse Polish notation calculations on grids
grdmath: phase_patch.grd landmask_ra_patch.grd MUL = phase_patch.grd
unwrapping phase with snaphu - higher threshold for faster unwrapping

```

```

snaphu v1.4.2
32 parameters input from file snaphu.conf.brief (297 lines total)
Reading wrapped phase from file phase.in
No weight file specified. Assuming uniform weights
Reading correlation data from file corr.in
Calculating deformation-mode cost parameters
Building range cost arrays
Building azimuth cost arrays
Initializing flows with MST algorithm
Running approximate minimum spanning tree solver
Running nonlinear network flow optimizer
Maximum flow on network: 3

```

Number of nodes in network: 4878776  
Flow increment: 1 (Total improvements: 0)  
Treesize: 4878776 Pivots: 242184 Improvements: 341  
Maximum flow on network: 3  
Flow increment: 2 (Total improvements: 341)  
Treesize: 4878776 Pivots: 12 Improvements: 4  
Maximum flow on network: 3  
Flow increment: 3 (Total improvements: 345)  
Treesize: 4878776 Pivots: 7 Improvements: 2  
Maximum flow on network: 3  
Total solution cost: 770583  
Integrating phase  
Writing output to file unwrap.out  
Program snaphu done  
Elapsed processor time: 0:01:40.36  
Elapsed wall clock time: 0:01:46  
grdmath: Perform reverse Polish notation calculations on grids  
grdmath: unwrap.grd landmask\_ra\_patch.grd MUL = tmp.grd  
SNAPHU.CSH - END

GEOCODE.CSH - START

threshold\_geocode: .45  
grdmath: Perform reverse Polish notation calculations on grids  
grdmath: corr.grd 0.45 GE 0 NAN mask.grd MUL = mask2.grd  
pscale: Warning: The -E option is deprecated but is accepted.  
pscale: For the current -D syntax you should use -D modifier +e instead.  
pscale: Note you cannot mix new-style modifiers (+e) with the old-style -D option.  
pscale: Warning: The -E option is deprecated but is accepted.  
pscale: For the current -D syntax you should use -D modifier +e instead.  
pscale: Note you cannot mix new-style modifiers (+e) with the old-style -D option.  
geocode.csh

project correlation, phase, unwrapped and amplitude back to lon lat coordinates  
remarked is by root on Mon May 21 10:24:22 JST 2018 with geocode.csh  
proj\_ra2ll.csh

surface: Provides 3, expects 3-column binary data  
surface: Grid domain: W: 144 E: 11296 S: 0 N: 27648 n\_columns: 697 n\_rows: 864 [gridline registration]  
surface: Warning: Your grid dimensions are mutually prime. Convergence is very unlikely.  
surface: Hint: Choosing -R-32/11488/0/27648 [n\_columns = 720, n\_rows = 864] might cut run time by a factor of 313.31004  
surface: Hint: Choosing -R-32/11488/-576/28224 [n\_columns = 720, n\_rows = 900] might cut run time by a factor of 296.03306  
surface: Hint: Choosing -R-416/11872/0/27648 [n\_columns = 768, n\_rows = 864] might cut run time by a factor of 293.90337  
surface: Hint: Choosing -R-32/11488/-1536/29184 [n\_columns = 720, n\_rows = 960] might cut run time by a factor of 281.91059  
surface: Hint: Choosing -R-672/12128/0/27648 [n\_columns = 800, n\_rows = 864] might cut run time by a factor of 279.79174  
surface: Hint: Choosing -R-32/11488/-1728/29376 [n\_columns = 720, n\_rows = 972] might cut run time by a factor of 272.41527  
surface: Hint: Choosing -R-272/11728/-576/28224 [n\_columns = 750, n\_rows = 900] might cut run time by a factor of 266.2878  
surface: Hint: Choosing -R-32/11488/-2176/29824 [n\_columns = 720, n\_rows = 1000] might cut run time by a factor of 265.80215  
surface: Hint: Choosing -R-416/11872/-1536/29184 [n\_columns = 768, n\_rows = 960] might cut run time by a factor of 264.62065  
surface: Hint: Choosing -R-1184/12640/0/27648 [n\_columns = 864, n\_rows = 864] might cut run time by a factor of 261.30766  
surface: Hint: After completion you can recover the desired region via gmt grdcut  
surface: Processing input table data  
surface: Input 3 columns via binary records using format fff  
surface: Minimum value of your dataset x,y,z at: surface: 140.659957886 27643.1582031 114.019996643  
surface: Maximum value of your dataset x,y,z at: surface: 11302.2324219 77.4909057617 114.921669006  
surface: 270406 unusable points were supplied; these will be ignored.  
surface: You should have pre-processed the data with block-mean, -median, or -mode.  
surface: Check that previous processing steps write results with enough decimals.  
surface: LS plane determined: z = 114.188 + (0.00105942 \* col) + (-0.000198537 \* row)  
surface: Grid Mode IterationMax Change Conv Limit Total Iterations  
surface: 1 D 24 2.95139085076e-07 3.23696105733e-07 24

surface: Fit info: N data points N nodes mean error rms error curvature  
surface: 601296 603770 -6.90514032337e-07 0.00652434965488 10756.6135043  
surface: Provides 3, expects 3-column binary data  
surface: Grid domain: W: 144 E: 11296 S: 0 N: 27648 n\_columns: 697 n\_rows: 864 [gridline registration]  
surface: Warning: Your grid dimensions are mutually prime. Convergence is very unlikely.  
surface: Hint: Choosing -R-32/11488/0/27648 [n\_columns = 720, n\_rows = 864] might cut run time by a factor of 313.31004  
surface: Hint: Choosing -R-32/11488/-576/28224 [n\_columns = 720, n\_rows = 900] might cut run time by a factor of 296.03306  
surface: Hint: Choosing -R-416/11872/0/27648 [n\_columns = 768, n\_rows = 864] might cut run time by a factor of 293.90337  
surface: Hint: Choosing -R-32/11488/-1536/29184 [n\_columns = 720, n\_rows = 960] might cut run time by a factor of 281.91059  
surface: Hint: Choosing -R-672/12128/0/27648 [n\_columns = 800, n\_rows = 864] might cut run time by a factor of 279.79174  
surface: Hint: Choosing -R-32/11488/-1728/29376 [n\_columns = 720, n\_rows = 972] might cut run time by a factor of 272.41527  
surface: Hint: Choosing -R-272/11728/-576/28224 [n\_columns = 750, n\_rows = 900] might cut run time by a factor of 266.2878  
surface: Hint: Choosing -R-32/11488/-2176/29824 [n\_columns = 720, n\_rows = 1000] might cut run time by a factor of 265.80215  
surface: Hint: Choosing -R-416/11872/-1536/29184 [n\_columns = 768, n\_rows = 960] might cut run time by a factor of 264.62065  
surface: Hint: Choosing -R-1184/12640/0/27648 [n\_columns = 864, n\_rows = 864] might cut run time by a factor of 261.30766  
surface: Hint: After completion you can recover the desired region via gmt grdcut  
surface: Processing input table data  
surface: Input 3 columns via binary records using format fff  
surface: Minimum value of your dataset x,y,z at: surface: 139.596466064 11.1603660583 -8.98166656494  
surface: Maximum value of your dataset x,y,z at: surface: 11264.6044922 27659.5566406 -8.03750038147  
surface: 270406 unusable points were supplied; these will be ignored.  
surface: You should have pre-processed the data with block-mean, -median, or -mode.  
surface: Check that previous processing steps write results with enough decimals.  
surface: LS plane determined: z = -8.98027 + (0.000239852 \* col) + (0.000900209 \* row)  
surface: Grid Mode IterationMax Change Conv Limit Total Iterations  
surface: 1 D 24 6.64131631207e-08 6.94063883989e-08 24

surface: Fit info: N data points N nodes mean error rms error curvature  
surface: 601296 603770 -5.52554381515e-06 0.012211329987 14839.7119146  
blockmedian: Provides 3, expects 3-column binary data  
blockmedian: Processing input table data  
blockmedian: W: 114.011111111 E: 114.922222222 S: -8.98611111111 N: -8.03472222222 n\_columns: 820 n\_rows: 1370  
blockmedian: Input 3 columns via binary records using format fff  
blockmedian: Output 3 columns via binary records using format fff  
blockmedian: N read: 4790307 N used: 4790307 outside\_area: 0 N cells filled: 779322

proj\_ra2ll.csh  
blockmedian: Provides 3, expects 3-column binary data  
blockmedian: Processing input table data  
blockmedian: W: 114.011111111 E: 114.922222222 S: -8.98611111111 N: -8.03472222222 n\_columns: 820 n\_rows: 1370  
blockmedian: Input 3 columns via binary records using format fff  
blockmedian: Output 3 columns via binary records using format fff  
blockmedian: N read: 4794775 N used: 4794775 outside\_area: 0 N cells filled: 780092

proj\_ra2ll.csh  
blockmedian: Provides 3, expects 3-column binary data  
blockmedian: Processing input table data  
blockmedian: W: 114.055555556 E: 114.811111111 S: -8.65972222222 N: -8.09027777778 n\_columns: 680 n\_rows: 820  
blockmedian: Input 3 columns via binary records using format fff  
blockmedian: Output 3 columns via binary records using format fff  
blockmedian: N read: 25744 N used: 25744 outside\_area: 0 N cells filled: 6949

proj\_ra2ll.csh  
blockmedian: Provides 3, expects 3-column binary data  
blockmedian: Processing input table data  
blockmedian: W: 114.011111111 E: 114.922222222 S: -8.98611111111 N: -8.03472222222 n\_columns: 820 n\_rows: 1370  
blockmedian: Input 3 columns via binary records using format fff  
blockmedian: Output 3 columns via binary records using format fff  
blockmedian: N read: 4817664 N used: 4817664 outside\_area: 0 N cells filled: 783741

proj\_ra2ll.csh  
blockmedian: Provides 3, expects 3-column binary data  
blockmedian: Processing input table data  
blockmedian: W: 114.055555556 E: 114.811111111 S: -8.65972222222 N: -8.09027777778 n\_columns: 680 n\_rows: 820  
blockmedian: Input 3 columns via binary records using format fff  
blockmedian: Output 3 columns via binary records using format fff

```

blockmedian: N read: 25691 N used: 25691 outside_area: 0 N cells filled: 6938
proj_ra2ll.csh
blockmedian: Provides 3, expects 3-column binary data
blockmedian: Processing input table data
blockmedian: W: 114.011111111 E: 114.844444444 S: -8.78472222222 N: -8.08333333333 n_columns: 750 n_rows: 1010
blockmedian: Input 3 columns via binary records using format fff
blockmedian: Output 3 columns via binary records using format fff
blockmedian: N read: 2133501 N used: 2133501 outside_area: 0 N cells filled: 350902
proj_ra2ll.csh
blockmedian: Provides 3, expects 3-column binary data
blockmedian: Processing input table data
blockmedian: W: 114.055555556 E: 114.811111111 S: -8.65972222222 N: -8.09027777778 n_columns: 680 n_rows: 820
blockmedian: Input 3 columns via binary records using format fff
blockmedian: Output 3 columns via binary records using format fff
blockmedian: N read: 25744 N used: 25744 outside_area: 0 N cells filled: 6949
geocode.csh
make the KML files for Google Earth
grdimage: Allocates memory and read data file display_amp_ll.grd
grdimage: Evaluate image pixel colors
grdimage: Creating 24-bit color image
Make display_amp_ll.kml and display_amp_ll.png
psconvert: Processing display_amp_ll.ps...
psconvert: Figure dimensions: Width: 65.58 points [0.910833 inch] Height: 68.52 points [0.951666 inch]
psconvert: gs -q -dSAFER -dNOPAUSE -dBATCH -dPDFSETTINGS=/prepress -dDownsampleColorImages=false -dDownsampleGrayImages=false -
dDownsampleMonoImages=false -dUseFlateCompression=true -dEmbedAllFonts=true -dSubsetFonts=true -dMonoImageFilter=/FlateEncode -
dAutoFilterGrayImages=false -dGrayImageFilter=/FlateEncode -dAutoFilterColorImages=false -dColorImageFilter=/FlateEncode -dSCANCONVERTERTYPE=2 -
dMaxBitmap=2147483647 -dUseFastColor=true -sDEVICE=pngalpha -g820x857 -r900 -sOutputFile='display_amp_ll.png' -f'./psconvert_23460d.eps'
psconvert: Done.
grdimage: Allocates memory and read data file corr_ll.grd
grdimage: Evaluate image pixel colors
grdimage: Creating 24-bit color image
PSL: Colormap of 255 colors created
Make corr_ll.kml and corr_ll.png
psconvert: Processing corr_ll.ps...
psconvert: Figure dimensions: Width: 65.58 points [0.910833 inch] Height: 68.52 points [0.951666 inch]
psconvert: gs -q -dSAFER -dNOPAUSE -dBATCH -dPDFSETTINGS=/prepress -dDownsampleColorImages=false -dDownsampleGrayImages=false -
dDownsampleMonoImages=false -dUseFlateCompression=true -dEmbedAllFonts=true -dSubsetFonts=true -dMonoImageFilter=/FlateEncode -
dAutoFilterGrayImages=false -dGrayImageFilter=/FlateEncode -dAutoFilterColorImages=false -dColorImageFilter=/FlateEncode -dSCANCONVERTERTYPE=2 -
dMaxBitmap=2147483647 -dUseFastColor=true -sDEVICE=pngalpha -g820x857 -r900 -sOutputFile='corr_ll.png' -f'./psconvert_32725d.eps'
psconvert: Done.
grdimage: Allocates memory and read data file phase_mask_ll.grd
grdimage: Evaluate image pixel colors
grdimage: Creating 24-bit color image
Make phase_mask_ll.kml and phase_mask_ll.png
psconvert: Processing phase_mask_ll.ps...
psconvert: Figure dimensions: Width: 54.42 points [0.755833 inch] Height: 40.98 points [0.569166 inch]
psconvert: gs -q -dSAFER -dNOPAUSE -dBATCH -dPDFSETTINGS=/prepress -dDownsampleColorImages=false -dDownsampleGrayImages=false -
dDownsampleMonoImages=false -dUseFlateCompression=true -dEmbedAllFonts=true -dSubsetFonts=true -dMonoImageFilter=/FlateEncode -
dAutoFilterGrayImages=false -dGrayImageFilter=/FlateEncode -dAutoFilterColorImages=false -dColorImageFilter=/FlateEncode -dSCANCONVERTERTYPE=2 -
dMaxBitmap=2147483647 -dUseFastColor=true -sDEVICE=pngalpha -g681x513 -r900 -sOutputFile='phase_mask_ll.png' -f'./psconvert_32986d.eps'
psconvert: Done.
grdimage: Allocates memory and read data file phasefilt_mask_ll.grd
grdimage: Evaluate image pixel colors
grdimage: Creating 24-bit color image
Make phasefilt_mask_ll.kml and phasefilt_mask_ll.png
psconvert: Processing phasefilt_mask_ll.ps...
psconvert: Figure dimensions: Width: 54.42 points [0.755833 inch] Height: 40.98 points [0.569166 inch]
psconvert: gs -q -dSAFER -dNOPAUSE -dBATCH -dPDFSETTINGS=/prepress -dDownsampleColorImages=false -dDownsampleGrayImages=false -
dDownsampleMonoImages=false -dUseFlateCompression=true -dEmbedAllFonts=true -dSubsetFonts=true -dMonoImageFilter=/FlateEncode -
dAutoFilterGrayImages=false -dGrayImageFilter=/FlateEncode -dAutoFilterColorImages=false -dColorImageFilter=/FlateEncode -dSCANCONVERTERTYPE=2 -
dMaxBitmap=2147483647 -dUseFastColor=true -sDEVICE=pngalpha -g681x513 -r900 -sOutputFile='phasefilt_mask_ll.png' -f'./psconvert_33159d.eps'
psconvert: Done.
grdimage: Allocates memory and read data file unwrap_mask_ll.grd
grdimage: Evaluate image pixel colors
grdimage: Creating 24-bit color image
Make unwrap_mask_ll.kml and unwrap_mask_ll.png
psconvert: Processing unwrap_mask_ll.ps...
psconvert: Figure dimensions: Width: 54.42 points [0.755833 inch] Height: 40.98 points [0.569166 inch]
psconvert: gs -q -dSAFER -dNOPAUSE -dBATCH -dPDFSETTINGS=/prepress -dDownsampleColorImages=false -dDownsampleGrayImages=false -
dDownsampleMonoImages=false -dUseFlateCompression=true -dEmbedAllFonts=true -dSubsetFonts=true -dMonoImageFilter=/FlateEncode -
dAutoFilterGrayImages=false -dGrayImageFilter=/FlateEncode -dAutoFilterColorImages=false -dColorImageFilter=/FlateEncode -dSCANCONVERTERTYPE=2 -
dMaxBitmap=2147483647 -dUseFastColor=true -sDEVICE=pngalpha -g681x513 -r900 -sOutputFile='unwrap_mask_ll.png' -f'./psconvert_33375d.eps'
psconvert: Done.
grdimage: Allocates memory and read data file phasefilt_mask_ll.grd
grdimage: Evaluate image pixel colors
grdimage: Creating 24-bit color image
Make phasefilt_mask_ll.kml and phasefilt_mask_ll.png
psconvert: Processing phasefilt_mask_ll.ps...
psconvert: Figure dimensions: Width: 54.42 points [0.755833 inch] Height: 40.98 points [0.569166 inch]
psconvert: gs -q -dSAFER -dNOPAUSE -dBATCH -dPDFSETTINGS=/prepress -dDownsampleColorImages=false -dDownsampleGrayImages=false -
dDownsampleMonoImages=false -dUseFlateCompression=true -dEmbedAllFonts=true -dSubsetFonts=true -dMonoImageFilter=/FlateEncode -
dAutoFilterGrayImages=false -dGrayImageFilter=/FlateEncode -dAutoFilterColorImages=false -dColorImageFilter=/FlateEncode -dSCANCONVERTERTYPE=2 -
dMaxBitmap=2147483647 -dUseFastColor=true -sDEVICE=pngalpha -g681x513 -r900 -sOutputFile='phasefilt_mask_ll.png' -f'./psconvert_33586d.eps'
psconvert: Done.
grdimage: Allocates memory and read data file los_ll.grd
grdimage: Evaluate image pixel colors
grdimage: Creating 24-bit color image
Make los_ll.kml and los_ll.png
psconvert: Processing los_ll.ps...
psconvert: Figure dimensions: Width: 54.42 points [0.755833 inch] Height: 40.98 points [0.569166 inch]
psconvert: gs -q -dSAFER -dNOPAUSE -dBATCH -dPDFSETTINGS=/prepress -dDownsampleColorImages=false -dDownsampleGrayImages=false -
dDownsampleMonoImages=false -dUseFlateCompression=true -dEmbedAllFonts=true -dSubsetFonts=true -dMonoImageFilter=/FlateEncode -
dAutoFilterGrayImages=false -dGrayImageFilter=/FlateEncode -dAutoFilterColorImages=false -dColorImageFilter=/FlateEncode -dSCANCONVERTERTYPE=2 -
dMaxBitmap=2147483647 -dUseFastColor=true -sDEVICE=pngalpha -g681x513 -r900 -sOutputFile='los_ll.png' -f'./psconvert_33809d.eps'
psconvert: Done.
GEOCODE.CSH - END

```

```

stack.list
cut_2007040_2007316.grd IMG-HH-ALPSRP055657010-H1.0_A.PRM IMG-HH-ALPSRP095917010-H1.0_A.PRM
cut_2007040_2008089.grd IMG-HH-ALPSRP055657010-H1.0_A.PRM IMG-HH-ALPSRP116047010-H1.0_A.PRM
cut_2007040_2008319.grd IMG-HH-ALPSRP055657010-H1.0_A.PRM IMG-HH-ALPSRP149597010-H1.0_A.PRM
cut_2007040_2008365.grd IMG-HH-ALPSRP055657010-H1.0_A.PRM IMG-HH-ALPSRP156307010-H1.0_A.PRM
cut_2007040_2009045.grd IMG-HH-ALPSRP055657010-H1.0_A.PRM IMG-HH-ALPSRP163017010-H1.0_A.PRM
cut_2007040_2009321.grd IMG-HH-ALPSRP055657010-H1.0_A.PRM IMG-HH-ALPSRP203277010-H1.0_A.PRM
cut_2007040_2010002.grd IMG-HH-ALPSRP055657010-H1.0_A.PRM IMG-HH-ALPSRP209987010-H1.0_A.PRM
cut_2007040_2010048.grd IMG-HH-ALPSRP055657010-H1.0_A.PRM IMG-HH-ALPSRP216697010-H1.0_A.PRM

```

```
bash stack_phase.bash stack.list mean.grd std.grd
```

```
compute the mean LOS velocity ..
```

```

time span (days) of cut_2007040_2007316.grd: 276
accumulative days in the stack: 276
time span (days) of cut_2007040_2008089.grd: 414
accumulative days in the stack: 690
time span (days) of cut_2007040_2008319.grd: 644
accumulative days in the stack: 1334
time span (days) of cut_2007040_2008365.grd: 690
accumulative days in the stack: 2024

```



time span (days) of cut\_2007040\_2009045.grd: 735  
accumulative days in the stack: 2759  
time span (days) of cut\_2007040\_2009321.grd: 1011  
accumulative days in the stack: 3770  
time span (days) of cut\_2007040\_2010002.grd: 1057  
accumulative days in the stack: 4827  
time span (days) of cut\_2007040\_2010048.grd: 1103  
accumulative days in the stack: 5930

compute the standard deviations ..

mean\_ll.grd  
std\_ll.grd  
los\_ll\_2007316.grd  
los\_ll\_2008089.grd  
los\_ll\_2008319.grd  
los\_ll\_2008365.grd  
los\_ll\_2009045.grd  
los\_ll\_2009321.grd  
los\_ll\_2010002.grd  
los\_ll\_2010048.grd

csf select\_pairs.csh baseline\_table.dat 950 1000

intf.tab

cut_2007040_2007316.grd	corcut_2007040_2007316.grd	2007040	2007316	-154.443018
cut_2007040_2008089.grd	corcut_2007040_2008089.grd	2007040	2008089	-992.090931
cut_2007040_2008319.grd	corcut_2007040_2008319.grd	2007040	2008319	838.266848
cut_2007040_2008365.grd	corcut_2007040_2008365.grd	2007040	2008365	279.200032
cut_2007040_2009045.grd	corcut_2007040_2009045.grd	2007040	2009045	454.752539
cut_2007316_2008089.grd	corcut_2007316_2008089.grd	2007316	2008089	-837.634256
cut_2007316_2008319.grd	corcut_2007316_2008319.grd	2007316	2008319	992.647698
cut_2007316_2008365.grd	corcut_2007316_2008365.grd	2007316	2008365	433.581243
cut_2007316_2009045.grd	corcut_2007316_2009045.grd	2007316	2009045	609.149582
cut_2007316_2009321.grd	corcut_2007316_2009321.grd	2007316	2009321	78.657579
cut_2007316_2010002.grd	corcut_2007316_2010002.grd	2007316	2010002	-27.005466
cut_2007316_2010048.grd	corcut_2007316_2010048.grd	2007316	2010048	-146.259667
cut_2008089_2009321.grd	corcut_2008089_2009321.grd	2008089	2009321	916.231145
cut_2008089_2010002.grd	corcut_2008089_2010002.grd	2008089	2010002	810.561468
cut_2008089_2010048.grd	corcut_2008089_2010048.grd	2008089	2010048	691.323086
cut_2008319_2008365.grd	corcut_2008319_2008365.grd	2008319	2008365	-559.088173
cut_2008319_2009045.grd	corcut_2008319_2009045.grd	2008319	2009045	-383.551557
cut_2008319_2009321.grd	corcut_2008319_2009321.grd	2008319	2009321	-914.106716
cut_2008365_2009045.grd	corcut_2008365_2009045.grd	2008365	2009045	175.530607
cut_2008365_2009321.grd	corcut_2008365_2009321.grd	2008365	2009321	-354.931583
cut_2008365_2010002.grd	corcut_2008365_2010002.grd	2008365	2010002	-460.576219
cut_2008365_2010048.grd	corcut_2008365_2010048.grd	2008365	2010048	-579.829560
cut_2009045_2009321.grd	corcut_2009045_2009321.grd	2009045	2009321	-530.538283
cut_2009045_2010002.grd	corcut_2009045_2010002.grd	2009045	2010002	-636.187896
cut_2009045_2010048.grd	corcut_2009045_2010048.grd	2009045	2010048	-755.468827
cut_2009321_2010002.grd	corcut_2009321_2010002.grd	2009321	2010002	-105.656240
cut_2009321_2010048.grd	corcut_2009321_2010048.grd	2009321	2010048	-224.912859
cut_2010002_2010048.grd	corcut_2010002_2010048.grd	2010002	2010048	-119.238730

scene.tab  
2007040 405  
2007316 681  
2008089 819  
2008319 1049  
2008365 1095  
2009045 1140  
2009321 1416  
2010002 1462  
2010048 1508

sbas intf.tab scene.tab 28 9 2826 1728 -smooth 1.0 -wavelength 0.2362 -incidence 34.3 -range 848965 -rms -dem -atm 1

compute RMS misfit  
compute DEM error

setting smoothing to 1.000  
setting radar wavelength to 0.236 m  
setting radar incidence angle to 34.300 degree  
setting range to 848965.000 m  
Memory Allocation Successful...  
read table file ...  
number of SAR scenes is 9  
number of interferograms is 28  
read phase and correlation grids ...  
fill the G matrix ...

Applying atmospheric correction by common point stacking...

Hit Matrix:  
2007040 0 1 1 1 1 1 0 0 0  
2007316 0 0 1 1 1 1 1 1 1  
2008089 0 0 0 0 0 0 1 1 1  
2008319 0 0 0 0 1 1 1 0 0  
2008365 0 0 0 0 0 1 1 1 1  
2009045 0 0 0 0 0 0 1 1 1  
2009321 0 0 0 0 0 0 0 1 1  
2010002 0 0 0 0 0 0 0 0 1  
2010048 0 0 0 0 0 0 0 0 0

Applying exponential relaxation on smoothing parameters

Setting smoothing parameter to 1000.000000...  
fill the G matrix ...  
Computing deformation time-series...  
run least-squares problem over 2826 by 1728 pixel (0) ...  
matrix is full rank: 9

Removing deformation time-series from original unwrapped phase...  
Computing atmospheric phase screen by common-point stacking...

Initial estimate of APS ...  
atm\_noise(NO.4) = 2.227145  
atm\_noise(NO.3) = 1.716612  
atm\_noise(NO.7) = 1.387921  
atm\_noise(NO.0) = 0.000000  
atm\_noise(NO.1) = 0.000000  
atm\_noise(NO.2) = 0.000000  
atm\_noise(NO.5) = 0.000000  
atm\_noise(NO.6) = 0.000000  
atm\_noise(NO.8) = 0.000000

```
atm_noise(NO.4) = 2.230879
atm_noise(NO.3) = 1.723571
atm_noise(NO.7) = 1.375030
atm_noise(NO.0) = 0.000000
atm_noise(NO.1) = 0.000000
atm_noise(NO.2) = 0.000000
atm_noise(NO.5) = 0.000000
atm_noise(NO.6) = 0.000000
atm_noise(NO.8) = 0.000000
```

```
Applying atmospheric phase screen to original unwrapped phase...
Setting smoothing parameter to 1.000000...
fill the G matrix ...
run least-squares problem over 2826 by 1728 pixel (2) ...
matrix is rank-deficient: 8
```

write output ...

```
raln.grd
ralt.grd
rms_ll.grd
dem.grd
vel_ll.grd
disp_2007040_ll.grd
disp_2007316_ll.grd
disp_2008089_ll.grd
disp_2008319_ll.grd
disp_2008365_ll.grd
disp_2009045_ll.grd
disp_2009321_ll.grd
disp_2010002_ll.grd
disp_2010048_ll.grd
aps_2007040.grd
aps_2007316.grd
aps_2008089.grd
aps_2008319.grd
aps_2008365.grd
aps_2009045.grd
aps_2009321.grd
aps_2010002.grd
aps_2010048.grd
```

## A.7 ALOS PALSAR (Path 424 Row 7020) in Bali, Indonesia

```
data.in
IMG-HH-ALPSRP055657020-H1.0__A
IMG-HH-ALPSRP095917020-H1.0__A
IMG-HH-ALPSRP116047020-H1.0__A
IMG-HH-ALPSRP149597020-H1.0__A
IMG-HH-ALPSRP156307020-H1.0__A
IMG-HH-ALPSRP163017020-H1.0__A
IMG-HH-ALPSRP203277020-H1.0__A
IMG-HH-ALPSRP209987020-H1.0__A
IMG-HH-ALPSRP216697020-H1.0__A
```

pre\_proc\_batch.csh ALOS data.in batch.config

START PREPROCESS A STACK OF IMAGES

```
preprocess master image
ledflag 1
.... swapping bytes
writing generic LED file: IMG-HH-ALPSRP055657020-H1.0__A.LED
.... calculating doppler for IMG-HH-ALPSRP055657020-H1.0__A.raw
Working on line 2000
Working on line 4000
Working on line 6000
Working on line 8000
Working on line 10000
Working on line 12000
Working on line 14000
Working on line 16000
Working on line 18000
Working on line 20000
Working on line 22000
Working on line 24000
Working on line 26000
Working on line 28000
Working on line 30000
Working on line 32000
Working on line 34000
pre_proc_batch.csh
preprocess slave images
setting fd1 to 29.328717
setting near_range to 848965.00
setting radius to 6377621.134085
setting npatches to 3
ledflag 1
.... swapping bytes
writing generic LED file: IMG-HH-ALPSRP095917020-H1.0__A.LED
near_range, shift = 849265 128
The range sampling rate for master and slave images are: 32000000
pre_proc_batch.csh
preprocess slave images
setting fd1 to 29.328717
setting near_range to 848965.00
setting radius to 6377621.134085
setting npatches to 3
ledflag 1
.... swapping bytes
writing generic LED file: IMG-HH-ALPSRP116047020-H1.0__A.LED
near_range, shift = 849265 128
near_range, shift = 848665 -128
The range sampling rate for master and slave images are: 32000000
pre_proc_batch.csh
preprocess slave images
setting fd1 to 29.328717
setting near_range to 848965.00
setting radius to 6377621.134085
setting npatches to 3
ledflag 1
.... swapping bytes
```

```
writing generic LED file: IMG-HH-ALPSRP149597020-H1.0_A.LED
The range sampling rate for master and slave images are: 32000000
pre_proc_batch.csh
preprocess slave images
  setting fd1 to 29.328717
  setting near_range to 848965.00
  setting radius to 6377621.134085
  setting npatches to 3
  ledflag 1
.... swapping bytes
writing generic LED file: IMG-HH-ALPSRP156307020-H1.0_A.LED
  near_range, shift = 848515 -192
The range sampling rate for master and slave images are: 32000000
pre_proc_batch.csh
preprocess slave images
  setting fd1 to 29.328717
  setting near_range to 848965.00
  setting radius to 6377621.134085
  setting npatches to 3
  ledflag 1
.... swapping bytes
writing generic LED file: IMG-HH-ALPSRP163017020-H1.0_A.LED
  near_range, shift = 849115 64
  near_range, shift = 848665 -128
The range sampling rate for master and slave images are: 32000000
pre_proc_batch.csh
preprocess slave images
  setting fd1 to 29.328717
  setting near_range to 848965.00
  setting radius to 6377621.134085
  setting npatches to 3
  ledflag 1
.... swapping bytes
writing generic LED file: IMG-HH-ALPSRP203277020-H1.0_A.LED
  near_range, shift = 849115 64
  near_range, shift = 848515 -192
The range sampling rate for master and slave images are: 32000000
pre_proc_batch.csh
preprocess slave images
  setting fd1 to 29.328717
  setting near_range to 848965.00
  setting radius to 6377621.134085
  setting npatches to 3
  ledflag 1
.... swapping bytes
writing generic LED file: IMG-HH-ALPSRP209987020-H1.0_A.LED
  near_range, shift = 848815 -64
The range sampling rate for master and slave images are: 32000000
pre_proc_batch.csh
preprocess slave images
  setting fd1 to 29.328717
  setting near_range to 848965.00
  setting radius to 6377621.134085
  setting npatches to 3
  ledflag 1
.... swapping bytes
writing generic LED file: IMG-HH-ALPSRP216697020-H1.0_A.LED
  near_range, shift = 849265 128
  near_range, shift = 848815 -64
The range sampling rate for master and slave images are: 32000000
```

END PREPROCESS A STACK OF IMAGES

```
baseline_table.dat
05565 2007040.6353306125 405 0.000000 0.000000
09591 2007316.6349412142 681 -48.728948 -133.910388
11604 2008089.6338296749 819 -735.405051 -955.833850
14959 2008319.6344884480 1049 634.428595 814.378031
15630 2008365.6350204272 1095 294.534204 259.936381
16301 2009045.6354324063 1140 340.358941 442.624606
20327 2009321.6365583555 1416 -13.484816 -70.677559
20998 2010002.6365291078 1462 -18.481623 -170.711935
21669 2010048.6364085753 1508 -155.775103 -283.339000
```

```
intf.in
IMG-HH-ALPSRP055657020-H1.0_A:IMG-HH-ALPSRP095917020-H1.0_A
IMG-HH-ALPSRP055657020-H1.0_A:IMG-HH-ALPSRP116047020-H1.0_A
IMG-HH-ALPSRP055657020-H1.0_A:IMG-HH-ALPSRP149597020-H1.0_A
IMG-HH-ALPSRP055657020-H1.0_A:IMG-HH-ALPSRP156307020-H1.0_A
IMG-HH-ALPSRP055657020-H1.0_A:IMG-HH-ALPSRP163017020-H1.0_A
IMG-HH-ALPSRP055657020-H1.0_A:IMG-HH-ALPSRP203277020-H1.0_A
IMG-HH-ALPSRP055657020-H1.0_A:IMG-HH-ALPSRP209987020-H1.0_A
IMG-HH-ALPSRP055657020-H1.0_A:IMG-HH-ALPSRP216697020-H1.0_A
IMG-HH-ALPSRP095917020-H1.0_A:IMG-HH-ALPSRP116047020-H1.0_A
IMG-HH-ALPSRP095917020-H1.0_A:IMG-HH-ALPSRP149597020-H1.0_A
IMG-HH-ALPSRP095917020-H1.0_A:IMG-HH-ALPSRP156307020-H1.0_A
IMG-HH-ALPSRP095917020-H1.0_A:IMG-HH-ALPSRP163017020-H1.0_A
IMG-HH-ALPSRP095917020-H1.0_A:IMG-HH-ALPSRP203277020-H1.0_A
IMG-HH-ALPSRP095917020-H1.0_A:IMG-HH-ALPSRP209987020-H1.0_A
IMG-HH-ALPSRP095917020-H1.0_A:IMG-HH-ALPSRP216697020-H1.0_A
IMG-HH-ALPSRP116047020-H1.0_A:IMG-HH-ALPSRP203277020-H1.0_A
IMG-HH-ALPSRP116047020-H1.0_A:IMG-HH-ALPSRP209987020-H1.0_A
IMG-HH-ALPSRP116047020-H1.0_A:IMG-HH-ALPSRP216697020-H1.0_A
IMG-HH-ALPSRP149597020-H1.0_A:IMG-HH-ALPSRP156307020-H1.0_A
IMG-HH-ALPSRP149597020-H1.0_A:IMG-HH-ALPSRP163017020-H1.0_A
IMG-HH-ALPSRP149597020-H1.0_A:IMG-HH-ALPSRP203277020-H1.0_A
IMG-HH-ALPSRP149597020-H1.0_A:IMG-HH-ALPSRP209987020-H1.0_A
IMG-HH-ALPSRP156307020-H1.0_A:IMG-HH-ALPSRP163017020-H1.0_A
IMG-HH-ALPSRP156307020-H1.0_A:IMG-HH-ALPSRP203277020-H1.0_A
IMG-HH-ALPSRP156307020-H1.0_A:IMG-HH-ALPSRP209987020-H1.0_A
IMG-HH-ALPSRP156307020-H1.0_A:IMG-HH-ALPSRP216697020-H1.0_A
IMG-HH-ALPSRP163017020-H1.0_A:IMG-HH-ALPSRP203277020-H1.0_A
IMG-HH-ALPSRP163017020-H1.0_A:IMG-HH-ALPSRP209987020-H1.0_A
IMG-HH-ALPSRP163017020-H1.0_A:IMG-HH-ALPSRP216697020-H1.0_A
IMG-HH-ALPSRP203277020-H1.0_A:IMG-HH-ALPSRP209987020-H1.0_A
IMG-HH-ALPSRP203277020-H1.0_A:IMG-HH-ALPSRP216697020-H1.0_A
IMG-HH-ALPSRP209987020-H1.0_A:IMG-HH-ALPSRP216697020-H1.0_A
```

```
align.in
IMG-HH-ALPSRP055657020-H1.0_A:IMG-HH-ALPSRP095917020-H1.0_A:IMG-HH-ALPSRP055657020-H1.0_A
IMG-HH-ALPSRP055657020-H1.0_A:IMG-HH-ALPSRP116047020-H1.0_A:IMG-HH-ALPSRP055657020-H1.0_A
IMG-HH-ALPSRP055657020-H1.0_A:IMG-HH-ALPSRP149597020-H1.0_A:IMG-HH-ALPSRP055657020-H1.0_A
IMG-HH-ALPSRP055657020-H1.0_A:IMG-HH-ALPSRP156307020-H1.0_A:IMG-HH-ALPSRP055657020-H1.0_A
IMG-HH-ALPSRP055657020-H1.0_A:IMG-HH-ALPSRP163017020-H1.0_A:IMG-HH-ALPSRP055657020-H1.0_A
IMG-HH-ALPSRP055657020-H1.0_A:IMG-HH-ALPSRP203277020-H1.0_A:IMG-HH-ALPSRP055657020-H1.0_A
IMG-HH-ALPSRP055657020-H1.0_A:IMG-HH-ALPSRP209987020-H1.0_A:IMG-HH-ALPSRP055657020-H1.0_A
IMG-HH-ALPSRP055657020-H1.0_A:IMG-HH-ALPSRP216697020-H1.0_A:IMG-HH-ALPSRP055657020-H1.0_A
IMG-HH-ALPSRP095917020-H1.0_A:IMG-HH-ALPSRP116047020-H1.0_A:IMG-HH-ALPSRP095917020-H1.0_A
IMG-HH-ALPSRP095917020-H1.0_A:IMG-HH-ALPSRP149597020-H1.0_A:IMG-HH-ALPSRP095917020-H1.0_A
```

IMG-HH-ALPSRP095917020-H1.0\_A:IMG-HH-ALPSRP156307020-H1.0\_A:IMG-HH-ALPSRP055657020-H1.0\_A  
IMG-HH-ALPSRP095917020-H1.0\_A:IMG-HH-ALPSRP163017020-H1.0\_A:IMG-HH-ALPSRP055657020-H1.0\_A  
IMG-HH-ALPSRP095917020-H1.0\_A:IMG-HH-ALPSRP203277020-H1.0\_A:IMG-HH-ALPSRP055657020-H1.0\_A  
IMG-HH-ALPSRP095917020-H1.0\_A:IMG-HH-ALPSRP209987020-H1.0\_A:IMG-HH-ALPSRP055657020-H1.0\_A  
IMG-HH-ALPSRP095917020-H1.0\_A:IMG-HH-ALPSRP216697020-H1.0\_A:IMG-HH-ALPSRP055657020-H1.0\_A  
IMG-HH-ALPSRP116047020-H1.0\_A:IMG-HH-ALPSRP203277020-H1.0\_A:IMG-HH-ALPSRP055657020-H1.0\_A  
IMG-HH-ALPSRP116047020-H1.0\_A:IMG-HH-ALPSRP209987020-H1.0\_A:IMG-HH-ALPSRP055657020-H1.0\_A  
IMG-HH-ALPSRP116047020-H1.0\_A:IMG-HH-ALPSRP216697020-H1.0\_A:IMG-HH-ALPSRP055657020-H1.0\_A  
IMG-HH-ALPSRP149597020-H1.0\_A:IMG-HH-ALPSRP156307020-H1.0\_A:IMG-HH-ALPSRP055657020-H1.0\_A  
IMG-HH-ALPSRP149597020-H1.0\_A:IMG-HH-ALPSRP163017020-H1.0\_A:IMG-HH-ALPSRP055657020-H1.0\_A  
IMG-HH-ALPSRP149597020-H1.0\_A:IMG-HH-ALPSRP203277020-H1.0\_A:IMG-HH-ALPSRP055657020-H1.0\_A  
IMG-HH-ALPSRP149597020-H1.0\_A:IMG-HH-ALPSRP209987020-H1.0\_A:IMG-HH-ALPSRP055657020-H1.0\_A  
IMG-HH-ALPSRP156307020-H1.0\_A:IMG-HH-ALPSRP163017020-H1.0\_A:IMG-HH-ALPSRP055657020-H1.0\_A  
IMG-HH-ALPSRP156307020-H1.0\_A:IMG-HH-ALPSRP203277020-H1.0\_A:IMG-HH-ALPSRP055657020-H1.0\_A  
IMG-HH-ALPSRP156307020-H1.0\_A:IMG-HH-ALPSRP209987020-H1.0\_A:IMG-HH-ALPSRP055657020-H1.0\_A  
IMG-HH-ALPSRP156307020-H1.0\_A:IMG-HH-ALPSRP216697020-H1.0\_A:IMG-HH-ALPSRP055657020-H1.0\_A  
IMG-HH-ALPSRP163017020-H1.0\_A:IMG-HH-ALPSRP203277020-H1.0\_A:IMG-HH-ALPSRP055657020-H1.0\_A  
IMG-HH-ALPSRP163017020-H1.0\_A:IMG-HH-ALPSRP209987020-H1.0\_A:IMG-HH-ALPSRP055657020-H1.0\_A  
IMG-HH-ALPSRP163017020-H1.0\_A:IMG-HH-ALPSRP216697020-H1.0\_A:IMG-HH-ALPSRP055657020-H1.0\_A  
IMG-HH-ALPSRP203277020-H1.0\_A:IMG-HH-ALPSRP209987020-H1.0\_A:IMG-HH-ALPSRP055657020-H1.0\_A  
IMG-HH-ALPSRP203277020-H1.0\_A:IMG-HH-ALPSRP216697020-H1.0\_A:IMG-HH-ALPSRP055657020-H1.0\_A  
IMG-HH-ALPSRP209987020-H1.0\_A:IMG-HH-ALPSRP216697020-H1.0\_A:IMG-HH-ALPSRP055657020-H1.0\_A

align\_batch.csh AL05 align.in

```
ALIGN.CSH - START
focussing master
Computing range reference function.
Processing patch 1
Processing Elapsed Time: 0 min 0.05 sec
Range Compression
Processing Elapsed Time: 0 min 5.17 sec
Azimuthal Transform
Processing Elapsed Time: 0 min 12.19 sec
Range Migration
Processing Elapsed Time: 0 min 21.79 sec
Azimuthal Compression
Processing Elapsed Time: 0 min 42.02 sec
Writing Data
Processing patch 2
Processing Elapsed Time: 0 min 43.90 sec
Range Compression
Processing Elapsed Time: 0 min 48.09 sec
Azimuthal Transform
Processing Elapsed Time: 0 min 54.96 sec
Range Migration
Processing Elapsed Time: 1 min 4.39 sec
Azimuthal Compression
Processing Elapsed Time: 1 min 23.77 sec
Writing Data
Processing patch 3
Processing Elapsed Time: 1 min 25.86 sec
Range Compression
Processing Elapsed Time: 1 min 30.13 sec
Azimuthal Transform
Processing Elapsed Time: 1 min 36.94 sec
Range Migration
Processing Elapsed Time: 1 min 46.39 sec
Azimuthal Compression
Processing Elapsed Time: 2 min 5.83 sec
Writing Data
Processing Elapsed Time: 2 min 7.61 sec
number of points clipped to short int 38
align.csh
focusing slave
Computing range reference function.
Processing patch 1
Processing Elapsed Time: 0 min 0.05 sec
Range Compression
Processing Elapsed Time: 0 min 5.68 sec
Azimuthal Transform
Processing Elapsed Time: 0 min 12.95 sec
Range Migration
Processing Elapsed Time: 0 min 22.65 sec
Azimuthal Compression
Processing Elapsed Time: 0 min 42.49 sec
Writing Data
Processing patch 2
Processing Elapsed Time: 0 min 44.53 sec
Range Compression
Processing Elapsed Time: 0 min 49.79 sec
Azimuthal Transform
Processing Elapsed Time: 0 min 56.65 sec
Range Migration
Processing Elapsed Time: 1 min 6.20 sec
Azimuthal Compression
Processing Elapsed Time: 1 min 25.64 sec
Writing Data
Processing patch 3
Processing Elapsed Time: 1 min 27.63 sec
Range Compression
Processing Elapsed Time: 1 min 32.83 sec
Azimuthal Transform
Processing Elapsed Time: 1 min 39.78 sec
Range Migration
Processing Elapsed Time: 1 min 49.27 sec
Azimuthal Compression
Processing Elapsed Time: 2 min 8.62 sec
Writing Data
Processing Elapsed Time: 2 min 10.74 sec
number of points clipped to short int 15
align.csh
correlate master and slave to find offset parameters
setting xsearch to 64
setting nx_corr to 128
setting ysearch to 64
setting ny_corr to 128
11304 27648 11304 27648 7 93 0.002151
locations n 512 nx 11304 nyl 32 nxl 16 x_inc 574 y_inc 826
elapsed time: 19.212068
align.csh
refocus slave
Computing range reference function.
Processing patch 1
Processing Elapsed Time: 0 min 0.05 sec
Range Compression
Processing Elapsed Time: 0 min 6.68 sec
Azimuthal Transform
Processing Elapsed Time: 0 min 13.58 sec
```

```
Range Migration
Processing Elapsed Time: 0 min 22.96 sec
Azimuthal Compression
Processing Elapsed Time: 0 min 45.15 sec
apply azimuth-dependent azimuth shift
Processing Elapsed Time: 1 min 2.48 sec
Writing Data
Processing patch 2
Processing Elapsed Time: 1 min 8.80 sec
Range Compression
Processing Elapsed Time: 1 min 13.50 sec
Azimuthal Transform
Processing Elapsed Time: 1 min 20.44 sec
Range Migration
Processing Elapsed Time: 1 min 29.99 sec
Azimuthal Compression
Processing Elapsed Time: 1 min 51.90 sec
apply azimuth-dependent azimuth shift
Processing Elapsed Time: 2 min 10.50 sec
Writing Data
Processing patch 3
Processing Elapsed Time: 2 min 17.11 sec
Range Compression
Processing Elapsed Time: 2 min 22.36 sec
Azimuthal Transform
Processing Elapsed Time: 2 min 29.56 sec
Range Migration
Processing Elapsed Time: 2 min 39.13 sec
Azimuthal Compression
Processing Elapsed Time: 3 min 2.01 sec
apply azimuth-dependent azimuth shift
Processing Elapsed Time: 3 min 19.99 sec
Writing Data
Processing Elapsed Time: 3 min 26.45 sec
number of points clipped to short int 16
rm: No match.
ALIGN.CSH - END
```

```
intf_batch.csh ALOS batch.config
clean up topo/ folder
```

```
DEM2TOPO_RA.CSH - START
USER SHOULD PROVIDE DEM FILE
  range decimation is: 2
blockmedian: Provides 3, expects 3-column binary data
blockmedian: Processing input table data
blockmedian: W: 0 E: 11304 S: 0 N: 27648 n_columns: 5652 n_rows: 6912
blockmedian: Input 3 columns via binary records using format ddd
blockmedian: Output 3 columns via binary records using format ddd
blockmedian: N read: 876576 N used: 873765 outside_area: 2811 N cells filled: 873729
surface: Provides 3, expects 3-column binary data
surface: Grid domain: W: 0 E: 11304 S: 0 N: 27648 n_columns: 5652 n_rows: 6912 [pixel registration]
surface: Processing input table data
surface: Input 3 columns via binary records using format ddd
surface: Minimum value of your dataset x,y,z at: surface: 4079.34350586 29.4696750641 87.177230835
surface: Maximum value of your dataset x,y,z at: surface: 347.312347412 12551.9707031 3381.46020508
surface: LS plane determined: z = 817.265 + (-0.130615 * col) + (-0.00775968 * row)
surface: Grid Mode IterationMax Change Conv Limit Total Iterations
surface: 36 D 74 0.00102558200731 0.0011772311755 74
surface: 12 I 29 0.00229282414267 0.0035316935266 103
surface: 12 D 217 0.00350996600763 0.0035316935266 320
surface: 4 I 27 0.00929507370964 0.0105950805799 347
surface: 4 D 463 0.0105799982936 0.0105950805799 810
surface: 2 I 20 0.0154308833046 0.0211901611598 830
surface: 2 D 155 0.0210317988359 0.0211901611598 985
surface: 1 I 18 0.0278734328297 0.0423803223195 1003
surface: 1 D 248 0.0421195920915 0.0423803223195 1251
surface: Fit info: N data points N nodes mean error rms error curvature
surface: 873729 39079189 6.79387433063e-06 0.00820823629261 23121.6638355
grd2cpt: Processing input grid(s)
grd2cpt: Mean and S.D. of data are 422.322843487 469.419145377
grdimage: Allocates memory and read data file topo_ra.grd
grdimage: Evaluate image pixel colors
grdimage: Creating 8-bit grayshade image
DEM2TOPO_RA.CSH - END
NO TOPO_RA SHIFT
```

```
START FORM A STACK OF INTERFEROGRAMS
```

```
INTF.CSH, FILTER.CSH - START
intf.csh
running phasediff...
reading topo topo_ra.grd
  xdim 11304, ydim 27648
filter.csh
gauss_300 4 2 (4 2)
making amplitudes...
filtering interferogram...
making amplitude...
making correlation...
making phase...
filtering phase...
INTF.CSH, FILTER.CSH - END
```

```
MAKE LANDMASK -- START
```

```
REQUIRE FULL RESOLUTION COASTLINE FROM GMT
```

```
grdlandmask: GSHHG version 2.3.7
Derived from World Vector Shoreline, CIA WDB-II, and Atlas of the Cryosphere
Processed by Paul Wessel and Walter H. F. Smith, 1994-2017
grdlandmask: Nodes in water will be set to NaN
grdlandmask: Nodes on land will be set to 1
grdlandmask: Level 0 contained 812640 nodes
grdlandmask: Level 1 contained 2478081 nodes
grdlandmask: Done!
surface: Provides 3, expects 3-column binary data
surface: Grid domain: W: 113.833333329 E: 117.416666662 S: -9.166666663 N: -7.416666663 n_columns: 4300 n_rows: 2100 [gridline registration]
surface: Processing input table data
surface: Input 3 columns via binary records using format fff
surface: Minimum value of your dataset x,y,z at: surface: 114.01499939 -8.25666713715 -9.99788951874
surface: Maximum value of your dataset x,y,z at: surface: 114.745002747 -8.02666664124 11313.9931641
surface: LS plane determined: z = -5760.95 + (12.1072 * col) + (2.73344 * row)
surface: Grid Mode IterationMax Change Conv Limit Total Iterations
surface: 100 D 15050 7.95390629687e-05 7.99866557348e-05 15050
surface: 20 I 84 0.000396339535357 0.000399933278674 15134
surface: 20 D 10000 0.000574572391921 0.000399933278674 25134
surface: 4 I 58 0.00192451159343 0.0019996663933 25192
```

```

surface: 4 D 2000 0.00388239622035 0.0019996663933 27192
surface: 2 I 17 0.00373777974225 0.0039993327867 27209
surface: 2 D 715 0.00399850656578 0.0039993327867 27924
surface: 1 I 15 0.00590702691402 0.0079986655734 27939
surface: 1 D 197 0.00798171715795 0.0079986655734 28136
surface: Fit info: N data points N nodes mean error rms error curvature
surface: 876576 9036401 0 0 9342.61905482
surface: Provides 3, expects 3-column binary data
surface: Grid domain: W: 113.83333329 E: 117.416666662 S: -9.166666663 N: -7.4166666637 n_columns: 4300 n_rows: 2100 [gridline registration]
surface: Processing input table data
surface: Input 3 columns via binary records using format fff
surface: Minimum value of your dataset x,y,z at: surface: 114.680000305 -8.35416698456 -19.9786300659
surface: Maximum value of your dataset x,y,z at: surface: 113.910003662 -7.71000003815 27667.9941406
surface: LS plane determined: z = -21072.2 + (-6.36047 * col) + (28.2227 * row)
surface: Grid Mode IterationMax Change Conv Limit Total Iterations
surface: 100 D 50000 3.44545802141e-06 2.71492099749e-06 50000
surface: 20 I 108 1.28473104737e-05 1.35746049874e-05 50108
surface: 20 D 10000 0.00027734520872 1.35746049874e-05 60108
surface: 4 I 77 6.28489295697e-05 6.78730249371e-05 60185
surface: 4 D 2000 0.00038165290949 6.78730249371e-05 62185
surface: 2 I 18 0.000103665807228 0.000135746049874 62203
surface: 2 D 1000 0.000164589056166 0.000135746049874 63203
surface: 1 I 16 0.000243787391865 0.000271492099749 63219
surface: 1 D 500 0.000277090339224 0.000271492099749 63719
surface: Fit info: N data points N nodes mean error rms error curvature
surface: 876576 9036401 0 0 524759.990928
MAKE LANDMASK -- END

```

```

SNAPHU.CSH - START
threshold_snaphu: .45
grdmath: Perform reverse Polish notation calculations on grids
grdmath: phase_patch.grd landmask_ra_patch.grd MUL = phase_patch.grd
unwrapping phase with snaphu - higher threshold for faster unwrapping

```

```

snaphu v1.4.2
32 parameters input from file snaphu.conf.brief (297 lines total)
Reading wrapped phase from file phase.in
No weight file specified. Assuming uniform weights
Reading correlation data from file corr.in
Calculating deformation-mode cost parameters
Building range cost arrays
Building azimuth cost arrays
Initializing flows with MST algorithm
Running approximate minimum spanning tree solver
Running nonlinear network flow optimizer
Maximum flow on network: 4
Number of nodes in network: 4878776
Flow increment: 1 (Total improvements: 0)
Treesize: 4878776 Pivots: 10621 Improvements: 412
Maximum flow on network: 3
Flow increment: 2 (Total improvements: 412)
Treesize: 4878776 Pivots: 2079 Improvements: 22
Maximum flow on network: 3
Flow increment: 3 (Total improvements: 434)
Treesize: 4878776 Pivots: 2 Improvements: 1
Maximum flow on network: 3
Total solution cost: 1057910
Integrating phase
Writing output to file unwrap.out
Program snaphu done
Elapsed processor time: 0:00:57.26
Elapsed wall clock time: 0:01:02
grdmath: Perform reverse Polish notation calculations on grids
grdmath: unwrap.grd landmask_ra_patch.grd MUL = tmp.grd
SNAPHU.CSH - END

```

```

GEOCODE.CSH - START
threshold_geocode: .45
grdmath: Perform reverse Polish notation calculations on grids
grdmath: corr.grd 0.45 GE 0 NAN mask.grd MUL = mask2.grd
psscale: Warning: The -E option is deprecated but is accepted.
psscale: For the current -D syntax you should use -D modifier +e instead.
psscale: Note you cannot mix new-style modifiers (+e) with the old-style -D option.
psscale: Warning: The -E option is deprecated but is accepted.
psscale: For the current -D syntax you should use -D modifier +e instead.
psscale: Note you cannot mix new-style modifiers (+e) with the old-style -D option.
geocode.csh
project correlation, phase, unwrapped and amplitude back to lon lat coordinates
remarked is by root on Mon May 21 09:30:51 JST 2018 with geocode.csh
proj_ra2ll.csh
surface: Provides 3, expects 3-column binary data
surface: Grid domain: W: 128 E: 11296 S: 0 N: 27648 n_columns: 698 n_rows: 864 [gridline registration]
surface: Processing input table data
surface: Input 3 columns via binary records using format fff
surface: Minimum value of your dataset x,y,z at: surface: 146.114242554 27660.1054688 113.900001526
surface: Maximum value of your dataset x,y,z at: surface: 11303.1259766 472.628265381 114.814163208
surface: 265719 unusable points were supplied; these will be ignored.
surface: You should have pre-processed the data with block-mean, -median, or -mode.
surface: Check that previous processing steps write results with enough decimals.
surface: LS plane determined: z = 114.086 + (0.00104637 * col) + (-0.000203008 * row)
surface: Grid Mode IterationMax Change Conv Limit Total Iterations
surface: 2 D 21 2.11677469738e-07 2.54173832244e-07 21
surface: 1 I 18 3.51165532003e-07 5.08347664488e-07 39
surface: 1 D 18 4.55228565389e-07 5.08347664488e-07 57
surface: Fit info: N data points N nodes mean error rms error curvature
surface: 598998 604635 2.85888505812e-06 0.00834228315715 10389.4432035
surface: Provides 3, expects 3-column binary data
surface: Grid domain: W: 128 E: 11296 S: 0 N: 27648 n_columns: 698 n_rows: 864 [gridline registration]
surface: Processing input table data
surface: Input 3 columns via binary records using format fff
surface: Minimum value of your dataset x,y,z at: surface: 127.394432068 -1.88170862198 -8.4908328247
surface: Maximum value of your dataset x,y,z at: surface: 11253.3925781 27660.6621094 -7.54750013351
surface: 265719 unusable points were supplied; these will be ignored.
surface: You should have pre-processed the data with block-mean, -median, or -mode.
surface: Check that previous processing steps write results with enough decimals.
surface: LS plane determined: z = -8.48753 + (0.000235839 * col) + (0.000899107 * row)
surface: Grid Mode IterationMax Change Conv Limit Total Iterations
surface: 2 D 21 4.72731083858e-08 5.68260967653e-08 21
surface: 1 I 18 8.10555445947e-08 1.13652193531e-07 39
surface: 1 D 18 1.02163467041e-07 1.13652193531e-07 57
surface: Fit info: N data points N nodes mean error rms error curvature
surface: 598998 604635 8.90645713269e-06 0.0103445668453 11665.3898877
blockmedian: Provides 3, expects 3-column binary data
blockmedian: Processing input table data
blockmedian: W: 113.9 E: 114.822222222 S: -8.49305555556 N: -7.54166666667 n_columns: 830 n_rows: 1370
blockmedian: Input 3 columns via binary records using format fff
blockmedian: Output 3 columns via binary records using format fff
blockmedian: N read: 4803326 N used: 4803326 outside_area: 0 N cells filled: 773864
proj_ra2ll.csh

```

```
blockmedian: Provides 3, expects 3-column binary data
blockmedian: Processing input table data
blockmedian: W: 113.9 E: 114.822222222 S: -8.49305555556 N: -7.54166666667 n_columns: 830 n_rows: 1370
blockmedian: Input 3 columns via binary records using format fff
blockmedian: Output 3 columns via binary records using format fff
blockmedian: N read: 4807662 N used: 4807662 outside_area: 0 N cells filled: 774628
proj_ra2ll.csh
blockmedian: Provides 3, expects 3-column binary data
blockmedian: Processing input table data
blockmedian: W: 113.911111111 E: 114.788888889 S: -8.48611111111 N: -7.66666666667 n_columns: 790 n_rows: 1180
blockmedian: Input 3 columns via binary records using format fff
blockmedian: Output 3 columns via binary records using format fff
blockmedian: N read: 119495 N used: 119495 outside_area: 0 N cells filled: 30605
proj_ra2ll.csh
blockmedian: Provides 3, expects 3-column binary data
blockmedian: Processing input table data
blockmedian: W: 113.888888889 E: 114.822222222 S: -8.49305555556 N: -7.54166666667 n_columns: 840 n_rows: 1370
blockmedian: Input 3 columns via binary records using format fff
blockmedian: Output 3 columns via binary records using format fff
blockmedian: N read: 4824576 N used: 4824576 outside_area: 0 N cells filled: 777375
proj_ra2ll.csh
blockmedian: Provides 3, expects 3-column binary data
blockmedian: Processing input table data
blockmedian: W: 113.911111111 E: 114.788888889 S: -8.48611111111 N: -7.66666666667 n_columns: 790 n_rows: 1180
blockmedian: Input 3 columns via binary records using format fff
blockmedian: Output 3 columns via binary records using format fff
blockmedian: N read: 119370 N used: 119370 outside_area: 0 N cells filled: 30585
proj_ra2ll.csh
blockmedian: Provides 3, expects 3-column binary data
blockmedian: Processing input table data
blockmedian: W: 113.9 E: 114.822222222 S: -8.49305555556 N: -7.66666666667 n_columns: 830 n_rows: 1190
blockmedian: Input 3 columns via binary records using format fff
blockmedian: Output 3 columns via binary records using format fff
blockmedian: N read: 3053505 N used: 3053505 outside_area: 0 N cells filled: 497996
proj_ra2ll.csh
blockmedian: Provides 3, expects 3-column binary data
blockmedian: Processing input table data
blockmedian: W: 113.911111111 E: 114.788888889 S: -8.48611111111 N: -7.66666666667 n_columns: 790 n_rows: 1180
blockmedian: Input 3 columns via binary records using format fff
blockmedian: Output 3 columns via binary records using format fff
blockmedian: N read: 119495 N used: 119495 outside_area: 0 N cells filled: 30605
geocode.csh
make the KML files for Google Earth
grdimage: Allocates memory and read data file display_amp_ll.grd
grdimage: Evaluate image pixel colors
grdimage: Creating 24-bit color image
PSL: Colormap of 256 colors created
Make display_amp_ll.kml and display_amp_ll.png
psconvert: Processing display_amp_ll.ps...
psconvert: Figure dimensions: Width: 67.2 points [0.933333 inch] Height: 68.52 points [0.951666 inch]
psconvert: gs -q -dSAFER -dNOPAUSE -dBATCH -dPDFSETTINGS=/prepress -dDownsampleColorImages=false -dDownsampleGrayImages=false -
dDownsampleMonoImages=false -dUseFlateCompression=true -dEmbedAllFonts=true -dSubsetFonts=true -dMonoImageFilter=/FlateEncode -
dAutoFilterGrayImages=false -dGrayImageFilter=/FlateEncode -dAutoFilterColorImages=false -dColorImageFilter=/FlateEncode -dSCANCONVERTERTYPE=2 -
dMaxBitmap=2147483647 -dUseFastColor=true -sDEVICE=pngalpha -g840x857 -r900 -sOutputFile='display_amp_ll.png' -f'./psconvert_31043d.eps'
psconvert: Done.
grdimage: Allocates memory and read data file corr_ll.grd
grdimage: Evaluate image pixel colors
grdimage: Creating 24-bit color image
PSL: Colormap of 255 colors created
Make corr_ll.kml and corr_ll.png
psconvert: Processing corr_ll.ps...
psconvert: Figure dimensions: Width: 66.42 points [0.9225 inch] Height: 68.52 points [0.951666 inch]
psconvert: gs -q -dSAFER -dNOPAUSE -dBATCH -dPDFSETTINGS=/prepress -dDownsampleColorImages=false -dDownsampleGrayImages=false -
dDownsampleMonoImages=false -dUseFlateCompression=true -dEmbedAllFonts=true -dSubsetFonts=true -dMonoImageFilter=/FlateEncode -
dAutoFilterGrayImages=false -dGrayImageFilter=/FlateEncode -dAutoFilterColorImages=false -dColorImageFilter=/FlateEncode -dSCANCONVERTERTYPE=2 -
dMaxBitmap=2147483647 -dUseFastColor=true -sDEVICE=pngalpha -g831x857 -r900 -sOutputFile='corr_ll.png' -f'./psconvert_31205d.eps'
psconvert: Done.
grdimage: Allocates memory and read data file phase_mask_ll.grd
grdimage: Evaluate image pixel colors
grdimage: Creating 24-bit color image
Make phase_mask_ll.kml and phase_mask_ll.png
psconvert: Processing phase_mask_ll.ps...
psconvert: Figure dimensions: Width: 63.18 points [0.8775 inch] Height: 58.98 points [0.819166 inch]
psconvert: gs -q -dSAFER -dNOPAUSE -dBATCH -dPDFSETTINGS=/prepress -dDownsampleColorImages=false -dDownsampleGrayImages=false -
dDownsampleMonoImages=false -dUseFlateCompression=true -dEmbedAllFonts=true -dSubsetFonts=true -dMonoImageFilter=/FlateEncode -
dAutoFilterGrayImages=false -dGrayImageFilter=/FlateEncode -dAutoFilterColorImages=false -dColorImageFilter=/FlateEncode -dSCANCONVERTERTYPE=2 -
dMaxBitmap=2147483647 -dUseFastColor=true -sDEVICE=pngalpha -g790x738 -r900 -sOutputFile='phase_mask_ll.png' -f'./psconvert_31397d.eps'
psconvert: Done.
grdimage: Allocates memory and read data file phasefilt_mask_ll.grd
grdimage: Evaluate image pixel colors
grdimage: Creating 24-bit color image
Make phasefilt_mask_ll.kml and phasefilt_mask_ll.png
psconvert: Processing phasefilt_mask_ll.ps...
psconvert: Figure dimensions: Width: 63.18 points [0.8775 inch] Height: 58.98 points [0.819166 inch]
psconvert: gs -q -dSAFER -dNOPAUSE -dBATCH -dPDFSETTINGS=/prepress -dDownsampleColorImages=false -dDownsampleGrayImages=false -
dDownsampleMonoImages=false -dUseFlateCompression=true -dEmbedAllFonts=true -dSubsetFonts=true -dMonoImageFilter=/FlateEncode -
dAutoFilterGrayImages=false -dGrayImageFilter=/FlateEncode -dAutoFilterColorImages=false -dColorImageFilter=/FlateEncode -dSCANCONVERTERTYPE=2 -
dMaxBitmap=2147483647 -dUseFastColor=true -sDEVICE=pngalpha -g790x738 -r900 -sOutputFile='phasefilt_mask_ll.png' -f'./psconvert_31660d.eps'
psconvert: Done.
grdimage: Allocates memory and read data file unwrap_mask_ll.grd
grdimage: Evaluate image pixel colors
grdimage: Creating 24-bit color image
Make unwrap_mask_ll.kml and unwrap_mask_ll.png
psconvert: Processing unwrap_mask_ll.ps...
psconvert: Figure dimensions: Width: 63.18 points [0.8775 inch] Height: 58.98 points [0.819166 inch]
psconvert: gs -q -dSAFER -dNOPAUSE -dBATCH -dPDFSETTINGS=/prepress -dDownsampleColorImages=false -dDownsampleGrayImages=false -
dDownsampleMonoImages=false -dUseFlateCompression=true -dEmbedAllFonts=true -dSubsetFonts=true -dMonoImageFilter=/FlateEncode -
dAutoFilterGrayImages=false -dGrayImageFilter=/FlateEncode -dAutoFilterColorImages=false -dColorImageFilter=/FlateEncode -dSCANCONVERTERTYPE=2 -
dMaxBitmap=2147483647 -dUseFastColor=true -sDEVICE=pngalpha -g790x738 -r900 -sOutputFile='unwrap_mask_ll.png' -f'./psconvert_31843d.eps'
psconvert: Done.
grdimage: Allocates memory and read data file phasefilt_mask_ll.grd
grdimage: Evaluate image pixel colors
grdimage: Creating 24-bit color image
Make phasefilt_mask_ll.kml and phasefilt_mask_ll.png
psconvert: Processing phasefilt_mask_ll.ps...
psconvert: Figure dimensions: Width: 63.18 points [0.8775 inch] Height: 58.98 points [0.819166 inch]
psconvert: gs -q -dSAFER -dNOPAUSE -dBATCH -dPDFSETTINGS=/prepress -dDownsampleColorImages=false -dDownsampleGrayImages=false -
dDownsampleMonoImages=false -dUseFlateCompression=true -dEmbedAllFonts=true -dSubsetFonts=true -dMonoImageFilter=/FlateEncode -
dAutoFilterGrayImages=false -dGrayImageFilter=/FlateEncode -dAutoFilterColorImages=false -dColorImageFilter=/FlateEncode -dSCANCONVERTERTYPE=2 -
dMaxBitmap=2147483647 -dUseFastColor=true -sDEVICE=pngalpha -g790x738 -r900 -sOutputFile='phasefilt_mask_ll.png' -f'./psconvert_31996d.eps'
psconvert: Done.
grdimage: Allocates memory and read data file los_ll.grd
grdimage: Evaluate image pixel colors
grdimage: Creating 24-bit color image
Make los_ll.kml and los_ll.png
psconvert: Processing los_ll.ps...
psconvert: Figure dimensions: Width: 63.18 points [0.8775 inch] Height: 58.98 points [0.819166 inch]
psconvert: gs -q -dSAFER -dNOPAUSE -dBATCH -dPDFSETTINGS=/prepress -dDownsampleColorImages=false -dDownsampleGrayImages=false -
dDownsampleMonoImages=false -dUseFlateCompression=true -dEmbedAllFonts=true -dSubsetFonts=true -dMonoImageFilter=/FlateEncode -
```

```
dAutoFilterGrayImages=false -dGrayImageFilter=/FlateEncode -dAutoFilterColorImages=false -dColorImageFilter=/FlateEncode -dSCANCONVERTERTYPE=2 -
dMaxBitmap=2147483647 -dUseFastColor=true -sDEVICE=pngalpha -g790x738 -r900 -sOutputFile='los_ll.png' -f'/psconvert_32245d.eps'
psconvert: Done.
GEOCODE.CSH - END
```

```
stack.list
cut_2007040_2007316.grd IMG-HH-ALPSRP055657020-H1.0_A.PRM IMG-HH-ALPSRP095917020-H1.0_A.PRM
cut_2007040_2008089.grd IMG-HH-ALPSRP055657020-H1.0_A.PRM IMG-HH-ALPSRP116047020-H1.0_A.PRM
cut_2007040_2008319.grd IMG-HH-ALPSRP055657020-H1.0_A.PRM IMG-HH-ALPSRP149597020-H1.0_A.PRM
cut_2007040_2008365.grd IMG-HH-ALPSRP055657020-H1.0_A.PRM IMG-HH-ALPSRP156307020-H1.0_A.PRM
cut_2007040_2009045.grd IMG-HH-ALPSRP055657020-H1.0_A.PRM IMG-HH-ALPSRP163017020-H1.0_A.PRM
cut_2007040_2009321.grd IMG-HH-ALPSRP055657020-H1.0_A.PRM IMG-HH-ALPSRP203277020-H1.0_A.PRM
cut_2007040_2010002.grd IMG-HH-ALPSRP055657020-H1.0_A.PRM IMG-HH-ALPSRP209987020-H1.0_A.PRM
cut_2007040_2010048.grd IMG-HH-ALPSRP055657020-H1.0_A.PRM IMG-HH-ALPSRP216697020-H1.0_A.PRM
```

```
bash stack_phase.bash stack.list mean.grd std.grd
```

```
compute the mean LOS velocity ..
```

```
time span (days) of cut_2007040_2007316.grd: 276
accumulative days in the stack: 276
time span (days) of cut_2007040_2008089.grd: 414
accumulative days in the stack: 690
time span (days) of cut_2007040_2008319.grd: 644
accumulative days in the stack: 1334
time span (days) of cut_2007040_2008365.grd: 690
accumulative days in the stack: 2024
time span (days) of cut_2007040_2009045.grd: 735
accumulative days in the stack: 2759
time span (days) of cut_2007040_2009321.grd: 1011
accumulative days in the stack: 3770
time span (days) of cut_2007040_2010002.grd: 1057
accumulative days in the stack: 4827
time span (days) of cut_2007040_2010048.grd: 1103
accumulative days in the stack: 5930
```

```
compute the standard deviations ..
```

```
mean_ll.grd
std_ll.grd
los_ll_2007316.grd
los_ll_2008089.grd
los_ll_2008319.grd
los_ll_2008365.grd
los_ll_2009045.grd
los_ll_2009321.grd
los_ll_2010002.grd
los_ll_2010048.grd
```

```
csf select_pairs.csh baseline_table.dat 950 1000
```

```
intf.tab
cut_2007040_2007316.grd corcut_2007040_2007316.grd 2007040 2007316 -133.910388
cut_2007040_2008089.grd corcut_2007040_2008089.grd 2007040 2008089 -955.833850
cut_2007040_2008319.grd corcut_2007040_2008319.grd 2007040 2008319 814.378031
cut_2007040_2008365.grd corcut_2007040_2008365.grd 2007040 2008365 259.936381
cut_2007040_2009045.grd corcut_2007040_2009045.grd 2007040 2009045 442.624606
cut_2007316_2008089.grd corcut_2007316_2008089.grd 2007316 2008089 -821.912307
cut_2007316_2008319.grd corcut_2007316_2008319.grd 2007316 2008319 948.235728
cut_2007316_2008365.grd corcut_2007316_2008365.grd 2007316 2008365 393.791788
cut_2007316_2009045.grd corcut_2007316_2009045.grd 2007316 2009045 576.496043
cut_2007316_2009321.grd corcut_2007316_2009321.grd 2007316 2009321 63.209294
cut_2007316_2010002.grd corcut_2007316_2010002.grd 2007316 2010002 -36.832156
cut_2007316_2010048.grd corcut_2007316_2010048.grd 2007316 2010048 -149.447189
cut_2008089_2009321.grd corcut_2008089_2009321.grd 2008089 2009321 885.063451
cut_2008089_2010002.grd corcut_2008089_2010002.grd 2008089 2010002 785.016995
cut_2008089_2010048.grd corcut_2008089_2010048.grd 2008089 2010048 672.417007
cut_2008319_2008365.grd corcut_2008319_2008365.grd 2008319 2008365 -554.460342
cut_2008319_2009045.grd corcut_2008319_2009045.grd 2008319 2009045 -371.787812
cut_2008319_2009321.grd corcut_2008319_2009321.grd 2008319 2009321 -885.130038
cut_2008319_2010002.grd corcut_2008319_2010002.grd 2008319 2010002 -985.156585
cut_2008365_2009045.grd corcut_2008365_2009045.grd 2008365 2009045 182.665119
cut_2008365_2009321.grd corcut_2008365_2009321.grd 2008365 2009321 -330.588772
cut_2008365_2010002.grd corcut_2008365_2010002.grd 2008365 2010002 -430.615682
cut_2008365_2010048.grd corcut_2008365_2010048.grd 2008365 2010048 -543.229643
cut_2009045_2009321.grd corcut_2009045_2009321.grd 2009045 2009321 -513.327391
cut_2009045_2010002.grd corcut_2009045_2010002.grd 2009045 2010002 -613.357860
cut_2009045_2010048.grd corcut_2009045_2010048.grd 2009045 2010048 -725.998255
cut_2009321_2010002.grd corcut_2009321_2010002.grd 2009321 2010002 -100.035858
cut_2009321_2010048.grd corcut_2009321_2010048.grd 2009321 2010048 -212.652996
cut_2010002_2010048.grd corcut_2010002_2010048.grd 2010002 2010048 -112.600301
```

```
scene.tab
2007040 405
2007316 681
2008089 819
2008319 1049
2008365 1095
2009045 1140
2009321 1416
2010002 1462
2010048 1508
```

```
sbas intf.tab scene.tab 29 9 2826 1728 -smooth 1.0 -wavelength 0.2362 -incidence 34.3 -range 848965 -rms -dem -atm 1
```

```
compute RMS misfit
compute DEM error
```

```
setting smoothing to 1.000
setting radar wavelength to 0.236 m
setting radar incidence angle to 34.300 degree
setting range to 848965.000 m
Memory Allocation Successful...
read table file ...
number of SAR scenes is 9
number of interferograms is 29
read phase and correlation grids ...
fill the G matrix ...
```

```
Applying atmospheric correction by common point stacking...
```

```
Hit Matrix:
2007040 0 1 1 1 1 0 0 0
2007316 0 0 1 1 1 1 1 1
2008089 0 0 0 0 0 1 1 1
```



```
2008319 0 0 0 0 1 1 1 1 0
2008365 0 0 0 0 0 1 1 1 1
2009045 0 0 0 0 0 0 1 1 1
2009321 0 0 0 0 0 0 0 1 1
2010002 0 0 0 0 0 0 0 0 1
2010048 0 0 0 0 0 0 0 0 0
```

Applying exponential relaxation on smoothing parameters

```
Setting smoothing parameter to 1000.000000...
fill the G matrix ...
Computing deformation time-series...
run least-squares problem over 2826 by 1728 pixel (0) ...
matrix is full rank: 9
```

```
Removing deformation time-series from original unwrapped phase...
Computing atmospheric phase screen by common-point stacking...
Initial estimate of APS...
atm_noise(NO.4) = 2.388532
atm_noise(NO.3) = 1.658535
atm_noise(NO.7) = 1.219377
atm_noise(NO.0) = 0.000000
atm_noise(NO.1) = 0.000000
atm_noise(NO.2) = 0.000000
atm_noise(NO.5) = 0.000000
atm_noise(NO.6) = 0.000000
atm_noise(NO.8) = 0.000000
```

```
atm_noise(NO.4) = 2.375551
atm_noise(NO.3) = 1.653585
atm_noise(NO.7) = 1.213044
atm_noise(NO.0) = 0.000000
atm_noise(NO.1) = 0.000000
atm_noise(NO.2) = 0.000000
atm_noise(NO.5) = 0.000000
atm_noise(NO.6) = 0.000000
atm_noise(NO.8) = 0.000000
```

```
Applying atmospheric phase screen to original unwrapped phase...
Setting smoothing parameter to 1.000000...
fill the G matrix ...
run least-squares problem over 2826 by 1728 pixel (2) ...
matrix is rank-deficient: 8
```

write output ...

```
raln.grd
ralt.grd
rms_ll.grd
dem.grd
vel_ll.grd
disp_2007040_ll.grd
disp_2007316_ll.grd
disp_2008089_ll.grd
disp_2008319_ll.grd
disp_2008365_ll.grd
disp_2009045_ll.grd
disp_2009321_ll.grd
disp_2010002_ll.grd
disp_2010048_ll.grd
aps_2007040.grd
aps_2007316.grd
aps_2008089.grd
aps_2008319.grd
aps_2008365.grd
aps_2009045.grd
aps_2009321.grd
aps_2010002.grd
aps_2010048.grd
```

## A.8 Sentinel-1A(Sub-swath F1) in Bali, Indonesia

```
data.in
s1a-iw1-slc-vv-20141016t104106-20141016t104134-002853-003393-001:S1A_OPER_AUX_POEORB_OPOD_20141106T123612_V20141015T225944_20141017T005944.EOF
s1a-iw1-slc-vv-20141028t104106-20141028t104134-003028-00374f-001:S1A_OPER_AUX_POEORB_OPOD_20141118T123725_V20141027T225944_20141029T005944.EOF
s1a-iw1-slc-vv-20141121t104106-20141121t104134-003378-003edb-001:S1A_OPER_AUX_POEORB_OPOD_20141212T123749_V20141120T225944_20141122T005944.EOF
s1a-iw1-slc-vv-20150225t104103-20150225t104131-004778-005eeb-001:S1A_OPER_AUX_POEORB_OPOD_20150318T123036_V20150224T225944_20150226T005944.EOF
s1a-iw1-slc-vv-20150321t104103-20150321t104131-005128-006757-001:S1A_OPER_AUX_POEORB_OPOD_20150411T123045_V20150320T225944_20150322T005944.EOF
s1a-iw1-slc-vv-20150508t104106-20150508t104133-005828-007800-001:S1A_OPER_AUX_POEORB_OPOD_20150529T122517_V20150507T225944_20150509T005944.EOF
s1a-iw1-slc-vv-20150601t104107-20150601t104135-006178-0080be-001:S1A_OPER_AUX_POEORB_OPOD_20150621T122558_V20150620T225944_20150602T005944.EOF
s1a-iw1-slc-vv-20150625t104109-20150625t104136-006528-008aad-001:S1A_OPER_AUX_POEORB_OPOD_20150715T122234_V20150624T225944_20150626T005944.EOF
s1a-iw1-slc-vv-20150719t104109-20150719t104137-006878-009494-001:S1A_OPER_AUX_POEORB_OPOD_20150808T122256_V20150718T225943_20150720T005943.EOF
s1a-iw1-slc-vv-20150812t104110-20150812t104138-007228-009e3f-001:S1A_OPER_AUX_POEORB_OPOD_20150901T122301_V20150811T225943_20150813T005943.EOF
s1a-iw1-slc-vv-20150929t104112-20150929t104140-007928-00b136-001:S1A_OPER_AUX_POEORB_OPOD_20151019T122431_V20150928T225943_20150930T005943.EOF
s1a-iw1-slc-vv-20151023t104112-20151023t104140-008278-00baaf-001:S1A_OPER_AUX_POEORB_OPOD_20151112T122405_V20151022T225943_20151024T005943.EOF
s1a-iw1-slc-vv-20151116t104106-20151116t104134-008628-00c418-001:S1A_OPER_AUX_POEORB_OPOD_20151206T122632_V20151115T225943_20151117T005943.EOF
s1a-iw1-slc-vv-20160103t104105-20160103t104133-009328-00d7c0-001:S1A_OPER_AUX_POEORB_OPOD_20160123T121722_V20160102T225943_20160104T005943.EOF
s1a-iw1-slc-vv-20160127t104104-20160127t104132-009678-00e1e3-001:S1A_OPER_AUX_POEORB_OPOD_20160216T121630_V20160126T225943_20160128T005943.EOF
s1a-iw1-slc-vv-20160220t104104-20160220t104132-010028-00ec16-001:S1A_OPER_AUX_POEORB_OPOD_20160311T121452_V20160219T225943_20160221T005943.EOF
s1a-iw1-slc-vv-20160408t104105-20160408t104133-010728-010026-001:S1A_OPER_AUX_POEORB_OPOD_20160428T121507_V20160407T225943_20160409T005943.EOF
s1a-iw1-slc-vv-20160502t104106-20160502t104134-011078-010af7-001:S1A_OPER_AUX_POEORB_OPOD_20160522T121449_V20160501T225943_20160503T005943.EOF
s1a-iw1-slc-vv-20160526t104107-20160526t104135-011428-011642-001:S1A_OPER_AUX_POEORB_OPOD_20160615T121532_V20160525T225943_20160527T005943.EOF
s1a-iw1-slc-vv-20160713t104110-20160713t104138-012128-012c99-001:S1A_OPER_AUX_POEORB_OPOD_20160802T121647_V20160712T225943_20160714T005943.EOF
s1a-iw1-slc-vv-20170121t104110-20170121t104138-014928-0185cf-001:S1A_OPER_AUX_POEORB_OPOD_20170210T121453_V20170120T225942_20170122T005942.EOF
```

```
preproc_batch_tops.csh data.in dem.grd 1
Reading in 4988 lines of info from XML...
Writing 17 lines for orbit...
Writing 58 lines of precise orbit for the LED file...
Successfully opened junk1
Reading in 4988 lines of info from XML...
Writing 17 lines for orbit...
Writing 58 lines of precise orbit for the LED file...
Successfully opened junk1
Reading in 4988 lines of info from XML...
Writing 17 lines for orbit...
Writing 58 lines of precise orbit for the LED file...
Successfully opened junk1
Reading in 4974 lines of info from XML...
Writing 16 lines for orbit...
Writing 58 lines of precise orbit for the LED file...
Successfully opened junk1
Reading in 5148 lines of info from XML...
Writing 32 lines for orbit...
```

```
Writing 58 lines of precise orbit for the LED file...
Successfully opened junk1
Reading in 5162 lines of info from XML...
Writing 32 lines for orbit...
Writing 58 lines of precise orbit for the LED file...
Successfully opened junk1
Reading in 5162 lines of info from XML...
Writing 32 lines for orbit...
Writing 58 lines of precise orbit for the LED file...
Successfully opened junk1
Reading in 5162 lines of info from XML...
Writing 32 lines for orbit...
Writing 59 lines of precise orbit for the LED file...
Successfully opened junk1
Reading in 5192 lines of info from XML...
Writing 32 lines for orbit...
Writing 59 lines of precise orbit for the LED file...
Successfully opened junk1
Reading in 5192 lines of info from XML...
Writing 32 lines for orbit...
Writing 59 lines of precise orbit for the LED file...
Successfully opened junk1
Reading in 5192 lines of info from XML...
Writing 32 lines for orbit...
Writing 58 lines of precise orbit for the LED file...
Successfully opened junk1
Reading in 5192 lines of info from XML...
Writing 32 lines for orbit...
Writing 58 lines of precise orbit for the LED file...
Successfully opened junk1
Reading in 5192 lines of info from XML...
Writing 32 lines for orbit...
Writing 58 lines of precise orbit for the LED file...
Successfully opened junk1
Reading in 4982 lines of info from XML...
Writing 17 lines for orbit...
Writing 58 lines of precise orbit for the LED file...
Successfully opened junk1
Reading in 4974 lines of info from XML...
Writing 16 lines for orbit...
Writing 58 lines of precise orbit for the LED file...
Successfully opened junk1
Reading in 4982 lines of info from XML...
Writing 17 lines for orbit...
Writing 58 lines of precise orbit for the LED file...
Successfully opened junk1
Reading in 4982 lines of info from XML...
Writing 17 lines for orbit...
Writing 58 lines of precise orbit for the LED file...
Successfully opened junk1
Reading in 4988 lines of info from XML...
Writing 17 lines for orbit...
Writing 58 lines of precise orbit for the LED file...
Successfully opened junk1
Reading in 4988 lines of info from XML...
Writing 17 lines for orbit...
Writing 59 lines of precise orbit for the LED file...
Successfully opened junk1
Reading in 4988 lines of info from XML...
Writing 17 lines for orbit...
Writing 59 lines of precise orbit for the LED file...
Successfully opened junk1
Reading in 4988 lines of info from XML...
Writing 17 lines for orbit...
Writing 58 lines of precise orbit for the LED file...
Successfully opened junk1
```

```
csh select_pairs.csh baseline_table.dat 250 100
intf.in
baseline.ps
```

```
baseline_table.dat
S1A20141016_ALL_F1 2014288.4452156418 288 0.000000 0.000000
S1A20141028_ALL_F1 2014300.4452141363 300 -21.669118 -25.794993
S1A20141121_ALL_F1 2014324.4452110576 324 -33.426980 -68.529590
S1A20150225_ALL_F1 2015055.4451773821 420 107.834308 128.258588
S1A20150321_ALL_F1 2015079.4451856010 444 -24.995214 -42.940559
S1A20150508_ALL_F1 2015127.4452092899 492 -1.832845 -28.307770
S1A20150601_ALL_F1 2015151.4452276966 516 -44.186964 -100.980561
S1A20150625_ALL_F1 2015175.4452440606 540 -30.891345 -58.143115
S1A20150719_ALL_F1 2015199.4452489563 564 -3.284813 -16.648726
S1A20150812_ALL_F1 2015223.4452642917 588 -1.937772 23.609184
S1A20150929_ALL_F1 2015271.4452840581 636 16.651560 16.250752
S1A20151023_ALL_F1 2015295.4452849580 660 53.455093 58.032623
S1A20151116_ALL_F1 2015319.4452184762 684 12.012287 -42.183869
S1A20160103_ALL_F1 2016002.4452002260 732 25.839979 -2.754282
S1A20160127_ALL_F1 2016026.4451877656 756 99.546853 113.414970
S1A20160220_ALL_F1 2016050.4451874956 780 -7.088722 -34.933552
S1A20160408_ALL_F1 2016098.4451989429 828 -26.915301 -59.874454
S1A20160502_ALL_F1 2016122.4452109376 852 -6.166273 -18.556871
S1A20160526_ALL_F1 2016146.4452258018 876 18.574571 28.857464
S1A20160713_ALL_F1 2016194.4452566183 924 41.476747 61.600292
S1A20170121_ALL_F1 2017020.4452583112 1115 57.417298 61.635328
```

```
preproc_batch_tops.csh data.in dem.grd 2
Reading in 4988 lines of info from XML...
Writing 17 lines for orbit...
Writing SLC..Image Size: 20500 X 13528...
Working on burst #1 #2 #3 #4 #5 #6 #7 #8 #9 #10
number of points clipped to short int 1
Writing 58 lines of precise orbit for the LED file...
Writing 58 lines of precise orbit for the LED file...
Successfully opened junk1
rm: No match.
Reading in 4988 lines of info from XML...
Writing 17 lines for orbit...
Writing 58 lines of precise orbit for the LED file...
Shifting the master PRM by 0 lines...
Successfully opened junk1.PRM
Successfully opened junk2.PRM
Successfully opened junk1
Successfully opened junk1
[1] 48152
[2] 48153
[2] + Done SAT_llt2rat S1A20141028_104106_F1.PRM 1 < topo.llt > tmp1.dat
[1] + Done SAT_llt2rat tmp.PRM 1 < topo.llt > tmpm.dat
[1] 48171
[2] 48172
[2] + Done gmt surface atmp.xyz -bi3d -R0/20500/0/13532 -I8/4 -Gatmp.grd -T0.5 -N1000 -r
```

```
[1] + Done          gmt surface rtmp.xyz -bi3d -R0/20500/0/13532 -I8/4 -Grtmp.grd -T0.5 -N1000 -r
Reading in 4988 lines of info from XML...
Writing 17 lines for orbit...
Reading in range and azimuth shifts table...
Writing SLC..Image Size: 20500 X 13532...
Working on burst #1 #2 #3 #4 #5 #6 #7 #8 #9 #10
number of points clipped to short int 2
Writing 58 lines of precise orbit for the LED file...
Successfully opened junk1
Reading in 4988 lines of info from XML...
Writing 17 lines for orbit...
Writing 58 lines of precise orbit for the LED file...
Shifting the master PRM by 0 lines...
Successfully opened junk1.PRM
Successfully opened junk2.PRM
Successfully opened junk1
Successfully opened junk1
[1] 48451
[2] 48452
[2] Done          SAT_llt2rat S1A20141121_104106_F1.PRM 1 < topo.llt > tmp1.dat
[1] + Done          SAT_llt2rat tmp.PRM 1 < topo.llt > tmpm.dat
[1] 48465
[2] 48466
[2] + Done          gmt surface atmp.xyz -bi3d -R0/20500/0/13532 -I8/4 -Gatmp.grd -T0.5 -N1000 -r
[1] + Done          gmt surface rtmp.xyz -bi3d -R0/20500/0/13532 -I8/4 -Grtmp.grd -T0.5 -N1000 -r
Reading in 4988 lines of info from XML...
Writing 17 lines for orbit...
Reading in range and azimuth shifts table...
Writing SLC..Image Size: 20500 X 13532...
Working on burst #1 #2 #3 #4 #5 #6 #7 #8 #9 #10
number of points clipped to short int 2
Writing 58 lines of precise orbit for the LED file...
Successfully opened junk1
Reading in 4974 lines of info from XML...
Writing 16 lines for orbit...
Writing 58 lines of precise orbit for the LED file...
Shifting the master PRM by 0 lines...
Successfully opened junk1.PRM
Successfully opened junk2.PRM
Successfully opened junk1
Successfully opened junk1
[1] 48740
[2] 48741
[2] Done          SAT_llt2rat S1A20150225_104103_F1.PRM 1 < topo.llt > tmp1.dat
[1] + Done          SAT_llt2rat tmp.PRM 1 < topo.llt > tmpm.dat
[1] 48754
[2] 48755
[2] Done          gmt surface atmp.xyz -bi3d -R0/20500/0/13532 -I8/4 -Gatmp.grd -T0.5 -N1000 -r
[1] + Done          gmt surface rtmp.xyz -bi3d -R0/20500/0/13532 -I8/4 -Grtmp.grd -T0.5 -N1000 -r
Reading in 4974 lines of info from XML...
Writing 16 lines for orbit...
Reading in range and azimuth shifts table...
Writing SLC..Image Size: 20500 X 13532...
Working on burst #1 #2 #3 #4 #5 #6 #7 #8 #9 #10
number of points clipped to short int 2
Writing 58 lines of precise orbit for the LED file...
Successfully opened junk1
Reading in 5148 lines of info from XML...
Writing 32 lines for orbit...
Writing 58 lines of precise orbit for the LED file...
Shifting the master PRM by 0 lines...
Successfully opened junk1.PRM
Successfully opened junk2.PRM
Successfully opened junk1
Successfully opened junk1
[1] 49029
[2] 49030
[2] + Done          SAT_llt2rat S1A20150321_104103_F1.PRM 1 < topo.llt > tmp1.dat
[1] + Done          SAT_llt2rat tmp.PRM 1 < topo.llt > tmpm.dat
[1] 49043
[2] 49044
[2] Done          gmt surface atmp.xyz -bi3d -R0/20500/0/13524 -I8/4 -Gatmp.grd -T0.5 -N1000 -r
[1] + Done          gmt surface rtmp.xyz -bi3d -R0/20500/0/13524 -I8/4 -Grtmp.grd -T0.5 -N1000 -r
Reading in 5148 lines of info from XML...
Writing 32 lines for orbit...
Reading in range and azimuth shifts table...
Writing SLC..Image Size: 20500 X 13524...
Working on burst #1 #2 #3 #4 #5 #6 #7 #8 #9 #10
number of points clipped to short int 4
Writing 58 lines of precise orbit for the LED file...
Successfully opened junk1
Reading in 5162 lines of info from XML...
Writing 32 lines for orbit...
Writing 58 lines of precise orbit for the LED file...
Shifting the master PRM by 0 lines...
Successfully opened junk1.PRM
Successfully opened junk2.PRM
Successfully opened junk1
Successfully opened junk1
[1] 49317
[2] 49318
[2] Done          SAT_llt2rat S1A20150508_104106_F1.PRM 1 < topo.llt > tmp1.dat
[1] + Done          SAT_llt2rat tmp.PRM 1 < topo.llt > tmpm.dat
[1] 49332
[2] 49333
[2] Done          gmt surface atmp.xyz -bi3d -R0/20500/0/13528 -I8/4 -Gatmp.grd -T0.5 -N1000 -r
[1] + Done          gmt surface rtmp.xyz -bi3d -R0/20500/0/13528 -I8/4 -Grtmp.grd -T0.5 -N1000 -r
Reading in 5162 lines of info from XML...
Writing 32 lines for orbit...
Reading in range and azimuth shifts table...
Writing SLC..Image Size: 20500 X 13528...
Working on burst #1 #2 #3 #4 #5 #6 #7 #8 #9 #10
number of points clipped to short int 3
Writing 58 lines of precise orbit for the LED file...
Successfully opened junk1
Reading in 5162 lines of info from XML...
Writing 32 lines for orbit...
Writing 58 lines of precise orbit for the LED file...
Shifting the master PRM by 0 lines...
Successfully opened junk1.PRM
Successfully opened junk2.PRM
Successfully opened junk1
Successfully opened junk1
[1] 49603
[2] 49604
[2] Done          SAT_llt2rat S1A20150601_104107_F1.PRM 1 < topo.llt > tmp1.dat
[1] + Done          SAT_llt2rat tmp.PRM 1 < topo.llt > tmpm.dat
[1] 49620
[2] 49621
```

```
[2] Done          gmt surface atmp.xyz -bi3d -R0/20500/0/13532 -I8/4 -Gatmp.grd -T0.5 -N1000 -r
[1] + Done          gmt surface rtmp.xyz -bi3d -R0/20500/0/13532 -I8/4 -Grtmp.grd -T0.5 -N1000 -r
Reading in 5162 lines of info from XML...
Writing 32 lines for orbit...
Reading in range and azimuth shifts table...
Writing SLC..Image Size: 20500 X 13532...
Working on burst #1 #2 #3 #4 #5 #6 #7 #8 #9 #10
number of points clipped to short int 3
Writing 58 lines of precise orbit for the LED file...
Successfully opened junk1
Reading in 5162 lines of info from XML...
Writing 32 lines for orbit...
Writing 59 lines of precise orbit for the LED file...
Shifting the master PRM by 0 lines...
Successfully opened junk1.PRM
Successfully opened junk2.PRM
Successfully opened junk1
Successfully opened junk1
[1] 49894
[2] 49895
[2] Done          SAT_llt2rat S1A20150625_104109_F1.PRM 1 < topo.llt > tmp1.dat
[1] + Done          SAT_llt2rat tmp.PRM 1 < topo.llt > tmpm.dat
[1] 49909
[2] 49910
[2] + Done          gmt surface atmp.xyz -bi3d -R0/20500/0/13524 -I8/4 -Gatmp.grd -T0.5 -N1000 -r
[1] + Done          gmt surface rtmp.xyz -bi3d -R0/20500/0/13524 -I8/4 -Grtmp.grd -T0.5 -N1000 -r
Reading in 5162 lines of info from XML...
Writing 32 lines for orbit...
Reading in range and azimuth shifts table...
Writing SLC..Image Size: 20500 X 13524...
Working on burst #1 #2 #3 #4 #5 #6 #7 #8 #9 #10
number of points clipped to short int 3
Writing 59 lines of precise orbit for the LED file...
Successfully opened junk1
Reading in 5192 lines of info from XML...
Writing 32 lines for orbit...
Writing 59 lines of precise orbit for the LED file...
Shifting the master PRM by 0 lines...
Successfully opened junk1.PRM
Successfully opened junk2.PRM
Successfully opened junk1
Successfully opened junk1
[1] 50132
[2] 50133
[2] Done          SAT_llt2rat S1A20150719_104109_F1.PRM 1 < topo.llt > tmp1.dat
[1] + Done          SAT_llt2rat tmp.PRM 1 < topo.llt > tmpm.dat
[1] 50194
[2] 50195
[2] Done          gmt surface atmp.xyz -bi3d -R0/20500/0/13524 -I8/4 -Gatmp.grd -T0.5 -N1000 -r
[1] + Done          gmt surface rtmp.xyz -bi3d -R0/20500/0/13524 -I8/4 -Grtmp.grd -T0.5 -N1000 -r
Reading in 5192 lines of info from XML...
Writing 32 lines for orbit...
Reading in range and azimuth shifts table...
Writing SLC..Image Size: 20500 X 13524...
Working on burst #1 #2 #3 #4 #5 #6 #7 #8 #9 #10
number of points clipped to short int 1
Writing 59 lines of precise orbit for the LED file...
Successfully opened junk1
Reading in 5192 lines of info from XML...
Writing 32 lines for orbit...
Writing 59 lines of precise orbit for the LED file...
Shifting the master PRM by 0 lines...
Successfully opened junk1.PRM
Successfully opened junk2.PRM
Successfully opened junk1
Successfully opened junk1
[1] 50421
[2] 50422
[2] Done          SAT_llt2rat S1A20150812_104110_F1.PRM 1 < topo.llt > tmp1.dat
[1] + Done          SAT_llt2rat tmp.PRM 1 < topo.llt > tmpm.dat
[1] 50435
[2] 50436
[2] + Done          gmt surface atmp.xyz -bi3d -R0/20500/0/13528 -I8/4 -Gatmp.grd -T0.5 -N1000 -r
[1] + Done          gmt surface rtmp.xyz -bi3d -R0/20500/0/13528 -I8/4 -Grtmp.grd -T0.5 -N1000 -r
Reading in 5192 lines of info from XML...
Writing 32 lines for orbit...
Reading in range and azimuth shifts table...
Writing SLC..Image Size: 20500 X 13528...
Working on burst #1 #2 #3 #4 #5 #6 #7 #8 #9 #10
number of points clipped to short int 4
Writing 59 lines of precise orbit for the LED file...
Successfully opened junk1
Reading in 5192 lines of info from XML...
Writing 32 lines for orbit...
Writing 58 lines of precise orbit for the LED file...
Shifting the master PRM by 0 lines...
Successfully opened junk1.PRM
Successfully opened junk2.PRM
Successfully opened junk1
Successfully opened junk1
[1] 50710
[2] 50711
[2] + Done          SAT_llt2rat S1A20150929_104112_F1.PRM 1 < topo.llt > tmp1.dat
[1] + Done          SAT_llt2rat tmp.PRM 1 < topo.llt > tmpm.dat
[1] 50724
[2] 50725
[2] Done          gmt surface atmp.xyz -bi3d -R0/20500/0/13528 -I8/4 -Gatmp.grd -T0.5 -N1000 -r
[1] + Done          gmt surface rtmp.xyz -bi3d -R0/20500/0/13528 -I8/4 -Grtmp.grd -T0.5 -N1000 -r
Reading in 5192 lines of info from XML...
Writing 32 lines for orbit...
Reading in range and azimuth shifts table...
Writing SLC..Image Size: 20500 X 13528...
Working on burst #1 #2 #3 #4 #5 #6 #7 #8 #9 #10
number of points clipped to short int 5
Writing 58 lines of precise orbit for the LED file...
Successfully opened junk1
Reading in 5192 lines of info from XML...
Writing 32 lines for orbit...
Writing 58 lines of precise orbit for the LED file...
Shifting the master PRM by 0 lines...
Successfully opened junk1.PRM
Successfully opened junk2.PRM
Successfully opened junk1
Successfully opened junk1
[1] 51000
[2] 51001
[2] + Done          SAT_llt2rat S1A20151023_104112_F1.PRM 1 < topo.llt > tmp1.dat
[1] + Done          SAT_llt2rat tmp.PRM 1 < topo.llt > tmpm.dat
[1] 51014
```

```
[2] 51015
[2] Done          gmt surface atmp.xyz -bi3d -R0/20500/0/13532 -I8/4 -Gatmp.grd -T0.5 -N1000 -r
[1] + Done          gmt surface rtmp.xyz -bi3d -R0/20500/0/13532 -I8/4 -Grtmp.grd -T0.5 -N1000 -r
Reading in 5192 lines of info from XML...
Writing 32 lines for orbit...
Reading in range and azimuth shifts table...
Writing SLC..Image Size: 20500 X 13532...
Working on burst #1 #2 #3 #4 #5 #6 #7 #8 #9 #10
number of points clipped to short int 4
Writing 58 lines of precise orbit for the LED file...
Successfully opened junk1
Reading in 5192 lines of info from XML...
Writing 32 lines for orbit...
Writing 58 lines of precise orbit for the LED file...
Shifting the master PRM by 0 lines...
Successfully opened junk1.PRM
Successfully opened junk2.PRM
Modifying master PRM by 2692 lines...
Successfully opened junk1
Successfully opened junk1
[1] 51382
[2] 51383
[2] + Done          SAT_llt2rat S1A20151116_104106_F1.PRM 1 < topo.llt > tmp1.dat
[1] + Done          SAT_llt2rat tmp.PRM 1 < topo.llt > tmpm.dat
[1] 51397
[2] 51398
[2] + Done          gmt surface atmp.xyz -bi3d -R0/20600/0/13528 -I8/4 -Gatmp.grd -T0.5 -N1000 -r
[1] + Done          gmt surface rtmp.xyz -bi3d -R0/20600/0/13528 -I8/4 -Grtmp.grd -T0.5 -N1000 -r
Reading in 5192 lines of info from XML...
Writing 32 lines for orbit...
Reading in range and azimuth shifts table...
Writing SLC..Image Size: 20600 X 13528...
Working on burst #1 #2 #3 #4 #5 #6 #7 #8 #9 #10
number of points clipped to short int 1
Writing 58 lines of precise orbit for the LED file...
Restoring 2692 lines shift to the image...
Successfully opened junk1
Reading in 4982 lines of info from XML...
Writing 17 lines for orbit...
Writing 58 lines of precise orbit for the LED file...
Shifting the master PRM by 0 lines...
Successfully opened junk1.PRM
Successfully opened junk2.PRM
Modifying master PRM by 2691 lines...
Successfully opened junk1
Successfully opened junk1
[1] 51723
[2] 51724
[2] + Done          SAT_llt2rat S1A20160103_104105_F1.PRM 1 < topo.llt > tmp1.dat
[1] + Done          SAT_llt2rat tmp.PRM 1 < topo.llt > tmpm.dat
[1] 51786
[2] 51787
[2] Done          gmt surface atmp.xyz -bi3d -R0/20600/0/13528 -I8/4 -Gatmp.grd -T0.5 -N1000 -r
[1] + Done          gmt surface rtmp.xyz -bi3d -R0/20600/0/13528 -I8/4 -Grtmp.grd -T0.5 -N1000 -r
Reading in 4982 lines of info from XML...
Writing 17 lines for orbit...
Reading in range and azimuth shifts table...
Writing SLC..Image Size: 20600 X 13528...
Working on burst #1 #2 #3 #4 #5 #6 #7 #8 #9 #10
number of points clipped to short int 2
Writing 58 lines of precise orbit for the LED file...
Restoring 2691 lines shift to the image...
Successfully opened junk1
Reading in 4974 lines of info from XML...
Writing 16 lines for orbit...
Writing 58 lines of precise orbit for the LED file...
Shifting the master PRM by 0 lines...
Successfully opened junk1.PRM
Successfully opened junk2.PRM
Modifying master PRM by 2700 lines...
Successfully opened junk1
Successfully opened junk1
[1] 52117
[2] 52118
[2] Done          SAT_llt2rat S1A20160127_104104_F1.PRM 1 < topo.llt > tmp1.dat
[1] + Done          SAT_llt2rat tmp.PRM 1 < topo.llt > tmpm.dat
[1] 52133
[2] 52134
[2] Done          gmt surface atmp.xyz -bi3d -R0/20600/0/13528 -I8/4 -Gatmp.grd -T0.5 -N1000 -r
[1] + Done          gmt surface rtmp.xyz -bi3d -R0/20600/0/13528 -I8/4 -Grtmp.grd -T0.5 -N1000 -r
Reading in 4974 lines of info from XML...
Writing 16 lines for orbit...
Reading in range and azimuth shifts table...
Writing SLC..Image Size: 20600 X 13528...
Working on burst #1 #2 #3 #4 #5 #6 #7 #8 #9 #10
number of points clipped to short int 4
Writing 58 lines of precise orbit for the LED file...
Restoring 2700 lines shift to the image...
Successfully opened junk1
Reading in 4982 lines of info from XML...
Writing 17 lines for orbit...
Writing 58 lines of precise orbit for the LED file...
Shifting the master PRM by 0 lines...
Successfully opened junk1.PRM
Successfully opened junk2.PRM
Modifying master PRM by 2699 lines...
Successfully opened junk1
Successfully opened junk1
[1] 52460
[2] 52461
[2] Done          SAT_llt2rat S1A20160220_104104_F1.PRM 1 < topo.llt > tmp1.dat
[1] + Done          SAT_llt2rat tmp.PRM 1 < topo.llt > tmpm.dat
[1] 52474
[2] 52475
[2] Done          gmt surface atmp.xyz -bi3d -R0/20600/0/13536 -I8/4 -Gatmp.grd -T0.5 -N1000 -r
[1] + Done          gmt surface rtmp.xyz -bi3d -R0/20600/0/13536 -I8/4 -Grtmp.grd -T0.5 -N1000 -r
Reading in 4982 lines of info from XML...
Writing 17 lines for orbit...
Reading in range and azimuth shifts table...
Writing SLC..Image Size: 20600 X 13536...
Working on burst #1 #2 #3 #4 #5 #6 #7 #8 #9 #10
number of points clipped to short int 0
Writing 58 lines of precise orbit for the LED file...
Restoring 2699 lines shift to the image...
Successfully opened junk1
Reading in 4982 lines of info from XML...
Writing 17 lines for orbit...
Writing 58 lines of precise orbit for the LED file...
Shifting the master PRM by 0 lines...
```

```
Successfully opened junk1.PRM
Successfully opened junk2.PRM
Modifying master PRM by 2697 lines...
Successfully opened junk1
Successfully opened junk1
[1] 52792
[2] 52793
[2] + Done          SAT_llt2rat S1A20160408_104105_F1.PRM 1 < topo.llt > tmp1.dat
[1] + Done          SAT_llt2rat tmp.PRM 1 < topo.llt > tmpm.dat
[1] 52807
[2] 52808
[2] + Done          gmt surface atmp.xyz -bi3d -R0/20600/0/13528 -I8/4 -Gatmp.grd -T0.5 -N1000 -r
[1] + Done          gmt surface rtmp.xyz -bi3d -R0/20600/0/13528 -I8/4 -Grtmp.grd -T0.5 -N1000 -r
Reading in 4982 lines of info from XML...
Writing 17 lines for orbit...
Reading in range and azimuth shifts table...
Writing SLC..Image Size: 20600 X 13528...
Working on burst #1 #2 #3 #4 #5 #6 #7 #8 #9 #10
number of points clipped to short int 1
Writing 58 lines of precise orbit for the LED file...
Restoring 2697 lines shift to the image...
Successfully opened junk1
Reading in 4988 lines of info from XML...
Writing 17 lines for orbit...
Writing 58 lines of precise orbit for the LED file...
Shifting the master PRM by 0 lines...
Successfully opened junk1.PRM
Successfully opened junk2.PRM
Modifying master PRM by 2697 lines...
Successfully opened junk1
Successfully opened junk1
[1] 53180
[2] 53181
[2] + Done          SAT_llt2rat S1A20160502_104106_F1.PRM 1 < topo.llt > tmp1.dat
[1] + Done          SAT_llt2rat tmp.PRM 1 < topo.llt > tmpm.dat
[1] 53194
[2] 53195
[2] + Done          gmt surface atmp.xyz -bi3d -R0/20600/0/13524 -I8/4 -Gatmp.grd -T0.5 -N1000 -r
[1] + Done          gmt surface rtmp.xyz -bi3d -R0/20600/0/13524 -I8/4 -Grtmp.grd -T0.5 -N1000 -r
Reading in 4988 lines of info from XML...
Writing 17 lines for orbit...
Reading in range and azimuth shifts table...
Writing SLC..Image Size: 20600 X 13524...
Working on burst #1 #2 #3 #4 #5 #6 #7 #8 #9 #10
number of points clipped to short int 2
Writing 58 lines of precise orbit for the LED file...
Restoring 2697 lines shift to the image...
Successfully opened junk1
Reading in 4988 lines of info from XML...
Writing 17 lines for orbit...
Writing 59 lines of precise orbit for the LED file...
Shifting the master PRM by 0 lines...
Successfully opened junk1.PRM
Successfully opened junk2.PRM
Modifying master PRM by 2693 lines...
Successfully opened junk1
Successfully opened junk1
[1] 53516
[2] 53517
[2] + Done          SAT_llt2rat S1A20160526_104107_F1.PRM 1 < topo.llt > tmp1.dat
[1] + Done          SAT_llt2rat tmp.PRM 1 < topo.llt > tmpm.dat
[1] 53530
[2] 53531
[2] + Done          gmt surface atmp.xyz -bi3d -R0/20600/0/13528 -I8/4 -Gatmp.grd -T0.5 -N1000 -r
[1] + Done          gmt surface rtmp.xyz -bi3d -R0/20600/0/13528 -I8/4 -Grtmp.grd -T0.5 -N1000 -r
Reading in 4988 lines of info from XML...
Writing 17 lines for orbit...
Reading in range and azimuth shifts table...
Writing SLC..Image Size: 20600 X 13528...
Working on burst #1 #2 #3 #4 #5 #6 #7 #8 #9 #10
number of points clipped to short int 2
Writing 59 lines of precise orbit for the LED file...
Restoring 2693 lines shift to the image...
Successfully opened junk1
Reading in 4988 lines of info from XML...
Writing 17 lines for orbit...
Writing 59 lines of precise orbit for the LED file...
Shifting the master PRM by 0 lines...
Successfully opened junk1.PRM
Successfully opened junk2.PRM
Modifying master PRM by 2686 lines...
Successfully opened junk1
Successfully opened junk1
[1] 53850
[2] 53851
[2] + Done          SAT_llt2rat S1A20160713_104110_F1.PRM 1 < topo.llt > tmp1.dat
[1] + Done          SAT_llt2rat tmp.PRM 1 < topo.llt > tmpm.dat
[1] 53864
[2] 53865
[2] + Done          gmt surface atmp.xyz -bi3d -R0/20600/0/13524 -I8/4 -Gatmp.grd -T0.5 -N1000 -r
[1] + Done          gmt surface rtmp.xyz -bi3d -R0/20600/0/13524 -I8/4 -Grtmp.grd -T0.5 -N1000 -r
Reading in 4988 lines of info from XML...
Writing 17 lines for orbit...
Reading in range and azimuth shifts table...
Writing SLC..Image Size: 20600 X 13524...
Working on burst #1 #2 #3 #4 #5 #6 #7 #8 #9 #10
number of points clipped to short int 2
Writing 59 lines of precise orbit for the LED file...
Restoring 2686 lines shift to the image...
Successfully opened junk1
Reading in 4988 lines of info from XML...
Writing 17 lines for orbit...
Writing 58 lines of precise orbit for the LED file...
Shifting the master PRM by 0 lines...
Successfully opened junk1.PRM
Successfully opened junk2.PRM
Modifying master PRM by 2691 lines...
Successfully opened junk1
Successfully opened junk1
[1] 54184
[2] 54185
[2] + Done          SAT_llt2rat S1A20170121_104110_F1.PRM 1 < topo.llt > tmp1.dat
[1] + Done          SAT_llt2rat tmp.PRM 1 < topo.llt > tmpm.dat
[1] 54246
[2] 54247
[2] + Done          gmt surface atmp.xyz -bi3d -R0/20600/0/13528 -I8/4 -Gatmp.grd -T0.5 -N1000 -r
[1] + Done          gmt surface rtmp.xyz -bi3d -R0/20600/0/13528 -I8/4 -Grtmp.grd -T0.5 -N1000 -r
Reading in 4988 lines of info from XML...
Writing 17 lines for orbit...
```

Reading in range and azimuth shifts table...  
Writing SLC..Image Size: 20600 X 13528...  
Working on burst #1 #2 #3 #4 #5 #6 #7 #8 #9 #10  
number of points clipped to short int 0  
Writing 58 lines of precise orbit for the LED file...  
Restoring 2691 lines shift to the image...  
Successfully opened junk1

intf\_tops.csh intf.in batch\_tops.config  
clean up topo/ folder

DEM2TOPOPHASE.CSH - START  
USER SHOULD PROVIDE DEM FILE  
range declination is: 2  
blockmedian: Provides 3, expects 3-column binary data  
blockmedian: Processing input table data  
blockmedian: W: 0 E: 20500 S: 0 N: 13528 n\_columns: 10250 n\_rows: 6764  
blockmedian: Input 3 columns via binary records using format ddd  
blockmedian: Output 3 columns via binary records using format ddd  
blockmedian: N read: 1951350 N used: 1943714 outside\_area: 7636 N cells filled: 1943459  
surface: Provides 3, expects 3-column binary data  
surface: Grid domain: W: 0 E: 20500 S: 0 N: 13528 n\_columns: 10250 n\_rows: 6764 [pixel registration]  
surface: Processing input table data  
surface: Input 3 columns via binary records using format ddd  
surface: Minimum value of your dataset x,y,z at: surface: 9.087203202582 3.80631566048 -4.24559545517  
surface: Maximum value of your dataset x,y,z at: surface: 17568.980469 7031.25976562 2382.2878418  
surface: LS plane determined: z = -10.8016 + (0.0132808 \* col) + (0.039174 \* row)  
surface: Grid Mode IterationMax Change Conv Limit Total Iterations  
surface: 2 D 349 0.0102886677188 0.0105022633649 349  
surface: 1 I 18 0.0143521364284 0.0210045267298 367  
surface: 1 D 315 0.0208256422956 0.0210045267298 682  
surface: Fit info: N data points N nodes mean error rms errorcurvature  
surface: 1943459 69348015 1.8855568431e-06 0.00746142954133 31783.0368027  
grd2cpt: Processing input grid(s)  
grd2cpt: Mean and S.D. of data are 189.346222536 229.128266265  
grdimage: Allocates memory and read data file topo\_ra.grd  
grdimage: Evaluate image pixel colors  
grdimage: Creating 8-bit grayshade image  
DEM2TOPOPHASE.CSH - END  
NO TOPOPHASE SHIFT

START FORM A STACK OF INTERFEROGRAMS

INTF.CSH, FILTER.CSH - START  
mkdir: 2014288\_2014300: File exists  
ln: ./S1A20141016\_ALL\_F1.LED: File exists  
ln: ./S1A20141028\_ALL\_F1.LED: File exists  
ln: ./S1A20141016\_ALL\_F1.SLC: File exists  
ln: ./S1A20141028\_ALL\_F1.SLC: File exists  
ln: ./topo\_ra.grd: File exists  
intf.csh  
running phasediff...  
reading topo topo\_ra.grd  
xdim 20500, ydim 13528  
filter.csh  
gauss\_300 4 6 (1 2)  
making amplitudes...  
filtering interferogram...  
making amplitude...  
making correlation...  
making phase...  
filtering phase...  
INTF.CSH, FILTER.CSH - END

MAKE LANDMASK -- START  
REQUIRE FULL RESOLUTION COASTLINE FROM GMT

grdlandmask: GSHHG version 2.3.7  
Derived from World Vector Shoreline, CIA WDB-II, and Atlas of the Cryosphere  
Processed by Paul Wessel and Walter H. F. Smith, 1994-2017  
grdlandmask: Nodes in water will be set to NaN  
grdlandmask: Nodes on land will be set to 1  
grdlandmask: Level 0 contained 8112640 nodes  
grdlandmask: Level 1 contained 2478081 nodes  
grdlandmask: Done!  
surface: Provides 3, expects 3-column binary data  
surface: Grid domain: W: 113.83333329 E: 117.416666662 S: -9.166666663 N: -7.4166666637 n\_columns: 4300 n\_rows: 2100 [gridline registration]  
surface: Processing input table data  
surface: Input 3 columns via binary records using format fff  
surface: Minimum value of your dataset x,y,z at: surface: 114.280830383 -7.92999982834 -9.99230003357  
surface: Maximum value of your dataset x,y,z at: surface: 115.052497864 -7.81833314896 20509.9980469  
surface: LS plane determined: z = -18491.1 + (21.2403 \* col) + (4.70208 \* row)  
surface: Grid Mode IterationMax Change Conv Limit Total Iterations  
surface: 100 D 12525 0.000127559532091 0.000129180713562 12525  
surface: 20 I 82 0.000634765875382 0.000645903567808 12607  
surface: 20 D 10000 0.002069698322 0.000645903567808 22607  
surface: 4 I 62 0.00308568304538 0.0032295178390 22669  
surface: 4 D 1805 0.00322851378894 0.0032295178390 24474  
surface: 2 I 18 0.0054122970447 0.00645903567808 24492  
surface: 2 D 653 0.00645208689182 0.0064590356780 25145  
surface: 1 I 14 0.011798358404 0.0129180713562 25159  
surface: 1 D 213 0.0129167500755 0.0129180713562 25372  
surface: Fit info: N data points N nodes mean error rms errorcurvature  
surface: 1821492 9036401 0 0 13547.3435574  
surface: Provides 3, expects 3-column binary data  
surface: Grid domain: W: 113.83333329 E: 117.416666662 S: -9.166666663 N: -7.4166666637 n\_columns: 4300 n\_rows: 2100 [gridline registration]  
surface: Processing input table data  
surface: Input 3 columns via binary records using format fff  
surface: Minimum value of your dataset x,y,z at: surface: 115.35333252 -9.16666698456 189.512191772  
surface: Maximum value of your dataset x,y,z at: surface: 114.444999695 -7.63000011444 13547.9990234  
surface: LS plane determined: z = 2798.48 + (-1.42891 \* col) + (6.39843 \* row)  
surface: Grid Mode IterationMax Change Conv Limit Total Iterations  
surface: 100 D 11537 7.92891904249e-07 7.97353770751e-07 11537  
surface: 20 I 84 3.74267157559e-06 3.98676885376e-06 11621  
surface: 20 D 10000 9.02122467258e-06 3.98676885376e-06 21621  
surface: 4 I 75 1.97806828705e-05 1.99338442688e-05 21696  
surface: 4 D 2000 0.000187696365708 1.99338442688e-05 23696  
surface: 2 I 11 3.62207438071e-05 3.98676885376e-05 24707  
surface: 2 D 1000 4.08256160202e-05 3.98676885376e-05 24707  
surface: 1 I 8 6.4429398092e-05 7.97353770751e-05 24715  
surface: 1 D 64 7.87402652595e-05 7.97353770751e-05 24779  
surface: Fit info: N data points N nodes mean error rms errorcurvature  
surface: 1821492 9036401 0 0 1353.58925599  
MAKE LANDMASK -- END  
ln: ./landmask\_ra.grd: File exists

SNAPHU.CSH - START

threshold\_snaphu: 0.45  
grdmath: Perform reverse Polish notation calculations on grids  
grdmath: phase\_patch.grd landmask\_ra\_patch.grd MUL = phase\_patch.grd  
unwrapping phase with snaphu - higher threshold for faster unwrapping

snaphu v1.4.2  
32 parameters input from file snaphu.conf.brief (297 lines total)  
Reading wrapped phase from file phase.in  
No weight file specified. Assuming uniform weights  
Reading correlation data from file corr.in  
Calculating deformation-mode cost parameters  
Building range cost arrays  
Building azimuth cost arrays  
Initializing flows with MST algorithm  
Running approximate minimum spanning tree solver  
Running nonlinear network flow optimizer  
Maximum flow on network: 4  
Number of nodes in network: 5774749  
Flow increment: 1 (Total improvements: 0)  
Treesize: 5774749 Pivots: 50605 Improvements: 536  
Maximum flow on network: 4  
Flow increment: 2 (Total improvements: 536)  
Treesize: 5774749 Pivots: 248 Improvements: 39  
Maximum flow on network: 4  
Flow increment: 3 (Total improvements: 575)  
Treesize: 5774749 Pivots: 32 Improvements: 10  
Maximum flow on network: 4  
Flow increment: 4 (Total improvements: 585)  
Treesize: 5774749 Pivots: 6 Improvements: 3  
Maximum flow on network: 4  
Total solution cost: 1276783  
Integrating phase  
Writing output to file unwrap.out  
Program snaphu done  
Elapsed processor time: 0:02:54.70  
Elapsed wall clock time: 0:02:56  
grdmath: Perform reverse Polish notation calculations on grids  
grdmath: unwrap.grd landmask\_ra\_patch.grd MUL = tmp.grd  
SNAPHU.CSH - END

GEOCODE.CSH - START

threshold\_geocode: .45  
grdmath: Perform reverse Polish notation calculations on grids  
grdmath: corr.grd 0.45 GE 0 NAN mask.grd MUL = mask2.grd  
psscale: Warning: The -E option is deprecated but is accepted.  
psscale: For the current -D syntax you should use -D modifier +e instead.  
psscale: Note you cannot mix new-style modifiers (+e) with the old-style -D option.  
psscale: Warning: The -E option is deprecated but is accepted.  
psscale: For the current -D syntax you should use -D modifier +e instead.  
psscale: Note you cannot mix new-style modifiers (+e) with the old-style -D option.  
geocode.csh  
project correlation, phase, unwrapped and amplitude back to lon lat coordinates  
remarked is by root on Mon May 14 20:03:52 JST 2018 with geocode.csh  
proj\_ra2ll.csh  
surface: Provides 3, expects 3-column binary data  
surface: Grid domain: W: 0 E: 20496 S: 0 N: 13536 n\_columns: 1281 n\_rows: 423 [gridline registration]  
surface: Processing input table data  
surface: Input 3 columns via binary records using format fff  
surface: Minimum value of your dataset x,y,z at: surface: 8.4292383194 13547.5927734 114.220001221  
surface: Maximum value of your dataset x,y,z at: surface: 20500.6113281 -12.4760046005 115.359169006  
surface: 1407751 unusable points were supplied; these will be ignored.  
surface: You should have pre-processed the data with block-mean, -median, or -mode.  
surface: Check that previous processing steps write results with enough decimals.  
surface: LS plane determined:  $z = 114.602 + (0.000597873 * \text{col}) + (-0.000879088 * \text{row})$   
surface: Grid Mode IterationMax Change Conv Limit Total Iterations  
surface: 3 D 18 1.09856571456e-07 1.60422700444e-07 18  
surface: 1 I 21 2.89638275712e-07 4.81268101333e-07 39  
surface: 1 D 18 3.26348538909e-07 4.81268101333e-07 57  
surface: Fit info: N data points N nodes mean error rms error curvature  
surface: 542268 543568 8.85633699404e-06 0.00844212721696 5237.0814115  
surface: Provides 3, expects 3-column binary data  
surface: Grid domain: W: 0 E: 20496 S: 0 N: 13536 n\_columns: 1281 n\_rows: 423 [gridline registration]  
surface: Processing input table data  
surface: Input 3 columns via binary records using format fff  
surface: Minimum value of your dataset x,y,z at: surface: -3.89805984497 -15.3827676773 -9.36416721344  
surface: Maximum value of your dataset x,y,z at: surface: 20489.9648438 13547.8720703 -7.51000022888  
surface: 1407751 unusable points were supplied; these will be ignored.  
surface: You should have pre-processed the data with block-mean, -median, or -mode.  
surface: Check that previous processing steps write results with enough decimals.  
surface: LS plane determined:  $z = -0.35961 + (0.000133549 * \text{col}) + (0.00397144 * \text{row})$   
surface: Grid Mode IterationMax Change Conv Limit Total Iterations  
surface: 3 D 18 2.40951585769e-08 3.4786119345e-08 18  
surface: 1 I 21 7.53017417096e-08 1.04358358035e-07 39  
surface: 1 D 18 9.66312061926e-08 1.04358358035e-07 57  
surface: Fit info: N data points N nodes mean error rms error curvature  
surface: 542268 543568 3.18630440715e-06 0.0100363693046 8547.88399102  
geocode.csh  
make the KML files for Google Earth  
grdimage: Allocates memory and read data file display\_amp\_ll.grd  
grdimage: Evaluate image pixel colors  
grdimage: Creating 24-bit color image  
Make display\_amp\_ll.kml and display\_amp\_ll.png  
psconvert: Processing display\_amp\_ll.ps...  
psconvert: Figure dimensions: Width: 82.5 points [1.14583 inch] Height: 133.8 points [1.85833 inch]  
psconvert: gs -q -dSAFER -dNOPAUSE -dBATCH -dPDFSETTINGS=/prepress -dDownsampleColorImages=false -dDownsampleGrayImages=false -dDownsampleMonoImages=false -dUseFlateCompression=true -dEmbedAllFonts=true -dSubsetFonts=true -dMonoImageFilter=/FlateEncode -dAutoFilterGrayImages=false -dGrayImageFilter=/FlateEncode -dAutoFilterColorImages=false -dColorImageFilter=/FlateEncode -dSCANCONVERTERTYPE=2 -dMaxBitmap=2147483647 -dUseFastColor=true -dDEVICE=pngalpha -g751x1218 -r655 -sOutputFile='display\_amp\_ll.png' -f'./psconvert\_49429d.eps'  
psconvert: Done.  
grdimage: Allocates memory and read data file corr\_ll.grd  
grdimage: Evaluate image pixel colors  
grdimage: Creating 24-bit color image  
PSL: Colormap of 255 colors created  
Make corr\_ll.kml and corr\_ll.png  
psconvert: Processing corr\_ll.ps...  
psconvert: Figure dimensions: Width: 82.5 points [1.14583 inch] Height: 133.8 points [1.85833 inch]  
psconvert: gs -q -dSAFER -dNOPAUSE -dBATCH -dPDFSETTINGS=/prepress -dDownsampleColorImages=false -dDownsampleGrayImages=false -dDownsampleMonoImages=false -dUseFlateCompression=true -dEmbedAllFonts=true -dSubsetFonts=true -dMonoImageFilter=/FlateEncode -dAutoFilterGrayImages=false -dGrayImageFilter=/FlateEncode -dAutoFilterColorImages=false -dColorImageFilter=/FlateEncode -dSCANCONVERTERTYPE=2 -dMaxBitmap=2147483647 -dUseFastColor=true -dDEVICE=pngalpha -g751x1218 -r655 -sOutputFile='corr\_ll.png' -f'./psconvert\_49443d.eps'  
psconvert: Done.  
grdimage: Allocates memory and read data file phase\_mask\_ll.grd  
grdimage: Evaluate image pixel colors  
grdimage: Creating 24-bit color image  
Make phase\_mask\_ll.kml and phase\_mask\_ll.png  
psconvert: Processing phase\_mask\_ll.ps...  
psconvert: Figure dimensions: Width: 74.8199 points [1.03917 inch] Height: 97.8 points [1.35833 inch]  
psconvert: gs -q -dSAFER -dNOPAUSE -dBATCH -dPDFSETTINGS=/prepress -dDownsampleColorImages=false -dDownsampleGrayImages=false -dDownsampleMonoImages=false -dUseFlateCompression=true -dEmbedAllFonts=true -dSubsetFonts=true -dMonoImageFilter=/FlateEncode -



```
dAutoFilterGrayImages=false -dGrayImageFilter=/FlateEncode -dAutoFilterColorImages=false -dColorImageFilter=/FlateEncode -dSCANCONVERTERTYPE=2 -dMaxBitmap=2147483647 -dUseFastColor=true -sDEVICE=pngalpha -g681x890 -r655 -sOutputFile='phase_mask_ll.png' -f'./psconvert_49460d.eps'
psconvert: Done.
grdimage: Allocates memory and read data file phasefilt_mask_ll.grd
grdimage: Evaluate image pixel colors
grdimage: Creating 24-bit color image
Make phasefilt_mask_ll.kml and phasefilt_mask_ll.png
psconvert: Processing phasefilt_mask_ll.ps...
psconvert: Figure dimensions: Width: 74.8199 points [1.03917 inch] Height: 97.8 points [1.35833 inch]
psconvert: gs -q -dSAFER -dNOPAUSE -dBATCH -dPDFSETTINGS=/prepress -dDownsampleColorImages=false -dDownsampleGrayImages=false -dDownsampleMonoImages=false -dUseFlateCompression=true -dEmbedAllFonts=true -dSubsetFonts=true -dMonoImageFilter=/FlateEncode -dAutoFilterGrayImages=false -dGrayImageFilter=/FlateEncode -dAutoFilterColorImages=false -dColorImageFilter=/FlateEncode -dSCANCONVERTERTYPE=2 -dMaxBitmap=2147483647 -dUseFastColor=true -sDEVICE=pngalpha -g681x890 -r655 -sOutputFile='phasefilt_mask_ll.png' -f'./psconvert_49478d.eps'
psconvert: Done.
grdimage: Allocates memory and read data file unwrap_mask_ll.grd
grdimage: Evaluate image pixel colors
grdimage: Creating 24-bit color image
Make unwrap_mask_ll.kml and unwrap_mask_ll.png
psconvert: Processing unwrap_mask_ll.ps...
psconvert: Figure dimensions: Width: 74.8199 points [1.03917 inch] Height: 82.8 points [1.15 inch]
psconvert: gs -q -dSAFER -dNOPAUSE -dBATCH -dPDFSETTINGS=/prepress -dDownsampleColorImages=false -dDownsampleGrayImages=false -dDownsampleMonoImages=false -dUseFlateCompression=true -dEmbedAllFonts=true -dSubsetFonts=true -dMonoImageFilter=/FlateEncode -dAutoFilterGrayImages=false -dGrayImageFilter=/FlateEncode -dAutoFilterColorImages=false -dColorImageFilter=/FlateEncode -dSCANCONVERTERTYPE=2 -dMaxBitmap=2147483647 -dUseFastColor=true -sDEVICE=pngalpha -g681x754 -r655 -sOutputFile='unwrap_mask_ll.png' -f'./psconvert_49507d.eps'
psconvert: Done.
grdimage: Allocates memory and read data file phasefilt_mask_ll.grd
grdimage: Evaluate image pixel colors
grdimage: Creating 24-bit color image
Make phasefilt_mask_ll.kml and phasefilt_mask_ll.png
psconvert: Processing phasefilt_mask_ll.ps...
psconvert: Figure dimensions: Width: 74.8199 points [1.03917 inch] Height: 97.8 points [1.35833 inch]
psconvert: gs -q -dSAFER -dNOPAUSE -dBATCH -dPDFSETTINGS=/prepress -dDownsampleColorImages=false -dDownsampleGrayImages=false -dDownsampleMonoImages=false -dUseFlateCompression=true -dEmbedAllFonts=true -dSubsetFonts=true -dMonoImageFilter=/FlateEncode -dAutoFilterGrayImages=false -dGrayImageFilter=/FlateEncode -dAutoFilterColorImages=false -dColorImageFilter=/FlateEncode -dSCANCONVERTERTYPE=2 -dMaxBitmap=2147483647 -dUseFastColor=true -sDEVICE=pngalpha -g681x890 -r655 -sOutputFile='phasefilt_mask_ll.png' -f'./psconvert_49537d.eps'
psconvert: Done.
grdimage: Allocates memory and read data file los_ll.grd
grdimage: Evaluate image pixel colors
grdimage: Creating 24-bit color image
Make los_ll.kml and los_ll.png
psconvert: Processing los_ll.ps...
psconvert: Figure dimensions: Width: 74.8199 points [1.03917 inch] Height: 82.8 points [1.15 inch]
psconvert: gs -q -dSAFER -dNOPAUSE -dBATCH -dPDFSETTINGS=/prepress -dDownsampleColorImages=false -dDownsampleGrayImages=false -dDownsampleMonoImages=false -dUseFlateCompression=true -dEmbedAllFonts=true -dSubsetFonts=true -dMonoImageFilter=/FlateEncode -dAutoFilterGrayImages=false -dGrayImageFilter=/FlateEncode -dAutoFilterColorImages=false -dColorImageFilter=/FlateEncode -dSCANCONVERTERTYPE=2 -dMaxBitmap=2147483647 -dUseFastColor=true -sDEVICE=pngalpha -g681x754 -r655 -sOutputFile='los_ll.png' -f'./psconvert_49565d.eps'
psconvert: Done.
```

```
stack.list
cut_2014288_2014300.grd S1A20141016_104106_F1.PRM S1A20141028_104106_F1.PRM
cut_2014288_2014324.grd S1A20141016_104106_F1.PRM S1A20141121_104106_F1.PRM
cut_2014288_2015055.grd S1A20141016_104106_F1.PRM S1A20150225_104103_F1.PRM
cut_2014288_2015079.grd S1A20141016_104106_F1.PRM S1A20150321_104103_F1.PRM
cut_2014288_2015127.grd S1A20141016_104106_F1.PRM S1A20150508_104106_F1.PRM
cut_2014288_2015151.grd S1A20141016_104106_F1.PRM S1A20150601_104107_F1.PRM
cut_2014288_2015175.grd S1A20141016_104106_F1.PRM S1A20150625_104109_F1.PRM
cut_2014288_2015199.grd S1A20141016_104106_F1.PRM S1A20150719_104109_F1.PRM
cut_2014288_2015223.grd S1A20141016_104106_F1.PRM S1A20150812_104110_F1.PRM
cut_2014288_2015271.grd S1A20141016_104106_F1.PRM S1A20150929_104112_F1.PRM
cut_2014288_2015295.grd S1A20141016_104106_F1.PRM S1A20151023_104112_F1.PRM
cut_2014288_2015319.grd S1A20141016_104106_F1.PRM S1A20151116_104106_F1.PRM
cut_2014288_2016002.grd S1A20141016_104106_F1.PRM S1A20160103_104105_F1.PRM
cut_2014288_2016026.grd S1A20141016_104106_F1.PRM S1A20160127_104104_F1.PRM
cut_2014288_2016050.grd S1A20141016_104106_F1.PRM S1A20160220_104104_F1.PRM
cut_2014288_2016098.grd S1A20141016_104106_F1.PRM S1A20160408_104105_F1.PRM
cut_2014288_2016122.grd S1A20141016_104106_F1.PRM S1A20160502_104106_F1.PRM
cut_2014288_2016146.grd S1A20141016_104106_F1.PRM S1A20160526_104107_F1.PRM
cut_2014288_2016194.grd S1A20141016_104106_F1.PRM S1A20160713_104110_F1.PRM
cut_2014288_2017020.grd S1A20141016_104106_F1.PRM S1A20170121_104110_F1.PRM
```

```
*sbas intf.tab scene.tab 20 21 1709 3382 -smooth 1.0 -wavelength 0.0554658 -incidence 30 -range 6377591.716445 -rms -dem
bash stack_phase.bash stack.list mean.grd std.grd
bash stack_phase.bash stack.list mean.grd std.grd
```

```
compute the mean LOS velocity ..
```

```
time span (days) of cut_2014288_2014300.grd: 12
accumulative days in the stack: 12
time span (days) of cut_2014288_2014324.grd: 36
accumulative days in the stack: 48
time span (days) of cut_2014288_2015055.grd: 132
accumulative days in the stack: 180
time span (days) of cut_2014288_2015079.grd: 156
accumulative days in the stack: 336
time span (days) of cut_2014288_2015127.grd: 204
accumulative days in the stack: 540
time span (days) of cut_2014288_2015151.grd: 228
accumulative days in the stack: 768
time span (days) of cut_2014288_2015175.grd: 252
accumulative days in the stack: 1020
time span (days) of cut_2014288_2015199.grd: 276
accumulative days in the stack: 1296
time span (days) of cut_2014288_2015223.grd: 300
accumulative days in the stack: 1596
time span (days) of cut_2014288_2015271.grd: 348
accumulative days in the stack: 1944
time span (days) of cut_2014288_2015295.grd: 372
accumulative days in the stack: 2316
time span (days) of cut_2014288_2015319.grd: 396
accumulative days in the stack: 2712
time span (days) of cut_2014288_2016002.grd: 444
accumulative days in the stack: 3156
time span (days) of cut_2014288_2016026.grd: 468
accumulative days in the stack: 3624
time span (days) of cut_2014288_2016050.grd: 492
accumulative days in the stack: 4116
time span (days) of cut_2014288_2016098.grd: 540
accumulative days in the stack: 4656
time span (days) of cut_2014288_2016122.grd: 564
accumulative days in the stack: 5220
time span (days) of cut_2014288_2016146.grd: 588
accumulative days in the stack: 5808
time span (days) of cut_2014288_2016194.grd: 636
accumulative days in the stack: 6444
time span (days) of cut_2014288_2017020.grd: 827
accumulative days in the stack: 7271
```

```
compute the standard deviations ..
```

mean\_ll.grd  
std\_ll.grd  
los\_ll\_2014288\_2014300.grd  
los\_ll\_2014288\_2014324.grd  
los\_ll\_2014288\_2015055.grd  
los\_ll\_2014288\_2015079.grd  
los\_ll\_2014288\_2015127.grd  
los\_ll\_2014288\_2015151.grd  
los\_ll\_2014288\_2015175.grd  
los\_ll\_2014288\_2015199.grd  
los\_ll\_2014288\_2015223.grd  
los\_ll\_2014288\_2015271.grd  
los\_ll\_2014288\_2015295.grd  
los\_ll\_2014288\_2015319.grd  
los\_ll\_2014288\_2016002.grd  
los\_ll\_2014288\_2016026.grd  
los\_ll\_2014288\_2016050.grd  
los\_ll\_2014288\_2016098.grd  
los\_ll\_2014288\_2016122.grd  
los\_ll\_2014288\_2016146.grd  
los\_ll\_2014288\_2016194.grd  
los\_ll\_2014288\_2017020.grd

intf.tab

./intf\_all/2014288\_2014300/unwrap.grd ./intf\_all/2014288\_2014300/corr.grd 2014288 2014300 -25.793575  
./intf\_all/2014288\_2014324/unwrap.grd ./intf\_all/2014288\_2014324/corr.grd 2014288 2014324 -68.527184  
./intf\_all/2014288\_2015079/unwrap.grd ./intf\_all/2014288\_2015079/corr.grd 2014288 2015079 -42.938555  
./intf\_all/2014288\_2015127/unwrap.grd ./intf\_all/2014288\_2015127/corr.grd 2014288 2015127 -28.307229  
./intf\_all/2014300\_2014324/unwrap.grd ./intf\_all/2014300\_2014324/corr.grd 2014300 2014324 -42.733691  
./intf\_all/2014300\_2015079/unwrap.grd ./intf\_all/2014300\_2015079/corr.grd 2014300 2015079 -17.144963  
./intf\_all/2014300\_2015127/unwrap.grd ./intf\_all/2014300\_2015127/corr.grd 2014300 2015127 -2.513575  
./intf\_all/2014300\_2015151/unwrap.grd ./intf\_all/2014300\_2015151/corr.grd 2014300 2015151 -75.185905  
./intf\_all/2014300\_2015175/unwrap.grd ./intf\_all/2014300\_2015175/corr.grd 2014300 2015175 -32.349513  
./intf\_all/2014324\_2015079/unwrap.grd ./intf\_all/2014324\_2015079/corr.grd 2014324 2015079 25.588436  
./intf\_all/2014324\_2015127/unwrap.grd ./intf\_all/2014324\_2015127/corr.grd 2014324 2015127 40.218891  
./intf\_all/2014324\_2015151/unwrap.grd ./intf\_all/2014324\_2015151/corr.grd 2014324 2015151 -32.451785  
./intf\_all/2014324\_2015175/unwrap.grd ./intf\_all/2014324\_2015175/corr.grd 2014324 2015175 10.384153  
./intf\_all/2014324\_2015199/unwrap.grd ./intf\_all/2014324\_2015199/corr.grd 2014324 2015199 51.873340  
./intf\_all/2015055\_2015295/unwrap.grd ./intf\_all/2015055\_2015295/corr.grd 2015055 2015295 -70.223660  
./intf\_all/2015079\_2015127/unwrap.grd ./intf\_all/2015079\_2015127/corr.grd 2015079 2015127 14.630962  
./intf\_all/2015079\_2015151/unwrap.grd ./intf\_all/2015079\_2015151/corr.grd 2015079 2015151 -58.046604  
./intf\_all/2015079\_2015175/unwrap.grd ./intf\_all/2015079\_2015175/corr.grd 2015079 2015175 -15.204398  
./intf\_all/2015079\_2015199/unwrap.grd ./intf\_all/2015079\_2015199/corr.grd 2015079 2015199 26.290388  
./intf\_all/2015079\_2015223/unwrap.grd ./intf\_all/2015079\_2015223/corr.grd 2015079 2015223 66.549255  
./intf\_all/2015079\_2015271/unwrap.grd ./intf\_all/2015079\_2015271/corr.grd 2015079 2015271 59.191624  
./intf\_all/2015079\_2015319/unwrap.grd ./intf\_all/2015079\_2015319/corr.grd 2015079 2015319 1.078339  
./intf\_all/2015127\_2015151/unwrap.grd ./intf\_all/2015127\_2015151/corr.grd 2015127 2015151 -72.670501  
./intf\_all/2015127\_2015175/unwrap.grd ./intf\_all/2015127\_2015175/corr.grd 2015127 2015175 -29.834678  
./intf\_all/2015127\_2015199/unwrap.grd ./intf\_all/2015127\_2015199/corr.grd 2015127 2015199 11.659498  
./intf\_all/2015127\_2015223/unwrap.grd ./intf\_all/2015127\_2015223/corr.grd 2015127 2015223 51.918316  
./intf\_all/2015127\_2015271/unwrap.grd ./intf\_all/2015127\_2015271/corr.grd 2015127 2015271 44.560277  
./intf\_all/2015127\_2015295/unwrap.grd ./intf\_all/2015127\_2015295/corr.grd 2015127 2015295 86.338989  
./intf\_all/2015127\_2015319/unwrap.grd ./intf\_all/2015127\_2015319/corr.grd 2015127 2015319 -13.553077  
./intf\_all/2015127\_2016002/unwrap.grd ./intf\_all/2015127\_2016002/corr.grd 2015127 2016002 25.847740  
./intf\_all/2015151\_2015175/unwrap.grd ./intf\_all/2015151\_2015175/corr.grd 2015151 2015175 42.835561  
./intf\_all/2015151\_2015199/unwrap.grd ./intf\_all/2015151\_2015199/corr.grd 2015151 2015199 84.329027  
./intf\_all/2015151\_2015319/unwrap.grd ./intf\_all/2015151\_2015319/corr.grd 2015151 2015319 59.116206  
./intf\_all/2015151\_2016002/unwrap.grd ./intf\_all/2015151\_2016002/corr.grd 2015151 2016002 98.516709  
./intf\_all/2015175\_2015199/unwrap.grd ./intf\_all/2015175\_2015199/corr.grd 2015175 2015199 41.494613  
./intf\_all/2015175\_2015223/unwrap.grd ./intf\_all/2015175\_2015223/corr.grd 2015175 2015223 81.753419  
./intf\_all/2015175\_2015271/unwrap.grd ./intf\_all/2015175\_2015271/corr.grd 2015175 2015271 74.395681  
./intf\_all/2015175\_2015319/unwrap.grd ./intf\_all/2015175\_2015319/corr.grd 2015175 2015319 16.282176  
./intf\_all/2015175\_2016002/unwrap.grd ./intf\_all/2015175\_2016002/corr.grd 2015175 2016002 55.683099  
./intf\_all/2015175\_2016050/unwrap.grd ./intf\_all/2015175\_2016050/corr.grd 2015175 2016050 23.999449  
./intf\_all/2015199\_2015223/unwrap.grd ./intf\_all/2015199\_2015223/corr.grd 2015199 2015223 40.258846  
./intf\_all/2015199\_2015271/unwrap.grd ./intf\_all/2015199\_2015271/corr.grd 2015199 2015271 32.901153  
./intf\_all/2015199\_2015295/unwrap.grd ./intf\_all/2015199\_2015295/corr.grd 2015199 2015295 74.680597  
./intf\_all/2015199\_2015319/unwrap.grd ./intf\_all/2015199\_2015319/corr.grd 2015199 2015319 -25.212244  
./intf\_all/2015199\_2016002/unwrap.grd ./intf\_all/2015199\_2016002/corr.grd 2015199 2016002 14.188838  
./intf\_all/2015199\_2016050/unwrap.grd ./intf\_all/2015199\_2016050/corr.grd 2015199 2016050 -17.495140  
./intf\_all/2015223\_2015271/unwrap.grd ./intf\_all/2015223\_2015271/corr.grd 2015223 2015271 -7.356583  
./intf\_all/2015223\_2015295/unwrap.grd ./intf\_all/2015223\_2015295/corr.grd 2015223 2015295 34.424907  
./intf\_all/2015223\_2015319/unwrap.grd ./intf\_all/2015223\_2015319/corr.grd 2015223 2015319 -65.470301  
./intf\_all/2015223\_2016002/unwrap.grd ./intf\_all/2015223\_2016002/corr.grd 2015223 2016002 -26.068547  
./intf\_all/2015223\_2016026/unwrap.grd ./intf\_all/2015223\_2016026/corr.grd 2015223 2016026 90.482883  
./intf\_all/2015223\_2016050/unwrap.grd ./intf\_all/2015223\_2016050/corr.grd 2015223 2016050 -57.754252  
./intf\_all/2015223\_2016098/unwrap.grd ./intf\_all/2015223\_2016098/corr.grd 2015223 2016098 -83.045664  
./intf\_all/2015271\_2015295/unwrap.grd ./intf\_all/2015271\_2015295/corr.grd 2015271 2015295 41.779842  
./intf\_all/2015271\_2015319/unwrap.grd ./intf\_all/2015271\_2015319/corr.grd 2015271 2015319 -58.113349  
./intf\_all/2015271\_2016002/unwrap.grd ./intf\_all/2015271\_2016002/corr.grd 2015271 2016002 -18.712141  
./intf\_all/2015271\_2016026/unwrap.grd ./intf\_all/2015271\_2016026/corr.grd 2015271 2016026 97.835638  
./intf\_all/2015271\_2016050/unwrap.grd ./intf\_all/2015271\_2016050/corr.grd 2015271 2016050 -50.396475  
./intf\_all/2015271\_2016098/unwrap.grd ./intf\_all/2015271\_2016098/corr.grd 2015271 2016098 -75.686997  
./intf\_all/2015271\_2016122/unwrap.grd ./intf\_all/2015271\_2016122/corr.grd 2015271 2016122 -34.408184  
./intf\_all/2015271\_2016146/unwrap.grd ./intf\_all/2015271\_2016146/corr.grd 2015271 2016146 12.985095  
./intf\_all/2015295\_2016002/unwrap.grd ./intf\_all/2015295\_2016002/corr.grd 2015295 2016002 -60.491807  
./intf\_all/2015295\_2016026/unwrap.grd ./intf\_all/2015295\_2016026/corr.grd 2015295 2016026 56.055332  
./intf\_all/2015295\_2016050/unwrap.grd ./intf\_all/2015295\_2016050/corr.grd 2015295 2016050 -92.175728  
./intf\_all/2015295\_2016122/unwrap.grd ./intf\_all/2015295\_2016122/corr.grd 2015295 2016122 -76.187412  
./intf\_all/2015295\_2016146/unwrap.grd ./intf\_all/2015295\_2016146/corr.grd 2015295 2016146 -28.794365  
./intf\_all/2015319\_2016002/unwrap.grd ./intf\_all/2015319\_2016002/corr.grd 2015319 2016002 39.401550  
./intf\_all/2015319\_2016050/unwrap.grd ./intf\_all/2015319\_2016050/corr.grd 2015319 2016050 7.716378  
./intf\_all/2015319\_2016098/unwrap.grd ./intf\_all/2015319\_2016098/corr.grd 2015319 2016098 -17.574619  
./intf\_all/2015319\_2016122/unwrap.grd ./intf\_all/2015319\_2016122/corr.grd 2015319 2016122 23.704791  
./intf\_all/2015319\_2016146/unwrap.grd ./intf\_all/2015319\_2016146/corr.grd 2015319 2016146 71.098744  
./intf\_all/2016002\_2016050/unwrap.grd ./intf\_all/2016002\_2016050/corr.grd 2016002 2016050 -31.686159  
./intf\_all/2016002\_2016098/unwrap.grd ./intf\_all/2016002\_2016098/corr.grd 2016002 2016098 -56.977804  
./intf\_all/2016002\_2016122/unwrap.grd ./intf\_all/2016002\_2016122/corr.grd 2016002 2016122 -15.697774  
./intf\_all/2016002\_2016146/unwrap.grd ./intf\_all/2016002\_2016146/corr.grd 2016002 2016146 31.697001  
./intf\_all/2016002\_2016194/unwrap.grd ./intf\_all/2016002\_2016194/corr.grd 2016002 2016194 64.094926  
./intf\_all/2016026\_2016146/unwrap.grd ./intf\_all/2016026\_2016146/corr.grd 2016026 2016146 -84.857491  
./intf\_all/2016026\_2016194/unwrap.grd ./intf\_all/2016026\_2016194/corr.grd 2016026 2016194 -52.458922  
./intf\_all/2016050\_2016098/unwrap.grd ./intf\_all/2016050\_2016098/corr.grd 2016050 2016098 -25.292021  
./intf\_all/2016050\_2016122/unwrap.grd ./intf\_all/2016050\_2016122/corr.grd 2016050 2016122 15.988366  
./intf\_all/2016050\_2016146/unwrap.grd ./intf\_all/2016050\_2016146/corr.grd 2016050 2016146 63.383523  
./intf\_all/2016050\_2016194/unwrap.grd ./intf\_all/2016050\_2016194/corr.grd 2016050 2016194 95.781868  
./intf\_all/2016098\_2016122/unwrap.grd ./intf\_all/2016098\_2016122/corr.grd 2016098 2016122 41.280364  
./intf\_all/2016098\_2016146/unwrap.grd ./intf\_all/2016098\_2016146/corr.grd 2016098 2016146 88.675516  
./intf\_all/2016122\_2016146/unwrap.grd ./intf\_all/2016122\_2016146/corr.grd 2016122 2016146 47.395653  
./intf\_all/2016122\_2016194/unwrap.grd ./intf\_all/2016122\_2016194/corr.grd 2016122 2016194 79.794414  
./intf\_all/2016146\_2016194/unwrap.grd ./intf\_all/2016146\_2016194/corr.grd 2016146 2016194 32.309235  
./intf\_all/2016146\_2017020/unwrap.grd ./intf\_all/2016146\_2017020/corr.grd 2016146 2017020 32.635742  
./intf\_all/2016194\_2017020/unwrap.grd ./intf\_all/2016194\_2017020/corr.grd 2016194 2017020 0.236469

scene.tab  
2014288 288  
2014300 300  
2014324 324  
2015055 420

```

2015079 444
2015127 492
2015151 516
2015175 540
2015199 564
2015223 588
2015271 636
2015295 660
2015319 684
2016002 732
2016026 756
2016050 780
2016098 828
2016122 852
2016146 876
2016194 924
2017020 1115

xdim 1709
ydim 3382
-smooth 1.0
-wavelength 0.0554658
-incidence 30
-range 6377591.716445
-atm 1

proc
#run dispersion.csh in the SLC/ folder to make amplitude dispersion index (full resolution).
#modify filter.csh to generate interferograms with real.grd and imag.grd file (full resolution).
#make a stack/ folder parallel to intf/, raw/, topo/ and SLC/
#run link.bash to move all the real.grd and imag.grd into stack/
#modify/run cut.bash to crop the real.grd and imag.grd to appropriate size and region
#link the scatter.grd to stack/
#modify/run mt_extract_info_gmtsar
#modify/run mt_extract_cands_gmtsar
#start matlab/stamps in stack/ and run stamps(1,8)

sbas intf.tab scene.tab 89 21 1709 3382 -smooth 1.0 -wavelength 0.0554658 -incidence 30 -range 6377591.716445 -rms -dem -atm 1

compute RMS misfit
compute DEM error

setting smoothing to 1.000
setting radar wavelength to 0.055 m
setting radar incidence angle to 30.000 degree
setting range to 6377591.716 m
Memory Allocation Successful...
read table file...
number of SAR scenes is 21
number of interferograms is 89
read phase and correlation grids ...
fill the G matrix ...

Applying atmospheric correction by common point stacking...

Hit Matrix:
2014288 0 1 1 0 1 1 0 0 0 0 0 0 0 0 0 0 0 0 0 0 0 0 0 0 0 0
2014300 0 0 1 0 1 1 1 1 0 0 0 0 0 0 0 0 0 0 0 0 0 0 0 0 0 0
2014324 0 0 0 0 1 1 1 1 1 0 0 0 0 0 0 0 0 0 0 0 0 0 0 0 0 0
2015055 0 0 0 0 0 0 0 0 0 0 0 0 0 1 0 0 0 0 0 0 0 0 0 0 0 0
2015079 0 0 0 0 0 1 1 1 1 1 1 0 1 0 0 0 0 0 0 0 0 0 0 0 0 0
2015127 0 0 0 0 0 0 1 1 1 1 1 1 1 1 0 0 0 0 0 0 0 0 0 0 0 0
2015151 0 0 0 0 0 0 0 1 1 0 0 0 1 1 0 0 0 0 0 0 0 0 0 0 0 0
2015175 0 0 0 0 0 0 0 0 0 1 1 1 0 1 1 0 1 0 0 0 0 0 0 0 0 0
2015199 0 0 0 0 0 0 0 0 0 0 1 1 1 1 0 1 0 1 0 0 0 0 0 0 0 0
2015223 0 0 0 0 0 0 0 0 0 0 0 1 1 1 1 1 1 1 0 0 0 0 0 0 0 0
2015271 0 0 0 0 0 0 0 0 0 0 0 0 1 1 1 1 1 1 1 0 0 0 0 0 0 0
2015295 0 0 0 0 0 0 0 0 0 0 0 0 0 0 1 1 1 1 1 0 0 0 0 0 0 0
2015319 0 0 0 0 0 0 0 0 0 0 0 0 0 0 1 0 1 1 1 1 0 0 0 0 0 0
2016002 0 0 0 0 0 0 0 0 0 0 0 0 0 0 0 0 0 0 1 1 1 1 0 0 0 0
2016026 0 0 0 0 0 0 0 0 0 0 0 0 0 0 0 0 0 0 0 0 0 1 1 0 0 0
2016050 0 0 0 0 0 0 0 0 0 0 0 0 0 0 0 0 0 0 0 0 1 1 1 0 0 0
2016098 0 0 0 0 0 0 0 0 0 0 0 0 0 0 0 0 0 0 0 0 1 1 0 0 0 0
2016122 0 0 0 0 0 0 0 0 0 0 0 0 0 0 0 0 0 0 0 0 1 1 0 0 0 0
2016146 0 0 0 0 0 0 0 0 0 0 0 0 0 0 0 0 0 0 0 0 0 0 1 1 0 0
2016194 0 0 0 0 0 0 0 0 0 0 0 0 0 0 0 0 0 0 0 0 0 0 0 1 0 0
2017020 0 0 0 0 0 0 0 0 0 0 0 0 0 0 0 0 0 0 0 0 0 0 0 0 0 0

Applying exponential relaxation on smoothing parameters

Setting smoothing parameter to 1000.000000...
fill the G matrix ...
Computing deformation time-series...
run least-squares problem over 1709 by 3382 pixel (0) ...
matrix is full rank: 21

Removing deformation time-series from original unwrapped phase...
Computing atmospheric phase screen by common-point stacking...
Initial estimate of APS...
atm_noise(NO.5) = 5.674039
atm_noise(NO.16) = 4.830041
atm_noise(NO.6) = 4.467123
atm_noise(NO.18) = 4.304721
atm_noise(NO.14) = 3.483975
atm_noise(NO.11) = 3.346816
atm_noise(NO.17) = 3.214240
atm_noise(NO.4) = 3.135152
atm_noise(NO.15) = 3.032790
atm_noise(NO.19) = 3.020215
atm_noise(NO.12) = 2.464828
atm_noise(NO.13) = 2.364944
atm_noise(NO.10) = 2.111712
atm_noise(NO.7) = 2.059721
atm_noise(NO.8) = 1.968782
atm_noise(NO.9) = 1.773309
atm_noise(NO.0) = 0.000000
atm_noise(NO.1) = 0.000000
atm_noise(NO.2) = 0.000000
atm_noise(NO.3) = 0.000000
atm_noise(NO.20) = 0.000000

atm_noise(NO.5) = 5.674218
atm_noise(NO.16) = 4.832845

```

```
atm_noise(NO.6) = 3.909472
atm_noise(NO.18) = 3.457782
atm_noise(NO.4) = 3.251456
atm_noise(NO.17) = 3.228142
atm_noise(NO.14) = 3.112467
atm_noise(NO.11) = 3.106750
atm_noise(NO.19) = 3.023728
atm_noise(NO.15) = 2.971523
atm_noise(NO.12) = 2.280923
atm_noise(NO.13) = 2.130611
atm_noise(NO.8) = 1.834218
atm_noise(NO.10) = 1.826735
atm_noise(NO.7) = 1.718904
atm_noise(NO.9) = 1.642878
atm_noise(NO.0) = 0.000000
atm_noise(NO.1) = 0.000000
atm_noise(NO.2) = 0.000000
atm_noise(NO.3) = 0.000000
atm_noise(NO.20) = 0.000000
```

```
Applying atmospheric phase screen to original unwrapped phase...
Setting smoothing parameter to 1.000000...
fill the G matrix ...
run least-squares problem over 1709 by 3382 pixel (15) ...
matrix is rank-deficient: 20
```

write output ...

```
raIn.grd
raLt.grd
rms_ll.grd
dem.grd
vel_ll.grd
disp_2014288_ll.grd
disp_2014300_ll.grd
disp_2014324_ll.grd
disp_2015055_ll.grd
disp_2015079_ll.grd
disp_2015127_ll.grd
disp_2015151_ll.grd
disp_2015175_ll.grd
disp_2015199_ll.grd
disp_2015223_ll.grd
disp_2015271_ll.grd
disp_2015295_ll.grd
disp_2015319_ll.grd
disp_2016002_ll.grd
disp_2016026_ll.grd
disp_2016050_ll.grd
disp_2016098_ll.grd
disp_2016122_ll.grd
disp_2016146_ll.grd
disp_2016194_ll.grd
disp_2017020_ll.grd
aps_2014288.grd
aps_2014300.grd
aps_2014324.grd
aps_2015055.grd
aps_2015079.grd
aps_2015127.grd
aps_2015151.grd
aps_2015175.grd
aps_2015199.grd
aps_2015223.grd
aps_2015271.grd
aps_2015295.grd
aps_2015319.grd
aps_2016002.grd
aps_2016026.grd
aps_2016050.grd
aps_2016098.grd
aps_2016122.grd
aps_2016146.grd
aps_2016194.grd
aps_2017020.grd
```

## A.9 Sentinel-1A (Sub-swath F2) in Bali, Indonesia

```
data.in
s1a-iw2-slc-vv-20141016t104107-20141016t104135-002853-003393-002:S1A_OPER_AUX_POEORB_OPOD_20141106T123612_V20141015T225944_20141017T005944.EOF
s1a-iw2-slc-vv-20141028t104107-20141028t104135-003028-00374f-002:S1A_OPER_AUX_POEORB_OPOD_20141118T123725_V20141027T225944_20141029T005944.EOF
s1a-iw2-slc-vv-20141121t104107-20141121t104135-003378-003edb-002:S1A_OPER_AUX_POEORB_OPOD_20141212T123749_V20141120T225944_20141122T005944.EOF
s1a-iw2-slc-vv-20150225t104104-20150225t104132-004778-005eeb-002:S1A_OPER_AUX_POEORB_OPOD_20150318T123036_V20150224T225944_20150226T005944.EOF
s1a-iw2-slc-vv-20150321t104104-20150321t104132-005128-006757-002:S1A_OPER_AUX_POEORB_OPOD_20150411T123045_V20150320T225944_20150322T005944.EOF
s1a-iw2-slc-vv-20150508t104106-20150508t104134-005828-007800-002:S1A_OPER_AUX_POEORB_OPOD_20150529T122517_V20150507T225944_20150509T005944.EOF
s1a-iw2-slc-vv-20150601t104108-20150601t104136-006178-0080be-002:S1A_OPER_AUX_POEORB_OPOD_20150621T122558_V20150531T225944_20150602T005944.EOF
s1a-iw2-slc-vv-20150625t104109-20150625t104137-006528-008ad5-002:S1A_OPER_AUX_POEORB_OPOD_20150715T122234_V20150624T225944_20150626T005944.EOF
s1a-iw2-slc-vv-20150719t104110-20150719t104138-006878-009494-002:S1A_OPER_AUX_POEORB_OPOD_20150808T122256_V20150718T225943_20150720T005943.EOF
s1a-iw2-slc-vv-20150812t104111-20150812t104139-007228-009e3f-002:S1A_OPER_AUX_POEORB_OPOD_20150901T122301_V20150811T225943_20150813T005943.EOF
s1a-iw2-slc-vv-20150929t104113-20150929t104141-007928-00b136-002:S1A_OPER_AUX_POEORB_OPOD_20151019T122431_V20150928T225943_20150930T005943.EOF
s1a-iw2-slc-vv-20151023t104113-20151023t104141-008278-00baaf-002:S1A_OPER_AUX_POEORB_OPOD_20151112T122405_V20151022T225943_20151024T005943.EOF
s1a-iw2-slc-vv-20151116t104107-20151116t104135-008628-00c418-002:S1A_OPER_AUX_POEORB_OPOD_20151206T122632_V20151115T225943_20151117T005943.EOF
s1a-iw2-slc-vv-20160103t104106-20160103t104134-009328-00d7c0-002:S1A_OPER_AUX_POEORB_OPOD_20160123T121722_V20160102T225943_20160104T005943.EOF
s1a-iw2-slc-vv-20160127t104105-20160127t104133-009678-00e1e3-002:S1A_OPER_AUX_POEORB_OPOD_20160216T121630_V20160126T225943_20160128T005943.EOF
s1a-iw2-slc-vv-20160220t104105-20160220t104133-010028-00ec16-002:S1A_OPER_AUX_POEORB_OPOD_20160311T121452_V20160219T225943_20160221T005943.EOF
s1a-iw2-slc-vv-20160408t104106-20160408t104133-010728-010026-002:S1A_OPER_AUX_POEORB_OPOD_20160428T121507_V20160407T225943_20160409T005943.EOF
s1a-iw2-slc-vv-20160502t104107-20160502t104135-011078-010af7-002:S1A_OPER_AUX_POEORB_OPOD_20160522T121449_V20160501T225943_20160503T005943.EOF
s1a-iw2-slc-vv-20160526t104108-20160526t104136-011428-011642-002:S1A_OPER_AUX_POEORB_OPOD_20160615T121532_V20160525T225943_20160527T005943.EOF
s1a-iw2-slc-vv-20160713t104111-20160713t104138-012128-012c99-002:S1A_OPER_AUX_POEORB_OPOD_20160802T121647_V20160712T225943_20160714T005943.EOF
s1a-iw2-slc-vv-20170121t104111-20170121t104139-014928-0185cf-002:S1A_OPER_AUX_POEORB_OPOD_20170210T121453_V20170120T225942_20170122T005942.EOF
```

```
preproc_batch_tops.csh data.in dem.grd 1
Reading in 5002 lines of info from XML...
Writing 17 lines for orbit...
Writing 58 lines of precise orbit for the LED file...
Successfully opened junk1
Reading in 5002 lines of info from XML...
Writing 17 lines for orbit...
Writing 58 lines of precise orbit for the LED file...
Successfully opened junk1
Reading in 5002 lines of info from XML...
Writing 17 lines for orbit...
Writing 58 lines of precise orbit for the LED file...
Successfully opened junk1
Reading in 4988 lines of info from XML...
Writing 16 lines for orbit...
```

```
Writing 58 lines of precise orbit for the LED file...
Successfully opened junk1
Reading in 5162 lines of info from XML...
Writing 32 lines for orbit...
Writing 58 lines of precise orbit for the LED file...
Successfully opened junk1
Reading in 5176 lines of info from XML...
Writing 32 lines for orbit...
Writing 58 lines of precise orbit for the LED file...
Successfully opened junk1
Reading in 5176 lines of info from XML...
Writing 32 lines for orbit...
Writing 59 lines of precise orbit for the LED file...
Successfully opened junk1
Reading in 5176 lines of info from XML...
Writing 32 lines for orbit...
Writing 59 lines of precise orbit for the LED file...
Successfully opened junk1
Reading in 5206 lines of info from XML...
Writing 32 lines for orbit...
Writing 59 lines of precise orbit for the LED file...
Successfully opened junk1
Reading in 5206 lines of info from XML...
Writing 32 lines for orbit...
Writing 58 lines of precise orbit for the LED file...
Successfully opened junk1
Reading in 5206 lines of info from XML...
Writing 32 lines for orbit...
Writing 58 lines of precise orbit for the LED file...
Successfully opened junk1
Reading in 5206 lines of info from XML...
Writing 32 lines for orbit...
Writing 58 lines of precise orbit for the LED file...
Successfully opened junk1
Reading in 5206 lines of info from XML...
Writing 32 lines for orbit...
Writing 59 lines of precise orbit for the LED file...
Successfully opened junk1
Reading in 4996 lines of info from XML...
Writing 17 lines for orbit...
Writing 58 lines of precise orbit for the LED file...
Successfully opened junk1
Reading in 5002 lines of info from XML...
Writing 17 lines for orbit...
Writing 58 lines of precise orbit for the LED file...
Successfully opened junk1
Reading in 4996 lines of info from XML...
Writing 17 lines for orbit...
Writing 58 lines of precise orbit for the LED file...
Successfully opened junk1
Reading in 4996 lines of info from XML...
Writing 17 lines for orbit...
Writing 58 lines of precise orbit for the LED file...
Successfully opened junk1
Reading in 4996 lines of info from XML...
Writing 17 lines for orbit...
Writing 58 lines of precise orbit for the LED file...
Successfully opened junk1
Reading in 5002 lines of info from XML...
Writing 17 lines for orbit...
Writing 59 lines of precise orbit for the LED file...
Successfully opened junk1
Reading in 5002 lines of info from XML...
Writing 17 lines for orbit...
Writing 59 lines of precise orbit for the LED file...
Successfully opened junk1
Reading in 5002 lines of info from XML...
Writing 17 lines for orbit...
Writing 58 lines of precise orbit for the LED file...
Successfully opened junk1
Reading in 5002 lines of info from XML...
Writing 17 lines for orbit...
Writing 58 lines of precise orbit for the LED file...
Successfully opened junk1
Reading in 5002 lines of info from XML...
Writing 17 lines for orbit...
Writing 58 lines of precise orbit for the LED file...
Successfully opened junk1
```

```
csh select_pairs.csh baseline_table.dat 250 100
intf.in
baseline.ps
```

```
baseline_table.dat
S1A20141016_ALL_F2 2014288.4452266330 288 0.000000 0.000000
S1A20141028_ALL_F2 2014300.4452252467 300 -23.930450 -23.573447
S1A20141121_ALL_F2 2014324.4452221205 324 -39.624132 -64.924527
S1A20150225_ALL_F2 2015055.4451884688 420 119.495739 117.497141
S1A20150321_ALL_F2 2015079.4451966877 444 -28.823404 -40.262032
S1A20150508_ALL_F2 2015127.4452203528 492 -4.408400 -27.947519
S1A20150601_ALL_F2 2015151.4452388070 516 -53.409230 -96.237064
S1A20150625_ALL_F2 2015175.4452550521 540 -36.202825 -54.966470
S1A20150719_ALL_F2 2015199.4452599715 564 -4.716440 -16.190551
S1A20150812_ALL_F2 2015223.4452753069 588 0.404026 23.743795
S1A20150929_ALL_F2 2015271.4452951448 636 18.274930 14.714526
S1A20151023_ALL_F2 2015295.4452959972 660 58.767590 52.766967
S1A20151116_ALL_F2 2015319.4452295154 684 8.007775 -43.077072
S1A20160103_ALL_F2 2016002.4452112177 732 25.457818 -5.131032
S1A20160127_ALL_F2 2016026.4451987334 756 109.867341 103.616339
S1A20160220_ALL_F2 2016050.4451985585 780 -10.248071 -33.981451
S1A20160408_ALL_F2 2016098.4452099584 828 -32.311985 -57.001825
S1A20160502_ALL_F2 2016122.4452219771 852 -7.768513 -17.833709
S1A20160526_ALL_F2 2016146.4452368170 876 21.335943 27.028632
S1A20160713_ALL_F2 2016194.4452676338 924 47.179038 57.406903
S1A20170121_ALL_F2 2017020.4452693502 1115 62.972856 55.978231
```

```
preproc_batch_tops.csh data.in dem.grd 2
Reading in 5002 lines of info from XML...
Writing 17 lines for orbit...
Writing SLC..Image Size: 24468 X 13528...
Working on burst #1 #2 #3 #4 #5 #6 #7 #8 #9 #10
number of points clipped to short int 0
Writing 58 lines of precise orbit for the LED file...
Writing 58 lines of precise orbit for the LED file...
Successfully opened junk1
rm: No match.
Reading in 5002 lines of info from XML...
Writing 17 lines for orbit...
Writing 58 lines of precise orbit for the LED file...
Shifting the master PRM by 0 lines...
Successfully opened junk1.PRM
Successfully opened junk2.PRM
Successfully opened junk1
Successfully opened junk1
[1] 39595
[2] 39596
[2] + Done
SAT_llt2rat S1A20141028_104107_F2.PRM 1 < topo.llt > tmp1.dat
```

```

[1] + Done          SAT_llt2rat tmp.PRM 1 < topo.llt > tmpm.dat
[1] 39609
[2] 39610
[2] Done          gmt surface atmp.xyz -bi3d -R0/24468/0/13528 -I8/4 -Gatmp.grd -T0.5 -N1000 -r
[1] + Done          gmt surface rtmp.xyz -bi3d -R0/24468/0/13528 -I8/4 -Grtmp.grd -T0.5 -N1000 -r
Reading in 5002 lines of info from XML...
Writing 17 lines for orbit...
Reading in range and azimuth shifts table...
Writing SLC..Image Size: 24468 X 13528...
Working on burst #1 #2 #3 #4 #5 #6 #7 #8 #9 #10
number of points clipped to short int 0
Writing 58 lines of precise orbit for the LED file...
Successfully opened junk1
Reading in 5002 lines of info from XML...
Writing 17 lines for orbit...
Writing 58 lines of precise orbit for the LED file...
Shifting the master PRM by 0 lines...
Successfully opened junk1.PRM
Successfully opened junk2.PRM
Successfully opened junk1
Successfully opened junk1
[1] 40246
[2] 40247          SAT_llt2rat S1A20141121_104107_F2.PRM 1 < topo.llt > tmp1.dat
[1] + Done          SAT_llt2rat tmp.PRM 1 < topo.llt > tmpm.dat
[1] 40260
[2] 40261          gmt surface atmp.xyz -bi3d -R0/24468/0/13528 -I8/4 -Gatmp.grd -T0.5 -N1000 -r
[1] + Done          gmt surface rtmp.xyz -bi3d -R0/24468/0/13528 -I8/4 -Grtmp.grd -T0.5 -N1000 -r
Reading in 5002 lines of info from XML...
Writing 17 lines for orbit...
Reading in range and azimuth shifts table...
Writing SLC..Image Size: 24468 X 13528...
Working on burst #1 #2 #3 #4 #5 #6 #7 #8 #9 #10
number of points clipped to short int 0
Writing 58 lines of precise orbit for the LED file...
Successfully opened junk1
Reading in 4988 lines of info from XML...
Writing 16 lines for orbit...
Writing 58 lines of precise orbit for the LED file...
Shifting the master PRM by 0 lines...
Successfully opened junk1.PRM
Successfully opened junk2.PRM
Successfully opened junk1
Successfully opened junk1
[1] 41379
[2] 41380          SAT_llt2rat S1A20150225_104104_F2.PRM 1 < topo.llt > tmp1.dat
[1] + Done          SAT_llt2rat tmp.PRM 1 < topo.llt > tmpm.dat
[1] 41393
[2] 41394          gmt surface atmp.xyz -bi3d -R0/24468/0/13528 -I8/4 -Gatmp.grd -T0.5 -N1000 -r
[1] + Done          gmt surface rtmp.xyz -bi3d -R0/24468/0/13528 -I8/4 -Grtmp.grd -T0.5 -N1000 -r
Reading in 4988 lines of info from XML...
Writing 16 lines for orbit...
Reading in range and azimuth shifts table...
Writing SLC..Image Size: 24468 X 13528...
Working on burst #1 #2 #3 #4 #5 #6 #7 #8 #9 #10
number of points clipped to short int 1
Writing 58 lines of precise orbit for the LED file...
Successfully opened junk1
Reading in 5162 lines of info from XML...
Writing 32 lines for orbit...
Writing 58 lines of precise orbit for the LED file...
Shifting the master PRM by 0 lines...
Successfully opened junk1.PRM
Successfully opened junk2.PRM
Successfully opened junk1
Successfully opened junk1
[1] 41740
[2] 41741          SAT_llt2rat S1A20150321_104104_F2.PRM 1 < topo.llt > tmp1.dat
[1] + Done          SAT_llt2rat tmp.PRM 1 < topo.llt > tmpm.dat
[1] 41754
[2] 41755          gmt surface atmp.xyz -bi3d -R0/24468/0/13520 -I8/4 -Gatmp.grd -T0.5 -N1000 -r
[1] + Done          gmt surface rtmp.xyz -bi3d -R0/24468/0/13520 -I8/4 -Grtmp.grd -T0.5 -N1000 -r
Reading in 5162 lines of info from XML...
Writing 32 lines for orbit...
Reading in range and azimuth shifts table...
Writing SLC..Image Size: 24468 X 13520...
Working on burst #1 #2 #3 #4 #5 #6 #7 #8 #9 #10
number of points clipped to short int 2
Writing 58 lines of precise orbit for the LED file...
Successfully opened junk1
Reading in 5176 lines of info from XML...
Writing 32 lines for orbit...
Writing 58 lines of precise orbit for the LED file...
Shifting the master PRM by 0 lines...
Successfully opened junk1.PRM
Successfully opened junk2.PRM
Successfully opened junk1
Successfully opened junk1
[1] 42047
[2] 42048          SAT_llt2rat S1A20150508_104106_F2.PRM 1 < topo.llt > tmp1.dat
[1] + Done          SAT_llt2rat tmp.PRM 1 < topo.llt > tmpm.dat
[1] 42063
[2] 42064          gmt surface atmp.xyz -bi3d -R0/24468/0/13528 -I8/4 -Gatmp.grd -T0.5 -N1000 -r
[1] + Done          gmt surface rtmp.xyz -bi3d -R0/24468/0/13528 -I8/4 -Grtmp.grd -T0.5 -N1000 -r
Reading in 5176 lines of info from XML...
Writing 32 lines for orbit...
Reading in range and azimuth shifts table...
Writing SLC..Image Size: 24468 X 13528...
Working on burst #1 #2 #3 #4 #5 #6 #7 #8 #9 #10
number of points clipped to short int 2
Writing 58 lines of precise orbit for the LED file...
Successfully opened junk1
Reading in 5176 lines of info from XML...
Writing 32 lines for orbit...
Writing 59 lines of precise orbit for the LED file...
Shifting the master PRM by 0 lines...
Successfully opened junk1.PRM
Successfully opened junk2.PRM
Successfully opened junk1
Successfully opened junk1
[1] 42349
[2] 42350

```

```

[2] Done SAT_llt2rat S1A20150601_104108_F2.PRM 1 < topo.llt > tmp1.dat
[1] + Done SAT_llt2rat tmp.PRM 1 < topo.llt > tmpm.dat
[1] 42365
[2] 42366
[2] Done gmt surface atmp.xyz -bi3d -R0/24468/0/13528 -I8/4 -Gatmp.grd -T0.5 -N1000 -r
[1] + Done gmt surface rtmp.xyz -bi3d -R0/24468/0/13528 -I8/4 -Grtmp.grd -T0.5 -N1000 -r
Reading in 5176 lines of info from XML...
Writing 32 lines for orbit...
Reading in range and azimuth shifts table...
Writing SLC..Image Size: 24468 X 13528...
Working on burst #1 #2 #3 #4 #5 #6 #7 #8 #9 #10
number of points clipped to short int 2
Writing 59 lines of precise orbit for the LED file...
Successfully opened junk1
Reading in 5176 lines of info from XML...
Writing 32 lines for orbit...
Writing 59 lines of precise orbit for the LED file...
Shifting the master PRM by 0 lines...
Successfully opened junk1.PRM
Successfully opened junk2.PRM
Successfully opened junk1
Successfully opened junk1
[1] 42647
[2] 42648
[2] + Done SAT_llt2rat S1A20150625_104109_F2.PRM 1 < topo.llt > tmp1.dat
[1] + Done SAT_llt2rat tmp.PRM 1 < topo.llt > tmpm.dat
[1] 42661
[2] 42662
[2] Done gmt surface atmp.xyz -bi3d -R0/24468/0/13524 -I8/4 -Gatmp.grd -T0.5 -N1000 -r
[1] + Done gmt surface rtmp.xyz -bi3d -R0/24468/0/13524 -I8/4 -Grtmp.grd -T0.5 -N1000 -r
Reading in 5176 lines of info from XML...
Writing 32 lines for orbit...
Reading in range and azimuth shifts table...
Writing SLC..Image Size: 24468 X 13524...
Working on burst #1 #2 #3 #4 #5 #6 #7 #8 #9 #10
number of points clipped to short int 1
Writing 59 lines of precise orbit for the LED file...
Successfully opened junk1
Reading in 5206 lines of info from XML...
Writing 32 lines for orbit...
Writing 59 lines of precise orbit for the LED file...
Shifting the master PRM by 0 lines...
Successfully opened junk1.PRM
Successfully opened junk2.PRM
Successfully opened junk1
Successfully opened junk1
[1] 42940
[2] 42941
[2] Done SAT_llt2rat S1A20150719_104110_F2.PRM 1 < topo.llt > tmp1.dat
[1] + Done SAT_llt2rat tmp.PRM 1 < topo.llt > tmpm.dat
[1] 42956
[2] 42957
[2] + Done gmt surface atmp.xyz -bi3d -R0/24468/0/13524 -I8/4 -Gatmp.grd -T0.5 -N1000 -r
[1] + Done gmt surface rtmp.xyz -bi3d -R0/24468/0/13524 -I8/4 -Grtmp.grd -T0.5 -N1000 -r
Reading in 5206 lines of info from XML...
Writing 32 lines for orbit...
Reading in range and azimuth shifts table...
Writing SLC..Image Size: 24468 X 13524...
Working on burst #1 #2 #3 #4 #5 #6 #7 #8 #9 #10
number of points clipped to short int 1
Writing 59 lines of precise orbit for the LED file...
Successfully opened junk1
Reading in 5206 lines of info from XML...
Writing 32 lines for orbit...
Writing 58 lines of precise orbit for the LED file...
Shifting the master PRM by 0 lines...
Successfully opened junk1.PRM
Successfully opened junk2.PRM
Successfully opened junk1
Successfully opened junk1
[1] 43283
[2] 43284
[2] Done SAT_llt2rat S1A20150812_104111_F2.PRM 1 < topo.llt > tmp1.dat
[1] + Done SAT_llt2rat tmp.PRM 1 < topo.llt > tmpm.dat
[1] 43297
[2] 43298
[2] Done gmt surface atmp.xyz -bi3d -R0/24468/0/13528 -I8/4 -Gatmp.grd -T0.5 -N1000 -r
[1] + Done gmt surface rtmp.xyz -bi3d -R0/24468/0/13528 -I8/4 -Grtmp.grd -T0.5 -N1000 -r
Reading in 5206 lines of info from XML...
Writing 32 lines for orbit...
Reading in range and azimuth shifts table...
Writing SLC..Image Size: 24468 X 13528...
Working on burst #1 #2 #3 #4 #5 #6 #7 #8 #9 #10
number of points clipped to short int 0
Writing 58 lines of precise orbit for the LED file...
Successfully opened junk1
Reading in 5206 lines of info from XML...
Writing 32 lines for orbit...
Writing 58 lines of precise orbit for the LED file...
Shifting the master PRM by 0 lines...
Successfully opened junk1.PRM
Successfully opened junk2.PRM
Successfully opened junk1
Successfully opened junk1
[1] 43584
[2] 43585
[2] Done SAT_llt2rat S1A20150929_104113_F2.PRM 1 < topo.llt > tmp1.dat
[1] + Done SAT_llt2rat tmp.PRM 1 < topo.llt > tmpm.dat
[1] 43598
[2] 43599
[2] Done gmt surface atmp.xyz -bi3d -R0/24468/0/13528 -I8/4 -Gatmp.grd -T0.5 -N1000 -r
[1] + Done gmt surface rtmp.xyz -bi3d -R0/24468/0/13528 -I8/4 -Grtmp.grd -T0.5 -N1000 -r
Reading in 5206 lines of info from XML...
Writing 32 lines for orbit...
Reading in range and azimuth shifts table...
Writing SLC..Image Size: 24468 X 13528...
Working on burst #1 #2 #3 #4 #5 #6 #7 #8 #9 #10
number of points clipped to short int 0
Writing 58 lines of precise orbit for the LED file...
Successfully opened junk1
Reading in 5206 lines of info from XML...
Writing 32 lines for orbit...
Writing 58 lines of precise orbit for the LED file...
Shifting the master PRM by 0 lines...
Successfully opened junk1.PRM
Successfully opened junk2.PRM
Successfully opened junk1
Successfully opened junk1
[1] 43877

```

```

[2] 43878
[2] + Done          SAT_llt2rat S1A20151023_104113_F2.PRM 1 < topo.llt > tmp1.dat
[1] + Done          SAT_llt2rat tmp.PRM 1 < topo.llt > tmpm.dat
[1] 43892
[2] 43893
[2] Done          gmt surface atmp.xyz -bi3d -R0/24468/0/13532 -I8/4 -Gatmp.grd -T0.5 -N1000 -r
[1] + Done          gmt surface rtmp.xyz -bi3d -R0/24468/0/13532 -I8/4 -Grtmp.grd -T0.5 -N1000 -r
Reading in 5206 lines of info from XML...
Writing 32 lines for orbit...
Reading in range and azimuth shifts table...
Writing SLC..Image Size: 24468 X 13532...
Working on burst #1 #2 #3 #4 #5 #6 #7 #8 #9 #10
number of points clipped to short int 3
Writing 58 lines of precise orbit for the LED file...
Successfully opened junk1
Reading in 5206 lines of info from XML...
Writing 32 lines for orbit...
Writing 59 lines of precise orbit for the LED file...
Shifting the master PRM by 0 lines...
Successfully opened junk1.PRM
Successfully opened junk2.PRM
Modifying master PRM by 2690 lines...
Successfully opened junk1
Successfully opened junk1
[1] 44218
[2] 44219
[2] Done          SAT_llt2rat S1A20151116_104107_F2.PRM 1 < topo.llt > tmp1.dat
[1] + Done          SAT_llt2rat tmp.PRM 1 < topo.llt > tmpm.dat
[1] 44279
[2] 44280
[2] Done          gmt surface atmp.xyz -bi3d -R0/24556/0/13528 -I8/4 -Gatmp.grd -T0.5 -N1000 -r
[1] + Done          gmt surface rtmp.xyz -bi3d -R0/24556/0/13528 -I8/4 -Grtmp.grd -T0.5 -N1000 -r
Reading in 5206 lines of info from XML...
Writing 32 lines for orbit...
Reading in range and azimuth shifts table...
Writing SLC..Image Size: 24556 X 13528...
Working on burst #1 #2 #3 #4 #5 #6 #7 #8 #9 #10
number of points clipped to short int 0
Writing 59 lines of precise orbit for the LED file...
Restoring 2690 lines shift to the image...
Successfully opened junk1
Reading in 4996 lines of info from XML...
Writing 17 lines for orbit...
Writing 58 lines of precise orbit for the LED file...
Shifting the master PRM by 0 lines...
Successfully opened junk1.PRM
Successfully opened junk2.PRM
Modifying master PRM by 2691 lines...
Successfully opened junk1
Successfully opened junk1
[1] 44603
[2] 44604
[2] + Done          SAT_llt2rat S1A20160103_104106_F2.PRM 1 < topo.llt > tmp1.dat
[1] + Done          SAT_llt2rat tmp.PRM 1 < topo.llt > tmpm.dat
[1] 44667
[2] 44668
[2] Done          gmt surface atmp.xyz -bi3d -R0/24556/0/13524 -I8/4 -Gatmp.grd -T0.5 -N1000 -r
[1] + Done          gmt surface rtmp.xyz -bi3d -R0/24556/0/13524 -I8/4 -Grtmp.grd -T0.5 -N1000 -r
Reading in 4996 lines of info from XML...
Writing 17 lines for orbit...
Reading in range and azimuth shifts table...
Writing SLC..Image Size: 24556 X 13524...
Working on burst #1 #2 #3 #4 #5 #6 #7 #8 #9 #10
number of points clipped to short int 0
Writing 58 lines of precise orbit for the LED file...
Restoring 2691 lines shift to the image...
Successfully opened junk1
Reading in 5002 lines of info from XML...
Writing 17 lines for orbit...
Writing 58 lines of precise orbit for the LED file...
Shifting the master PRM by 0 lines...
Successfully opened junk1.PRM
Successfully opened junk2.PRM
Modifying master PRM by 2701 lines...
Successfully opened junk1
Successfully opened junk1
[1] 44996
[2] 44997
[2] + Done          SAT_llt2rat S1A20160127_104105_F2.PRM 1 < topo.llt > tmp1.dat
[1] + Done          SAT_llt2rat tmp.PRM 1 < topo.llt > tmpm.dat
[1] 45010
[2] 45011
[2] Done          gmt surface atmp.xyz -bi3d -R0/24556/0/13528 -I8/4 -Gatmp.grd -T0.5 -N1000 -r
[1] + Done          gmt surface rtmp.xyz -bi3d -R0/24556/0/13528 -I8/4 -Grtmp.grd -T0.5 -N1000 -r
Reading in 5002 lines of info from XML...
Writing 17 lines for orbit...
Reading in range and azimuth shifts table...
Writing SLC..Image Size: 24556 X 13528...
Working on burst #1 #2 #3 #4 #5 #6 #7 #8 #9 #10
number of points clipped to short int 1
Writing 58 lines of precise orbit for the LED file...
Restoring 2701 lines shift to the image...
Successfully opened junk1
Reading in 4996 lines of info from XML...
Writing 17 lines for orbit...
Writing 58 lines of precise orbit for the LED file...
Shifting the master PRM by 0 lines...
Successfully opened junk1.PRM
Successfully opened junk2.PRM
Modifying master PRM by 2697 lines...
Successfully opened junk1
Successfully opened junk1
[1] 45475
[2] 45476
[2] + Done          SAT_llt2rat S1A20160220_104105_F2.PRM 1 < topo.llt > tmp1.dat
[1] + Done          SAT_llt2rat tmp.PRM 1 < topo.llt > tmpm.dat
[1] 45490
[2] 45491
[2] + Done          gmt surface atmp.xyz -bi3d -R0/24556/0/13536 -I8/4 -Gatmp.grd -T0.5 -N1000 -r
[1] + Done          gmt surface rtmp.xyz -bi3d -R0/24556/0/13536 -I8/4 -Grtmp.grd -T0.5 -N1000 -r
Reading in 4996 lines of info from XML...
Writing 17 lines for orbit...
Reading in range and azimuth shifts table...
Writing SLC..Image Size: 24556 X 13536...
Working on burst #1 #2 #3 #4 #5 #6 #7 #8 #9 #10
number of points clipped to short int 0
Writing 58 lines of precise orbit for the LED file...
Restoring 2697 lines shift to the image...
Successfully opened junk1

```



```

Reading in 4996 lines of info from XML...
Writing 17 lines for orbit...
Writing 58 lines of precise orbit for the LED file...
Shifting the master PRM by 0 lines...
Successfully opened junk1.PRM
Successfully opened junk2.PRM
Modifying master PRM by 2696 lines...
Successfully opened junk1
Successfully opened junk1
[1] 46023
[2] 46024
[2] + Done          SAT_llt2rat S1A20160408_104106_F2.PRM 1 < topo.llt > tmp1.dat
[1] + Done          SAT_llt2rat tmp.PRM 1 < topo.llt > tmpm.dat
[1] 46114
[2] 46115
[2] + Done          gmt surface atmp.xyz -bi3d -R0/24556/0/13528 -I8/4 -Gatmp.grd -T0.5 -N1000 -r
[1] + Done          gmt surface rtmp.xyz -bi3d -R0/24556/0/13528 -I8/4 -Grtmp.grd -T0.5 -N1000 -r
Reading in 4996 lines of info from XML...
Writing 17 lines for orbit...
Reading in range and azimuth shifts table...
Writing SLC..Image Size: 24556 X 13528...
Working on burst #1 #2 #3 #4 #5 #6 #7 #8 #9 #10
number of points clipped to short int 1
Writing 58 lines of precise orbit for the LED file...
Restoring 2696 lines shift to the image...
Successfully opened junk1
Reading in 5002 lines of info from XML...
Writing 17 lines for orbit...
Writing 59 lines of precise orbit for the LED file...
Shifting the master PRM by 0 lines...
Successfully opened junk1.PRM
Successfully opened junk2.PRM
Modifying master PRM by 2695 lines...
Successfully opened junk1
Successfully opened junk1
[1] 46613
[2] 46614
[2] + Done          SAT_llt2rat S1A20160502_104107_F2.PRM 1 < topo.llt > tmp1.dat
[1] + Done          SAT_llt2rat tmp.PRM 1 < topo.llt > tmpm.dat
[1] 46627
[2] 46628
[2] + Done          gmt surface atmp.xyz -bi3d -R0/24556/0/13528 -I8/4 -Gatmp.grd -T0.5 -N1000 -r
[1] + Done          gmt surface rtmp.xyz -bi3d -R0/24556/0/13528 -I8/4 -Grtmp.grd -T0.5 -N1000 -r
Reading in 5002 lines of info from XML...
Writing 17 lines for orbit...
Reading in range and azimuth shifts table...
Writing SLC..Image Size: 24556 X 13528...
Working on burst #1 #2 #3 #4 #5 #6 #7 #8 #9 #10
number of points clipped to short int 0
Writing 59 lines of precise orbit for the LED file...
Restoring 2695 lines shift to the image...
Successfully opened junk1
Reading in 5002 lines of info from XML...
Writing 17 lines for orbit...
Writing 59 lines of precise orbit for the LED file...
Shifting the master PRM by 0 lines...
Successfully opened junk1.PRM
Successfully opened junk2.PRM
Modifying master PRM by 2692 lines...
Successfully opened junk1
Successfully opened junk1
[1] 46961
[2] 46962
[2] + Done          SAT_llt2rat S1A20160526_104108_F2.PRM 1 < topo.llt > tmp1.dat
[1] + Done          SAT_llt2rat tmp.PRM 1 < topo.llt > tmpm.dat
[1] 47028
[2] 47029
[2] + Done          gmt surface atmp.xyz -bi3d -R0/24556/0/13532 -I8/4 -Gatmp.grd -T0.5 -N1000 -r
[1] + Done          gmt surface rtmp.xyz -bi3d -R0/24556/0/13532 -I8/4 -Grtmp.grd -T0.5 -N1000 -r
Reading in 5002 lines of info from XML...
Writing 17 lines for orbit...
Reading in range and azimuth shifts table...
Writing SLC..Image Size: 24556 X 13528...
Working on burst #1 #2 #3 #4 #5 #6 #7 #8 #9 #10
number of points clipped to short int 0
Writing 59 lines of precise orbit for the LED file...
Restoring 2692 lines shift to the image...
Successfully opened junk1
Reading in 5002 lines of info from XML...
Writing 17 lines for orbit...
Writing 58 lines of precise orbit for the LED file...
Shifting the master PRM by 0 lines...
Successfully opened junk1.PRM
Successfully opened junk2.PRM
Modifying master PRM by 2685 lines...
Successfully opened junk1
Successfully opened junk1
[1] 47358
[2] 47359
[2] + Done          SAT_llt2rat S1A20160713_104111_F2.PRM 1 < topo.llt > tmp1.dat
[1] + Done          SAT_llt2rat tmp.PRM 1 < topo.llt > tmpm.dat
[1] 47373
[2] 47374
[2] + Done          gmt surface atmp.xyz -bi3d -R0/24556/0/13528 -I8/4 -Gatmp.grd -T0.5 -N1000 -r
[1] + Done          gmt surface rtmp.xyz -bi3d -R0/24556/0/13528 -I8/4 -Grtmp.grd -T0.5 -N1000 -r
Reading in 5002 lines of info from XML...
Writing 17 lines for orbit...
Reading in range and azimuth shifts table...
Writing SLC..Image Size: 24556 X 13528...
Working on burst #1 #2 #3 #4 #5 #6 #7 #8 #9 #10
number of points clipped to short int 0
Writing 58 lines of precise orbit for the LED file...
Restoring 2685 lines shift to the image...
Successfully opened junk1
Reading in 5002 lines of info from XML...
Writing 17 lines for orbit...
Writing 58 lines of precise orbit for the LED file...
Shifting the master PRM by 0 lines...
Successfully opened junk1.PRM
Successfully opened junk2.PRM
Modifying master PRM by 2689 lines...
Successfully opened junk1
Successfully opened junk1
[1] 47959
[2] 47960
[2] + Done          SAT_llt2rat S1A20170121_104111_F2.PRM 1 < topo.llt > tmp1.dat
[1] + Done          SAT_llt2rat tmp.PRM 1 < topo.llt > tmpm.dat
[1] 47976
[2] 47977

```

```
[2] Done gmt surface atmp.xyz -bi3d -R0/24556/0/13528 -I8/4 -Gatmp.grd -T0.5 -N1000 -r
[1] + Done gmt surface rtmp.xyz -bi3d -R0/24556/0/13528 -I8/4 -Grtmp.grd -T0.5 -N1000 -r
Reading in 5002 lines of info from XML...
Writing 17 lines for orbit...
Reading in range and azimuth shifts table...
Writing SLC..Image Size: 24556 X 13528...
Working on burst #1 #2 #3 #4 #5 #6 #7 #8 #9 #10
number of points clipped to short int 0
Writing 58 lines of precise orbit for the LED file...
Restoring 2689 lines shift to the image...
Successfully opened junk1
```

```
intf_tops.csh intf.in batch_tops.config
clean up topo/ folder
```

```
DEM2TOPOPHASE.CSH - START
USER SHOULD PROVIDE DEM FILE
range decimation is: 2
blockmedian: Provides 3, expects 3-column binary data
blockmedian: Processing input table data
blockmedian: W: 0 E: 20500 S: 0 N: 13528 n_columns: 10250 n_rows: 6764
blockmedian: Input 3 columns via binary records using format ddd
blockmedian: Output 3 columns via binary records using format ddd
blockmedian: N read: 1951350 N used: 1943714 outside_area: 7636 N cells filled: 1943459
surface: Provides 3, expects 3-column binary data
surface: Grid domain: W: 0 E: 20500 S: 0 N: 13528 n_columns: 10250 n_rows: 6764 [pixel registration]
surface: Processing input table data
surface: Input 3 columns via binary records using format ddd
surface: Minimum value of your dataset x,y,z at: surface: 9.08720302582 3.80631566048 -4.24559545517
surface: Maximum value of your dataset x,y,z at: surface: 17568.9980469 7031.25976562 2382.2878418
surface: LS plane determined: z = -10.8016 + (0.0132808 * col) + (0.039174 * row)
surface: Grid Mode IterationMax Change Conv Limit Total Iterations
surface: 2 D 349 0.0102886677188 0.0105022633649 349
surface: 1 I 18 0.0143521364284 0.0210045267298 367
surface: 1 D 315 0.0208256422956 0.0210045267298 682
surface: Fit info: N data points N nodes mean error rms error curvature
surface: 1943459 69348015 1.8855568431e-06 0.00746142954133 31783.0368027
grd2cpt: Processing input grid(s)
grd2cpt: Mean and S.D. of data are 189.346222536 229.128266265
grdimage: Allocates memory and read data file topo_ra.grd
grdimage: Evaluate image pixel colors
grdimage: Creating 8-bit grayshade image
DEM2TOPOPHASE.CSH - END
NO TOPOPHASE SHIFT
```

```
START FORM A STACK OF INTERFEROGRAMS
```

```
INTF.CSH, FILTER.CSH - START
mkdir: 2014288_2014300
ln: ./S1A20141016_ALL_F2.LED: File exists
ln: ./S1A20141028_ALL_F2.LED: File exists
ln: ./S1A20141016_ALL_F2.SLC: File exists
ln: ./S1A20141028_ALL_F2.SLC: File exists
ln: ./topo_ra.grd: File exists
intf.csh
running phasediff...
reading topo topo_ra.grd
_xdim 20500, ydim 13528
filter.csh
gauss_300 4 6 (1 2)
making amplitudes...
filtering interferogram...
making amplitude...
making correlation...
making phase...
filtering phase...
INTF.CSH, FILTER.CSH - END
```

```
MAKE LANDMASK -- START
REQUIRE FULL RESOLUTION COASTLINE FROM GMT
```

```
grdlandmask: GSHHG version 2.3.7
Derived from World Vector Shoreline, CIA WDB-II, and Atlas of the Cryosphere
Processed by Paul Wessel and Walter H. F. Smith, 1994-2017
grdlandmask: Nodes in water will be set to NaN
grdlandmask: Nodes on land will be set to 1
grdlandmask: Level 0 contained 8112640 nodes
grdlandmask: Level 1 contained 2478081 nodes
grdlandmask: Done!
surface: Provides 3, expects 3-column binary data
surface: Grid domain: W: 113.83333329 E: 117.416666662 S: -9.166666663 N: -7.4166666637 n_columns: 4300 n_rows: 2100 [gridline registration]
surface: Processing input table data
surface: Input 3 columns via binary records using format fff
surface: Minimum value of your dataset x,y,z at: surface: 114.280830383 -7.92999982834 -9.99230003357
surface: Maximum value of your dataset x,y,z at: surface: 115.052497864 -7.8183314896 20509.9980469
surface: LS plane determined: z = -18491.1 + (21.2403 * col) + (4.70208 * row)
surface: Grid Mode IterationMax Change Conv Limit Total Iterations
surface: 100 D 12525 0.000127559532091 0.000129180713562 12525
surface: 20 I 82 0.000634765875382 0.000645903567808 12607
surface: 20 D 10000 0.002069698322 0.000645903567808 22607
surface: 4 I 62 0.00308568304538 0.0032295178390 22669
surface: 4 D 1805 0.00322851378894 0.0032295178390 24474
surface: 2 I 18 0.0054122970447 0.00645903567808 24492
surface: 2 D 653 0.00645208689182 0.0064590356780 25145
surface: 1 I 14 0.011798358404 0.0129180713562 25159
surface: 1 D 213 0.0129167500755 0.0129180713562 25372
surface: Fit info: N data points N nodes mean error rms error curvature
surface: 1821492 9036401 0 13547.3435574
surface: Provides 3, expects 3-column binary data
surface: Grid domain: W: 113.83333329 E: 117.416666662 S: -9.166666663 N: -7.4166666637 n_columns: 4300 n_rows: 2100 [gridline registration]
surface: Processing input table data
surface: Input 3 columns via binary records using format fff
surface: Minimum value of your dataset x,y,z at: surface: 115.35333252 -9.16666698456 189.512191772
surface: Maximum value of your dataset x,y,z at: surface: 114.444999695 -7.63000011444 13547.9990234
surface: LS plane determined: z = 2798.48 + (-1.42891 * col) + (6.39843 * row)
surface: Grid Mode IterationMax Change Conv Limit Total Iterations
surface: 100 D 11537 7.92891904249e-07 7.97353770751e-07 11537
surface: 20 I 84 3.74267157559e-06 3.98676885376e-06 11621
surface: 20 D 10000 9.02122467258e-06 3.98676885376e-06 21621
surface: 4 I 75 1.97886828705e-05 1.99338442688e-05 21696
surface: 4 D 2000 0.000187696365708 1.99338442688e-05 23696
surface: 2 I 11 3.62207438071e-05 3.98676885376e-05 23707
surface: 2 D 1000 4.08256160202e-05 3.98676885376e-05 24707
surface: 1 I 8 6.4429398092e-05 7.97353770751e-05 24715
surface: 1 D 64 7.87402652595e-05 7.97353770751e-05 24779
surface: Fit info: N data points N nodes mean error rms error curvature
surface: 1821492 9036401 0 1353.58925599
MAKE LANDMASK -- END
```

ln: ./landmask\_ra.grd: File exists

SNAPHU.CSH - START  
threshold\_snaphu: 0.45  
grdmath: Perform reverse Polish notation calculations on grids  
grdmath: phase\_patch.grd landmask\_ra\_patch.grd MUL = phase\_patch.grd  
unwrapping phase with snaphu - higher threshold for faster unwrapping

snaphu v1.4.2  
32 parameters input from file snaphu.conf.brief (297 lines total)  
Reading wrapped phase from file phase.in  
No weight file specified. Assuming uniform weights  
Reading correlation data from file corr.in  
Calculating deformation-mode cost parameters  
Building range cost arrays  
Building azimuth cost arrays  
Initializing flows with MST algorithm  
Running approximate minimum spanning tree solver  
Running nonlinear network flow optimizer  
Maximum flow on network: 4  
Number of nodes in network: 5774749  
Flow increment: 1 (Total improvements: 0)  
Treesize: 5774749 Pivots: 50605 Improvements: 536  
Maximum flow on network: 4  
Flow increment: 2 (Total improvements: 536)  
Treesize: 5774749 Pivots: 248 Improvements: 39  
Maximum flow on network: 4  
Flow increment: 3 (Total improvements: 575)  
Treesize: 5774749 Pivots: 32 Improvements: 10  
Maximum flow on network: 4  
Flow increment: 4 (Total improvements: 585)  
Treesize: 5774749 Pivots: 6 Improvements: 3  
Maximum flow on network: 4  
Total solution cost: 1276783  
Integrating phase  
Writing output to file unwrap.out  
Program snaphu done  
Elapsed processor time: 0:02:54.70  
Elapsed wall clock time: 0:02:56  
grdmath: Perform reverse Polish notation calculations on grids  
grdmath: unwrap.grd landmask\_ra\_patch.grd MUL = tmp.grd  
SNAPHU.CSH - END

GEOCODE.CSH - START  
threshold\_geocode: .45  
grdmath: Perform reverse Polish notation calculations on grids  
grdmath: corr.grd 0.45 GE 0 NAN mask.grd MUL = mask2.grd  
psccale: Warning: The -E option is deprecated but is accepted.  
psccale: For the current -D syntax you should use -D modifier +e instead.  
psccale: Note you cannot mix new-style modifiers (+e) with the old-style -D option.  
psccale: Warning: The -E option is deprecated but is accepted.  
psccale: For the current -D syntax you should use -D modifier +e instead.  
psccale: Note you cannot mix new-style modifiers (+e) with the old-style -D option.  
geocode.csh  
project correlation, phase, unwrapped and amplitude back to lon lat coordinates  
remarked is by root on Mon May 14 20:03:52 JST 2018 with geocode.csh  
proj\_ra2ll.csh  
surface: Provides 3, expects 3-column binary data  
surface: Grid domain: W: 0 E: 20496 S: 0 N: 13536 n\_columns: 1281 n\_rows: 423 [gridline registration]  
surface: Processing input table data  
surface: Input 3 columns via binary records using format fff  
surface: Minimum value of your dataset x,y,z at: surface: 8.4292383194 13547.5927734 114.220001221  
surface: Maximum value of your dataset x,y,z at: surface: 20500.6113281 -12.4760046005 115.359169006  
surface: 1407751 unusable points were supplied; these will be ignored.  
surface: You should have pre-processed the data with block-mean, -median, or -mode.  
surface: Check that previous processing steps write results with enough decimals.  
surface: LS plane determined: z = 114.602 + (0.000597873 \* col) + (-0.000879088 \* row)  
surface: Grid Mode IterationMax Change Conv Limit Total Iterations  
surface: 3 D 18 1.09856571456e-07 1.60422700444e-07 18  
surface: 1 I 21 2.89638275712e-07 4.81268101333e-07 39  
surface: 1 D 18 3.26348538909e-07 4.81268101333e-07 57  
surface: Fit info: N data points N nodes mean error rms error curvature  
surface: 542268 543568 8.85633699404e-06 0.00844212721696 5237.0814115  
surface: Provides 3, expects 3-column binary data  
surface: Grid domain: W: 0 E: 20496 S: 0 N: 13536 n\_columns: 1281 n\_rows: 423 [gridline registration]  
surface: Processing input table data  
surface: Input 3 columns via binary records using format fff  
surface: Minimum value of your dataset x,y,z at: surface: -3.89805984497 -15.3827676773 -9.36416721344  
surface: Maximum value of your dataset x,y,z at: surface: 20489.9648438 13547.8720703 -7.51000022888  
surface: 1407751 unusable points were supplied; these will be ignored.  
surface: You should have pre-processed the data with block-mean, -median, or -mode.  
surface: Check that previous processing steps write results with enough decimals.  
surface: LS plane determined: z = -9.35961 + (0.000133549 \* col) + (0.00397144 \* row)  
surface: Grid Mode IterationMax Change Conv Limit Total Iterations  
surface: 3 D 18 2.40951585769e-08 3.4786119345e-08 18  
surface: 1 I 21 7.53017417096e-08 1.04358358035e-07 39  
surface: 1 D 18 9.66312061926e-08 1.04358358035e-07 57  
surface: Fit info: N data points N nodes mean error rms error curvature  
surface: 542268 543568 3.18630440715e-06 0.0100363693046 8547.88399102  
geocode.csh  
make the KML files for Google Earth  
grdimage: Allocates memory and read data file display\_amp\_ll.grd  
grdimage: Evaluate image pixel colors  
grdimage: Creating 24-bit color image  
Make display\_amp\_ll.kml and display\_amp\_ll.png  
psconvert: Processing display\_amp\_ll.ps...  
psconvert: Figure dimensions: Width: 82.5 points [1.14583 inch] Height: 133.8 points [1.85833 inch]  
psconvert: gs -q -dSAFER -dNOPAUSE -dBATCH -dPDFSETTINGS=/prepress -dDownsampleColorImages=false -dDownsampleGrayImages=false -dDownsampleMonoImages=false -dUseFlateCompression=true -dEmbedAllFonts=true -dSubsetFonts=true -dMonoImageFilter=/FlateEncode -dAutoFilterGrayImages=false -dGrayImageFilter=/FlateEncode -dAutoFilterColorImages=false -dColorImageFilter=/FlateEncode -dSCANCONVERTERTYPE=2 -dMaxBitmap=2147483647 -dUseFastColor=true -sDEVICE=pngalpha -g751x1218 -r655 -sOutputFile='display\_amp\_ll.png' -f'./psconvert\_49429d.eps'  
psconvert: Done.  
grdimage: Allocates memory and read data file corr\_ll.grd  
grdimage: Evaluate image pixel colors  
grdimage: Creating 24-bit color image  
PSL: Colormap of 255 colors created  
Make corr\_ll.kml and corr\_ll.png  
psconvert: Processing corr\_ll.ps...  
psconvert: Figure dimensions: Width: 82.5 points [1.14583 inch] Height: 133.8 points [1.85833 inch]  
psconvert: gs -q -dSAFER -dNOPAUSE -dBATCH -dPDFSETTINGS=/prepress -dDownsampleColorImages=false -dDownsampleGrayImages=false -dDownsampleMonoImages=false -dUseFlateCompression=true -dEmbedAllFonts=true -dSubsetFonts=true -dMonoImageFilter=/FlateEncode -dAutoFilterGrayImages=false -dGrayImageFilter=/FlateEncode -dAutoFilterColorImages=false -dColorImageFilter=/FlateEncode -dSCANCONVERTERTYPE=2 -dMaxBitmap=2147483647 -dUseFastColor=true -sDEVICE=pngalpha -g751x1218 -r655 -sOutputFile='corr\_ll.png' -f'./psconvert\_49443d.eps'  
psconvert: Done.  
grdimage: Allocates memory and read data file phase\_mask\_ll.grd  
grdimage: Evaluate image pixel colors  
grdimage: Creating 24-bit color image  
Make phase\_mask\_ll.kml and phase\_mask\_ll.png  
psconvert: Processing phase\_mask\_ll.ps...

```

psconvert: Figure dimensions: Width: 74.8199 points [1.03917 inch] Height: 97.8 points [1.35833 inch]
psconvert: gs -q -dSAFER -dNOPAUSE -dBATCH -dPDFSETTINGS=/prepress -dDownsampleColorImages=false -dDownsampleGrayImages=false -
dDownsampleMonoImages=false -dUseFlateCompression=true -dEmbedAllFonts=true -dSubsetFonts=true -dMonoImageFilter=/FlateEncode -
dAutoFilterGrayImages=false -dGrayImageFilter=/FlateEncode -dAutoFilterColorImages=false -dColorImageFilter=/FlateEncode -dSCANCONVERTERTYPE=2 -
dMaxBitmap=2147483647 -dUseFastColor=true -sDEVICE=pngalpha -g681x890 -r655 -sOutputFile='phase_mask_ll.png' -f'./psconvert_49460d.eps'
psconvert: Done.
grdimage: Allocates memory and read data file phasefilt_mask_ll.grd
grdimage: Evaluate image pixel colors
grdimage: Creating 24-bit color image
Make phasefilt_mask_ll.kml and phasefilt_mask_ll.png
psconvert: Processing phasefilt_mask_ll.ps...
psconvert: Figure dimensions: Width: 74.8199 points [1.03917 inch] Height: 97.8 points [1.35833 inch]
psconvert: gs -q -dSAFER -dNOPAUSE -dBATCH -dPDFSETTINGS=/prepress -dDownsampleColorImages=false -dDownsampleGrayImages=false -
dDownsampleMonoImages=false -dUseFlateCompression=true -dEmbedAllFonts=true -dSubsetFonts=true -dMonoImageFilter=/FlateEncode -
dAutoFilterGrayImages=false -dGrayImageFilter=/FlateEncode -dAutoFilterColorImages=false -dColorImageFilter=/FlateEncode -dSCANCONVERTERTYPE=2 -
dMaxBitmap=2147483647 -dUseFastColor=true -sDEVICE=pngalpha -g681x890 -r655 -sOutputFile='phasefilt_mask_ll.png' -f'./psconvert_49478d.eps'
psconvert: Done.
grdimage: Allocates memory and read data file unwrap_mask_ll.grd
grdimage: Evaluate image pixel colors
grdimage: Creating 24-bit color image
Make unwrap_mask_ll.kml and unwrap_mask_ll.png
psconvert: Processing unwrap_mask_ll.ps...
psconvert: Figure dimensions: Width: 74.8199 points [1.03917 inch] Height: 82.8 points [1.15 inch]
psconvert: gs -q -dSAFER -dNOPAUSE -dBATCH -dPDFSETTINGS=/prepress -dDownsampleColorImages=false -dDownsampleGrayImages=false -
dDownsampleMonoImages=false -dUseFlateCompression=true -dEmbedAllFonts=true -dSubsetFonts=true -dMonoImageFilter=/FlateEncode -
dAutoFilterGrayImages=false -dGrayImageFilter=/FlateEncode -dAutoFilterColorImages=false -dColorImageFilter=/FlateEncode -dSCANCONVERTERTYPE=2 -
dMaxBitmap=2147483647 -dUseFastColor=true -sDEVICE=pngalpha -g681x754 -r655 -sOutputFile='unwrap_mask_ll.png' -f'./psconvert_49507d.eps'
psconvert: Done.
grdimage: Allocates memory and read data file phasefilt_mask_ll.grd
grdimage: Evaluate image pixel colors
grdimage: Creating 24-bit color image
Make phasefilt_mask_ll.kml and phasefilt_mask_ll.png
psconvert: Processing phasefilt_mask_ll.ps...
psconvert: Figure dimensions: Width: 74.8199 points [1.03917 inch] Height: 97.8 points [1.35833 inch]
psconvert: gs -q -dSAFER -dNOPAUSE -dBATCH -dPDFSETTINGS=/prepress -dDownsampleColorImages=false -dDownsampleGrayImages=false -
dDownsampleMonoImages=false -dUseFlateCompression=true -dEmbedAllFonts=true -dSubsetFonts=true -dMonoImageFilter=/FlateEncode -
dAutoFilterGrayImages=false -dGrayImageFilter=/FlateEncode -dAutoFilterColorImages=false -dColorImageFilter=/FlateEncode -dSCANCONVERTERTYPE=2 -
dMaxBitmap=2147483647 -dUseFastColor=true -sDEVICE=pngalpha -g681x890 -r655 -sOutputFile='phasefilt_mask_ll.png' -f'./psconvert_49537d.eps'
psconvert: Done.
grdimage: Allocates memory and read data file los_ll.grd
grdimage: Evaluate image pixel colors
grdimage: Creating 24-bit color image
Make los_ll.kml and los_ll.png
psconvert: Processing los_ll.ps...
psconvert: Figure dimensions: Width: 74.8199 points [1.03917 inch] Height: 82.8 points [1.15 inch]
psconvert: gs -q -dSAFER -dNOPAUSE -dBATCH -dPDFSETTINGS=/prepress -dDownsampleColorImages=false -dDownsampleGrayImages=false -
dDownsampleMonoImages=false -dUseFlateCompression=true -dEmbedAllFonts=true -dSubsetFonts=true -dMonoImageFilter=/FlateEncode -
dAutoFilterGrayImages=false -dGrayImageFilter=/FlateEncode -dAutoFilterColorImages=false -dColorImageFilter=/FlateEncode -dSCANCONVERTERTYPE=2 -
dMaxBitmap=2147483647 -dUseFastColor=true -sDEVICE=pngalpha -g681x754 -r655 -sOutputFile='los_ll.png' -f'./psconvert_49565d.eps'
psconvert: Done.

```

stack.list

```

unwrap_2014288_2014300.grd S1A20141016_104107_F2.PRM S1A20141028_104107_F2.PRM
unwrap_2014288_2014324.grd S1A20141016_104107_F2.PRM S1A20141121_104107_F2.PRM
unwrap_2014288_2015055.grd S1A20141016_104107_F2.PRM S1A20150225_104104_F2.PRM
unwrap_2014288_2015079.grd S1A20141016_104107_F2.PRM S1A20150321_104104_F2.PRM
unwrap_2014288_2015127.grd S1A20141016_104107_F2.PRM S1A20150508_104106_F2.PRM
unwrap_2014288_2015151.grd S1A20141016_104107_F2.PRM S1A20150601_104108_F2.PRM
unwrap_2014288_2015175.grd S1A20141016_104107_F2.PRM S1A20150625_104109_F2.PRM
unwrap_2014288_2015199.grd S1A20141016_104107_F2.PRM S1A20150719_104110_F2.PRM
unwrap_2014288_2015223.grd S1A20141016_104107_F2.PRM S1A20150812_104111_F2.PRM
unwrap_2014288_2015271.grd S1A20141016_104107_F2.PRM S1A20150929_104113_F2.PRM
unwrap_2014288_2015295.grd S1A20141016_104107_F2.PRM S1A20151023_104113_F2.PRM
unwrap_2014288_2015319.grd S1A20141016_104107_F2.PRM S1A20151116_104107_F2.PRM
unwrap_2014288_2016002.grd S1A20141016_104107_F2.PRM S1A20160103_104106_F2.PRM
unwrap_2014288_2016026.grd S1A20141016_104107_F2.PRM S1A20160127_104105_F2.PRM
unwrap_2014288_2016050.grd S1A20141016_104107_F2.PRM S1A20160220_104105_F2.PRM
unwrap_2014288_2016098.grd S1A20141016_104107_F2.PRM S1A20160408_104106_F2.PRM
unwrap_2014288_2016122.grd S1A20141016_104107_F2.PRM S1A20160502_104107_F2.PRM
unwrap_2014288_2016146.grd S1A20141016_104107_F2.PRM S1A20160526_104108_F2.PRM
unwrap_2014288_2016194.grd S1A20141016_104107_F2.PRM S1A20160713_104111_F2.PRM
unwrap_2014288_2017020.grd S1A20141016_104107_F2.PRM S1A20170121_104111_F2.PRM

```

```
bash stack_phase.bash stack.list mean.grd std.grd
```

```
compute the mean LOS velocity ..
```

```

time span (days) of unwrap_2014288_2014300.grd: 12
accumulative days in the stack: 12
time span (days) of unwrap_2014288_2014324.grd: 36
accumulative days in the stack: 48
time span (days) of unwrap_2014288_2015055.grd: 132
accumulative days in the stack: 180
time span (days) of unwrap_2014288_2015079.grd: 156
accumulative days in the stack: 336
time span (days) of unwrap_2014288_2015127.grd: 204
accumulative days in the stack: 540
time span (days) of unwrap_2014288_2015151.grd: 228
accumulative days in the stack: 768
time span (days) of unwrap_2014288_2015175.grd: 252
accumulative days in the stack: 1020
time span (days) of unwrap_2014288_2015199.grd: 276
accumulative days in the stack: 1296
time span (days) of unwrap_2014288_2015223.grd: 300
accumulative days in the stack: 1596
time span (days) of unwrap_2014288_2015271.grd: 348
accumulative days in the stack: 1944
time span (days) of unwrap_2014288_2015295.grd: 372
accumulative days in the stack: 2316
time span (days) of unwrap_2014288_2015319.grd: 396
accumulative days in the stack: 2712
time span (days) of unwrap_2014288_2016002.grd: 444
accumulative days in the stack: 3156
time span (days) of unwrap_2014288_2016026.grd: 468
accumulative days in the stack: 3624
time span (days) of unwrap_2014288_2016050.grd: 492
accumulative days in the stack: 4116
time span (days) of unwrap_2014288_2016098.grd: 540
accumulative days in the stack: 4656
time span (days) of unwrap_2014288_2016122.grd: 564
accumulative days in the stack: 5220
time span (days) of unwrap_2014288_2016146.grd: 588
accumulative days in the stack: 5808
time span (days) of unwrap_2014288_2016194.grd: 636
accumulative days in the stack: 6444
time span (days) of unwrap_2014288_2017020.grd: 827
accumulative days in the stack: 7271

```

```
compute the standard deviations ..
```

mean\_ll.grd  
std\_ll.grd  
los\_ll\_2014288\_2014300.grd  
los\_ll\_2014288\_2014324.grd  
los\_ll\_2014288\_2015055.grd  
los\_ll\_2014288\_2015079.grd  
los\_ll\_2014288\_2015127.grd  
los\_ll\_2014288\_2015151.grd  
los\_ll\_2014288\_2015175.grd  
los\_ll\_2014288\_2015199.grd  
los\_ll\_2014288\_2015223.grd  
los\_ll\_2014288\_2015271.grd  
los\_ll\_2014288\_2015295.grd  
los\_ll\_2014288\_2015319.grd  
los\_ll\_2014288\_2016002.grd  
los\_ll\_2014288\_2016026.grd  
los\_ll\_2014288\_2016050.grd  
los\_ll\_2014288\_2016098.grd  
los\_ll\_2014288\_2016122.grd  
los\_ll\_2014288\_2016146.grd  
los\_ll\_2014288\_2016194.grd  
los\_ll\_2014288\_2017020.grd

intf.tab

```
../intf_all/2014288_2014300/unwrap.grd ../intf_all/2014288_2014300/corr.grd 2014288 2014300 -23.929581
../intf_all/2014288_2014324/unwrap.grd ../intf_all/2014288_2014324/corr.grd 2014288 2014324 -39.622878
../intf_all/2014288_2015079/unwrap.grd ../intf_all/2014288_2015079/corr.grd 2014288 2015079 -28.822636
../intf_all/2014288_2015127/unwrap.grd ../intf_all/2014288_2015127/corr.grd 2014288 2015127 -4.408254
../intf_all/2014288_2015151/unwrap.grd ../intf_all/2014288_2015151/corr.grd 2014288 2015151 -53.409349
../intf_all/2014300_2014324/unwrap.grd ../intf_all/2014300_2014324/corr.grd 2014300 2014324 -15.693259
../intf_all/2014300_2015079/unwrap.grd ../intf_all/2014300_2015079/corr.grd 2014300 2015079 -4.893107
../intf_all/2014300_2015127/unwrap.grd ../intf_all/2014300_2015127/corr.grd 2014300 2015127 19.521330
../intf_all/2014300_2015151/unwrap.grd ../intf_all/2014300_2015151/corr.grd 2014300 2015151 -29.479652
../intf_all/2014300_2015175/unwrap.grd ../intf_all/2014300_2015175/corr.grd 2014300 2015175 -12.272183
../intf_all/2014324_2015079/unwrap.grd ../intf_all/2014324_2015079/corr.grd 2014324 2015079 10.800900
../intf_all/2014324_2015127/unwrap.grd ../intf_all/2014324_2015127/corr.grd 2014324 2015127 35.215843
../intf_all/2014324_2015151/unwrap.grd ../intf_all/2014324_2015151/corr.grd 2014324 2015151 -13.787436
../intf_all/2014324_2015175/unwrap.grd ../intf_all/2014324_2015175/corr.grd 2014324 2015175 3.421466
../intf_all/2014324_2015199/unwrap.grd ../intf_all/2014324_2015199/corr.grd 2014324 2015199 34.909165
../intf_all/2015055_2015223/unwrap.grd ../intf_all/2015055_2015223/corr.grd 2015055 2015223 -119.091274
../intf_all/2015055_2015295/unwrap.grd ../intf_all/2015055_2015295/corr.grd 2015055 2015295 -60.728597
../intf_all/2015079_2015127/unwrap.grd ../intf_all/2015079_2015127/corr.grd 2015079 2015127 24.414670
../intf_all/2015079_2015151/unwrap.grd ../intf_all/2015079_2015151/corr.grd 2015079 2015151 -24.587381
../intf_all/2015079_2015175/unwrap.grd ../intf_all/2015079_2015175/corr.grd 2015079 2015175 -7.379231
../intf_all/2015079_2015199/unwrap.grd ../intf_all/2015079_2015199/corr.grd 2015079 2015199 24.107786
../intf_all/2015079_2015223/unwrap.grd ../intf_all/2015079_2015223/corr.grd 2015079 2015223 29.230344
../intf_all/2015079_2015271/unwrap.grd ../intf_all/2015079_2015271/corr.grd 2015079 2015271 47.100960
../intf_all/2015079_2015295/unwrap.grd ../intf_all/2015079_2015295/corr.grd 2015079 2015295 87.593036
../intf_all/2015079_2015319/unwrap.grd ../intf_all/2015079_2015319/corr.grd 2015079 2015319 37.022386
../intf_all/2015127_2015151/unwrap.grd ../intf_all/2015127_2015151/corr.grd 2015127 2015151 -49.003384
../intf_all/2015127_2015175/unwrap.grd ../intf_all/2015127_2015175/corr.grd 2015127 2015175 -31.794448
../intf_all/2015127_2015199/unwrap.grd ../intf_all/2015127_2015199/corr.grd 2015127 2015199 -0.306636
../intf_all/2015127_2015223/unwrap.grd ../intf_all/2015127_2015223/corr.grd 2015127 2015223 4.816707
../intf_all/2015127_2015271/unwrap.grd ../intf_all/2015127_2015271/corr.grd 2015127 2015271 22.687164
../intf_all/2015127_2015295/unwrap.grd ../intf_all/2015127_2015295/corr.grd 2015127 2015295 63.179951
../intf_all/2015127_2015319/unwrap.grd ../intf_all/2015127_2015319/corr.grd 2015127 2015319 12.607361
../intf_all/2015127_2016002/unwrap.grd ../intf_all/2015127_2016002/corr.grd 2015127 2016002 29.828351
../intf_all/2015151_2015175/unwrap.grd ../intf_all/2015151_2015175/corr.grd 2015151 2015175 17.209856
../intf_all/2015151_2015199/unwrap.grd ../intf_all/2015151_2015199/corr.grd 2015151 2015199 48.698465
../intf_all/2015151_2015319/unwrap.grd ../intf_all/2015151_2015319/corr.grd 2015151 2015319 61.611962
../intf_all/2015151_2016002/unwrap.grd ../intf_all/2015151_2016002/corr.grd 2015151 2016002 78.833764
../intf_all/2015175_2015199/unwrap.grd ../intf_all/2015175_2015199/corr.grd 2015175 2015199 31.487492
../intf_all/2015175_2015223/unwrap.grd ../intf_all/2015175_2015223/corr.grd 2015175 2015223 36.610415
../intf_all/2015175_2015271/unwrap.grd ../intf_all/2015175_2015271/corr.grd 2015175 2015271 54.481010
../intf_all/2015175_2015319/unwrap.grd ../intf_all/2015175_2015319/corr.grd 2015175 2015319 44.401703
../intf_all/2015175_2016002/unwrap.grd ../intf_all/2015175_2016002/corr.grd 2015175 2016002 61.622258
../intf_all/2015175_2016050/unwrap.grd ../intf_all/2015175_2016050/corr.grd 2015175 2016050 26.581792
../intf_all/2015199_2015223/unwrap.grd ../intf_all/2015199_2015223/corr.grd 2015199 2015223 5.122707
../intf_all/2015199_2015271/unwrap.grd ../intf_all/2015199_2015271/corr.grd 2015199 2015271 22.993278
../intf_all/2015199_2015295/unwrap.grd ../intf_all/2015199_2015295/corr.grd 2015199 2015295 63.485504
../intf_all/2015199_2015319/unwrap.grd ../intf_all/2015199_2015319/corr.grd 2015199 2015319 12.914493
../intf_all/2015199_2016002/unwrap.grd ../intf_all/2015199_2016002/corr.grd 2015199 2016002 30.134888
../intf_all/2015199_2016050/unwrap.grd ../intf_all/2015199_2016050/corr.grd 2015199 2016050 -4.905553
../intf_all/2015223_2015271/unwrap.grd ../intf_all/2015223_2015271/corr.grd 2015223 2015271 17.871054
../intf_all/2015223_2015295/unwrap.grd ../intf_all/2015223_2015295/corr.grd 2015223 2015295 58.361397
../intf_all/2015223_2015319/unwrap.grd ../intf_all/2015223_2015319/corr.grd 2015223 2015319 7.794955
../intf_all/2015223_2016002/unwrap.grd ../intf_all/2015223_2016002/corr.grd 2015223 2016002 25.013444
../intf_all/2015223_2016026/unwrap.grd ../intf_all/2015223_2016026/corr.grd 2015223 2016026 109.774303
../intf_all/2015223_2016050/unwrap.grd ../intf_all/2015223_2016050/corr.grd 2015223 2016050 -10.025526
../intf_all/2015223_2016098/unwrap.grd ../intf_all/2015223_2016098/corr.grd 2015223 2016098 -31.913717
../intf_all/2015271_2015295/unwrap.grd ../intf_all/2015271_2015295/corr.grd 2015271 2015295 40.491950
../intf_all/2015271_2015319/unwrap.grd ../intf_all/2015271_2015319/corr.grd 2015271 2015319 -10.078201
../intf_all/2015271_2016002/unwrap.grd ../intf_all/2015271_2016002/corr.grd 2015271 2016002 7.141869
../intf_all/2015271_2016026/unwrap.grd ../intf_all/2015271_2016026/corr.grd 2015271 2016026 91.906905
../intf_all/2015271_2016050/unwrap.grd ../intf_all/2015271_2016050/corr.grd 2015271 2016050 -27.898382
../intf_all/2015271_2016098/unwrap.grd ../intf_all/2015271_2016098/corr.grd 2015271 2016098 -49.787536
../intf_all/2015271_2016122/unwrap.grd ../intf_all/2015271_2016122/corr.grd 2015271 2016122 -25.333091
../intf_all/2015271_2016146/unwrap.grd ../intf_all/2015271_2016146/corr.grd 2015271 2016146 3.750374
../intf_all/2015295_2015319/unwrap.grd ../intf_all/2015295_2015319/corr.grd 2015295 2015319 -50.570813
../intf_all/2015295_2016002/unwrap.grd ../intf_all/2015295_2016002/corr.grd 2015295 2016002 -33.350564
../intf_all/2015295_2016026/unwrap.grd ../intf_all/2015295_2016026/corr.grd 2015295 2016026 51.415248
../intf_all/2015295_2016050/unwrap.grd ../intf_all/2015295_2016050/corr.grd 2015295 2016050 -68.390828
../intf_all/2015295_2016122/unwrap.grd ../intf_all/2015295_2016122/corr.grd 2015295 2016122 -65.825398
../intf_all/2015295_2016146/unwrap.grd ../intf_all/2015295_2016146/corr.grd 2015295 2016146 -36.741653
../intf_all/2015319_2016002/unwrap.grd ../intf_all/2015319_2016002/corr.grd 2015319 2016002 17.219139
../intf_all/2015319_2016050/unwrap.grd ../intf_all/2015319_2016050/corr.grd 2015319 2016050 -17.820271
../intf_all/2015319_2016098/unwrap.grd ../intf_all/2015319_2016098/corr.grd 2015319 2016098 -39.708795
../intf_all/2015319_2016122/unwrap.grd ../intf_all/2015319_2016122/corr.grd 2015319 2016122 -15.255229
../intf_all/2015319_2016146/unwrap.grd ../intf_all/2015319_2016146/corr.grd 2015319 2016146 13.827216
../intf_all/2016002_2016050/unwrap.grd ../intf_all/2016002_2016050/corr.grd 2016002 2016050 -35.038533
../intf_all/2016002_2016098/unwrap.grd ../intf_all/2016002_2016098/corr.grd 2016002 2016098 -56.926412
../intf_all/2016002_2016122/unwrap.grd ../intf_all/2016002_2016122/corr.grd 2016002 2016122 -32.473956
../intf_all/2016002_2016146/unwrap.grd ../intf_all/2016002_2016146/corr.grd 2016002 2016146 -3.392717
../intf_all/2016002_2016194/unwrap.grd ../intf_all/2016002_2016194/corr.grd 2016002 2016194 22.162687
../intf_all/2016026_2016146/unwrap.grd ../intf_all/2016026_2016146/corr.grd 2016026 2016146 -88.150628
../intf_all/2016026_2016194/unwrap.grd ../intf_all/2016026_2016194/corr.grd 2016026 2016194 -62.595934
../intf_all/2016050_2016098/unwrap.grd ../intf_all/2016050_2016098/corr.grd 2016050 2016098 -21.687674
../intf_all/2016050_2016122/unwrap.grd ../intf_all/2016050_2016122/corr.grd 2016050 2016122 2.564343
../intf_all/2016050_2016146/unwrap.grd ../intf_all/2016050_2016146/corr.grd 2016050 2016146 31.645037
../intf_all/2016050_2016194/unwrap.grd ../intf_all/2016050_2016194/corr.grd 2016050 2016194 57.200168
../intf_all/2016098_2016122/unwrap.grd ../intf_all/2016098_2016122/corr.grd 2016098 2016122 24.452062
../intf_all/2016098_2016146/unwrap.grd ../intf_all/2016098_2016146/corr.grd 2016098 2016146 53.532806
../intf_all/2016122_2016146/unwrap.grd ../intf_all/2016122_2016146/corr.grd 2016122 2016146 29.079938
../intf_all/2016122_2016194/unwrap.grd ../intf_all/2016122_2016194/corr.grd 2016122 2016194 54.634573
../intf_all/2016146_2016194/unwrap.grd ../intf_all/2016146_2016194/corr.grd 2016146 2016194 25.554067
../intf_all/2016146_2017020/unwrap.grd ../intf_all/2016146_2017020/corr.grd 2016146 2017020 40.890653
../intf_all/2016194_2017020/unwrap.grd ../intf_all/2016194_2017020/corr.grd 2016194 2017020 15.336519
```

```
scene.tab
2014288 288
2014300 300
2014324 324
2015055 420
2015079 444
2015127 492
2015151 516
2015175 540
2015199 564
2015223 588
2015271 636
2015295 660
2015319 684
2016002 732
2016026 756
2016050 780
2016098 828
2016122 852
2016146 876
2016194 924
2017020 1115
```

```
xdim 2039
ydim 3382
-smooth 1.0
-wavelength 0.0554658
-incidence 30
-range 6377591.716445
-atm 1
```

```
sbas intf.tab scene.tab 93 21 2039 3382 -smooth 1.0 -wavelength 0.0554658 -incidence 30 -range 6377598.430062 -rms -dem -atm 1
```

```
compute RMS misfit
compute DEM error
```

```
setting smoothing to 1.000
setting radar wavelength to 0.055 m
setting radar incidence angle to 30.000 degree
setting range to 6377598.430 m
Memory Allocation Successful...
read table file ...
number of SAR scenes is 21
number of interferograms is 93
read phase and correlation grids ...
fill the G matrix ...
```

Applying atmospheric correction by common point stacking...

Hit Matrix:

```
2014288 0 1 1 0 1 1 1 0 0 0 0 0 0 0 0 0 0 0 0 0 0 0 0 0 0 0 0
2014300 0 0 1 0 1 1 1 1 0 0 0 0 0 0 0 0 0 0 0 0 0 0 0 0 0 0 0
2014324 0 0 0 0 1 1 1 1 1 0 0 0 0 0 0 0 0 0 0 0 0 0 0 0 0 0 0
2015055 0 0 0 0 0 0 0 0 0 1 0 1 0 0 0 0 0 0 0 0 0 0 0 0 0 0 0
2015079 0 0 0 0 0 1 1 1 1 1 1 1 0 0 0 0 0 0 0 0 0 0 0 0 0 0 0
2015127 0 0 0 0 0 0 1 1 1 1 1 1 1 1 0 0 0 0 0 0 0 0 0 0 0 0 0
2015151 0 0 0 0 0 0 0 1 1 0 0 0 1 1 0 0 0 0 0 0 0 0 0 0 0 0 0
2015175 0 0 0 0 0 0 0 0 1 1 1 0 1 1 0 1 0 1 0 0 0 0 0 0 0 0 0
2015199 0 0 0 0 0 0 0 0 0 1 1 1 1 1 0 1 0 1 0 0 0 0 0 0 0 0 0
2015223 0 0 0 0 0 0 0 0 0 0 1 1 1 1 1 1 1 1 1 0 0 0 0 0 0 0 0
2015271 0 0 0 0 0 0 0 0 0 0 0 1 1 1 1 1 1 1 1 1 0 0 0 0 0 0 0
2015295 0 0 0 0 0 0 0 0 0 0 0 0 0 1 1 1 1 1 0 1 0 0 0 0 0 0 0
2015319 0 0 0 0 0 0 0 0 0 0 0 0 0 0 1 0 1 1 1 1 0 0 0 0 0 0 0
2016002 0 0 0 0 0 0 0 0 0 0 0 0 0 0 0 0 0 0 0 0 1 1 1 1 1 1 0
2016026 0 0 0 0 0 0 0 0 0 0 0 0 0 0 0 0 0 0 0 0 0 0 1 1 1 1 0
2016050 0 0 0 0 0 0 0 0 0 0 0 0 0 0 0 0 0 0 0 0 0 0 1 1 1 1 0
2016098 0 0 0 0 0 0 0 0 0 0 0 0 0 0 0 0 0 0 0 0 0 0 1 1 1 0 0
2016122 0 0 0 0 0 0 0 0 0 0 0 0 0 0 0 0 0 0 0 0 0 0 0 0 1 1 0
2016146 0 0 0 0 0 0 0 0 0 0 0 0 0 0 0 0 0 0 0 0 0 0 0 0 0 1 1
2016194 0 0 0 0 0 0 0 0 0 0 0 0 0 0 0 0 0 0 0 0 0 0 0 0 0 0 1
2017020 0 0 0 0 0 0 0 0 0 0 0 0 0 0 0 0 0 0 0 0 0 0 0 0 0 0 0
```

Applying exponential relaxation on smoothing parameters

```
Setting smoothing parameter to 1000.000000...
fill the G matrix ...
Computing deformation time-series...
run least-squares problem over 2039 by 3382 pixel (0) ...
matrix is full rank: 21
```

```
Removing deformation time-series from original unwrapped phase...
Computing atmospheric phase screen by common-point stacking...
```

```
Initial estimate of APS...
atm_noise(NO.5) = 5.536704
atm_noise(NO.10) = 5.063536
atm_noise(NO.6) = 3.690576
atm_noise(NO.16) = 3.480332
atm_noise(NO.12) = 3.470815
atm_noise(NO.11) = 3.461461
atm_noise(NO.17) = 3.101115
atm_noise(NO.14) = 3.099292
atm_noise(NO.19) = 3.059327
atm_noise(NO.13) = 3.025417
atm_noise(NO.4) = 2.845336
atm_noise(NO.18) = 2.668153
atm_noise(NO.15) = 2.663929
atm_noise(NO.8) = 2.504027
atm_noise(NO.7) = 2.260086
atm_noise(NO.9) = 1.370297
atm_noise(NO.0) = 0.000000
atm_noise(NO.1) = 0.000000
atm_noise(NO.2) = 0.000000
atm_noise(NO.3) = 0.000000
atm_noise(NO.20) = 0.000000
```

```
atm_noise(NO.5) = 5.492509
atm_noise(NO.10) = 5.168353
atm_noise(NO.6) = 4.418743
atm_noise(NO.16) = 3.476375
atm_noise(NO.11) = 3.406650
atm_noise(NO.19) = 3.058821
atm_noise(NO.17) = 3.036520
atm_noise(NO.13) = 2.904932
```

```
atm_noise(N0.4) = 2.850295
atm_noise(N0.12) = 2.745037
atm_noise(N0.18) = 2.547410
atm_noise(N0.14) = 2.539950
atm_noise(N0.8) = 2.415565
atm_noise(N0.15) = 2.174427
atm_noise(N0.7) = 1.954733
atm_noise(N0.9) = 1.429744
atm_noise(N0.0) = 0.000000
atm_noise(N0.1) = 0.000000
atm_noise(N0.2) = 0.000000
atm_noise(N0.3) = 0.000000
atm_noise(N0.20) = 0.000000
```

```
Applying atmospheric phase screen to original unwrapped phase...
Setting smoothing parameter to 1.000000...
fill the G matrix ...
run least-squares problem over 2039 by 3382 pixel (15) ...
matrix is rank-deficient: 20
```

```
write output ...
```

```
raln.grd
ralt.grd
rms_ll.grd
dem.grd
vel_ll.grd
disp_2014288_ll.grd
disp_2014300_ll.grd
disp_2014324_ll.grd
disp_2015055_ll.grd
disp_2015079_ll.grd
disp_2015127_ll.grd
disp_2015151_ll.grd
disp_2015175_ll.grd
disp_2015199_ll.grd
disp_2015223_ll.grd
disp_2015271_ll.grd
disp_2015295_ll.grd
disp_2015319_ll.grd
disp_2016002_ll.grd
disp_2016026_ll.grd
disp_2016050_ll.grd
disp_2016098_ll.grd
disp_2016122_ll.grd
disp_2016146_ll.grd
disp_2016194_ll.grd
disp_2017020_ll.grd
aps_2014288.grd
aps_2014300.grd
aps_2014324.grd
aps_2015055.grd
aps_2015079.grd
aps_2015127.grd
aps_2015151.grd
aps_2015175.grd
aps_2015199.grd
aps_2015223.grd
aps_2015271.grd
aps_2015295.grd
aps_2015319.grd
aps_2016002.grd
aps_2016026.grd
aps_2016050.grd
aps_2016098.grd
aps_2016122.grd
aps_2016146.grd
aps_2016194.grd
aps_2017020.grd
```

## A.10 ALOS PALSAR in Talcahuano, Chile

```
data.in
IMG-HH-ALPSRP220276440-H1.0__A
IMG-HH-ALPSRP166596440-H1.0__A
IMG-HH-ALPSRP226986440-H1.0__A
IMG-HH-ALPSRP267246440-H1.0__A
IMG-HH-ALPSRP273956440-H1.0__A
```

```
pre_proc_batch.csh ALOS data.in batch.config
```

```
START PREPROCESS A STACK OF IMAGES
```

```
preprocess master image
ledflag 1
.... swapping bytes
writing generic LED file: IMG-HH-ALPSRP220276440-H1.0__A.LED
near_range, shift = 861706 -448
.... Calculating doppler for IMG-HH-ALPSRP220276440-H1.0__A.raw
Working on line 2000
Working on line 4000
Working on line 6000
Working on line 8000
Working on line 10000
Working on line 12000
Working on line 14000
Working on line 16000
Working on line 18000
Working on line 20000
Working on line 22000
Working on line 24000
Working on line 26000
Working on line 28000
Working on line 30000
Working on line 32000
Working on line 34000
pre_proc_batch.csh
preprocess slave images
setting fd1 to -9.335909
setting near_range to 862755.00
setting radius to 6370170.480921
setting npatches to 3
ledflag 1
```

```
.... swapping bytes
writing generic LED file: IMG-HH-ALPSRP166596440-H1.0__A.LED
near_range, shift = 861856 -384
The range sampling rate for master and slave images are: 32000000
pre_proc_batch.csh
preprocess slave images
setting fd1 to -9.335909
setting near_range to 862755.00
setting radius to 6370170.480921
setting npatches to 3
ledflag 1
.... swapping bytes
writing generic LED file: IMG-HH-ALPSRP226986440-H1.0__A.LED
near_range, shift = 862456 -128
near_range, shift = 861406 -576
The range sampling rate for master and slave images are: 32000000
pre_proc_batch.csh
preprocess slave images
setting fd1 to -9.335909
setting near_range to 862755.00
setting radius to 6370170.480921
setting npatches to 3
ledflag 1
.... swapping bytes
writing generic LED file: IMG-HH-ALPSRP267246440-H1.0__A.LED
near_range, shift = 862456 -128
near_range, shift = 861406 -576
The range sampling rate for master and slave images are: 32000000
pre_proc_batch.csh
preprocess slave images
setting fd1 to -9.335909
setting near_range to 862755.00
setting radius to 6370170.480921
setting npatches to 3
ledflag 1
.... swapping bytes
writing generic LED file: IMG-HH-ALPSRP273956440-H1.0__A.LED
near_range, shift = 862456 -128
near_range, shift = 861406 -576
The range sampling rate for master and slave images are: 32000000
```

END PREPROCESS A STACK OF IMAGES

```
baseline_table.dat
22027 2010073.1732441077 1533 0.000000 0.000000
16659 2009070.1725686332 1165 1587.186736 2053.815036
22698 2010119.1729807514 1579 -435.197819 -450.437285
26724 2011030.1702765152 1855 -1439.155674 -1847.689031
27395 2011076.1695306008 1901 -1603.662440 -2071.893898
```

```
intf.in
IMG-HH-ALPSRP220276440-H1.0__A:IMG-HH-ALPSRP166596440-H1.0__A
IMG-HH-ALPSRP220276440-H1.0__A:IMG-HH-ALPSRP226986440-H1.0__A
IMG-HH-ALPSRP220276440-H1.0__A:IMG-HH-ALPSRP267246440-H1.0__A
IMG-HH-ALPSRP220276440-H1.0__A:IMG-HH-ALPSRP273956440-H1.0__A
IMG-HH-ALPSRP166596440-H1.0__A:IMG-HH-ALPSRP220276440-H1.0__A
IMG-HH-ALPSRP226986440-H1.0__A:IMG-HH-ALPSRP267246440-H1.0__A
IMG-HH-ALPSRP226986440-H1.0__A:IMG-HH-ALPSRP273956440-H1.0__A
IMG-HH-ALPSRP267246440-H1.0__A:IMG-HH-ALPSRP273956440-H1.0__A
```

```
align.in
IMG-HH-ALPSRP220276440-H1.0__A:IMG-HH-ALPSRP166596440-H1.0__A:IMG-HH-ALPSRP220276440-H1.0__A
IMG-HH-ALPSRP220276440-H1.0__A:IMG-HH-ALPSRP226986440-H1.0__A:IMG-HH-ALPSRP220276440-H1.0__A
IMG-HH-ALPSRP220276440-H1.0__A:IMG-HH-ALPSRP267246440-H1.0__A:IMG-HH-ALPSRP220276440-H1.0__A
IMG-HH-ALPSRP220276440-H1.0__A:IMG-HH-ALPSRP273956440-H1.0__A:IMG-HH-ALPSRP220276440-H1.0__A
IMG-HH-ALPSRP166596440-H1.0__A:IMG-HH-ALPSRP220276440-H1.0__A:IMG-HH-ALPSRP220276440-H1.0__A
IMG-HH-ALPSRP226986440-H1.0__A:IMG-HH-ALPSRP267246440-H1.0__A:IMG-HH-ALPSRP220276440-H1.0__A
IMG-HH-ALPSRP226986440-H1.0__A:IMG-HH-ALPSRP267246440-H1.0__A:IMG-HH-ALPSRP220276440-H1.0__A
IMG-HH-ALPSRP226986440-H1.0__A:IMG-HH-ALPSRP273956440-H1.0__A:IMG-HH-ALPSRP220276440-H1.0__A
IMG-HH-ALPSRP267246440-H1.0__A:IMG-HH-ALPSRP273956440-H1.0__A:IMG-HH-ALPSRP220276440-H1.0__A
```

align\_batch.csh AL05 align.in

```
ALIGN.CSH - START
focussing master
Computing range reference function.
Processing patch 1
Processing Elapsed Time: 0 min 0.03 sec
Range Compression
Processing Elapsed Time: 0 min 5.07 sec
Azimuthal Transform
Processing Elapsed Time: 0 min 12.32 sec
Range Migration
Processing Elapsed Time: 0 min 21.76 sec
Azimuthal Compression
Processing Elapsed Time: 0 min 42.49 sec
Writing Data
Processing patch 2
Processing Elapsed Time: 0 min 43.33 sec
Range Compression
Processing Elapsed Time: 0 min 47.47 sec
Azimuthal Transform
Processing Elapsed Time: 0 min 54.56 sec
Range Migration
Processing Elapsed Time: 1 min 3.90 sec
Azimuthal Compression
Processing Elapsed Time: 1 min 24.75 sec
Writing Data
Processing patch 3
Processing Elapsed Time: 1 min 25.59 sec
Range Compression
Processing Elapsed Time: 1 min 29.76 sec
Azimuthal Transform
Processing Elapsed Time: 1 min 36.78 sec
Range Migration
Processing Elapsed Time: 1 min 46.25 sec
Azimuthal Compression
Processing Elapsed Time: 2 min 7.16 sec
Writing Data
Processing Elapsed Time: 2 min 8.01 sec
number of points clipped to short int 168
align.csh
focussing slave
Computing range reference function.
Processing patch 1
Processing Elapsed Time: 0 min 0.03 sec
Range Compression
Processing Elapsed Time: 0 min 5.08 sec
Azimuthal Transform
Processing Elapsed Time: 0 min 12.37 sec
```



```

Range Migration
Processing Elapsed Time: 0 min 21.87 sec
Azimuthal Compression
Processing Elapsed Time: 0 min 42.74 sec
Writing Data
Processing patch 2
Processing Elapsed Time: 0 min 43.59 sec
Range Compression
Processing Elapsed Time: 0 min 47.89 sec
Azimuthal Transform
Processing Elapsed Time: 0 min 55.16 sec
Range Migration
Processing Elapsed Time: 1 min 4.68 sec
Azimuthal Compression
Processing Elapsed Time: 1 min 25.27 sec
Writing Data
Processing patch 3
Processing Elapsed Time: 1 min 26.10 sec
Range Compression
Processing Elapsed Time: 1 min 30.32 sec
Azimuthal Transform
Processing Elapsed Time: 1 min 37.50 sec
Range Migration
Processing Elapsed Time: 1 min 46.90 sec
Azimuthal Compression
Processing Elapsed Time: 2 min 7.89 sec
Writing Data
Processing Elapsed Time: 2 min 8.72 sec
number of points clipped to short int 0
align.csh
correlate master and slave to find offset parameters
  setting xsearch to 64
  setting nx_corr to 128
  setting ysearch to 64
  setting ny_corr to 128
  11304 27648 11304 27648 224 50 0.002114
  locations n 512 nx 11304 nyl 32 nxl 16 x_inc 574 y_inc 826
  elapsed time: 18.176372
align.csh
refocus slave
Computing range reference function.
Processing patch 1
Processing Elapsed Time: 0 min 0.03 sec
Range Compression
Processing Elapsed Time: 0 min 5.08 sec
Azimuthal Transform
Processing Elapsed Time: 0 min 12.51 sec
Range Migration
Processing Elapsed Time: 0 min 21.95 sec
Azimuthal Compression
Processing Elapsed Time: 0 min 43.23 sec
Writing Data
Processing patch 2
Processing Elapsed Time: 0 min 44.08 sec
Range Compression
Processing Elapsed Time: 0 min 48.25 sec
Azimuthal Transform
Processing Elapsed Time: 0 min 55.62 sec
Range Migration
Processing Elapsed Time: 1 min 4.92 sec
Azimuthal Compression
Processing Elapsed Time: 1 min 26.88 sec
Writing Data
Processing patch 3
Processing Elapsed Time: 1 min 27.72 sec
Range Compression
Processing Elapsed Time: 1 min 31.95 sec
Azimuthal Transform
Processing Elapsed Time: 1 min 39.11 sec
Range Migration
Processing Elapsed Time: 1 min 48.73 sec
Azimuthal Compression
Processing Elapsed Time: 2 min 10.08 sec
Writing Data
Processing Elapsed Time: 2 min 10.92 sec
number of points clipped to short int 0
rm: No match.
ALIGN.CSH - END

intf_batch.csh ALOS batch.config
clean up topo/ folder

DEM2TOPO_RA.CSH - START
USER SHOULD PROVIDE DEM FILE
  range decimation is: 2
blockmedian: Provides 3, expects 3-column binary data
blockmedian: Processing input table data
blockmedian: W: 0 E: 11304 S: 0 N: 27648 n_columns: 5652 n_rows: 6912
blockmedian: Input 3 columns via binary records using format ddd
blockmedian: Output 3 columns via binary records using format ddd
blockmedian: N read: 820604 N used: 819846 outside_area: 758 N cells filled: 819846
surface: Provides 3, expects 3-column binary data
surface: Grid domain: W: 0 E: 11304 S: 0 N: 27648 n_columns: 5652 n_rows: 6912 [pixel registration]
surface: Processing input table data
surface: Input 3 columns via binary records using format ddd
surface: Minimum value of your dataset x,y,z at: surface: 1.12547659874 5630.14648438 251.258743286
surface: Maximum value of your dataset x,y,z at: surface: 10325.4550781 19196.9160156 1368.26428223
surface: LS plane determined: z = 277.179 + (0.0531511 * col) + (0.0234857 * row)
surface:


| Grid        | Mode | Iteration | Max Change        | Conv Limit        | Total Iterations |
|-------------|------|-----------|-------------------|-------------------|------------------|
| surface: 36 | D    | 15326     | 0.000302695363147 | 0.000303042456691 | 15326            |
| surface: 12 | I    | 30        | 0.0007684972502   | 0.000909127370074 | 15356            |
| surface: 12 | D    | 5349      | 0.000907706771858 | 0.000909127370074 | 20705            |
| surface: 4  | I    | 24        | 0.00259984212886  | 0.0027273821102   | 20729            |
| surface: 4  | D    | 1741      | 0.00271894782305  | 0.0027273821102   | 22470            |
| surface: 2  | I    | 18        | 0.00411256030944  | 0.0054547642204   | 22488            |
| surface: 2  | D    | 396       | 0.00544386989678  | 0.0054547642204   | 22884            |
| surface: 1  | I    | 15        | 0.00889034868035  | 0.0109095284409   | 22899            |
| surface: 1  | D    | 239       | 0.0109077407916   | 0.0109095284409   | 23138            |


surface: Fit info: N data points N nodes mean error rms error curvature
surface: 819846 39079189 2.53831261513e-06 0.00557076836902 96122.1752609
gridcpt: Processing input grid(s)
gridcpt: Mean and S.D. of data are 514.775373751 149.61184721
gridimage: Allocates memory and read data file topo_ra.grd
gridimage: Evaluate image pixel colors
gridimage: Creating 8-bit grayshade image
DEM2TOPO_RA.CSH - END
NO TOPO_RA SHIFT

START FORM A STACK OF INTERFEROGRAMS

```

INTF.CSH, FILTER.CSH - START

```
intf.csh
running phasediff...
reading topo topo_ra.grd
  xdim 11304, ydim 27648
filter.csh
gauss_300 4 2 (4 2)
making amplitudes...
filtering interferogram...
making amplitude...
making correlation...
making phase...
filtering phase...
INTF.CSH, FILTER.CSH - END
```

SNAPHU.CSH - START

```
threshold_snaphu: .16
grdmath: Perform reverse Polish notation calculations on grids
grdmath: phase_patch.grd landmask_ra_patch.grd MUL = phase_patch.grd
unwrapping phase with snaphu - higher threshold for faster unwrapping
```

snaphu v1.4.2

32 parameters input from file snaphu.conf.brief (297 lines total)

Reading wrapped phase from file phase.in

No weight file specified. Assuming uniform weights

Reading correlation data from file corr.in

Calculating deformation-mode cost parameters

Building range cost arrays

Building azimuth cost arrays

Initializing flows with MST algorithm

Running approximate minimum spanning tree solver

Running nonlinear network flow optimizer

Maximum flow on network: 2

Number of nodes in network: 4878776

Flow increment: 1 (Total improvements: 0)

Treesize: 4878776 Pivots: 340919 Improvements: 123

Maximum flow on network: 2

Flow increment: 2 (Total improvements: 123)

Treesize: 4878776 Pivots: 7 Improvements: 2

Maximum flow on network: 2

Total solution cost: 1565955

Integrating phase

Writing output to file unwrap.out

Program snaphu done

Elapsed processor time: 0:01:01.56

Elapsed wall clock time: 0:01:02

grdmath: Perform reverse Polish notation calculations on grids

grdmath: unwrap.grd landmask\_ra\_patch.grd MUL = tmp.grd

SNAPHU.CSH - END

GEOCODE.CSH - START

threshold\_geocode: .16

grdmath: Perform reverse Polish notation calculations on grids

grdmath: corr.grd 0.16 GE 0 NAN mask.grd MUL = mask2.grd

psscale: Warning: The -E option is deprecated but is accepted.

psscale: For the current -D syntax you should use -D modifier +e instead.

psscale: Note you cannot mix new-style modifiers (+e) with the old-style -D option.

psscale: Warning: The -E option is deprecated but is accepted.

psscale: For the current -D syntax you should use -D modifier +e instead.

psscale: Note you cannot mix new-style modifiers (+e) with the old-style -D option.

geocode.csh

project correlation, phase, unwrapped and amplitude back to lon lat coordinates

remarked is by root on Sat May 19 12:23:56 JST 2018 with geocode.csh

proj\_ra2ll.csh

surface: Provides 3, expects 3-column binary data

surface: Grid domain: W: 48 E: 11216 S: 0 N: 27648 n\_columns: 698 n\_rows: 864 [gridline registration]

surface: Processing input table data

surface: Input 3 columns via binary records using format fff

surface: Minimum value of your dataset x,y,z at: surface: 1157.27636719 27641.6796875 -73.3199996948

surface: Maximum value of your dataset x,y,z at: surface: 11220.6337891 13819.7900391 -72.3799972534

surface: 368121 unusable points were supplied; these will be ignored.

surface: You should have pre-processed the data with block-mean, -median, or -mode.

surface: Check that previous processing steps write results with enough decimals.

surface: LS plane determined: z = -73.123 + (0.00128341 \* col) + (-0.000329582 \* row)

surface: Grid	Mode	Iteration	Max Change	Conv Limit	Total Iterations
2	D	1000	3.6513143853e-06	1.99723167218e-07	1000
1	I	15	2.58214989051e-07	3.99446334437e-07	1015
1	D	500	8.33893307477e-07	3.99446334437e-07	1515

surface: Fit info: N data points N nodes mean error rms error/curvature

surface: 457037 604635 -2.53484679499e-06 0.00681102227394 9592.91231207

surface: Provides 3, expects 3-column binary data

surface: Grid domain: W: 48 E: 11216 S: 0 N: 27648 n\_columns: 698 n\_rows: 864 [gridline registration]

surface: Processing input table data

surface: Input 3 columns via binary records using format fff

surface: Minimum value of your dataset x,y,z at: surface: 47.4586181641 5829.44580078 -36.9000015259

surface: Maximum value of your dataset x,y,z at: surface: 1380.12194824 27663.7246094 -36.2599983215

surface: 368121 unusable points were supplied; these will be ignored.

surface: You should have pre-processed the data with block-mean, -median, or -mode.

surface: Check that previous processing steps write results with enough decimals.

surface: LS plane determined: z = -37.0614 + (0.000309001 \* col) + (0.000897308 \* row)

surface: Grid	Mode	Iteration	Max Change	Conv Limit	Total Iterations
2	D	1000	6.31386177158e-07	3.58320659535e-08	1000
1	I	15	6.11068715462e-08	7.16641319071e-08	1015
1	D	500	1.44489694472e-07	7.16641319071e-08	1515

surface: Fit info: N data points N nodes mean error rms error/curvature

surface: 457037 604635 -2.06139269364e-05 0.0153010106888 18915.9940995

blockmedian: Provides 3, expects 3-column binary data

blockmedian: Processing input table data

blockmedian: W: 286.588888889 E: 287.777777778 S: -37.0625 N: -36.0694444444 n\_columns: 1070 n\_rows: 1430

blockmedian: Input 3 columns via binary records using format fff

blockmedian: Output 3 columns via binary records using format fff

blockmedian: N read: 4761772 N used: 4761772 outside\_area: 0 N cells filled: 969780

proj\_ra2ll.csh

blockmedian: Provides 3, expects 3-column binary data

blockmedian: Processing input table data

blockmedian: W: 286.588888889 E: 287.777777778 S: -37.0625 N: -36.0694444444 n\_columns: 1070 n\_rows: 1430

blockmedian: Input 3 columns via binary records using format fff

blockmedian: Output 3 columns via binary records using format fff

blockmedian: N read: 4766582 N used: 4766582 outside\_area: 0 N cells filled: 970774

proj\_ra2ll.csh

blockmedian: Provides 3, expects 3-column binary data

blockmedian: Processing input table data

blockmedian: W: 286.7 E: 287.766666667 S: -37.0625 N: -36.0694444444 n\_columns: 960 n\_rows: 1430

blockmedian: Input 3 columns via binary records using format fff

blockmedian: Output 3 columns via binary records using format fff

blockmedian: N read: 3186539 N used: 3186539 outside\_area: 0 N cells filled: 653430

proj\_ra2ll.csh

```
blockmedian: Provides 3, expects 3-column binary data
blockmedian: Processing input table data
blockmedian: W: 286.58888889 E: 287.77777778 S: -37.0625 N: -36.069444444 n_columns: 1070 n_rows: 1430
blockmedian: Input 3 columns via binary records using format fff
blockmedian: Output 3 columns via binary records using format fff
blockmedian: N read: 4824576 N used: 4824576 outside_area: 0 N cells filled: 982440
proj_ra2ll.csh
blockmedian: Provides 3, expects 3-column binary data
blockmedian: Processing input table data
blockmedian: W: 286.77777778 E: 287.63333333 S: -36.909722222 N: -36.25 n_columns: 770 n_rows: 950
blockmedian: Input 3 columns via binary records using format fff
blockmedian: Output 3 columns via binary records using format fff
blockmedian: N read: 2411902 N used: 2411902 outside_area: 0 N cells filled: 489615
proj_ra2ll.csh
blockmedian: Provides 3, expects 3-column binary data
blockmedian: Processing input table data
blockmedian: W: 286.76666667 E: 287.63333333 S: -36.909722222 N: -36.25 n_columns: 780 n_rows: 950
blockmedian: Input 3 columns via binary records using format fff
blockmedian: Output 3 columns via binary records using format fff
blockmedian: N read: 2502145 N used: 2502145 outside_area: 0 N cells filled: 504307
proj_ra2ll.csh
blockmedian: Provides 3, expects 3-column binary data
blockmedian: Processing input table data
blockmedian: W: 286.7 E: 287.76666667 S: -37.0625 N: -36.069444444 n_columns: 960 n_rows: 1430
blockmedian: Input 3 columns via binary records using format fff
blockmedian: Output 3 columns via binary records using format fff
blockmedian: N read: 3186539 N used: 3186539 outside_area: 0 N cells filled: 653430
geocode.csh
make the KML files for Google Earth
grdimage: Allocates memory and read data file display_amp_ll.grd
grdimage: Evaluate image pixel colors
grdimage: Creating 24-bit color image
PSL: Colormap of 253 colors created
Make display_amp_ll.kml and display_amp_ll.png
psconvert: Processing display_amp_ll.ps...
psconvert: Figure dimensions: Width: 85.626 points [1.18925 inch] Height: 71.52 points [0.993333 inch]
psconvert: gs -q -dSAFER -dNOPAUSE -dBATCH -dPDFSETTINGS=/prepress -dDownsampleColorImages=false -dDownsampleGrayImages=false -dDownsampleMonoImages=false -dUseFlateCompression=true -dEmbedAllFonts=true -dSubsetFonts=true -dMonoImageFilter=/FlateEncode -dAutoFilterGrayImages=false -dGrayImageFilter=/FlateEncode -dAutoFilterColorImages=false -dColorImageFilter=/FlateEncode -dSCANCONVERTERTYPE=2 -dMaxBitmap=2147483647 -dUseFastColor=true -sDEVICE=pngalpha -g1071x894 -r900 -sOutputFile='display_amp_ll.png' -f'./psconvert_45245d.eps'
psconvert: Done.
grdimage: Allocates memory and read data file corr_ll.grd
grdimage: Evaluate image pixel colors
grdimage: Creating 24-bit color image
Make corr_ll.kml and corr_ll.png
psconvert: Processing corr_ll.ps...
psconvert: Figure dimensions: Width: 85.626 points [1.18925 inch] Height: 71.52 points [0.993333 inch]
psconvert: gs -q -dSAFER -dNOPAUSE -dBATCH -dPDFSETTINGS=/prepress -dDownsampleColorImages=false -dDownsampleGrayImages=false -dDownsampleMonoImages=false -dUseFlateCompression=true -dEmbedAllFonts=true -dSubsetFonts=true -dMonoImageFilter=/FlateEncode -dAutoFilterGrayImages=false -dGrayImageFilter=/FlateEncode -dAutoFilterColorImages=false -dColorImageFilter=/FlateEncode -dSCANCONVERTERTYPE=2 -dMaxBitmap=2147483647 -dUseFastColor=true -sDEVICE=pngalpha -g1071x894 -r900 -sOutputFile='corr_ll.png' -f'./psconvert_45259d.eps'
psconvert: Done.
grdimage: Allocates memory and read data file phase_mask_ll.grd
grdimage: Evaluate image pixel colors
grdimage: Creating 24-bit color image
Make phase_mask_ll.kml and phase_mask_ll.png
psconvert: Processing phase_mask_ll.ps...
psconvert: Figure dimensions: Width: 76.806 points [1.06675 inch] Height: 71.52 points [0.993333 inch]
psconvert: gs -q -dSAFER -dNOPAUSE -dBATCH -dPDFSETTINGS=/prepress -dDownsampleColorImages=false -dDownsampleGrayImages=false -dDownsampleMonoImages=false -dUseFlateCompression=true -dEmbedAllFonts=true -dSubsetFonts=true -dMonoImageFilter=/FlateEncode -dAutoFilterGrayImages=false -dGrayImageFilter=/FlateEncode -dAutoFilterColorImages=false -dColorImageFilter=/FlateEncode -dSCANCONVERTERTYPE=2 -dMaxBitmap=2147483647 -dUseFastColor=true -sDEVICE=pngalpha -g961x894 -r900 -sOutputFile='phase_mask_ll.png' -f'./psconvert_45273d.eps'
psconvert: Done.
grdimage: Allocates memory and read data file phasefilt_mask_ll.grd
grdimage: Evaluate image pixel colors
grdimage: Creating 24-bit color image
Make phasefilt_mask_ll.kml and phasefilt_mask_ll.png
psconvert: Processing phasefilt_mask_ll.ps...
psconvert: Figure dimensions: Width: 76.806 points [1.06675 inch] Height: 71.52 points [0.993333 inch]
psconvert: gs -q -dSAFER -dNOPAUSE -dBATCH -dPDFSETTINGS=/prepress -dDownsampleColorImages=false -dDownsampleGrayImages=false -dDownsampleMonoImages=false -dUseFlateCompression=true -dEmbedAllFonts=true -dSubsetFonts=true -dMonoImageFilter=/FlateEncode -dAutoFilterGrayImages=false -dGrayImageFilter=/FlateEncode -dAutoFilterColorImages=false -dColorImageFilter=/FlateEncode -dSCANCONVERTERTYPE=2 -dMaxBitmap=2147483647 -dUseFastColor=true -sDEVICE=pngalpha -g961x894 -r900 -sOutputFile='phasefilt_mask_ll.png' -f'./psconvert_45287d.eps'
psconvert: Done.
grdimage: Allocates memory and read data file unwrap_mask_ll.grd
grdimage: Evaluate image pixel colors
grdimage: Creating 24-bit color image
Make unwrap_mask_ll.kml and unwrap_mask_ll.png
psconvert: Processing unwrap_mask_ll.ps...
psconvert: Figure dimensions: Width: 61.62 points [0.855833 inch] Height: 47.52 points [0.66 inch]
psconvert: gs -q -dSAFER -dNOPAUSE -dBATCH -dPDFSETTINGS=/prepress -dDownsampleColorImages=false -dDownsampleGrayImages=false -dDownsampleMonoImages=false -dUseFlateCompression=true -dEmbedAllFonts=true -dSubsetFonts=true -dMonoImageFilter=/FlateEncode -dAutoFilterGrayImages=false -dGrayImageFilter=/FlateEncode -dAutoFilterColorImages=false -dColorImageFilter=/FlateEncode -dSCANCONVERTERTYPE=2 -dMaxBitmap=2147483647 -dUseFastColor=true -sDEVICE=pngalpha -g771x594 -r900 -sOutputFile='unwrap_mask_ll.png' -f'./psconvert_45301d.eps'
psconvert: Done.
grdimage: Allocates memory and read data file phasefilt_mask_ll.grd
grdimage: Evaluate image pixel colors
grdimage: Creating 24-bit color image
Make phasefilt_mask_ll.kml and phasefilt_mask_ll.png
psconvert: Processing phasefilt_mask_ll.ps...
psconvert: Figure dimensions: Width: 76.806 points [1.06675 inch] Height: 71.52 points [0.993333 inch]
psconvert: gs -q -dSAFER -dNOPAUSE -dBATCH -dPDFSETTINGS=/prepress -dDownsampleColorImages=false -dDownsampleGrayImages=false -dDownsampleMonoImages=false -dUseFlateCompression=true -dEmbedAllFonts=true -dSubsetFonts=true -dMonoImageFilter=/FlateEncode -dAutoFilterGrayImages=false -dGrayImageFilter=/FlateEncode -dAutoFilterColorImages=false -dColorImageFilter=/FlateEncode -dSCANCONVERTERTYPE=2 -dMaxBitmap=2147483647 -dUseFastColor=true -sDEVICE=pngalpha -g961x894 -r900 -sOutputFile='phasefilt_mask_ll.png' -f'./psconvert_45315d.eps'
psconvert: Done.
grdimage: Allocates memory and read data file los_ll.grd
grdimage: Evaluate image pixel colors
grdimage: Creating 24-bit color image
Make los_ll.kml and los_ll.png
psconvert: Processing los_ll.ps...
psconvert: Figure dimensions: Width: 61.62 points [0.855833 inch] Height: 47.52 points [0.66 inch]
psconvert: gs -q -dSAFER -dNOPAUSE -dBATCH -dPDFSETTINGS=/prepress -dDownsampleColorImages=false -dDownsampleGrayImages=false -dDownsampleMonoImages=false -dUseFlateCompression=true -dEmbedAllFonts=true -dSubsetFonts=true -dMonoImageFilter=/FlateEncode -dAutoFilterGrayImages=false -dGrayImageFilter=/FlateEncode -dAutoFilterColorImages=false -dColorImageFilter=/FlateEncode -dSCANCONVERTERTYPE=2 -dMaxBitmap=2147483647 -dUseFastColor=true -sDEVICE=pngalpha -g771x594 -r900 -sOutputFile='los_ll.png' -f'./psconvert_45331d.eps'
psconvert: Done.
GEOCODE.CSH - END
```

```
stack.list
cut_2010073_2009070.grd IMG-HH-ALPSRP220276440-H1_0_A.PRM IMG-HH-ALPSRP166596440-H1_0_A.PRM
cut_2010073_2010119.grd IMG-HH-ALPSRP220276440-H1_0_A.PRM IMG-HH-ALPSRP226986440-H1_0_A.PRM
cut_2010073_2011030.grd IMG-HH-ALPSRP220276440-H1_0_A.PRM IMG-HH-ALPSRP267246440-H1_0_A.PRM
cut_2010073_2011076.grd IMG-HH-ALPSRP220276440-H1_0_A.PRM IMG-HH-ALPSRP273956440-H1_0_A.PRM
```

```
bash stack_phase.bash stack.list mean.grd std.grd
```

```
compute the mean LOS velocity ..
```

```

time span (days) of cut_2010073_2009070.grd: 368
accumulative days in the stack: 368
time span (days) of cut_2010073_2010119.grd: 46
accumulative days in the stack: 414
time span (days) of cut_2010073_2011030.grd: 322
accumulative days in the stack: 736
time span (days) of cut_2010073_2011076.grd: 368
accumulative days in the stack: 1104

compute the standard deviations ..

mean_ll.grd
std_ll.grd
los_ll_2009070.grd
los_ll_2010119.grd
los_ll_2011030.grd
los_ll_2011076.grd

csh select_pairs.csh baseline_table.dat 1000 2059

intf.tab
cut_2010073_2010119.grd corcut_2010073_2010119.grd 2010073 2010119 -450.437285
cut_2010073_2011030.grd corcut_2010073_2011030.grd 2010073 2011030 -1847.689031
cut_2009070_2010073.grd corcut_2009070_2010073.grd 2009070 2010073 -2054.587109
cut_2010119_2011030.grd corcut_2010119_2011030.grd 2010119 2011030 -1397.267474
cut_2010119_2011076.grd corcut_2010119_2011076.grd 2010119 2011076 -1621.473370
cut_2011030_2011076.grd corcut_2011030_2011076.grd 2011030 2011076 -224.198309

scene.tab
2010073 1533
2009070 1165
2010119 1579
2011030 1855
2011076 1901

sbas intf.tab scene.tab 6 5 750 500 -smooth 1.0 -wavelength 0.2362 -incidence 34.3 -range 862755 -rms -dem -atm 1

compute RMS misfit
compute DEM error

setting smoothing to 1.000
setting radar wavelength to 0.236 m
setting radar incidence angle to 34.300 degree
setting range to 862755.000 m
Memory Allocation Successful...
read table file ...
number of SAR scenes is 5
number of interferograms is 6
read phase and correlation grids ...
fill the G matrix ...

Applying atmospheric correction by common point stacking...

Hit Matrix:
2010073 0 0 1 1 0
2009070 1 0 0 0 0
2010119 0 0 0 1 1
2011030 0 0 0 0 1
2011076 0 0 0 0 0

Applying exponential relaxation on smoothing parameters

Setting smoothing parameter to 1000.000000...
fill the G matrix ...
Computing deformation time-series...
run least-squares problem over 750 by 500 pixel (0) ...
matrix is full rank: 5

Removing deformation time-series from original unwrapped phase...
Computing atmospheric phase screen by common-point stacking...
Initial estimate of APS...
atm_noise(NO.0) = 0.000000
atm_noise(NO.1) = 0.000000
atm_noise(NO.2) = 0.000000
atm_noise(NO.3) = 0.000000
atm_noise(NO.4) = 0.000000

atm_noise(NO.0) = 0.000000
atm_noise(NO.1) = 0.000000
atm_noise(NO.2) = 0.000000
atm_noise(NO.3) = 0.000000
atm_noise(NO.4) = 0.000000

Applying atmospheric phase screen to original unwrapped phase...
Setting smoothing parameter to 1.000000...
fill the G matrix ...
run least-squares problem over 750 by 500 pixel (0) ...
matrix is rank-deficient: 4

write output ...

raln.grd
ralt.grd
rms_ll.grd
dem.grd
vel_ll.grd
disp_2009070_ll.grd
disp_2010073_ll.grd
disp_2010119_ll.grd
disp_2011030_ll.grd
disp_2011076_ll.grd
aps_2009070.grd
aps_2010073.grd
aps_2010119.grd
aps_2011030.grd
aps_2011076.grd

```

# APPENDIX B. RTK-GNSS PROCESSING

## B.1 CPBI station

RINEX Observation		RINEX *NAV/CLK, SP3 or SBS/EMS			EOP data file	Date	Height (m)
Rover	Base station	IGS_NAV	IGS_EPH	IGS_CLK_30s			
cpbi1870.08o	csrj1870.08o	brdc1870.08n	igs14870.sp3	igs14870.clk_30s	igs14877.erp	2008/07/06	277.7797
cpbi1880.08o	csrj1880.08o	brdc1880.08n	igs14873.sp3	igs14873.clk_30s	igs14877.erp	2008/07/09	279.8512
cpbi1960.08o	csrj1960.08o	brdc1960.08n	igs14881.sp3	igs14881.clk_30s	igs14887.erp	2008/07/14	277.0775
cpbi1970.08o	csrj1970.08o	brdc1970.08n	igs14882.sp3	igs14882.clk_30s	igs14887.erp	2008/07/15	278.2781
cpbi2020.08o	csrj2020.08o	brdc2020.08n	igs14890.sp3	igs14890.clk_30s	igs14897.erp	2008/07/20	278.2367
cpbi2030.08o	csrj2030.08o	brdc2030.08n	igs14891.sp3	igs14891.clk_30s	igs14897.erp	2008/07/21	280.3650
cpbi2040.08o	csrj2040.08o	brdc2040.08n	igs14892.sp3	igs14892.clk_30s	igs14897.erp	2008/07/22	280.1233
cpbi2090.08o	csrj2090.08o	brdc2090.08n	igs14900.sp3	igs14900.clk_30s	igs14907.erp	2008/07/27	278.2861
cpbi2190.08o	csrj2190.08o	brdc2190.08n	igs14913.sp3	igs14913.clk_30s	igs14917.erp	2008/08/06	278.7607
cpbi2200.08o	csrj2200.08o	brdc2200.08n	igs14914.sp3	igs14914.clk_30s	igs14917.erp	2008/08/07	278.0443
cpbi2290.08o	csrj2290.08o	brdc2290.08n	igs14926.sp3	igs14926.clk_30s	igs14927.erp	2008/08/16	279.1849
cpbi2360.08o	csrj2360.08o	brdc2360.08n	igs14936.sp3	igs14936.clk_30s	igs14937.erp	2008/08/23	279.2658
cpbi2400.08o	csrj2400.08o	brdc2400.08n	igs14943.sp3	igs14943.clk_30s	igs14947.erp	2008/08/27	278.4913
cpbi2470.08o	csrj2470.08o	brdc2470.08n	igs14953.sp3	igs14953.clk_30s	igs14957.erp	2008/09/03	278.9343
cpbi2480.08o	csrj2480.08o	brdc2480.08n	igs14954.sp3	igs14954.clk_30s	igs14957.erp	2008/09/04	277.9543
cpbi2500.08o	csrj2500.08o	brdc2500.08n	igs14956.sp3	igs14956.clk_30s	igs14957.erp	2008/09/06	277.8994
cpbi2540.08o	csrj2540.08o	brdc2540.08n	igs14963.sp3	igs14963.clk_30s	igs14967.erp	2008/09/10	276.7304
cpbi2560.08o	csrj2560.08o	brdc2560.08n	igs14965.sp3	igs14965.clk_30s	igs14967.erp	2008/09/12	278.9137
cpbi2580.08o	csrj2580.08o	brdc2580.08n	igs14970.sp3	igs14970.clk_30s	igs14977.erp	2008/09/14	276.9904
cpbi2590.08o	csrj2590.08o	brdc2590.08n	igs14971.sp3	igs14971.clk_30s	igs14977.erp	2008/09/15	279.5108
cpbi2610.08o	csrj2610.08o	brdc2610.08n	igs14973.sp3	igs14973.clk_30s	igs14977.erp	2008/09/17	278.1275
cpbi2620.08o	csrj2620.08o	brdc2620.08n	igs14974.sp3	igs14974.clk_30s	igs14977.erp	2008/09/18	278.0126
cpbi2630.08o	csrj2630.08o	brdc2630.08n	igs14975.sp3	igs14975.clk_30s	igs14977.erp	2008/09/19	279.1329
cpbi2640.08o	csrj2640.08o	brdc2640.08n	igs14976.sp3	igs14976.clk_30s	igs14977.erp	2008/09/20	279.0781
cpbi2650.08o	csrj2650.08o	brdc2650.08n	igs14980.sp3	igs14980.clk_30s	igs14987.erp	2008/09/21	279.0045
cpbi2660.08o	csrj2660.08o	brdc2660.08n	igs14981.sp3	igs14981.clk_30s	igs14987.erp	2008/09/22	279.2188
cpbi2670.08o	csrj2670.08o	brdc2670.08n	igs14982.sp3	igs14982.clk_30s	igs14987.erp	2008/09/23	279.7788
cpbi2680.08o	csrj2680.08o	brdc2680.08n	igs14983.sp3	igs14983.clk_30s	igs14987.erp	2008/09/24	277.6786
cpbi2690.08o	csrj2690.08o	brdc2690.08n	igs14984.sp3	igs14984.clk_30s	igs14987.erp	2008/09/26	279.7905
cpbi2710.08o	csrj2710.08o	brdc2710.08n	igs14986.sp3	igs14986.clk_30s	igs14987.erp	2008/09/27	279.5899
cpbi2720.08o	csrj2720.08o	brdc2720.08n	igs14990.sp3	igs14990.clk_30s	igs14997.erp	2008/09/28	279.4947
cpbi2730.08o	csrj2730.08o	brdc2730.08n	igs14991.sp3	igs14991.clk_30s	igs14997.erp	2008/09/29	280.3855
cpbi2790.08o	csrj2790.08o	brdc2790.08n	igs15000.sp3	igs15000.clk_30s	igs15007.erp	2008/10/05	279.6836
cpbi2800.08o	csrj2800.08o	brdc2800.08n	igs15001.sp3	igs15001.clk_30s	igs15007.erp	2008/10/06	277.1232
cpbi2820.08o	csrj2820.08o	brdc2820.08n	igs15003.sp3	igs15003.clk_30s	igs15007.erp	2008/10/08	279.6530
cpbi2840.08o	csrj2840.08o	brdc2840.08n	igs15005.sp3	igs15005.clk_30s	igs15007.erp	2008/10/10	279.1972
cpbi2850.08o	csrj2850.08o	brdc2850.08n	igs15006.sp3	igs15006.clk_30s	igs15007.erp	2008/10/11	278.9930
cpbi2860.08o	csrj2860.08o	brdc2860.08n	igs15010.sp3	igs15010.clk_30s	igs15017.erp	2008/10/12	279.5867
cpbi2870.08o	csrj2870.08o	brdc2870.08n	igs15011.sp3	igs15011.clk_30s	igs15017.erp	2008/10/13	278.5433
cpbi2900.08o	csrj2900.08o	brdc2900.08n	igs15014.sp3	igs15014.clk_30s	igs15017.erp	2008/10/16	279.4995
cpbi2910.08o	csrj2910.08o	brdc2910.08n	igs15015.sp3	igs15015.clk_30s	igs15017.erp	2008/10/17	277.6874
cpbi2920.08o	csrj2920.08o	brdc2920.08n	igs15016.sp3	igs15016.clk_30s	igs15017.erp	2008/10/18	276.9413
cpbi2950.08o	csrj2950.08o	brdc2950.08n	igs15022.sp3	igs15022.clk_30s	igs15027.erp	2008/10/21	278.3526
cpbi2960.08o	csrj2960.08o	brdc2960.08n	igs15023.sp3	igs15023.clk_30s	igs15027.erp	2008/10/22	279.2640
cpbi2980.08o	csrj2980.08o	brdc2980.08n	igs15025.sp3	igs15025.clk_30s	igs15027.erp	2008/10/24	277.4998
cpbi2990.08o	csrj2990.08o	brdc2990.08n	igs15026.sp3	igs15026.clk_30s	igs15027.erp	2008/10/25	278.8279
cpbi3030.08o	csrj3030.08o	brdc3030.08n	igs15033.sp3	igs15033.clk_30s	igs15037.erp	2008/10/29	280.3840
cpbi3070.08o	csrj3070.08o	brdc3070.08n	igs15040.sp3	igs15040.clk_30s	igs15047.erp	2008/11/02	278.8934
cpbi3080.08o	csrj3080.08o	brdc3080.08n	igs15041.sp3	igs15041.clk_30s	igs15047.erp	2008/11/03	279.0908
cpbi3090.08o	csrj3090.08o	brdc3090.08n	igs15042.sp3	igs15042.clk_30s	igs15047.erp	2008/11/04	278.2646
cpbi0690.09o	csrj0690.09o	brdc0690.09n	igs15222.sp3	igs15222.clk_30s	igs15227.erp	2009/03/10	278.5618
cpbi0700.09o	csrj0700.09o	brdc0700.09n	igs15223.sp3	igs15223.clk_30s	igs15227.erp	2009/03/11	278.8484
cpbi0710.09o	csrj0710.09o	brdc0710.09n	igs15224.sp3	igs15224.clk_30s	igs15227.erp	2009/03/12	278.7923
cpbi0720.09o	csrj0720.09o	brdc0720.09n	igs15225.sp3	igs15225.clk_30s	igs15227.erp	2009/03/13	278.7242
cpbi0730.09o	csrj0730.09o	brdc0730.09n	igs15226.sp3	igs15226.clk_30s	igs15227.erp	2009/03/14	279.0224
cpbi0740.09o	csrj0740.09o	brdc0740.09n	igs15230.sp3	igs15230.clk_30s	igs15237.erp	2009/03/15	278.7391
cpbi0750.09o	csrj0750.09o	brdc0750.09n	igs15231.sp3	igs15231.clk_30s	igs15237.erp	2009/03/16	278.8065
cpbi0760.09o	csrj0760.09o	brdc0760.09n	igs15232.sp3	igs15232.clk_30s	igs15237.erp	2009/03/17	278.8067
cpbi0770.09o	csrj0770.09o	brdc0770.09n	igs15233.sp3	igs15233.clk_30s	igs15237.erp	2009/03/18	278.8586
cpbi0780.09o	csrj0780.09o	brdc0780.09n	igs15234.sp3	igs15234.clk_30s	igs15237.erp	2009/03/19	278.6982
cpbi0790.09o	csrj0790.09o	brdc0790.09n	igs15235.sp3	igs15235.clk_30s	igs15237.erp	2009/03/20	278.7153
cpbi0800.09o	csrj0800.09o	brdc0800.09n	igs15236.sp3	igs15236.clk_30s	igs15237.erp	2009/03/21	278.6944
cpbi0810.09o	csrj0810.09o	brdc0810.09n	igs15240.sp3	igs15240.clk_30s	igs15247.erp	2009/03/22	278.6133

cpbi0820.09o	csrj0820.09o	brdc0820.09n	igs15241.sp3	igs15241.clk_30s	igs15247.erp	2009/03/23	278.7907
cpbi0830.09o	csrj0830.09o	brdc0830.09n	igs15242.sp3	igs15242.clk_30s	igs15247.erp	2009/03/24	278.7733
cpbi0840.09o	csrj0840.09o	brdc0840.09n	igs15243.sp3	igs15243.clk_30s	igs15247.erp	2009/03/25	278.7529
cpbi0850.09o	csrj0850.09o	brdc0850.09n	igs15244.sp3	igs15244.clk_30s	igs15247.erp	2009/03/26	278.8456
cpbi0890.09o	csrj0890.09o	brdc0890.09n	igs15251.sp3	igs15251.clk_30s	igs15257.erp	2009/03/30	278.5433
cpbi0900.09o	csrj0900.09o	brdc0900.09n	igs15252.sp3	igs15252.clk_30s	igs15257.erp	2009/03/31	278.6507
cpbi0910.09o	csrj0910.09o	brdc0910.09n	igs15253.sp3	igs15253.clk_30s	igs15257.erp	2009/04/01	278.5794
cpbi0920.09o	csrj0920.09o	brdc0920.09n	igs15254.sp3	igs15254.clk_30s	igs15257.erp	2009/04/02	278.7165
cpbi0930.09o	csrj0930.09o	brdc0930.09n	igs15255.sp3	igs15255.clk_30s	igs15257.erp	2009/04/03	278.7317
cpbi0940.09o	csrj0940.09o	brdc0940.09n	igs15256.sp3	igs15256.clk_30s	igs15257.erp	2009/04/04	278.7863
cpbi0950.09o	csrj0950.09o	brdc0950.09n	igs15260.sp3	igs15260.clk_30s	igs15267.erp	2009/04/05	278.7594
cpbi0960.09o	csrj0960.09o	brdc0960.09n	igs15261.sp3	igs15261.clk_30s	igs15267.erp	2009/04/06	278.7255
cpbi0980.09o	csrj0980.09o	brdc0980.09n	igs15263.sp3	igs15263.clk_30s	igs15267.erp	2009/04/08	278.7984
cpbi0990.09o	csrj0990.09o	brdc0990.09n	igs15264.sp3	igs15264.clk_30s	igs15267.erp	2009/04/09	278.7278
cpbi1010.09o	csrj1010.09o	brdc1010.09n	igs15266.sp3	igs15266.clk_30s	igs15267.erp	2009/04/11	278.7672
cpbi1020.09o	csrj1020.09o	brdc1020.09n	igs15270.sp3	igs15270.clk_30s	igs15277.erp	2009/04/12	278.6101
cpbi1030.09o	csrj1030.09o	brdc1030.09n	igs15271.sp3	igs15271.clk_30s	igs15277.erp	2009/04/13	278.9428
cpbi1040.09o	csrj1040.09o	brdc1040.09n	igs15272.sp3	igs15272.clk_30s	igs15277.erp	2009/04/14	278.9840
cpbi1050.09o	csrj1050.09o	brdc1050.09n	igs15273.sp3	igs15273.clk_30s	igs15277.erp	2009/04/15	278.6335
cpbi1060.09o	csrj1060.09o	brdc1060.09n	igs15274.sp3	igs15274.clk_30s	igs15277.erp	2009/04/16	278.5670
cpbi1070.09o	csrj1070.09o	brdc1070.09n	igs15275.sp3	igs15275.clk_30s	igs15277.erp	2009/04/17	278.6267
cpbi1080.09o	csrj1080.09o	brdc1080.09n	igs15276.sp3	igs15276.clk_30s	igs15277.erp	2009/04/18	278.7502
cpbi1090.09o	csrj1090.09o	brdc1090.09n	igs15280.sp3	igs15280.clk_30s	igs15287.erp	2009/04/19	278.9118
cpbi1100.09o	csrj1100.09o	brdc1100.09n	igs15281.sp3	igs15281.clk_30s	igs15287.erp	2009/04/20	278.7399
cpbi1120.09o	csrj1120.09o	brdc1120.09n	igs15283.sp3	igs15283.clk_30s	igs15287.erp	2009/04/22	278.8463
cpbi1130.09o	csrj1130.09o	brdc1130.09n	igs15284.sp3	igs15284.clk_30s	igs15287.erp	2009/04/23	278.7632
cpbi1140.09o	csrj1140.09o	brdc1140.09n	igs15285.sp3	igs15285.clk_30s	igs15287.erp	2009/04/24	278.7611
cpbi1150.09o	csrj1150.09o	brdc1150.09n	igs15286.sp3	igs15286.clk_30s	igs15287.erp	2009/04/25	278.6705
cpbi1160.09o	csrj1160.09o	brdc1160.09n	igs15290.sp3	igs15290.clk_30s	igs15297.erp	2009/04/26	278.8925
cpbi1170.09o	csrj1170.09o	brdc1170.09n	igs15291.sp3	igs15291.clk_30s	igs15297.erp	2009/04/27	278.7460
cpbi1180.09o	csrj1180.09o	brdc1180.09n	igs15292.sp3	igs15292.clk_30s	igs15297.erp	2009/04/28	278.7049
cpbi1190.09o	csrj1190.09o	brdc1190.09n	igs15293.sp3	igs15293.clk_30s	igs15297.erp	2009/04/29	278.7366
cpbi0510.10o	csrj0510.10o	brdc0510.10n	igs15716.sp3	igs15716.clk_30s	igs15717.erp	2010/02/20	278.3779
cpbi0520.10o	csrj0520.10o	brdc0520.10n	igs15720.sp3	igs15720.clk_30s	igs15727.erp	2010/02/21	278.5648
cpbi0530.10o	csrj0530.10o	brdc0530.10n	igs15721.sp3	igs15721.clk_30s	igs15727.erp	2010/02/22	278.7788
cpbi0540.10o	csrj0540.10o	brdc0540.10n	igs15722.sp3	igs15722.clk_30s	igs15727.erp	2010/02/23	279.1310
cpbi0560.10o	csrj0560.10o	brdc0560.10n	igs15724.sp3	igs15724.clk_30s	igs15727.erp	2010/02/25	279.3105
cpbi0570.10o	csrj0570.10o	brdc0570.10n	igs15725.sp3	igs15725.clk_30s	igs15727.erp	2010/02/26	278.8310
cpbi0580.10o	csrj0580.10o	brdc0580.10n	igs15726.sp3	igs15726.clk_30s	igs15727.erp	2010/02/27	278.9032
cpbi0590.10o	csrj0590.10o	brdc0590.10n	igs15730.sp3	igs15730.clk_30s	igs15737.erp	2010/02/28	278.0917
cpbi0600.10o	csrj0600.10o	brdc0600.10n	igs15731.sp3	igs15731.clk_30s	igs15737.erp	2010/03/01	279.2088
cpbi0610.10o	csrj0610.10o	brdc0610.10n	igs15732.sp3	igs15732.clk_30s	igs15737.erp	2010/03/02	278.3792
cpbi0620.10o	csrj0620.10o	brdc0620.10n	igs15733.sp3	igs15733.clk_30s	igs15737.erp	2010/03/03	278.6049
cpbi0630.10o	csrj0630.10o	brdc0630.10n	igs15734.sp3	igs15734.clk_30s	igs15737.erp	2010/03/04	279.2046
cpbi0640.10o	csrj0640.10o	brdc0640.10n	igs15735.sp3	igs15735.clk_30s	igs15737.erp	2010/03/05	279.1595
cpbi0650.10o	csrj0650.10o	brdc0650.10n	igs15736.sp3	igs15736.clk_30s	igs15737.erp	2010/03/06	278.4043
cpbi0660.10o	csrj0660.10o	brdc0660.10n	igs15740.sp3	igs15740.clk_30s	igs15747.erp	2010/03/07	277.8677
cpbi0670.10o	csrj0670.10o	brdc0670.10n	igs15741.sp3	igs15741.clk_30s	igs15747.erp	2010/03/08	278.7124
cpbi0680.10o	csrj0680.10o	brdc0680.10n	igs15742.sp3	igs15742.clk_30s	igs15747.erp	2010/03/09	279.0107
cpbi0690.10o	csrj0690.10o	brdc0690.10n	igs15743.sp3	igs15743.clk_30s	igs15747.erp	2010/03/10	278.5174
cpbi0710.10o	csrj0710.10o	brdc0710.10n	igs15745.sp3	igs15745.clk_30s	igs15747.erp	2010/03/12	278.6700
cpbi0720.10o	csrj0720.10o	brdc0720.10n	igs15746.sp3	igs15746.clk_30s	igs15747.erp	2010/03/13	278.5503
cpbi0730.10o	csrj0730.10o	brdc0730.10n	igs15750.sp3	igs15750.clk_30s	igs15757.erp	2010/03/14	279.0192
cpbi0740.10o	csrj0740.10o	brdc0740.10n	igs15751.sp3	igs15751.clk_30s	igs15757.erp	2010/03/15	278.0436
cpbi0750.10o	csrj0750.10o	brdc0750.10n	igs15752.sp3	igs15752.clk_30s	igs15757.erp	2010/03/16	278.0089
cpbi0760.10o	csrj0760.10o	brdc0760.10n	igs15753.sp3	igs15753.clk_30s	igs15757.erp	2010/03/17	277.7333
cpbi0770.10o	csrj0770.10o	brdc0770.10n	igs15754.sp3	igs15754.clk_30s	igs15757.erp	2010/03/18	279.2725
cpbi0780.10o	csrj0780.10o	brdc0780.10n	igs15755.sp3	igs15755.clk_30s	igs15757.erp	2010/03/19	279.6083
cpbi0790.10o	csrj0790.10o	brdc0790.10n	igs15756.sp3	igs15756.clk_30s	igs15757.erp	2010/03/20	278.7130
cpbi0800.10o	csrj0800.10o	brdc0800.10n	igs15760.sp3	igs15760.clk_30s	igs15767.erp	2010/03/21	279.6012
cpbi0810.10o	csrj0810.10o	brdc0810.10n	igs15761.sp3	igs15761.clk_30s	igs15767.erp	2010/03/22	279.0131
cpbi0820.10o	csrj0820.10o	brdc0820.10n	igs15762.sp3	igs15762.clk_30s	igs15767.erp	2010/03/23	279.3848
cpbi0830.10o	csrj0830.10o	brdc0830.10n	igs15763.sp3	igs15763.clk_30s	igs15767.erp	2010/03/24	278.9222
cpbi0850.10o	csrj0850.10o	brdc0850.10n	igs15765.sp3	igs15765.clk_30s	igs15767.erp	2010/03/26	279.3747
cpbi0860.10o	csrj0860.10o	brdc0860.10n	igs15766.sp3	igs15766.clk_30s	igs15767.erp	2010/03/27	278.0894
cpbi0870.10o	csrj0870.10o	brdc0870.10n	igs15770.sp3	igs15770.clk_30s	igs15777.erp	2010/03/28	278.2786
cpbi0880.10o	csrj0880.10o	brdc0880.10n	igs15771.sp3	igs15771.clk_30s	igs15777.erp	2010/03/29	278.3963
cpbi0890.10o	csrj0890.10o	brdc0890.10n	igs15772.sp3	igs15772.clk_30s	igs15777.erp	2010/03/30	279.2214
cpbi0940.10o	csrj0940.10o	brdc0940.10n	igs15780.sp3	igs15780.clk_30s	igs15787.erp	2010/04/04	278.8894
cpbi0980.10o	csrj0980.10o	brdc0980.10n	igs15784.sp3	igs15784.clk_30s	igs15787.erp	2010/04/08	278.5559

cpbi0990.10o	csrj0990.10o	brdc0990.10n	igs15785.sp3	igs15785.clk_30s	igs15787.erp	2010/04/09	279.2550
cpbi1000.10o	csrj1000.10o	brdc1000.10n	igs15786.sp3	igs15786.clk_30s	igs15787.erp	2010/04/10	278.6750
cpbi1010.10o	csrj1010.10o	brdc1010.10n	igs15790.sp3	igs15790.clk_30s	igs15797.erp	2010/04/11	278.4057
cpbi1020.10o	csrj1020.10o	brdc1020.10n	igs15791.sp3	igs15791.clk_30s	igs15797.erp	2010/04/12	278.5832
cpbi1040.10o	csrj1040.10o	brdc1040.10n	igs15793.sp3	igs15793.clk_30s	igs15797.erp	2010/04/14	278.7768
cpbi1050.10o	csrj1050.10o	brdc1050.10n	igs15794.sp3	igs15794.clk_30s	igs15797.erp	2010/04/15	279.4035
cpbi1060.10o	csrj1060.10o	brdc1060.10n	igs15795.sp3	igs15795.clk_30s	igs15797.erp	2010/04/16	279.2014
cpbi1070.10o	csrj1070.10o	brdc1070.10n	igs15796.sp3	igs15796.clk_30s	igs15797.erp	2010/04/17	278.3343
cpbi1080.10o	csrj1080.10o	brdc1080.10n	igs15801.sp3	igs15801.clk_30s	igs15807.erp	2010/04/18	277.9750
cpbi1090.10o	csrj1090.10o	brdc1090.10n	igs15802.sp3	igs15802.clk_30s	igs15807.erp	2010/04/19	279.0195
cpbi1100.10o	csrj1100.10o	brdc1100.10n	igs15803.sp3	igs15803.clk_30s	igs15807.erp	2010/04/20	279.1210
cpbi1110.10o	csrj1110.10o	brdc1110.10n	igs15804.sp3	igs15804.clk_30s	igs15807.erp	2010/04/21	278.6455
cpbi1120.10o	csrj1120.10o	brdc1120.10n	igs15805.sp3	igs15805.clk_30s	igs15807.erp	2010/04/22	278.6124
cpbi1130.10o	csrj1130.10o	brdc1130.10n	igs15806.sp3	igs15806.clk_30s	igs15807.erp	2010/04/23	279.4519
cpbi1140.10o	csrj1140.10o	brdc1140.10n	igs15807.sp3	igs15807.clk_30s	igs15807.erp	2010/04/24	278.5059
cpbi1150.10o	csrj1150.10o	brdc1150.10n	igs15810.sp3	igs15810.clk_30s	igs15817.erp	2010/04/25	278.4447
cpbi1160.10o	csrj1160.10o	brdc1160.10n	igs15811.sp3	igs15811.clk_30s	igs15817.erp	2010/04/26	279.4595
cpbi1170.10o	csrj1170.10o	brdc1170.10n	igs15812.sp3	igs15812.clk_30s	igs15817.erp	2010/04/27	278.5441
cpbi1180.10o	csrj1180.10o	brdc1180.10n	igs15813.sp3	igs15813.clk_30s	igs15817.erp	2010/04/28	278.5215
cpbi1190.10o	csrj1190.10o	brdc1190.10n	igs15814.sp3	igs15814.clk_30s	igs15817.erp	2010/04/29	278.6141
cpbi1200.10o	csrj1200.10o	brdc1200.10n	igs15815.sp3	igs15815.clk_30s	igs15817.erp	2010/04/30	278.2028
cpbi1210.10o	csrj1210.10o	brdc1210.10n	igs15816.sp3	igs15816.clk_30s	igs15817.erp	2010/05/01	278.3162
cpbi1220.10o	csrj1220.10o	brdc1220.10n	igs15820.sp3	igs15820.clk_30s	igs15827.erp	2010/05/02	278.3434
cpbi1230.10o	csrj1230.10o	brdc1230.10n	igs15821.sp3	igs15821.clk_30s	igs15827.erp	2010/05/03	279.9808
cpbi1240.10o	csrj1240.10o	brdc1240.10n	igs15822.sp3	igs15822.clk_30s	igs15827.erp	2010/05/04	279.1342
cpbi1250.10o	csrj1250.10o	brdc1250.10n	igs15823.sp3	igs15823.clk_30s	igs15827.erp	2010/05/05	278.3185
cpbi1260.10o	csrj1260.10o	brdc1260.10n	igs15824.sp3	igs15824.clk_30s	igs15827.erp	2010/05/06	278.3638
cpbi1270.10o	csrj1270.10o	brdc1270.10n	igs15825.sp3	igs15825.clk_30s	igs15827.erp	2010/05/07	278.7405
cpbi1280.10o	csrj1280.10o	brdc1280.10n	igs15826.sp3	igs15826.clk_30s	igs15827.erp	2010/05/08	278.6507
cpbi1290.10o	csrj1290.10o	brdc1290.10n	igs15830.sp3	igs15830.clk_30s	igs15837.erp	2010/05/09	278.5711
cpbi1300.10o	csrj1300.10o	brdc1300.10n	igs15831.sp3	igs15831.clk_30s	igs15837.erp	2010/05/10	278.9306
cpbi1310.10o	csrj1310.10o	brdc1310.10n	igs15832.sp3	igs15832.clk_30s	igs15837.erp	2010/05/11	278.5744
cpbi1320.10o	csrj1320.10o	brdc1320.10n	igs15833.sp3	igs15833.clk_30s	igs15837.erp	2010/05/12	278.3851
cpbi1330.10o	csrj1330.10o	brdc1330.10n	igs15834.sp3	igs15834.clk_30s	igs15837.erp	2010/05/13	278.3725
cpbi1340.10o	csrj1340.10o	brdc1340.10n	igs15835.sp3	igs15835.clk_30s	igs15837.erp	2010/05/14	278.9573
cpbi1350.10o	csrj1350.10o	brdc1350.10n	igs15836.sp3	igs15836.clk_30s	igs15837.erp	2010/05/15	278.6692
cpbi1360.10o	csrj1360.10o	brdc1360.10n	igs15840.sp3	igs15840.clk_30s	igs15847.erp	2010/05/16	278.8026
cpbi1370.10o	csrj1370.10o	brdc1370.10n	igs15841.sp3	igs15841.clk_30s	igs15847.erp	2010/05/17	278.5773
cpbi1380.10o	csrj1380.10o	brdc1380.10n	igs15842.sp3	igs15842.clk_30s	igs15847.erp	2010/05/18	278.4707
cpbi1390.10o	csrj1390.10o	brdc1390.10n	igs15843.sp3	igs15843.clk_30s	igs15847.erp	2010/05/19	278.8308
cpbi1400.10o	csrj1400.10o	brdc1400.10n	igs15844.sp3	igs15844.clk_30s	igs15847.erp	2010/05/20	278.9452
cpbi1410.10o	csrj1410.10o	brdc1410.10n	igs15845.sp3	igs15845.clk_30s	igs15847.erp	2010/05/21	278.5371
cpbi1420.10o	csrj1420.10o	brdc1420.10n	igs15846.sp3	igs15846.clk_30s	igs15847.erp	2010/05/22	278.9735
cpbi1430.10o	csrj1430.10o	brdc1430.10n	igs15850.sp3	igs15850.clk_30s	igs15857.erp	2010/05/23	278.8059
cpbi1440.10o	csrj1440.10o	brdc1440.10n	igs15851.sp3	igs15851.clk_30s	igs15857.erp	2010/05/24	279.0550
cpbi1450.10o	csrj1450.10o	brdc1450.10n	igs15852.sp3	igs15852.clk_30s	igs15857.erp	2010/05/25	279.3435
cpbi1460.10o	csrj1460.10o	brdc1460.10n	igs15853.sp3	igs15853.clk_30s	igs15857.erp	2010/05/26	278.3753
cpbi1470.10o	csrj1470.10o	brdc1470.10n	igs15854.sp3	igs15854.clk_30s	igs15857.erp	2010/05/27	279.0225
cpbi1480.10o	csrj1480.10o	brdc1480.10n	igs15855.sp3	igs15855.clk_30s	igs15857.erp	2010/05/28	278.9796
cpbi1490.10o	csrj1490.10o	brdc1490.10n	igs15856.sp3	igs15856.clk_30s	igs15857.erp	2010/05/29	278.3388
cpbi1500.10o	csrj1500.10o	brdc1500.10n	igs15860.sp3	igs15860.clk_30s	igs15867.erp	2010/05/30	278.6264
cpbi1510.10o	csrj1510.10o	brdc1510.10n	igs15861.sp3	igs15861.clk_30s	igs15867.erp	2010/05/31	279.2147
cpbi1520.10o	csrj1520.10o	brdc1520.10n	igs15862.sp3	igs15862.clk_30s	igs15867.erp	2010/06/01	278.9581
cpbi1530.10o	csrj1530.10o	brdc1530.10n	igs15863.sp3	igs15863.clk_30s	igs15867.erp	2010/06/02	279.1662
cpbi1540.10o	csrj1540.10o	brdc1540.10n	igs15864.sp3	igs15864.clk_30s	igs15867.erp	2010/06/03	279.1185
cpbi1550.10o	csrj1550.10o	brdc1550.10n	igs15865.sp3	igs15865.clk_30s	igs15867.erp	2010/06/04	278.7226
cpbi1560.10o	csrj1560.10o	brdc1560.10n	igs15866.sp3	igs15866.clk_30s	igs15867.erp	2010/06/05	278.5765
cpbi1570.10o	csrj1570.10o	brdc1570.10n	igs15870.sp3	igs15870.clk_30s	igs15877.erp	2010/06/06	278.5386
cpbi1580.10o	csrj1580.10o	brdc1580.10n	igs15871.sp3	igs15871.clk_30s	igs15877.erp	2010/06/07	278.2601
cpbi1590.10o	csrj1590.10o	brdc1590.10n	igs15872.sp3	igs15872.clk_30s	igs15877.erp	2010/06/08	278.8579
cpbi1600.10o	csrj1600.10o	brdc1600.10n	igs15873.sp3	igs15873.clk_30s	igs15877.erp	2010/06/09	278.9994
cpbi1610.10o	csrj1610.10o	brdc1610.10n	igs15874.sp3	igs15874.clk_30s	igs15877.erp	2010/06/10	279.2641
cpbi1620.10o	csrj1620.10o	brdc1620.10n	igs15875.sp3	igs15875.clk_30s	igs15877.erp	2010/06/11	278.9922
cpbi1630.10o	csrj1630.10o	brdc1630.10n	igs15876.sp3	igs15876.clk_30s	igs15877.erp	2010/06/12	278.8067
cpbi1640.10o	csrj1640.10o	brdc1640.10n	igs15880.sp3	igs15880.clk_30s	igs15887.erp	2010/06/13	279.0765
cpbi1650.10o	csrj1650.10o	brdc1650.10n	igs15881.sp3	igs15881.clk_30s	igs15887.erp	2010/06/14	278.8329
cpbi1660.10o	csrj1660.10o	brdc1660.10n	igs15882.sp3	igs15882.clk_30s	igs15887.erp	2010/06/15	278.4272
cpbi1670.10o	csrj1670.10o	brdc1670.10n	igs15883.sp3	igs15883.clk_30s	igs15887.erp	2010/06/16	279.0982
cpbi1690.10o	csrj1690.10o	brdc1690.10n	igs15885.sp3	igs15885.clk_30s	igs15887.erp	2010/06/18	278.1612
cpbi1700.10o	csrj1700.10o	brdc1700.10n	igs15886.sp3	igs15886.clk_30s	igs15887.erp	2010/06/19	278.1991

cpbi1710.10o	csrj1710.10o	brdc1710.10n	igs15890.sp3	igs15890.clk_30s	igs15897.erp	2010/06/20	278.5793
cpbi1720.10o	csrj1720.10o	brdc1720.10n	igs15891.sp3	igs15891.clk_30s	igs15897.erp	2010/06/21	278.1788
cpbi1730.10o	csrj1730.10o	brdc1730.10n	igs15892.sp3	igs15892.clk_30s	igs15897.erp	2010/06/22	277.9150
cpbi1740.10o	csrj1740.10o	brdc1740.10n	igs15893.sp3	igs15893.clk_30s	igs15897.erp	2010/06/23	278.8999
cpbi1750.10o	csrj1750.10o	brdc1750.10n	igs15894.sp3	igs15894.clk_30s	igs15897.erp	2010/06/24	278.5875
cpbi1760.10o	csrj1760.10o	brdc1760.10n	igs15895.sp3	igs15895.clk_30s	igs15897.erp	2010/06/25	278.8825
cpbi1770.10o	csrj1770.10o	brdc1770.10n	igs15896.sp3	igs15896.clk_30s	igs15897.erp	2010/06/26	279.1385
cpbi1780.10o	csrj1780.10o	brdc1780.10n	igs15900.sp3	igs15900.clk_30s	igs15907.erp	2010/06/27	279.1773
cpbi1790.10o	csrj1790.10o	brdc1790.10n	igs15901.sp3	igs15901.clk_30s	igs15907.erp	2010/06/28	279.3616
cpbi1800.10o	csrj1800.10o	brdc1800.10n	igs15902.sp3	igs15902.clk_30s	igs15907.erp	2010/06/29	278.1532
cpbi0120.11o	csrj0120.11o	brdc0120.11n	igs16183.sp3	igs16183.clk_30s	igs16187.erp	2011/01/12	278.9445
cpbi0130.11o	csrj0130.11o	brdc0130.11n	igs16184.sp3	igs16184.clk_30s	igs16187.erp	2011/01/13	277.6664
cpbi0140.11o	csrj0140.11o	brdc0140.11n	igs16185.sp3	igs16185.clk_30s	igs16187.erp	2011/01/14	279.1724
cpbi0150.11o	csrj0150.11o	brdc0150.11n	igs16186.sp3	igs16186.clk_30s	igs16187.erp	2011/01/15	278.5765
cpbi0160.11o	csrj0160.11o	brdc0160.11n	igs16190.sp3	igs16190.clk_30s	igs16197.erp	2011/01/16	278.1819
cpbi0170.11o	csrj0170.11o	brdc0170.11n	igs16191.sp3	igs16191.clk_30s	igs16197.erp	2011/01/17	278.7307
cpbi0180.11o	csrj0180.11o	brdc0180.11n	igs16192.sp3	igs16192.clk_30s	igs16197.erp	2011/01/18	279.0230
cpbi0190.11o	csrj0190.11o	brdc0190.11n	igs16193.sp3	igs16193.clk_30s	igs16197.erp	2011/01/19	279.6121
cpbi0200.11o	csrj0200.11o	brdc0200.11n	igs16194.sp3	igs16194.clk_30s	igs16197.erp	2011/01/20	279.3389
cpbi0210.11o	csrj0210.11o	brdc0210.11n	igs16195.sp3	igs16195.clk_30s	igs16197.erp	2011/01/21	279.0128
cpbi0220.11o	csrj0220.11o	brdc0220.11n	igs16196.sp3	igs16196.clk_30s	igs16197.erp	2011/01/22	278.8124
cpbi0230.11o	csrj0230.11o	brdc0230.11n	igs16200.sp3	igs16200.clk_30s	igs16207.erp	2011/01/23	278.7469
cpbi0240.11o	csrj0240.11o	brdc0240.11n	igs16201.sp3	igs16201.clk_30s	igs16207.erp	2011/01/24	277.7155
cpbi0250.11o	csrj0250.11o	brdc0250.11n	igs16202.sp3	igs16202.clk_30s	igs16207.erp	2011/01/25	278.6820
cpbi0260.11o	csrj0260.11o	brdc0260.11n	igs16203.sp3	igs16203.clk_30s	igs16207.erp	2011/01/26	278.7403
cpbi0270.11o	csrj0270.11o	brdc0270.11n	igs16204.sp3	igs16204.clk_30s	igs16207.erp	2011/01/27	278.7957
cpbi0280.11o	csrj0280.11o	brdc0280.11n	igs16205.sp3	igs16205.clk_30s	igs16207.erp	2011/01/28	278.9517

## B.2 CDNP station

RINEX Observation		RINEX *NAV/CLK, SP3 or SBS/EMS			EOP data file	Date	Height (m)
Rover	Base station	IGS_NAV	IGS_EPH	IGS_CLK_30s			
cdnp1800.10o	csrj1800.10o	brdc1800.10n	igs15902.sp3	igs15902.clk_30s	igs15907.erp	2010/06/29	234.5200
cdnp1810.10o	csrj1810.10o	brdc1810.10n	igs15903.sp3	igs15903.clk_30s	igs15907.erp	2010/06/30	234.5181
cdnp1820.10o	csrj1820.10o	brdc1820.10n	igs15904.sp3	igs15904.clk_30s	igs15907.erp	2010/07/01	234.5187
cdnp1830.10o	csrj1830.10o	brdc1830.10n	igs15905.sp3	igs15905.clk_30s	igs15907.erp	2010/07/02	234.5180
cdnp1840.10o	csrj1840.10o	brdc1840.10n	igs15906.sp3	igs15906.clk_30s	igs15907.erp	2010/07/03	234.5118
cdnp1850.10o	csrj1850.10o	brdc1850.10n	igs15910.sp3	igs15910.clk_30s	igs15917.erp	2010/07/04	234.5035
cdnp1860.10o	csrj1860.10o	brdc1860.10n	igs15911.sp3	igs15911.clk_30s	igs15917.erp	2010/07/05	234.5110
cdnp1870.10o	csrj1870.10o	brdc1870.10n	igs15912.sp3	igs15912.clk_30s	igs15917.erp	2010/07/06	234.5250
cdnp1880.10o	csrj1880.10o	brdc1880.10n	igs15913.sp3	igs15913.clk_30s	igs15917.erp	2010/07/07	234.5200
cdnp1890.10o	csrj1890.10o	brdc1890.10n	igs15914.sp3	igs15914.clk_30s	igs15917.erp	2010/07/08	234.5295
cdnp1900.10o	csrj1900.10o	brdc1900.10n	igs15915.sp3	igs15915.clk_30s	igs15917.erp	2010/07/09	234.4651
cdnp1910.10o	csrj1910.10o	brdc1910.10n	igs15916.sp3	igs15916.clk_30s	igs15917.erp	2010/07/10	234.5246
cdnp1920.10o	csrj1920.10o	brdc1920.10n	igs15920.sp3	igs15920.clk_30s	igs15927.erp	2010/07/11	234.5508
cdnp1930.10o	csrj1930.10o	brdc1930.10n	igs15921.sp3	igs15921.clk_30s	igs15927.erp	2010/07/12	234.5179
cdnp1940.10o	csrj1940.10o	brdc1940.10n	igs15922.sp3	igs15922.clk_30s	igs15927.erp	2010/07/13	234.5229
cdnp1950.10o	csrj1950.10o	brdc1950.10n	igs15923.sp3	igs15923.clk_30s	igs15927.erp	2010/07/14	234.5241
cdnp1960.10o	csrj1960.10o	brdc1960.10n	igs15924.sp3	igs15924.clk_30s	igs15927.erp	2010/07/15	234.5244
cdnp1970.10o	csrj1970.10o	brdc1970.10n	igs15925.sp3	igs15925.clk_30s	igs15927.erp	2010/07/16	234.5241
cdnp1980.10o	csrj1980.10o	brdc1980.10n	igs15926.sp3	igs15926.clk_30s	igs15927.erp	2010/07/17	234.5276
cdnp1990.10o	csrj1990.10o	brdc1990.10n	igs15930.sp3	igs15930.clk_30s	igs15937.erp	2010/07/18	234.5151
cdnp2000.10o	csrj2000.10o	brdc2000.10n	igs15931.sp3	igs15931.clk_30s	igs15937.erp	2010/07/19	234.5163
cdnp2010.10o	csrj2010.10o	brdc2010.10n	igs15932.sp3	igs15932.clk_30s	igs15937.erp	2010/07/20	234.5166
cdnp2020.10o	csrj2020.10o	brdc2020.10n	igs15933.sp3	igs15933.clk_30s	igs15937.erp	2010/07/21	234.5050
cdnp2030.10o	csrj2030.10o	brdc2030.10n	igs15934.sp3	igs15934.clk_30s	igs15937.erp	2010/07/22	234.5237
cdnp2040.10o	csrj2040.10o	brdc2040.10n	igs15935.sp3	igs15935.clk_30s	igs15937.erp	2010/07/23	234.5254
cdnp2050.10o	csrj2050.10o	brdc2050.10n	igs15936.sp3	igs15936.clk_30s	igs15937.erp	2010/07/24	234.5181
cdnp2060.10o	csrj2060.10o	brdc2060.10n	igs15940.sp3	igs15940.clk_30s	igs15947.erp	2010/07/25	234.5264
cdnp2070.10o	csrj2070.10o	brdc2070.10n	igs15941.sp3	igs15941.clk_30s	igs15947.erp	2010/07/26	234.5298
cdnp2080.10o	csrj2080.10o	brdc2080.10n	igs15942.sp3	igs15942.clk_30s	igs15947.erp	2010/07/27	234.5202
cdnp2090.10o	csrj2090.10o	brdc2090.10n	igs15943.sp3	igs15943.clk_30s	igs15947.erp	2010/07/28	234.5028
cdnp2100.10o	csrj2100.10o	brdc2100.10n	igs15944.sp3	igs15944.clk_30s	igs15947.erp	2010/07/29	234.5382
cdnp2110.10o	csrj2110.10o	brdc2110.10n	igs15945.sp3	igs15945.clk_30s	igs15947.erp	2010/07/30	234.5246
cdnp2120.10o	csrj2120.10o	brdc2120.10n	igs15946.sp3	igs15946.clk_30s	igs15947.erp	2010/07/31	234.5056
cdnp2130.10o	csrj2130.10o	brdc2130.10n	igs15950.sp3	igs15950.clk_30s	igs15957.erp	2010/08/01	234.5095
cdnp2140.10o	csrj2140.10o	brdc2140.10n	igs15951.sp3	igs15951.clk_30s	igs15957.erp	2010/08/02	234.5109
cdnp2150.10o	csrj2150.10o	brdc2150.10n	igs15952.sp3	igs15952.clk_30s	igs15957.erp	2010/08/03	234.5158
cdnp2160.10o	csrj2160.10o	brdc2160.10n	igs15953.sp3	igs15953.clk_30s	igs15957.erp	2010/08/04	234.5468



cdnp2170.10o	csrj2170.10o	brdc2170.10n	igs15954.sp3	igs15954.clk_30s	igs15957.erp	2010/08/05	234.5226
cdnp2180.10o	csrj2180.10o	brdc2180.10n	igs15955.sp3	igs15955.clk_30s	igs15957.erp	2010/08/06	234.5312
cdnp2190.10o	csrj2190.10o	brdc2190.10n	igs15956.sp3	igs15956.clk_30s	igs15957.erp	2010/08/07	234.5313
cdnp2200.10o	csrj2200.10o	brdc2200.10n	igs15960.sp3	igs15960.clk_30s	igs15967.erp	2010/08/08	234.5272
cdnp2210.10o	csrj2210.10o	brdc2210.10n	igs15961.sp3	igs15961.clk_30s	igs15967.erp	2010/08/09	234.5391
cdnp2220.10o	csrj2220.10o	brdc2220.10n	igs15962.sp3	igs15962.clk_30s	igs15967.erp	2010/08/10	234.5292
cdnp2230.10o	csrj2230.10o	brdc2230.10n	igs15963.sp3	igs15963.clk_30s	igs15967.erp	2010/08/11	234.5192
cdnp2240.10o	csrj2240.10o	brdc2240.10n	igs15964.sp3	igs15964.clk_30s	igs15967.erp	2010/08/12	234.5069
cdnp2250.10o	csrj2250.10o	brdc2250.10n	igs15965.sp3	igs15965.clk_30s	igs15967.erp	2010/08/13	234.5372
cdnp2260.10o	csrj2260.10o	brdc2260.10n	igs15966.sp3	igs15966.clk_30s	igs15967.erp	2010/08/14	234.5229
cdnp2270.10o	csrj2270.10o	brdc2270.10n	igs15970.sp3	igs15970.clk_30s	igs15977.erp	2010/08/15	234.5211
cdnp2280.10o	csrj2280.10o	brdc2280.10n	igs15971.sp3	igs15971.clk_30s	igs15977.erp	2010/08/16	234.5157
cdnp2290.10o	csrj2290.10o	brdc2290.10n	igs15972.sp3	igs15972.clk_30s	igs15977.erp	2010/08/17	234.5048
cdnp2300.10o	csrj2300.10o	brdc2300.10n	igs15973.sp3	igs15973.clk_30s	igs15977.erp	2010/08/18	234.5278
cdnp2310.10o	csrj2310.10o	brdc2310.10n	igs15974.sp3	igs15974.clk_30s	igs15977.erp	2010/08/19	234.5064
cdnp2320.10o	csrj2320.10o	brdc2320.10n	igs15975.sp3	igs15975.clk_30s	igs15977.erp	2010/08/20	234.5030
cdnp2330.10o	csrj2330.10o	brdc2330.10n	igs15976.sp3	igs15976.clk_30s	igs15977.erp	2010/08/21	234.4916
cdnp2340.10o	csrj2340.10o	brdc2340.10n	igs15980.sp3	igs15980.clk_30s	igs15987.erp	2010/08/22	234.5153
cdnp2350.10o	csrj2350.10o	brdc2350.10n	igs15981.sp3	igs15981.clk_30s	igs15987.erp	2010/08/23	234.5248
cdnp2360.10o	csrj2360.10o	brdc2360.10n	igs15982.sp3	igs15982.clk_30s	igs15987.erp	2010/08/24	234.5305
cdnp2370.10o	csrj2370.10o	brdc2370.10n	igs15983.sp3	igs15983.clk_30s	igs15987.erp	2010/08/25	234.5247
cdnp2380.10o	csrj2380.10o	brdc2380.10n	igs15984.sp3	igs15984.clk_30s	igs15987.erp	2010/08/26	234.5288
cdnp2390.10o	csrj2390.10o	brdc2390.10n	igs15985.sp3	igs15985.clk_30s	igs15987.erp	2010/08/27	234.5106
cdnp2400.10o	csrj2400.10o	brdc2400.10n	igs15986.sp3	igs15986.clk_30s	igs15987.erp	2010/08/28	234.5185
cdnp2410.10o	csrj2410.10o	brdc2410.10n	igs15990.sp3	igs15990.clk_30s	igs15997.erp	2010/08/29	234.5121
cdnp2420.10o	csrj2420.10o	brdc2420.10n	igs15991.sp3	igs15991.clk_30s	igs15997.erp	2010/08/30	234.4746
cdnp2430.10o	csrj2430.10o	brdc2430.10n	igs15992.sp3	igs15992.clk_30s	igs15997.erp	2010/08/31	234.5177
cdnp2450.10o	csrj2450.10o	brdc2450.10n	igs15994.sp3	igs15994.clk_30s	igs15997.erp	2010/09/02	234.4773
cdnp2460.10o	csrj2460.10o	brdc2460.10n	igs15995.sp3	igs15995.clk_30s	igs15997.erp	2010/09/03	234.4912
cdnp2470.10o	csrj2470.10o	brdc2470.10n	igs15996.sp3	igs15996.clk_30s	igs15997.erp	2010/09/04	234.4895
cdnp2480.10o	csrj2480.10o	brdc2480.10n	igs16000.sp3	igs16000.clk_30s	igs16007.erp	2010/09/05	234.4933
cdnp2490.10o	csrj2490.10o	brdc2490.10n	igs16001.sp3	igs16001.clk_30s	igs16007.erp	2010/09/06	234.5128
cdnp2500.10o	csrj2500.10o	brdc2500.10n	igs16002.sp3	igs16002.clk_30s	igs16007.erp	2010/09/07	234.5049
cdnp2510.10o	csrj2510.10o	brdc2510.10n	igs16003.sp3	igs16003.clk_30s	igs16007.erp	2010/09/08	234.4906
cdnp2520.10o	csrj2520.10o	brdc2520.10n	igs16004.sp3	igs16004.clk_30s	igs16007.erp	2010/09/09	234.5144
cdnp2530.10o	csrj2530.10o	brdc2530.10n	igs16005.sp3	igs16005.clk_30s	igs16007.erp	2010/09/10	234.5028
cdnp2540.10o	csrj2540.10o	brdc2540.10n	igs16006.sp3	igs16006.clk_30s	igs16007.erp	2010/09/11	234.4870
cdnp2550.10o	csrj2550.10o	brdc2550.10n	igs16010.sp3	igs16010.clk_30s	igs16017.erp	2010/09/12	234.5146
cdnp2560.10o	csrj2560.10o	brdc2560.10n	igs16011.sp3	igs16011.clk_30s	igs16017.erp	2010/09/14	234.4705
cdnp2580.10o	csrj2580.10o	brdc2580.10n	igs16012.sp3	igs16012.clk_30s	igs16017.erp	2010/09/15	234.4702
cdnp2590.10o	csrj2590.10o	brdc2590.10n	igs16013.sp3	igs16013.clk_30s	igs16017.erp	2010/09/16	234.5414
cdnp2600.10o	csrj2600.10o	brdc2600.10n	igs16014.sp3	igs16014.clk_30s	igs16017.erp	2010/09/18	234.5454
cdnp2620.10o	csrj2620.10o	brdc2620.10n	igs16020.sp3	igs16020.clk_30s	igs16027.erp	2010/09/19	234.5646
cdnp2630.10o	csrj2630.10o	brdc2630.10n	igs16021.sp3	igs16021.clk_30s	igs16027.erp	2010/09/20	234.5534
cdnp2640.10o	csrj2640.10o	brdc2640.10n	igs16022.sp3	igs16022.clk_30s	igs16027.erp	2010/09/21	234.5508
cdnp2650.10o	csrj2650.10o	brdc2650.10n	igs16023.sp3	igs16023.clk_30s	igs16027.erp	2010/09/22	234.5606
cdnp2660.10o	csrj2660.10o	brdc2660.10n	igs16024.sp3	igs16024.clk_30s	igs16027.erp	2010/09/23	234.5508
cdnp2670.10o	csrj2670.10o	brdc2670.10n	igs16025.sp3	igs16025.clk_30s	igs16027.erp	2010/09/24	234.5357
cdnp2680.10o	csrj2680.10o	brdc2680.10n	igs16026.sp3	igs16026.clk_30s	igs16027.erp	2010/09/25	234.5461
cdnp2690.10o	csrj2690.10o	brdc2690.10n	igs16030.sp3	igs16030.clk_30s	igs16037.erp	2010/09/26	234.5214
cdnp2700.10o	csrj2700.10o	brdc2700.10n	igs16031.sp3	igs16031.clk_30s	igs16037.erp	2010/09/27	234.5282
cdnp2710.10o	csrj2710.10o	brdc2710.10n	igs16032.sp3	igs16032.clk_30s	igs16037.erp	2010/09/28	234.5297
cdnp2720.10o	csrj2720.10o	brdc2720.10n	igs16033.sp3	igs16033.clk_30s	igs16037.erp	2010/09/29	234.5495
cdnp2730.10o	csrj2730.10o	brdc2730.10n	igs16034.sp3	igs16034.clk_30s	igs16037.erp	2010/09/30	234.5251
cdnp2740.10o	csrj2740.10o	brdc2740.10n	igs16035.sp3	igs16035.clk_30s	igs16037.erp	2010/10/01	234.5148
cdnp2760.10o	csrj2760.10o	brdc2760.10n	igs16040.sp3	igs16040.clk_30s	igs16047.erp	2010/10/03	234.5143
cdnp2770.10o	csrj2770.10o	brdc2770.10n	igs16041.sp3	igs16041.clk_30s	igs16047.erp	2010/10/04	234.5049
cdnp2780.10o	csrj2780.10o	brdc2780.10n	igs16042.sp3	igs16042.clk_30s	igs16047.erp	2010/10/05	234.5045
cdnp2790.10o	csrj2790.10o	brdc2790.10n	igs16043.sp3	igs16043.clk_30s	igs16047.erp	2010/10/06	234.5287
cdnp2800.10o	csrj2800.10o	brdc2800.10n	igs16044.sp3	igs16044.clk_30s	igs16047.erp	2010/10/07	234.5744
cdnp2810.10o	csrj2810.10o	brdc2810.10n	igs16045.sp3	igs16045.clk_30s	igs16047.erp	2010/10/08	234.5405
cdnp2820.10o	csrj2820.10o	brdc2820.10n	igs16046.sp3	igs16046.clk_30s	igs16047.erp	2010/10/10	234.5390
cdnp2830.10o	csrj2830.10o	brdc2830.10n	igs16050.sp3	igs16050.clk_30s	igs16057.erp	2010/10/11	234.5073
cdnp2850.10o	csrj2850.10o	brdc2850.10n	igs16052.sp3	igs16052.clk_30s	igs16057.erp	2010/10/12	234.5143
cdnp2860.10o	csrj2860.10o	brdc2860.10n	igs16053.sp3	igs16053.clk_30s	igs16057.erp	2010/10/13	234.5378
cdnp2870.10o	csrj2870.10o	brdc2870.10n	igs16054.sp3	igs16054.clk_30s	igs16057.erp	2010/10/14	234.5198
cdnp2880.10o	csrj2880.10o	brdc2880.10n	igs16055.sp3	igs16055.clk_30s	igs16057.erp	2010/10/15	234.5458
cdnp2890.10o	csrj2890.10o	brdc2890.10n	igs16056.sp3	igs16056.clk_30s	igs16057.erp	2010/10/16	234.5235
cdnp2900.10o	csrj2900.10o	brdc2900.10n	igs16060.sp3	igs16060.clk_30s	igs16067.erp	2010/10/17	234.4943
cdnp2910.10o	csrj2910.10o	brdc2910.10n	igs16061.sp3	igs16061.clk_30s	igs16067.erp	2010/10/18	234.5088

cdnp2920.10o	csrj2920.10o	brdc2920.10n	igs16062.sp3	igs16062.clk_30s	igs16067.erp	2010/10/19	234.5125
cdnp2930.10o	csrj2930.10o	brdc2930.10n	igs16063.sp3	igs16063.clk_30s	igs16067.erp	2010/10/20	234.5259
cdnp2940.10o	csrj2940.10o	brdc2940.10n	igs16064.sp3	igs16064.clk_30s	igs16067.erp	2010/10/21	234.5062
cdnp2950.10o	csrj2950.10o	brdc2950.10n	igs16065.sp3	igs16065.clk_30s	igs16067.erp	2010/10/22	234.5026
cdnp2960.10o	csrj2960.10o	brdc2960.10n	igs16066.sp3	igs16066.clk_30s	igs16067.erp	2010/10/23	234.4989
cdnp2970.10o	csrj2970.10o	brdc2970.10n	igs16070.sp3	igs16070.clk_30s	igs16077.erp	2010/10/24	234.5134
cdnp2980.10o	csrj2980.10o	brdc2980.10n	igs16071.sp3	igs16071.clk_30s	igs16077.erp	2010/10/25	234.5046
cdnp2990.10o	csrj2990.10o	brdc2990.10n	igs16072.sp3	igs16072.clk_30s	igs16077.erp	2010/10/26	234.5346
cdnp3000.10o	csrj3000.10o	brdc3000.10n	igs16073.sp3	igs16073.clk_30s	igs16077.erp	2010/10/27	234.5385
cdnp3010.10o	csrj3010.10o	brdc3010.10n	igs16074.sp3	igs16074.clk_30s	igs16077.erp	2010/10/28	234.5154
cdnp3020.10o	csrj3020.10o	brdc3020.10n	igs16075.sp3	igs16075.clk_30s	igs16077.erp	2010/10/29	234.4932
cdnp3030.10o	csrj3030.10o	brdc3030.10n	igs16076.sp3	igs16076.clk_30s	igs16077.erp	2010/10/30	234.5155
cdnp3040.10o	csrj3040.10o	brdc3040.10n	igs16080.sp3	igs16080.clk_30s	igs16087.erp	2010/10/31	234.5542
cdnp3050.10o	csrj3050.10o	brdc3050.10n	igs16081.sp3	igs16081.clk_30s	igs16087.erp	2010/11/01	234.5650
cdnp3060.10o	csrj3060.10o	brdc3060.10n	igs16082.sp3	igs16082.clk_30s	igs16087.erp	2010/11/02	234.5364
cdnp3070.10o	csrj3070.10o	brdc3070.10n	igs16083.sp3	igs16083.clk_30s	igs16087.erp	2010/11/03	234.5204
cdnp3080.10o	csrj3080.10o	brdc3080.10n	igs16084.sp3	igs16084.clk_30s	igs16087.erp	2010/11/04	234.5435
cdnp3090.10o	csrj3090.10o	brdc3090.10n	igs16085.sp3	igs16085.clk_30s	igs16087.erp	2010/11/05	234.5403
cdnp3100.10o	csrj3100.10o	brdc3100.10n	igs16086.sp3	igs16086.clk_30s	igs16087.erp	2010/11/06	234.5314
cdnp3110.10o	csrj3110.10o	brdc3110.10n	igs16090.sp3	igs16090.clk_30s	igs16097.erp	2010/11/07	234.4958
cdnp3120.10o	csrj3120.10o	brdc3120.10n	igs16091.sp3	igs16091.clk_30s	igs16097.erp	2010/11/08	234.4938
cdnp3130.10o	csrj3130.10o	brdc3130.10n	igs16092.sp3	igs16092.clk_30s	igs16097.erp	2010/11/09	234.5004
cdnp3140.10o	csrj3140.10o	brdc3140.10n	igs16093.sp3	igs16093.clk_30s	igs16097.erp	2010/11/10	234.4968
cdnp3150.10o	csrj3150.10o	brdc3150.10n	igs16094.sp3	igs16094.clk_30s	igs16097.erp	2010/11/11	234.5165
cdnp3160.10o	csrj3160.10o	brdc3160.10n	igs16095.sp3	igs16095.clk_30s	igs16097.erp	2010/11/12	234.5491
cdnp3170.10o	csrj3170.10o	brdc3170.10n	igs16096.sp3	igs16096.clk_30s	igs16097.erp	2010/11/13	234.5059
cdnp3180.10o	csrj3180.10o	brdc3180.10n	igs16100.sp3	igs16100.clk_30s	igs16107.erp	2010/11/14	234.5649
cdnp3190.10o	csrj3190.10o	brdc3190.10n	igs16101.sp3	igs16101.clk_30s	igs16107.erp	2010/11/15	234.5184
cdnp3200.10o	csrj3200.10o	brdc3200.10n	igs16102.sp3	igs16102.clk_30s	igs16107.erp	2010/11/16	234.5085
cdnp3210.10o	csrj3210.10o	brdc3210.10n	igs16103.sp3	igs16103.clk_30s	igs16107.erp	2010/11/17	234.4886
cdnp3220.10o	csrj3220.10o	brdc3220.10n	igs16104.sp3	igs16104.clk_30s	igs16107.erp	2010/11/18	234.4720
cdnp3230.10o	csrj3230.10o	brdc3230.10n	igs16105.sp3	igs16105.clk_30s	igs16107.erp	2010/11/19	234.5069
cdnp3240.10o	csrj3240.10o	brdc3240.10n	igs16106.sp3	igs16106.clk_30s	igs16107.erp	2010/11/20	234.5044
cdnp3250.10o	csrj3250.10o	brdc3250.10n	igs16110.sp3	igs16110.clk_30s	igs16117.erp	2010/11/21	234.5253
cdnp3260.10o	csrj3260.10o	brdc3260.10n	igs16111.sp3	igs16111.clk_30s	igs16117.erp	2010/11/22	234.5269
cdnp3270.10o	csrj3270.10o	brdc3270.10n	igs16112.sp3	igs16112.clk_30s	igs16117.erp	2010/11/23	234.4984
cdnp3280.10o	csrj3280.10o	brdc3280.10n	igs16113.sp3	igs16113.clk_30s	igs16117.erp	2010/11/24	234.5239
cdnp3290.10o	csrj3290.10o	brdc3290.10n	igs16114.sp3	igs16114.clk_30s	igs16117.erp	2010/11/25	234.5260
cdnp3300.10o	csrj3300.10o	brdc3300.10n	igs16115.sp3	igs16115.clk_30s	igs16117.erp	2010/11/26	234.5313
cdnp3310.10o	csrj3310.10o	brdc3310.10n	igs16116.sp3	igs16116.clk_30s	igs16117.erp	2010/11/27	234.5308
cdnp3320.10o	csrj3320.10o	brdc3320.10n	igs16120.sp3	igs16120.clk_30s	igs16127.erp	2010/11/28	234.5522
cdnp3330.10o	csrj3330.10o	brdc3330.10n	igs16121.sp3	igs16121.clk_30s	igs16127.erp	2010/11/29	234.4899
cdnp3340.10o	csrj3340.10o	brdc3340.10n	igs16122.sp3	igs16122.clk_30s	igs16127.erp	2010/11/30	234.5325
cdnp3350.10o	csrj3350.10o	brdc3350.10n	igs16123.sp3	igs16123.clk_30s	igs16127.erp	2010/12/01	234.5116
cdnp3360.10o	csrj3360.10o	brdc3360.10n	igs16124.sp3	igs16124.clk_30s	igs16127.erp	2010/12/02	234.5260
cdnp3370.10o	csrj3370.10o	brdc3370.10n	igs16125.sp3	igs16125.clk_30s	igs16127.erp	2010/12/03	234.5100
cdnp3380.10o	csrj3380.10o	brdc3380.10n	igs16126.sp3	igs16126.clk_30s	igs16127.erp	2010/12/04	234.4962
cdnp3390.10o	csrj3390.10o	brdc3390.10n	igs16130.sp3	igs16130.clk_30s	igs16137.erp	2010/12/05	234.4980
cdnp3400.10o	csrj3400.10o	brdc3400.10n	igs16131.sp3	igs16131.clk_30s	igs16137.erp	2010/12/06	234.5535
cdnp3410.10o	csrj3410.10o	brdc3410.10n	igs16132.sp3	igs16132.clk_30s	igs16137.erp	2010/12/07	234.5313
cdnp3420.10o	csrj3420.10o	brdc3420.10n	igs16133.sp3	igs16133.clk_30s	igs16137.erp	2010/12/08	234.5552
cdnp3430.10o	csrj3430.10o	brdc3430.10n	igs16134.sp3	igs16134.clk_30s	igs16137.erp	2010/12/09	234.5402
cdnp3440.10o	csrj3440.10o	brdc3440.10n	igs16135.sp3	igs16135.clk_30s	igs16137.erp	2010/12/10	234.4955
cdnp3450.10o	csrj3450.10o	brdc3450.10n	igs16136.sp3	igs16136.clk_30s	igs16137.erp	2010/12/11	234.4977
cdnp3460.10o	csrj3460.10o	brdc3460.10n	igs16140.sp3	igs16140.clk_30s	igs16147.erp	2010/12/12	234.5087
cdnp3470.10o	csrj3470.10o	brdc3470.10n	igs16141.sp3	igs16141.clk_30s	igs16147.erp	2010/12/13	234.5193
cdnp3480.10o	csrj3480.10o	brdc3480.10n	igs16142.sp3	igs16142.clk_30s	igs16147.erp	2010/12/14	234.5285
cdnp3490.10o	csrj3490.10o	brdc3490.10n	igs16143.sp3	igs16143.clk_30s	igs16147.erp	2010/12/15	234.5252
cdnp3500.10o	csrj3500.10o	brdc3500.10n	igs16144.sp3	igs16144.clk_30s	igs16147.erp	2010/12/16	234.4811
cdnp3510.10o	csrj3510.10o	brdc3510.10n	igs16145.sp3	igs16145.clk_30s	igs16147.erp	2010/12/17	234.4937
cdnp3520.10o	csrj3520.10o	brdc3520.10n	igs16146.sp3	igs16146.clk_30s	igs16147.erp	2010/12/18	234.5002
cdnp3530.10o	csrj3530.10o	brdc3530.10n	igs16150.sp3	igs16150.clk_30s	igs16157.erp	2010/12/19	234.5430
cdnp3540.10o	csrj3540.10o	brdc3540.10n	igs16151.sp3	igs16151.clk_30s	igs16157.erp	2010/12/20	234.5287
cdnp3550.10o	csrj3550.10o	brdc3550.10n	igs16152.sp3	igs16152.clk_30s	igs16157.erp	2010/12/21	234.5078
cdnp3560.10o	csrj3560.10o	brdc3560.10n	igs16153.sp3	igs16153.clk_30s	igs16157.erp	2010/12/22	234.5392
cdnp3570.10o	csrj3570.10o	brdc3570.10n	igs16154.sp3	igs16154.clk_30s	igs16157.erp	2010/12/23	234.4654
cdnp3580.10o	csrj3580.10o	brdc3580.10n	igs16155.sp3	igs16155.clk_30s	igs16157.erp	2010/12/24	234.4901
cdnp3590.10o	csrj3590.10o	brdc3590.10n	igs16156.sp3	igs16156.clk_30s	igs16157.erp	2010/12/25	234.5038
cdnp3600.10o	csrj3600.10o	brdc3600.10n	igs16160.sp3	igs16160.clk_30s	igs16167.erp	2010/12/26	234.5756
cdnp3610.10o	csrj3610.10o	brdc3610.10n	igs16161.sp3	igs16161.clk_30s	igs16167.erp	2010/12/27	234.5450

cdnp3620.10o	csrj3620.10o	brdc3620.10n	igs16162.sp3	igs16162.clk_30s	igs16167.erp	2010/12/28	234.5419
cdnp3630.10o	csrj3630.10o	brdc3630.10n	igs16163.sp3	igs16163.clk_30s	igs16167.erp	2010/12/29	234.5259
cdnp3640.10o	csrj3640.10o	brdc3640.10n	igs16164.sp3	igs16164.clk_30s	igs16167.erp	2010/12/30	234.5551
cdnp3650.10o	csrj3650.10o	brdc3650.10n	igs16165.sp3	igs16165.clk_30s	igs16167.erp	2010/12/31	234.5101
cdnp0120.11o	csrj0120.11o	brdc0120.11n	igs16170.sp3	igs16170.clk_30s	igs16177.erp	2011/01/12	234.4172
cdnp0280.11o	csrj0280.11o	brdc0280.11n	igs16205.sp3	igs16205.clk_30s	igs16207.erp	2011/01/28	234.6211
cdnp2250.11o	csrj2250.11o	brdc2250.11n	igs16486.sp3	igs16486.clk_30s	igs16487.erp	2011/08/13	234.5309
cdnp2260.11o	csrj2260.11o	brdc2260.11n	igs16490.sp3	igs16490.clk_30s	igs16497.erp	2011/08/14	234.5238
cdnp2270.11o	csrj2270.11o	brdc2270.11n	igs16491.sp3	igs16491.clk_30s	igs16497.erp	2011/08/15	234.5239
cdnp2280.11o	csrj2280.11o	brdc2280.11n	igs16492.sp3	igs16492.clk_30s	igs16497.erp	2011/08/16	234.5220
cdnp2290.11o	csrj2290.11o	brdc2290.11n	igs16493.sp3	igs16493.clk_30s	igs16497.erp	2011/08/17	234.5429
cdnp2300.11o	csrj2300.11o	brdc2300.11n	igs16494.sp3	igs16494.clk_30s	igs16497.erp	2011/08/18	234.5142
cdnp2310.11o	csrj2310.11o	brdc2310.11n	igs16495.sp3	igs16495.clk_30s	igs16497.erp	2011/08/19	234.5250
cdnp2320.11o	csrj2320.11o	brdc2320.11n	igs16496.sp3	igs16496.clk_30s	igs16497.erp	2011/08/20	234.5161
cdnp2330.11o	csrj2330.11o	brdc2330.11n	igs16500.sp3	igs16500.clk_30s	igs16507.erp	2011/08/21	234.5118
cdnp2340.11o	csrj2340.11o	brdc2340.11n	igs16501.sp3	igs16501.clk_30s	igs16507.erp	2011/08/22	234.5360
cdnp2350.11o	csrj2350.11o	brdc2350.11n	igs16502.sp3	igs16502.clk_30s	igs16507.erp	2011/08/23	234.5203
cdnp2360.11o	csrj2360.11o	brdc2360.11n	igs16503.sp3	igs16503.clk_30s	igs16507.erp	2011/08/24	234.5371
cdnp2370.11o	csrj2370.11o	brdc2370.11n	igs16504.sp3	igs16504.clk_30s	igs16507.erp	2011/08/25	234.5384
cdnp2380.11o	csrj2380.11o	brdc2380.11n	igs16505.sp3	igs16505.clk_30s	igs16507.erp	2011/08/26	234.4884
cdnp2390.11o	csrj2390.11o	brdc2390.11n	igs16506.sp3	igs16506.clk_30s	igs16507.erp	2011/08/27	234.5140
cdnp2400.11o	csrj2400.11o	brdc2400.11n	igs16510.sp3	igs16510.clk_30s	igs16517.erp	2011/08/28	234.5451
cdnp2410.11o	csrj2410.11o	brdc2410.11n	igs16511.sp3	igs16511.clk_30s	igs16517.erp	2011/08/29	234.4901
cdnp2420.11o	csrj2420.11o	brdc2420.11n	igs16512.sp3	igs16512.clk_30s	igs16517.erp	2011/08/30	234.5094
cdnp2430.11o	csrj2430.11o	brdc2430.11n	igs16513.sp3	igs16513.clk_30s	igs16517.erp	2011/08/31	234.4622
cdnp2440.11o	csrj2440.11o	brdc2440.11n	igs16514.sp3	igs16514.clk_30s	igs16517.erp	2011/09/01	234.5339
cdnp2450.11o	csrj2450.11o	brdc2450.11n	igs16515.sp3	igs16515.clk_30s	igs16517.erp	2011/09/02	234.5385
cdnp2460.11o	csrj2460.11o	brdc2460.11n	igs16516.sp3	igs16516.clk_30s	igs16517.erp	2011/09/03	234.5275
cdnp2470.11o	csrj2470.11o	brdc2470.11n	igs16520.sp3	igs16520.clk_30s	igs16527.erp	2011/09/04	234.5054
cdnp2480.11o	csrj2480.11o	brdc2480.11n	igs16521.sp3	igs16521.clk_30s	igs16527.erp	2011/09/05	234.5007
cdnp2490.11o	csrj2490.11o	brdc2490.11n	igs16522.sp3	igs16522.clk_30s	igs16527.erp	2011/09/06	234.4996
cdnp2500.11o	csrj2500.11o	brdc2500.11n	igs16523.sp3	igs16523.clk_30s	igs16527.erp	2011/09/07	234.5074
cdnp2510.11o	csrj2510.11o	brdc2510.11n	igs16524.sp3	igs16524.clk_30s	igs16527.erp	2011/09/08	234.4804
cdnp2520.11o	csrj2520.11o	brdc2520.11n	igs16525.sp3	igs16525.clk_30s	igs16527.erp	2011/09/09	234.4903
cdnp2530.11o	csrj2530.11o	brdc2530.11n	igs16526.sp3	igs16526.clk_30s	igs16527.erp	2011/09/10	234.5163
cdnp2540.11o	csrj2540.11o	brdc2540.11n	igs16530.sp3	igs16530.clk_30s	igs16537.erp	2011/09/11	234.4984
cdnp2550.11o	csrj2550.11o	brdc2550.11n	igs16531.sp3	igs16531.clk_30s	igs16537.erp	2011/09/12	234.5138
cdnp2560.11o	csrj2560.11o	brdc2560.11n	igs16532.sp3	igs16532.clk_30s	igs16537.erp	2011/09/13	234.5220
cdnp2570.11o	csrj2570.11o	brdc2570.11n	igs16533.sp3	igs16533.clk_30s	igs16537.erp	2011/09/14	234.5414
cdnp2580.11o	csrj2580.11o	brdc2580.11n	igs16534.sp3	igs16534.clk_30s	igs16537.erp	2011/09/15	234.5161
cdnp2590.11o	csrj2590.11o	brdc2590.11n	igs16535.sp3	igs16535.clk_30s	igs16537.erp	2011/09/16	234.5121
cdnp2600.11o	csrj2600.11o	brdc2600.11n	igs16536.sp3	igs16536.clk_30s	igs16537.erp	2011/09/17	234.5195
cdnp2610.11o	csrj2610.11o	brdc2610.11n	igs16540.sp3	igs16540.clk_30s	igs16547.erp	2011/09/18	234.5681
cdnp2620.11o	csrj2620.11o	brdc2620.11n	igs16541.sp3	igs16541.clk_30s	igs16547.erp	2011/09/19	234.5302
cdnp2630.11o	csrj2630.11o	brdc2630.11n	igs16542.sp3	igs16542.clk_30s	igs16547.erp	2011/09/20	234.5220
cdnp2640.11o	csrj2640.11o	brdc2640.11n	igs16543.sp3	igs16543.clk_30s	igs16547.erp	2011/09/21	234.5427
cdnp2650.11o	csrj2650.11o	brdc2650.11n	igs16544.sp3	igs16544.clk_30s	igs16547.erp	2011/09/22	234.5597
cdnp2660.11o	csrj2660.11o	brdc2660.11n	igs16545.sp3	igs16545.clk_30s	igs16547.erp	2011/09/23	234.4948
cdnp2670.11o	csrj2670.11o	brdc2670.11n	igs16546.sp3	igs16546.clk_30s	igs16547.erp	2011/09/24	234.5145
cdnp2680.11o	csrj2680.11o	brdc2680.11n	igs16550.sp3	igs16550.clk_30s	igs16557.erp	2011/09/25	234.4895
cdnp2690.11o	csrj2690.11o	brdc2690.11n	igs16551.sp3	igs16551.clk_30s	igs16557.erp	2011/09/26	234.5095
cdnp2700.11o	csrj2700.11o	brdc2700.11n	igs16552.sp3	igs16552.clk_30s	igs16557.erp	2011/09/27	234.5124
cdnp2710.11o	csrj2710.11o	brdc2710.11n	igs16553.sp3	igs16553.clk_30s	igs16557.erp	2011/09/28	234.5119
cdnp2720.11o	csrj2720.11o	brdc2720.11n	igs16554.sp3	igs16554.clk_30s	igs16557.erp	2011/09/29	234.5240
cdnp2730.11o	csrj2730.11o	brdc2730.11n	igs16555.sp3	igs16555.clk_30s	igs16557.erp	2011/09/30	234.5619
cdnp2740.11o	csrj2740.11o	brdc2740.11n	igs16556.sp3	igs16556.clk_30s	igs16557.erp	2011/10/01	234.5539
cdnp2750.11o	csrj2750.11o	brdc2750.11n	igs16560.sp3	igs16560.clk_30s	igs16567.erp	2011/10/02	234.5272
cdnp2760.11o	csrj2760.11o	brdc2760.11n	igs16561.sp3	igs16561.clk_30s	igs16567.erp	2011/10/03	234.5031
cdnp2770.11o	csrj2770.11o	brdc2770.11n	igs16562.sp3	igs16562.clk_30s	igs16567.erp	2011/10/04	234.4844
cdnp2780.11o	csrj2780.11o	brdc2780.11n	igs16563.sp3	igs16563.clk_30s	igs16567.erp	2011/10/05	234.5344
cdnp2790.11o	csrj2790.11o	brdc2790.11n	igs16564.sp3	igs16564.clk_30s	igs16567.erp	2011/10/06	234.4796
cdnp2800.11o	csrj2800.11o	brdc2800.11n	igs16565.sp3	igs16565.clk_30s	igs16577.erp	2011/10/07	234.5296
cdnp2810.11o	csrj2810.11o	brdc2810.11n	igs16566.sp3	igs16566.clk_30s	igs16577.erp	2011/10/08	234.5140
cdnp2820.11o	csrj2820.11o	brdc2820.11n	igs16570.sp3	igs16570.clk_30s	igs16577.erp	2011/10/09	234.5124
cdnp2830.11o	csrj2830.11o	brdc2830.11n	igs16571.sp3	igs16571.clk_30s	igs16577.erp	2011/10/10	234.5449
cdnp2840.11o	csrj2840.11o	brdc2840.11n	igs16572.sp3	igs16572.clk_30s	igs16577.erp	2011/10/11	234.5225
cdnp2850.11o	csrj2850.11o	brdc2850.11n	igs16573.sp3	igs16573.clk_30s	igs16577.erp	2011/10/12	234.5190
cdnp2860.11o	csrj2860.11o	brdc2860.11n	igs16574.sp3	igs16574.clk_30s	igs16577.erp	2011/10/13	234.5205
cdnp2870.11o	csrj2870.11o	brdc2870.11n	igs16575.sp3	igs16575.clk_30s	igs16577.erp	2011/10/14	234.5404
cdnp2880.11o	csrj2880.11o	brdc2880.11n	igs16576.sp3	igs16576.clk_30s	igs16577.erp	2011/10/15	234.4973

cdnp2890.11o	csrj2890.11o	brdc2890.11n	igs16580.sp3	igs16580.clk_30s	igs16587.erp	2011/10/16	234.5140
cdnp2900.11o	csrj2900.11o	brdc2900.11n	igs16581.sp3	igs16581.clk_30s	igs16587.erp	2011/10/17	234.5365
cdnp2910.11o	csrj2910.11o	brdc2910.11n	igs16582.sp3	igs16582.clk_30s	igs16587.erp	2011/10/18	234.4928
cdnp2920.11o	csrj2920.11o	brdc2920.11n	igs16583.sp3	igs16583.clk_30s	igs16587.erp	2011/10/19	234.4981
cdnp2930.11o	csrj2930.11o	brdc2930.11n	igs16584.sp3	igs16584.clk_30s	igs16587.erp	2011/10/20	234.5496
cdnp2940.11o	csrj2940.11o	brdc2940.11n	igs16585.sp3	igs16585.clk_30s	igs16587.erp	2011/10/21	234.4836
cdnp2950.11o	csrj2950.11o	brdc2950.11n	igs16586.sp3	igs16586.clk_30s	igs16587.erp	2011/10/22	234.4892
cdnp2960.11o	csrj2960.11o	brdc2960.11n	igs16590.sp3	igs16590.clk_30s	igs16597.erp	2011/10/23	234.5125
cdnp2970.11o	csrj2970.11o	brdc2970.11n	igs16591.sp3	igs16591.clk_30s	igs16597.erp	2011/10/24	234.5057
cdnp2980.11o	csrj2980.11o	brdc2980.11n	igs16592.sp3	igs16592.clk_30s	igs16597.erp	2011/10/25	234.5328
cdnp2990.11o	csrj2990.11o	brdc2990.11n	igs16593.sp3	igs16593.clk_30s	igs16597.erp	2011/10/26	234.5153
cdnp3000.11o	csrj3000.11o	brdc3000.11n	igs16594.sp3	igs16594.clk_30s	igs16597.erp	2011/10/27	234.5049
cdnp3010.11o	csrj3010.11o	brdc3010.11n	igs16595.sp3	igs16595.clk_30s	igs16597.erp	2011/10/28	234.5395
cdnp3020.11o	csrj3020.11o	brdc3020.11n	igs16596.sp3	igs16596.clk_30s	igs16597.erp	2011/10/29	234.5322
cdnp3030.11o	csrj3030.11o	brdc3030.11n	igs16600.sp3	igs16600.clk_30s	igs16597.erp	2011/10/30	234.5799
cdnp3040.11o	csrj3040.11o	brdc3040.11n	igs16601.sp3	igs16601.clk_30s	igs16607.erp	2011/10/31	234.4860
cdnp3050.11o	csrj3050.11o	brdc3050.11n	igs16602.sp3	igs16602.clk_30s	igs16607.erp	2011/11/01	234.5306
cdnp3060.11o	csrj3060.11o	brdc3060.11n	igs16603.sp3	igs16603.clk_30s	igs16607.erp	2011/11/02	234.4872
cdnp3070.11o	csrj3070.11o	brdc3070.11n	igs16604.sp3	igs16604.clk_30s	igs16607.erp	2011/11/03	234.5126
cdnp3080.11o	csrj3080.11o	brdc3080.11n	igs16605.sp3	igs16605.clk_30s	igs16607.erp	2011/11/04	234.4824
cdnp3090.11o	csrj3090.11o	brdc3090.11n	igs16606.sp3	igs16606.clk_30s	igs16607.erp	2011/11/05	234.5122
cdnp3100.11o	csrj3100.11o	brdc3100.11n	igs16610.sp3	igs16610.clk_30s	igs16617.erp	2011/11/06	234.5200
cdnp3110.11o	csrj3110.11o	brdc3110.11n	igs16611.sp3	igs16611.clk_30s	igs16617.erp	2011/11/07	234.5492
cdnp3120.11o	csrj3120.11o	brdc3120.11n	igs16612.sp3	igs16612.clk_30s	igs16617.erp	2011/11/08	234.5098
cdnp3130.11o	csrj3130.11o	brdc3130.11n	igs16613.sp3	igs16613.clk_30s	igs16617.erp	2011/11/09	234.4831
cdnp3140.11o	csrj3140.11o	brdc3140.11n	igs16614.sp3	igs16614.clk_30s	igs16617.erp	2011/11/10	234.4822
cdnp3150.11o	csrj3150.11o	brdc3150.11n	igs16615.sp3	igs16615.clk_30s	igs16617.erp	2011/11/11	234.4562
cdnp3160.11o	csrj3160.11o	brdc3160.11n	igs16616.sp3	igs16616.clk_30s	igs16617.erp	2011/11/12	234.4977
cdnp3170.11o	csrj3170.11o	brdc3170.11n	igs16620.sp3	igs16620.clk_30s	igs16617.erp	2011/11/13	234.4831
cdnp3180.11o	csrj3180.11o	brdc3180.11n	igs16621.sp3	igs16621.clk_30s	igs16627.erp	2011/11/14	234.5117
cdnp3190.11o	csrj3190.11o	brdc3190.11n	igs16622.sp3	igs16622.clk_30s	igs16627.erp	2011/11/15	234.5764
cdnp3200.11o	csrj3200.11o	brdc3200.11n	igs16623.sp3	igs16623.clk_30s	igs16627.erp	2011/11/16	234.5468
cdnp3210.11o	csrj3210.11o	brdc3210.11n	igs16624.sp3	igs16624.clk_30s	igs16627.erp	2011/11/17	234.5843
cdnp3220.11o	csrj3220.11o	brdc3220.11n	igs16625.sp3	igs16625.clk_30s	igs16627.erp	2011/11/18	234.4175
cdnp3230.11o	csrj3230.11o	brdc3230.11n	igs16626.sp3	igs16626.clk_30s	igs16627.erp	2011/11/19	234.5894
cdnp3240.11o	csrj3240.11o	brdc3240.11n	igs16630.sp3	igs16630.clk_30s	igs16637.erp	2011/11/20	234.5539
cdnp3250.11o	csrj3250.11o	brdc3250.11n	igs16631.sp3	igs16631.clk_30s	igs16637.erp	2011/11/21	234.5173
cdnp3260.11o	csrj3260.11o	brdc3260.11n	igs16632.sp3	igs16632.clk_30s	igs16637.erp	2011/11/22	234.5351
cdnp3270.11o	csrj3270.11o	brdc3270.11n	igs16633.sp3	igs16633.clk_30s	igs16637.erp	2011/11/23	234.5527
cdnp3280.11o	csrj3280.11o	brdc3280.11n	igs16634.sp3	igs16634.clk_30s	igs16637.erp	2011/11/24	234.5032
cdnp3290.11o	csrj3290.11o	brdc3290.11n	igs16635.sp3	igs16635.clk_30s	igs16637.erp	2011/11/25	234.5457
cdnp3300.11o	csrj3300.11o	brdc3300.11n	igs16636.sp3	igs16636.clk_30s	igs16637.erp	2011/11/26	234.5369
cdnp3310.11o	csrj3310.11o	brdc3310.11n	igs16640.sp3	igs16640.clk_30s	igs16647.erp	2011/11/27	234.5076
cdnp3320.11o	csrj3320.11o	brdc3320.11n	igs16641.sp3	igs16641.clk_30s	igs16647.erp	2011/11/28	234.5252
cdnp3330.11o	csrj3330.11o	brdc3330.11n	igs16642.sp3	igs16642.clk_30s	igs16647.erp	2011/11/29	234.5218
cdnp3340.11o	csrj3340.11o	brdc3340.11n	igs16643.sp3	igs16643.clk_30s	igs16647.erp	2011/11/30	234.5181
cdnp3350.11o	csrj3350.11o	brdc3350.11n	igs16644.sp3	igs16644.clk_30s	igs16647.erp	2011/12/01	234.5028
cdnp3360.11o	csrj3360.11o	brdc3360.11n	igs16645.sp3	igs16645.clk_30s	igs16647.erp	2011/12/02	234.5747
cdnp3370.11o	csrj3370.11o	brdc3370.11n	igs16646.sp3	igs16646.clk_30s	igs16647.erp	2011/12/03	234.5979
cdnp3380.11o	csrj3380.11o	brdc3380.11n	igs16650.sp3	igs16650.clk_30s	igs16657.erp	2011/12/04	234.5587
cdnp3390.11o	csrj3390.11o	brdc3390.11n	igs16651.sp3	igs16651.clk_30s	igs16657.erp	2011/12/05	234.6456
cdnp3400.11o	csrj3400.11o	brdc3400.11n	igs16652.sp3	igs16652.clk_30s	igs16657.erp	2011/12/06	234.5452
cdnp3410.11o	csrj3410.11o	brdc3410.11n	igs16653.sp3	igs16653.clk_30s	igs16657.erp	2011/12/07	234.5721
cdnp3420.11o	csrj3420.11o	brdc3420.11n	igs16654.sp3	igs16654.clk_30s	igs16657.erp	2011/12/08	234.6192
cdnp3430.11o	csrj3430.11o	brdc3430.11n	igs16655.sp3	igs16655.clk_30s	igs16657.erp	2011/12/09	234.5583
cdnp3440.11o	csrj3440.11o	brdc3440.11n	igs16656.sp3	igs16656.clk_30s	igs16657.erp	2011/12/10	234.6163
cdnp3450.11o	csrj3450.11o	brdc3450.11n	igs16660.sp3	igs16660.clk_30s	igs16667.erp	2011/12/11	234.4601
cdnp3460.11o	csrj3460.11o	brdc3460.11n	igs16661.sp3	igs16661.clk_30s	igs16667.erp	2011/12/12	234.6246
cdnp3470.11o	csrj3470.11o	brdc3470.11n	igs16662.sp3	igs16662.clk_30s	igs16667.erp	2011/12/13	234.5466
cdnp3480.11o	csrj3480.11o	brdc3480.11n	igs16663.sp3	igs16663.clk_30s	igs16667.erp	2011/12/14	234.6515
cdnp3490.11o	csrj3490.11o	brdc3490.11n	igs16664.sp3	igs16664.clk_30s	igs16667.erp	2011/12/15	234.5776
cdnp3500.11o	csrj3500.11o	brdc3500.11n	igs16665.sp3	igs16665.clk_30s	igs16667.erp	2011/12/16	234.5625
cdnp3510.11o	csrj3510.11o	brdc3510.11n	igs16666.sp3	igs16666.clk_30s	igs16667.erp	2011/12/17	234.4735
cdnp3520.11o	csrj3520.11o	brdc3520.11n	igs16670.sp3	igs16670.clk_30s	igs16677.erp	2011/12/18	234.4534
cdnp3530.11o	csrj3530.11o	brdc3530.11n	igs16671.sp3	igs16671.clk_30s	igs16677.erp	2011/12/19	234.4627
cdnp3540.11o	csrj3540.11o	brdc3540.11n	igs16672.sp3	igs16672.clk_30s	igs16677.erp	2011/12/20	234.4601
cdnp3550.11o	csrj3550.11o	brdc3550.11n	igs16673.sp3	igs16673.clk_30s	igs16677.erp	2011/12/21	234.3773
cdnp3560.11o	csrj3560.11o	brdc3560.11n	igs16674.sp3	igs16674.clk_30s	igs16677.erp	2011/12/22	234.4331
cdnp3570.11o	csrj3570.11o	brdc3570.11n	igs16675.sp3	igs16675.clk_30s	igs16677.erp	2011/12/23	234.4648
cdnp3580.11o	csrj3580.11o	brdc3580.11n	igs16676.sp3	igs16676.clk_30s	igs16677.erp	2011/12/24	234.4741

cdnp3590.11o	csrj3590.11o	brdc3590.11n	igs16680.sp3	igs16680.clk_30s	igs16687.erp	2011/12/25	234.4749
cdnp3600.11o	csrj3600.11o	brdc3600.11n	igs16681.sp3	igs16681.clk_30s	igs16687.erp	2011/12/26	234.4610
cdnp3610.11o	csrj3610.11o	brdc3610.11n	igs16682.sp3	igs16682.clk_30s	igs16687.erp	2011/12/27	234.4746
cdnp3620.11o	csrj3620.11o	brdc3620.11n	igs16683.sp3	igs16683.clk_30s	igs16687.erp	2011/12/28	234.4389
cdnp3630.11o	csrj3630.11o	brdc3630.11n	igs16684.sp3	igs16684.clk_30s	igs16687.erp	2011/12/29	234.4419
cdnp3640.11o	csrj3640.11o	brdc3640.11n	igs16685.sp3	igs16685.clk_30s	igs16687.erp	2011/12/30	234.4704
cdnp3650.11o	csrj3650.11o	brdc3650.11n	igs16686.sp3	igs16686.clk_30s	igs16687.erp	2011/12/31	234.4695
cdnp0050.12o	csrj0050.12o	brdc0050.12n	igs16694.sp3	igs16694.clk_30s	igs16697.erp	2012/01/05	235.9412
cdnp0060.12o	csrj0060.12o	brdc0060.12n	igs16695.sp3	igs16695.clk_30s	igs16697.erp	2012/01/06	236.4543
cdnp0070.12o	csrj0070.12o	brdc0070.12n	igs16696.sp3	igs16696.clk_30s	igs16697.erp	2012/01/07	234.9945
cdnp0080.12o	csrj0080.12o	brdc0080.12n	igs16700.sp3	igs16700.clk_30s	igs16707.erp	2012/01/08	234.8079
cdnp0090.12o	csrj0090.12o	brdc0090.12n	igs16701.sp3	igs16701.clk_30s	igs16707.erp	2012/01/09	234.6224
cdnp0100.12o	csrj0100.12o	brdc0100.12n	igs16702.sp3	igs16702.clk_30s	igs16707.erp	2012/01/10	233.6126
cdnp0110.12o	csrj0110.12o	brdc0110.12n	igs16704.sp3	igs16704.clk_30s	igs16707.erp	2012/01/11	234.0508
cdnp0130.12o	csrj0130.12o	brdc0130.12n	igs16705.sp3	igs16705.clk_30s	igs16707.erp	2012/01/13	235.4518
cdnp0140.12o	csrj0140.12o	brdc0140.12n	igs16706.sp3	igs16706.clk_30s	igs16707.erp	2012/01/14	234.9681
cdnp0150.12o	csrj0150.12o	brdc0150.12n	igs16710.sp3	igs16710.clk_30s	igs16717.erp	2012/01/15	235.2936
cdnp0160.12o	csrj0160.12o	brdc0160.12n	igs16711.sp3	igs16711.clk_30s	igs16717.erp	2012/01/16	234.6371
cdnp0180.12o	csrj0180.12o	brdc0180.12n	igs16713.sp3	igs16713.clk_30s	igs16717.erp	2012/01/18	234.3646
cdnp0200.12o	csrj0200.12o	brdc0200.12n	igs16715.sp3	igs16715.clk_30s	igs16717.erp	2012/01/20	233.6403
cdnp0220.12o	csrj0220.12o	brdc0220.12n	igs16720.sp3	igs16720.clk_30s	igs16727.erp	2012/01/22	236.6536
cdnp0230.12o	csrj0230.12o	brdc0230.12n	igs16721.sp3	igs16721.clk_30s	igs16727.erp	2012/01/23	234.0458
cdnp0240.12o	csrj0240.12o	brdc0240.12n	igs16722.sp3	igs16722.clk_30s	igs16727.erp	2012/01/24	233.8455
cdnp0250.12o	csrj0250.12o	brdc0250.12n	igs16723.sp3	igs16723.clk_30s	igs16727.erp	2012/01/25	233.7934
cdnp0260.12o	csrj0260.12o	brdc0260.12n	igs16724.sp3	igs16724.clk_30s	igs16727.erp	2012/01/26	235.6518
cdnp0270.12o	csrj0270.12o	brdc0270.12n	igs16725.sp3	igs16725.clk_30s	igs16727.erp	2012/01/27	236.0626
cdnp0280.12o	csrj0280.12o	brdc0280.12n	igs16726.sp3	igs16726.clk_30s	igs16727.erp	2012/01/28	235.4891
cdnp0290.12o	csrj0290.12o	brdc0290.12n	igs16730.sp3	igs16730.clk_30s	igs16737.erp	2012/01/29	231.9763
cdnp0300.12o	csrj0300.12o	brdc0300.12n	igs16731.sp3	igs16731.clk_30s	igs16737.erp	2012/01/30	233.4142
cdnp0310.12o	csrj0310.12o	brdc0310.12n	igs16732.sp3	igs16732.clk_30s	igs16737.erp	2012/01/31	233.1211
cdnp0330.12o	csrj0330.12o	brdc0330.12n	igs16734.sp3	igs16734.clk_30s	igs16737.erp	2012/02/02	236.5242
cdnp0350.12o	csrj0350.12o	brdc0350.12n	igs16736.sp3	igs16736.clk_30s	igs16737.erp	2012/02/04	233.7770
cdnp0380.12o	csrj0380.12o	brdc0380.12n	igs16742.sp3	igs16742.clk_30s	igs16747.erp	2012/02/07	234.1420
cdnp0390.12o	csrj0390.12o	brdc0390.12n	igs16743.sp3	igs16743.clk_30s	igs16747.erp	2012/02/08	232.6563
cdnp0400.12o	csrj0400.12o	brdc0400.12n	igs16744.sp3	igs16744.clk_30s	igs16747.erp	2012/02/09	238.4121
cdnp0420.12o	csrj0420.12o	brdc0420.12n	igs16746.sp3	igs16746.clk_30s	igs16747.erp	2012/02/11	232.2736
cdnp0430.12o	csrj0430.12o	brdc0430.12n	igs16750.sp3	igs16750.clk_30s	igs16757.erp	2012/02/12	231.6164
cdnp0440.12o	csrj0440.12o	brdc0440.12n	igs16751.sp3	igs16751.clk_30s	igs16757.erp	2012/02/13	236.5731
cdnp0450.12o	csrj0450.12o	brdc0450.12n	igs16752.sp3	igs16752.clk_30s	igs16757.erp	2012/02/14	233.3987
cdnp0460.12o	csrj0460.12o	brdc0460.12n	igs16753.sp3	igs16753.clk_30s	igs16757.erp	2012/02/15	236.1088
cdnp0480.12o	csrj0480.12o	brdc0480.12n	igs16755.sp3	igs16755.clk_30s	igs16757.erp	2012/02/17	236.6511
cdnp0490.12o	csrj0490.12o	brdc0490.12n	igs16756.sp3	igs16756.clk_30s	igs16757.erp	2012/02/18	234.4283
cdnp0500.12o	csrj0500.12o	brdc0500.12n	igs16760.sp3	igs16760.clk_30s	igs16767.erp	2012/02/19	231.2074
cdnp0510.12o	csrj0510.12o	brdc0510.12n	igs16761.sp3	igs16761.clk_30s	igs16767.erp	2012/02/20	232.8916
cdnp0520.12o	csrj0520.12o	brdc0520.12n	igs16762.sp3	igs16762.clk_30s	igs16767.erp	2012/02/21	232.5231
cdnp0540.12o	csrj0540.12o	brdc0540.12n	igs16764.sp3	igs16764.clk_30s	igs16767.erp	2012/02/23	235.1159
cdnp0550.12o	csrj0550.12o	brdc0550.12n	igs16765.sp3	igs16765.clk_30s	igs16767.erp	2012/02/24	238.4716
cdnp0650.12o	csrj0650.12o	brdc0650.12n	igs16781.sp3	igs16781.clk_30s	igs16787.erp	2012/03/05	235.8946
cdnp0660.12o	csrj0660.12o	brdc0660.12n	igs16782.sp3	igs16782.clk_30s	igs16787.erp	2012/03/06	235.3072
cdnp0670.12o	csrj0670.12o	brdc0670.12n	igs16783.sp3	igs16783.clk_30s	igs16787.erp	2012/03/07	234.7676
cdnp0680.12o	csrj0680.12o	brdc0680.12n	igs16784.sp3	igs16784.clk_30s	igs16787.erp	2012/03/08	234.6865
cdnp0700.12o	csrj0700.12o	brdc0700.12n	igs16786.sp3	igs16786.clk_30s	igs16787.erp	2012/03/10	233.5879
cdnp0710.12o	csrj0710.12o	brdc0710.12n	igs16790.sp3	igs16790.clk_30s	igs16797.erp	2012/03/11	232.9945
cdnp0740.12o	csrj0740.12o	brdc0740.12n	igs16793.sp3	igs16793.clk_30s	igs16797.erp	2012/03/14	233.9755
cdnp0750.12o	csrj0750.12o	brdc0750.12n	igs16794.sp3	igs16794.clk_30s	igs16797.erp	2012/03/15	232.7527
cdnp0760.12o	csrj0760.12o	brdc0760.12n	igs16795.sp3	igs16795.clk_30s	igs16797.erp	2012/03/16	236.6860
cdnp0010.13o	csrj0010.13o	brdc0010.13n	igs17212.sp3	igs17212.clk_30s	igs17217.erp	2013/01/01	234.4976
cdnp0020.13o	csrj0020.13o	brdc0020.13n	igs17213.sp3	igs17213.clk_30s	igs17217.erp	2013/01/02	234.5121
cdnp0030.13o	csrj0030.13o	brdc0030.13n	igs17214.sp3	igs17214.clk_30s	igs17217.erp	2013/01/03	234.5234
cdnp0040.13o	csrj0040.13o	brdc0040.13n	igs17215.sp3	igs17215.clk_30s	igs17217.erp	2013/01/04	234.4862
cdnp0050.13o	csrj0050.13o	brdc0050.13n	igs17216.sp3	igs17216.clk_30s	igs17217.erp	2013/01/05	234.5110
cdnp0060.13o	csrj0060.13o	brdc0060.13n	igs17220.sp3	igs17220.clk_30s	igs17227.erp	2013/01/06	234.5041
cdnp0070.13o	csrj0070.13o	brdc0070.13n	igs17221.sp3	igs17221.clk_30s	igs17227.erp	2013/01/07	234.5199
cdnp0080.13o	csrj0080.13o	brdc0080.13n	igs17222.sp3	igs17222.clk_30s	igs17227.erp	2013/01/08	234.5342
cdnp0090.13o	csrj0090.13o	brdc0090.13n	igs17223.sp3	igs17223.clk_30s	igs17227.erp	2013/01/09	234.5346
cdnp0100.13o	csrj0100.13o	brdc0100.13n	igs17224.sp3	igs17224.clk_30s	igs17227.erp	2013/01/10	234.5356
cdnp0110.13o	csrj0110.13o	brdc0110.13n	igs17225.sp3	igs17225.clk_30s	igs17227.erp	2013/01/11	234.5279
cdnp0120.13o	csrj0120.13o	brdc0120.13n	igs17226.sp3	igs17226.clk_30s	igs17227.erp	2013/01/12	234.5142
cdnp0130.13o	csrj0130.13o	brdc0130.13n	igs17230.sp3	igs17230.clk_30s	igs17237.erp	2013/01/13	234.5105
cdnp0140.13o	csrj0140.13o	brdc0140.13n	igs17231.sp3	igs17231.clk_30s	igs17237.erp	2013/01/14	234.5349

cdnp0150.13o	csrj0150.13o	brdc0150.13n	igs17232.sp3	igs17232.clk_30s	igs17237.erp	2013/01/15	234.5210
cdnp0160.13o	csrj0160.13o	brdc0160.13n	igs17233.sp3	igs17233.clk_30s	igs17237.erp	2013/01/16	234.5174
cdnp0170.13o	csrj0170.13o	brdc0170.13n	igs17234.sp3	igs17234.clk_30s	igs17237.erp	2013/01/17	234.5111
cdnp0180.13o	csrj0180.13o	brdc0180.13n	igs17235.sp3	igs17235.clk_30s	igs17237.erp	2013/01/18	234.5428
cdnp0190.13o	csrj0190.13o	brdc0190.13n	igs17236.sp3	igs17236.clk_30s	igs17237.erp	2013/01/19	234.5139
cdnp0200.13o	csrj0200.13o	brdc0200.13n	igs17240.sp3	igs17240.clk_30s	igs17247.erp	2013/01/20	234.5367
cdnp0210.13o	csrj0210.13o	brdc0210.13n	igs17241.sp3	igs17241.clk_30s	igs17247.erp	2013/01/21	234.5198
cdnp0220.13o	csrj0220.13o	brdc0220.13n	igs17242.sp3	igs17242.clk_30s	igs17247.erp	2013/01/22	234.5205
cdnp0230.13o	csrj0230.13o	brdc0230.13n	igs17243.sp3	igs17243.clk_30s	igs17247.erp	2013/01/23	234.5199
cdnp0240.13o	csrj0240.13o	brdc0240.13n	igs17244.sp3	igs17244.clk_30s	igs17247.erp	2013/01/24	234.5027
cdnp0250.13o	csrj0250.13o	brdc0250.13n	igs17245.sp3	igs17245.clk_30s	igs17247.erp	2013/01/25	234.4835
cdnp0260.13o	csrj0260.13o	brdc0260.13n	igs17246.sp3	igs17246.clk_30s	igs17247.erp	2013/01/26	234.4866
cdnp0270.13o	csrj0270.13o	brdc0270.13n	igs17250.sp3	igs17250.clk_30s	igs17257.erp	2013/01/27	234.5280
cdnp0280.13o	csrj0280.13o	brdc0280.13n	igs17251.sp3	igs17251.clk_30s	igs17257.erp	2013/01/28	234.5212
cdnp0290.13o	csrj0290.13o	brdc0290.13n	igs17252.sp3	igs17252.clk_30s	igs17257.erp	2013/01/29	234.5240
cdnp0300.13o	csrj0300.13o	brdc0300.13n	igs17253.sp3	igs17253.clk_30s	igs17257.erp	2013/01/30	234.5173
cdnp0310.13o	csrj0310.13o	brdc0310.13n	igs17254.sp3	igs17254.clk_30s	igs17257.erp	2013/01/31	234.4963
cdnp0320.13o	csrj0320.13o	brdc0320.13n	igs17255.sp3	igs17255.clk_30s	igs17257.erp	2013/02/01	234.5340
cdnp0330.13o	csrj0330.13o	brdc0330.13n	igs17256.sp3	igs17256.clk_30s	igs17257.erp	2013/02/02	234.5063
cdnp0350.13o	csrj0350.13o	brdc0350.13n	igs17261.sp3	igs17261.clk_30s	igs17267.erp	2013/02/04	234.5189
cdnp0360.13o	csrj0360.13o	brdc0360.13n	igs17262.sp3	igs17262.clk_30s	igs17267.erp	2013/02/05	234.5141
cdnp0370.13o	csrj0370.13o	brdc0370.13n	igs17263.sp3	igs17263.clk_30s	igs17267.erp	2013/02/06	234.5345
cdnp0380.13o	csrj0380.13o	brdc0380.13n	igs17264.sp3	igs17264.clk_30s	igs17267.erp	2013/02/07	234.5254
cdnp0390.13o	csrj0390.13o	brdc0390.13n	igs17265.sp3	igs17265.clk_30s	igs17267.erp	2013/02/08	234.5169
cdnp0400.13o	csrj0400.13o	brdc0400.13n	igs17266.sp3	igs17266.clk_30s	igs17267.erp	2013/02/09	234.5288
cdnp0410.13o	csrj0410.13o	brdc0410.13n	igs17270.sp3	igs17270.clk_30s	igs17277.erp	2013/02/10	234.4777
cdnp0420.13o	csrj0420.13o	brdc0420.13n	igs17271.sp3	igs17271.clk_30s	igs17277.erp	2013/02/11	234.5395
cdnp0430.13o	csrj0430.13o	brdc0430.13n	igs17272.sp3	igs17272.clk_30s	igs17277.erp	2013/02/12	234.5277
cdnp0440.13o	csrj0440.13o	brdc0440.13n	igs17273.sp3	igs17273.clk_30s	igs17277.erp	2013/02/13	234.5097
cdnp0450.13o	csrj0450.13o	brdc0450.13n	igs17274.sp3	igs17274.clk_30s	igs17277.erp	2013/02/14	234.5244
cdnp0460.13o	csrj0460.13o	brdc0460.13n	igs17275.sp3	igs17275.clk_30s	igs17277.erp	2013/02/15	234.4873
cdnp0470.13o	csrj0470.13o	brdc0470.13n	igs17276.sp3	igs17276.clk_30s	igs17277.erp	2013/02/16	234.5282
cdnp0480.13o	csrj0480.13o	brdc0480.13n	igs17280.sp3	igs17280.clk_30s	igs17287.erp	2013/02/17	234.5155
cdnp0490.13o	csrj0490.13o	brdc0490.13n	igs17281.sp3	igs17281.clk_30s	igs17287.erp	2013/02/18	234.5114
cdnp0500.13o	csrj0500.13o	brdc0500.13n	igs17282.sp3	igs17282.clk_30s	igs17287.erp	2013/02/19	234.4968
cdnp0510.13o	csrj0510.13o	brdc0510.13n	igs17283.sp3	igs17283.clk_30s	igs17287.erp	2013/02/20	234.5139
cdnp0520.13o	csrj0520.13o	brdc0520.13n	igs17284.sp3	igs17284.clk_30s	igs17287.erp	2013/02/21	234.4929
cdnp0530.13o	csrj0530.13o	brdc0530.13n	igs17285.sp3	igs17285.clk_30s	igs17287.erp	2013/02/22	234.5214
cdnp0540.13o	csrj0540.13o	brdc0540.13n	igs17286.sp3	igs17286.clk_30s	igs17287.erp	2013/02/23	234.5038
cdnp0550.13o	csrj0550.13o	brdc0550.13n	igs17290.sp3	igs17290.clk_30s	igs17297.erp	2013/02/24	234.5186
cdnp0560.13o	csrj0560.13o	brdc0560.13n	igs17291.sp3	igs17291.clk_30s	igs17297.erp	2013/02/25	234.5191
cdnp0570.13o	csrj0570.13o	brdc0570.13n	igs17292.sp3	igs17292.clk_30s	igs17297.erp	2013/02/26	234.5288
cdnp0580.13o	csrj0580.13o	brdc0580.13n	igs17293.sp3	igs17293.clk_30s	igs17297.erp	2013/02/27	234.5069
cdnp0590.13o	csrj0590.13o	brdc0590.13n	igs17294.sp3	igs17294.clk_30s	igs17297.erp	2013/02/28	234.5319
cdnp0600.13o	csrj0600.13o	brdc0600.13n	igs17295.sp3	igs17295.clk_30s	igs17297.erp	2013/03/01	234.5256
cdnp0610.13o	csrj0610.13o	brdc0610.13n	igs17296.sp3	igs17296.clk_30s	igs17297.erp	2013/03/02	234.5210
cdnp0730.13o	csrj0730.13o	brdc0730.13n	igs17314.sp3	igs17314.clk_30s	igs17317.erp	2013/03/14	234.5125
cdnp0740.13o	csrj0740.13o	brdc0740.13n	igs17315.sp3	igs17315.clk_30s	igs17317.erp	2013/03/15	234.5194
cdnp0750.13o	csrj0750.13o	brdc0750.13n	igs17316.sp3	igs17316.clk_30s	igs17317.erp	2013/03/16	234.5324
cdnp0760.9o	csrj0760.13o	brdc0760.13n	igs17320.sp3	igs17320.clk_30s	igs17327.erp	2013/03/17	234.5181
cdnp0770.13o	csrj0770.13o	brdc0770.13n	igs17321.sp3	igs17321.clk_30s	igs17327.erp	2013/03/18	234.5154
cdnp0780.13o	csrj0780.13o	brdc0780.13n	igs17322.sp3	igs17322.clk_30s	igs17327.erp	2013/03/19	234.5365
cdnp0790.13o	csrj0790.13o	brdc0790.13n	igs17323.sp3	igs17323.clk_30s	igs17327.erp	2013/03/20	234.5172
cdnp0800.13o	csrj0800.13o	brdc0800.13n	igs17324.sp3	igs17324.clk_30s	igs17327.erp	2013/03/21	234.5276
cdnp0810.13o	csrj0810.13o	brdc0810.13n	igs17325.sp3	igs17325.clk_30s	igs17327.erp	2013/03/22	234.5121
cdnp0820.13o	csrj0820.13o	brdc0820.13n	igs17326.sp3	igs17326.clk_30s	igs17327.erp	2013/03/23	234.4933
cdnp0830.13o	csrj0830.13o	brdc0830.13n	igs17330.sp3	igs17330.clk_30s	igs17330.erp	2013/03/24	234.5001
cdnp0840.13o	csrj0840.13o	brdc0840.13n	igs17331.sp3	igs17331.clk_30s	igs17330.erp	2013/03/25	234.4919
cdnp0850.13o	csrj0850.13o	brdc0850.13n	igs17332.sp3	igs17332.clk_30s	igs17330.erp	2013/03/26	234.5151
cdnp0860.13o	csrj0860.13o	brdc0860.13n	igs17333.sp3	igs17333.clk_30s	igs17330.erp	2013/03/27	234.5115
cdnp0870.13o	csrj0870.13o	brdc0870.13n	igs17334.sp3	igs17334.clk_30s	igs17330.erp	2013/03/28	234.5310
cdnp0880.13o	csrj0880.13o	brdc0880.13n	igs17335.sp3	igs17335.clk_30s	igs17330.erp	2013/03/29	234.5163
cdnp0890.13o	csrj0890.13o	brdc0890.13n	igs17336.sp3	igs17336.clk_30s	igs17330.erp	2013/03/30	234.5247
cdnp0900.13o	csrj0900.13o	brdc0900.13n	igs17340.sp3	igs17340.clk_30s	igs17337.erp	2013/03/31	234.5092
cdnp0910.13o	csrj0910.13o	brdc0910.13n	igs17341.sp3	igs17341.clk_30s	igs17337.erp	2013/04/01	234.4969
cdnp0920.13o	csrj0920.13o	brdc0920.13n	igs17342.sp3	igs17342.clk_30s	igs17337.erp	2013/04/02	234.5035
cdnp0930.13o	csrj0930.13o	brdc0930.13n	igs17343.sp3	igs17343.clk_30s	igs17337.erp	2013/04/03	234.5089
cdnp0940.13o	csrj0940.13o	brdc0940.13n	igs17344.sp3	igs17344.clk_30s	igs17337.erp	2013/04/04	234.5146
cdnp0950.13o	csrj0950.13o	brdc0950.13n	igs17345.sp3	igs17345.clk_30s	igs17337.erp	2013/04/05	234.5286
cdnp0960.13o	csrj0960.13o	brdc0960.13n	igs17346.sp3	igs17346.clk_30s	igs17347.erp	2013/04/06	234.5229

cdnp0970.13o	csrj0970.13o	brdc0970.13n	igs17350.sp3	igs17350.clk_30s	igs17357.erp	2013/04/07	234.5162
cdnp0980.13o	csrj0980.13o	brdc0980.13n	igs17351.sp3	igs17351.clk_30s	igs17357.erp	2013/04/08	234.5203
cdnp0990.13o	csrj0990.13o	brdc0990.13n	igs17352.sp3	igs17352.clk_30s	igs17357.erp	2013/04/09	234.5258
cdnp1000.13o	csrj1000.13o	brdc1000.13n	igs17353.sp3	igs17353.clk_30s	igs17357.erp	2013/04/10	234.5170
cdnp1010.13o	csrj1010.13o	brdc1010.13n	igs17354.sp3	igs17354.clk_30s	igs17357.erp	2013/04/11	234.5059
cdnp1020.13o	csrj1020.13o	brdc1020.13n	igs17355.sp3	igs17355.clk_30s	igs17357.erp	2013/04/12	234.5029
cdnp1030.13o	csrj1030.13o	brdc1030.13n	igs17356.sp3	igs17356.clk_30s	igs17357.erp	2013/04/13	234.5204
cdnp1040.13o	csrj1040.13o	brdc1040.13n	igs17360.sp3	igs17360.clk_30s	igs17367.erp	2013/04/14	234.5231
cdnp1050.13o	csrj1050.13o	brdc1050.13n	igs17361.sp3	igs17361.clk_30s	igs17367.erp	2013/04/15	234.5204
cdnp1060.13o	csrj1060.13o	brdc1060.13n	igs17362.sp3	igs17362.clk_30s	igs17367.erp	2013/04/16	234.5016
cdnp1070.13o	csrj1070.13o	brdc1070.13n	igs17363.sp3	igs17363.clk_30s	igs17367.erp	2013/04/17	234.5179
cdnp1080.13o	csrj1080.13o	brdc1080.13n	igs17364.sp3	igs17364.clk_30s	igs17367.erp	2013/04/18	234.5102
cdnp1090.13o	csrj1090.13o	brdc1090.13n	igs17365.sp3	igs17365.clk_30s	igs17367.erp	2013/04/19	234.5169
cdnp1100.13o	csrj1100.13o	brdc1100.13n	igs17366.sp3	igs17366.clk_30s	igs17367.erp	2013/04/20	234.5068
cdnp1110.13o	csrj1110.13o	brdc1110.13n	igs17370.sp3	igs17370.clk_30s	igs17377.erp	2013/04/21	234.5212
cdnp1120.13o	csrj1120.13o	brdc1120.13n	igs17371.sp3	igs17371.clk_30s	igs17377.erp	2013/04/22	234.5364
cdnp1130.13o	csrj1130.13o	brdc1130.13n	igs17372.sp3	igs17372.clk_30s	igs17377.erp	2013/04/23	234.5136
cdnp1140.13o	csrj1140.13o	brdc1140.13n	igs17373.sp3	igs17373.clk_30s	igs17377.erp	2013/04/24	234.5308
cdnp1150.13o	csrj1150.13o	brdc1150.13n	igs17374.sp3	igs17374.clk_30s	igs17377.erp	2013/04/25	234.5076
cdnp1160.9o	csrj1160.9o	brdc1160.9o	igs17375.sp3	igs17375.clk_30s	igs17377.erp	2013/04/26	234.5280
cdnp1170.13o	csrj1170.13o	brdc1170.13n	igs17376.sp3	igs17376.clk_30s	igs17377.erp	2013/04/27	234.5304
cdnp1180.13o	csrj1180.13o	brdc1180.13n	igs17380.sp3	igs17380.clk_30s	igs17387.erp	2013/04/28	234.5196
cdnp1190.13o	csrj1190.13o	brdc1190.13n	igs17381.sp3	igs17381.clk_30s	igs17387.erp	2013/04/29	234.5282
cdnp1200.13o	csrj1200.13o	brdc1200.13n	igs17382.sp3	igs17382.clk_30s	igs17387.erp	2013/04/30	234.5064
cdnp1210.13o	csrj1210.13o	brdc1210.13n	igs17383.sp3	igs17383.clk_30s	igs17387.erp	2013/05/01	234.5240
cdnp1220.13o	csrj1220.13o	brdc1220.13n	igs17384.sp3	igs17384.clk_30s	igs17387.erp	2013/05/02	234.5241
cdnp1230.13o	csrj1230.13o	brdc1230.13n	igs17385.sp3	igs17385.clk_30s	igs17387.erp	2013/05/03	234.5114
cdnp1240.13o	csrj1240.13o	brdc1240.13n	igs17386.sp3	igs17386.clk_30s	igs17387.erp	2013/05/04	234.5304
cdnp1250.13o	csrj1250.13o	brdc1250.13n	igs17390.sp3	igs17390.clk_30s	igs17397.erp	2013/05/05	234.5327
cdnp1260.13o	csrj1260.13o	brdc1260.13n	igs17391.sp3	igs17391.clk_30s	igs17397.erp	2013/05/06	234.5245
cdnp1270.13o	csrj1270.13o	brdc1270.13n	igs17392.sp3	igs17392.clk_30s	igs17397.erp	2013/05/07	234.5350
cdnp1280.13o	csrj1280.13o	brdc1280.13n	igs17393.sp3	igs17393.clk_30s	igs17397.erp	2013/05/08	234.5099
cdnp1290.13o	csrj1290.13o	brdc1290.13n	igs17394.sp3	igs17394.clk_30s	igs17397.erp	2013/05/09	234.5162
cdnp1300.13o	csrj1300.13o	brdc1300.13n	igs17395.sp3	igs17395.clk_30s	igs17397.erp	2013/05/10	234.4986
cdnp1310.13o	csrj1310.13o	brdc1310.13n	igs17396.sp3	igs17396.clk_30s	igs17397.erp	2013/05/11	234.4910
cdnp1320.13o	csrj1320.13o	brdc1320.13n	igs17400.sp3	igs17400.clk_30s	igs17407.erp	2013/05/12	234.5302
cdnp1330.13o	csrj1330.13o	brdc1330.13n	igs17401.sp3	igs17401.clk_30s	igs17407.erp	2013/05/13	234.5211
cdnp1340.13o	csrj1340.13o	brdc1340.13n	igs17402.sp3	igs17402.clk_30s	igs17407.erp	2013/05/14	234.5195
cdnp1350.13o	csrj1350.13o	brdc1350.13n	igs17403.sp3	igs17403.clk_30s	igs17407.erp	2013/05/15	234.5227
cdnp1360.13o	csrj1360.13o	brdc1360.13n	igs17404.sp3	igs17404.clk_30s	igs17407.erp	2013/05/16	234.5076
cdnp1370.13o	csrj1370.13o	brdc1370.13n	igs17405.sp3	igs17405.clk_30s	igs17407.erp	2013/05/17	234.5040
cdnp1380.13o	csrj1380.13o	brdc1380.13n	igs17406.sp3	igs17406.clk_30s	igs17407.erp	2013/05/18	234.5183
cdnp1390.13o	csrj1390.13o	brdc1390.13n	igs17410.sp3	igs17410.clk_30s	igs17417.erp	2013/05/19	234.5207
cdnp1400.13o	csrj1400.13o	brdc1400.13n	igs17411.sp3	igs17411.clk_30s	igs17417.erp	2013/05/20	234.5180
cdnp1420.13o	csrj1410.13o	brdc1410.13n	igs17412.sp3	igs17412.clk_30s	igs17417.erp	2013/05/21	234.5202
cdnp1410.13o	csrj1420.13o	brdc1420.13n	igs17413.sp3	igs17413.clk_30s	igs17417.erp	2013/05/22	234.5064
cdnp1430.13o	csrj1430.13o	brdc1430.13n	igs17414.sp3	igs17414.clk_30s	igs17417.erp	2013/05/23	234.4961
cdnp1460.13o	csrj1460.13o	brdc1460.13n	igs17420.sp3	igs17420.clk_30s	igs17427.erp	2013/05/24	234.5138
cdnp1470.13o	csrj1470.13o	brdc1470.13n	igs17421.sp3	igs17421.clk_30s	igs17427.erp	2013/05/25	234.4937
cdnp1460.13o	csrj1460.13o	brdc1460.13n	igs17422.sp3	igs17422.clk_30s	igs17427.erp	2013/05/26	234.5161
cdnp1470.13o	csrj1470.13o	brdc1470.13n	igs17423.sp3	igs17423.clk_30s	igs17427.erp	2013/05/27	234.5209
cdnp1480.13o	csrj1480.13o	brdc1480.13n	igs17424.sp3	igs17424.clk_30s	igs17427.erp	2013/05/28	234.5219
cdnp1490.13o	csrj1490.13o	brdc1490.13n	igs17425.sp3	igs17425.clk_30s	igs17427.erp	2013/05/29	234.5132
cdnp1500.13o	csrj1500.13o	brdc1500.13n	igs17426.sp3	igs17426.clk_30s	igs17427.erp	2013/05/30	234.5080
cdnp1510.13o	csrj1510.13o	brdc1510.13n	igs17427.sp3	igs17427.clk_30s	igs17427.erp	2013/05/31	234.5223
cdnp1520.13o	csrj1520.13o	brdc1520.13n	igs17428.sp3	igs17428.clk_30s	igs17427.erp	2013/06/01	234.5175
cdnp1530.13o	csrj1530.13o	brdc1530.13n	igs17430.sp3	igs17430.clk_30s	igs17437.erp	2013/06/02	234.5524
cdnp1540.13o	csrj1540.13o	brdc1540.13n	igs17431.sp3	igs17431.clk_30s	igs17437.erp	2013/06/03	234.5170
cdnp1660.13o	csrj1660.13o	brdc1660.13n	igs17446.sp3	igs17446.clk_30s	igs17447.erp	2013/06/15	234.4977
cdnp1670.13o	csrj1670.13o	brdc1670.13n	igs17450.sp3	igs17450.clk_30s	igs17457.erp	2013/06/16	234.5062
cdnp1680.13o	csrj1680.13o	brdc1680.13n	igs17451.sp3	igs17451.clk_30s	igs17457.erp	2013/06/17	234.5430
cdnp1690.13o	csrj1690.13o	brdc1690.13n	igs17452.sp3	igs17452.clk_30s	igs17457.erp	2013/06/18	234.5148
cdnp1700.13o	csrj1700.13o	brdc1700.13n	igs17453.sp3	igs17453.clk_30s	igs17457.erp	2013/06/19	234.5179
cdnp1710.13o	csrj1710.13o	brdc1710.13n	igs17454.sp3	igs17454.clk_30s	igs17457.erp	2013/06/20	234.5078
cdnp1720.13o	csrj1720.13o	brdc1720.13n	igs17455.sp3	igs17455.clk_30s	igs17457.erp	2013/06/21	234.5001
cdnp1730.13o	csrj1730.13o	brdc1730.13n	igs17456.sp3	igs17456.clk_30s	igs17457.erp	2013/06/22	234.5134
cdnp1740.13o	csrj1740.13o	brdc1740.13n	igs17460.sp3	igs17460.clk_30s	igs17467.erp	2013/06/23	234.5203
cdnp1750.13o	csrj1750.13o	brdc1750.13n	igs17461.sp3	igs17461.clk_30s	igs17467.erp	2013/06/24	234.5007
cdnp1760.13o	csrj1760.13o	brdc1760.13n	igs17462.sp3	igs17462.clk_30s	igs17467.erp	2013/06/25	234.5146
cdnp1770.13o	csrj1770.13o	brdc1770.13n	igs17463.sp3	igs17463.clk_30s	igs17467.erp	2013/06/26	234.5299

cdnp1780.13o	csrj1780.13o	brdc1780.13n	igs17464.sp3	igs17464.clk_30s	igs17467.erp	2013/06/27	234.5029
cdnp1790.13o	csrj1790.13o	brdc1790.13n	igs17465.sp3	igs17465.clk_30s	igs17467.erp	2013/06/28	234.5446
cdnp1800.13o	csrj1800.13o	brdc1800.13n	igs17466.sp3	igs17466.clk_30s	igs17467.erp	2013/06/29	234.5135
cdnp1810.13o	csrj1810.13o	brdc1810.13n	igs17470.sp3	igs17470.clk_30s	igs17477.erp	2013/06/30	234.4812
cdnp1820.13o	csrj1820.13o	brdc1820.13n	igs17471.sp3	igs17471.clk_30s	igs17477.erp	2013/07/01	234.5087
cdnp1830.13o	csrj1830.13o	brdc1830.13n	igs17472.sp3	igs17472.clk_30s	igs17477.erp	2013/07/02	234.5137
cdnp1840.13o	csrj1840.13o	brdc1840.13n	igs17473.sp3	igs17473.clk_30s	igs17477.erp	2013/07/03	234.5156
cdnp1850.13o	csrj1850.13o	brdc1850.13n	igs17474.sp3	igs17474.clk_30s	igs17477.erp	2013/07/04	234.5047
cdnp1860.13o	csrj1860.13o	brdc1860.13n	igs17475.sp3	igs17475.clk_30s	igs17477.erp	2013/07/05	234.5098
cdnp1870.13o	csrj1870.13o	brdc1870.13n	igs17476.sp3	igs17476.clk_30s	igs17477.erp	2013/07/06	234.5182
cdnp1880.13o	csrj1880.13o	brdc1880.13n	igs17480.sp3	igs17480.clk_30s	igs17487.erp	2013/07/07	234.5219
cdnp1890.13o	csrj1890.13o	brdc1890.13n	igs17481.sp3	igs17481.clk_30s	igs17487.erp	2013/07/08	234.4932
cdnp1900.13o	csrj1900.13o	brdc1900.13n	igs17482.sp3	igs17482.clk_30s	igs17487.erp	2013/07/09	234.5187
cdnp1910.13o	csrj1910.13o	brdc1910.13n	igs17483.sp3	igs17483.clk_30s	igs17487.erp	2013/07/10	234.5382
cdnp1920.13o	csrj1920.13o	brdc1920.13n	igs17484.sp3	igs17484.clk_30s	igs17487.erp	2013/07/11	234.5190
cdnp1930.13o	csrj1930.13o	brdc1930.13n	igs17485.sp3	igs17485.clk_30s	igs17487.erp	2013/07/12	234.5069
cdnp1940.13o	csrj1940.13o	brdc1940.13n	igs17486.sp3	igs17486.clk_30s	igs17487.erp	2013/07/13	234.5130
cdnp1950.13o	csrj1950.13o	brdc1950.13n	igs17487.sp3	igs17487.clk_30s	igs17487.erp	2013/07/14	234.5334
cdnp1960.13o	csrj1960.13o	brdc1960.13n	igs17491.sp3	igs17491.clk_30s	igs17487.erp	2013/07/15	234.5169
cdnp1970.13o	csrj1970.13o	brdc1970.13n	igs17492.sp3	igs17492.clk_30s	igs17487.erp	2013/07/16	234.5143
cdnp1980.13o	csrj1980.13o	brdc1980.13n	igs17493.sp3	igs17493.clk_30s	igs17487.erp	2013/07/17	234.5085
cdnp1990.13o	csrj1990.13o	brdc1990.13n	igs17494.sp3	igs17494.clk_30s	igs17497.erp	2013/07/18	234.5078
cdnp2000.13o	csrj2000.13o	brdc2000.13n	igs17495.sp3	igs17495.clk_30s	igs17497.erp	2013/07/19	234.5114
cdnp2010.13o	csrj2010.13o	brdc2010.13n	igs17496.sp3	igs17496.clk_30s	igs17497.erp	2013/07/20	234.5059
cdnp2020.13o	csrj2020.13o	brdc2020.13n	igs17500.sp3	igs17500.clk_30s	igs17507.erp	2013/07/21	234.5212
cdnp2030.13o	csrj2030.13o	brdc2030.13n	igs17501.sp3	igs17501.clk_30s	igs17507.erp	2013/07/22	234.5212
cdnp2040.13o	csrj2040.13o	brdc2040.13n	igs17502.sp3	igs17502.clk_30s	igs17507.erp	2013/07/23	234.5213
cdnp2050.13o	csrj2050.13o	brdc2050.13n	igs17503.sp3	igs17503.clk_30s	igs17507.erp	2013/07/24	234.5229
cdnp2060.13o	csrj2060.13o	brdc2060.13n	igs17504.sp3	igs17504.clk_30s	igs17507.erp	2013/07/25	234.5167
cdnp2070.13o	csrj2070.13o	brdc2070.13n	igs17505.sp3	igs17505.clk_30s	igs17507.erp	2013/07/26	234.5146
cdnp2080.13o	csrj2080.13o	brdc2080.13n	igs17506.sp3	igs17506.clk_30s	igs17507.erp	2013/07/27	234.5159
cdnp2090.13o	csrj2090.13o	brdc2090.13n	igs17510.sp3	igs17510.clk_30s	igs17517.erp	2013/07/28	234.5144
cdnp2100.13o	csrj2100.13o	brdc2100.13n	igs17511.sp3	igs17511.clk_30s	igs17517.erp	2013/07/30	234.5169
cdnp2120.13o	csrj2120.13o	brdc2120.13n	igs17513.sp3	igs17513.clk_30s	igs17527.erp	2013/07/31	234.5235
cdnp2130.13o	csrj2130.13o	brdc2130.13n	igs17514.sp3	igs17514.clk_30s	igs17527.erp	2013/08/01	234.5205
cdnp2140.13o	csrj2140.13o	brdc2140.13n	igs17515.sp3	igs17515.clk_30s	igs17527.erp	2013/08/02	234.5247
cdnp2150.13o	csrj2150.13o	brdc2150.13n	igs17516.sp3	igs17516.clk_30s	igs17527.erp	2013/08/03	234.5151
cdnp2160.13o	csrj2160.13o	brdc2160.13n	igs17520.sp3	igs17520.clk_30s	igs17527.erp	2013/08/04	234.5113
cdnp2170.13o	csrj2170.13o	brdc2170.13n	igs17521.sp3	igs17521.clk_30s	igs17527.erp	2013/08/05	234.5144
cdnp2180.13o	csrj2180.13o	brdc2180.13n	igs17522.sp3	igs17522.clk_30s	igs17527.erp	2013/08/06	234.5119
cdnp2190.13o	csrj2190.13o	brdc2190.13n	igs17523.sp3	igs17523.clk_30s	igs17527.erp	2013/08/07	234.5210
cdnp2210.13o	csrj2210.13o	brdc2210.13n	igs17525.sp3	igs17525.clk_30s	igs17527.erp	2013/08/09	234.5122
cdnp2220.13o	csrj2220.13o	brdc2220.13n	igs17526.sp3	igs17526.clk_30s	igs17527.erp	2013/08/10	234.5217
cdnp2230.13o	csrj2230.13o	brdc2230.13n	igs17530.sp3	igs17530.clk_30s	igs17537.erp	2013/08/11	234.5235
cdnp2240.13o	csrj2240.13o	brdc2240.13n	igs17531.sp3	igs17531.clk_30s	igs17537.erp	2013/08/12	234.5178
cdnp2250.13o	csrj2250.13o	brdc2250.13n	igs17532.sp3	igs17532.clk_30s	igs17537.erp	2013/08/13	234.5047
cdnp2260.13o	csrj2260.13o	brdc2260.13n	igs17533.sp3	igs17533.clk_30s	igs17537.erp	2013/08/14	234.5244
cdnp2270.13o	csrj2270.13o	brdc2270.13n	igs17534.sp3	igs17534.clk_30s	igs17537.erp	2013/08/15	234.4955
cdnp2280.13o	csrj2280.13o	brdc2280.13n	igs17535.sp3	igs17535.clk_30s	igs17537.erp	2013/08/16	234.5157
cdnp2290.13o	csrj2290.13o	brdc2290.13n	igs17536.sp3	igs17536.clk_30s	igs17537.erp	2013/08/17	234.5067
cdnp2300.13o	csrj2300.13o	brdc2300.13n	igs17540.sp3	igs17540.clk_30s	igs17547.erp	2013/08/18	234.5139
cdnp2310.13o	csrj2310.13o	brdc2310.13n	igs17541.sp3	igs17541.clk_30s	igs17547.erp	2013/08/19	234.5075
cdnp2320.13o	csrj2320.13o	brdc2320.13n	igs17542.sp3	igs17542.clk_30s	igs17547.erp	2013/08/20	234.5216
cdnp2330.13o	csrj2330.13o	brdc2330.13n	igs17543.sp3	igs17543.clk_30s	igs17547.erp	2013/08/21	234.5145
cdnp2340.13o	csrj2340.13o	brdc2340.13n	igs17544.sp3	igs17544.clk_30s	igs17547.erp	2013/08/22	234.5095
cdnp2350.13o	csrj2350.13o	brdc2350.13n	igs17545.sp3	igs17545.clk_30s	igs17547.erp	2013/08/23	234.5151
cdnp2360.13o	csrj2360.13o	brdc2360.13n	igs17546.sp3	igs17546.clk_30s	igs17547.erp	2013/08/24	234.5158
cdnp2370.13o	csrj2370.13o	brdc2370.13n	igs17550.sp3	igs17550.clk_30s	igs17547.erp	2013/08/25	234.5265
cdnp2380.13o	csrj2380.13o	brdc2380.13n	igs17551.sp3	igs17551.clk_30s	igs17547.erp	2013/08/26	234.5077
cdnp2390.13o	csrj2390.13o	brdc2390.13n	igs17552.sp3	igs17552.clk_30s	igs17547.erp	2013/08/27	234.5164
cdnp2400.13o	csrj2400.13o	brdc2400.13n	igs17553.sp3	igs17553.clk_30s	igs17547.erp	2013/08/28	234.5120
cdnp2410.13o	csrj2410.13o	brdc2410.13n	igs17554.sp3	igs17554.clk_30s	igs17547.erp	2013/08/29	234.4962
cdnp2420.13o	csrj2420.13o	brdc2420.13n	igs17555.sp3	igs17555.clk_30s	igs17557.erp	2013/08/30	234.5277
cdnp2430.13o	csrj2430.13o	brdc2430.13n	igs17556.sp3	igs17556.clk_30s	igs17557.erp	2013/08/31	234.5154
cdnp2440.13o	csrj2440.13o	brdc2440.13n	igs17560.sp3	igs17560.clk_30s	igs17557.erp	2013/09/01	234.5192
cdnp2450.13o	csrj2450.13o	brdc2450.13n	igs17561.sp3	igs17561.clk_30s	igs17557.erp	2013/09/02	234.5227
cdnp2460.13o	csrj2460.13o	brdc2460.13n	igs17562.sp3	igs17562.clk_30s	igs17557.erp	2013/09/03	234.5160
cdnp2470.13o	csrj2470.13o	brdc2470.13n	igs17563.sp3	igs17563.clk_30s	igs17557.erp	2013/09/04	234.5126
cdnp2480.13o	csrj2480.13o	brdc2480.13n	igs17564.sp3	igs17564.clk_30s	igs17567.erp	2013/09/05	234.5108
cdnp2490.13o	csrj2490.13o	brdc2490.13n	igs17565.sp3	igs17565.clk_30s	igs17567.erp	2013/09/06	234.5124



cdnp2500.13o	csrj2500.13o	brdc2500.13n	igs17566.sp3	igs17566.clk_30s	igs17567.erp	2013/09/07	234.5049
cdnp2510.13o	csrj2510.13o	brdc2510.13n	igs17570.sp3	igs17570.clk_30s	igs17577.erp	2013/09/08	234.5157
cdnp2520.13o	csrj2520.13o	brdc2520.13n	igs17571.sp3	igs17571.clk_30s	igs17577.erp	2013/09/09	234.5064
cdnp2530.13o	csrj2530.13o	brdc2530.13n	igs17572.sp3	igs17572.clk_30s	igs17577.erp	2013/09/10	234.5299
cdnp2540.13o	csrj2540.13o	brdc2540.13n	igs17573.sp3	igs17573.clk_30s	igs17577.erp	2013/09/11	234.5139
cdnp2550.13o	csrj2550.13o	brdc2550.13n	igs17574.sp3	igs17574.clk_30s	igs17577.erp	2013/09/12	234.5080
cdnp2560.13o	csrj2560.13o	brdc2560.13n	igs17575.sp3	igs17575.clk_30s	igs17577.erp	2013/09/13	234.5075
cdnp2570.13o	csrj2570.13o	brdc2570.13n	igs17576.sp3	igs17576.clk_30s	igs17577.erp	2013/09/14	234.5299
cdnp2580.13o	csrj2580.13o	brdc2580.13n	igs17580.sp3	igs17580.clk_30s	igs17577.erp	2013/09/15	234.5177
cdnp2590.13o	csrj2590.13o	brdc2590.13n	igs17581.sp3	igs17581.clk_30s	igs17587.erp	2013/09/16	234.5174
cdnp2600.13o	csrj2600.13o	brdc2600.13n	igs17582.sp3	igs17582.clk_30s	igs17587.erp	2013/09/17	234.5290
cdnp2610.13o	csrj2610.13o	brdc2610.13n	igs17583.sp3	igs17583.clk_30s	igs17587.erp	2013/09/18	234.5183
cdnp2620.13o	csrj2620.13o	brdc2620.13n	igs17584.sp3	igs17584.clk_30s	igs17587.erp	2013/09/19	234.5240
cdnp2630.13o	csrj2630.13o	brdc2630.13n	igs17585.sp3	igs17585.clk_30s	igs17587.erp	2013/09/20	234.5216
cdnp2640.13o	csrj2640.13o	brdc2640.13n	igs17586.sp3	igs17586.clk_30s	igs17587.erp	2013/09/21	234.5098
cdnp2650.13o	csrj2650.13o	brdc2650.13n	igs17590.sp3	igs17590.clk_30s	igs17597.erp	2013/09/22	234.5106
cdnp2660.13o	csrj2660.13o	brdc2660.13n	igs17591.sp3	igs17591.clk_30s	igs17597.erp	2013/09/23	234.5121
cdnp2670.13o	csrj2670.13o	brdc2670.13n	igs17592.sp3	igs17592.clk_30s	igs17597.erp	2013/09/24	234.5096
cdnp2680.13o	csrj2680.13o	brdc2680.13n	igs17593.sp3	igs17593.clk_30s	igs17597.erp	2013/09/25	234.5100
cdnp2690.13o	csrj2690.13o	brdc2690.13n	igs17594.sp3	igs17594.clk_30s	igs17597.erp	2013/09/26	234.5144
cdnp2700.13o	csrj2700.13o	brdc2700.13n	igs17595.sp3	igs17595.clk_30s	igs17597.erp	2013/09/27	234.5122
cdnp0010.14o	csrj0010.14o	brdc0010.14n	igs17733.sp3	igs17733.clk_30s	igs17737.erp	2014/01/01	234.5279
cdnp0030.14o	csrj0030.14o	brdc0030.erp	igs17735.sp3	igs17735.clk_30s	igs17737.erp	2014/01/03	234.6026
cdnp0040.14o	csrj0040.14o	brdc0040.erp	igs17736.sp3	igs17736.clk_30s	igs17737.erp	2014/01/04	234.6698
cdnp0050.14o	csrj0050.14o	brdc0050.erp	igs17740.sp3	igs17740.clk_30s	igs17747.erp	2014/01/05	234.6679
cdnp0060.14o	csrj0060.14o	brdc0060.erp	igs17741.sp3	igs17741.clk_30s	igs17747.erp	2014/01/06	234.6865
cdnp0070.14o	csrj0070.14o	brdc0070.erp	igs17742.sp3	igs17742.clk_30s	igs17747.erp	2014/01/07	233.9736
cdnp0080.14o	csrj0080.14o	brdc0080.erp	igs17743.sp3	igs17743.clk_30s	igs17747.erp	2014/01/08	234.3203
cdnp0090.14o	csrj0090.14o	brdc0090.erp	igs17744.sp3	igs17744.clk_30s	igs17747.erp	2014/01/09	234.3200
cdnp0100.14o	csrj0100.14o	brdc0100.erp	igs17745.sp3	igs17745.clk_30s	igs17747.erp	2014/01/10	234.6557
cdnp0110.14o	csrj0110.14o	brdc0110.erp	igs17746.sp3	igs17746.clk_30s	igs17747.erp	2014/01/11	234.6713
cdnp0120.14o	csrj0120.14o	brdc0120.erp	igs17750.sp3	igs17750.clk_30s	igs17757.erp	2014/01/12	234.6784
cdnp0130.14o	csrj0130.14o	brdc0130.erp	igs17751.sp3	igs17751.clk_30s	igs17757.erp	2014/01/13	234.6696
cdnp0140.14o	csrj0140.14o	brdc0140.erp	igs17752.sp3	igs17752.clk_30s	igs17757.erp	2014/01/14	234.3260
cdnp0150.14o	csrj0150.14o	brdc0150.erp	igs17753.sp3	igs17753.clk_30s	igs17757.erp	2014/01/15	234.5299
cdnp0160.14o	csrj0160.14o	brdc0160.erp	igs17754.sp3	igs17754.clk_30s	igs17757.erp	2014/01/16	234.6650
cdnp0170.14o	csrj0170.14o	brdc0170.erp	igs17755.sp3	igs17755.clk_30s	igs17757.erp	2014/01/17	234.6742
cdnp0180.14o	csrj0180.14o	brdc0180.erp	igs17756.sp3	igs17756.clk_30s	igs17757.erp	2014/01/18	234.6846
cdnp0190.14o	csrj0190.14o	brdc0190.erp	igs17760.sp3	igs17760.clk_30s	igs17767.erp	2014/01/19	234.6629
cdnp0200.14o	csrj0200.14o	brdc0200.erp	igs17761.sp3	igs17761.clk_30s	igs17767.erp	2014/01/20	234.4260
cdnp0210.14o	csrj0210.14o	brdc0210.erp	igs17762.sp3	igs17762.clk_30s	igs17767.erp	2014/01/21	234.8046
cdnp0260.14o	csrj0260.14o	brdc0260.erp	igs17770.sp3	igs17770.clk_30s	igs17777.erp	2014/01/26	234.6338
cdnp0270.14o	csrj0270.14o	brdc0270.erp	igs17771.sp3	igs17771.clk_30s	igs17777.erp	2014/01/27	234.2666
cdnp0280.14o	csrj0280.14o	brdc0280.erp	igs17772.sp3	igs17772.clk_30s	igs17777.erp	2014/01/28	234.6355
cdnp0290.14o	csrj0290.14o	brdc0290.erp	igs17773.sp3	igs17773.clk_30s	igs17777.erp	2014/01/29	234.3359
cdnp0300.14o	csrj0300.14o	brdc0300.erp	igs17774.sp3	igs17774.clk_30s	igs17777.erp	2014/01/30	234.1452
cdnp0310.14o	csrj0310.14o	brdc0310.erp	igs17775.sp3	igs17775.clk_30s	igs17777.erp	2014/01/31	234.1452
cdnp0320.14o	csrj0320.14o	brdc0320.erp	igs17776.sp3	igs17776.clk_30s	igs17777.erp	2014/02/01	233.8121
cdnp0330.14o	csrj0330.14o	brdc0330.erp	igs17780.sp3	igs17780.clk_30s	igs17787.erp	2014/02/02	234.6544
cdnp0340.14o	csrj0340.14o	brdc0340.erp	igs17781.sp3	igs17781.clk_30s	igs17787.erp	2014/02/03	233.8823
cdnp0350.14o	csrj0350.14o	brdc0350.erp	igs17782.sp3	igs17782.clk_30s	igs17787.erp	2014/02/04	233.8823
cdnp0370.14o	csrj0370.14o	brdc0370.erp	igs17784.sp3	igs17784.clk_30s	igs17787.erp	2014/02/06	233.8452
cdnp0380.14o	csrj0380.14o	brdc0380.erp	igs17785.sp3	igs17785.clk_30s	igs17787.erp	2014/02/07	233.9421
cdnp0400.14o	csrj0400.14o	brdc0400.erp	igs17790.sp3	igs17790.clk_30s	igs17797.erp	2014/02/09	234.4984
cdnp0410.14o	csrj0410.14o	brdc0410.erp	igs17791.sp3	igs17791.clk_30s	igs17797.erp	2014/02/10	235.1319
cdnp0430.14o	csrj0430.14o	brdc0430.erp	igs17793.sp3	igs17793.clk_30s	igs17797.erp	2014/02/12	234.4301
cdnp0440.14o	csrj0440.14o	brdc0440.erp	igs17794.sp3	igs17794.clk_30s	igs17797.erp	2014/02/13	235.3241
cdnp0450.14o	csrj0450.14o	brdc0450.erp	igs17795.sp3	igs17795.clk_30s	igs17797.erp	2014/02/14	234.2105
cdnp0460.14o	csrj0460.14o	brdc0460.erp	igs17796.sp3	igs17796.clk_30s	igs17797.erp	2014/02/15	234.1578
cdnp0470.14o	csrj0470.14o	brdc0470.erp	igs17800.sp3	igs17800.clk_30s	igs17807.erp	2014/02/16	234.9534
cdnp0490.14o	csrj0490.14o	brdc0490.erp	igs17802.sp3	igs17802.clk_30s	igs17807.erp	2014/02/18	234.9534
cdnp0510.14o	csrj0510.14o	brdc0510.erp	igs17804.sp3	igs17804.clk_30s	igs17807.erp	2014/02/20	234.4632
cdnp0560.14o	csrj0560.14o	brdc0560.erp	igs17812.sp3	igs17812.clk_30s	igs17817.erp	2014/02/24	235.2862
cdnp0590.14o	csrj0590.14o	brdc0590.erp	igs17815.sp3	igs17815.clk_30s	igs17817.erp	2014/02/28	235.3160
cdnp0600.14o	csrj0600.14o	brdc0600.erp	igs17816.sp3	igs17816.clk_30s	igs17817.erp	2014/03/01	234.1324
cdnp0610.14o	csrj0610.14o	brdc0610.erp	igs17820.sp3	igs17820.clk_30s	igs17827.erp	2014/03/02	234.3284
cdnp0630.14o	csrj0630.14o	brdc0630.erp	igs17822.sp3	igs17822.clk_30s	igs17827.erp	2014/03/04	234.6347
cdnp0640.14o	csrj0640.14o	brdc0640.erp	igs17823.sp3	igs17823.clk_30s	igs17827.erp	2014/03/05	234.7591
cdnp0650.14o	csrj0650.14o	brdc0650.erp	igs17824.sp3	igs17824.clk_30s	igs17827.erp	2014/03/06	234.2713
cdnp0660.14o	csrj0660.14o	brdc0660.erp	igs17825.sp3	igs17825.clk_30s	igs17827.erp	2014/03/07	235.0254

cdnp0670.14o	csrj0670.14o	brdc0670.erp	igs17826.sp3	igs17826.clk_30s	igs17827.erp	2014/03/08	233.5775
cdnp0680.14o	csrj0680.14o	brdc0680.erp	igs17830.sp3	igs17830.clk_30s	igs17837.erp	2014/03/09	233.9549
cdnp0740.14o	csrj0740.14o	brdc0740.erp	igs17836.sp3	igs17836.clk_30s	igs17837.erp	2014/03/15	234.8487
cdnp0750.14o	csrj0750.14o	brdc0750.erp	igs17840.sp3	igs17840.clk_30s	igs17847.erp	2014/03/16	235.0005
cdnp0810.14o	csrj0810.14o	brdc0810.erp	igs17846.sp3	igs17846.clk_30s	igs17847.erp	2014/03/22	234.7711
cdnp0820.14o	csrj0820.14o	brdc0820.erp	igs17850.sp3	igs17850.clk_30s	igs17857.erp	2014/03/23	234.4049
cdnp0830.14o	csrj0830.14o	brdc0830.erp	igs17851.sp3	igs17851.clk_30s	igs17857.erp	2014/03/24	234.4049
cdnp0880.14o	csrj0880.14o	brdc0880.erp	igs17856.sp3	igs17856.clk_30s	igs17857.erp	2014/03/29	234.8309
cdnp0890.14o	csrj0890.14o	brdc0890.erp	igs17860.sp3	igs17860.clk_30s	igs17867.erp	2014/03/30	234.7527
cdnp0910.14o	csrj0910.14o	brdc0910.erp	igs17862.sp3	igs17862.clk_30s	igs17867.erp	2014/04/01	233.4858
cdnp0950.14o	csrj0950.14o	brdc0950.erp	igs17866.sp3	igs17866.clk_30s	igs17867.erp	2014/04/05	234.3763
cdnp0990.14o	csrj0990.14o	brdc0990.erp	igs17873.sp3	igs17873.clk_30s	igs1787.erp7	2014/04/09	234.2948
cdnp1000.14o	csrj1000.14o	brdc1000.erp	igs17874.sp3	igs17874.clk_30s	igs1787.erp7	2014/04/10	233.7476
cdnp1040.14o	csrj1040.14o	brdc1040.erp	igs17881.sp3	igs17881.clk_30s	igs17887.erp	2014/04/14	235.1969
cdnp1050.14o	csrj1050.14o	brdc1050.erp	igs17882.sp3	igs17882.clk_30s	igs17887.erp	2014/04/15	234.7870
cdnp1070.14o	csrj1070.14o	brdc1070.erp	igs17884.sp3	igs17884.clk_30s	igs17887.erp	2014/04/17	234.6810
cdnp1120.14o	csrj1120.14o	brdc1120.erp	igs17892.sp3	igs17892.clk_30s	igs17897.erp	2014/04/22	235.3107
cdnp1140.14o	csrj1140.14o	brdc1140.erp	igs17894.sp3	igs17894.clk_30s	igs17897.erp	2014/04/24	234.0914
cdnp1150.14o	csrj1150.14o	brdc1150.erp	igs17895.sp3	igs17895.clk_30s	igs17897.erp	2014/04/25	235.1575
cdnp1210.14o	csrj1210.14o	brdc1210.erp	igs17904.sp3	igs17904.clk_30s	igs17907.erp	2014/05/01	234.8609
cdnp1230.14o	csrj1230.14o	brdc1230.erp	igs17906.sp3	igs17906.clk_30s	igs17907.erp	2014/05/03	234.4680
cdnp1250.14o	csrj1250.14o	brdc1250.erp	igs17911.sp3	igs17911.clk_30s	igs17917.erp	2014/05/05	234.4920
cdnp1260.14o	csrj1260.14o	brdc1260.erp	igs17912.sp3	igs17912.clk_30s	igs17917.erp	2014/05/06	235.3014
cdnp1280.14o	csrj1280.14o	brdc1280.erp	igs17914.sp3	igs17914.clk_30s	igs17917.erp	2014/05/08	234.8956
cdnp1290.14o	csrj1290.14o	brdc1290.erp	igs17915.sp3	igs17915.clk_30s	igs17917.erp	2014/05/09	235.0214
cdnp1310.14o	csrj1310.14o	brdc1310.erp	igs17920.sp3	igs17920.clk_30s	igs17927.erp	2014/05/11	234.6379
cdnp1320.14o	csrj1320.14o	brdc1320.erp	igs17921.sp3	igs17921.clk_30s	igs17927.erp	2014/05/12	234.4918
cdnp1340.14o	csrj1340.14o	brdc1340.erp	igs17923.sp3	igs17923.clk_30s	igs17927.erp	2014/05/14	234.0742
cdnp1350.14o	csrj1350.14o	brdc1350.erp	igs17924.sp3	igs17924.clk_30s	igs17927.erp	2014/05/15	234.0713
cdnp1370.14o	csrj1370.14o	brdc1370.erp	igs17926.sp3	igs17926.clk_30s	igs17927.erp	2014/05/17	234.3201
cdnp1390.14o	csrj1390.14o	brdc1390.erp	igs17931.sp3	igs17931.clk_30s	igs17937.erp	2014/05/19	234.4771
cdnp1400.14o	csrj1400.14o	brdc1400.erp	igs17932.sp3	igs17932.clk_30s	igs17937.erp	2014/05/20	234.6867
cdnp1420.14o	csrj1420.14o	brdc1420.erp	igs17934.sp3	igs17934.clk_30s	igs17937.erp	2014/05/22	234.5635
cdnp1430.14o	csrj1430.14o	brdc1430.erp	igs17935.sp3	igs17935.clk_30s	igs17937.erp	2014/05/23	234.6256
cdnp1480.14o	csrj1480.14o	brdc1480.erp	igs17943.sp3	igs17943.clk_30s	igs17947.erp	2014/05/28	234.0862
cdnp1490.14o	csrj1490.14o	brdc1490.erp	igs17944.sp3	igs17944.clk_30s	igs17947.erp	2014/05/29	234.2760
cdnp1500.14o	csrj1500.14o	brdc1500.erp	igs17945.sp3	igs17945.clk_30s	igs17947.erp	2014/05/30	233.8890
cdnp1520.14o	csrj1520.14o	brdc1520.erp	igs17950.sp3	igs17950.clk_30s	igs17957.erp	2014/06/01	233.9156
cdnp1540.14o	csrj1540.14o	brdc1540.erp	igs17952.sp3	igs17952.clk_30s	igs17957.erp	2014/06/03	234.7873
cdnp1560.14o	csrj1560.14o	brdc1560.erp	igs17954.sp3	igs17954.clk_30s	igs17957.erp	2014/06/05	234.4029
cdnp1570.14o	csrj1570.14o	brdc1570.erp	igs17955.sp3	igs17955.clk_30s	igs17957.erp	2014/06/06	234.5866
cdnp1590.14o	csrj1590.14o	brdc1590.erp	igs17960.sp3	igs17960.clk_30s	igs17967.erp	2014/06/08	234.4076
cdnp1610.14o	csrj1610.14o	brdc1610.erp	igs17962.sp3	igs17962.clk_30s	igs17967.erp	2014/06/10	234.8062
cdnp1630.14o	csrj1630.14o	brdc1630.erp	igs17964.sp3	igs17964.clk_30s	igs17967.erp	2014/06/12	234.8945
cdnp1640.14o	csrj1640.14o	brdc1640.erp	igs17965.sp3	igs17965.clk_30s	igs17967.erp	2014/06/13	234.6881
cdnp1650.14o	csrj1650.14o	brdc1650.erp	igs17966.sp3	igs17966.clk_30s	igs17967.erp	2014/06/14	234.6981
cdnp1670.14o	csrj1670.14o	brdc1670.erp	igs17971.sp3	igs17971.clk_30s	igs17977.erp	2014/06/16	234.5983
cdnp1680.14o	csrj1680.14o	brdc1680.erp	igs17972.sp3	igs17972.clk_30s	igs17977.erp	2014/06/17	234.6917
cdnp1700.14o	csrj1700.14o	brdc1700.erp	igs17974.sp3	igs17974.clk_30s	igs17977.erp	2014/06/19	234.3354
cdnp1720.14o	csrj1720.14o	brdc1720.erp	igs17976.sp3	igs17976.clk_30s	igs17977.erp	2014/06/21	234.5208
cdnp1730.14o	csrj1730.14o	brdc1730.erp	igs17980.sp3	igs17980.clk_30s	igs17987.erp	2014/06/22	234.4464
cdnp1750.14o	csrj1750.14o	brdc1750.erp	igs17982.sp3	igs17982.clk_30s	igs17987.erp	2014/06/24	234.9409
cdnp1770.14o	csrj1770.14o	brdc1770.erp	igs17984.sp3	igs17984.clk_30s	igs17987.erp	2014/06/26	233.8479
cdnp1790.14o	csrj1790.14o	brdc1790.erp	igs17986.sp3	igs17986.clk_30s	igs17987.erp	2014/06/28	234.1621
cdnp1810.14o	csrj1810.14o	brdc1810.erp	igs17991.sp3	igs17991.clk_30s	igs17997.erp	2014/06/30	234.4985
cdnp1830.14o	csrj1830.14o	brdc1830.erp	igs17993.sp3	igs17993.clk_30s	igs17997.erp	2014/07/02	234.3323
cdnp1840.14o	csrj1840.14o	brdc1840.erp	igs17994.sp3	igs17994.clk_30s	igs17997.erp	2014/07/03	235.3248
cdnp1860.14o	csrj1860.14o	brdc1860.erp	igs17996.sp3	igs17996.clk_30s	igs17997.erp	2014/07/05	235.1344
cdnp1870.14o	csrj1870.14o	brdc1870.erp	igs18000.sp3	igs18000.clk_30s	igs18007.erp	2014/07/06	234.2057
cdnp1880.14o	csrj1880.14o	brdc1880.erp	igs18001.sp3	igs18001.clk_30s	igs18007.erp	2014/07/07	234.6834
cdnp1900.14o	csrj1900.14o	brdc1900.erp	igs18003.sp3	igs18003.clk_30s	igs18007.erp	2014/07/09	235.0929
cdnp1910.14o	csrj1910.14o	brdc1910.erp	igs18004.sp3	igs18004.clk_30s	igs18007.erp	2014/07/10	235.3793
cdnp1930.14o	csrj1930.14o	brdc1930.erp	igs18006.sp3	igs18006.clk_30s	igs18007.erp	2014/07/12	234.7985
cdnp1960.14o	csrj1960.14o	brdc1960.erp	igs18012.sp3	igs18012.clk_30s	igs18017.erp	2014/07/15	234.1947
cdnp1980.14o	csrj1980.14o	brdc1980.erp	igs18014.sp3	igs18014.clk_30s	igs18017.erp	2014/07/17	234.3688
cdnp1990.14o	csrj1990.14o	brdc1990.erp	igs18015.sp3	igs18015.clk_30s	igs18017.erp	2014/07/18	234.1853
cdnp2000.14o	csrj2000.14o	brdc2000.erp	igs18016.sp3	igs18016.clk_30s	igs18017.erp	2014/07/19	234.7802
cdnp2020.14o	csrj2020.14o	brdc2020.erp	igs18021.sp3	igs18021.clk_30s	igs18027.erp	2014/07/21	234.1340
cdnp2040.14o	csrj2040.14o	brdc2040.erp	igs18023.sp3	igs18023.clk_30s	igs18027.erp	2014/07/23	233.0706
cdnp2060.14o	csrj2060.14o	brdc2060.erp	igs18025.sp3	igs18025.clk_30s	igs18027.erp	2014/07/25	234.1646

cdnp2070.14o	csrj2070.14o	brdc2070.erp	igs18026.sp3	igs18026.clk_30s	igs18027.erp	2014/07/26	234.3241
cdnp3250.14o	csrj3250.14o	brdc3250.erp	igs18195.sp3	igs18195.clk_30s	igs18197.erp	2014/11/21	234.5294
cdnp3260.14o	csrj3260.14o	brdc3260.erp	igs18196.sp3	igs18196.clk_30s	igs18197.erp	2014/11/22	234.5877
cdnp3270.14o	csrj3270.14o	brdc3270.erp	igs18200.sp3	igs18200.clk_30s	igs18207.erp	2014/11/23	234.6114
cdnp3280.14o	csrj3280.14o	brdc3280.erp	igs18201.sp3	igs18201.clk_30s	igs18207.erp	2014/11/24	234.5996
cdnp3290.14o	csrj3290.14o	brdc3290.erp	igs18202.sp3	igs18202.clk_30s	igs18207.erp	2014/11/25	234.6398
cdnp3300.14o	csrj3300.14o	brdc3300.erp	igs18203.sp3	igs18203.clk_30s	igs18207.erp	2014/11/26	233.6038
cdnp3310.14o	csrj3310.14o	brdc3310.erp	igs18204.sp3	igs18204.clk_30s	igs18207.erp	2014/11/27	234.6152
cdnp3330.14o	csrj3330.14o	brdc3330.erp	igs18206.sp3	igs18206.clk_30s	igs18207.erp	2014/11/29	234.8396
cdnp3340.14o	csrj3340.14o	brdc3340.erp	igs18210.sp3	igs18210.clk_30s	igs18217.erp	2014/11/30	234.5817
cdnp3350.14o	csrj3350.14o	brdc3350.erp	igs18211.sp3	igs18211.clk_30s	igs18217.erp	2014/12/01	234.4121
cdnp3450.14o	csrj3450.14o	brdc3450.erp	igs18224.sp3	igs18224.clk_30s	igs18227.erp	2014/12/11	234.4272
cdnp3470.14o	csrj3470.14o	brdc3470.erp	igs18226.sp3	igs18226.clk_30s	igs18227.erp	2014/12/13	234.5232
cdnp3480.14o	csrj3480.14o	brdc3480.erp	igs18230.sp3	igs18230.clk_30s	igs18227.erp	2014/12/14	234.4552
cdnp3490.14o	csrj3490.14o	brdc3490.erp	igs18231.sp3	igs18231.clk_30s	igs18227.erp	2014/12/15	234.4873
cdnp3500.14o	csrj3500.14o	brdc3500.erp	igs18232.sp3	igs18232.clk_30s	igs18227.erp	2014/12/16	234.4982
cdnp3510.14o	csrj3510.14o	brdc3510.erp	igs18233.sp3	igs18233.clk_30s	igs18227.erp	2014/12/17	234.4647
cdnp3520.14o	csrj3520.14o	brdc3520.erp	igs18234.sp3	igs18234.clk_30s	igs18237.erp	2014/12/18	234.8237
cdnp0010.15o	csrj0010.15o	brdc0010.erp	igs18254.sp3	igs18254.clk_30s	igs18257.erp	2015/01/01	234.5266
cdnp0040.15o	csrj0040.15o	brdc0040.erp	igs18260.sp3	igs18260.clk_30s	igs18267.erp	2015/01/04	234.5144
cdnp0070.15o	csrj0070.15o	brdc0070.erp	igs18263.sp3	igs18263.clk_30s	igs18267.erp	2015/01/07	234.5075
cdnp0080.15o	csrj0080.15o	brdc0080.erp	igs18264.sp3	igs18264.clk_30s	igs18267.erp	2015/01/08	234.5221
cdnp0110.15o	csrj0110.15o	brdc0110.erp	igs18270.sp3	igs18270.clk_30s	igs18277.erp	2015/01/11	234.5338
cdnp0120.15o	csrj0120.15o	brdc0120.erp	igs18271.sp3	igs18271.clk_30s	igs18277.erp	2015/01/12	234.5506
cdnp0130.15o	csrj0130.15o	brdc0130.erp	igs18272.sp3	igs18272.clk_30s	igs18277.erp	2015/01/13	234.5412
cdnp0140.15o	csrj0140.15o	brdc0140.erp	igs18273.sp3	igs18273.clk_30s	igs18277.erp	2015/01/14	234.5222
cdnp0160.15o	csrj0160.15o	brdc0160.erp	igs18274.sp3	igs18274.clk_30s	igs18277.erp	2015/01/16	234.5092
cdnp0170.15o	csrj0170.15o	brdc0170.erp	igs18275.sp3	igs18275.clk_30s	igs18277.erp	2015/01/17	234.5152
cdnp0180.15o	csrj0180.15o	brdc0180.erp	igs18280.sp3	igs18280.clk_30s	igs18287.erp	2015/01/18	234.4919
cdnp0200.15o	csrj0200.15o	brdc0200.erp	igs18282.sp3	igs18282.clk_30s	igs18287.erp	2015/01/20	234.5152
cdnp0220.15o	csrj0220.15o	brdc0220.erp	igs18284.sp3	igs18284.clk_30s	igs18287.erp	2015/01/22	234.5113
cdnp0230.15o	csrj0230.15o	brdc0230.erp	igs18285.sp3	igs18285.clk_30s	igs18287.erp	2015/01/23	234.5215
cdnp0250.15o	csrj0250.15o	brdc0250.erp	igs18290.sp3	igs18290.clk_30s	igs18297.erp	2015/01/25	234.4597
cdnp0260.15o	csrj0260.15o	brdc0260.erp	igs18291.sp3	igs18291.clk_30s	igs18297.erp	2015/01/26	234.5160
cdnp0280.15o	csrj0280.15o	brdc0280.erp	igs18293.sp3	igs18293.clk_30s	igs18297.erp	2015/01/28	234.4523
cdnp0300.15o	csrj0300.15o	brdc0300.erp	igs18295.sp3	igs18295.clk_30s	igs18297.erp	2015/01/30	234.5006
cdnp0310.15o	csrj0310.15o	brdc0310.erp	igs18296.sp3	igs18296.clk_30s	igs18297.erp	2015/01/31	234.4860
cdnp0320.15o	csrj0320.15o	brdc0320.erp	igs18300.sp3	igs18300.clk_30s	igs18307.erp	2015/02/01	234.4991
cdnp0330.15o	csrj0330.15o	brdc0330.erp	igs18301.sp3	igs18301.clk_30s	igs18307.erp	2015/02/02	234.5750
cdnp0340.15o	csrj0340.15o	brdc0340.erp	igs18302.sp3	igs18302.clk_30s	igs18307.erp	2015/02/03	234.5034
cdnp0350.15o	csrj0350.15o	brdc0350.erp	igs18303.sp3	igs18303.clk_30s	igs18307.erp	2015/02/04	234.5033
cdnp0360.15o	csrj0360.15o	brdc0360.erp	igs18304.sp3	igs18304.clk_30s	igs18307.erp	2015/02/05	234.5156
cdnp0370.15o	csrj0370.15o	brdc0370.erp	igs18305.sp3	igs18305.clk_30s	igs18307.erp	2015/02/06	234.4285
cdnp0380.15o	csrj0380.15o	brdc0380.erp	igs18306.sp3	igs18306.clk_30s	igs18307.erp	2015/02/07	234.5151
cdnp0390.15o	csrj0390.15o	brdc0390.erp	igs18310.sp3	igs18310.clk_30s	igs18317.erp	2015/02/08	234.5257
cdnp0420.15o	csrj0420.15o	brdc0420.erp	igs18313.sp3	igs18313.clk_30s	igs18317.erp	2015/02/11	234.5120
cdnp0440.15o	csrj0440.15o	brdc0440.erp	igs18315.sp3	igs18315.clk_30s	igs18317.erp	2015/02/13	234.5067
cdnp0450.15o	csrj0450.15o	brdc0450.erp	igs18316.sp3	igs18316.clk_30s	igs18317.erp	2015/02/14	234.5121
cdnp0470.15o	csrj0470.15o	brdc0470.erp	igs18321.sp3	igs18321.clk_30s	igs18327.erp	2015/02/16	234.5372
cdnp0490.15o	csrj0490.15o	brdc0490.erp	igs18323.sp3	igs18323.clk_30s	igs18327.erp	2015/02/18	234.5159
cdnp0510.15o	csrj0510.15o	brdc0510.erp	igs18325.sp3	igs18325.clk_30s	igs18327.erp	2015/02/20	234.5042
cdnp0530.15o	csrj0530.15o	brdc0530.erp	igs18330.sp3	igs18330.clk_30s	igs18347.erp	2015/02/22	234.4716
cdnp0540.15o	csrj0540.15o	brdc0540.erp	igs18331.sp3	igs18331.clk_30s	igs18347.erp	2015/02/23	234.5140
cdnp0560.15o	csrj0560.15o	brdc0560.erp	igs18333.sp3	igs18333.clk_30s	igs18347.erp	2015/02/25	234.4953
cdnp0580.15o	csrj0580.15o	brdc0580.erp	igs18335.sp3	igs18335.clk_30s	igs18347.erp	2015/02/27	234.5195
cdnp0600.15o	csrj0600.15o	brdc0600.erp	igs18340.sp3	igs18340.clk_30s	igs18347.erp	2015/03/01	234.5332
cdnp0620.15o	csrj0620.15o	brdc0620.erp	igs18342.sp3	igs18342.clk_30s	igs18347.erp	2015/03/03	234.5228
cdnp0630.15o	csrj0630.15o	brdc0630.erp	igs18343.sp3	igs18343.clk_30s	igs18347.erp	2015/03/04	234.5011
cdnp0650.15o	csrj0650.15o	brdc0650.erp	igs18345.sp3	igs18345.clk_30s	igs18347.erp	2015/03/06	234.5324
cdnp0670.15o	csrj0670.15o	brdc0670.erp	igs18350.sp3	igs18350.clk_30s	igs18357.erp	2015/03/08	234.5042
cdnp0690.15o	csrj0690.15o	brdc0690.erp	igs18352.sp3	igs18352.clk_30s	igs18357.erp	2015/03/10	234.5002
cdnp0710.15o	csrj0710.15o	brdc0710.erp	igs18354.sp3	igs18354.clk_30s	igs18357.erp	2015/03/12	234.5041
cdnp0720.15o	csrj0720.15o	brdc0720.erp	igs18355.sp3	igs18355.clk_30s	igs18357.erp	2015/03/13	234.5100
cdnp0740.15o	csrj0740.15o	brdc0740.erp	igs18360.sp3	igs18360.clk_30s	igs18367.erp	2015/03/15	234.5459
cdnp0760.15o	csrj0760.15o	brdc0760.erp	igs18362.sp3	igs18362.clk_30s	igs18367.erp	2015/03/17	234.4973
cdnp0780.15o	csrj0780.15o	brdc0780.erp	igs18364.sp3	igs18364.clk_30s	igs18367.erp	2015/03/19	234.5783
cdnp0800.15o	csrj0800.15o	brdc0800.erp	igs18366.sp3	igs18366.clk_30s	igs18367.erp	2015/03/21	234.5078
cdnp0810.15o	csrj0810.15o	brdc0810.erp	igs18370.sp3	igs18370.clk_30s	igs18377.erp	2015/03/22	234.4945
cdnp0830.15o	csrj0830.15o	brdc0830.erp	igs18372.sp3	igs18372.clk_30s	igs18377.erp	2015/03/24	234.4773
cdnp0850.15o	csrj0850.15o	brdc0850.erp	igs18374.sp3	igs18374.clk_30s	igs18377.erp	2015/03/26	234.5022

cdnp0860.15o	csrj0860.15o	brdc0860.erp	igs18375.sp3	igs18375.clk_30s	igs18377.erp	2015/03/27	234.4823
cdnp0870.15o	csrj0870.15o	brdc0870.erp	igs18376.sp3	igs18376.clk_30s	igs18377.erp	2015/03/28	234.5030
cdnp0880.15o	csrj0880.15o	brdc0880.erp	igs18380.sp3	igs18380.clk_30s	igs18387.erp	2015/03/29	234.4829
cdnp0890.15o	csrj0890.15o	brdc0890.erp	igs18381.sp3	igs18381.clk_30s	igs18387.erp	2015/03/30	234.5033
cdnp0900.15o	csrj0900.15o	brdc0900.erp	igs18382.sp3	igs18382.clk_30s	igs18387.erp	2015/03/31	234.5028
cdnp0910.15o	csrj0910.15o	brdc0910.erp	igs18383.sp3	igs18383.clk_30s	igs18387.erp	2015/04/01	234.5359
cdnp0920.15o	csrj0920.15o	brdc0920.erp	igs18384.sp3	igs18384.clk_30s	igs18387.erp	2015/04/02	234.5711
cdnp0930.15o	csrj0930.15o	brdc0930.erp	igs18385.sp3	igs18385.clk_30s	igs18387.erp	2015/04/03	234.5085
cdnp0940.15o	csrj0940.15o	brdc0940.erp	igs18386.sp3	igs18386.clk_30s	igs18387.erp	2015/04/04	234.4919
cdnp0950.15o	csrj0950.15o	brdc0950.erp	igs18390.sp3	igs18390.clk_30s	igs18397.erp	2015/04/05	234.5097
cdnp0960.15o	csrj0960.15o	brdc0960.erp	igs18391.sp3	igs18391.clk_30s	igs18397.erp	2015/04/06	234.5170
cdnp0970.15o	csrj0970.15o	brdc0970.erp	igs18392.sp3	igs18392.clk_30s	igs18397.erp	2015/04/07	234.5139
cdnp0980.15o	csrj0980.15o	brdc0980.erp	igs18393.sp3	igs18393.clk_30s	igs18397.erp	2015/04/08	234.5116
cdnp0990.15o	csrj0990.15o	brdc0990.erp	igs18394.sp3	igs18394.clk_30s	igs18397.erp	2015/04/09	234.5008
cdnp1000.15o	csrj1000.15o	brdc1000.erp	igs18395.sp3	igs18395.clk_30s	igs18397.erp	2015/04/10	234.5023
cdnp1010.15o	csrj1010.15o	brdc1010.erp	igs18396.sp3	igs18396.clk_30s	igs18397.erp	2015/04/11	234.5105
cdnp1020.15o	csrj1020.15o	brdc1020.erp	igs18400.sp3	igs18400.clk_30s	igs18407.erp	2015/04/12	234.4877
cdnp1030.15o	csrj1030.15o	brdc1030.erp	igs18401.sp3	igs18401.clk_30s	igs18407.erp	2015/04/13	234.5491
cdnp1040.15o	csrj1040.15o	brdc1040.erp	igs18402.sp3	igs18402.clk_30s	igs18407.erp	2015/04/14	234.5638
cdnp1050.15o	csrj1050.15o	brdc1050.erp	igs18403.sp3	igs18403.clk_30s	igs18407.erp	2015/04/15	234.4999
cdnp1060.15o	csrj1060.15o	brdc1060.erp	igs18404.sp3	igs18404.clk_30s	igs18407.erp	2015/04/16	234.4949
cdnp1070.15o	csrj1070.15o	brdc1070.erp	igs18405.sp3	igs18405.clk_30s	igs18407.erp	2015/04/17	234.5178
cdnp1080.15o	csrj1080.15o	brdc1080.erp	igs18406.sp3	igs18406.clk_30s	igs18407.erp	2015/04/18	234.5005
cdnp1090.15o	csrj1090.15o	brdc1090.erp	igs18410.sp3	igs18410.clk_30s	igs18417.erp	2015/04/19	234.4892
cdnp1100.15o	csrj1100.15o	brdc1100.erp	igs18411.sp3	igs18411.clk_30s	igs18417.erp	2015/04/20	234.4944
cdnp1110.15o	csrj1110.15o	brdc1110.erp	igs18412.sp3	igs18412.clk_30s	igs18417.erp	2015/04/21	234.5058
cdnp1120.15o	csrj1120.15o	brdc1120.erp	igs18413.sp3	igs18413.clk_30s	igs18417.erp	2015/04/22	234.5046
cdnp1130.15o	csrj1130.15o	brdc1130.erp	igs18414.sp3	igs18414.clk_30s	igs18417.erp	2015/04/23	234.5130
cdnp1140.15o	csrj1140.15o	brdc1140.erp	igs18415.sp3	igs18415.clk_30s	igs18417.erp	2015/04/24	234.5152
cdnp1150.15o	csrj1150.15o	brdc1150.erp	igs18416.sp3	igs18416.clk_30s	igs18417.erp	2015/04/25	234.4895
cdnp1160.15o	csrj1160.15o	brdc1160.erp	igs18420.sp3	igs18420.clk_30s	igs18427.erp	2015/04/26	234.5320
cdnp1170.15o	csrj1170.15o	brdc1170.erp	igs18421.sp3	igs18421.clk_30s	igs18427.erp	2015/04/27	234.5056
cdnp1190.15o	csrj1190.15o	brdc1190.erp	igs18423.sp3	igs18423.clk_30s	igs18427.erp	2015/04/29	234.4741
cdnp1200.15o	csrj1200.15o	brdc1200.erp	igs18424.sp3	igs18424.clk_30s	igs18427.erp	2015/04/30	234.4515
cdnp1210.15o	csrj1210.15o	brdc1210.erp	igs18425.sp3	igs18425.clk_30s	igs18427.erp	2015/05/01	234.4925
cdnp1220.15o	csrj1220.15o	brdc1220.erp	igs18426.sp3	igs18426.clk_30s	igs18427.erp	2015/05/02	234.4925
cdnp1230.15o	csrj1230.15o	brdc1230.erp	igs18430.sp3	igs18430.clk_30s	igs18437.erp	2015/05/03	234.5006
cdnp1240.15o	csrj1240.15o	brdc1240.erp	igs18431.sp3	igs18431.clk_30s	igs18437.erp	2015/05/04	234.5106
cdnp1250.15o	csrj1250.15o	brdc1250.erp	igs18432.sp3	igs18432.clk_30s	igs18437.erp	2015/05/05	234.5021
cdnp1260.15o	csrj1260.15o	brdc1260.erp	igs18433.sp3	igs18433.clk_30s	igs18437.erp	2015/05/06	234.5025
cdnp1270.15o	csrj1270.15o	brdc1270.erp	igs18434.sp3	igs18434.clk_30s	igs18437.erp	2015/05/07	234.4872
cdnp1280.15o	csrj1280.15o	brdc1280.erp	igs18435.sp3	igs18435.clk_30s	igs18437.erp	2015/05/08	234.5096
cdnp1290.15o	csrj1290.15o	brdc1290.erp	igs18436.sp3	igs18436.clk_30s	igs18437.erp	2015/05/09	234.5211
cdnp1300.15o	csrj1300.15o	brdc1300.erp	igs18440.sp3	igs18440.clk_30s	igs18447.erp	2015/05/10	234.4954
cdnp1310.15o	csrj1310.15o	brdc1310.erp	igs18441.sp3	igs18441.clk_30s	igs18447.erp	2015/05/11	234.5197
cdnp1320.15o	csrj1320.15o	brdc1320.erp	igs18442.sp3	igs18442.clk_30s	igs18447.erp	2015/05/12	234.4939
cdnp1340.15o	csrj1340.15o	brdc1340.erp	igs18444.sp3	igs18444.clk_30s	igs18447.erp	2015/05/14	234.5056
cdnp1350.15o	csrj1350.15o	brdc1350.erp	igs18445.sp3	igs18445.clk_30s	igs18447.erp	2015/05/15	234.5183
cdnp1360.15o	csrj1360.15o	brdc1360.erp	igs18446.sp3	igs18446.clk_30s	igs18447.erp	2015/05/16	234.5232
cdnp1370.15o	csrj1370.15o	brdc1370.erp	igs18450.sp3	igs18450.clk_30s	igs18457.erp	2015/05/17	234.5132
cdnp1380.15o	csrj1380.15o	brdc1380.erp	igs18451.sp3	igs18451.clk_30s	igs18457.erp	2015/05/18	234.5121
cdnp1390.15o	csrj1390.15o	brdc1390.erp	igs18452.sp3	igs18452.clk_30s	igs18457.erp	2015/05/19	234.5109
cdnp1400.15o	csrj1400.15o	brdc1400.erp	igs18453.sp3	igs18453.clk_30s	igs18457.erp	2015/05/20	234.5226
cdnp1410.15o	csrj1410.15o	brdc1410.erp	igs18454.sp3	igs18454.clk_30s	igs18457.erp	2015/05/21	234.5178
cdnp1420.15o	csrj1420.15o	brdc1420.erp	igs18455.sp3	igs18455.clk_30s	igs18457.erp	2015/05/22	234.5133
cdnp1430.15o	csrj1430.15o	brdc1430.erp	igs18456.sp3	igs18456.clk_30s	igs18457.erp	2015/05/23	234.5212
cdnp1440.15o	csrj1440.15o	brdc1440.erp	igs18460.sp3	igs18460.clk_30s	igs18467.erp	2015/05/24	234.5268
cdnp1450.15o	csrj1450.15o	brdc1450.erp	igs18461.sp3	igs18461.clk_30s	igs18467.erp	2015/05/25	234.5162
cdnp1460.15o	csrj1460.15o	brdc1460.erp	igs18462.sp3	igs18462.clk_30s	igs18467.erp	2015/05/26	234.5006
cdnp1470.15o	csrj1470.15o	brdc1470.erp	igs18463.sp3	igs18463.clk_30s	igs18467.erp	2015/05/27	234.5052
cdnp1480.15o	csrj1480.15o	brdc1480.erp	igs18464.sp3	igs18464.clk_30s	igs18467.erp	2015/05/28	234.5091
cdnp1490.15o	csrj1490.15o	brdc1490.erp	igs18465.sp3	igs18465.clk_30s	igs18467.erp	2015/05/29	234.4983
cdnp1500.15o	csrj1500.15o	brdc1500.erp	igs18466.sp3	igs18466.clk_30s	igs18467.erp	2015/05/30	234.5142
cdnp1510.15o	csrj1510.15o	brdc1510.erp	igs18470.sp3	igs18470.clk_30s	igs18477.erp	2015/05/31	234.5202
cdnp1520.15o	csrj1520.15o	brdc1520.erp	igs18471.sp3	igs18471.clk_30s	igs18477.erp	2015/06/01	234.5110
cdnp1540.15o	csrj1540.15o	brdc1540.erp	igs18473.sp3	igs18473.clk_30s	igs18477.erp	2015/06/03	234.5135
cdnp1550.15o	csrj1550.15o	brdc1550.erp	igs18474.sp3	igs18474.clk_30s	igs18477.erp	2015/06/04	234.5070
cdnp1560.15o	csrj1560.15o	brdc1560.erp	igs18475.sp3	igs18475.clk_30s	igs18477.erp	2015/06/05	234.4992
cdnp1580.15o	csrj1580.15o	brdc1580.erp	igs18480.sp3	igs18480.clk_30s	igs18487.erp	2015/06/07	234.5130
cdnp1590.15o	csrj1590.15o	brdc1590.erp	igs18481.sp3	igs18481.clk_30s	igs18487.erp	2015/06/08	234.5122

cdnp1600.15o	csrj1600.15o	brdc1600.erp	igs18482.sp3	igs18482.clk_30s	igs18487.erp	2015/06/09	234.5021
cdnp1610.15o	csrj1610.15o	brdc1610.erp	igs18483.sp3	igs18483.clk_30s	igs18487.erp	2015/06/10	234.5096
cdnp1840.15o	csrj1840.15o	brdc1840.erp	igs18515.sp3	igs18515.clk_30s	igs18517.erp	2015/07/03	234.5135
cdnp1850.15o	csrj1850.15o	brdc1850.erp	igs18516.sp3	igs18516.clk_30s	igs18517.erp	2015/07/04	234.5207
cdnp1860.15o	csrj1860.15o	brdc1860.erp	igs18520.sp3	igs18520.clk_30s	igs18527.erp	2015/07/05	234.5180
cdnp1870.15o	csrj1870.15o	brdc1870.erp	igs18521.sp3	igs18521.clk_30s	igs18527.erp	2015/07/06	234.5054
cdnp1890.15o	csrj1890.15o	brdc1890.erp	igs18523.sp3	igs18523.clk_30s	igs18527.erp	2015/07/08	234.5241
cdnp1900.15o	csrj1900.15o	brdc1900.erp	igs18524.sp3	igs18524.clk_30s	igs18527.erp	2015/07/09	234.5129
cdnp1910.15o	csrj1910.15o	brdc1910.erp	igs18525.sp3	igs18525.clk_30s	igs18527.erp	2015/07/10	234.5108
cdnp1920.15o	csrj1920.15o	brdc1920.erp	igs18526.sp3	igs18526.clk_30s	igs18527.erp	2015/07/11	234.5194
cdnp1930.15o	csrj1930.15o	brdc1930.erp	igs18530.sp3	igs18530.clk_30s	igs18537.erp	2015/07/12	234.5153
cdnp1940.15o	csrj1940.15o	brdc1940.erp	igs18531.sp3	igs18531.clk_30s	igs18537.erp	2015/07/13	234.5197
cdnp1950.15o	csrj1950.15o	brdc1950.erp	igs18532.sp3	igs18532.clk_30s	igs18537.erp	2015/07/14	234.4747
cdnp1960.15o	csrj1960.15o	brdc1960.erp	igs18533.sp3	igs18533.clk_30s	igs18537.erp	2015/07/15	234.5061
cdnp1970.15o	csrj1970.15o	brdc1970.erp	igs18534.sp3	igs18534.clk_30s	igs18537.erp	2015/07/16	234.5127
cdnp1980.15o	csrj1980.15o	brdc1980.erp	igs18535.sp3	igs18535.clk_30s	igs18537.erp	2015/07/17	234.5139
cdnp1990.15o	csrj1990.15o	brdc1990.erp	igs18536.sp3	igs18536.clk_30s	igs18537.erp	2015/07/18	234.5066
cdnp2000.15o	csrj2000.15o	brdc2000.erp	igs18540.sp3	igs18540.clk_30s	igs18547.erp	2015/07/19	234.5051
cdnp2010.15o	csrj2010.15o	brdc2010.erp	igs18541.sp3	igs18541.clk_30s	igs18547.erp	2015/07/20	234.5121
cdnp2020.15o	csrj2020.15o	brdc2020.erp	igs18542.sp3	igs18542.clk_30s	igs18547.erp	2015/07/21	234.5094
cdnp2030.15o	csrj2030.15o	brdc2030.erp	igs18543.sp3	igs18543.clk_30s	igs18547.erp	2015/07/22	234.5010
cdnp2040.15o	csrj2040.15o	brdc2040.erp	igs18544.sp3	igs18544.clk_30s	igs18547.erp	2015/07/23	234.5212
cdnp2050.15o	csrj2050.15o	brdc2050.erp	igs18545.sp3	igs18545.clk_30s	igs18547.erp	2015/07/24	234.5055
cdnp2070.15o	csrj2070.15o	brdc2070.erp	igs18550.sp3	igs18550.clk_30s	igs18557.erp	2015/07/26	234.5128
cdnp2080.15o	csrj2080.15o	brdc2080.erp	igs18551.sp3	igs18551.clk_30s	igs18557.erp	2015/07/27	234.5019
cdnp2090.15o	csrj2090.15o	brdc2090.erp	igs18552.sp3	igs18552.clk_30s	igs18557.erp	2015/07/28	234.5097
cdnp2100.15o	csrj2100.15o	brdc2100.erp	igs18553.sp3	igs18553.clk_30s	igs18557.erp	2015/07/29	234.5020
cdnp2110.15o	csrj2110.15o	brdc2110.erp	igs18554.sp3	igs18554.clk_30s	igs18557.erp	2015/07/30	234.5030
cdnp2120.15o	csrj2120.15o	brdc2120.erp	igs18555.sp3	igs18555.clk_30s	igs18557.erp	2015/07/31	234.4318
cdnp2140.15o	csrj2140.15o	brdc2140.erp	igs18560.sp3	igs18560.clk_30s	igs18567.erp	2015/08/02	234.5116
cdnp2150.15o	csrj2150.15o	brdc2150.erp	igs18561.sp3	igs18561.clk_30s	igs18567.erp	2015/08/03	234.5002
cdnp2160.15o	csrj2160.15o	brdc2160.erp	igs18562.sp3	igs18562.clk_30s	igs18567.erp	2015/08/04	234.5195
cdnp2170.15o	csrj2170.15o	brdc2170.erp	igs18563.sp3	igs18563.clk_30s	igs18567.erp	2015/08/05	234.5052
cdnp2180.15o	csrj2180.15o	brdc2180.erp	igs18564.sp3	igs18564.clk_30s	igs18567.erp	2015/08/06	234.4993
cdnp2190.15o	csrj2190.15o	brdc2190.erp	igs18565.sp3	igs18565.clk_30s	igs18567.erp	2015/08/07	234.5129
cdnp2200.15o	csrj2200.15o	brdc2200.erp	igs18566.sp3	igs18566.clk_30s	igs18567.erp	2015/08/08	234.5086
cdnp2210.15o	csrj2210.15o	brdc2210.erp	igs18570.sp3	igs18570.clk_30s	igs18577.erp	2015/08/09	234.5049
cdnp2220.15o	csrj2220.15o	brdc2220.erp	igs18571.sp3	igs18571.clk_30s	igs18577.erp	2015/08/10	234.5109
cdnp2240.15o	csrj2240.15o	brdc2240.erp	igs18573.sp3	igs18573.clk_30s	igs18577.erp	2015/08/12	234.5065
cdnp2250.15o	csrj2250.15o	brdc2250.erp	igs18574.sp3	igs18574.clk_30s	igs18577.erp	2015/08/13	234.5035
cdnp2260.15o	csrj2260.15o	brdc2260.erp	igs18575.sp3	igs18575.clk_30s	igs18577.erp	2015/08/14	234.5125
cdnp2270.15o	csrj2270.15o	brdc2270.erp	igs18576.sp3	igs18576.clk_30s	igs18577.erp	2015/08/15	234.4981
cdnp2280.15o	csrj2280.15o	brdc2280.erp	igs18580.sp3	igs18580.clk_30s	igs18587.erp	2015/08/16	234.5136
cdnp2290.15o	csrj2290.15o	brdc2290.erp	igs18581.sp3	igs18581.clk_30s	igs18587.erp	2015/08/17	234.5066
cdnp2310.15o	csrj2310.15o	brdc2310.erp	igs18583.sp3	igs18583.clk_30s	igs18587.erp	2015/08/19	234.5048
cdnp2320.15o	csrj2320.15o	brdc2320.erp	igs18584.sp3	igs18584.clk_30s	igs18587.erp	2015/08/20	234.5042
cdnp2330.15o	csrj2330.15o	brdc2330.erp	igs18585.sp3	igs18585.clk_30s	igs18587.erp	2015/08/21	234.5063
cdnp2340.15o	csrj2340.15o	brdc2340.erp	igs18586.sp3	igs18586.clk_30s	igs18587.erp	2015/08/22	234.5056
cdnp2350.15o	csrj2350.15o	brdc2350.erp	igs18590.sp3	igs18590.clk_30s	igs18597.erp	2015/08/23	234.5135
cdnp2360.15o	csrj2360.15o	brdc2360.erp	igs18591.sp3	igs18591.clk_30s	igs18597.erp	2015/08/24	234.5173
cdnp2370.15o	csrj2370.15o	brdc2370.erp	igs18592.sp3	igs18592.clk_30s	igs18597.erp	2015/08/25	234.4984
cdnp2380.15o	csrj2380.15o	brdc2380.erp	igs18593.sp3	igs18593.clk_30s	igs18597.erp	2015/08/26	234.5070
cdnp2390.15o	csrj2390.15o	brdc2390.erp	igs18594.sp3	igs18594.clk_30s	igs18597.erp	2015/08/27	234.5134
cdnp2400.15o	csrj2400.15o	brdc2400.erp	igs18595.sp3	igs18595.clk_30s	igs18597.erp	2015/08/28	234.5259
cdnp2420.15o	csrj2420.15o	brdc2420.erp	igs18600.sp3	igs18600.clk_30s	igs18607.erp	2015/08/30	234.5082
cdnp2430.15o	csrj2430.15o	brdc2430.erp	igs18601.sp3	igs18601.clk_30s	igs18607.erp	2015/08/31	234.5012
cdnp2440.15o	csrj2440.15o	brdc2440.erp	igs18602.sp3	igs18602.clk_30s	igs18607.erp	2015/09/01	234.5121
cdnp2450.15o	csrj2450.15o	brdc2450.erp	igs18603.sp3	igs18603.clk_30s	igs18607.erp	2015/09/02	234.4985
cdnp2460.15o	csrj2460.15o	brdc2460.erp	igs18604.sp3	igs18604.clk_30s	igs18607.erp	2015/09/03	234.5084
cdnp2480.15o	csrj2480.15o	brdc2480.erp	igs18606.sp3	igs18606.clk_30s	igs18607.erp	2015/09/05	234.5098
cdnp2490.15o	csrj2490.15o	brdc2490.erp	igs18610.sp3	igs18610.clk_30s	igs18617.erp	2015/09/06	234.5092
cdnp2500.15o	csrj2500.15o	brdc2500.erp	igs18611.sp3	igs18611.clk_30s	igs18617.erp	2015/09/07	234.5036
cdnp2510.15o	csrj2510.15o	brdc2510.erp	igs18612.sp3	igs18612.clk_30s	igs18617.erp	2015/09/08	234.5138
cdnp2520.15o	csrj2520.15o	brdc2520.erp	igs18613.sp3	igs18613.clk_30s	igs18617.erp	2015/09/09	234.5093
cdnp2530.15o	csrj2530.15o	brdc2530.erp	igs18614.sp3	igs18614.clk_30s	igs18617.erp	2015/09/10	234.5141
cdnp2540.15o	csrj2540.15o	brdc2540.erp	igs18615.sp3	igs18615.clk_30s	igs18617.erp	2015/09/11	234.5039
cdnp2550.15o	csrj2550.15o	brdc2550.erp	igs18616.sp3	igs18616.clk_30s	igs18617.erp	2015/09/12	234.5076
cdnp2560.15o	csrj2560.15o	brdc2560.erp	igs18620.sp3	igs18620.clk_30s	igs18627.erp	2015/09/13	234.4997
cdnp2570.15o	csrj2570.15o	brdc2570.erp	igs18621.sp3	igs18621.clk_30s	igs18627.erp	2015/09/14	234.5028
cdnp2590.15o	csrj2590.15o	brdc2590.erp	igs18623.sp3	igs18623.clk_30s	igs18627.erp	2015/09/16	234.5073

cdnp2600.15o	csrj2600.15o	brdc2600.erp	igs18624.sp3	igs18624.clk_30s	igs18627.erp	2015/09/17	234.5021
cdnp2610.15o	csrj2610.15o	brdc2610.erp	igs18625.sp3	igs18625.clk_30s	igs18627.erp	2015/09/18	234.5145
cdnp2620.15o	csrj2620.15o	brdc2620.erp	igs18626.sp3	igs18626.clk_30s	igs18627.erp	2015/09/19	234.5018
cdnp2630.15o	csrj2630.15o	brdc2630.erp	igs18630.sp3	igs18630.clk_30s	igs18637.erp	2015/09/20	234.5094
cdnp2650.15o	csrj2650.15o	brdc2650.erp	igs18632.sp3	igs18632.clk_30s	igs18637.erp	2015/09/22	234.5009
cdnp2660.15o	csrj2660.15o	brdc2660.erp	igs18633.sp3	igs18633.clk_30s	igs18637.erp	2015/09/23	234.4945
cdnp2670.15o	csrj2670.15o	brdc2670.erp	igs18634.sp3	igs18634.clk_30s	igs18637.erp	2015/09/24	234.5069
cdnp2680.15o	csrj2680.15o	brdc2680.erp	igs18635.sp3	igs18635.clk_30s	igs18637.erp	2015/09/25	234.5043
cdnp2690.15o	csrj2690.15o	brdc2690.erp	igs18636.sp3	igs18636.clk_30s	igs18637.erp	2015/09/26	234.5069
cdnp2700.15o	csrj2700.15o	brdc2700.erp	igs18640.sp3	igs18640.clk_30s	igs18647.erp	2015/09/27	234.5199
cdnp2720.15o	csrj2720.15o	brdc2720.erp	igs18642.sp3	igs18642.clk_30s	igs18647.erp	2015/09/29	234.5230
cdnp2730.15o	csrj2730.15o	brdc2730.erp	igs18643.sp3	igs18643.clk_30s	igs18647.erp	2015/09/30	234.5126
cdnp2750.15o	csrj2750.15o	brdc2750.erp	igs18644.sp3	igs18644.clk_30s	igs18647.erp	2015/10/02	234.4938
cdnp2760.15o	csrj2760.15o	brdc2760.erp	igs18645.sp3	igs18645.clk_30s	igs18647.erp	2015/10/03	234.5062
cdnp2770.15o	csrj2770.15o	brdc2770.erp	igs18650.sp3	igs18650.clk_30s	igs18657.erp	2015/10/04	234.5095
cdnp2780.15o	csrj2780.15o	brdc2780.erp	igs18651.sp3	igs18651.clk_30s	igs18657.erp	2015/10/05	234.5058
cdnp2790.15o	csrj2790.15o	brdc2790.erp	igs18652.sp3	igs18652.clk_30s	igs18657.erp	2015/10/06	234.5051
cdnp2800.15o	csrj2800.15o	brdc2800.erp	igs18653.sp3	igs18653.clk_30s	igs18657.erp	2015/10/07	234.4989
cdnp2810.15o	csrj2810.15o	brdc2810.erp	igs18654.sp3	igs18654.clk_30s	igs18657.erp	2015/10/08	234.5022
cdnp2830.15o	csrj2830.15o	brdc2830.erp	igs18656.sp3	igs18656.clk_30s	igs18657.erp	2015/10/10	234.5114
cdnp2840.15o	csrj2840.15o	brdc2840.erp	igs18660.sp3	igs18660.clk_30s	igs18667.erp	2015/10/11	234.5078
cdnp2850.15o	csrj2850.15o	brdc2850.erp	igs18661.sp3	igs18661.clk_30s	igs18667.erp	2015/10/12	234.4975
cdnp2860.15o	csrj2860.15o	brdc2860.erp	igs18662.sp3	igs18662.clk_30s	igs18667.erp	2015/10/13	234.4989
cdnp2870.15o	csrj2870.15o	brdc2870.erp	igs18663.sp3	igs18663.clk_30s	igs18667.erp	2015/10/14	234.5044
cdnp2880.15o	csrj2880.15o	brdc2880.erp	igs18664.sp3	igs18664.clk_30s	igs18667.erp	2015/10/15	234.5241
cdnp2900.15o	csrj2900.15o	brdc2900.erp	igs18666.sp3	igs18666.clk_30s	igs18667.erp	2015/10/17	234.5110
cdnp2910.15o	csrj2910.15o	brdc2910.erp	igs18670.sp3	igs18670.clk_30s	igs18677.erp	2015/10/18	234.5200
cdnp2920.15o	csrj2920.15o	brdc2920.erp	igs18671.sp3	igs18671.clk_30s	igs18677.erp	2015/10/19	234.4932
cdnp2930.15o	csrj2930.15o	brdc2930.erp	igs18672.sp3	igs18672.clk_30s	igs18677.erp	2015/10/20	234.5157
cdnp2940.15o	csrj2940.15o	brdc2940.erp	igs18673.sp3	igs18673.clk_30s	igs18677.erp	2015/10/21	234.5169
cdnp2950.15o	csrj2950.15o	brdc2950.erp	igs18674.sp3	igs18674.clk_30s	igs18677.erp	2015/10/22	234.5100
cdnp2960.15o	csrj2960.15o	brdc2960.erp	igs18675.sp3	igs18675.clk_30s	igs18677.erp	2015/10/23	234.5164
cdnp2970.15o	csrj2970.15o	brdc2970.erp	igs18676.sp3	igs18676.clk_30s	igs18677.erp	2015/10/24	234.5137
cdnp2980.15o	csrj2980.15o	brdc2980.erp	igs18680.sp3	igs18680.clk_30s	igs18687.erp	2015/10/25	234.4886
cdnp2990.15o	csrj2990.15o	brdc2990.erp	igs18681.sp3	igs18681.clk_30s	igs18687.erp	2015/10/26	234.5137
cdnp3000.15o	csrj3000.15o	brdc3000.erp	igs18682.sp3	igs18682.clk_30s	igs18687.erp	2015/10/27	234.5046
cdnp3010.15o	csrj3010.15o	brdc3010.erp	igs18683.sp3	igs18683.clk_30s	igs18687.erp	2015/10/28	234.5021
cdnp3020.15o	csrj3020.15o	brdc3020.erp	igs18684.sp3	igs18684.clk_30s	igs18687.erp	2015/10/29	234.5047
cdnp3030.15o	csrj3030.15o	brdc3030.erp	igs18685.sp3	igs18685.clk_30s	igs18687.erp	2015/10/30	234.4868
cdnp3040.15o	csrj3040.15o	brdc3040.erp	igs18686.sp3	igs18686.clk_30s	igs18687.erp	2015/10/31	234.5353
cdnp3050.15o	csrj3050.15o	brdc3050.erp	igs18690.sp3	igs18690.clk_30s	igs18697.erp	2015/11/01	234.5072
cdnp3060.15o	csrj3060.15o	brdc3060.erp	igs18691.sp3	igs18691.clk_30s	igs18697.erp	2015/11/02	234.5090
cdnp3080.15o	csrj3080.15o	brdc3080.erp	igs18693.sp3	igs18693.clk_30s	igs18697.erp	2015/11/04	234.5129
cdnp3090.15o	csrj3090.15o	brdc3090.erp	igs18694.sp3	igs18694.clk_30s	igs18697.erp	2015/11/05	234.5121
cdnp3100.15o	csrj3100.15o	brdc3100.erp	igs18695.sp3	igs18695.clk_30s	igs18697.erp	2015/11/06	234.5030
cdnp3110.15o	csrj3110.15o	brdc3110.erp	igs18696.sp3	igs18696.clk_30s	igs18697.erp	2015/11/07	234.5293
cdnp3120.15o	csrj3120.15o	brdc3120.erp	igs18700.sp3	igs18700.clk_30s	igs18707.erp	2015/11/08	234.5309
cdnp3130.15o	csrj3130.15o	brdc3130.erp	igs18701.sp3	igs18701.clk_30s	igs18707.erp	2015/11/09	234.5020
cdnp3140.15o	csrj3140.15o	brdc3140.erp	igs18702.sp3	igs18702.clk_30s	igs18707.erp	2015/11/10	234.4835
cdnp3150.15o	csrj3150.15o	brdc3150.erp	igs18703.sp3	igs18703.clk_30s	igs18707.erp	2015/11/11	234.4674
cdnp3160.15o	csrj3160.15o	brdc3160.erp	igs18704.sp3	igs18704.clk_30s	igs18707.erp	2015/11/12	234.5083
cdnp3170.15o	csrj3170.15o	brdc3170.erp	igs18705.sp3	igs18705.clk_30s	igs18707.erp	2015/11/13	234.4921
cdnp3180.15o	csrj3180.15o	brdc3180.erp	igs18706.sp3	igs18706.clk_30s	igs18707.erp	2015/11/14	234.5233
cdnp3190.15o	csrj3190.15o	brdc3190.erp	igs18710.sp3	igs18710.clk_30s	igs18717.erp	2015/11/15	234.5016
cdnp3200.15o	csrj3200.15o	brdc3200.erp	igs18711.sp3	igs18711.clk_30s	igs18717.erp	2015/11/16	234.5086
cdnp3210.15o	csrj3210.15o	brdc3210.erp	igs18712.sp3	igs18712.clk_30s	igs18717.erp	2015/11/17	234.5412
cdnp3230.15o	csrj3230.15o	brdc3230.erp	igs18714.sp3	igs18714.clk_30s	igs18717.erp	2015/11/19	234.4917
cdnp3240.15o	csrj3240.15o	brdc3240.erp	igs18715.sp3	igs18715.clk_30s	igs18717.erp	2015/11/20	234.4705
cdnp3250.15o	csrj3250.15o	brdc3250.erp	igs18716.sp3	igs18716.clk_30s	igs18717.erp	2015/11/21	234.5194
cdnp3260.15o	csrj3260.15o	brdc3260.erp	igs18720.sp3	igs18720.clk_30s	igs18727.erp	2015/11/22	234.5241
cdnp3270.15o	csrj3270.15o	brdc3270.erp	igs18721.sp3	igs18721.clk_30s	igs18727.erp	2015/11/23	234.5122
cdnp3280.15o	csrj3280.15o	brdc3280.erp	igs18722.sp3	igs18722.clk_30s	igs18727.erp	2015/11/24	234.4892
cdnp3290.15o	csrj3290.15o	brdc3290.erp	igs18723.sp3	igs18723.clk_30s	igs18727.erp	2015/11/25	234.4962
cdnp3300.15o	csrj3300.15o	brdc3300.erp	igs18724.sp3	igs18724.clk_30s	igs18727.erp	2015/11/26	234.4997
cdnp3310.15o	csrj3310.15o	brdc3310.erp	igs18725.sp3	igs18725.clk_30s	igs18727.erp	2015/11/27	234.5170
cdnp3320.15o	csrj3320.15o	brdc3320.erp	igs18726.sp3	igs18726.clk_30s	igs18727.erp	2015/11/28	234.5380
cdnp3330.15o	csrj3330.15o	brdc3330.erp	igs18730.sp3	igs18730.clk_30s	igs18737.erp	2015/11/29	234.5057
cdnp3340.15o	csrj3340.15o	brdc3340.erp	igs18731.sp3	igs18731.clk_30s	igs18737.erp	2015/11/30	234.5080
cdnp3350.15o	csrj3350.15o	brdc3350.erp	igs18732.sp3	igs18732.clk_30s	igs18737.erp	2015/12/01	234.5089
cdnp3360.15o	csrj3360.15o	brdc3360.erp	igs18733.sp3	igs18733.clk_30s	igs18737.erp	2015/12/02	234.5123

cdnp3370.15o	csrj3370.15o	brdc3370.erp	igs18734.sp3	igs18734.clk_30s	igs18737.erp	2015/12/03	234.5163
cdnp3380.15o	csrj3380.15o	brdc3380.erp	igs18735.sp3	igs18735.clk_30s	igs18737.erp	2015/12/04	234.4984
cdnp3390.15o	csrj3390.15o	brdc3390.erp	igs18736.sp3	igs18736.clk_30s	igs18737.erp	2015/12/05	234.5148
cdnp3400.15o	csrj3400.15o	brdc3400.erp	igs18740.sp3	igs18740.clk_30s	igs18747.erp	2015/12/06	234.5275
cdnp3410.15o	csrj3410.15o	brdc3410.erp	igs18741.sp3	igs18741.clk_30s	igs18747.erp	2015/12/07	234.5066
cdnp3430.15o	csrj3430.15o	brdc3430.erp	igs18743.sp3	igs18743.clk_30s	igs18747.erp	2015/12/09	234.4864
cdnp3440.15o	csrj3440.15o	brdc3440.erp	igs18744.sp3	igs18744.clk_30s	igs18747.erp	2015/12/10	234.5144
cdnp3450.15o	csrj3450.15o	brdc3450.erp	igs18745.sp3	igs18745.clk_30s	igs18747.erp	2015/12/11	234.5034
cdnp3460.15o	csrj3460.15o	brdc3460.erp	igs18746.sp3	igs18746.clk_30s	igs18747.erp	2015/12/12	234.5126
cdnp3470.15o	csrj3470.15o	brdc3470.erp	igs18750.sp3	igs18750.clk_30s	igs18757.erp	2015/12/13	234.5055
cdnp3480.15o	csrj3480.15o	brdc3480.erp	igs18751.sp3	igs18751.clk_30s	igs18757.erp	2015/12/14	234.4878
cdnp3490.15o	csrj3490.15o	brdc3490.erp	igs18752.sp3	igs18752.clk_30s	igs18757.erp	2015/12/15	234.5452
cdnp3510.15o	csrj3510.15o	brdc3510.erp	igs18754.sp3	igs18754.clk_30s	igs18757.erp	2015/12/17	234.5078
cdnp3520.15o	csrj3520.15o	brdc3520.erp	igs18755.sp3	igs18755.clk_30s	igs18757.erp	2015/12/18	234.4811
cdnp3530.15o	csrj3530.15o	brdc3530.erp	igs18756.sp3	igs18756.clk_30s	igs18757.erp	2015/12/19	234.5335
cdnp3540.15o	csrj3540.15o	brdc3540.erp	igs18760.sp3	igs18760.clk_30s	igs18767.erp	2015/12/20	234.4815
cdnp3550.15o	csrj3550.15o	brdc3550.erp	igs18761.sp3	igs18761.clk_30s	igs18767.erp	2015/12/21	234.4999
cdnp3560.15o	csrj3560.15o	brdc3560.erp	igs18762.sp3	igs18762.clk_30s	igs18767.erp	2015/12/22	234.5177
cdnp3570.15o	csrj3570.15o	brdc3570.erp	igs18763.sp3	igs18763.clk_30s	igs18767.erp	2015/12/23	234.5151
cdnp3580.15o	csrj3580.15o	brdc3580.erp	igs18764.sp3	igs18764.clk_30s	igs18767.erp	2015/12/24	234.5272
cdnp3590.15o	csrj3590.15o	brdc3590.erp	igs18765.sp3	igs18765.clk_30s	igs18767.erp	2015/12/25	234.5172
cdnp3610.15o	csrj3610.15o	brdc3610.erp	igs18770.sp3	igs18770.clk_30s	igs18777.erp	2015/12/27	234.4668
cdnp3620.15o	csrj3620.15o	brdc3620.erp	igs18771.sp3	igs18771.clk_30s	igs18777.erp	2015/12/28	234.4792
cdnp3630.15o	csrj3630.15o	brdc3630.erp	igs18772.sp3	igs18772.clk_30s	igs18777.erp	2015/12/29	234.5079
cdnp3640.15o	csrj3640.15o	brdc3640.erp	igs18773.sp3	igs18773.clk_30s	igs18777.erp	2015/12/30	234.5043
cdnp3650.15o	csrj3650.15o	brdc3650.erp	igs18774.sp3	igs18774.clk_30s	igs18777.erp	2015/12/31	234.5042
cdnp0010.16o	csrj0010.16o	brdc0010.16n	igs18775.sp3	igs18775.clk_30s	igs18777.erp	2016/01/01	234.4770
cdnp0020.16o	csrj0020.16o	brdc0020.16n	igs18776.sp3	igs18776.clk_30s	igs18777.erp	2016/01/02	234.5034
cdnp0030.16o	csrj0030.16o	brdc0030.16n	igs18780.sp3	igs18780.clk_30s	igs18787.erp	2016/01/03	234.5335
cdnp0040.16o	csrj0040.16o	brdc0040.16n	igs18781.sp3	igs18781.clk_30s	igs18787.erp	2016/01/04	234.5067
cdnp0060.16o	csrj0060.16o	brdc0060.16n	igs18783.sp3	igs18783.clk_30s	igs18787.erp	2016/01/06	234.4987
cdnp0070.16o	csrj0070.16o	brdc0070.16n	igs18784.sp3	igs18784.clk_30s	igs18787.erp	2016/01/07	234.5258
cdnp0080.16o	csrj0080.16o	brdc0080.16n	igs18785.sp3	igs18785.clk_30s	igs18787.erp	2016/01/08	234.4733
cdnp0090.16o	csrj0090.16o	brdc0090.16n	igs18786.sp3	igs18786.clk_30s	igs18787.erp	2016/01/09	234.5217
cdnp0100.16o	csrj0100.16o	brdc0100.16n	igs18790.sp3	igs18790.clk_30s	igs18797.erp	2016/01/10	234.5297
cdnp0110.16o	csrj0110.16o	brdc0110.16n	igs18791.sp3	igs18791.clk_30s	igs18797.erp	2016/01/11	234.5082
cdnp0120.16o	csrj0120.16o	brdc0120.16n	igs18792.sp3	igs18792.clk_30s	igs18797.erp	2016/01/12	234.5149
cdnp0130.16o	csrj0130.16o	brdc0130.16n	igs18793.sp3	igs18793.clk_30s	igs18797.erp	2016/01/13	234.5333
cdnp0140.16o	csrj0140.16o	brdc0140.16n	igs18794.sp3	igs18794.clk_30s	igs18797.erp	2016/01/14	234.5321
cdnp0150.16o	csrj0150.16o	brdc0150.16n	igs18795.sp3	igs18795.clk_30s	igs18797.erp	2016/01/15	234.5001
cdnp0170.16o	csrj0170.16o	brdc0170.16n	igs18800.sp3	igs18800.clk_30s	igs18807.erp	2016/01/17	234.5083
cdnp0180.16o	csrj0180.16o	brdc0180.16n	igs18801.sp3	igs18801.clk_30s	igs18807.erp	2016/01/18	234.5325
cdnp0190.16o	csrj0190.16o	brdc0190.16n	igs18802.sp3	igs18802.clk_30s	igs18807.erp	2016/01/19	234.5151
cdnp0200.16o	csrj0200.16o	brdc0200.16n	igs18803.sp3	igs18803.clk_30s	igs18807.erp	2016/01/20	234.5291
cdnp0210.16o	csrj0210.16o	brdc0210.16n	igs18804.sp3	igs18804.clk_30s	igs18807.erp	2016/01/21	234.5099
cdnp0220.16o	csrj0220.16o	brdc0220.16n	igs18805.sp3	igs18805.clk_30s	igs18807.erp	2016/01/22	234.4654
cdnp0240.16o	csrj0240.16o	brdc0240.16n	igs18810.sp3	igs18810.clk_30s	igs18817.erp	2016/01/24	234.4775
cdnp0250.16o	csrj0250.16o	brdc0250.16n	igs18811.sp3	igs18811.clk_30s	igs18817.erp	2016/01/25	234.5000
cdnp0260.16o	csrj0260.16o	brdc0260.16n	igs18812.sp3	igs18812.clk_30s	igs18817.erp	2016/01/26	234.4989
cdnp0270.16o	csrj0270.16o	brdc0270.16n	igs18813.sp3	igs18813.clk_30s	igs18817.erp	2016/01/27	234.4964
cdnp0280.16o	csrj0280.16o	brdc0280.16n	igs18814.sp3	igs18814.clk_30s	igs18817.erp	2016/01/28	234.4890
cdnp0290.16o	csrj0290.16o	brdc0290.16n	igs18815.sp3	igs18815.clk_30s	igs18817.erp	2016/01/29	234.4999
cdnp0300.16o	csrj0300.16o	brdc0300.16n	igs18816.sp3	igs18816.clk_30s	igs18817.erp	2016/01/30	234.4930
cdnp0320.16o	csrj0320.16o	brdc0320.16n	igs18821.sp3	igs18821.clk_30s	igs18827.erp	2016/02/01	234.5030
cdnp0330.16o	csrj0330.16o	brdc0330.16n	igs18822.sp3	igs18822.clk_30s	igs18827.erp	2016/02/02	234.4955
cdnp0370.16o	csrj0370.16o	brdc0370.16n	igs18826.sp3	igs18826.clk_30s	igs18827.erp	2016/02/06	234.5044
cdnp0390.16o	csrj0390.16o	brdc0390.16n	igs18831.sp3	igs18831.clk_30s	igs18837.erp	2016/02/08	234.5017
cdnp0400.16o	csrj0400.16o	brdc0400.16n	igs18832.sp3	igs18832.clk_30s	igs18837.erp	2016/02/09	234.5075
cdnp0410.16o	csrj0410.16o	brdc0410.16n	igs18833.sp3	igs18833.clk_30s	igs18837.erp	2016/02/10	234.5099
cdnp0420.16o	csrj0420.16o	brdc0420.16n	igs18834.sp3	igs18834.clk_30s	igs18837.erp	2016/02/11	234.4786
cdnp0430.16o	csrj0430.16o	brdc0430.16n	igs18835.sp3	igs18835.clk_30s	igs18837.erp	2016/02/12	234.5563
cdnp0440.16o	csrj0440.16o	brdc0440.16n	igs18836.sp3	igs18836.clk_30s	igs18837.erp	2016/02/13	234.4842
cdnp0450.16o	csrj0450.16o	brdc0450.16n	igs18840.sp3	igs18840.clk_30s	igs18847.erp	2016/02/14	234.5074
cdnp0480.16o	csrj0480.16o	brdc0480.16n	igs18843.sp3	igs18843.clk_30s	igs18847.erp	2016/02/17	234.5117
cdnp0510.16o	csrj0510.16o	brdc0510.16n	igs18846.sp3	igs18846.clk_30s	igs18847.erp	2016/02/20	234.4982
cdnp0540.16o	csrj0540.16o	brdc0540.16n	igs18852.sp3	igs18852.clk_30s	igs18857.erp	2016/02/23	234.4829
cdnp0550.16o	csrj0550.16o	brdc0550.16n	igs18853.sp3	igs18853.clk_30s	igs18857.erp	2016/02/24	234.5181
cdnp0560.16o	csrj0560.16o	brdc0560.16n	igs18854.sp3	igs18854.clk_30s	igs18857.erp	2016/02/25	234.4923
cdnp0570.16o	csrj0570.16o	brdc0570.16n	igs18855.sp3	igs18855.clk_30s	igs18857.erp	2016/02/26	234.5070
cdnp0590.16o	csrj0590.16o	brdc0590.16n	igs18860.sp3	igs18860.clk_30s	igs18867.erp	2016/02/28	234.5069

cdnp0600.16o	csrj0600.16o	brdc0600.16n	igs18861.sp3	igs18861.clk_30s	igs18867.erp	2016/02/29	234.5191
cdnp0610.16o	csrj0610.16o	brdc0610.16n	igs18862.sp3	igs18862.clk_30s	igs18867.erp	2016/03/01	234.4978
cdnp0620.16o	csrj0620.16o	brdc0620.16n	igs18863.sp3	igs18863.clk_30s	igs18867.erp	2016/03/02	234.4900
cdnp0630.16o	csrj0630.16o	brdc0630.16n	igs18864.sp3	igs18864.clk_30s	igs18867.erp	2016/03/03	234.5215
cdnp0640.16o	csrj0640.16o	brdc0640.16n	igs18865.sp3	igs18865.clk_30s	igs18867.erp	2016/03/04	234.5152
cdnp0650.16o	csrj0650.16o	brdc0650.16n	igs18866.sp3	igs18866.clk_30s	igs18867.erp	2016/03/05	234.4952
cdnp0660.16o	csrj0660.16o	brdc0660.16n	igs18870.sp3	igs18870.clk_30s	igs18877.erp	2016/03/06	234.4850
cdnp0670.16o	csrj0670.16o	brdc0670.16n	igs18871.sp3	igs18871.clk_30s	igs18877.erp	2016/03/07	234.5127
cdnp0680.16o	csrj0680.16o	brdc0680.16n	igs18872.sp3	igs18872.clk_30s	igs18877.erp	2016/03/08	234.5082
cdnp0690.16o	csrj0690.16o	brdc0690.16n	igs18873.sp3	igs18873.clk_30s	igs18877.erp	2016/03/09	234.5129
cdnp0700.16o	csrj0700.16o	brdc0700.16n	igs18874.sp3	igs18874.clk_30s	igs18877.erp	2016/03/10	234.5123
cdnp0720.16o	csrj0720.16o	brdc0720.16n	igs18876.sp3	igs18876.clk_30s	igs18877.erp	2016/03/12	234.5199
cdnp0730.16o	csrj0730.16o	brdc0730.16n	igs18880.sp3	igs18880.clk_30s	igs18887.erp	2016/03/13	234.5219
cdnp0740.16o	csrj0740.16o	brdc0740.16n	igs18881.sp3	igs18881.clk_30s	igs18887.erp	2016/03/14	234.5098
cdnp0750.16o	csrj0750.16o	brdc0750.16n	igs18882.sp3	igs18882.clk_30s	igs18887.erp	2016/03/15	234.4963
cdnp0760.16o	csrj0760.16o	brdc0760.16n	igs18883.sp3	igs18883.clk_30s	igs18887.erp	2016/03/16	234.5128
cdnp0770.16o	csrj0770.16o	brdc0770.16n	igs18884.sp3	igs18884.clk_30s	igs18887.erp	2016/03/17	234.4964
cdnp0780.16o	csrj0780.16o	brdc0780.16n	igs18885.sp3	igs18885.clk_30s	igs18887.erp	2016/03/18	234.4940
cdnp0790.16o	csrj0790.16o	brdc0790.16n	igs18886.sp3	igs18886.clk_30s	igs18887.erp	2016/03/19	234.5166
cdnp0800.16o	csrj0800.16o	brdc0800.16n	igs18890.sp3	igs18890.clk_30s	igs18897.erp	2016/03/20	234.5201
cdnp0810.16o	csrj0810.16o	brdc0810.16n	igs18891.sp3	igs18891.clk_30s	igs18897.erp	2016/03/21	234.5094
cdnp0820.16o	csrj0820.16o	brdc0820.16n	igs18892.sp3	igs18892.clk_30s	igs18897.erp	2016/03/22	234.5032
cdnp0830.16o	csrj0830.16o	brdc0830.16n	igs18893.sp3	igs18893.clk_30s	igs18897.erp	2016/03/23	234.4757
cdnp0840.16o	csrj0840.16o	brdc0840.16n	igs18894.sp3	igs18894.clk_30s	igs18897.erp	2016/03/24	234.4960
cdnp0850.16o	csrj0850.16o	brdc0850.16n	igs18895.sp3	igs18895.clk_30s	igs18897.erp	2016/03/25	234.5138
cdnp0860.16o	csrj0860.16o	brdc0860.16n	igs18896.sp3	igs18896.clk_30s	igs18897.erp	2016/03/26	234.5301
cdnp0870.16o	csrj0870.16o	brdc0870.16n	igs18900.sp3	igs18900.clk_30s	igs18907.erp	2016/03/27	234.4825
cdnp0880.16o	csrj0880.16o	brdc0880.16n	igs18901.sp3	igs18901.clk_30s	igs18907.erp	2016/03/28	234.5067
cdnp0890.16o	csrj0890.16o	brdc0890.16n	igs18902.sp3	igs18902.clk_30s	igs18907.erp	2016/03/29	234.4794
cdnp0900.16o	csrj0900.16o	brdc0900.16n	igs18903.sp3	igs18903.clk_30s	igs18907.erp	2016/03/30	234.5168
cdnp0910.16o	csrj0910.16o	brdc0910.16n	igs18904.sp3	igs18904.clk_30s	igs18907.erp	2016/03/31	234.5094
cdnp0920.16o	csrj0920.16o	brdc0920.16n	igs18905.sp3	igs18905.clk_30s	igs18907.erp	2016/04/01	234.4579
cdnp0930.16o	csrj0930.16o	brdc0930.16n	igs18906.sp3	igs18906.clk_30s	igs18907.erp	2016/04/02	234.4659
cdnp0940.16o	csrj0940.16o	brdc0940.16n	igs18910.sp3	igs18910.clk_30s	igs18917.erp	2016/04/03	234.4932
cdnp0950.16o	csrj0950.16o	brdc0950.16n	igs18911.sp3	igs18911.clk_30s	igs18917.erp	2016/04/04	234.5363
cdnp0960.16o	csrj0960.16o	brdc0960.16n	igs18912.sp3	igs18912.clk_30s	igs18917.erp	2016/04/05	234.5126
cdnp0970.16o	csrj0970.16o	brdc0970.16n	igs18913.sp3	igs18913.clk_30s	igs18917.erp	2016/04/06	234.4756
cdnp0980.16o	csrj0980.16o	brdc0980.16n	igs18914.sp3	igs18914.clk_30s	igs18917.erp	2016/04/07	234.5160
cdnp0990.16o	csrj0990.16o	brdc0990.16n	igs18915.sp3	igs18915.clk_30s	igs18917.erp	2016/04/08	234.5090
cdnp1000.16o	csrj1000.16o	brdc1000.16n	igs18916.sp3	igs18916.clk_30s	igs18917.erp	2016/04/09	234.5032
cdnp1010.16o	csrj1010.16o	brdc1010.16n	igs18920.sp3	igs18920.clk_30s	igs18927.erp	2016/04/10	234.4846
cdnp1020.16o	csrj1020.16o	brdc1020.16n	igs18921.sp3	igs18921.clk_30s	igs18927.erp	2016/04/11	234.4971
cdnp1030.16o	csrj1030.16o	brdc1030.16n	igs18922.sp3	igs18922.clk_30s	igs18927.erp	2016/04/12	234.5170
cdnp1040.16o	csrj1040.16o	brdc1040.16n	igs18923.sp3	igs18923.clk_30s	igs18927.erp	2016/04/13	234.5211
cdnp1050.16o	csrj1050.16o	brdc1050.16n	igs18924.sp3	igs18924.clk_30s	igs18927.erp	2016/04/14	234.5079
cdnp1060.16o	csrj1060.16o	brdc1060.16n	igs18925.sp3	igs18925.clk_30s	igs18927.erp	2016/04/15	234.5332
cdnp1070.16o	csrj1070.16o	brdc1070.16n	igs18926.sp3	igs18926.clk_30s	igs18927.erp	2016/04/16	234.5020
cdnp1080.16o	csrj1080.16o	brdc1080.16n	igs18930.sp3	igs18930.clk_30s	igs18937.erp	2016/04/17	234.5150
cdnp1090.16o	csrj1090.16o	brdc1090.16n	igs18931.sp3	igs18931.clk_30s	igs18937.erp	2016/04/18	234.4999
cdnp1100.16o	csrj1100.16o	brdc1100.16n	igs18932.sp3	igs18932.clk_30s	igs18937.erp	2016/04/19	234.5267
cdnp1110.16o	csrj1110.16o	brdc1110.16n	igs18933.sp3	igs18933.clk_30s	igs18937.erp	2016/04/20	234.5367
cdnp1120.16o	csrj1120.16o	brdc1120.16n	igs18934.sp3	igs18934.clk_30s	igs18937.erp	2016/04/21	234.5061
cdnp1130.16o	csrj1130.16o	brdc1130.16n	igs18935.sp3	igs18935.clk_30s	igs18937.erp	2016/04/22	234.5046
cdnp1140.16o	csrj1140.16o	brdc1140.16n	igs18936.sp3	igs18936.clk_30s	igs18937.erp	2016/04/23	234.5013
cdnp1150.16o	csrj1150.16o	brdc1150.16n	igs18940.sp3	igs18940.clk_30s	igs18947.erp	2016/04/24	234.5124
cdnp1160.16o	csrj1160.16o	brdc1160.16n	igs18941.sp3	igs18941.clk_30s	igs18947.erp	2016/04/25	234.5208
cdnp1170.16o	csrj1170.16o	brdc1170.16n	igs18942.sp3	igs18942.clk_30s	igs18947.erp	2016/04/26	234.5248
cdnp1180.16o	csrj1180.16o	brdc1180.16n	igs18943.sp3	igs18943.clk_30s	igs18947.erp	2016/04/27	234.4988
cdnp1190.16o	csrj1190.16o	brdc1190.16n	igs18944.sp3	igs18944.clk_30s	igs18947.erp	2016/04/28	234.5122
cdnp1200.16o	csrj1200.16o	brdc1200.16n	igs18945.sp3	igs18945.clk_30s	igs18947.erp	2016/04/29	234.4790
cdnp1210.16o	csrj1210.16o	brdc1210.16n	igs18946.sp3	igs18946.clk_30s	igs18947.erp	2016/04/30	234.5006
cdnp1220.16o	csrj1220.16o	brdc1220.16n	igs18950.sp3	igs18950.clk_30s	igs18957.erp	2016/05/01	234.4965
cdnp1230.16o	csrj1230.16o	brdc1230.16n	igs18951.sp3	igs18951.clk_30s	igs18957.erp	2016/05/02	234.5212
cdnp1240.16o	csrj1240.16o	brdc1240.16n	igs18952.sp3	igs18952.clk_30s	igs18957.erp	2016/05/03	234.5203
cdnp1250.16o	csrj1250.16o	brdc1250.16n	igs18953.sp3	igs18953.clk_30s	igs18957.erp	2016/05/04	234.5130
cdnp1260.16o	csrj1260.16o	brdc1260.16n	igs18954.sp3	igs18954.clk_30s	igs18957.erp	2016/05/05	234.4842
cdnp1270.16o	csrj1270.16o	brdc1270.16n	igs18955.sp3	igs18955.clk_30s	igs18957.erp	2016/05/06	234.5008
cdnp1280.16o	csrj1280.16o	brdc1280.16n	igs18956.sp3	igs18956.clk_30s	igs18957.erp	2016/05/07	234.5052
cdnp1290.16o	csrj1290.16o	brdc1290.16n	igs18960.sp3	igs18960.clk_30s	igs18967.erp	2016/05/08	234.4936
cdnp1300.16o	csrj1300.16o	brdc1300.16n	igs18961.sp3	igs18961.clk_30s	igs18967.erp	2016/05/09	234.5247



cdnp1310.16o	csrj1310.16o	brdc1310.16n	igs18962.sp3	igs18962.clk_30s	igs18967.erp	2016/05/10	234.4888
cdnp1320.16o	csrj1320.16o	brdc1320.16n	igs18963.sp3	igs18963.clk_30s	igs18967.erp	2016/05/11	234.5041
cdnp1330.16o	csrj1330.16o	brdc1330.16n	igs18964.sp3	igs18964.clk_30s	igs18967.erp	2016/05/12	234.4969
cdnp1340.16o	csrj1340.16o	brdc1340.16n	igs18965.sp3	igs18965.clk_30s	igs18967.erp	2016/05/13	234.4881
cdnp1350.16o	csrj1350.16o	brdc1350.16n	igs18966.sp3	igs18966.clk_30s	igs18967.erp	2016/05/14	234.5169
cdnp1360.16o	csrj1360.16o	brdc1360.16n	igs18970.sp3	igs18970.clk_30s	igs18977.erp	2016/05/15	234.5491
cdnp1370.16o	csrj1370.16o	brdc1370.16n	igs18971.sp3	igs18971.clk_30s	igs18977.erp	2016/05/16	234.4961
cdnp1380.16o	csrj1380.16o	brdc1380.16n	igs18972.sp3	igs18972.clk_30s	igs18977.erp	2016/05/17	234.4909
cdnp1390.16o	csrj1390.16o	brdc1390.16n	igs18973.sp3	igs18973.clk_30s	igs18977.erp	2016/05/18	234.5151
cdnp1400.16o	csrj1400.16o	brdc1400.16n	igs18974.sp3	igs18974.clk_30s	igs18977.erp	2016/05/19	234.5028
cdnp1410.16o	csrj1410.16o	brdc1410.16n	igs18975.sp3	igs18975.clk_30s	igs18977.erp	2016/05/20	234.5238
cdnp1420.16o	csrj1420.16o	brdc1420.16n	igs18976.sp3	igs18976.clk_30s	igs18977.erp	2016/05/21	234.4843
cdnp1430.16o	csrj1430.16o	brdc1430.16n	igs18980.sp3	igs18980.clk_30s	igs18987.erp	2016/05/22	234.4838
cdnp1440.16o	csrj1440.16o	brdc1440.16n	igs18981.sp3	igs18981.clk_30s	igs18987.erp	2016/05/23	234.4815
cdnp1450.16o	csrj1450.16o	brdc1450.16n	igs18982.sp3	igs18982.clk_30s	igs18987.erp	2016/05/24	234.4999
cdnp1460.16o	csrj1460.16o	brdc1460.16n	igs18983.sp3	igs18983.clk_30s	igs18987.erp	2016/05/25	234.4776
cdnp1470.16o	csrj1470.16o	brdc1470.16n	igs18984.sp3	igs18984.clk_30s	igs18987.erp	2016/05/26	234.5065
cdnp1480.16o	csrj1480.16o	brdc1480.16n	igs18985.sp3	igs18985.clk_30s	igs18987.erp	2016/05/27	234.5236
cdnp1490.16o	csrj1490.16o	brdc1490.16n	igs18986.sp3	igs18986.clk_30s	igs18987.erp	2016/05/28	234.5075
cdnp1500.16o	csrj1500.16o	brdc1500.16n	igs18990.sp3	igs18990.clk_30s	igs18997.erp	2016/05/29	234.4972
cdnp1510.16o	csrj1510.16o	brdc1510.16n	igs18991.sp3	igs18991.clk_30s	igs18997.erp	2016/05/30	234.5177
cdnp1520.16o	csrj1520.16o	brdc1520.16n	igs18992.sp3	igs18992.clk_30s	igs18997.erp	2016/05/31	234.5273
cdnp1530.16o	csrj1530.16o	brdc1530.16n	igs18993.sp3	igs18993.clk_30s	igs18997.erp	2016/06/01	234.5090
cdnp1540.16o	csrj1540.16o	brdc1540.16n	igs18994.sp3	igs18994.clk_30s	igs18997.erp	2016/06/02	234.5039
cdnp1550.16o	csrj1550.16o	brdc1550.16n	igs18995.sp3	igs18995.clk_30s	igs18997.erp	2016/06/03	234.4933
cdnp1560.16o	csrj1560.16o	brdc1560.16n	igs18996.sp3	igs18996.clk_30s	igs18997.erp	2016/06/04	234.5301
cdnp1570.16o	csrj1570.16o	brdc1570.16n	igs19000.sp3	igs19000.clk_30s	igs19007.erp	2016/06/05	234.4977
cdnp1580.16o	csrj1580.16o	brdc1580.16n	igs19001.sp3	igs19001.clk_30s	igs19007.erp	2016/06/06	234.5033
cdnp1590.16o	csrj1590.16o	brdc1590.16n	igs19002.sp3	igs19002.clk_30s	igs19007.erp	2016/06/07	234.5034
cdnp1600.16o	csrj1600.16o	brdc1600.16n	igs19003.sp3	igs19003.clk_30s	igs19007.erp	2016/06/08	234.4957
cdnp1610.16o	csrj1610.16o	brdc1610.16n	igs19004.sp3	igs19004.clk_30s	igs19007.erp	2016/06/09	234.4963
cdnp1620.16o	csrj1620.16o	brdc1620.16n	igs19005.sp3	igs19005.clk_30s	igs19007.erp	2016/06/10	234.4999
cdnp1630.16o	csrj1630.16o	brdc1630.16n	igs19006.sp3	igs19006.clk_30s	igs19007.erp	2016/06/11	234.5067
cdnp1640.16o	csrj1640.16o	brdc1640.16n	igs19010.sp3	igs19010.clk_30s	igs19017.erp	2016/06/12	234.5130
cdnp1650.16o	csrj1650.16o	brdc1650.16n	igs19011.sp3	igs19011.clk_30s	igs19017.erp	2016/06/13	234.4936
cdnp1660.16o	csrj1660.16o	brdc1660.16n	igs19012.sp3	igs19012.clk_30s	igs19017.erp	2016/06/14	234.5126
cdnp1670.16o	csrj1670.16o	brdc1670.16n	igs19013.sp3	igs19013.clk_30s	igs19017.erp	2016/06/15	234.5095
cdnp1680.16o	csrj1680.16o	brdc1680.16n	igs19014.sp3	igs19014.clk_30s	igs19017.erp	2016/06/16	234.4907
cdnp1690.16o	csrj1690.16o	brdc1690.16n	igs19015.sp3	igs19015.clk_30s	igs19017.erp	2016/06/17	234.5208
cdnp1700.16o	csrj1700.16o	brdc1700.16n	igs19016.sp3	igs19016.clk_30s	igs19017.erp	2016/06/18	234.5044
cdnp1710.16o	csrj1710.16o	brdc1710.16n	igs19020.sp3	igs19020.clk_30s	igs19027.erp	2016/06/19	234.4960
cdnp1720.16o	csrj1720.16o	brdc1720.16n	igs19021.sp3	igs19021.clk_30s	igs19027.erp	2016/06/20	234.5077
cdnp1730.16o	csrj1730.16o	brdc1730.16n	igs19022.sp3	igs19022.clk_30s	igs19027.erp	2016/06/21	234.4858
cdnp1740.16o	csrj1740.16o	brdc1740.16n	igs19023.sp3	igs19023.clk_30s	igs19027.erp	2016/06/22	234.4877
cdnp1750.16o	csrj1750.16o	brdc1750.16n	igs19024.sp3	igs19024.clk_30s	igs19027.erp	2016/06/23	234.4940
cdnp1760.16o	csrj1760.16o	brdc1760.16n	igs19025.sp3	igs19025.clk_30s	igs19027.erp	2016/06/24	234.4972
cdnp1770.16o	csrj1770.16o	brdc1770.16n	igs19026.sp3	igs19026.clk_30s	igs19027.erp	2016/06/25	234.5029
cdnp1780.16o	csrj1780.16o	brdc1780.16n	igs19030.sp3	igs19030.clk_30s	igs19037.erp	2016/06/26	234.5102
cdnp1790.16o	csrj1790.16o	brdc1790.16n	igs19031.sp3	igs19031.clk_30s	igs19037.erp	2016/06/27	234.5115
cdnp1800.16o	csrj1800.16o	brdc1800.16n	igs19032.sp3	igs19032.clk_30s	igs19037.erp	2016/06/28	234.5150
cdnp1810.16o	csrj1810.16o	brdc1810.16n	igs19033.sp3	igs19033.clk_30s	igs19037.erp	2016/06/29	234.5244
cdnp1820.16o	csrj1820.16o	brdc1820.16n	igs19034.sp3	igs19034.clk_30s	igs19037.erp	2016/06/30	234.4982
cdnp1830.16o	csrj1830.16o	brdc1830.16n	igs19035.sp3	igs19035.clk_30s	igs19037.erp	2016/07/01	234.5293
cdnp1840.16o	csrj1840.16o	brdc1840.16n	igs19036.sp3	igs19036.clk_30s	igs19037.erp	2016/07/02	234.4975
cdnp1850.16o	csrj1850.16o	brdc1850.16n	igs19040.sp3	igs19040.clk_30s	igs19047.erp	2016/07/03	234.5102
cdnp1860.16o	csrj1860.16o	brdc1860.16n	igs19041.sp3	igs19041.clk_30s	igs19047.erp	2016/07/04	234.5079
cdnp1870.16o	csrj1870.16o	brdc1870.16n	igs19042.sp3	igs19042.clk_30s	igs19047.erp	2016/07/05	234.4420
cdnp1880.16o	csrj1880.16o	brdc1880.16n	igs19043.sp3	igs19043.clk_30s	igs19047.erp	2016/07/06	234.5148
cdnp1890.16o	csrj1890.16o	brdc1890.16n	igs19044.sp3	igs19044.clk_30s	igs19047.erp	2016/07/07	234.5223
cdnp1900.16o	csrj1900.16o	brdc1900.16n	igs19045.sp3	igs19045.clk_30s	igs19047.erp	2016/07/08	234.5047
cdnp1910.16o	csrj1910.16o	brdc1910.16n	igs19046.sp3	igs19046.clk_30s	igs19047.erp	2016/07/09	234.4846
cdnp1920.16o	csrj1920.16o	brdc1920.16n	igs19050.sp3	igs19050.clk_30s	igs19057.erp	2016/07/10	234.4776
cdnp1930.16o	csrj1930.16o	brdc1930.16n	igs19051.sp3	igs19051.clk_30s	igs19057.erp	2016/07/11	234.5300
cdnp1960.16o	csrj1960.16o	brdc1960.16n	igs19054.sp3	igs19054.clk_30s	igs19057.erp	2016/07/14	234.4848
cdnp1970.16o	csrj1970.16o	brdc1970.16n	igs19055.sp3	igs19055.clk_30s	igs19057.erp	2016/07/15	234.5461
cdnp1980.16o	csrj1980.16o	brdc1980.16n	igs19056.sp3	igs19056.clk_30s	igs19057.erp	2016/07/16	234.5068
cdnp1990.16o	csrj1990.16o	brdc1990.16n	igs19060.sp3	igs19060.clk_30s	igs19067.erp	2016/07/17	234.4321
cdnp2000.16o	csrj2000.16o	brdc2000.16n	igs19061.sp3	igs19061.clk_30s	igs19067.erp	2016/07/18	234.5089
cdnp2010.16o	csrj2010.16o	brdc2010.16n	igs19062.sp3	igs19062.clk_30s	igs19067.erp	2016/07/19	234.5464
cdnp2030.16o	csrj2030.16o	brdc2030.16n	igs19064.sp3	igs19064.clk_30s	igs19067.erp	2016/07/21	234.5201

cdnp2050.16o	csrj2050.16o	brdc2050.16n	igs19066.sp3	igs19066.clk_30s	igs19067.erp	2016/07/23	234.4970
cdnp2060.16o	csrj2060.16o	brdc2060.16n	igs19070.sp3	igs19070.clk_30s	igs19067.erp	2016/07/24	234.5061
cdnp2070.16o	csrj2070.16o	brdc2070.16n	igs19071.sp3	igs19071.clk_30s	igs19077.erp	2016/07/25	234.5219
cdnp2080.16o	csrj2080.16o	brdc2080.16n	igs19072.sp3	igs19072.clk_30s	igs19077.erp	2016/07/26	234.4997
cdnp2090.16o	csrj2090.16o	brdc2090.16n	igs19073.sp3	igs19073.clk_30s	igs19077.erp	2016/07/27	234.4978
cdnp2100.16o	csrj2100.16o	brdc2100.16n	igs19074.sp3	igs19074.clk_30s	igs19077.erp	2016/07/28	234.5209
cdnp2110.16o	csrj2110.16o	brdc2110.16n	igs19075.sp3	igs19075.clk_30s	igs19077.erp	2016/07/29	234.4851
cdnp2120.16o	csrj2120.16o	brdc2120.16n	igs19076.sp3	igs19076.clk_30s	igs19077.erp	2016/07/30	234.5115
cdnp2130.16o	csrj2130.16o	brdc2130.16n	igs19080.sp3	igs19080.clk_30s	igs19087.erp	2016/07/31	234.5077
cdnp2140.16o	csrj2140.16o	brdc2140.16n	igs19081.sp3	igs19081.clk_30s	igs19087.erp	2016/08/01	234.5011
cdnp2150.16o	csrj2150.16o	brdc2150.16n	igs19082.sp3	igs19082.clk_30s	igs19087.erp	2016/08/02	234.5110
cdnp2160.16o	csrj2160.16o	brdc2160.16n	igs19083.sp3	igs19083.clk_30s	igs19087.erp	2016/08/03	234.5012
cdnp2170.16o	csrj2170.16o	brdc2170.16n	igs19084.sp3	igs19084.clk_30s	igs19087.erp	2016/08/04	234.5058
cdnp2180.16o	csrj2180.16o	brdc2180.16n	igs19085.sp3	igs19085.clk_30s	igs19087.erp	2016/08/05	234.4765
cdnp2190.16o	csrj2190.16o	brdc2190.16n	igs19086.sp3	igs19086.clk_30s	igs19087.erp	2016/08/06	234.4894
cdnp2200.16o	csrj2200.16o	brdc2200.16n	igs19090.sp3	igs19090.clk_30s	igs19097.erp	2016/08/07	234.5193
cdnp2210.16o	csrj2210.16o	brdc2210.16n	igs19091.sp3	igs19091.clk_30s	igs19097.erp	2016/08/08	234.5163
cdnp2220.16o	csrj2220.16o	brdc2220.16n	igs19092.sp3	igs19092.clk_30s	igs19097.erp	2016/08/09	234.5057
cdnp2230.16o	csrj2230.16o	brdc2230.16n	igs19093.sp3	igs19093.clk_30s	igs19097.erp	2016/08/10	234.5200
cdnp2240.16o	csrj2240.16o	brdc2240.16n	igs19094.sp3	igs19094.clk_30s	igs19097.erp	2016/08/11	234.5156
cdnp2250.16o	csrj2250.16o	brdc2250.16n	igs19095.sp3	igs19095.clk_30s	igs19097.erp	2016/08/12	234.4674
cdnp2260.16o	csrj2260.16o	brdc2260.16n	igs19096.sp3	igs19096.clk_30s	igs19097.erp	2016/08/13	234.4991
cdnp2270.16o	csrj2270.16o	brdc2270.16n	igs19100.sp3	igs19100.clk_30s	igs19107.erp	2016/08/14	234.5192
cdnp2280.16o	csrj2280.16o	brdc2280.16n	igs19101.sp3	igs19101.clk_30s	igs19107.erp	2016/08/15	234.5110
cdnp2290.16o	csrj2290.16o	brdc2290.16n	igs19102.sp3	igs19102.clk_30s	igs19107.erp	2016/08/16	234.5103
cdnp2300.16o	csrj2300.16o	brdc2300.16n	igs19103.sp3	igs19103.clk_30s	igs19107.erp	2016/08/17	234.4931
cdnp2310.16o	csrj2310.16o	brdc2310.16n	igs19104.sp3	igs19104.clk_30s	igs19107.erp	2016/08/18	234.4989
cdnp2320.16o	csrj2320.16o	brdc2320.16n	igs19105.sp3	igs19105.clk_30s	igs19107.erp	2016/08/19	234.5000
cdnp2330.16o	csrj2330.16o	brdc2330.16n	igs19106.sp3	igs19106.clk_30s	igs19107.erp	2016/08/20	234.4893
cdnp2340.16o	csrj2340.16o	brdc2340.16n	igs19110.sp3	igs19110.clk_30s	igs19117.erp	2016/08/21	234.5126
cdnp2350.16o	csrj2350.16o	brdc2350.16n	igs19111.sp3	igs19111.clk_30s	igs19117.erp	2016/08/22	234.5099
cdnp2360.16o	csrj2360.16o	brdc2360.16n	igs19112.sp3	igs19112.clk_30s	igs19117.erp	2016/08/23	234.4949
cdnp2370.16o	csrj2370.16o	brdc2370.16n	igs19113.sp3	igs19113.clk_30s	igs19127.erp	2016/08/24	234.5017
cdnp2380.16o	csrj2380.16o	brdc2380.16n	igs19114.sp3	igs19114.clk_30s	igs19127.erp	2016/08/25	234.5209
cdnp2390.16o	csrj2390.16o	brdc2390.16n	igs19115.sp3	igs19115.clk_30s	igs19127.erp	2016/08/26	234.4867
cdnp2400.16o	csrj2400.16o	brdc2400.16n	igs19116.sp3	igs19116.clk_30s	igs19127.erp	2016/08/27	234.5053
cdnp2410.16o	csrj2410.16o	brdc2410.16n	igs19120.sp3	igs19120.clk_30s	igs19127.erp	2016/08/28	234.5030
cdnp2420.16o	csrj2420.16o	brdc2420.16n	igs19121.sp3	igs19121.clk_30s	igs19127.erp	2016/08/29	234.4939
cdnp2430.16o	csrj2430.16o	brdc2430.16n	igs19122.sp3	igs19122.clk_30s	igs19127.erp	2016/08/30	234.4896
cdnp2440.16o	csrj2440.16o	brdc2440.16n	igs19123.sp3	igs19123.clk_30s	igs19127.erp	2016/08/31	234.5194
cdnp2450.16o	csrj2450.16o	brdc2450.16n	igs19124.sp3	igs19124.clk_30s	igs19127.erp	2016/09/01	234.5005
cdnp2460.16o	csrj2460.16o	brdc2460.16n	igs19125.sp3	igs19125.clk_30s	igs19127.erp	2016/09/02	234.4921
cdnp2470.16o	csrj2470.16o	brdc2470.16n	igs19126.sp3	igs19126.clk_30s	igs19127.erp	2016/09/03	234.4998
cdnp2480.16o	csrj2480.16o	brdc2480.16n	igs19130.sp3	igs19130.clk_30s	igs19137.erp	2016/09/04	234.4943
cdnp2490.16o	csrj2490.16o	brdc2490.16n	igs19131.sp3	igs19131.clk_30s	igs19137.erp	2016/09/05	234.5005
cdnp2500.16o	csrj2500.16o	brdc2500.16n	igs19132.sp3	igs19132.clk_30s	igs19137.erp	2016/09/06	234.4747
cdnp2510.16o	csrj2510.16o	brdc2510.16n	igs19133.sp3	igs19133.clk_30s	igs19137.erp	2016/09/07	234.4909
cdnp2520.16o	csrj2520.16o	brdc2520.16n	igs19134.sp3	igs19134.clk_30s	igs19137.erp	2016/09/08	234.4876
cdnp2530.16o	csrj2530.16o	brdc2530.16n	igs19135.sp3	igs19135.clk_30s	igs19137.erp	2016/09/09	234.5087
cdnp2540.16o	csrj2540.16o	brdc2540.16n	igs19136.sp3	igs19136.clk_30s	igs19137.erp	2016/09/10	234.4968
cdnp2550.16o	csrj2550.16o	brdc2550.16n	igs19140.sp3	igs19140.clk_30s	igs19147.erp	2016/09/11	234.5310
cdnp2560.16o	csrj2560.16o	brdc2560.16n	igs19141.sp3	igs19141.clk_30s	igs19147.erp	2016/09/12	234.5098
cdnp2570.16o	csrj2570.16o	brdc2570.16n	igs19142.sp3	igs19142.clk_30s	igs19147.erp	2016/09/13	234.5098
cdnp2580.16o	csrj2580.16o	brdc2580.16n	igs19143.sp3	igs19143.clk_30s	igs19147.erp	2016/09/14	234.5233
cdnp2590.16o	csrj2590.16o	brdc2590.16n	igs19144.sp3	igs19144.clk_30s	igs19147.erp	2016/09/15	234.4994
cdnp2600.16o	csrj2600.16o	brdc2600.16n	igs19145.sp3	igs19145.clk_30s	igs19147.erp	2016/09/16	234.5254
cdnp2610.16o	csrj2610.16o	brdc2610.16n	igs19146.sp3	igs19146.clk_30s	igs19147.erp	2016/09/17	234.4934
cdnp2620.16o	csrj2620.16o	brdc2620.16n	igs19150.sp3	igs19150.clk_30s	igs19157.erp	2016/09/18	234.5247
cdnp2630.16o	csrj2630.16o	brdc2630.16n	igs19151.sp3	igs19151.clk_30s	igs19157.erp	2016/09/19	234.4519
cdnp2640.16o	csrj2640.16o	brdc2640.16n	igs19152.sp3	igs19152.clk_30s	igs19157.erp	2016/09/20	234.4863
cdnp2650.16o	csrj2650.16o	brdc2650.16n	igs19153.sp3	igs19153.clk_30s	igs19157.erp	2016/09/21	234.5539
cdnp2660.16o	csrj2660.16o	brdc2660.16n	igs19154.sp3	igs19154.clk_30s	igs19157.erp	2016/09/22	234.4986
cdnp2670.16o	csrj2670.16o	brdc2670.16n	igs19155.sp3	igs19155.clk_30s	igs19157.erp	2016/09/23	234.5477
cdnp2690.16o	csrj2690.16o	brdc2690.16n	igs19160.sp3	igs19160.clk_30s	igs19167.erp	2016/09/25	234.4880
cdnp2700.16o	csrj2700.16o	brdc2700.16n	igs19161.sp3	igs19161.clk_30s	igs19167.erp	2016/09/26	234.4944
cdnp2710.16o	csrj2710.16o	brdc2710.16n	igs19162.sp3	igs19162.clk_30s	igs19167.erp	2016/09/27	234.4693
cdnp2720.16o	csrj2720.16o	brdc2720.16n	igs19163.sp3	igs19163.clk_30s	igs19167.erp	2016/09/28	234.5179
cdnp2730.16o	csrj2730.16o	brdc2730.16n	igs19164.sp3	igs19164.clk_30s	igs19167.erp	2016/09/29	234.4745
cdnp2740.16o	csrj2740.16o	brdc2740.16n	igs19165.sp3	igs19165.clk_30s	igs19167.erp	2016/09/30	234.5112
cdnp2750.16o	csrj2750.16o	brdc2750.16n	igs19166.sp3	igs19166.clk_30s	igs19167.erp	2016/10/01	234.4556

cdnp2760.16o	csrj2760.16o	brdc2760.16n	igs19170.sp3	igs19170.clk_30s	igs1917.erp7	2016/10/02	234.4475
cdnp2780.16o	csrj2780.16o	brdc2780.16n	igs19172.sp3	igs19172.clk_30s	igs1917.erp7	2016/10/04	234.5671
cdnp2790.16o	csrj2790.16o	brdc2790.16n	igs19173.sp3	igs19173.clk_30s	igs1917.erp7	2016/10/05	234.5386
cdnp2800.16o	csrj2800.16o	brdc2800.16n	igs19174.sp3	igs19174.clk_30s	igs1917.erp7	2016/10/06	234.4915
cdnp2810.16o	csrj2810.16o	brdc2810.16n	igs19175.sp3	igs19175.clk_30s	igs1917.erp7	2016/10/07	234.4626
cdnp2820.16o	csrj2820.16o	brdc2820.16n	igs19176.sp3	igs19176.clk_30s	igs1917.erp7	2016/10/08	234.5202
cdnp2830.16o	csrj2830.16o	brdc2830.16n	igs19180.sp3	igs19180.clk_30s	igs19187.erp	2016/10/09	234.5327
cdnp2840.16o	csrj2840.16o	brdc2840.16n	igs19181.sp3	igs19181.clk_30s	igs19187.erp	2016/10/10	234.4596
cdnp2850.16o	csrj2850.16o	brdc2850.16n	igs19182.sp3	igs19182.clk_30s	igs19187.erp	2016/10/11	234.4801
cdnp2860.16o	csrj2860.16o	brdc2860.16n	igs19183.sp3	igs19183.clk_30s	igs19187.erp	2016/10/12	234.4996
cdnp2880.16o	csrj2880.16o	brdc2880.16n	igs19185.sp3	igs19185.clk_30s	igs19187.erp	2016/10/14	234.5272
cdnp2890.16o	csrj2890.16o	brdc2890.16n	igs19186.sp3	igs19186.clk_30s	igs19187.erp	2016/10/15	234.4918
cdnp2900.16o	csrj2900.16o	brdc2900.16n	igs19190.sp3	igs19190.clk_30s	igs19197.erp	2016/10/16	234.5270
cdnp2930.16o	csrj2930.16o	brdc2930.16n	igs19193.sp3	igs19193.clk_30s	igs19197.erp	2016/10/19	234.5028
cdnp2940.16o	csrj2940.16o	brdc2940.16n	igs19194.sp3	igs19194.clk_30s	igs19197.erp	2016/10/20	234.5306
cdnp2950.16o	csrj2950.16o	brdc2950.16n	igs19195.sp3	igs19195.clk_30s	igs19197.erp	2016/10/21	234.5008
cdnp2960.16o	csrj2960.16o	brdc2960.16n	igs19196.sp3	igs19196.clk_30s	igs19197.erp	2016/10/22	234.5194
cdnp2970.16o	csrj2970.16o	brdc2970.16n	igs19200.sp3	igs19200.clk_30s	igs19207.erp	2016/10/23	234.5132
cdnp2980.16o	csrj2980.16o	brdc2980.16n	igs19201.sp3	igs19201.clk_30s	igs19207.erp	2016/10/24	234.4940
cdnp2990.16o	csrj2990.16o	brdc2990.16n	igs19202.sp3	igs19202.clk_30s	igs19207.erp	2016/10/25	234.4864
cdnp3000.16o	csrj3000.16o	brdc3000.16n	igs19203.sp3	igs19203.clk_30s	igs19207.erp	2016/10/26	234.4716
cdnp3010.16o	csrj3010.16o	brdc3010.16n	igs19204.sp3	igs19204.clk_30s	igs19207.erp	2016/10/27	234.5236
cdnp3020.16o	csrj3020.16o	brdc3020.16n	igs19205.sp3	igs19205.clk_30s	igs19207.erp	2016/10/28	234.5116
cdnp3030.16o	csrj3030.16o	brdc3030.16n	igs19206.sp3	igs19206.clk_30s	igs19207.erp	2016/10/29	234.4874
cdnp3040.16o	csrj3040.16o	brdc3040.16n	igs19210.sp3	igs19210.clk_30s	igs19217.erp	2016/10/30	234.4949
cdnp3050.16o	csrj3050.16o	brdc3050.16n	igs19211.sp3	igs19211.clk_30s	igs19217.erp	2016/10/31	234.5263
cdnp3060.16o	csrj3060.16o	brdc3060.16n	igs19212.sp3	igs19212.clk_30s	igs19217.erp	2016/11/01	234.5038
cdnp3070.16o	csrj3070.16o	brdc3070.16n	igs19213.sp3	igs19213.clk_30s	igs19217.erp	2016/11/02	234.4911
cdnp3080.16o	csrj3080.16o	brdc3080.16n	igs19214.sp3	igs19214.clk_30s	igs19217.erp	2016/11/03	234.5081
cdnp3090.16o	csrj3090.16o	brdc3090.16n	igs19215.sp3	igs19215.clk_30s	igs19217.erp	2016/11/04	234.5140
cdnp3100.16o	csrj3100.16o	brdc3100.16n	igs19216.sp3	igs19216.clk_30s	igs19217.erp	2016/11/05	234.5308
cdnp3110.16o	csrj3110.16o	brdc3110.16n	igs19220.sp3	igs19220.clk_30s	igs19227.erp	2016/11/06	234.4882
cdnp3130.16o	csrj3130.16o	brdc3130.16n	igs19222.sp3	igs19222.clk_30s	igs19227.erp	2016/11/08	234.4909
cdnp3140.16o	csrj3140.16o	brdc3140.16n	igs19223.sp3	igs19223.clk_30s	igs19227.erp	2016/11/09	234.4935
cdnp3150.16o	csrj3150.16o	brdc3150.16n	igs19224.sp3	igs19224.clk_30s	igs19227.erp	2016/11/10	234.5178
cdnp3160.16o	csrj3160.16o	brdc3160.16n	igs19225.sp3	igs19225.clk_30s	igs19227.erp	2016/11/11	234.4983
cdnp3170.16o	csrj3170.16o	brdc3170.16n	igs19226.sp3	igs19226.clk_30s	igs19227.erp	2016/11/12	234.4946
cdnp3200.16o	csrj3200.16o	brdc3200.16n	igs19232.sp3	igs19232.clk_30s	igs19237.erp	2016/11/15	234.5682
cdnp3210.16o	csrj3210.16o	brdc3210.16n	igs19233.sp3	igs19233.clk_30s	igs19237.erp	2016/11/16	234.4585
cdnp3220.16o	csrj3220.16o	brdc3220.16n	igs19234.sp3	igs19234.clk_30s	igs19237.erp	2016/11/17	234.5118
cdnp3230.16o	csrj3230.16o	brdc3230.16n	igs19235.sp3	igs19235.clk_30s	igs19237.erp	2016/11/18	234.5239
cdnp3240.16o	csrj3240.16o	brdc3240.16n	igs19236.sp3	igs19236.clk_30s	igs19237.erp	2016/11/19	234.5061
cdnp3250.16o	csrj3250.16o	brdc3250.16n	igs19240.sp3	igs19240.clk_30s	igs19247.erp	2016/11/20	234.5121
cdnp3260.16o	csrj3260.16o	brdc3260.16n	igs19241.sp3	igs19241.clk_30s	igs19247.erp	2016/11/21	234.5378
cdnp3270.16o	csrj3270.16o	brdc3270.16n	igs19242.sp3	igs19242.clk_30s	igs19247.erp	2016/11/22	234.4773
cdnp3280.16o	csrj3280.16o	brdc3280.16n	igs19243.sp3	igs19243.clk_30s	igs19247.erp	2016/11/23	234.4979
cdnp3290.16o	csrj3290.16o	brdc3290.16n	igs19244.sp3	igs19244.clk_30s	igs19247.erp	2016/11/24	234.4925
cdnp3300.16o	csrj3300.16o	brdc3300.16n	igs19245.sp3	igs19245.clk_30s	igs19247.erp	2016/11/25	234.4814
cdnp3310.16o	csrj3310.16o	brdc3310.16n	igs19246.sp3	igs19246.clk_30s	igs19247.erp	2016/11/26	234.4930
cdnp3330.16o	csrj3330.16o	brdc3330.16n	igs19251.sp3	igs19251.clk_30s	igs19257.erp	2016/11/28	234.4993
cdnp3340.16o	csrj3340.16o	brdc3340.16n	igs19252.sp3	igs19252.clk_30s	igs19257.erp	2016/11/29	234.4876
cdnp3350.16o	csrj3350.16o	brdc3350.16n	igs19253.sp3	igs19253.clk_30s	igs19257.erp	2016/11/30	234.4976
cdnp3360.16o	csrj3360.16o	brdc3360.16n	igs19254.sp3	igs19254.clk_30s	igs19257.erp	2016/12/01	234.4881
cdnp3370.16o	csrj3370.16o	brdc3370.16n	igs19255.sp3	igs19255.clk_30s	igs19257.erp	2016/12/02	234.5075
cdnp3380.16o	csrj3380.16o	brdc3380.16n	igs19256.sp3	igs19256.clk_30s	igs19257.erp	2016/12/03	234.5100
cdnp3390.16o	csrj3390.16o	brdc3390.16n	igs19260.sp3	igs19260.clk_30s	igs19267.erp	2016/12/04	234.5108
cdnp3400.16o	csrj3400.16o	brdc3400.16n	igs19261.sp3	igs19261.clk_30s	igs19267.erp	2016/12/05	234.5226
cdnp3410.16o	csrj3410.16o	brdc3410.16n	igs19262.sp3	igs19262.clk_30s	igs19267.erp	2016/12/06	234.5069
cdnp3420.16o	csrj3420.16o	brdc3420.16n	igs19263.sp3	igs19263.clk_30s	igs19267.erp	2016/12/07	234.5010
cdnp3430.16o	csrj3430.16o	brdc3430.16n	igs19264.sp3	igs19264.clk_30s	igs19267.erp	2016/12/08	234.5189
cdnp3440.16o	csrj3440.16o	brdc3440.16n	igs19265.sp3	igs19265.clk_30s	igs19267.erp	2016/12/09	234.4926
cdnp3450.16o	csrj3450.16o	brdc3450.16n	igs19266.sp3	igs19266.clk_30s	igs19267.erp	2016/12/10	234.4963
cdnp3460.16o	csrj3460.16o	brdc3460.16n	igs19270.sp3	igs19270.clk_30s	igs19277.erp	2016/12/11	234.5267
cdnp3470.16o	csrj3470.16o	brdc3470.16n	igs19271.sp3	igs19271.clk_30s	igs19277.erp	2016/12/12	234.4784
cdnp3480.16o	csrj3480.16o	brdc3480.16n	igs19272.sp3	igs19272.clk_30s	igs19277.erp	2016/12/13	234.5051
cdnp3490.16o	csrj3490.16o	brdc3490.16n	igs19273.sp3	igs19273.clk_30s	igs19277.erp	2016/12/14	234.4979
cdnp3530.16o	csrj3530.16o	brdc3530.16n	igs19280.sp3	igs19280.clk_30s	igs19287.erp	2016/12/18	234.5012
cdnp3540.16o	csrj3540.16o	brdc3540.16n	igs19281.sp3	igs19281.clk_30s	igs19287.erp	2016/12/19	234.5357
cdnp3550.16o	csrj3550.16o	brdc3550.16n	igs19282.sp3	igs19282.clk_30s	igs19287.erp	2016/12/20	234.4937
cdnp3560.16o	csrj3560.16o	brdc3560.16n	igs19283.sp3	igs19283.clk_30s	igs19287.erp	2016/12/21	234.5038

cdnp3570.16o	csrj3570.16o	brdc3570.16n	igs19284.sp3	igs19284.clk_30s	igs19287.erp	2016/12/22	234.5032
cdnp3580.16o	csrj3580.16o	brdc3580.16n	igs19285.sp3	igs19285.clk_30s	igs19287.erp	2016/12/23	234.4958
cdnp3590.16o	csrj3590.16o	brdc3590.16n	igs19286.sp3	igs19286.clk_30s	igs19287.erp	2016/12/24	234.4868
cdnp3620.16o	csrj3620.16o	brdc3620.16n	igs19292.sp3	igs19292.clk_30s	igs19297.erp	2016/12/27	234.4641
cdnp3630.16o	csrj3630.16o	brdc3630.16n	igs19293.sp3	igs19293.clk_30s	igs19297.erp	2016/12/28	234.4819
cdnp3640.16o	csrj3640.16o	brdc3640.16n	igs19294.sp3	igs19294.clk_30s	igs19297.erp	2016/12/29	234.5142
cdnp0240.17o	csrj0240.17o	brdc0240.17n	igs19332.sp3	igs19332.clk_30s	igs19337.erp	2017/01/24	234.5021
cdnp0320.17o	blng032x.17o	brdc0320.17n	igs19343.sp3	igs19343.clk_30s	igs19347.erp	2017/02/01	233.9093
cdnp0330.17o	blng033x.17o	brdc0330.17n	igs19344.sp3	igs19344.clk_30s	igs19347.erp	2017/02/02	233.7403
cdnp0340.17o	blng034x.17o	brdc0340.17n	igs19345.sp3	igs19345.clk_30s	igs19347.erp	2017/02/03	233.9194
cdnp0360.17o	blng036x.17o	brdc0360.17n	igs19350.sp3	igs19350.clk_30s	igs19357.erp	2017/02/05	234.2191
cdnp0370.17o	blng037x.17o	brdc0370.17n	igs19351.sp3	igs19351.clk_30s	igs19357.erp	2017/02/06	234.0546
cdnp0390.17o	blng039x.17o	brdc0390.17n	igs19353.sp3	igs19353.clk_30s	igs19357.erp	2017/02/08	233.8934
cdnp0400.17o	blng040x.17o	brdc0400.17n	igs19354.sp3	igs19354.clk_30s	igs19357.erp	2017/02/09	233.9805
cdnp0410.17o	blng041x.17o	brdc0410.17n	igs19355.sp3	igs19355.clk_30s	igs19357.erp	2017/02/10	234.1746
cdnp0420.17o	blng042x.17o	brdc0420.17n	igs19356.sp3	igs19356.clk_30s	igs19357.erp	2017/02/11	234.2829
cdnp0430.17o	blng043x.17o	brdc0430.17n	igs19360.sp3	igs19360.clk_30s	igs19367.erp	2017/02/12	234.0708
cdnp0440.17o	blng044j.17o	brdc0440.17n	igs19361.sp3	igs19361.clk_30s	igs19367.erp	2017/02/13	234.0472
cdnp0450.17o	blng045x.17o	brdc0450.17n	igs19362.sp3	igs19362.clk_30s	igs19367.erp	2017/02/14	233.9943
cdnp0470.17o	blng047x.17o	brdc0470.17n	igs19364.sp3	igs19364.clk_30s	igs19367.erp	2017/02/16	234.0214
cdnp0480.17o	blng048x.17o	brdc0480.17n	igs19365.sp3	igs19365.clk_30s	igs19367.erp	2017/02/17	235.1624
cdnp0490.17o	blng049x.17o	brdc0490.17n	igs19366.sp3	igs19366.clk_30s	igs19367.erp	2017/02/18	234.2250
cdnp0500.17o	blng050x.17o	brdc0500.17n	igs19370.sp3	igs19370.clk_30s	igs19377.erp	2017/02/19	235.1155
cdnp0510.17o	blng051x.17o	brdc0510.17n	igs19371.sp3	igs19371.clk_30s	igs19377.erp	2017/02/20	234.5945
cdnp0520.17o	blng052x.17o	brdc0520.17n	igs19372.sp3	igs19372.clk_30s	igs19377.erp	2017/02/21	235.1533
cdnp0530.17o	blng053x.17o	brdc0530.17n	igs19373.sp3	igs19373.clk_30s	igs19377.erp	2017/02/22	235.3782
cdnp0540.17o	blng054x.17o	brdc0540.17n	igs19374.sp3	igs19374.clk_30s	igs19377.erp	2017/02/23	234.9068
cdnp0560.17o	blng056x.17o	brdc0560.17n	igs19376.sp3	igs19376.clk_30s	igs19377.erp	2017/02/24	235.4457
cdnp0570.17o	blng057x.17o	brdc0570.17n	igs19380.sp3	igs19380.clk_30s	igs19377.erp	2017/02/25	235.3947
cdnp0580.17o	blng058x.17o	brdc0580.17n	igs19381.sp3	igs19381.clk_30s	igs19387.erp	2017/02/26	234.6328
cdnp0590.17o	blng059x.17o	brdc0590.17n	igs19382.sp3	igs19382.clk_30s	igs19387.erp	2017/02/27	235.5051
cdnp0600.17o	blng060x.17o	brdc0600.17n	igs19383.sp3	igs19383.clk_30s	igs19387.erp	2017/02/28	234.7545
cdnp0610.17o	blng061x.17o	brdc0610.17n	igs19384.sp3	igs19384.clk_30s	igs19387.erp	2017/03/01	234.0875
cdnp0620.17o	blng062w.17o	brdc0620.17n	igs19385.sp3	igs19385.clk_30s	igs19387.erp	2017/03/02	234.5803
cdnp0630.17o	blng063x.17o	brdc0630.17n	igs19386.sp3	igs19386.clk_30s	igs19387.erp	2017/03/03	234.4493
cdnp0640.17o	blng064x.17o	brdc0640.17n	igs19390.sp3	igs19390.clk_30s	igs19397.erp	2017/03/04	235.1763
cdnp0650.17o	blng065x.17o	brdc0650.17n	igs19391.sp3	igs19391.clk_30s	igs19397.erp	2017/03/05	235.2375
cdnp0660.17o	blng066x.17o	brdc0660.17n	igs19392.sp3	igs19392.clk_30s	igs19397.erp	2017/03/06	234.4901
cdnp0670.17o	blng067x.17o	brdc0670.17n	igs19393.sp3	igs19393.clk_30s	igs19397.erp	2017/03/07	234.6319
cdnp0680.17o	blng068x.17o	brdc0680.17n	igs19394.sp3	igs19394.clk_30s	igs19397.erp	2017/03/08	234.7436
cdnp0690.17o	blng069x.17o	brdc0690.17n	igs19395.sp3	igs19395.clk_30s	igs19397.erp	2017/03/09	234.4023
cdnp0700.17o	blng070x.17o	brdc0700.17n	igs19396.sp3	igs19396.clk_30s	igs19397.erp	2017/03/10	234.4254
cdnp0710.17o	blng071x.17o	brdc0710.17n	igs19400.sp3	igs19400.clk_30s	igs19407.erp	2017/03/11	234.3973
cdnp0720.17o	blng072x.17o	brdc0720.17n	igs19401.sp3	igs19401.clk_30s	igs19407.erp	2017/03/12	234.0975
cdnp0730.17o	blng073x.17o	brdc0730.17n	igs19402.sp3	igs19402.clk_30s	igs19407.erp	2017/03/13	233.8106
cdnp0740.17o	blng074x.17o	brdc0740.17n	igs19403.sp3	igs19403.clk_30s	igs19407.erp	2017/03/14	233.8124
cdnp0750.17o	blng075x.17o	brdc0750.17n	igs19404.sp3	igs19404.clk_30s	igs19407.erp	2017/03/15	234.3730
cdnp0760.17o	blng076i.17o	brdc0760.17n	igs19405.sp3	igs19405.clk_30s	igs19407.erp	2017/03/16	234.1108
cdnp0890.17o	blng089x.17o	brdc0890.17n	igs19424.sp3	igs19424.clk_30s	igs19427.erp	2017/03/30	235.2578
cdnp0900.17o	blng090x.17o	brdc0900.17n	igs19425.sp3	igs19425.clk_30s	igs19427.erp	2017/03/31	234.9585
cdnp0910.17o	blng091x.17o	brdc0910.17n	igs19426.sp3	igs19426.clk_30s	igs19427.erp	2017/04/01	234.7841
cdnp0920.17o	blng092a.17o	brdc0920.17n	igs19430.sp3	igs19430.clk_30s	igs19437.erp	2017/04/02	233.9168
cdnp0930.17o	blng093x.17o	brdc0930.17n	igs19431.sp3	igs19431.clk_30s	igs19437.erp	2017/04/03	234.1143
cdnp0950.17o	blng095x.17o	brdc0950.17n	igs19433.sp3	igs19433.clk_30s	igs19437.erp	2017/04/05	234.1085
cdnp0960.17o	blng096x.17o	brdc0960.17n	igs19434.sp3	igs19434.clk_30s	igs19437.erp	2017/04/06	233.6409
cdnp1020.17o	blng102x.17o	brdc1020.17n	igs19443.sp3	igs19443.clk_30s	igs19447.erp	2017/04/12	234.6803
cdnp1030.17o	blng103x.17o	brdc1030.17n	igs19444.sp3	igs19444.clk_30s	igs19447.erp	2017/04/13	234.4968
cdnp1040.17o	blng104x.17o	brdc1040.17n	igs19445.sp3	igs19445.clk_30s	igs19447.erp	2017/04/14	234.1279
cdnp1050.17o	blng105x.17o	brdc1050.17n	igs19446.sp3	igs19446.clk_30s	igs19447.erp	2017/04/15	234.6016
cdnp1060.17o	blng106x.17o	brdc1060.17n	igs19450.sp3	igs19450.clk_30s	igs19457.erp	2017/04/16	235.1993
cdnp1070.17o	blng107x.17o	brdc1070.17n	igs19451.sp3	igs19451.clk_30s	igs19457.erp	2017/04/17	234.4039
cdnp1080.17o	blng108x.17o	brdc1080.17n	igs19452.sp3	igs19452.clk_30s	igs19457.erp	2017/04/18	234.1852
cdnp1160.17o	blng116x.17o	brdc1160.17n	igs19463.sp3	igs19463.clk_30s	igs19467.erp	2017/04/26	235.2434
cdnp1170.17o	blng117x.17o	brdc1170.17n	igs19464.sp3	igs19464.clk_30s	igs19467.erp	2017/04/27	234.7465
cdnp1180.17o	blng118x.17o	brdc1180.17n	igs19465.sp3	igs19465.clk_30s	igs19467.erp	2017/04/28	234.8831
cdnp1190.17o	blng119x.17o	brdc1190.17n	igs19466.sp3	igs19466.clk_30s	igs19467.erp	2017/04/29	234.2550
cdnp1200.17o	blng120x.17o	brdc1200.17n	igs19470.sp3	igs19470.clk_30s	igs19477.erp	2017/04/30	235.1446
cdnp1210.17o	blng121x.17o	brdc1210.17n	igs19471.sp3	igs19471.clk_30s	igs19477.erp	2017/05/01	234.5024

### B.3 JMB0 station

RINEX Observation		RINEX *NAV/CLK, SP3 or SBS/EMS			EOP data file	Date	Height (m)
Rover	Base station	IGS_NAV	IGS_EPH	IGS_CLK_30s			
jmb0200x.16o	csrj2000.16o	brdc2000.16n	igs19061.sp3	igs19061.clk_30s	igs19067.erp	2016/07/18	61.5787
jmb0201f.16o	csrj2010.16o	brdc2010.16n	igs19062.sp3	igs19062.clk_30s	igs19067.erp	2016/07/19	60.7949
jmb0204x.16o	csrj2040.16o	brdc2040.16n	igs19065.sp3	igs19065.clk_30s	igs19067.erp	2016/07/22	60.0453
jmb0205x.16o	csrj2050.16o	brdc2050.16n	igs19066.sp3	igs19066.clk_30s	igs19067.erp	2016/07/23	60.5278
jmb0206x.16o	csrj2060.16o	brdc2060.16n	igs19070.sp3	igs19070.clk_30s	igs19067.erp	2016/07/24	60.5835
jmb0207x.16o	csrj2070.16o	brdc2070.16n	igs19071.sp3	igs19071.clk_30s	igs19077.erp	2016/07/25	60.8644
jmb0208x.16o	csrj2080.16o	brdc2080.16n	igs19072.sp3	igs19072.clk_30s	igs19077.erp	2016/07/26	60.4672
jmb0209x.16o	csrj2090.16o	brdc2090.16n	igs19073.sp3	igs19073.clk_30s	igs19077.erp	2016/07/27	60.0651
jmb0210x.16o	csrj2100.16o	brdc2100.16n	igs19074.sp3	igs19074.clk_30s	igs19077.erp	2016/07/28	59.9389
jmb0211x.16o	csrj2110.16o	brdc2110.16n	igs19075.sp3	igs19075.clk_30s	igs19077.erp	2016/07/29	61.1085
jmb0212b.16o	csrj2120.16o	brdc2120.16n	igs19076.sp3	igs19076.clk_30s	igs19077.erp	2016/07/30	60.6329
jmb0223x.16o	csrj2230.16o	brdc2230.16n	igs19093.sp3	igs19093.clk_30s	igs19097.erp	2016/08/10	60.3828
jmb0224x.16o	csrj2240.16o	brdc2240.16n	igs19094.sp3	igs19094.clk_30s	igs19097.erp	2016/08/11	60.5440
jmb0225x.16o	csrj2250.16o	brdc2250.16n	igs19095.sp3	igs19095.clk_30s	igs19097.erp	2016/08/12	60.8021
jmb0226x.16o	csrj2260.16o	brdc2260.16n	igs19096.sp3	igs19096.clk_30s	igs19097.erp	2016/08/13	61.2460
jmb0227x.16o	csrj2270.16o	brdc2270.16n	igs19100.sp3	igs19100.clk_30s	igs19107.erp	2016/08/14	60.3366
jmb0228x.16o	csrj2280.16o	brdc2280.16n	igs19101.sp3	igs19101.clk_30s	igs19107.erp	2016/08/15	60.7781
jmb0229x.16o	csrj2290.16o	brdc2290.16n	igs19102.sp3	igs19102.clk_30s	igs19107.erp	2016/08/16	60.8956
jmb0230x.16o	csrj2300.16o	brdc2300.16n	igs19103.sp3	igs19103.clk_30s	igs19107.erp	2016/08/17	60.0634
jmb0231x.16o	csrj2310.16o	brdc2310.16n	igs19104.sp3	igs19104.clk_30s	igs19107.erp	2016/08/18	61.4695
jmb0232f.16o	csrj2320.16o	brdc2320.16n	igs19105.sp3	igs19105.clk_30s	igs19107.erp	2016/08/19	59.9121
jmb0237x.16o	csrj2370.16o	brdc2370.16n	igs19113.sp3	igs19113.clk_30s	igs19127.erp	2016/08/24	60.5543
jmb0238x.16o	csrj2380.16o	brdc2380.16n	igs19114.sp3	igs19114.clk_30s	igs19127.erp	2016/08/25	60.2814
jmb0239x.16o	csrj2390.16o	brdc2390.16n	igs19115.sp3	igs19115.clk_30s	igs19127.erp	2016/08/26	60.0306
jmb0240g.16o	csrj2400.16o	brdc2400.16n	igs19116.sp3	igs19116.clk_30s	igs19127.erp	2016/08/27	60.7232
jmb0244x.16o	csrj2440.16o	brdc2440.16n	igs19123.sp3	igs19123.clk_30s	igs19127.erp	2016/08/31	60.9964
jmb0245x.16o	csrj2450.16o	brdc2450.16n	igs19124.sp3	igs19124.clk_30s	igs19127.erp	2016/09/01	60.8392
jmb0246x.16o	csrj2460.16o	brdc2460.16n	igs19125.sp3	igs19125.clk_30s	igs19127.erp	2016/09/02	60.5395
jmb0247x.16o	csrj2470.16o	brdc2470.16n	igs19126.sp3	igs19126.clk_30s	igs19127.erp	2016/09/03	59.7864
jmb0248x.16o	csrj2480.16o	brdc2480.16n	igs19130.sp3	igs19130.clk_30s	igs19137.erp	2016/09/04	61.3506
jmb0249x.16o	csrj2490.16o	brdc2490.16n	igs19131.sp3	igs19131.clk_30s	igs19137.erp	2016/09/05	59.5126
jmb0250x.16o	csrj2500.16o	brdc2500.16n	igs19132.sp3	igs19132.clk_30s	igs19137.erp	2016/09/06	60.7987
jmb0251x.16o	csrj2510.16o	brdc2510.16n	igs19133.sp3	igs19133.clk_30s	igs19137.erp	2016/09/07	61.2777
jmb0252x.16o	csrj2520.16o	brdc2520.16n	igs19134.sp3	igs19134.clk_30s	igs19137.erp	2016/09/08	60.4558
jmb0253x.16o	csrj2530.16o	brdc2530.16n	igs19135.sp3	igs19135.clk_30s	igs19137.erp	2016/09/09	61.5430
jmb0254x.16o	csrj2540.16o	brdc2540.16n	igs19136.sp3	igs19136.clk_30s	igs19137.erp	2016/09/10	59.2811
jmb0255x.16o	csrj2550.16o	brdc2550.16n	igs19140.sp3	igs19140.clk_30s	igs19147.erp	2016/09/11	59.2187
jmb0256x.16o	csrj2560.16o	brdc2560.16n	igs19141.sp3	igs19141.clk_30s	igs19147.erp	2016/09/12	60.8212
jmb0257x.16o	csrj2570.16o	brdc2570.16n	igs19142.sp3	igs19142.clk_30s	igs19147.erp	2016/09/13	60.4363
jmb0258x.16o	csrj2580.16o	brdc2580.16n	igs19143.sp3	igs19143.clk_30s	igs19147.erp	2016/09/14	61.8337
jmb0259x.16o	csrj2590.16o	brdc2590.16n	igs19144.sp3	igs19144.clk_30s	igs19147.erp	2016/09/15	61.9606
jmb0260x.16o	csrj2600.16o	brdc2600.16n	igs19145.sp3	igs19145.clk_30s	igs19147.erp	2016/09/16	60.3479
jmb0261h.16o	csrj2610.16o	brdc2610.16n	igs19146.sp3	igs19146.clk_30s	igs19147.erp	2016/09/17	59.9355
jmb0263x.16o	csrj2630.16o	brdc2630.16n	igs19151.sp3	igs19151.clk_30s	igs19157.erp	2016/09/19	59.9031
jmb0264x.16o	csrj2640.16o	brdc2640.16n	igs19152.sp3	igs19152.clk_30s	igs19157.erp	2016/09/20	62.0971
jmb0265x.16o	csrj2650.16o	brdc2650.16n	igs19153.sp3	igs19153.clk_30s	igs19157.erp	2016/09/21	61.5400
jmb0266x.16o	csrj2660.16o	brdc2660.16n	igs19154.sp3	igs19154.clk_30s	igs19157.erp	2016/09/22	60.0577
jmb0267x.16o	csrj2670.16o	brdc2670.16n	igs19155.sp3	igs19155.clk_30s	igs19157.erp	2016/09/23	61.5090
jmb0268x.16o	csrj2680.16o	brdc2680.16n	igs19156.sp3	igs19156.clk_30s	igs19157.erp	2016/09/24	60.1067
jmb0269x.16o	csrj2690.16o	brdc2690.16n	igs19160.sp3	igs19160.clk_30s	igs19167.erp	2016/09/25	60.1638
jmb0270x.16o	csrj2700.16o	brdc2700.16n	igs19161.sp3	igs19161.clk_30s	igs19167.erp	2016/09/26	60.7223
jmb0271x.16o	csrj2710.16o	brdc2710.16n	igs19162.sp3	igs19162.clk_30s	igs19167.erp	2016/09/27	61.6583
jmb0272x.16o	csrj2720.16o	brdc2720.16n	igs19163.sp3	igs19163.clk_30s	igs19167.erp	2016/09/28	60.7181
jmb0273x.16o	csrj2730.16o	brdc2730.16n	igs19164.sp3	igs19164.clk_30s	igs19167.erp	2016/09/29	59.6477
jmb0274x.16o	csrj2740.16o	brdc2740.16n	igs19165.sp3	igs19165.clk_30s	igs19167.erp	2016/09/30	59.3638
jmb0275x.16o	csrj2750.16o	brdc2750.16n	igs19166.sp3	igs19166.clk_30s	igs19167.erp	2016/10/01	60.5267
jmb0276x.16o	csrj2760.16o	brdc2760.16n	igs19170.sp3	igs19170.clk_30s	igs19177.erp	2016/10/02	61.9874
jmb0277x.16o	csrj2770.16o	brdc2770.16n	igs19171.sp3	igs19171.clk_30s	igs19177.erp	2016/10/03	60.9853
jmb0278g.16o	csrj2780.16o	brdc2780.16n	igs19172.sp3	igs19172.clk_30s	igs19177.erp	2016/10/04	61.5195
jmb0292x.16o	csrj2920.16o	brdc2920.16n	igs19192.sp3	igs19192.clk_30s	igs19197.erp	2016/10/18	60.0937
jmb0293x.16o	csrj2930.16o	brdc2930.16n	igs19193.sp3	igs19193.clk_30s	igs19197.erp	2016/10/19	61.1668
jmb0294x.16o	csrj2940.16o	brdc2940.16n	igs19194.sp3	igs19194.clk_30s	igs19197.erp	2016/10/20	59.4050

jmb0295x.16o	csrj2950.16o	brdc2950.16n	igs19195.sp3	igs19195.clk_30s	igs19197.erp	2016/10/21	60.5176
jmb0296x.16o	csrj2960.16o	brdc2960.16n	igs19196.sp3	igs19196.clk_30s	igs19197.erp	2016/10/22	60.4730
jmb0297e.16o	csrj2970.16o	brdc2970.16n	igs19200.sp3	igs19200.clk_30s	igs19207.erp	2016/10/23	60.2574
jmb0302x.16o	csrj3020.16o	brdc3020.16n	igs19205.sp3	igs19205.clk_30s	igs19207.erp	2016/10/28	59.4327
jmb0303x.16o	csrj3030.16o	brdc3030.16n	igs19206.sp3	igs19206.clk_30s	igs19207.erp	2016/10/29	60.4331
jmb0304x.16o	csrj3040.16o	brdc3040.16n	igs19210.sp3	igs19210.clk_30s	igs19217.erp	2016/10/30	61.0785
jmb0305x.16o	csrj3050.16o	brdc3050.16n	igs19211.sp3	igs19211.clk_30s	igs19217.erp	2016/10/31	60.5251
jmb0306x.16o	csrj3060.16o	brdc3060.16n	igs19212.sp3	igs19212.clk_30s	igs19217.erp	2016/11/01	61.9604
jmb0307x.16o	csrj3070.16o	brdc3070.16n	igs19213.sp3	igs19213.clk_30s	igs19217.erp	2016/11/02	60.4775
jmb0308x.16o	csrj3080.16o	brdc3080.16n	igs19214.sp3	igs19214.clk_30s	igs19217.erp	2016/11/03	61.1421
jmb0309x.16o	csrj3090.16o	brdc3090.16n	igs19215.sp3	igs19215.clk_30s	igs19217.erp	2016/11/04	60.7810
jmb0310x.16o	csrj3100.16o	brdc3100.16n	igs19216.sp3	igs19216.clk_30s	igs19217.erp	2016/11/05	60.0569
jmb0311x.16o	csrj3110.16o	brdc3110.16n	igs19220.sp3	igs19220.clk_30s	igs19227.erp	2016/11/06	60.7573
jmb0312x.16o	csrj3120.16o	brdc3120.16n	igs19221.sp3	igs19221.clk_30s	igs19227.erp	2016/11/07	59.7719
jmb0314x.16o	csrj3140.16o	brdc3140.16n	igs19223.sp3	igs19223.clk_30s	igs19227.erp	2016/11/09	60.2676
jmb0315x.16o	csrj3150.16o	brdc3150.16n	igs19224.sp3	igs19224.clk_30s	igs19227.erp	2016/11/10	60.5728
jmb0316x.16o	csrj3160.16o	brdc3160.16n	igs19225.sp3	igs19225.clk_30s	igs19227.erp	2016/11/11	61.2676
jmb0317x.16o	csrj3170.16o	brdc3170.16n	igs19226.sp3	igs19226.clk_30s	igs19227.erp	2016/11/12	61.2800
jmb0318x.16o	csrj3180.16o	brdc3180.16n	igs19230.sp3	igs19230.clk_30s	igs19237.erp	2016/11/13	60.5763
jmb0319x.16o	csrj3190.16o	brdc3190.16n	igs19231.sp3	igs19231.clk_30s	igs19237.erp	2016/11/14	60.0836
jmb0320x.16o	csrj3200.16o	brdc3200.16n	igs19232.sp3	igs19232.clk_30s	igs19237.erp	2016/11/15	59.8820
jmb0321x.16o	csrj3210.16o	brdc3210.16n	igs19233.sp3	igs19233.clk_30s	igs19237.erp	2016/11/16	60.5608
jmb0322x.16o	csrj3220.16o	brdc3220.16n	igs19234.sp3	igs19234.clk_30s	igs19237.erp	2016/11/17	60.4851
jmb0323c.16o	csrj3230.16o	brdc3230.16n	igs19235.sp3	igs19235.clk_30s	igs19237.erp	2016/11/18	60.2344
jmb0328x.16o	csrj3280.16o	brdc3280.16n	igs19236.sp3	igs19236.clk_30s	igs19237.erp	2016/11/19	61.4857
jmb0329x.16o	csrj3290.16o	brdc3290.16n	igs19244.sp3	igs19244.clk_30s	igs19247.erp	2016/11/24	60.6081
jmb0330x.16o	csrj3300.16o	brdc3300.16n	igs19245.sp3	igs19245.clk_30s	igs19247.erp	2016/11/25	60.6021
jmb0331x.16o	csrj3310.16o	brdc3310.16n	igs19246.sp3	igs19246.clk_30s	igs19247.erp	2016/11/26	60.7479
jmb0332x.16o	csrj3320.16o	brdc3320.16n	igs19250.sp3	igs19250.clk_30s	igs19257.erp	2016/11/27	60.6832
jmb0333x.16o	csrj3330.16o	brdc3330.16n	igs19251.sp3	igs19251.clk_30s	igs19257.erp	2016/11/28	59.5620
jmb0334x.16o	csrj3340.16o	brdc3340.16n	igs19252.sp3	igs19252.clk_30s	igs19257.erp	2016/11/29	60.3329
jmb0335x.16o	csrj3350.16o	brdc3350.16n	igs19253.sp3	igs19253.clk_30s	igs19257.erp	2016/11/30	60.8067
jmb0336x.16o	csrj3360.16o	brdc3360.16n	igs19254.sp3	igs19254.clk_30s	igs19257.erp	2016/12/01	60.5351
jmb0337x.16o	csrj3370.16o	brdc3370.16n	igs19255.sp3	igs19255.clk_30s	igs19257.erp	2016/12/02	60.7213
jmb0338x.16o	csrj3380.16o	brdc3380.16n	igs19256.sp3	igs19256.clk_30s	igs19257.erp	2016/12/03	60.5988
jmb0339x.16o	csrj3390.16o	brdc3390.16n	igs19260.sp3	igs19260.clk_30s	igs19267.erp	2016/12/04	60.6638
jmb0340x.16o	csrj3400.16o	brdc3400.16n	igs19261.sp3	igs19261.clk_30s	igs19267.erp	2016/12/05	60.4078
jmb0341q.16o	csrj3410.16o	brdc3410.16n	igs19262.sp3	igs19262.clk_30s	igs19267.erp	2016/12/06	60.6487
jmb0342x.16o	csrj3420.16o	brdc3420.16n	igs19263.sp3	igs19263.clk_30s	igs19267.erp	2016/12/07	61.0146
jmb0343x.16o	csrj3430.16o	brdc3430.16n	igs19264.sp3	igs19264.clk_30s	igs19267.erp	2016/12/08	60.4996
jmb0344x.16o	csrj3440.16o	brdc3440.16n	igs19265.sp3	igs19265.clk_30s	igs19267.erp	2016/12/09	60.0089
jmb0345x.16o	csrj3450.16o	brdc3450.16n	igs19266.sp3	igs19266.clk_30s	igs19267.erp	2016/12/10	60.6773
jmb0346x.16o	csrj3460.16o	brdc3460.16n	igs19270.sp3	igs19270.clk_30s	igs19277.erp	2016/12/11	60.7410
jmb0347x.16o	csrj3470.16o	brdc3470.16n	igs19271.sp3	igs19271.clk_30s	igs19277.erp	2016/12/12	61.0063
jmb0348x.16o	csrj3480.16o	brdc3480.16n	igs19272.sp3	igs19272.clk_30s	igs19277.erp	2016/12/13	60.2717
jmb0349f.16o	csrj3490.16o	brdc3490.16n	igs19273.sp3	igs19273.clk_30s	igs19277.erp	2016/12/14	60.6011

#### B.4 KLG station

RINEX Observation		RINEX *NAV/CLK, SP3 or SBS/EMS			EOP data file	Date	Height (m)
Rover	Base station	IGS_NAV	IGS_EPH	IGS_CLK_30s			
klg_200x.16o	csrj_2000.16o	brdc_2000.16n	igs19061.sp3	igs19061.clk_30s	igs19067.erp	2016/07/18	173.8872
klg_201x.16o	csrj_2010.16o	brdc_2010.16n	igs19062.sp3	igs19062.clk_30s	igs19067.erp	2016/07/19	173.1497
klg_202x.16o	csrj_2020.16o	brdc_2020.16n	igs19063.sp3	igs19063.clk_30s	igs19067.erp	2016/07/20	173.2319
klg_203x.16o	csrj_2030.16o	brdc_2030.16n	igs19064.sp3	igs19064.clk_30s	igs19067.erp	2016/07/21	173.5011
klg_204x.16o	csrj_2040.16o	brdc_2040.16n	igs19065.sp3	igs19065.clk_30s	igs19067.erp	2016/07/22	172.3836
klg_205x.16o	csrj_2050.16o	brdc_2050.16n	igs19066.sp3	igs19066.clk_30s	igs19067.erp	2016/07/23	172.8363
klg_206x.16o	csrj_2060.16o	brdc_2060.16n	igs19070.sp3	igs19070.clk_30s	igs19067.erp	2016/07/24	172.8920
klg_207x.16o	csrj_2070.16o	brdc_2070.16n	igs19071.sp3	igs19071.clk_30s	igs19077.erp	2016/07/25	173.1729
klg_208x.16o	csrj_2080.16o	brdc_2080.16n	igs19072.sp3	igs19072.clk_30s	igs19077.erp	2016/07/26	172.7757
klg_209x.16o	csrj_2090.16o	brdc_2090.16n	igs19073.sp3	igs19073.clk_30s	igs19077.erp	2016/07/27	172.3736
klg_210x.16o	csrj_2100.16o	brdc_2100.16n	igs19074.sp3	igs19074.clk_30s	igs19077.erp	2016/07/28	172.2474
klg_211x.16o	csrj_2110.16o	brdc_2110.16n	igs19075.sp3	igs19075.clk_30s	igs19077.erp	2016/07/29	173.4170
klg_212x.16o	csrj_2120.16o	brdc_2120.16n	igs19076.sp3	igs19076.clk_30s	igs19077.erp	2016/07/30	172.9934
klg_213x.16o	csrj_2130.16o	brdc_2130.16n	igs19080.sp3	igs19080.clk_30s	igs19087.erp	2016/07/31	171.9626
klg_214x.16o	csrj_2140.16o	brdc_2140.16n	igs19081.sp3	igs19081.clk_30s	igs19087.erp	2016/08/01	172.0686

klg_215x.16o	csrj_2150.16o	brdc_2150.16n	igs19082.sp3	igs19082.clk_30s	igs19087.erp	2016/08/02	171.5994
klg_216x.16o	csrj_2160.16o	brdc_2160.16n	igs19083.sp3	igs19083.clk_30s	igs19087.erp	2016/08/03	173.1440
klg_217x.16o	csrj_2170.16o	brdc_2170.16n	igs19084.sp3	igs19084.clk_30s	igs19087.erp	2016/08/04	173.4012
klg_218x.16o	csrj_2180.16o	brdc_2180.16n	igs19085.sp3	igs19085.clk_30s	igs19087.erp	2016/08/05	173.6932
klg_219x.16o	csrj_2190.16o	brdc_2190.16n	igs19086.sp3	igs19086.clk_30s	igs19087.erp	2016/08/06	172.9848
klg_220x.16o	csrj_2200.16o	brdc_2200.16n	igs19090.sp3	igs19090.clk_30s	igs19097.erp	2016/08/07	172.2202
klg_221x.16o	csrj_2210.16o	brdc_2210.16n	igs19091.sp3	igs19091.clk_30s	igs19097.erp	2016/08/08	173.1249
klg_222x.16o	csrj_2220.16o	brdc_2220.16n	igs19092.sp3	igs19092.clk_30s	igs19097.erp	2016/08/09	172.3219
klg_223x.16o	csrj_2230.16o	brdc_2230.16n	igs19093.sp3	igs19093.clk_30s	igs19097.erp	2016/08/10	173.0474
klg_224x.16o	csrj_2240.16o	brdc_2240.16n	igs19094.sp3	igs19094.clk_30s	igs19097.erp	2016/08/11	173.2086
klg_225x.16o	csrj_2250.16o	brdc_2250.16n	igs19095.sp3	igs19095.clk_30s	igs19097.erp	2016/08/12	173.4667
klg_226x.16o	csrj_2260.16o	brdc_2260.16n	igs19096.sp3	igs19096.clk_30s	igs19097.erp	2016/08/13	173.9106
klg_227x.16o	csrj_2270.16o	brdc_2270.16n	igs19100.sp3	igs19100.clk_30s	igs19107.erp	2016/08/14	173.0012
klg_228x.16o	csrj_2280.16o	brdc_2280.16n	igs19101.sp3	igs19101.clk_30s	igs19107.erp	2016/08/15	173.4427
klg_229x.16o	csrj_2290.16o	brdc_2290.16n	igs19102.sp3	igs19102.clk_30s	igs19107.erp	2016/08/16	173.5602
klg_230x.16o	csrj_2300.16o	brdc_2300.16n	igs19103.sp3	igs19103.clk_30s	igs19107.erp	2016/08/17	172.7280
klg_231x.16o	csrj_2310.16o	brdc_2310.16n	igs19104.sp3	igs19104.clk_30s	igs19107.erp	2016/08/18	174.1341
klg_232x.16o	csrj_2320.16o	brdc_2320.16n	igs19105.sp3	igs19105.clk_30s	igs19107.erp	2016/08/19	172.6779
klg_233x.16o	csrj_2330.16o	brdc_2330.16n	igs19106.sp3	igs19106.clk_30s	igs19107.erp	2016/08/20	172.7982
klg_234x.16o	csrj_2340.16o	brdc_2340.16n	igs19110.sp3	igs19110.clk_30s	igs19117.erp	2016/08/21	172.4885
klg_235x.16o	csrj_2350.16o	brdc_2350.16n	igs19111.sp3	igs19111.clk_30s	igs19117.erp	2016/08/22	171.8042
klg_236x.16o	csrj_2360.16o	brdc_2360.16n	igs19112.sp3	igs19112.clk_30s	igs19117.erp	2016/08/23	171.9231
klg_237x.16o	csrj_2370.16o	brdc_2370.16n	igs19113.sp3	igs19113.clk_30s	igs19127.erp	2016/08/24	173.1248
klg_238x.16o	csrj_2380.16o	brdc_2380.16n	igs19114.sp3	igs19114.clk_30s	igs19127.erp	2016/08/25	172.8634
klg_239x.16o	csrj_2390.16o	brdc_2390.16n	igs19115.sp3	igs19115.clk_30s	igs19127.erp	2016/08/26	172.6259
klg_240x.16o	csrj_2400.16o	brdc_2400.16n	igs19116.sp3	igs19116.clk_30s	igs19127.erp	2016/08/27	173.3987
klg_241x.16o	csrj_2410.16o	brdc_2410.16n	igs19120.sp3	igs19120.clk_30s	igs19127.erp	2016/08/28	172.7011
klg_242x.16o	csrj_2420.16o	brdc_2420.16n	igs19121.sp3	igs19121.clk_30s	igs19127.erp	2016/08/29	173.0199
klg_243x.16o	csrj_2430.16o	brdc_2430.16n	igs19122.sp3	igs19122.clk_30s	igs19127.erp	2016/08/30	173.0450
klg_245x.16o	csrj_2450.16o	brdc_2450.16n	igs19124.sp3	igs19124.clk_30s	igs19127.erp	2016/09/01	173.1757
klg_246x.16o	csrj_2460.16o	brdc_2460.16n	igs19125.sp3	igs19125.clk_30s	igs19127.erp	2016/09/02	172.8760
klg_247x.16o	csrj_2470.16o	brdc_2470.16n	igs19126.sp3	igs19126.clk_30s	igs19127.erp	2016/09/03	172.1229
klg_248x.16o	csrj_2480.16o	brdc_2480.16n	igs19130.sp3	igs19130.clk_30s	igs19137.erp	2016/09/04	173.6871
klg_249x.16o	csrj_2490.16o	brdc_2490.16n	igs19131.sp3	igs19131.clk_30s	igs19137.erp	2016/09/05	171.8491
klg_250x.16o	csrj_2500.16o	brdc_2500.16n	igs19132.sp3	igs19132.clk_30s	igs19137.erp	2016/09/06	173.1352
klg_251x.16o	csrj_2510.16o	brdc_2510.16n	igs19133.sp3	igs19133.clk_30s	igs19137.erp	2016/09/07	173.6923
klg_252x.16o	csrj_2520.16o	brdc_2520.16n	igs19134.sp3	igs19134.clk_30s	igs19137.erp	2016/09/08	172.6559
klg_253x.16o	csrj_2530.16o	brdc_2530.16n	igs19135.sp3	igs19135.clk_30s	igs19137.erp	2016/09/09	173.8346
klg_254x.16o	csrj_2540.16o	brdc_2540.16n	igs19136.sp3	igs19136.clk_30s	igs19137.erp	2016/09/10	171.6176
klg_255x.16o	csrj_2550.16o	brdc_2550.16n	igs19140.sp3	igs19140.clk_30s	igs19147.erp	2016/09/11	171.5552
klg_256x.16o	csrj_2560.16o	brdc_2560.16n	igs19141.sp3	igs19141.clk_30s	igs19147.erp	2016/09/12	173.1577
klg_257x.16o	csrj_2570.16o	brdc_2570.16n	igs19142.sp3	igs19142.clk_30s	igs19147.erp	2016/09/13	172.7728
klg_258x.16o	csrj_2580.16o	brdc_2580.16n	igs19143.sp3	igs19143.clk_30s	igs19147.erp	2016/09/14	174.0319
klg_259x.16o	csrj_2590.16o	brdc_2590.16n	igs19144.sp3	igs19144.clk_30s	igs19147.erp	2016/09/15	174.1542
klg_260x.16o	csrj_2600.16o	brdc_2600.16n	igs19145.sp3	igs19145.clk_30s	igs19147.erp	2016/09/16	172.6844
klg_261h.16o	csrj_2610.16o	brdc_2610.16n	igs19146.sp3	igs19146.clk_30s	igs19147.erp	2016/09/17	172.2270
klg_263x.16o	csrj_2630.16o	brdc_2630.16n	igs19151.sp3	igs19151.clk_30s	igs19157.erp	2016/09/19	172.1899
klg_264x.16o	csrj_2640.16o	brdc_2640.16n	igs19152.sp3	igs19152.clk_30s	igs19157.erp	2016/09/20	174.4336
klg_265x.16o	csrj_2650.16o	brdc_2650.16n	igs19153.sp3	igs19153.clk_30s	igs19157.erp	2016/09/21	173.8765
klg_266x.16o	csrj_2660.16o	brdc_2660.16n	igs19154.sp3	igs19154.clk_30s	igs19157.erp	2016/09/22	172.3942
klg_267x.16o	csrj_2670.16o	brdc_2670.16n	igs19155.sp3	igs19155.clk_30s	igs19157.erp	2016/09/23	173.8455
klg_268o.16o	csrj_2680.16o	brdc_2680.16n	igs19156.sp3	igs19156.clk_30s	igs19157.erp	2016/09/24	172.5825
klg_269x.16o	csrj_2690.16o	brdc_2690.16n	igs19160.sp3	igs19160.clk_30s	igs19167.erp	2016/09/25	172.5852
klg_270x.16o	csrj_2700.16o	brdc_2700.16n	igs19161.sp3	igs19161.clk_30s	igs19167.erp	2016/09/26	173.0588
klg_271x.16o	csrj_2710.16o	brdc_2710.16n	igs19162.sp3	igs19162.clk_30s	igs19167.erp	2016/09/27	173.8635
klg_272x.16o	csrj_2720.16o	brdc_2720.16n	igs19163.sp3	igs19163.clk_30s	igs19167.erp	2016/09/28	172.9633
klg_273x.16o	csrj_2730.16o	brdc_2730.16n	igs19164.sp3	igs19164.clk_30s	igs19167.erp	2016/09/29	171.9368
klg_274x.16o	csrj_2740.16o	brdc_2740.16n	igs19165.sp3	igs19165.clk_30s	igs19167.erp	2016/09/30	171.6688
klg_275x.16o	csrj_2750.16o	brdc_2750.16n	igs19166.sp3	igs19166.clk_30s	igs19167.erp	2016/10/01	173.0625
klg_276x.16o	csrj_2760.16o	brdc_2760.16n	igs19170.sp3	igs19170.clk_30s	igs19177.erp	2016/10/02	174.4292
klg_277x.16o	csrj_2770.16o	brdc_2770.16n	igs19171.sp3	igs19171.clk_30s	igs19177.erp	2016/10/03	173.4697
klg_278g.16o	csrj_2780.16o	brdc_2780.16n	igs19172.sp3	igs19172.clk_30s	igs19177.erp	2016/10/04	173.9769
klg_280x.16o	csrj_2800.16o	brdc_2800.16n	igs19174.sp3	igs19174.clk_30s	igs1917.erp7	2016/10/06	172.5403
klg_281x.16o	csrj_2810.16o	brdc_2810.16n	igs19175.sp3	igs19175.clk_30s	igs1917.erp7	2016/10/07	172.1686
klg_282x.16o	csrj_2820.16o	brdc_2820.16n	igs19176.sp3	igs19176.clk_30s	igs1917.erp7	2016/10/08	172.9912
klg_283x.16o	csrj_2830.16o	brdc_2830.16n	igs19180.sp3	igs19180.clk_30s	igs19187.erp	2016/10/09	172.8071
klg_284x.16o	csrj_2840.16o	brdc_2840.16n	igs19181.sp3	igs19181.clk_30s	igs19187.erp	2016/10/10	172.1934

klg_285x.16o	csrj_2850.16o	brdc_2850.16n	igs19182.sp3	igs19182.clk_30s	igs19187.erp	2016/10/11	171.9827
klg_286x.16o	csrj_2860.16o	brdc_2860.16n	igs19183.sp3	igs19183.clk_30s	igs19187.erp	2016/10/12	172.2251
klg_287x.16o	csrj_2870.16o	brdc_2870.16n	igs19184.sp3	igs19184.clk_30s	igs19187.erp	2016/10/13	173.0904
klg_289x.16o	csrj_2890.16o	brdc_2890.16n	igs19186.sp3	igs19186.clk_30s	igs19187.erp	2016/10/15	171.9467
klg_290x.16o	csrj_2900.16o	brdc_2900.16n	igs19190.sp3	igs19190.clk_30s	igs19197.erp	2016/10/16	172.1520
klg_292x.16o	csrj_2920.16o	brdc_2920.16n	igs19192.sp3	igs19192.clk_30s	igs19197.erp	2016/10/18	172.6127
klg_293x.16o	csrj_2930.16o	brdc_2930.16n	igs19193.sp3	igs19193.clk_30s	igs19197.erp	2016/10/19	173.6414
klg_294x.16o	csrj_2940.16o	brdc_2940.16n	igs19194.sp3	igs19194.clk_30s	igs19197.erp	2016/10/20	171.9522
klg_295x.16o	csrj_2950.16o	brdc_2950.16n	igs19195.sp3	igs19195.clk_30s	igs19197.erp	2016/10/21	173.0189
klg_296x.16o	csrj_2960.16o	brdc_2960.16n	igs19196.sp3	igs19196.clk_30s	igs19197.erp	2016/10/22	172.9764
klg_297x.16o	csrj_2970.16o	brdc_2970.16n	igs19200.sp3	igs19200.clk_30s	igs19207.erp	2016/10/23	172.7690
klg_298x.16o	csrj_2980.16o	brdc_2980.16n	igs19201.sp3	igs19201.clk_30s	igs19207.erp	2016/10/24	174.0845
klg_299x.16o	csrj_2990.16o	brdc_2990.16n	igs19202.sp3	igs19202.clk_30s	igs19207.erp	2016/10/25	174.1769
klg_300x.16o	csrj_3000.16o	brdc_3000.16n	igs19203.sp3	igs19203.clk_30s	igs19207.erp	2016/10/26	172.7643
klg_301x.16o	csrj_3010.16o	brdc_3010.16n	igs19204.sp3	igs19204.clk_30s	igs19207.erp	2016/10/27	173.1166
klg_302x.16o	csrj_3020.16o	brdc_3020.16n	igs19205.sp3	igs19205.clk_30s	igs19207.erp	2016/10/28	171.9773
klg_303x.16o	csrj_3030.16o	brdc_3030.16n	igs19206.sp3	igs19206.clk_30s	igs19207.erp	2016/10/29	172.9258
klg_304x.16o	csrj_3040.16o	brdc_3040.16n	igs19210.sp3	igs19210.clk_30s	igs19217.erp	2016/10/30	173.5597
klg_305x.16o	csrj_3050.16o	brdc_3050.16n	igs19211.sp3	igs19211.clk_30s	igs19217.erp	2016/10/31	173.0193
klg_306x.16o	csrj_3060.16o	brdc_3060.16n	igs19212.sp3	igs19212.clk_30s	igs19217.erp	2016/11/01	173.8762
klg_307x.16o	csrj_3070.16o	brdc_3070.16n	igs19213.sp3	igs19213.clk_30s	igs19217.erp	2016/11/02	172.4577
klg_308s.16o	csrj_3080.16o	brdc_3080.16n	igs19214.sp3	igs19214.clk_30s	igs19217.erp	2016/11/03	173.1520
klg_314x.16o	csrj_3140.16o	brdc_3140.16n	igs19223.sp3	igs19223.clk_30s	igs19227.erp	2016/11/09	172.2562
klg_315x.16o	csrj_3150.16o	brdc_3150.16n	igs19224.sp3	igs19224.clk_30s	igs19227.erp	2016/11/10	172.5490
klg_316x.16o	csrj_3160.16o	brdc_3160.16n	igs19225.sp3	igs19225.clk_30s	igs19227.erp	2016/11/11	173.2160
klg_317x.16o	csrj_3170.16o	brdc_3170.16n	igs19226.sp3	igs19226.clk_30s	igs19227.erp	2016/11/12	173.2354
klg_318o.16o	csrj_3180.16o	brdc_3180.16n	igs19230.sp3	igs19230.clk_30s	igs19237.erp	2016/11/13	172.5749

## B.5 TBN0 station

RINEX Observation		RINEX *NAV/CLK, SP3 or SBS/EMS			EOP data file	Date	Height (m)
Rover	Base station	IGS_NAV	IGS_EPH	IGS_CLK_30s			
tbn0206x.16o	csrj2060.16o	brdc2060.16n	igs19070.sp3	igs19070.clk_30s	igs19067.erp	2016/07/24	60.7786
tbn0208x.16o	csrj2080.16o	brdc2080.16n	igs19072.sp3	igs19072.clk_30s	igs19077.erp	2016/07/26	60.5449
tbn0211x.16o	csrj2110.16o	brdc2110.16n	igs19075.sp3	igs19075.clk_30s	igs19077.erp	2016/07/29	61.1027
tbn0212x.16o	csrj2120.16o	brdc2120.16n	igs19076.sp3	igs19076.clk_30s	igs19077.erp	2016/07/30	60.7121
tbn0213x.16o	csrj2130.16o	brdc2130.16n	igs19080.sp3	igs19080.clk_30s	igs19087.erp	2016/07/31	59.8492
tbn0214x.16o	csrj2140.16o	brdc2140.16n	igs19081.sp3	igs19081.clk_30s	igs19087.erp	2016/08/01	59.7065
tbn0215x.16o	csrj2150.16o	brdc2150.16n	igs19082.sp3	igs19082.clk_30s	igs19087.erp	2016/08/02	59.2373
tbn0216x.16o	csrj2160.16o	brdc2160.16n	igs19083.sp3	igs19083.clk_30s	igs19087.erp	2016/08/03	60.7819
tbn0217x.16o	csrj2170.16o	brdc2170.16n	igs19084.sp3	igs19084.clk_30s	igs19087.erp	2016/08/04	61.0391
tbn0218x.16o	csrj2180.16o	brdc2180.16n	igs19085.sp3	igs19085.clk_30s	igs19087.erp	2016/08/05	61.3311
tbn0219x.16o	csrj2190.16o	brdc2190.16n	igs19086.sp3	igs19086.clk_30s	igs19087.erp	2016/08/06	60.6227
tbn0220x.16o	csrj2200.16o	brdc2200.16n	igs19090.sp3	igs19090.clk_30s	igs19097.erp	2016/08/07	59.8581
tbn0221x.16o	csrj2210.16o	brdc2210.16n	igs19091.sp3	igs19091.clk_30s	igs19097.erp	2016/08/08	60.7628
tbn0222x.16o	csrj2220.16o	brdc2220.16n	igs19092.sp3	igs19092.clk_30s	igs19097.erp	2016/08/09	59.9598
tbn0223x.16o	csrj2230.16o	brdc2230.16n	igs19093.sp3	igs19093.clk_30s	igs19097.erp	2016/08/10	60.6853
tbn0224x.16o	csrj2240.16o	brdc2240.16n	igs19094.sp3	igs19094.clk_30s	igs19097.erp	2016/08/11	60.8465
tbn0225x.16o	csrj2250.16o	brdc2250.16n	igs19095.sp3	igs19095.clk_30s	igs19097.erp	2016/08/12	61.1046
tbn0226x.16o	csrj2260.16o	brdc2260.16n	igs19096.sp3	igs19096.clk_30s	igs19097.erp	2016/08/13	61.5485
tbn0227x.16o	csrj2270.16o	brdc2270.16n	igs19100.sp3	igs19100.clk_30s	igs19107.erp	2016/08/14	60.6391
tbn0228x.16o	csrj2280.16o	brdc2280.16n	igs19101.sp3	igs19101.clk_30s	igs19107.erp	2016/08/15	61.0806
tbn0229x.16o	csrj2290.16o	brdc2290.16n	igs19102.sp3	igs19102.clk_30s	igs19107.erp	2016/08/16	61.1993
tbn0230x.16o	csrj2300.16o	brdc2300.16n	igs19103.sp3	igs19103.clk_30s	igs19107.erp	2016/08/17	60.3659
tbn0231x.16o	csrj2310.16o	brdc2310.16n	igs19104.sp3	igs19104.clk_30s	igs19107.erp	2016/08/18	61.7720
tbn0232x.16o	csrj2320.16o	brdc2320.16n	igs19105.sp3	igs19105.clk_30s	igs19107.erp	2016/08/19	60.3158
tbn0233x.16o	csrj2330.16o	brdc2330.16n	igs19106.sp3	igs19106.clk_30s	igs19107.erp	2016/08/20	60.4361
tbn0234x.16o	csrj2340.16o	brdc2340.16n	igs19110.sp3	igs19110.clk_30s	igs19117.erp	2016/08/21	60.1264
tbn0235x.16o	csrj2350.16o	brdc2350.16n	igs19111.sp3	igs19111.clk_30s	igs19117.erp	2016/08/22	59.4421
tbn0236x.16o	csrj2360.16o	brdc2360.16n	igs19112.sp3	igs19112.clk_30s	igs19117.erp	2016/08/23	59.5979
tbn0237x.16o	csrj2370.16o	brdc2370.16n	igs19113.sp3	igs19113.clk_30s	igs19127.erp	2016/08/24	60.8578
tbn0238x.16o	csrj2380.16o	brdc2380.16n	igs19114.sp3	igs19114.clk_30s	igs19127.erp	2016/08/25	60.5839
tbn0239x.16o	csrj2390.16o	brdc2390.16n	igs19115.sp3	igs19115.clk_30s	igs19127.erp	2016/08/26	60.3331
tbn0240x.16o	csrj2400.16o	brdc2400.16n	igs19116.sp3	igs19116.clk_30s	igs19127.erp	2016/08/27	61.1401
tbn0241x.16o	csrj2410.16o	brdc2410.16n	igs19120.sp3	igs19120.clk_30s	igs19127.erp	2016/08/28	60.4152
tbn0242x.16o	csrj2420.16o	brdc2420.16n	igs19121.sp3	igs19121.clk_30s	igs19127.erp	2016/08/29	60.7464



tbn0243x.16o	csrj2430.16o	brdc2430.16n	igs19122.sp3	igs19122.clk_30s	igs19127.erp	2016/08/30	60.7732
tbn0244x.16o	csrj2440.16o	brdc2440.16n	igs19123.sp3	igs19123.clk_30s	igs19127.erp	2016/08/31	61.2989
tbn0245x.16o	csrj2450.16o	brdc2450.16n	igs19124.sp3	igs19124.clk_30s	igs19127.erp	2016/09/01	60.8362
tbn0246x.16o	csrj2460.16o	brdc2460.16n	igs19125.sp3	igs19125.clk_30s	igs19127.erp	2016/09/02	60.4378
tbn0247x.16o	csrj2470.16o	brdc2470.16n	igs19126.sp3	igs19126.clk_30s	igs19127.erp	2016/09/03	59.7834
tbn0248x.16o	csrj2480.16o	brdc2480.16n	igs19130.sp3	igs19130.clk_30s	igs19137.erp	2016/09/04	61.3476
tbn0249x.16o	csrj2490.16o	brdc2490.16n	igs19131.sp3	igs19131.clk_30s	igs19137.erp	2016/09/05	59.5096
tbn0250x.16o	csrj2500.16o	brdc2500.16n	igs19132.sp3	igs19132.clk_30s	igs19137.erp	2016/09/06	60.7957
tbn0251x.16o	csrj2510.16o	brdc2510.16n	igs19133.sp3	igs19133.clk_30s	igs19137.erp	2016/09/07	61.3528
tbn0252x.16o	csrj2520.16o	brdc2520.16n	igs19134.sp3	igs19134.clk_30s	igs19137.erp	2016/09/08	60.4528
tbn0253x.16o	csrj2530.16o	brdc2530.16n	igs19135.sp3	igs19135.clk_30s	igs19137.erp	2016/09/09	61.5400
tbn0254x.16o	csrj2540.16o	brdc2540.16n	igs19136.sp3	igs19136.clk_30s	igs19137.erp	2016/09/10	59.2781
tbn0255x.16o	csrj2550.16o	brdc2550.16n	igs19140.sp3	igs19140.clk_30s	igs19147.erp	2016/09/11	59.2157
tbn0256x.16o	csrj2560.16o	brdc2560.16n	igs19141.sp3	igs19141.clk_30s	igs19147.erp	2016/09/12	60.8182
tbn0257x.16o	csrj2570.16o	brdc2570.16n	igs19142.sp3	igs19142.clk_30s	igs19147.erp	2016/09/13	60.4333
tbn0258x.16o	csrj2580.16o	brdc2580.16n	igs19143.sp3	igs19143.clk_30s	igs19147.erp	2016/09/14	61.8307
tbn0259x.16o	csrj2590.16o	brdc2590.16n	igs19144.sp3	igs19144.clk_30s	igs19147.erp	2016/09/15	61.9576
tbn0260x.16o	csrj2600.16o	brdc2600.16n	igs19145.sp3	igs19145.clk_30s	igs19147.erp	2016/09/16	60.3449
tbn0261h.16o	csrj2610.16o	brdc2610.16n	igs19146.sp3	igs19146.clk_30s	igs19147.erp	2016/09/17	59.9350
tbn0263x.16o	csrj2630.16o	brdc2630.16n	igs19151.sp3	igs19151.clk_30s	igs19157.erp	2016/09/19	59.9001
tbn0264x.16o	csrj2640.16o	brdc2640.16n	igs19152.sp3	igs19152.clk_30s	igs19157.erp	2016/09/20	62.0941
tbn0265x.16o	csrj2650.16o	brdc2650.16n	igs19153.sp3	igs19153.clk_30s	igs19157.erp	2016/09/21	61.5370
tbn0266x.16o	csrj2660.16o	brdc2660.16n	igs19154.sp3	igs19154.clk_30s	igs19157.erp	2016/09/22	60.0547
tbn0267x.16o	csrj2670.16o	brdc2670.16n	igs19155.sp3	igs19155.clk_30s	igs19157.erp	2016/09/23	61.5060
tbn0268x.16o	csrj2680.16o	brdc2680.16n	igs19156.sp3	igs19156.clk_30s	igs19157.erp	2016/09/24	60.1037
tbn0269x.16o	csrj2690.16o	brdc2690.16n	igs19160.sp3	igs19160.clk_30s	igs19167.erp	2016/09/25	60.1608
tbn0270x.16o	csrj2700.16o	brdc2700.16n	igs19161.sp3	igs19161.clk_30s	igs19167.erp	2016/09/26	60.7193
tbn0271x.16o	csrj2710.16o	brdc2710.16n	igs19162.sp3	igs19162.clk_30s	igs19167.erp	2016/09/27	61.6553
tbn0272x.16o	csrj2720.16o	brdc2720.16n	igs19163.sp3	igs19163.clk_30s	igs19167.erp	2016/09/28	60.7151
tbn0273x.16o	csrj2730.16o	brdc2730.16n	igs19164.sp3	igs19164.clk_30s	igs19167.erp	2016/09/29	59.6447
tbn0274x.16o	csrj2740.16o	brdc2740.16n	igs19165.sp3	igs19165.clk_30s	igs19167.erp	2016/09/30	59.3608
tbn0275x.16o	csrj2750.16o	brdc2750.16n	igs19166.sp3	igs19166.clk_30s	igs19167.erp	2016/10/01	60.7907
tbn0276x.16o	csrj2760.16o	brdc2760.16n	igs19170.sp3	igs19170.clk_30s	igs19177.erp7	2016/10/02	62.2514
tbn0277x.16o	csrj2770.16o	brdc2770.16n	igs19171.sp3	igs19171.clk_30s	igs19177.erp8	2016/10/03	61.2493
tbn0278g.16o	csrj2780.16o	brdc2780.16n	igs19172.sp3	igs19172.clk_30s	igs19177.erp7	2016/10/04	61.7779
tbn0280x.16o	csrj2800.16o	brdc2800.16n	igs19174.sp3	igs19174.clk_30s	igs19177.erp7	2016/10/06	60.2806
tbn0281x.16o	csrj2810.16o	brdc2810.16n	igs19175.sp3	igs19175.clk_30s	igs19177.erp7	2016/10/07	59.9734
tbn0282x.16o	csrj2820.16o	brdc2820.16n	igs19176.sp3	igs19176.clk_30s	igs19177.erp7	2016/10/08	60.7179
tbn0283x.16o	csrj2830.16o	brdc2830.16n	igs19180.sp3	igs19180.clk_30s	igs19187.erp	2016/10/09	60.5539
tbn0284x.16o	csrj2840.16o	brdc2840.16n	igs19181.sp3	igs19181.clk_30s	igs19187.erp	2016/10/10	59.9571
tbn0285x.16o	csrj2850.16o	brdc2850.16n	igs19182.sp3	igs19182.clk_30s	igs19187.erp	2016/10/11	59.6710
tbn0286x.16o	csrj2860.16o	brdc2860.16n	igs19183.sp3	igs19183.clk_30s	igs19187.erp	2016/10/12	59.9262
tbn0289x.16o	csrj2890.16o	brdc2890.16n	igs19186.sp3	igs19186.clk_30s	igs19187.erp	2016/10/15	59.6212
tbn0290j.16o	csrj2900.16o	brdc2900.16n	igs19190.sp3	igs19190.clk_30s	igs19197.erp	2016/10/16	59.8228
tbn0291x.16o	csrj2910.16o	brdc2910.16n	igs19191.sp3	igs19191.clk_30s	igs19197.erp	2016/10/17	59.2545
tbn0292x.16o	csrj2920.16o	brdc2920.16n	igs19192.sp3	igs19192.clk_30s	igs19197.erp	2016/10/18	60.3415
tbn0293x.16o	csrj2930.16o	brdc2930.16n	igs19193.sp3	igs19193.clk_30s	igs19197.erp	2016/10/19	61.3816
tbn0294x.16o	csrj2940.16o	brdc2940.16n	igs19194.sp3	igs19194.clk_30s	igs19197.erp	2016/10/20	59.6215
tbn0295x.16o	csrj2950.16o	brdc2950.16n	igs19195.sp3	igs19195.clk_30s	igs19197.erp	2016/10/21	60.7362
tbn0296x.16o	csrj2960.16o	brdc2960.16n	igs19196.sp3	igs19196.clk_30s	igs19197.erp	2016/10/22	60.7310
tbn0297x.16o	csrj2970.16o	brdc2970.16n	igs19200.sp3	igs19200.clk_30s	igs19207.erp	2016/10/23	60.5007
tbn0298x.16o	csrj2980.16o	brdc2980.16n	igs19201.sp3	igs19201.clk_30s	igs19207.erp	2016/10/24	61.9003
tbn0299x.16o	csrj2990.16o	brdc2990.16n	igs19202.sp3	igs19202.clk_30s	igs19207.erp	2016/10/25	61.9762
tbn0300x.16o	csrj3000.16o	brdc3000.16n	igs19203.sp3	igs19203.clk_30s	igs19207.erp	2016/10/26	60.5777
tbn0301x.16o	csrj3010.16o	brdc3010.16n	igs19204.sp3	igs19204.clk_30s	igs19207.erp	2016/10/27	60.9873
tbn0302x.16o	csrj3020.16o	brdc3020.16n	igs19205.sp3	igs19205.clk_30s	igs19207.erp	2016/10/28	59.8188
tbn0303x.16o	csrj3030.16o	brdc3030.16n	igs19206.sp3	igs19206.clk_30s	igs19207.erp	2016/10/29	60.5484
tbn0304x.16o	csrj3040.16o	brdc3040.16n	igs19210.sp3	igs19210.clk_30s	igs19217.erp	2016/10/30	61.2428
tbn0305x.16o	csrj3050.16o	brdc3050.16n	igs19211.sp3	igs19211.clk_30s	igs19217.erp	2016/10/31	60.7824
tbn0306x.16o	csrj3060.16o	brdc3060.16n	igs19212.sp3	igs19212.clk_30s	igs19217.erp	2016/11/01	61.9764
tbn0307x.16o	csrj3070.16o	brdc3070.16n	igs19213.sp3	igs19213.clk_30s	igs19217.erp	2016/11/02	60.4697
tbn0308x.16o	csrj3080.16o	brdc3080.16n	igs19214.sp3	igs19214.clk_30s	igs19217.erp	2016/11/03	61.1948
tbn0309x.16o	csrj3090.16o	brdc3090.16n	igs19215.sp3	igs19215.clk_30s	igs19217.erp	2016/11/04	60.8368
tbn0310x.16o	csrj3100.16o	brdc3100.16n	igs19216.sp3	igs19216.clk_30s	igs19217.erp	2016/11/05	60.1632
tbn0311x.16o	csrj3110.16o	brdc3110.16n	igs19220.sp3	igs19220.clk_30s	igs19227.erp	2016/11/06	60.7797
tbn0312x.16o	csrj3120.16o	brdc3120.16n	igs19221.sp3	igs19221.clk_30s	igs19227.erp	2016/11/07	59.7626
tbn0313l.16o	csrj3130.16o	brdc3130.16n	igs19222.sp3	igs19222.clk_30s	igs19227.erp	2016/11/08	60.5776

tbn0314x.16o	csrj3140.16o	brdc3140.16n	igs19223.sp3	igs19223.clk_30s	igs19227.erp	2016/11/09	60.3263
tbn0315x.16o	csrj3150.16o	brdc3150.16n	igs19224.sp3	igs19224.clk_30s	igs19227.erp	2016/11/10	60.6118
tbn0316x.16o	csrj3160.16o	brdc3160.16n	igs19225.sp3	igs19225.clk_30s	igs19227.erp	2016/11/11	61.3066
tbn0317x.16o	csrj3170.16o	brdc3170.16n	igs19226.sp3	igs19226.clk_30s	igs19227.erp	2016/11/12	61.3190
tbn0318x.16o	csrj3180.16o	brdc3180.16n	igs19230.sp3	igs19230.clk_30s	igs19237.erp	2016/11/13	60.6153
tbn0319x.16o	csrj3190.16o	brdc3190.16n	igs19231.sp3	igs19231.clk_30s	igs19237.erp	2016/11/14	60.1226
tbn0320x.16o	csrj3200.16o	brdc3200.16n	igs19232.sp3	igs19232.clk_30s	igs19237.erp	2016/11/15	59.9210
tbn0321x.16o	csrj3210.16o	brdc3210.16n	igs19233.sp3	igs19233.clk_30s	igs19237.erp	2016/11/16	60.5998
tbn0322x.16o	csrj3220.16o	brdc3220.16n	igs19234.sp3	igs19234.clk_30s	igs19237.erp	2016/11/17	60.5241
tbn0323x.16o	csrj3230.16o	brdc3230.16n	igs19235.sp3	igs19235.clk_30s	igs19237.erp	2016/11/18	60.3172
tbn0324x.16o	csrj3240.16o	brdc3240.16n	igs19236.sp3	igs19236.clk_30s	igs19237.erp	2016/11/19	60.3812
tbn0325x.16o	csrj3250.16o	brdc3250.16n	igs19240.sp3	igs19240.clk_30s	igs19247.erp	2016/11/20	59.8671
tbn0326x.16o	csrj3260.16o	brdc3260.16n	igs19241.sp3	igs19241.clk_30s	igs19247.erp	2016/11/21	60.6304
tbn0327x.16o	csrj3270.16o	brdc3270.16n	igs19242.sp3	igs19242.clk_30s	igs19247.erp	2016/11/22	61.0752
tbn0328x.16o	csrj3280.16o	brdc3280.16n	igs19243.sp3	igs19243.clk_30s	igs19247.erp	2016/11/23	61.5247
tbn0329x.16o	csrj3290.16o	brdc3290.16n	igs19244.sp3	igs19244.clk_30s	igs19247.erp	2016/11/24	60.6471
tbn0330x.16o	csrj3300.16o	brdc3300.16n	igs19245.sp3	igs19245.clk_30s	igs19247.erp	2016/11/25	60.6411
tbn0331x.16o	csrj3310.16o	brdc3310.16n	igs19246.sp3	igs19246.clk_30s	igs19247.erp	2016/11/26	60.7869
tbn0332x.16o	csrj3320.16o	brdc3320.16n	igs19250.sp3	igs19250.clk_30s	igs19257.erp	2016/11/27	60.6070
tbn0333x.16o	csrj3330.16o	brdc3330.16n	igs19251.sp3	igs19251.clk_30s	igs19257.erp	2016/11/28	59.5337
tbn0334x.16o	csrj3340.16o	brdc3340.16n	igs19252.sp3	igs19252.clk_30s	igs19257.erp	2016/11/29	60.2759
tbn0335x.16o	csrj3350.16o	brdc3350.16n	igs19253.sp3	igs19253.clk_30s	igs19257.erp	2016/11/30	60.8457
tbn0336x.16o	csrj3360.16o	brdc3360.16n	igs19254.sp3	igs19254.clk_30s	igs19257.erp	2016/12/01	60.5424
tbn0337d.16o	csrj3370.16o	brdc3370.16n	igs19255.sp3	igs19255.clk_30s	igs19257.erp	2016/12/02	60.6600

## B.6 CSRJ station

RINEX Observation		RINEX *NAV/CLK, SP3 or SBS/EMS			EOP data file	Date	Height (m)
Rover	Base station	IGS_NAV	IGS_EPH	IGS_CLK_30s			
csrj2060.16o	tbn0206x.16o	brdc2060.16n	igs19070.sp3	igs19070.clk_30s	igs19067.erp	2016/07/24	60.5072
csrj2080.16o	tbn0208x.16o	brdc2080.16n	igs19072.sp3	igs19072.clk_30s	igs19077.erp	2016/07/26	60.2735
csrj2110.16o	tbn0211x.16o	brdc2110.16n	igs19075.sp3	igs19075.clk_30s	igs19077.erp	2016/07/29	60.8313
csrj2120.16o	tbn0212x.16o	brdc2120.16n	igs19076.sp3	igs19076.clk_30s	igs19077.erp	2016/07/30	60.4407
csrj2130.16o	tbn0213x.16o	brdc2130.16n	igs19080.sp3	igs19080.clk_30s	igs19087.erp	2016/07/31	59.5778
csrj2140.16o	tbn0214x.16o	brdc2140.16n	igs19081.sp3	igs19081.clk_30s	igs19087.erp	2016/08/01	59.4351
csrj2150.16o	tbn0215x.16o	brdc2150.16n	igs19082.sp3	igs19082.clk_30s	igs19087.erp	2016/08/02	58.9659
csrj2160.16o	tbn0216x.16o	brdc2160.16n	igs19083.sp3	igs19083.clk_30s	igs19087.erp	2016/08/03	60.5105
csrj2170.16o	tbn0217x.16o	brdc2170.16n	igs19084.sp3	igs19084.clk_30s	igs19087.erp	2016/08/04	60.7677
csrj2180.16o	tbn0218x.16o	brdc2180.16n	igs19085.sp3	igs19085.clk_30s	igs19087.erp	2016/08/05	61.0597
csrj2190.16o	tbn0219x.16o	brdc2190.16n	igs19086.sp3	igs19086.clk_30s	igs19087.erp	2016/08/06	60.3513
csrj2200.16o	tbn0220x.16o	brdc2200.16n	igs19090.sp3	igs19090.clk_30s	igs19097.erp	2016/08/07	59.5867
csrj2210.16o	tbn0221x.16o	brdc2210.16n	igs19091.sp3	igs19091.clk_30s	igs19097.erp	2016/08/08	60.4914
csrj2220.16o	tbn0222x.16o	brdc2220.16n	igs19092.sp3	igs19092.clk_30s	igs19097.erp	2016/08/09	59.6884
csrj2230.16o	tbn0223x.16o	brdc2230.16n	igs19093.sp3	igs19093.clk_30s	igs19097.erp	2016/08/10	60.4139
csrj2240.16o	tbn0224x.16o	brdc2240.16n	igs19094.sp3	igs19094.clk_30s	igs19097.erp	2016/08/11	60.5751
csrj2250.16o	tbn0225x.16o	brdc2250.16n	igs19095.sp3	igs19095.clk_30s	igs19097.erp	2016/08/12	60.8332
csrj2260.16o	tbn0226x.16o	brdc2260.16n	igs19096.sp3	igs19096.clk_30s	igs19097.erp	2016/08/13	61.2771
csrj2270.16o	tbn0227x.16o	brdc2270.16n	igs19100.sp3	igs19100.clk_30s	igs19107.erp	2016/08/14	60.3677
csrj2280.16o	tbn0228x.16o	brdc2280.16n	igs19101.sp3	igs19101.clk_30s	igs19107.erp	2016/08/15	60.8092
csrj2290.16o	tbn0229x.16o	brdc2290.16n	igs19102.sp3	igs19102.clk_30s	igs19107.erp	2016/08/16	60.9279
csrj2300.16o	tbn0230x.16o	brdc2300.16n	igs19103.sp3	igs19103.clk_30s	igs19107.erp	2016/08/17	60.0945
csrj2310.16o	tbn0231x.16o	brdc2310.16n	igs19104.sp3	igs19104.clk_30s	igs19107.erp	2016/08/18	61.5006
csrj2320.16o	tbn0232x.16o	brdc2320.16n	igs19105.sp3	igs19105.clk_30s	igs19107.erp	2016/08/19	60.0444
csrj2330.16o	tbn0233x.16o	brdc2330.16n	igs19106.sp3	igs19106.clk_30s	igs19107.erp	2016/08/20	60.1647
csrj2340.16o	tbn0234x.16o	brdc2340.16n	igs19110.sp3	igs19110.clk_30s	igs19117.erp	2016/08/21	59.8550
csrj2350.16o	tbn0235x.16o	brdc2350.16n	igs19111.sp3	igs19111.clk_30s	igs19117.erp	2016/08/22	59.1707
csrj2360.16o	tbn0236x.16o	brdc2360.16n	igs19112.sp3	igs19112.clk_30s	igs19117.erp	2016/08/23	59.3265
csrj2370.16o	tbn0237x.16o	brdc2370.16n	igs19113.sp3	igs19113.clk_30s	igs19127.erp	2016/08/24	60.5864
csrj2380.16o	tbn0238x.16o	brdc2380.16n	igs19114.sp3	igs19114.clk_30s	igs19127.erp	2016/08/25	60.3125
csrj2390.16o	tbn0239x.16o	brdc2390.16n	igs19115.sp3	igs19115.clk_30s	igs19127.erp	2016/08/26	60.0617
csrj2400.16o	tbn0240x.16o	brdc2400.16n	igs19116.sp3	igs19116.clk_30s	igs19127.erp	2016/08/27	60.8687
csrj2410.16o	tbn0241x.16o	brdc2410.16n	igs19120.sp3	igs19120.clk_30s	igs19127.erp	2016/08/28	60.1438
csrj2420.16o	tbn0242x.16o	brdc2420.16n	igs19121.sp3	igs19121.clk_30s	igs19127.erp	2016/08/29	60.4750
csrj2430.16o	tbn0243x.16o	brdc2430.16n	igs19122.sp3	igs19122.clk_30s	igs19127.erp	2016/08/30	60.5018
csrj2440.16o	tbn0244x.16o	brdc2440.16n	igs19123.sp3	igs19123.clk_30s	igs19127.erp	2016/08/31	61.0275
csrj2450.16o	tbn0245x.16o	brdc2450.16n	igs19124.sp3	igs19124.clk_30s	igs19127.erp	2016/09/01	60.5648

csrj2460.16o	tbn0246h.16o	brdc2460.16n	igs19125.sp3	igs19125.clk_30s	igs19127.erp	2016/09/02	60.1664
csrj2470.16o	tbn0247x.16o	brdc2470.16n	igs19126.sp3	igs19126.clk_30s	igs19127.erp	2016/09/03	59.5120
csrj2480.16o	tbn0248x.16o	brdc2480.16n	igs19130.sp3	igs19130.clk_30s	igs19137.erp	2016/09/04	61.0762
csrj2490.16o	tbn0249x.16o	brdc2490.16n	igs19131.sp3	igs19131.clk_30s	igs19137.erp	2016/09/05	59.2382
csrj2500.16o	tbn0250x.16o	brdc2500.16n	igs19132.sp3	igs19132.clk_30s	igs19137.erp	2016/09/06	60.5243
csrj2510.16o	tbn0251x.16o	brdc2510.16n	igs19133.sp3	igs19133.clk_30s	igs19137.erp	2016/09/07	61.0814
csrj2520.16o	tbn0252x.16o	brdc2520.16n	igs19134.sp3	igs19134.clk_30s	igs19137.erp	2016/09/08	60.1814
csrj2530.16o	tbn0253x.16o	brdc2530.16n	igs19135.sp3	igs19135.clk_30s	igs19137.erp	2016/09/09	61.2686
csrj2540.16o	tbn0254x.16o	brdc2540.16n	igs19136.sp3	igs19136.clk_30s	igs19137.erp	2016/09/10	59.0067
csrj2550.16o	tbn0255x.16o	brdc2550.16n	igs19140.sp3	igs19140.clk_30s	igs19147.erp	2016/09/11	58.9443
csrj2560.16o	tbn0256x.16o	brdc2560.16n	igs19141.sp3	igs19141.clk_30s	igs19147.erp	2016/09/12	60.5468
csrj2570.16o	tbn0257x.16o	brdc2570.16n	igs19142.sp3	igs19142.clk_30s	igs19147.erp	2016/09/13	60.1619
csrj2580.16o	tbn0258x.16o	brdc2580.16n	igs19143.sp3	igs19143.clk_30s	igs19147.erp	2016/09/14	61.5593
csrj2590.16o	tbn0259x.16o	brdc2590.16n	igs19144.sp3	igs19144.clk_30s	igs19147.erp	2016/09/15	61.6862
csrj2600.16o	tbn0260x.16o	brdc2600.16n	igs19145.sp3	igs19145.clk_30s	igs19147.erp	2016/09/16	60.0735
csrj2610.16o	tbn0261h.16o	brdc2610.16n	igs19146.sp3	igs19146.clk_30s	igs19147.erp	2016/09/17	59.6636
csrj2630.16o	tbn0263x.16o	brdc2630.16n	igs19151.sp3	igs19151.clk_30s	igs19157.erp	2016/09/19	59.6287
csrj2640.16o	tbn0264x.16o	brdc2640.16n	igs19152.sp3	igs19152.clk_30s	igs19157.erp	2016/09/20	61.8227
csrj2650.16o	tbn0265x.16o	brdc2650.16n	igs19153.sp3	igs19153.clk_30s	igs19157.erp	2016/09/21	61.2656
csrj2660.16o	tbn0266x.16o	brdc2660.16n	igs19154.sp3	igs19154.clk_30s	igs19157.erp	2016/09/22	59.7833
csrj2670.16o	tbn0267x.16o	brdc2670.16n	igs19155.sp3	igs19155.clk_30s	igs19157.erp	2016/09/23	61.2346
csrj2680.16o	tbn0268x.16o	brdc2680.16n	igs19156.sp3	igs19156.clk_30s	igs19157.erp	2016/09/24	59.8323
csrj2690.16o	tbn0269x.16o	brdc2690.16n	igs19160.sp3	igs19160.clk_30s	igs19167.erp	2016/09/25	59.8894
csrj2700.16o	tbn0270x.16o	brdc2700.16n	igs19161.sp3	igs19161.clk_30s	igs19167.erp	2016/09/26	60.4479
csrj2710.16o	tbn0271x.16o	brdc2710.16n	igs19162.sp3	igs19162.clk_30s	igs19167.erp	2016/09/27	61.3839
csrj2720.16o	tbn0272x.16o	brdc2720.16n	igs19163.sp3	igs19163.clk_30s	igs19167.erp	2016/09/28	60.4437
csrj2730.16o	tbn0273x.16o	brdc2730.16n	igs19164.sp3	igs19164.clk_30s	igs19167.erp	2016/09/29	59.3733
csrj2740.16o	tbn0274x.16o	brdc2740.16n	igs19165.sp3	igs19165.clk_30s	igs19167.erp	2016/09/30	59.0894
csrj2750.16o	tbn0275x.16o	brdc2750.16n	igs19166.sp3	igs19166.clk_30s	igs19167.erp	2016/10/01	60.5193
csrj2760.16o	tbn0276x.16o	brdc2760.16n	igs19170.sp3	igs19170.clk_30s	igs19177.erp7	2016/10/02	61.9800
csrj2770.16o	tbn0277x.16o	brdc2770.16n	igs19171.sp3	igs19171.clk_30s	igs19177.erp8	2016/10/03	60.9779
csrj2780.16o	tbn0278g.16o	brdc2780.16n	igs19172.sp3	igs19172.clk_30s	igs19177.erp7	2016/10/04	61.5065
csrj2800.16o	tbn0280x.16o	brdc2800.16n	igs19174.sp3	igs19174.clk_30s	igs19177.erp7	2016/10/06	60.0092
csrj2810.16o	tbn0281x.16o	brdc2810.16n	igs19175.sp3	igs19175.clk_30s	igs19177.erp7	2016/10/07	59.7020
csrj2820.16o	tbn0282x.16o	brdc2820.16n	igs19176.sp3	igs19176.clk_30s	igs19177.erp7	2016/10/08	60.4465
csrj2830.16o	tbn0283x.16o	brdc2830.16n	igs19180.sp3	igs19180.clk_30s	igs19187.erp	2016/10/09	60.2825
csrj2840.16o	tbn0284x.16o	brdc2840.16n	igs19181.sp3	igs19181.clk_30s	igs19187.erp	2016/10/10	59.6857
csrj2850.16o	tbn0285x.16o	brdc2850.16n	igs19182.sp3	igs19182.clk_30s	igs19187.erp	2016/10/11	59.3996
csrj2860.16o	tbn0286x.16o	brdc2860.16n	igs19183.sp3	igs19183.clk_30s	igs19187.erp	2016/10/12	59.6548
csrj2890.16o	tbn0289x.16o	brdc2890.16n	igs19186.sp3	igs19186.clk_30s	igs19187.erp	2016/10/15	59.3498
csrj2900.16o	tbn0290j.16o	brdc2900.16n	igs19190.sp3	igs19190.clk_30s	igs19197.erp	2016/10/16	59.5514
csrj2910.16o	tbn0291x.16o	brdc2910.16n	igs19191.sp3	igs19191.clk_30s	igs19197.erp	2016/10/17	58.9831
csrj2920.16o	tbn0292x.16o	brdc2920.16n	igs19192.sp3	igs19192.clk_30s	igs19197.erp	2016/10/18	60.0701
csrj2930.16o	tbn0293x.16o	brdc2930.16n	igs19193.sp3	igs19193.clk_30s	igs19197.erp	2016/10/19	61.1102
csrj2940.16o	tbn0294x.16o	brdc2940.16n	igs19194.sp3	igs19194.clk_30s	igs19197.erp	2016/10/20	59.3501
csrj2950.16o	tbn0295x.16o	brdc2950.16n	igs19195.sp3	igs19195.clk_30s	igs19197.erp	2016/10/21	60.4648
csrj2960.16o	tbn0296x.16o	brdc2960.16n	igs19196.sp3	igs19196.clk_30s	igs19197.erp	2016/10/22	60.4596
csrj2970.16o	tbn0297x.16o	brdc2970.16n	igs19200.sp3	igs19200.clk_30s	igs19207.erp	2016/10/23	60.2293
csrj2980.16o	tbn0298x.16o	brdc2980.16n	igs19201.sp3	igs19201.clk_30s	igs19207.erp	2016/10/24	61.6289
csrj2990.16o	tbn0299x.16o	brdc2990.16n	igs19202.sp3	igs19202.clk_30s	igs19207.erp	2016/10/25	61.7048
csrj3000.16o	tbn0300x.16o	brdc3000.16n	igs19203.sp3	igs19203.clk_30s	igs19207.erp	2016/10/26	60.3063
csrj3010.16o	tbn0301x.16o	brdc3010.16n	igs19204.sp3	igs19204.clk_30s	igs19207.erp	2016/10/27	60.7159
csrj3020.16o	tbn0302x.16o	brdc3020.16n	igs19205.sp3	igs19205.clk_30s	igs19207.erp	2016/10/28	59.5474
csrj3030.16o	tbn0303x.16o	brdc3030.16n	igs19206.sp3	igs19206.clk_30s	igs19207.erp	2016/10/29	60.2770
csrj3040.16o	tbn0304x.16o	brdc3040.16n	igs19210.sp3	igs19210.clk_30s	igs19217.erp	2016/10/30	60.9714
csrj3050.16o	tbn0305x.16o	brdc3050.16n	igs19211.sp3	igs19211.clk_30s	igs19217.erp	2016/10/31	60.5110
csrj3060.16o	tbn0306x.16o	brdc3060.16n	igs19212.sp3	igs19212.clk_30s	igs19217.erp	2016/11/01	61.7050
csrj3070.16o	tbn0307x.16o	brdc3070.16n	igs19213.sp3	igs19213.clk_30s	igs19217.erp	2016/11/02	60.1983
csrj3080.16o	tbn0308x.16o	brdc3080.16n	igs19214.sp3	igs19214.clk_30s	igs19217.erp	2016/11/03	60.9234
csrj3090.16o	tbn0309x.16o	brdc3090.16n	igs19215.sp3	igs19215.clk_30s	igs19217.erp	2016/11/04	60.5654
csrj3100.16o	tbn0310x.16o	brdc3100.16n	igs19216.sp3	igs19216.clk_30s	igs19217.erp	2016/11/05	59.8918
csrj3110.16o	tbn0311x.16o	brdc3110.16n	igs19220.sp3	igs19220.clk_30s	igs19227.erp	2016/11/06	60.5083
csrj3120.16o	tbn0312x.16o	brdc3120.16n	igs19221.sp3	igs19221.clk_30s	igs19227.erp	2016/11/07	59.4912
csrj3130.16o	tbn0313l.16o	brdc3130.16n	igs19222.sp3	igs19222.clk_30s	igs19227.erp	2016/11/08	60.3062
csrj3140.16o	tbn0314x.16o	brdc3140.16n	igs19223.sp3	igs19223.clk_30s	igs19227.erp	2016/11/09	60.0549
csrj3150.16o	tbn0315x.16o	brdc3150.16n	igs19224.sp3	igs19224.clk_30s	igs19227.erp	2016/11/10	60.3404
csrj3160.16o	tbn0316x.16o	brdc3160.16n	igs19225.sp3	igs19225.clk_30s	igs19227.erp	2016/11/11	61.0352

csrj3170.16o	tbn0317x.16o	brdc3170.16n	igs19226.sp3	igs19226.clk_30s	igs19227.erp	2016/11/12	61.0476
csrj3180.16o	tbn0318x.16o	brdc3180.16n	igs19230.sp3	igs19230.clk_30s	igs19237.erp	2016/11/13	60.3439
csrj3190.16o	tbn0319x.16o	brdc3190.16n	igs19231.sp3	igs19231.clk_30s	igs19237.erp	2016/11/14	59.8512
csrj3200.16o	tbn0320x.16o	brdc3200.16n	igs19232.sp3	igs19232.clk_30s	igs19237.erp	2016/11/15	59.6496
csrj3210.16o	tbn0321x.16o	brdc3210.16n	igs19233.sp3	igs19233.clk_30s	igs19237.erp	2016/11/16	60.3284
csrj3220.16o	tbn0322x.16o	brdc3220.16n	igs19234.sp3	igs19234.clk_30s	igs19237.erp	2016/11/17	60.2527
csrj3230.16o	tbn0323x.16o	brdc3230.16n	igs19235.sp3	igs19235.clk_30s	igs19237.erp	2016/11/18	60.0458
csrj3240.16o	tbn0324x.16o	brdc3240.16n	igs19236.sp3	igs19236.clk_30s	igs19237.erp	2016/11/19	60.1098
csrj3250.16o	tbn0325x.16o	brdc3250.16n	igs19240.sp3	igs19240.clk_30s	igs19247.erp	2016/11/20	59.5957
csrj3260.16o	tbn0326x.16o	brdc3260.16n	igs19241.sp3	igs19241.clk_30s	igs19247.erp	2016/11/21	60.3590
csrj3270.16o	tbn0327x.16o	brdc3270.16n	igs19242.sp3	igs19242.clk_30s	igs19247.erp	2016/11/22	60.8038
csrj3280.16o	tbn0328x.16o	brdc3280.16n	igs19243.sp3	igs19243.clk_30s	igs19247.erp	2016/11/23	61.2533
csrj3290.16o	tbn0329x.16o	brdc3290.16n	igs19244.sp3	igs19244.clk_30s	igs19247.erp	2016/11/24	60.3757
csrj3300.16o	tbn0330x.16o	brdc3300.16n	igs19245.sp3	igs19245.clk_30s	igs19247.erp	2016/11/25	60.3697
csrj3310.16o	tbn0331x.16o	brdc3310.16n	igs19246.sp3	igs19246.clk_30s	igs19247.erp	2016/11/26	60.5155
csrj3320.16o	tbn0332x.16o	brdc3320.16n	igs19250.sp3	igs19250.clk_30s	igs19257.erp	2016/11/27	60.3356
csrj3330.16o	tbn0333x.16o	brdc3330.16n	igs19251.sp3	igs19251.clk_30s	igs19257.erp	2016/11/28	59.2623
csrj3340.16o	tbn0334x.16o	brdc3340.16n	igs19252.sp3	igs19252.clk_30s	igs19257.erp	2016/11/29	60.0045
csrj3350.16o	tbn0335x.16o	brdc3350.16n	igs19253.sp3	igs19253.clk_30s	igs19257.erp	2016/11/30	60.5743
csrj3360.16o	tbn0336x.16o	brdc3360.16n	igs19254.sp3	igs19254.clk_30s	igs19257.erp	2016/12/01	60.2710
csrj3370.16o	tbn0337d.16o	brdc3370.16n	igs19255.sp3	igs19255.clk_30s	igs19257.erp	2016/12/02	60.3886